North Atlantic deep-water circulation during the Messinian Stage (the latest Miocene) - Possible cause and effect: Foraminiferal and stable isotope evidence

by

Jijun Zhang

Submitted in partial fulfillment of the requirements
for the degree of Doctor of Philosophy

at

Dalhousie University
Halifax, Nova Scotia

ISBN 0-612-15860-8

Name Tijun Zhang

Dissertation Abstracts International and *Masters Abstracts International* are arranged by broad, general subject categories. Please select the one subject which most nearly describes the content of your dissertation or thesis. Enter the corresponding four-digit code in the spaces provided.

Geology

SUBJECT TERM

0 1 7 2 UMI

SUBJECT CODE

Subject Categories

THE HUMANITIES AND SOCIAL SCIENCES

COMMUNICATIONS AND THE ARTS
Architecture 0729
Art History 0377
Cinema 0900
Dance 0378
Fine Arts 0357
Information Science 0723
Journalism 0391
Library Science 0399
Mass Communications 0708
Music 0413
Speech Communication 0459
Theater 0465

EDUCATION
General 0515
Administration 0514
Adult and Continuing 0516
Agricultural 0517
Art 0273
Bilingual and Multicultural 0282
Business 0688
Community College 0275
Curriculum and Instruction 0727
Early Childhood 0518
Elementary 0524
Finance 0277
Guidance and Counseling 0519
Health 0680
Higher 0745
History of 0520
Home Economics 0278
Industrial 0521
Language and Literature 0279
Mathematics 0280
Music 0522
Philosophy of 0998
Physical 0523
Psychology 0525
Reading 0535
Religious 0527
Sciences 0714
Secondary 0533
Social Sciences 0534
Sociology of 0340
Special 0529
Teacher Training 0530
Technology 0710
Tests and Measurements 0288
Vocational 0747

LANGUAGE, LITERATURE AND LINGUISTICS
Language
- General 0679
- Ancient 0289
- Linguistics 0290
- Modern 0291

Literature
- General 0401
- Classical 0294
- Comparative 0295
- Medieval 0297
- Modern 0298
- African 0316
- American 0591
- Asian 0305
- Canadian (English) 0352
- Canadian (French) 0355
- English 0593
- Germanic 0311
- Latin American 0312
- Middle Eastern 0315
- Romance 0313
- Slavic and East European 0314

PHILOSOPHY, RELIGION AND THEOLOGY
Philosophy 0422
Religion
- General 0318
- Biblical Studies 0321
- Clergy 0319
- History of 0320
- Philosophy of 0322

Theology 0469

SOCIAL SCIENCES
American Studies 0323
Anthropology
- Archaeology 0324
- Cultural 0326
- Physical 0327

Business Administration
- General 0310
- Accounting 0272
- Banking 0770
- Management 0454
- Marketing 0338

Canadian Studies 0385
Economics
- General 0501
- Agricultural 0503
- Commerce-Business 0505
- Finance 0508
- History 0509
- Labor 0510
- Theory 0511

Folklore 0358
Geography 0366
Gerontology 0351
History
- General 0578
- Ancient 0579
- Medieval 0581
- Modern 0582
- Black 0328
- African 0331
- Asia, Australia and Oceania 0332
- Canadian 0334
- European 0335
- Latin American 0336
- Middle Eastern 0333
- United States 0337

History of Science 0585
Law 0398
Political Science
- General 0615
- International Law and Relations 0616
- Public Administration 0617

Recreation 0814
Social Work 0452
Sociology
- General 0626
- Criminology and Penology 0627
- Demography 0938
- Ethnic and Racial Studies 0631
- Individual and Family Studies 0628
- Industrial and Labor Relations 0629
- Public and Social Welfare 0630
- Social Structure and Development 0700
- Theory and Methods 0344

Transportation 0709
Urban and Regional Planning 0999
Women's Studies 0453

THE SCIENCES AND ENGINEERING

BIOLOGICAL SCIENCES
Agriculture
- General 0473
- Agronomy 0285
- Animal Culture and Nutrition 0475
- Animal Pathology 0476
- Food Science and Technology 0359
- Forestry and Wildlife 0478
- Plant Culture 0479
- Plant Pathology 0480
- Plant Physiology 0817
- Range Management 0777
- Wood Technology 0746

Biology
- General 0306
- Anatomy 0287
- Biostatistics 0308
- Botany 0309
- Cell 0379
- Ecology 0329
- Entomology 0353
- Genetics 0369
- Limnology 0793
- Microbiology 0410
- Molecular 0307
- Neuroscience 0317
- Oceanography 0416
- Physiology 0433
- Radiation 0821
- Veterinary Science 0778
- Zoology 0472

Biophysics
- General 0786
- Medical 0760

EARTH SCIENCES
Biogeochemistry 0425
Geochemistry 0996
Geodesy 0370
Geology 0372
Geophysics 0373
Hydrology 0388
Mineralogy 0411
Paleobotany 0345
Paleoecology 0426
Paleontology 0418
Paleozoology 0985
Palynology 0427
Physical Geography 0368
Physical Oceanography 0415

HEALTH AND ENVIRONMENTAL SCIENCES
Environmental Sciences 0768
Health Sciences
- General 0566
- Audiology 0300
- Chemotherapy 0992
- Dentistry 0567
- Education 0350
- Hospital Management 0769
- Human Development 0758
- Immunology 0982
- Medicine and Surgery 0564
- Mental Health 0347
- Nursing 0569
- Nutrition 0570
- Obstetrics and Gynecology 0380
- Occupational Health and Therapy 0354
- Ophthalmology 0381
- Pathology 0571
- Pharmacology 0419
- Pharmacy 0572
- Physical Therapy 0382
- Public Health 0573
- Radiology 0574
- Recreation 0575
- Speech Pathology 0460
- Toxicology 0383

Home Economics 0386

PHYSICAL SCIENCES
Pure Sciences
Chemistry
- General 0485
- Agricultural 0749
- Analytical 0486
- Biochemistry 0487
- Inorganic 0488
- Nuclear 0738
- Organic 0490
- Pharmaceutical 0491
- Physical 0494
- Polymer 0495
- Radiation 0754

Mathematics 0405
Physics
- General 0605
- Acoustics 0986
- Astronomy and Astrophysics 0606
- Atmospheric Science 0608
- Atomic 0748
- Electronics and Electricity 0607
- Elementary Particles and High Energy 0798
- Fluid and Plasma 0759
- Molecular 0609
- Nuclear 0610
- Optics 0752
- Radiation 0756
- Solid State 0611

Statistics 0463

Applied Sciences
Applied Mechanics 0346
Computer Science 0984
Engineering
- General 0537
- Aerospace 0538
- Agricultural 0539
- Automotive 0540
- Biomedical 0541
- Chemical 0542
- Civil 0543
- Electronics and Electrical 0544
- Heat and Thermodynamics 0348
- Hydraulic 0545
- Industrial 0546
- Marine 0547
- Materials Science 0794
- Mechanical 0548
- Metallurgy 0743
- Mining 0551
- Nuclear 0552
- Packaging 0549
- Petroleum 0765
- Sanitary and Municipal 0554
- System Science 0790

Geotechnology 0428
Operations Research 0796
Plastics Technology 0795
Textile Technology 0994

PSYCHOLOGY
General 0621
Behavioral 0384
Clinical 0622
Developmental 0620
Experimental 0623
Industrial 0624
Personality 0625
Physiological 0989
Psychobiology 0349
Psychometrics 0632
Social 0451

TABLE OF CONTENTS

LIST OF FIGURES

LIST OF TABLES

ABSTRACT

Quantitative studies of benthic foraminifera and stable isotopes from 4 DSDP/ODP holes (552A, 608, 547A, 646B in the North Atlantic Ocean), and one inland borehole (Salé Briquetterie, Morocco) have been conducted to determine the deep-water circulation in the North Atlantic and its possible relationship to the Mediterranean Salinity Crisis during the Messinian. The Messinian sequences in these holes are well controlled by integrated magneto-, isotope- and bio-stratigraphy. Our data show a distinct relationship between the Atlantic deep-water circulation and the Mediterranean Salinity Crisis.

Benthic foraminifera from Salé core clearly show three major stages of water exchange, which are constrained by local tectonic movements during the Messinian: Stage 1 occurred between 7.12–6.2 Ma is characterized by paleo-Mediterranean outflow water (PMOW) leaking, suggesting an anti-estuarine circulation system. This model suggests that the paleo–Mediterranean Basin probably was equivalent to an euxinic environment where the bottom water had become stagnant and poorly oxygenated below sill depth. Stage 2 (6.2–5.9 Ma) is marked by a reversed current (i.e., Atlantic inflow into the Mediterranean). This reversed current reflects a strong negative water balance in the Mediterranean Basin caused by strong evaporation, and marks the onset of the Mediterranean salinity crisis. Stage 3 (5.9–5.32 Ma) is characterized by a significant uplift of Morocco and salinity crisis in the Mediterranean Basin. In Stage 3, seven glacioeustatic sea-level lowerings occurred, once every 100,000 yrs, coinciding with the eccentricity orbital parameter. These sea-level fluctuations may have served as an "automatic choke" in controlling the Atlantic water infilling, and have caused the cyclic evaporite deposits in the Mediterranean Basin. At about 5.6 Ma, a major transgression is observed in Salé core, which is considered to have caused the unconformity that separates the Lower and Upper Evaporites in the Mediterranean Basin. Such sea-level changes are also observed in abyssal North Atlantic indicated by similar numbers of deep-water turbidite cycles at Site 646 and climate cycles recorded at Site 552. It is clear that the cause of the Mediterranean Salinity Crisis has been associated with both Moroccan uplift and sea–level lowerings that coincide with eccentricity forcing.

In the deep ocean, three major paleoceanographic phases similar to those in Morocco are also determined in the intervals of 7.12-6.2 (Stage 1), 6.2-5.9 (Stage 2), and 5.9-5.32 Ma (Stage 3), respectively. During Stage 1, the North Atlantic was characterized by relatively strong, altered North Atlantic Deep Water (NADW) and Antarctic Bottom Water (AABW) fluxes, indicating relatively good ventilation in the open ocean. This is also supported by the presence of an unconformity at Site 547 that cut off the early Messinian section (7.12-6.2 Ma). AABW may have pinched out at least as far as 60°N in the North Atlantic Ocean at this time. During Stage 2, AABW was significantly reduced during the onset of Mediterranean Salinity Crisis. In Stage 3, deep-water circulation varied significantly. In particular, both NADW and AABW were greatly reduced at 5.75 and 5.55 Ma, respectively. These two major reductions are coeval with two major glaciations recorded in stable oxygen isotopes, indicating the cause coupled with climate cooling and Mediterranean Salinity Crisis. The salinity crisis could have caused open ocean to be more sluggish. However, brief returns of NADW and AABW have occurred during the "interglacial" at about 5.6 Ma. This return has been linked to the major unconformity (resulting from inundation) that separates the Lower and Upper Evaporites in the Mediterranean Basin.

Acknowledgments

I would like to take this opportunity to thank my supervisor Dr. David. B. Scott for suggesting this research topic to me, for discussing major issues of the project, and for providing invaluable advice and criticism. I would like to acknowledge my committee members, Drs. Franco Medioli, Peta Mudie and Peter H. Reynolds for their discussions, criticisms, and encouragement. Many thanks also go to Dr. Martin Gibling for his contribution of the early phase of the project and his review, and to Dr. Richard K. Olsson (Rutgers University, USA), Dr. Pat J.C. Ryall (Departmental Chair), and Dr. Dave Piper (Bedford Institution of Oceanography/BIO) for their reviews and invaluable suggestions.

I thank Dr. William A. Berggren at Woods Hole Oceanographic Institution (WHOI), Woods Hole, MA for discussion of biostratigraphy and confirmation of the Messinian planktonic foraminiferal taxa for DSDP Holes 608 and 547A and partial review of my thesis, and to thank Dr. M.-P. Aubry (WHOI) for her re-interpretation of nannofossil biostratigraphy of DSDP Hole 608. Many thanks are to Drs Kenneth G. Miller and C. Liu for running Sr stable isotope of ODP Site 646B at Rutgers University, NJ; to Dr. David A. Hodell at the University of Florida for running stable isotopes for DSDP Site 608; to Dr. Lloyd D. Keigwin (WHOI) for providing me original stable isotope data of DSDP Site 552A; and Dr. Nick J. Shackleton at University of Cambridge, England for providing his unpublished work of ODP Site 846. Dr. Richard H. Benson at the Smithsonian Institution, Washington, D.C. is greatly acknowledged for providing me Salé (Morocco) drilling material and continuous invaluable discussion on Messinian biostratigraphic and paleoceanographic issues as well as critical review of chapters 4 and 5 which were sent to *Paleoceanography* and *Marine Micropaleontology, respectively* for publication. Dr. Zehui Huang (BIO) is acknowledged for his kind assistance in time series analysis for DSDP Site 552A and Salé borehole and for his partial review of Chapter 2.

Dr. Kenneth J. Hsü at Geological Institute, ETH, Zürich, Switzerland, and Fritz J. Hilgen at University of Utrecht, Netherlands are greatly thanked for providing helpful suggestions for this study. Dr. K.G. Miller, Dr. Ellen Thomas at Yale University, and Dr. Michael Kaminski at University College, London, England are thanked for their review of Chapter 5 that was sent to Paleoceanography for publication. I thank Drs. Dan Kelley and Barry Ruddick at the Department of Oceanography, Dalhousie University for discussion of some physical oceanographic issues. I thank Chloe Younger for her technical expertise in the processing all the samples both for micropaleontological and stable isotopic studies. Thanks are to Ms Lynne Maillet at Dalhousie University who allowed me to use the departmental scanning electronic microscope, and Ms Julie Richards at Lamont-Doherty Earth Observatory of Columbia University who helped me to sample DSDP/ODP cores.

I would express my thanks to Dr. K.G. Miller, Dr. W.A. Berggren and Dr. John A. van Couvering at Micropaleontology Press, American Museum of Natural History, NY, for encouraging me to pursue Ph.D. degree at Dalhousie University. I would like to thank Dr. Dave Scott and his wife Dr. Kumiko Azetsu Scott, Dr. Franco S. Medioli, Jane Barrett, Eric Collins, Emmanuelle Javaux, Ana Putar-Roberts, Neil Tibert, Neil Banerjee, and other professors as well as students in the Department of Earth Sciences, with whom I shared joyfulness and happiness during the 4-year Ph.D. mission at Dalhousie University.

Finally, I would like to thank all my family members for different kinds of support; particularly, my mother-in-law who took care of my little son and almost all of the home work, and my wife Lisha Zheng who provided continued support, encouragement and voluntary work that greatly fulfill this project and benefit the geosciences.

This project was supported by Izzak Waiton Killam Memorial Trust Scholarship at Dalhousie University and partially supported by 1994 GSA Student Award and 1993 Cushman Foundation Student Award, together with funds from a Natural Sciences and Engineering Research Council research grant to D.B. Scott.

CHAPTER 1

GENERAL INTRODUCTION

1.1. This study

1.1.1. Importance and problems of the Messinian deepwater circulation

The Messinian Stage is considered to be one of the most important intervals of the Neogene, where a number of paleoceanographic and paleoclimatic events, termed "Terminal Miocene events" (Van Couvering et al., 1976; Kennett, 1983) occurred. In particular, the formation of the Giant Salt in the Mediterranean Sea could have drained off more than six percent of dissolved salts and turned the world oceans less alkaline, resulting in deep waters that were more undersaturated in calcium carbonate, and thus caused more extensive carbonate dissolution in deep oceans (Ryan, 1973). The concurrent freshening of surface sea water resulting from the loss of the salts may have enhanced the formation of high latitude sea ice, leading to the great burst of glaciation in Antarctica, and further to the formation of global deep water circulation (Kennett, 1983).

Messinian deep water circulation has not only been closely related to tectonic movement, marine sedimentation patterns, and faunal migrations, but also to redistribution of salt and heat on a global scale. The latter is particularly crucial to the modulation of paleoclimate. Various scientists (e.g., Stommel, 1958a, b; Blanc and Duplessy, 1982; Hooper and Weaver, 1987; D.B. Scott, pers. comm., 1993; K.J. Hsü, pers. comm., 1992; Ryan, 1973) postulated that the shutting–off of the Paleo–Mediterranean Outflow Water (PMOW) into the Atlantic Ocean and salt extraction during the Messinian Salinity Crisis could have caused a series of paleoceanographic changes in the world oceans and changes of global climate. Some important recent studies suggest that glacial and interglacial cycles may have been linked with deep water circulation (Broecker and Denton, 1990; Broecker et al., 1990; Lehman and Keigwin, 1992a; Lehman and Keigwin, 1992b;

Lehman and Keigwin, 1992c; Veum et al., 1992), rather than with Milankovitch forcing alone (i.e., precession, eccentricity and obliquity). Broecker and Denton (1989) estimated that the production of the North Atlantic Deep Water (NADW) releases an amount of heat to the North Atlantic north of 35^{o}N which is equivalent to 25% of incoming solar radiation.

However, after over twenty years of study, our knowledge of the Messinian deep water circulation in the North Atlantic and its relationship to the Messinian Salinity Crisis is still limited, leaving various assumptions poorly understood. This may be attributed to: 1) incomplete stratigraphic sections in oceanic basins and misinterpreted stratigraphic records; 2) low sampling resolution; 3) concentration on large size fractions (>150 μm) for benthic foraminiferal studies, which eliminates ~80% of the small population of total benthic fauna (Kurihara and Kennett, 1992; Schröder et al., 1987); and 4) difficult stratigraphic correlation between open ocean and the Mediterranean due to the isolation of the Mediterranean Sea from the Atlantic Ocean during the Messinian.

1.1.2. Objectives and approaches

The primary objectives of the study were: 1) to determine the response of the North Atlantic bottom waters, namely the North Atlantic Deep Water (NADW), the Mediterranean Outflow Water (MOW), and the Antarctic Bottom Water (AABW) to the Messinian Salinity Crisis; and 2) to evaluate the relationships between the Messinian bottom water masses, paleoclimate, and tectonic evolution in the North Atlantic Ocean and inland Morocco. A secondary objective of the project was to procure accurate Messinian stratigraphic control based on an integration of biostratigraphy, magnetostratigraphy, and isotopic stratigraphy. To achieve the above objectives, four approaches were undertaken:

1. Continuous and complete (or nearly so) Messinian sections were selected from stratigraphically important locations which may have been influenced by deep water masses;

2. High sampling resolution. Low sampling resolution obviously does not satisfy the frequent connections and isolations between the Atlantic and Mediterranean Sea, resulting from highly fluctuating Messinian climate and tectonic activities during Messinian time;

3. Foraminiferal and stable isotope analyses. Deep water masses are distinguished in today's oceans by combinations of temperature, salinity, and geochemical tracers (such as $\delta^{18}O$ and $\delta^{13}C$). However, reconstructions of water masses in past oceans rely primarily on deep–water organism biofacies and deep–water benthic foraminiferal isotope analyses (i.e., geochemical tracers). Study of benthic foraminifera is essential because stable isotopic studies alone yield uncertain conclusions resulting from the difficulties of separating isotopic value from temperature fluctuation and ice volume variation. Certain benthic foraminiferal assemblages are considered bottom water indicators because they are sensitive to environmental parameters such as oxygen content, temperature and salinity, which are expected to have replaced each other when the bottom waters changed during pre–"desiccation", "desiccation", and post–"desiccation" of the Messinian.

The variation of oxygen and carbon stable isotope values recorded in benthic calcareous fossil tests results from changes in the isotopic composition of the seawater caused by environmental changes. The isotopes provide information not only for stratigraphic correlation, but also for paleoenvironmental gradients. AABW is distinguished from NADW by its strongly positive $\delta^{18}O$, lower $\delta^{13}C$ and high nutrients (Worthington, 1970). MOW is even higher (averaging ~1.5‰) in $\delta^{13}C$ than NADW due to low productivity in the Mediterranean (Hodell et al, 1989). These isotope criteria are used to determine bottom water characteristics in my study. In addition, oxygen isotope values in planktonic foraminiferal tests indicate climatic changes. For example, a high $\delta^{18}O$ value implies a low temperature, and vice versa, in the surface dwellers planktonic foraminifera.

4. Messinian stratigraphic control. To determine the bottom water characteristics at selected time slices within the Messinian, a reliable integrated stratigraphic scheme was

investigated. Planktonic foraminiferal biostratigraphy for all selected sites both from abyssal basin and inland, and isotope stratigraphy for Site 608 are investigated in this study, while nannofossil biostratigraphy, magnetostratigraphy and isotope stratigraphy for the remaining selected sites (or whichever possible) are reinterpreted based on the available data obtained during each DSDP/ODP leg, and the latest development of Messinian stratigraphy and chronology.

1.2. Brief geological background of the North Atlantic Ocean

In this introductory chapter, I will provide brief geological and physical oceanographic background information, which may be potentially necessary for interpretation of data in this study.

1.2.1. Tectonics

The opening of the North Atlantic began in the Middle Jurassic, some 165 million years ago, although the central Atlantic, Caribbean and Gulf of Mexico might have formed little earlier (Sclater and Tapscott, 1979). The Norwegian–Greenland seas started to open between 60–63 Ma. Most of the major topographic features of the Atlantic had formed and the Vema Channel between the Rio Grande Rise and South America subsided to the depth below 4000 m by 36 Ma, allowing AABW formed in the Weddell Sea to enter the North Atlantic Basin. An important change at this time was the change in motion between Greenland and North America. Greenland changed from a rotation about northern Baffin Bay to a rotation about a pole near the center of the Sahara. This movement resulted in the opening of the Baffin Bay and Labrador Sea. During the early to middle Miocene overflow water from the Norwegian–Greenland seas began to flow in significant quantities into the North Atlantic, creating basic circulation patterns existing in the modern Atlantic Ocean (Kennett, 1983).

By the late Miocene, the North Atlantic basin had attained its approximate present size, shape, and depth. The circum–equatorial seaways were virtually closed at about 5.5 Ma. Major tectonic subsidence of the Iceland–Faeroe ridge caused by sea–floor spreading between Greenland and Scandinavia (Vogt, 1972; Talwani, Udintsev et al., 1976; Nilsen and Kerr, 1978; van Hinte, 1979; Thiede, 1980) in the North Atlantic is considered to have occurred during the middle Miocene, although the subsidence might have been initiated during the Oligocene.

Several important fracture zones along the Mid–Atlantic Ridge (Fig. 1-1), such as the Romanche Fracture Zone at the equator north of the Brazil Basin, Vema Fracture Zone at ~11^{O}N, and Charlie–Gibbs Fracture Zone at ~52^{O}N, may have served an important role in deep water circulation. Miller et al. (1987) suggested that AABW could have entered into the eastern North Atlantic from the western Atlantic across the Romanche Fracture Zone during the Miocene. In addition, McCartney et al. (1991) and McCartney (1992) determined that AABW diluted by NADW in the western North Atlantic Basin, enters the northeastern North Atlantic through the Vema and Romanche Fracture zones at ~ 11^{O}N and near the equator, respectively. They observed that the abyssal circulation in the northeastern Atlantic basins such as Gambia Abyssal Plain, South Canary Basin, and North Canary Basin is strongly influenced by the Vema Fracture Zone. The Charlie–Gibbs Fracture Zone serves as a major conduit through which the Norwegian Sea overflow water moves into the Irminger Basin, and then into the Labrador Basin in the western North Atlantic Ocean (Broecker and Peng, 1982; McCave and Tucholke, 1986; Arthur et al., 1989).

The Mediterranean Sea, which played a particularly important role in late Miocene paleoceanography and paleoclimatology, has experienced great changes in its configuration since the Miocene. This inland Sea has been considered a relic sea transferred from the Tethys as a result of the northward movement of the Africa plate (Suess, 1901). On the contrary, Argand (1924) considered that the Tethys was completely terminated by the Alpine Orogeny, and the modern Mediterranean basins were formed during a major

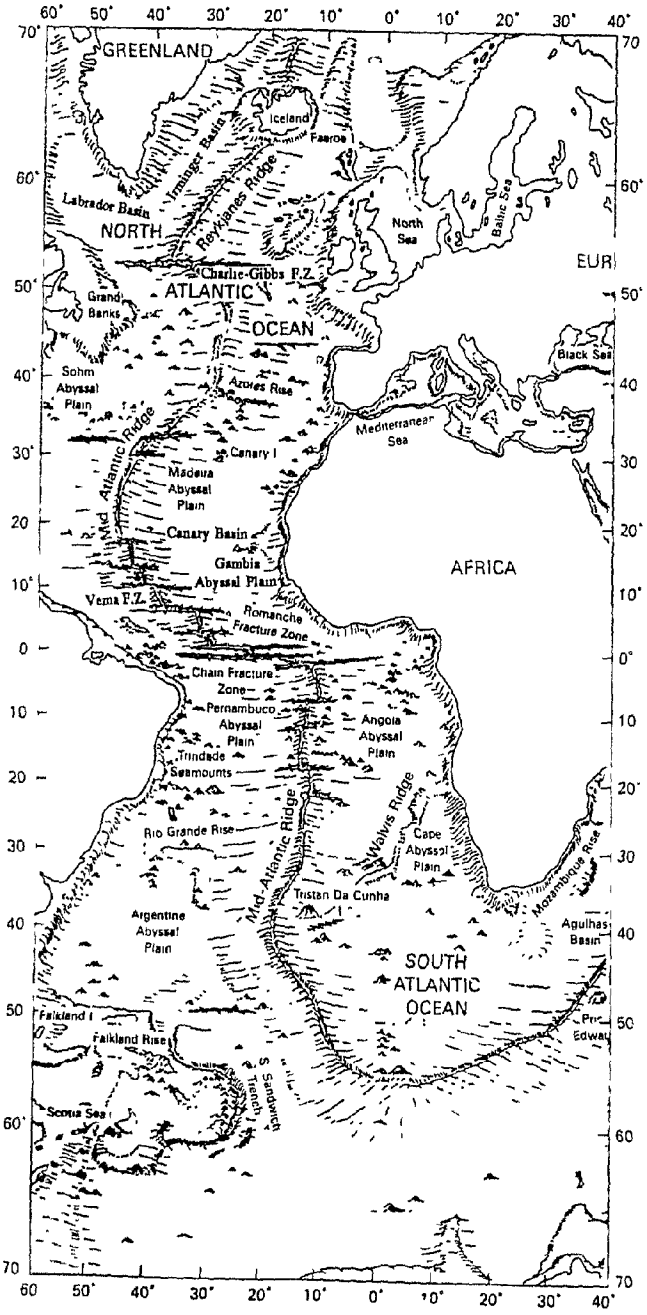

Fig. 1-1. Atlantic ocean floor (from Kennett, 1983).

extensional phase in late Oligocene and early Miocene. However, the study of heat flow (Erickson and Von Herzen, 1978) during DSDP Leg 42A suggested that the Mediterranean basins originated a quite different geological times. Hsü and Bernoulli (1978) suggested that only Levantine and Ionian seas in the Eastern Mediterranean may represent relics of Tethys, while the Tyrrhenian, Balearic and Aegean seas were formed during the late Cenozoic as evidenced by high heat flow. The Aegean Sea, lacking oceanic crust, is the youngest, mainly having subsided during the Quaternary. Hsü and Bernoulli (1978) reported that the Tyrrhenian Sea was formed as a back–arc basin largely prior to the Messinian salinity crisis. There are some crucial controversies for the origin of the Balearic Basin. Hsü et al. (1978) claimed a subsidence of the Balearic in early Miocene, whereas Stanley (1974) suggested a foundering in the Pliocene. This is a critical issue for the genesis of the Giant Salt in the Balearic basin as to whether or not the deep Mediterranean basins were desiccated as Hsü, Ryan and Cita (1973) proposed.

1.2.2. Seaways

The history of basin development in the Cenozoic North Atlantic is a history not only of the progressive tectonic enlargement, but also of the opening of seaways that apparently are important in exchanging surface and deep water between the oceanic basins (Berggren and Hollister, 1974; Miller and Tucholke, 1983; Miller et al., 1987). Deep water exchange between the oceanic basins via seaways may result in differential chemical fractionation of water masses, local and global climatic fluctuations, and changing biogeographic provincialism. During the Messinian Stage, several seaways are considered to be crucial in Atlantic and Mediterranean paleoceanography, such as the Panamanian Isthmus, the Gibraltar Strait, the Iceland–Faeroe Channel, the Denmark Strait, and the Vema Channel.

The Panamanian Isthmus served as a communication conduit of seawater between the Atlantic and Pacific before Pliocene time. This conduit shoaled since the late Miocene

causing a possible global decrease of carbon–13 (Bender and Keigwin, 1979), and its final closure took place at about 3.5 to 2.5 Ma (late Pliocene), triggering the initiation of the Northern Hemisphere glaciation (Keigwin, 1978; Marshall, 1988; Coates et al., 1992; Collins, 1993). Many studies (e.g., Gartner et al., 1987; Duque–Caro, 1990; Coates et al., 1992) show that the benthic assemblages pattern on the Atlantic side became quite different from that on Pacific side when the shoaling of the Panamanian Strait took place.

The Iceland–Faeroe Sill (about 600–1000 m below present sea level), once above sea level, began to subside about 28 Ma, as a result of sea–floor spreading, linking the Arctic Ocean as a heat sink to the Atlantic, and thus the world oceans. The main body of the Iceland–Faeroe Ridge subsided below the sea level by the middle Miocene (Vogt, 1972; Talwani, Udintsev et al., 1976; Thiede, 1980; van Hinte, 1979), although there is a possibility that some of the deeper sills such as the Denmark Sill and Faeroe Bank Channel may have subsided earlier (Roberts et al., 1983; Write and McKenzie, 1989). This significant subsidence allowed fundamental deep–water mass exchanges between the Arctic and the other oceans (Schnitker, 1980).

The base of Denmark Strait is about 600 m below the present sea level. The history of its evolution is least well documented. It has been suggested to have begun a rifting since Anomaly 24, some 56 million years ago (White and McKenzie, 1989), but it did not subside below the sea level until 35 Ma (Miller et al., 1987). The Denmark Strait probably reached its present depth during the late Miocene.

The Strait of Gibraltar (about 300–400 m below present sea level) is the only passage between the Mediterranean Sea and the world ocean at the present time. Major water exchange between the inland sea and open ocean depends on this passage. However this strait is geologically young. It was opened only some 5 million years ago (at the beginning of the Pliocene). Prior to the Pliocene, two seaways, namely the Betic Passage in southern Spain, and Rifian Corridor in northwestern Morocco, existed for water exchange between the Atlantic and the Mediterranean Sea. These coupled seaways have

been called the "Twin–channel" (Benson et al., 1991). These twin–channels completely closed at the end of the Messinian (~ 5.3 Ma) as a result of the uplift of the Betic–Rifian Orogeny, immediately followed by the opening of the Gibraltar Strait. The uplifting and restricting of the twin–channel probably, in part, caused the isolation of the Mediterranean Sea from the Atlantic Ocean at this time.

1.3. Physical Oceanography of the North Atlantic and Mediterranean Sea

1.3.1. Deep–water circulation

Deep water circulation is driven by temperature- and salinity-related density differences, which may result in global climate change through redistribution of oceanic heat and salt. There are three major source areas in the world ocean producing deep water masses, namely the Norwegian-Greenland seas in the north, the Weddell Sea and the Ross Sea in the Antarctic, which produce super-cooled, high salinity, high density waters that sink to the deep ocean. Today's North Atlantic Ocean is dominated by three major deep water masses, i.e., the northward–flowing Antarctic Bottom Water (AABW; Fig. 1-2), the southward–flowing North Atlantic Deep Water (NADW; Figs. 1-2; 1-3) with a branch entering the eastern North Atlantic Ocean is known as Northeast Atlantic Deep Water (Fig. 1-3), and by the Mediterranean Outflow Water (MOW; Fig. 1-4; also see "Overflow" below for more details).

The Antarctic Bottom Water is one of two principal components of Southern Ocean circulation, the other being the Antarctic Circumpolar Water (CPW) (Pudsey et al.. 1988). This southern hemisphere thermohaline flow is cold and nutrient–enriched, formed mainly (~70%) in the Weddell Sea by the increase of salinity and density due to the sea ice formation, and associated with the melting and freezing at the bottom of ice shelves in the Antarctic (Gordon, 1975; Foldvik and Gammelsrod, 1988). Although AABW (density σ_t = 27.9) is not as dense as the deep waters in either the Norwegian–Greenland seas or the Mediterranean Sea, it does not have to pass over shallow ridges or through straits where

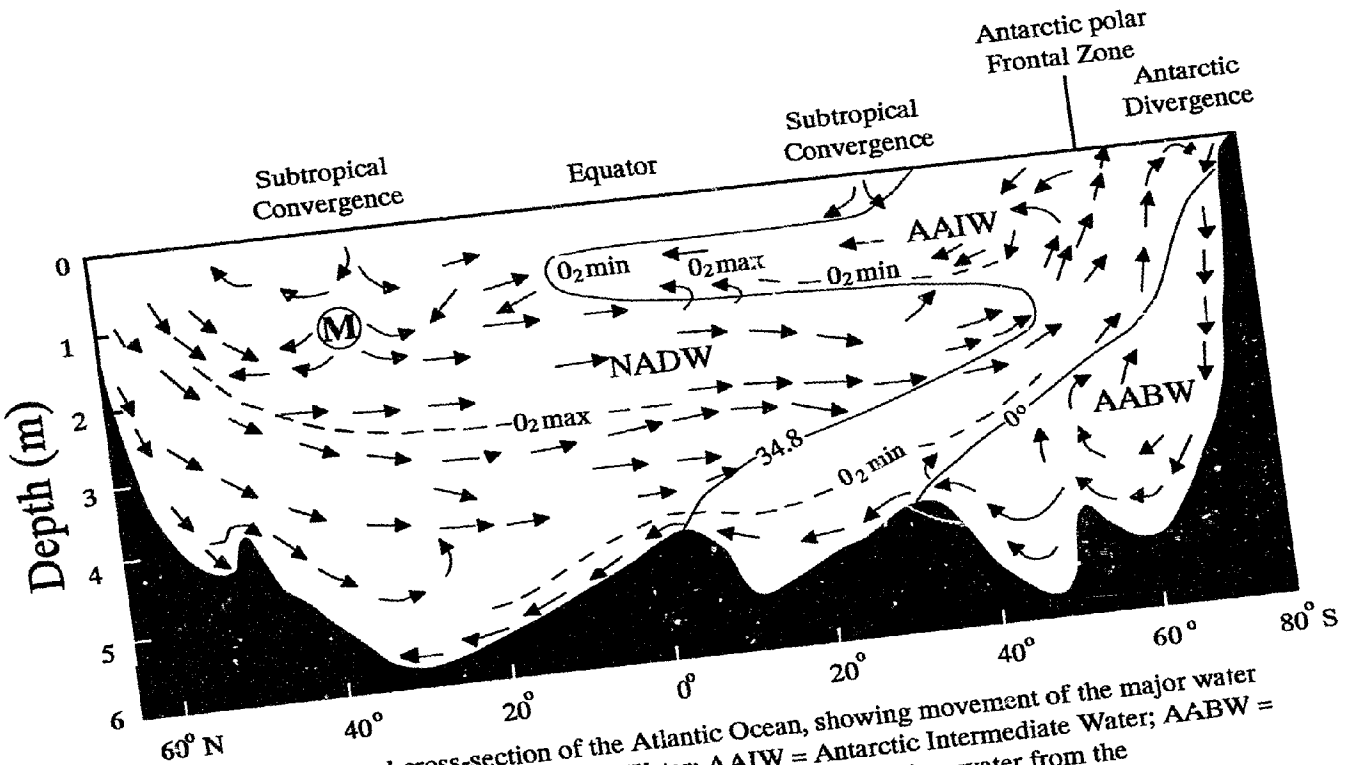

Fig. 1-2. Meridional cross-section of the Atlantic Ocean, showing movement of the major water masses; NADW = North Atlantic Deep Water; AAIW = Antarctic Intermediate Water; AABW = Antarctic Bottom Water; The M at about 35°N indicates the outflow water from the Mediterranean Sea (after Open University, 1989).

Fig. 1-3. Schematic map showing the main paths followed by the two types of North Atlantic Deep Water - North-East Atlantic Deep Water (NEADW) and North-West Atlantic Bottom Water (NWABW) - in relation to the topography of the sea floor and the flow of Labrador Sea Water (LSW). Flow data are from Open University (1989).

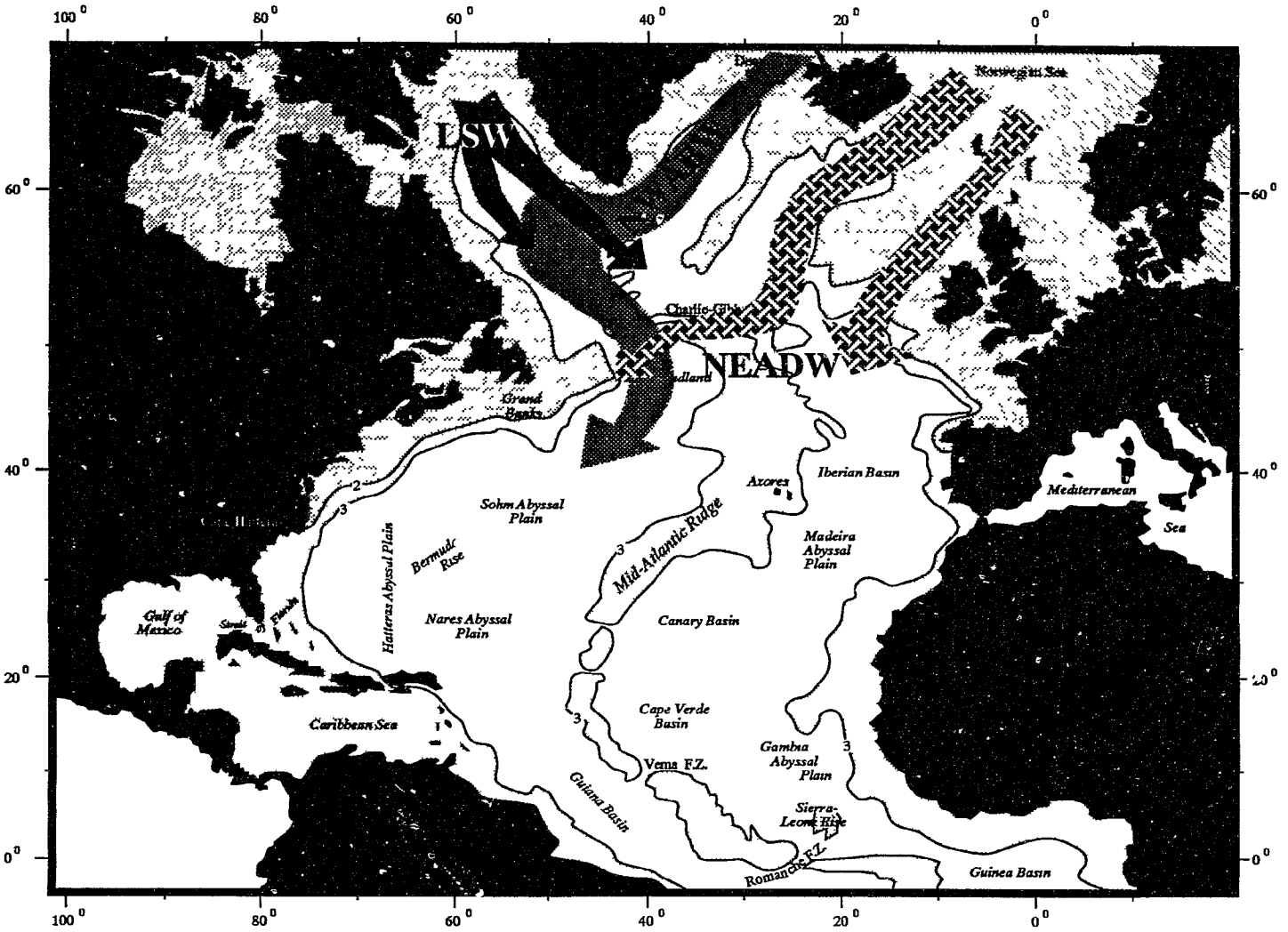
100°
80°
60°
40°
20°
0°
60°
40°
20°
0°
LSW
NEADW
Norwegian Sea
Charlie Gibbs
Grand Banks
Iberian Basin
Azores
Mediterranean Sea
Sohm Abyssal Plain
Bermuda Rise
Hatteras Abyssal Plain
Mid-Atlantic Ridge
Madeira Abyssal Plain
Gulf of Mexico
Nares Abyssal Plain
Canary Basin
Caribbean Sea
Cape Verde Basin
Vema F.Z.
Gambia Abyssal Plain
Guiana Basin
Sierra-Leone Rise
Romanche F.Z.
Guinea Basin

Fig. 1-4. Distribution of (a) temperature (^{0}C) and (b) salinity (‰) at 1000m depth in the North Atlantic, showing the spread of Mediterranean Outflow Water (MOW) (after Open University, 1989).

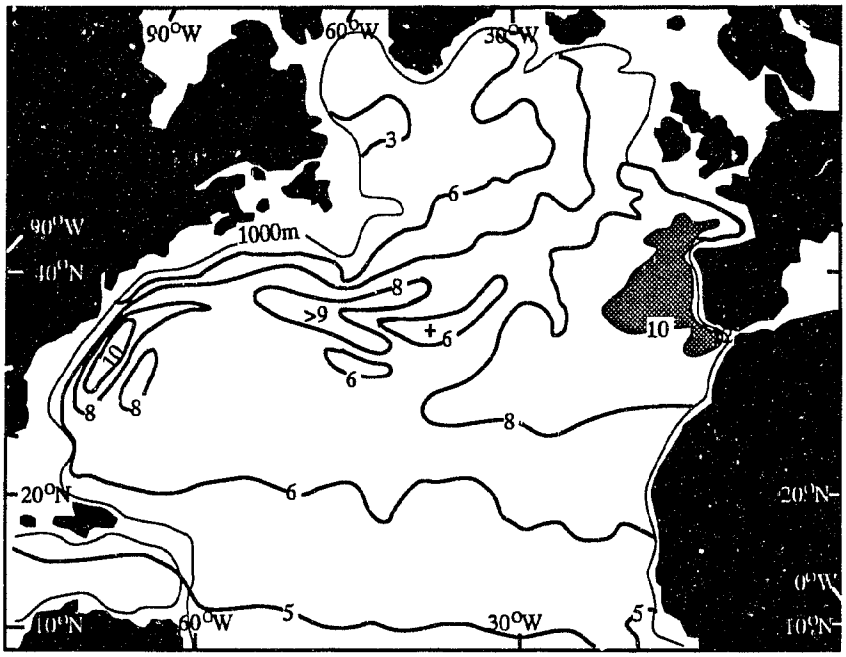
90°W
60°W
30°W
90°W
40°N
1000m
3
6
8
>9
6
10
10
6
8
8
8
20°N
6
20°N
0°W
10°N
60°W
5
30°W
5
10°N

(A)

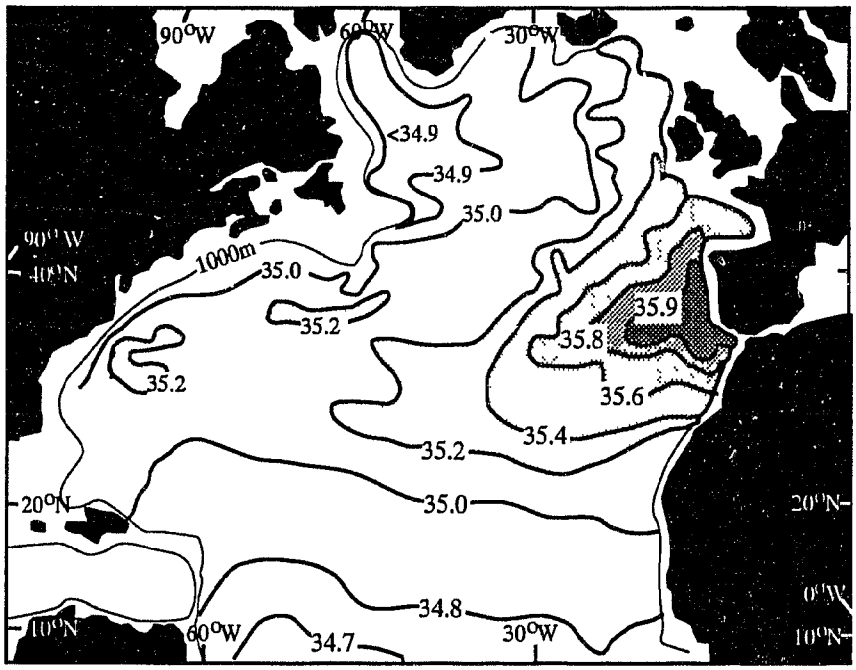
90°W
60°W
30°W
<34.9
34.9
35.0
90°W
40°N
1000m
35.0
35.2
35.9
35.8
35.6
35.2
35.4
35.2
20°N
35.0
20°N
0°W
34.8
10°N
60°W
34.7
30°W
10°N

(B)

large quantities of less dense water become entrained in it, and thus it is the most dense water in deep open ocean (Open University Course Team, 1978). AABW flows northwards after leaving the Weddell Sea, and reaches about 40°N in the North Atlantic Ocean through the Argentine Basin and Vema Channel north of the Brazil Basin (Gordon, 1975). As mentioned earlier, this water also enters into the eastern North Atlantic through Vema and Romanche Fracture zones in the Mid–Atlantic Ridge. It becomes stronger during interglacial periods (Pudsey et al., 1988).

During Messinian time, AABW not only occurred in the western North Atlantic, but also in the eastern North Atlantic (Murray et al., 1986, Murray, 1986). This type of water was also suggested to be in the Labrador Sea during the Tortonian (Kaminski et al., 1989).

The history of circulation of AABW is equivocal. One idea is that AABW entered the North Atlantic when the Vema Channel subsided during the Pliocene (McCoy and Zimmerman, 1977). Other suggestions are that it flowed into the North Atlantic during the middle Miocene. Murray et al. (1986) reported that the earliest AABW was recorded at 10 Ma. AABW moved northward progressively, and reached about 57^0 N at 5.0 Ma when MOW was shut off.

The North Atlantic Deep Water (NADW) is a nutrient–enriched and cold deep water mass. It is initiated in the Norwegian-Greenland seas when the Mediterranean Outflow Water and the Gulf Stream enter there through the Iceland–Faeroe Ridge and sink to the bottom as they cool (Gordon, 1975). This denser water mass feeds back across the Iceland–Faeroe Ridge and Denmark Strait to the Atlantic Ocean, and combines with intermediate water south of the Ridge to form NADW (Turnau and Ledbetter, 1989), although Zahn et al. (1987) suggested a contrast for the late Quaternary. Characteristics of NADW are apparent in the western boundary current as far as 40°S. Eventually, a part of the water mass flows further southward, and is entrained within CPW entering the other major oceans.

In the North Atlantic Ocean, however, two types of NADW have been recognized. They are the North East Atlantic Deep Water (NEADW) and North West Atlantic Bottom Water (NWABW). NEADW crosses the sill between Iceland and Scotland with temperature about 2.5°C and salinity about 35.03‰. Some of this water continues south in the eastern basin, whereas the remainder flows into the western basin. NWABW crosses the sill between Iceland and Greenland. It is considered to be a combination of Norwegian–Greenland Deep water (NGDW), NEADW and Labrador Sea Water (LSW), with temperature 1°C and salinity 34.91‰ (Open University Course Team, 1978)(refer to "Overflow" for more details).

Most recently, some scientists (Broecker et al., 1990; Broecker, 1990; Lehman and Keigwin, 1992a; Lehman and Keigwin, 1992b; Lehman and Keigwin, 1992c) have proposed a twist to the model of the conveyor–belt/salt–oscillator hypothesis. This conveyor model contains two subsurface belts in the North Atlantic Ocean, which carry NADW southwards. The upper belt is fed mainly by open ocean convection in the Labrador Sea, and the lower one primarily by convection within the Norwegian Basin (Lehman and Keigwin, 1992b). The movement of these subsurface belts eventually are driven by warm salty surface water which includes the Gulf Stream and Mediterranean Outflow. Schmitz and McCartney (1993) hypothesized that most NADW may upwell in the Antarctic Circumpolar Current regime, eventually to form Antarctic Intermediate Water (AAIW) and AABW, while small amounts continue into the Pacific and Indian oceans. A similar conveyor belt was originally suggested by Gordon (1986) and Broecker (1987) (Fig. 1-5).

NADW production began prior to the late Miocene (Schnitker, 1980; Blanc and Duplessy, 1982; Miller and Fairbanks, 1985; Wooddruff and Savin, 1989). However, it has experienced great changes since then. For example, there has been an abrupt increase in its production rate immediately prior to the large scale melting of the Northern Hemisphere ice sheets and a reduction during the last glacial maximum recorded in the Southern Ocean

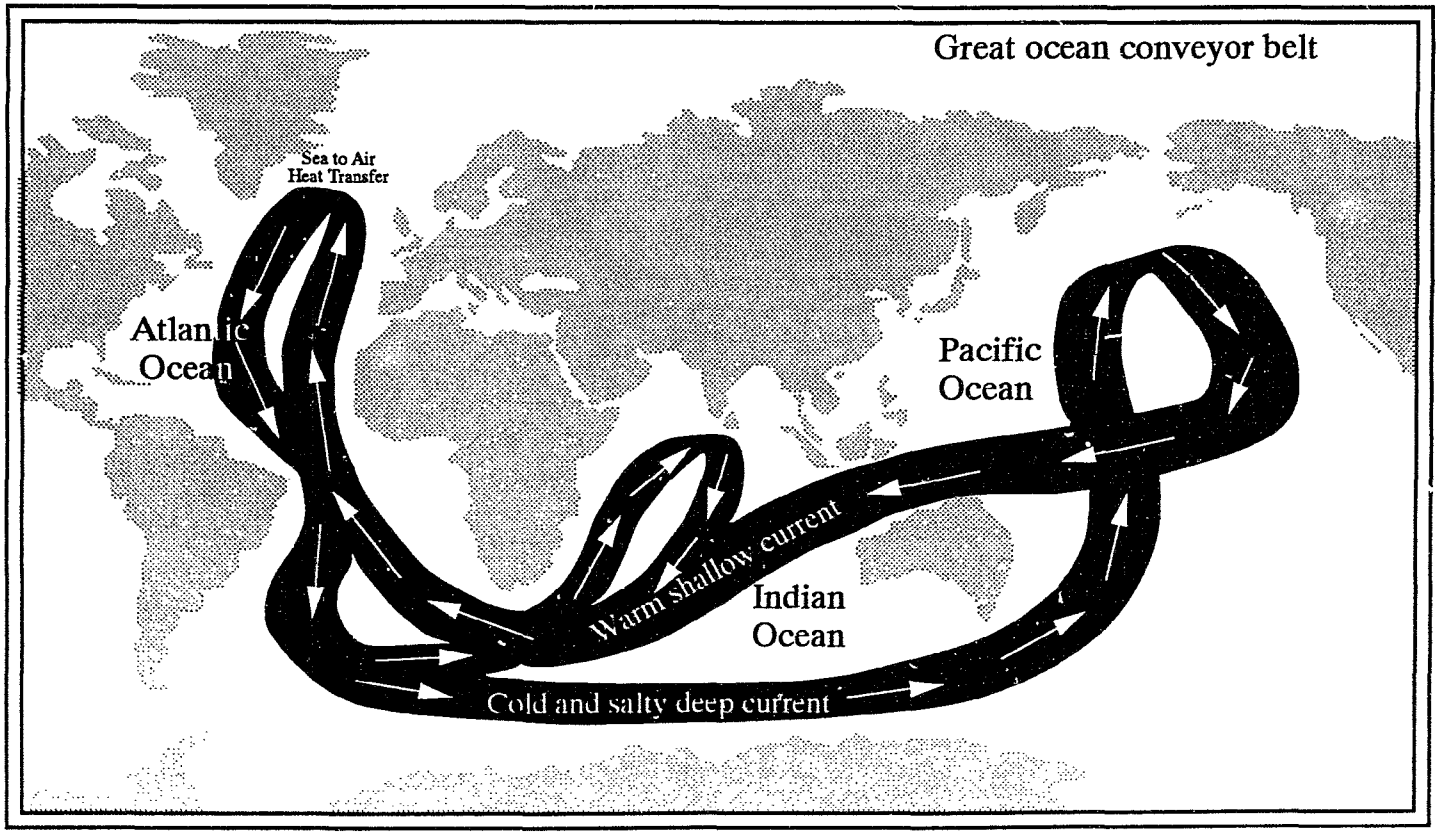

Fig. 1-5. The great ocean conveyor logo (after Broecker, 1987)

(Charles and Fairbanks, 1992). In addition, Wright et al. (1991) suggest a complete shutdown at 8.6 Ma, and highest productions at 9.8–9.3 Ma, 7.8–7.0 Ma, and after 5.8 Ma during the late Miocene. During the middle Miocene, NADW dominated the entire North Atlantic Ocean and it is considered to have been initiated when the main Iceland–Faeroe ridge subsided. NADW seems to have been much stronger in the Messinian than in the middle Miocene.

1.3.2. Surface Circulation in the North Atlantic Ocean

1.3.2.1. The Subtropical Gyre

The North Atlantic Subtropical gyre (Fig. 1-6) is the main clockwise surface oceanic circulation system in the area, which is related to the overlying regions of high pressure in the atmosphere, and to the anticyclonic wind fields where the westerlies blow eastward from North America at 45°N and trade winds westward from Africa at 15°N. Because the center of the mid–latitudes anticyclone in the atmosphere tends to be located over the eastern rather than the western side of the ocean, whereas the Subtropical gyre is nearly centered in the western side, the gyre becomes asymmetrical in physical characteristics between the east and west. In the east of the gyre, relatively slow, wide, shallow and diffuse currents occur (known as the eastern boundary currents, such as the Canary Current), whereas fast, narrow, deep and intense currents are developed in west of the gyre (known as the western boundary currents, such as the Gulf Stream)(Open University Course Team, 1989). The western boundary current is typically only some 100 km in width but has a velocity greater than 2 m s^{-1}. The eastern boundary current (the Canary Current) is more than 1000 km wide with a velocity of less than 0.25 m s^{-1} (Open University Course Team, 1978). The central water mass in the North Atlantic subtropical gyre is situated in the Sargasso Sea. It serves as a 700–800 m deep warm water pool in which the upper layer of most of the North Atlantic Ocean is produced (Pickard and Emery,

1982). This water mass is characterized by high temperature (about 25–28°C), low nutrients, low biological productivity, and little terrigenous input.

1.3.2.2. The Gulf Stream

The Gulf Stream (Fig. 1-6) plays an extremely important role in the formation of Atlantic deep water circulation (e.g., Worthington, 1976; McCartney, 1992). This stream is originally derived from the North Equatorial Current joined by some of the South Equatorial Current across the Equator as a function of the deflection by the Brazilian coastline. Much of the North Equatorial Current enters the Caribbean Sea through the passage between the Lesser Antiles, and continues through the Yucatan Channel into the Gulf of Mexico. The outlet from the Gulf of Mexico is through the Strait of Florida, most of the water taking a direct path from the Yucatan Channel into the Strait of Florida and not taking part in the circulation of the Gulf of Mexico itself (Open University Course Team, 1978). The Gulf Stream (s.s.) may be considered to extend from the Strait of Florida to the Grand Banks of Newfoundland (~55°N). It has two sections separated by a line east of the Cape Hatteras. In the first section between Florida and Cape Hatteras, the current runs along the Blake Plateau following the continental slope with a depth limited to about 800 m, and remains narrow and well–defined, and meanders are restricted to a maximum of 55 km amplitudes. In the second section beyond Cape Hatteras, after leaving the continental slope, the flow moves into deeper water (~4000–5000 m), and becomes more complex in chemophysical nature, with meanders commonly over 350 km in amplitude. The meanders between Cape Hatteras and the Grand Banks often break off as independent eddies with estimated lifetimes of more than 2 years after separating from the Gulf Stream (Open University Course Team, 1978).

By the time Gulf Stream reaches the Grand Banks of Newfoundland, the it has broadened considerably and become more diffuse. East of this area it is more correctly referred to as the North Atlantic Current (or North Atlantic Drift). The North Atlantic

Fig. 1-6. The Gulf Stream in relation to the surface circulation of the Atlantic; the Stream consists of water from the equatorial current system (much of which comes via the Caribbean/Gulf of Mexico) and water that has recirculated in the North Atlantic subtropical gyre. The broken lines represent cool currents (after Open University, 1989).

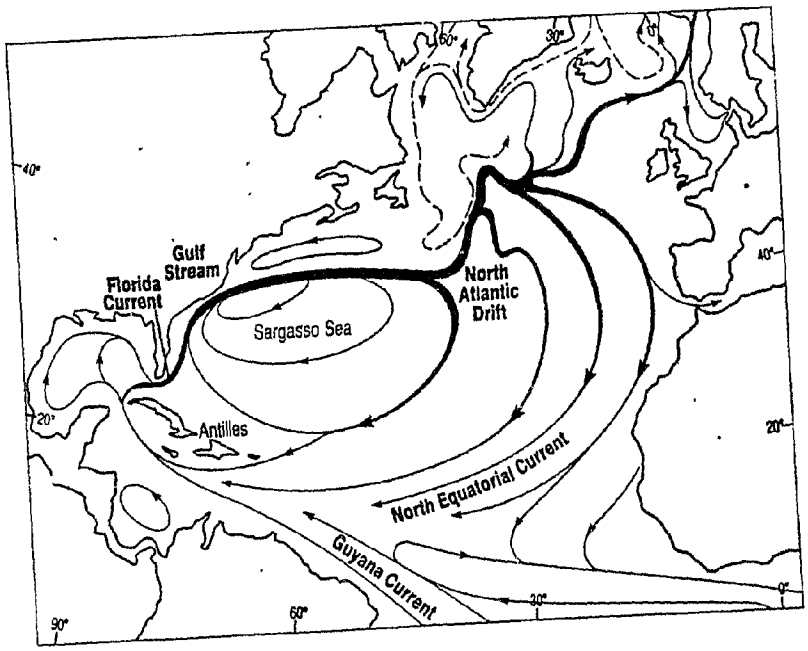
60°
30°
0°
40°
Gulf Stream
Florida Current
Sargasso Sea
North Atlantic Drift
40°
20°
Antilles
20°
North Equatorial Current
Guyana Current
0°
90°
60°
30°

(a)

Current divides into a number of branches. Most of the water turns south–eastwards to contribute to the Canary Current and to recirculate in the subtropical gyre (Open University Course Team, 1978). One branch turns westward into the Irminger and Labrador Basins across the Mid–Atlantic Ridge from the northeastern Atlantic region (Lehman and Keigwin, 1992; McCartney and Talley, 1984). Other branches continue north–eastwards into the Greenland–Norwegian Sea through the Iceland–Faeroe Channel, and then sink to the bottom as they are super-cooled.

1.3.3. Overflows

In the North Atlantic Ocean, six overflow waters have been described (Worthington and Wright, 1970; Worthington, 1976): 1) Denmark Overflow; 2) Norwegian–Greenland Overflow; 3) Mediterranean Sea Outflow through the Strait of Gibraltar; 4) Labrador Sea Water; and 5) Inflow of AABW north of the Brazil Basin (refer to 1.3.1. Deep water circulation for details). All these sources contribute to the North Atlantic Deep Water.

The Denmark Strait Overflow (about 50 km in width near the sill) is mainly composed of Arctic Intermediate Water spilling out primarily through Denmark Strait (Price and Baringer, in prep.). This overflow joins the Iceland–Faeroe Overflow in the western Irminger Basin, and is pushed southward along the continental slope of Greenland by Coriolis force.

The dense Norwegian Sea Deep Water spills out mainly through Iceland–Faeroe Channel at rate of 0.8 m per second (Price and Baringer, in prep.), termed the Norwegian-Greenland Overflow. It is strongly steered by Coriolis force along the east side of the Mid–Atlantic Ridge (i.e. the Reykjanes Ridge). This water returns northward along the west side of the Reykjanes Ridge after passing the Charlie–Gibbs Fracture Zone, and then is joined by the Denmark Strait Overflow in the northeastern Irminger Basin. Another eastern branch of the Iceland–Faeroe Overflow moves around the Rockall Plateau, and later merges into the western one in the east side of the Reykjanes Ridge (Stow and Holbrook, 1984).

Labrador Sea Water is formed when water from the surface of the Labrador Sea sinks to the bottom of the western arm of the western North Atlantic Basin. This water was mistaken to be the major source of the North Atlantic Deep and Bottom Water (e.g., Defant, 1941; Worthington, 1954; Stommel, 1958c). Since the work of Cooper in 1955, the Norwegian Sea overflows have come to be recognized as the main northern source of deep bottom water for the Atlantic and, in fact, the world ocean (Cooper, 1955; Worthington, 1976). This water mixes with the Denmark Strait and Iceland–Faeroe overflows in the northwestern North Atlantic Basin to form NADW which enters the main western basin along the continental margin of the North America (Worthington, 1976; Price and Baringer, in prep.; Price, 1992; Broecker and Peng, 1982).

Mediterranean Outflow Water contributes to the NADW as a significant source. During winters, cooling and evaporation, associated particularly with the dry Mistral wind, can lead to convection right down to the sea floor. The deep water thus formed has T–S characteristics of 12.8°C and 38.4‰, corresponding to σ_t = 29.1. (Open University Course Team, 1978). The water flowing into the Atlantic through the Strait of Gibraltar (at a rate of 1.3 m per second; Price et al., 1993) is called the Mediterranean Outflow Water (MOW). When it mixes with Atlantic water, it is reduced to about 11°C in temperature and about 36.5‰ in salinity, corresponding to σ_t = 27.8 in density. It measures about 100 m in thickness near the Strait of Gibraltar (Price et al., 1993). At present, MOW flows out through the bottom of the Strait, while Atlantic water into the Mediterranean rides over the MOW, forming an anti-estuarine pattern. MOW contains two major branches, one that flows westward into the western basin across the Mid–Ocean Ridge, and another that goes into the Norwegian Sea contributing to Norwegian Sea overflows (Reid, 1979; Loubere, 1987). Thus this outflow serves as an important driving force for oceanographic and climatic changes, locally and globaliy, resulting from the redistribution of its heat and salt.

During the Messinian Stage, this MOW is envisioned to have stopped due to the closing of the seaways between Spain and Morocco and to eustatic sea–level lowering. As

a result, the open ocean became less saline and more undersaturated in calcium carbonate, and thus increased oceanic carbonate dissolution (Ryan, 1973; Thunell et al., 1987). Mediterranean Messinian deep waters outflow were interpreted by Hodell et al. (1989) and Benson et al. (1991) from foraminiferal and ostracod assemblages, and their stable isotope values in northwestern Morocco. MOW stopped entering the North Atlantic Ocean near the Tortonian/Messinian boundary, corresponding to the carbon–13 shift, which implies that cold water of the North Atlantic entered the Mediterranean Sea via a siphon between 6.4 and 5.7 Ma in the Rifian Corridor of north western Morocco (Benson et al., 1991). In addition, Benson et al. (1991) proposed a "twin–channel" model (see above for definition) to interpret the water balance between the Atlantic Ocean and Mediterranean Sea. They speculated that the Atlantic inflow entered the Mediterranean Sea through the Rifian Corridor in Morocco, while the Mediterranean Outflow came out via the Betic Passage in southern Spain driven by Coriolis ·rce.

1.4. Geological and paleoceanographic background of the Messinian Stage

1.4.1. Development of the Messinian Stage

The term "Messinian" was first introduced by Mayer–Eymar of Zurich in 1868 for the sulfurous gypsum, brackish, and fresh water deposits near Messina in Sicily (Italy) that straddled the Miocene/Pliocene boundary. This term was not commonly used in geological community until 1959 when the Congress of the Committee of Mediterranean Neogene Stratigraphy was held in Vienna, Austria. Selli (1960), almost immediately after the Congress, proposed a composite reference section as a neostratotype at Pasqueasia and Capodarso in central Sicily, and defined the Messinian as the only stage suitable for the Mediterranean upper Miocene between the Tortonian and the lower Pliocene. This section contains the Tripoli diatomites, evaporites, and brackish deposits (the so-called *Lago Mare* deposits), overlain by the lowermost Pliocene normal marine marls (known as the Trubi Marl) which resulted from the permanent inundation by Atlantic water into the

Mediterranean Sea (also called "Zanclean Deluge" by Benson and Rakic–El Bied, 1991a) following the Mediterranean Salinity Crisis. The incomplete stratigraphic records of the neostratotype led Colalongo et al. (1979) to establish the Falconara section in Sicily as the Messinian Stage boundary stratotype.

The presently accepted Messinian/Pliocene boundary stratotype was proposed by Cita (1975). She defined the boundary at the base of the Trubi Marl at Capo Rossello, Realmonte, Province of Agrigento, Sicily. This was once considered to be the best land section then available in the Mediterranean region. Cita (1975; 1976) suggested that Miocene/Pliocene boundary is associated with the base of the *Sphaeroidinellopsis* Acme Zone within the upper part of paleomagnetic polarity Chron 5, estimated to have an age of 5.3–5.4 Ma based on the cross–correlation of Capo Rossello section and DSDP sites 125 and 132. Others (Berggren et al., 1976; Saito et al., 1975) suggest the boundary at the last occurrence (LO) of *Globoquadrina dehiscens* and first occurrence (FO) of *Globorotalia tumida,* with an age estimate of 5.3 Ma. Most recently, Benson et al. (in press.) found that this section still fails to meet the operational requirements of Global Section Boundary Stratigraphy and Point (GSSP) because of some important limitations of the section. For example, diachronous biostratigraphic markers, missing paleomagnetic chrons, and no marine record that precede the boundary datum, an unconformity between the Trubi Marl and Arenazzolo Formation–the last non–marine *Lago Mare* deposits, and no significant stable isotope changes correlatable outside of the Mediterranean. These critical problems have led Benson et al. to suggest the composite Bou Regreg Section of northern Morocco near Rabat as a global Miocene/Pliocene boundary stratotype (Benson et al., in press).

The Bou Regreg reference section begins in the upper Tortonian (Chron 7, ca. 7 Ma), and is continuous throughout the Messinian, well into the upper Zanclean (Cochiti Subchron; ca. 3.7 Ma), with abundant and well preserved bathyal and outer neritic microfauna characterized by well– known biostratigraphic markers (Benson et al., in press). The Miocene/Pliocene (M/P) boundary is placed in the paleomagnetic polarity

reversal between the Chron 5N1 and Gilbert Chron, marked by the beginning of the *Globorotalia margaritae* Acme Zone, estimated to have an age of 5.35 Ma. The age estimate for the stratotype is close to the new geomagnetic polarity time scale (GPTS; 5.16 Ma; Cande and Kent, 1992; =4.86 Ma of Berggren et al., 1985), and close to the astronomical time scale (5.32 Ma; Hilgen and Langereis, 1993) and to the GPTS of Berggren et al. (5.3 Ma; 1995).

The Tortonian/Messinian boundary is suggested to be marked by the first occurrence (FO) of *Globorotalia conomiozea* (D'Onofrio, 1975), and this has been widely accepted by most of the recent workers (Benson and Rakic–El Bied, 1991a; Krijgsman et al., 1994; Colalongo et al., 1979; Hilgen and Langereis, 1988; 1993; Hodell et al., 1994, and Berggren et al., 1995). However, the FO of the species is considered not to be used as a zonal marker to define the lower limit of the Messinian in the Southwest Pacific and New Zealand (Roberts et al., 1994) due to its marked diachrony (FO = 6.05 Ma). This observation led Roberts et al. (1994) to conclude that the FO of *G. conomiozea* is not suitable for global correlation between ocean basins.

Several age estimates marking important Messinian boundaries and events were recently accepted by the International Conference on the Biotic and Climatic Effects of the Messinian Event on the Circum–Mediterranean in Benghazi, Libya, January, 1995. These will be adopted in this study: 1) the beginning of the Messinian Stage, 7.12 Ma (ref. Berggren et al., 1995); 2) the end of the Messinian Stage, 5.32 Ma (ref. Berggren et al., 1995); and 3) the first postulated cut–off of Atlantic Inflow into the Mediterranean basin, 5.8 Ma (Gautier et al., 1994; or near paleomagnetic Subchronozone C3An.1n, 5.5894 Ma (Berggren et al., 1995). However Benson et al. (1995) calibrated this level to 5.94 Ma based on the study of the orbital precession from Salé Briquetterie section, Morocco.

DSDP/ODP (Deep Sea Drilling Project and Oceanic Drilling Program) drilling in the North Atlantic reveals that the Messinian sections are not well preserved in abyssal and bathyal depths, and most of them may contain incomplete Messinian section as a result of

bottom water erosion and strong carbonate dissolution. Only very few DSDP/ODP sites display a continuous Messinian section, such as DSDP Site 552A in the Atlantic (Keigwin, 1987), 588 in the Pacific (Hodell et al., 1986), and ODP Site 758 (Farrell et al., 1995). These sites, therefore, have become the most important ones to reveal the mystery of the Messinian paleoceanographic history. In this thesis I provide an integrated magneto–, bio– and isotope stratigraphy with good stratigraphic resolution in defining the Tortonian/Messinian and Pliocene/Messinian boundaries from some selected DSDP/ODP Holes and a land borehole in Morocco. I expect that my stratigraphic study will furnish a strong basis for re-construction of paleoceanographic history and for further evaluation of the relationship between the global deep water circulation and Mediterranean Salinity Crisis during the Messinian Stage.

1.4.2 The Mediterranean Salinity Crisis

Messinian Salinity Crisis has been considered to be a spectacular geological event, which resulted in the deposition of a large volume of evaporites (about 2000m–3000m thick; also known as "Giant Salt") in the Mediterranean Sea. Such Messinian evaporites are not only encountered in the abyssal Mediterranean basins, but also in the circum–Mediterranean lands and islands in the Eastern Mediterranean Sea, such as Italy, Crete, Sicily, Cyprus and so on. This Giant Salt has led Hsü and his DSDP (Legs 13 and 42A) colleagues, Ryan and Cita (Hsü et al., 1973a, Hsü et al., 1973b, Hsü, 1973, Hsü, 1978, Hsü, 1987, Hsü, 1988) to formulate a spectacular hypothesis – the desiccation of the Mediterranean Sea (also known as "Deep–basin/shallow–water model") to explain the formation of the Giant Salt. This model has been highly questioned, because it requires at least 13 interludes of Atlantic water inundating the desiccated Mediterranean Sea. As a result, these 13 interludes should generate the same number of evaporitic depositional cycles, but these have not been unearthed either in the deep sea or on the land. Four other models have also been proposed to explain the origin of the evaporites, namely: 1)

shallow–basin/shallow–water proposed (Bourcart, 1962; Neseroff, 1973a, b; Montadert et al., 1978; Drooger, 1975; and Fabricus et al., 1978); 2) deep–water/deep basin (Bandy, 1973; Van Couvering et al., 1976; and Ruggeri and Sprovieri, 1976; and Rouchy, 1982a, b); 3) Barred basin (Selli, 1973); and 4) endorheic basins (Gvirtzmann and Buchbinder; 1978; Sonnenfeld, 1975; Dietz and Woodhouse, 1988; and Drooger, 1975). Benson and Raki-El Bied (1991a) describe the diagnostic characteristics, evidence, and mechanisms of these models. Although the origin of the "Giant Salt" is controversial, it is evident that the Messinian Salinity Crisis plays an important role in Late Miocene paleoceanography.

1.4.3. Global Carbon–13 Shift

The carbon–13 shift is another important Messinian paleoceanographic event which occurred in deep marine regimes, and shows a permanently decreased oceanic ^{13}C value at ~ 6.3 Ma (Berggren et al. 1985 time scale), slightly above the Messinian/Tortonian boundary (Loutit and Kennett, 1979; Loutit and Keigwin, 1982; Keigwin, 1979; Keigwin, 1987; Keigwin and Shackleton, 1980; Haq et al., 1980; Hodell et al., 1986; Hodell and Kennett, 1986; Hodell et al., 1989). The major cause of the shift has not been well established, however, it is widely accepted that the shift may be linked to sea–level lowering that may have increased the influx of organic matter from the continents into the open oceans (Loutit and Keigwin, 1982; Benson et al., 1991). Bender and Keigwin (1979) suggested that the ^{13}C shift may indicate a different abyssal circulation pattern before the shift resulting from the shoaling of the Isthmus of Panama, or a global decrease in upwelling rate. Other factors, such as increase of bottom circulation rates, and increase in biogenic silica removal in the Southern Ocean high productivity zone have been also considered to have affected the oceanic ^{13}C value (Loutit and Keigwin, 1982). Stratigraphically, this shift can be used as a constraint of the lower Messinian for global correlation because no diachroneity has been recognized between basins.

1.4.4. Global cooling

Microfossils (Kennett, 1967a; Ingle, 1967; Kennett and Vella, 1975; Barron and Keller, 1983) and evidence for expansion of Antarctic glaciation (Mercer, 1978; Mercer and Sutter, 1982; Shackleton and Kennett, 1975; Kennett, 1977) indicate global cooling in the Late Miocene. The global cooling could have resulted in a major relative sea–level lowering by about 70m (Vail et al., 1977; Hodell and Kennett, 1986; Cita and Ryan, 1978). In the deep North Atlantic and Pacific oceans two possible glacial events occurred at 5.2 Ma and 4.8 Ma, respectively (Keigwin, 1987). The former glacial (5.2 Ma) also has been determined in northeastern Morocco by Hodell et al. (1989, 1994). The study of a raised coral atoll of Niue in the South Pacific shows eight episodes of the sea-level fluctuations in the intra–Messinian suggested by eight unconformities (Aharon et al., 1993); in Mallorca of the Western Mediterranean Sea, Pomar and Ward (1994) determined three six–order depositional cycles; and most recently, ODP Leg 151 shipboard scientists (1994) discovered that the first significant quantities of dropstones appeared in the Norwegian Sea near the late Miocene/Pliocene boundary, probably indicating glacial expansion of the Arctic. Obviously all this evidence may have been linked to global climate deterioration.

CHAPTER 2

STUDY METHODS AND MATERIAL

2.1. Methods

2.1.1. Foraminiferal analysis

All samples were washed through a 63μm mesh using tap water, and dried in an oven at temperature of 40°C. Benthic foraminifera greater than 63μm from all sites were examined. Samples for benthic foraminiferal analysis were split with mini-microfossil splitter, and an aliquot was procured to obtain the desired number of specimens (~300) for counting and identification. Samples were not soaked in hydrogen peroxide solution to avoid artificial destruction of shells during lab preparation. Planktonic foraminifera greater than 63μm from all sites were studied for biostratigraphy.

2.1.2. Oxygen and carbon stable isotope analysis

72 samples both for benthic and planktonic foraminifera from Site 608 with a resolution of 5–7 samples in each core were picked for oxygen and carbon stable isotope analysis. Stable isotopic analyses were conducted at the University of Florida, USA, by Dr. David A. Hodell. Specimens of the benthic foraminifera *Cibicidoides* spp. and *Planulina wuellerstorfi* greater than 212μm (some of them are >150μm when specimens are insufficient) were measured for stable isotopes on the mass spectrometer after 3 seconds of cleaning in an ultrasound bath. The planktonic foraminifera *Globigerina bulloides* (size range 212–250μm) for the intervals from samples 12–2 to 17–2 and from 19–5 to 24–6 were also measured. However, for the interval from Sample 17–1 to 20–2, we substituted *Orbulina* (size range 212–250μm) because of insufficient specimens of *G. bulloides* resulting from intense carbonate dissolution. It is considered that *Orbulina* probably has similar isotope values to *G. bulloides* because both species inhabit surface waters.

Necessary overlaps have been taken for isotope value correlation between the two taxa. All these samples were washed in a ultrasound bath for 1 second because of their delicate tests, prior to analysis in the mass spectrometer.

Samples were reacted in a common acid bath of ortho–phosphoric acid at 70^0C using a VG Isogas autocarbonate preparation system. Isotopic ratios of purified CO_2 gas were measured on– line by a triple–collector VG Isogas Precision Isotope Ratio Mass Spectrometer (PRISM). All results are reported in standard delta notation and corrected to PDB (Hodell et al., 1994). Analytical precision, based on routine analysis of an internal carbonate standard (Carrara Marble), was ±0.07 for $\delta^{18}O$ and ±0.03 for $\delta^{13}C$ (see Hodell et al., 1994).

The stable isotopic data for ODP Hole 646B, DSDP Hole 552A, and Salé Borehole of Morocco are from Aksu and Hillaire-Marcel (1989), Keigwin (1987) and Hodell et al. (1994), respectively.

2.1.3. Strontium stable isotope analysis

Sr isotope analyses for Hole 646B were performed on more than 200 specimens of mixed calcareous benthic and planktonic foraminifera picked from the greater than 150μm size fraction and dissolved in 1.5 N NHL. Standard ion exchange techniques (*fide* Miller et al., 1991) were used to separate strontium for analyses on a VG Sector mass spectrometer at Rutgers University, NJ, USA. Internal precision (inter-run variability) is approximately ±0.000008 (mean 2σ error; Miller et al., 1991); external precision (inter-run variability) is approximately ±0.000030 or better (see Miller et al., 1991). At Rutgers, NBS 987 is routinely measured as 0.710252 (2σ standard deviation 0.000026; n = 35; Miller et al., 1991) normalized to $^{87}Sr/^{86}Sr$ of 0.1194. Farrell et al. (1995) estimated that the rate of increase of $^{87}Sr/^{86}Sr$ during the Messinian (from 4.8 Ma to 7.0 Ma) was ~0.00005/m.y., yielding a stratigraphic resolution of 0.44 Ma. The rate of increase of $^{87}Sr/^{86}Sr$ was low for the interval from 2.5 to 4.8 Ma, yielding a stratigraphic resolution of 1.69 m.y. Sr-

isotope age estimates were determined using these equations calculated from the regression of Farrell et al. (1995):

Age=59941.95-(Sr 87/86)x84530.85 (Sr=0.709080-0.709056)

for 2.5-4.8 Ma (Miller, pers. comm. based on Farrell et al. data, 1994)

Age=15640.06-(Sr 87/86)x22050.72 (Sr=0.709056-0.708955)

for 4.8-7.3 Ma (Miller, pers. comm. based on Farrell et al. data, 1994)

2.1.4. Paleomagnetics

Paleomagnetic data are available for all sites selected for this study, except for DSDP Hole 547A. These published data were used to solve the chronostratigraphic problems with necessary re-interpretation. The Messinian Stage includes Chronozone C3r (=the lower reversal of Gilbert Chron), Chronozone C3An (=Chron 5), Chronozones C3Ar, C3Bn and the upper part of C3Br (=Chron 6). Age estimates of the chronozones are after Berggren et al. (1995).

2.1.5. Time series analysis

In Salé Borehole of Morocco, time series for the interval from the top of Chronozone C3Bn to the top of C3An (6.935-5.894 Ma) were analyzed by Hodell et al. (1994) because the age of the interval is well controlled magnetically. The time series for Hole 552A was studied by Beaufort and Aubry (1990) based on the old time scale of Berggren et al. (1985). In this study, standard time series analysis techniques were used to estimate the power spectral density as a function of frequency for oxygen-18 and carbon-13 stable isotopic signals (interval from the lowermost C3r to the top of the Messinian; 5.894-5.32 Ma) for DSDP Hole 552A, and planktonic/benthic (P/B) ratio, oxygen-18 and

carbonate signals (interval from the middle of C3Ar to the top of the Messinian; ~6.7 to 5.32 Ma) for Salé Borehole.

In the present study, depth is interpolated uniformly to make the number of data points equal to power of 2 for fast Fourier transformation. All signals from Hole 552A and Salé core were linearly detrended. The power spectrum for all signals reveals relatively significant peaks at 100-kyr in the Salé core, and 123-kyr at DSDP Hole 552A, which correspond to the Milankovitch cycles of orbital eccentricity (100-kyr and 123-kyr, respectively). My results of Hole 552A are similar to those given by Beaufort and Aubry (1990).

2.2. Material

Four DSDP/ODP (Deep Sea Drilling Project/Oceanic Drilling Programs) holes, namely 552A, 547A, 608 and 646B (Fig. 2-1) have been carefully selected for this study from all Atlantic DSDP/ODP sites drilled before 1990. These sites are considered either to have good Messinian sedimentary records or good locations where deep water masses may have been recorded. Another borehole drilled in the Bou Regreg Valley of northwestern Morocco, where some excursions of Atlantic and Mediterranean water exchange are expected to have been taken place during Messinian time, was provided by Dr. R. H. Benson at the Smithsonian Institution, Washington, D.C..

2.2.1. DSDP Hole 552A: Core location and description

DSDP Hole 552A (Leg 81) was drilled on the Hatton Drift at the base of Hatton Bank, west margin of the Rockall Plateau (56°02.56'N, 23°13.88'W; water depth 2301 m), south of Iceland– Faeroe Ridge (Fig. 2-1). It was hydraulically piston cored to 183.5 m, yielding almost 100% recovery. One of the major objectives to drill this site was to understand the evolution of Quaternary/Tertiary paleoclimate and deep water circulation based on a consideration of the outflow of the Norwegian Sea Water plunging into the

North Atlantic Ocean across the Iceland–Faeroe Ridge. The Hatton Drift is envisioned to have been deposited under the influence of bottom currents flowing northeastward against the slope of the Hatton Bank. Deep waters at this site lie above the southward–flowing North Atlantic Deep Water that fills the deeper part of the Iceland Basin and mantles the Reykjanes Ridge south of Iceland (Roberts, Schnitker et al., 1984).

Hole 552A contains a continuous late Miocene–Pliocene sedimentary record and no turbidites or hiatuses have been determined in this interval although possible slumping may have occurred in the Pliocene from core 17 to 24 (Stow and Holbrook, 1984). However, two hiatuses are present within the middle Miocene and between the middle Miocene and the Oligocene. It was lithologically divided into four sediment units and the interval of the late Miocene–Pliocene is attributed to Subunit IIa ranging from 44 to 168.5 m in subbottom depth (Shipboard Scientific Party, 1984a). This subunit is composed of relatively uniform foraminiferal–nannofossil ooze and nannofossil ooze, with minor (about 10%) component of biogenic silica. The dominant color is bluish white, and carbonate content remains at more than 90% throughout the subunit. Laminations recognized by color are abundant in cores 11 to 29, but rare or absent in the base of the subunit (cores 30–36).

2.2.2. Moroccan Borehole: Core location and description

The Salé Moroccan borehole was provided by Dr. R.H. Benson of the Smithsonian Institute of National Museum of Natural History, Washington, D.C., USA for benthic and planktonic foraminiferal analyses of this study. It was drilled from a large brick quarry (the Salé Briquetterie) on the road to the airport just east of Rabat, northeastern Morocco. The objective for this hole was to reconstruct the history of water exchange between the Mediterranean Sea and Atlantic Ocean for the Messinian Salinity Crisis. Because this hole is situated in the one of two gateways (called the Rifian Corridor; another one in southern Spain that is called Betic Passage) between the Mediterranean and Atlantic during the Messinian ; it could have recorded important information on water circulation at this time

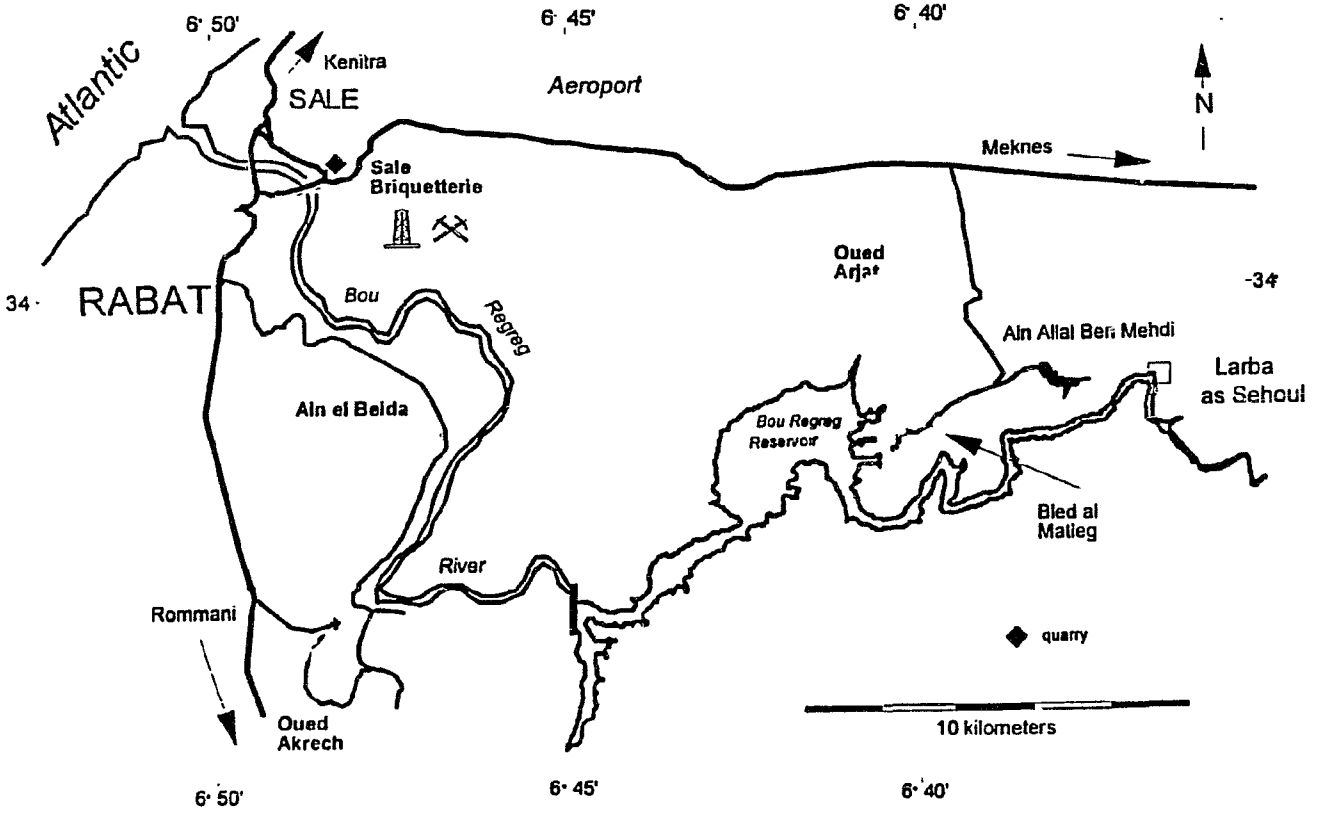

Fig. 2-2. Detailed location of the Salé Briqueterie Borehole in northwestern Morocco.

(Hodell et al., 1989; Benson and Rakic–El Bied, 1991a, b). The drilling was accomplished in two phases in April 1987 and September 1988 under contract to SOLMAROC, a local drilling company. The section was cored by continuous "mazier" drilling (cookie cutter bit) using a one metre barrel with a diameter of 74 mm. During the first phase of drilling, 72 cores were recovered to a maximum depth of ~75 m below the quarry floor. These cores are designated as S–series. During the second phase of drilling the first 60 m were drilled without recovery and 104 cores were recovered below this level reaching a maximum depth of approximately 170 m. These cores are designated as B–series. The lowermost part of the B– series was drilled by destructive rotary drilling and only spot cores were obtained. The overlap between the S– and B–series drilling is about 7m (between 66 and 73 m below the base of the quarry floor. The depth offset between the two holes is ~ 5m and this amount was added to all the core depths measured in the field for the B–series samples (Hodell et al., 1994).

Deposits ranging from the upper Tortonian to the Zanclean consist predominately of blue marine marls that outcrop in high bluffs along the Bou Regreg River and its tributaries in brick clay quarries on the southern flank of the Gharb Basin, with abundant and well preserved outer shelf and upper bathyal microfossil faunas. This sequence is continuously deposited and no sedimentation gaps have been determined, because it was deposited on the Atlantic side of Morocco, rather than on the Mediterranean side. In addition the sedimentation rate in the Salé borehole is high. For example, the rate during the lower Gilbert exceeded 13 cm/kyr, which results in a sampling frequency of ~4,000 years. During Chron C3An and C3Ar, the sedimentation rate averaged about 5 cm/kyr, yielding a sample spacing of about 10,000 years (Hodell et al., 1994).

Stable isotopes were measured with benthic foraminiferal species, *Planulina ariminensis* from the S and B series samples by Hodell et al. (1994). Planktonic foraminifera are inadequate for isotope measurements because of poor preservation.

2.2.3. DSDP Site 608: Core location and description

Hole 608 was drilled during DSDP Leg 94, 1983 on the southern flank of the King's Trough tectonic complex near the axis of the Mid–Atlantic Ridge (42°50.205'N, 23°05.252'W; water depth 3541.8 m). The major purposes to drill the hole were to determine the geological history of the intraplate King's Trough tectonic complex and to test for east–west differences in polar–front movement and sea–surface temperature changes. The hole was continuously cored with the variable–length hydraulic piston core (VLHPC) for cores 1–16 (core recovery over 95%), and with extended core barrel (XCB) that extended into basement at 530.9 m sub–bottom (cores 17–57, with core recovery averaged over 86% for the late Miocene interval). The interval of the late Miocene and early Pliocene is recognized within the lithologic Unit II, equivalent to the acoustic Unit C that is relatively transparent. The lithologic Unit II contains high carbonate content (90–95%), and is virtually featureless below 140 m (subbottom). It has been subdivided into 2 subunits: Subunit IIa (76–220 m) is white to very light gray foraminiferal–nannofossil ooze to 122 m and nannofossil ooze below, and the Unit IIb, beginning at 220 m and ending at 257 m, consists of white nannofossil chalk. A graded foraminiferal sand layer (about 30 cm) occurs at ca. 115 m (Pliocene), which has been interpreted as a possible turbidite or as a result of deep water activity (Ruddiman et al., 1987a, b). No hiatuses have been reported in this interval selected in this study.

2.2.4. DSDP Hole 547A: Core location and description

DSDP Hole 547A (Leg 79) was drilled in the Moroccan Basin, the northwestern part of Mazagan Plateau off the Moroccan coast (33°46.84'N, 09°20.98'W; water depth 3948 m) and southwest of the Strait of Gibraltar. It is expected that this region was influenced by paleo–Mediterranean Outflow Water (PMOW). Hole 547A was hydraulically piston cored to 674.5 m, and achieved core recovery of 49.4% in average. The late Miocene–early Pliocene section has been lithologically recognized in lower Unit I and

DSDP Hole 608

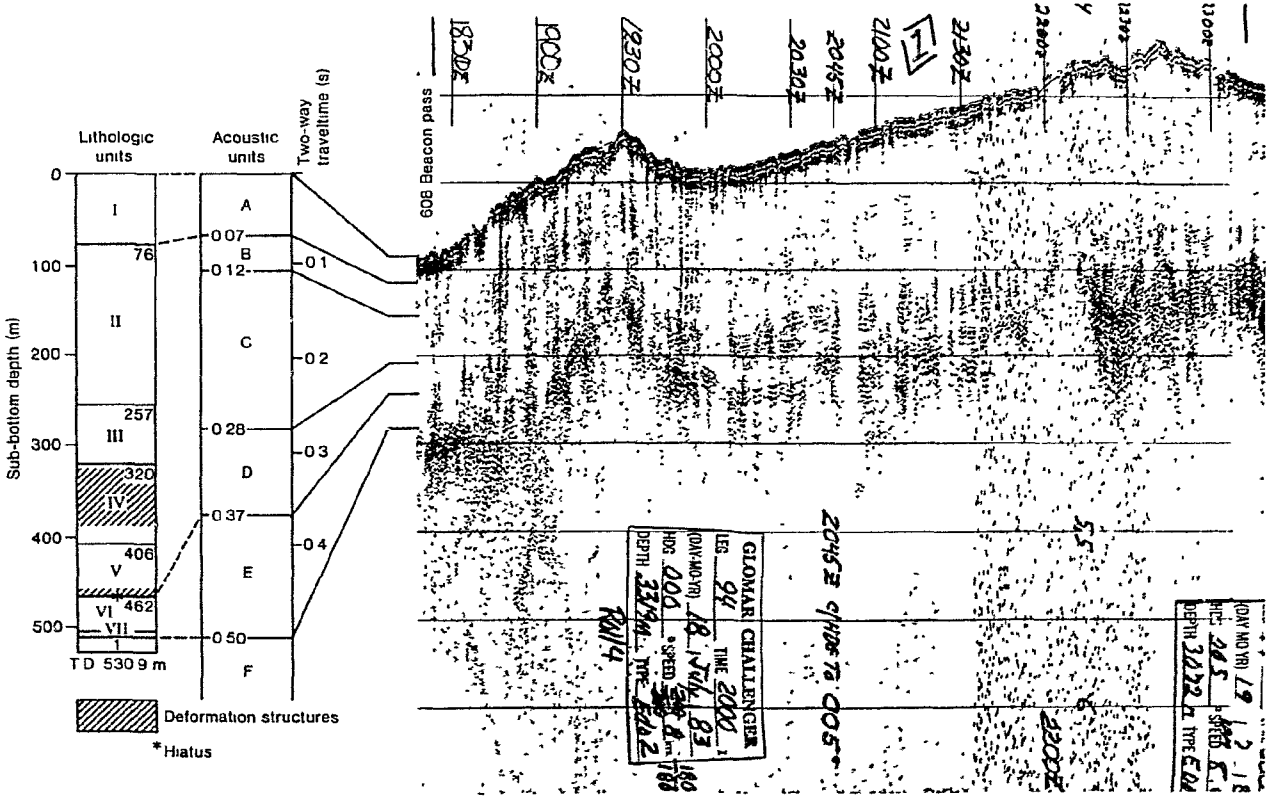

Fig. 2-3. Seismic stratigraphy and comparison with lithologic units at DSDP Site 608 (After Ruddiman et al., 1987a).

upper Unit II. These sediment units are equivalent to the seismic sequences Ma 1.3 and Ma 1.2, respectively (Shipboard Scientific Party, 1984b). The sediments in this section are well oxidized foraminiferal–nannofossil ooze, generally slightly clayey, with about 25% terrigenous detritus. These sediments were interpreted to be deposited at an accumulation rate of ~22 m/m.y. above the foraminiferal lysocline where the dissolution of foraminiferal skeletons increases rapidly. Two hiatuses have been suggested by Hinz et al. (1984): one situated right above 100 m (subbottom depth) may cut much of the Pliocene, and another one is situated between the middle and late Miocene. The interval from 50–210 m is characterized by calcite overgrowth and cementation with subordinate clay overgrowth, but fossils were not reported to be recrystallized (Moore, 1984). Cementation must be related to the depth of burial, not the range of sediment (Moore, 1984). No detailed biostratigraphy of planktonic foraminifera was conducted during the Leg 79 cruise for the late Miocene.

2.2.5. ODP Hole 646B: Core location and description

Hole 646B was drilled during ODP Leg 105, 1985 on the northern flank of the Erik Ridge in the southeastern part of the Labrador Sea and southwest of Greenland (58°12.559'N, 48°22.147'W; water depth 3461.3 m). One of the major objectives for this hole was to determine the history of paleocirculation in the North Atlantic and the Arctic oceans because it is located in the region where maximum influence from Norwegian–Greenland Sea Overflow Water is expected (Shipboard Scientific Party, 1986). Because of the difficulty of pulling core barrel from the bottom, the interval below the lowermost Pleistocene (HPC core 14) was drilled with XCB (extended core barrel) coring, which yields poorer core recovery (only 48%). In this hole, the late Miocene reportedly ranges from ~500 m (subbottom depth) to the base of the hole, which is bracketed by the seismic reflector R3/4 and R2, while the early Pliocene occurred approximately between R2 and R1. Both the late Miocene and early Pliocene have been attributed to the seismic Unit 3, equivalent to lithologic Unit II. Unit II is lithologically dominated by terrigenous clay–rich

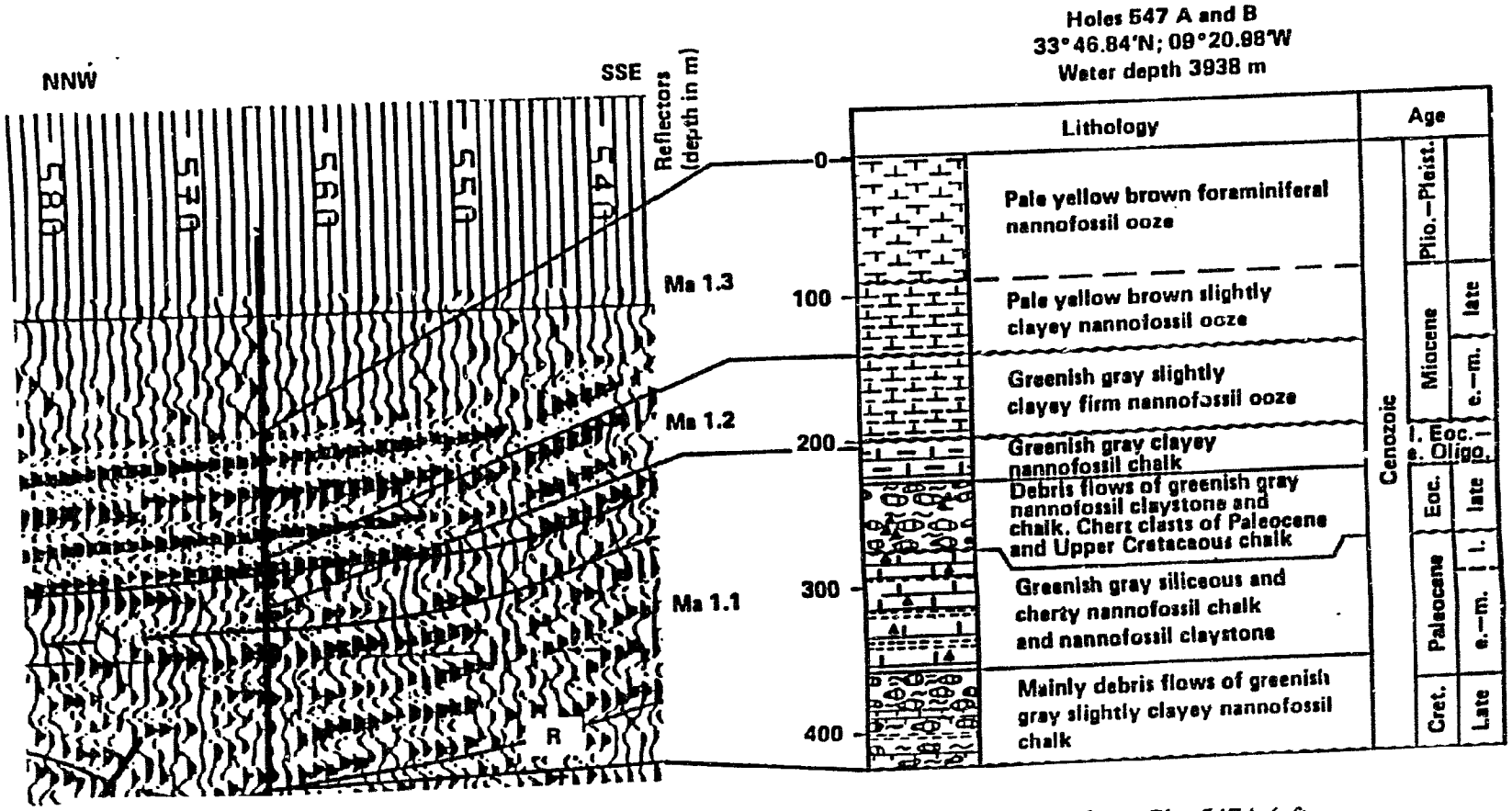

Fig. 2-4. Correlation of seismic sequences and reflectors with results at Site 547A (after Hinz et al., 1984).

sediments. Major lithofacies are silty clay (69%), clayey silt (11.5%), clay (11%), and nannofossil silty clay and clayey silt (6%). Nannofossils in the unit are the main biogenic component, which reaches about 50% of total fauna and flora in abundance. The terrigenous detritus deposits are suggested to have been carried for some distance along the continental margin of Greenland in a bottom nepheloid layer, and periodic contributions to the nepheloid layer may have been from river discharge or from low–concentration turbidity currents or from plumes of turbid water originating on the shelf (Srivastava et al., 1986). In addition, this unit shows very little variation in either texture or sedimentary structure. Except for a few thin paralleled–laminated layers, all sediment is bioturbated (Srivastava et al., 1986).

Fig. 2-5. Correlation between physical property measurement (density, water content, porosity, velocity), major reflectors and seismic units, with lithology, Hole 646B (After Srivastava et al., 1989a).

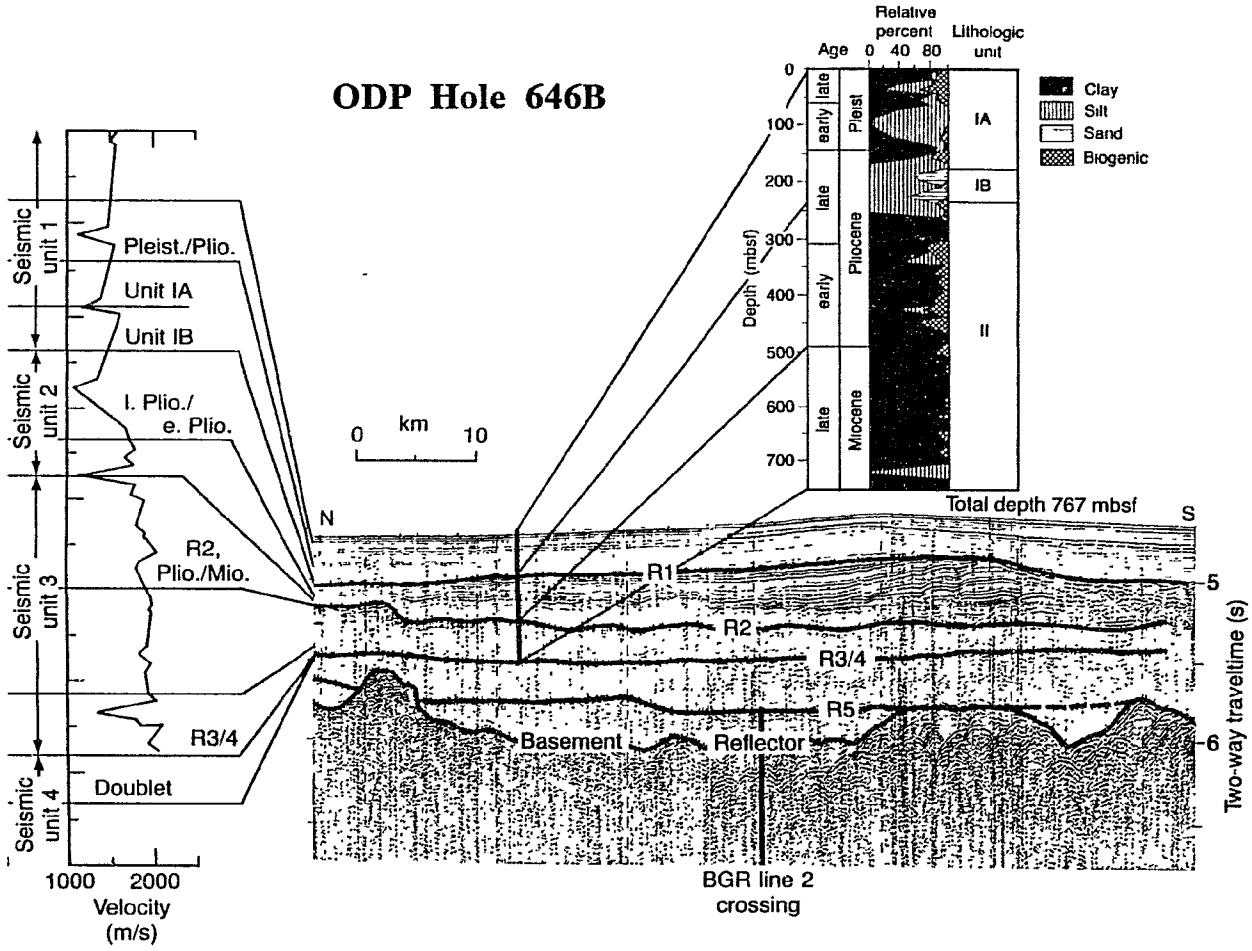
ODP Hole 646B
Relative percent
Lithologic unit
Age
0 40 80
Clay
Silt
Sand
Biogenic
Depth (mbsf)
0
100
200
300
400
500
600
700
early
late
Pleist
Pliocene
Miocene
IA
IB
II
Seismic unit 1
Seismic unit 2
Seismic unit 3
Seismic unit 4
Pleist./Plio.
Unit IA
Unit IB
I. Plio./ e. Plio.
R2, Plio./Mio.
R3/4
Doublet
1000 2000
Velocity (m/s)
0 km 10
N
S
Total depth 767 mbsf
R1
R2
R3/4
R5
Basement
Reflector
5
6
Two-way traveltime (s)
BGR line 2 crossing

CHAPTER 3

RESULTS OF MICROPALEONTOLOGY AND STABLE ISOTOPES

3.1. Salé borehole, Morocco

3.1.1. Distribution of Moroccan benthic foraminifera

In this study, 124 samples for the interval from 3 m to 173 m were quantitatively analyzed for benthic foraminifera greater than 63μm, providing an average sampling spacing of 1.37m. Over 100 species have been identified (see Appendix A) in these samples, and these are the basis for paleobathymetric and paleoceanographic reconstruction in the Rifian Corridor of Morocco. As shown in Fig. 3-1A, foraminiferal abundance increases rapidly above Chron 5 (equivalent to the upper Messinian), but highly variable. The abundance decreases dramatically to about 5,000 per cc on average below the Chron 5/Gilbert boundary, and remains constantly low during Chrons 5 and 6. During the earliest Messinian (lower Chron 6), it reaches the minimum. In the interval of the upper Tortonian the benthic foraminiferal abundance increase rapidly again. Two major peaks occur between 40 and 50 m during the late Messinian, and 160– 170 m during the upper Tortonian (Fig. 3-1A).

Benthic foraminiferal percentages of total fauna (benthic plus planktonic) increases rapidly from the bottom to the top, with 7 major stepwise fluctuations throughout the core (Fig. 3-1B). Similar to the abundance distribution, a distinct shift of the benthic/planktonic ratio occurs in Chron 5. During the Chron Gilbert, the ratios range from 30% to 55%, while less than 25% during lower Chron 5 through Chron 7, except for 2 spikes in this interval, indicating that the planktonic foraminifera dominate the lower Messinian and uppermost Tortonian (Fig. 3-1B). This percentage is attributed to the change of paleobathymetry. Smaller benthic values indicate deeper water depth, and greater values indicate shallower water depth. Note that the spike in Chron 6 is associated with carbonate

Fig. 3-1. Distribution of benthic foraminiferal abundance (A) and benthic foraminiferal percentage in the total foraminiferal fauna (B) in Salé core, northwestern Morocco.

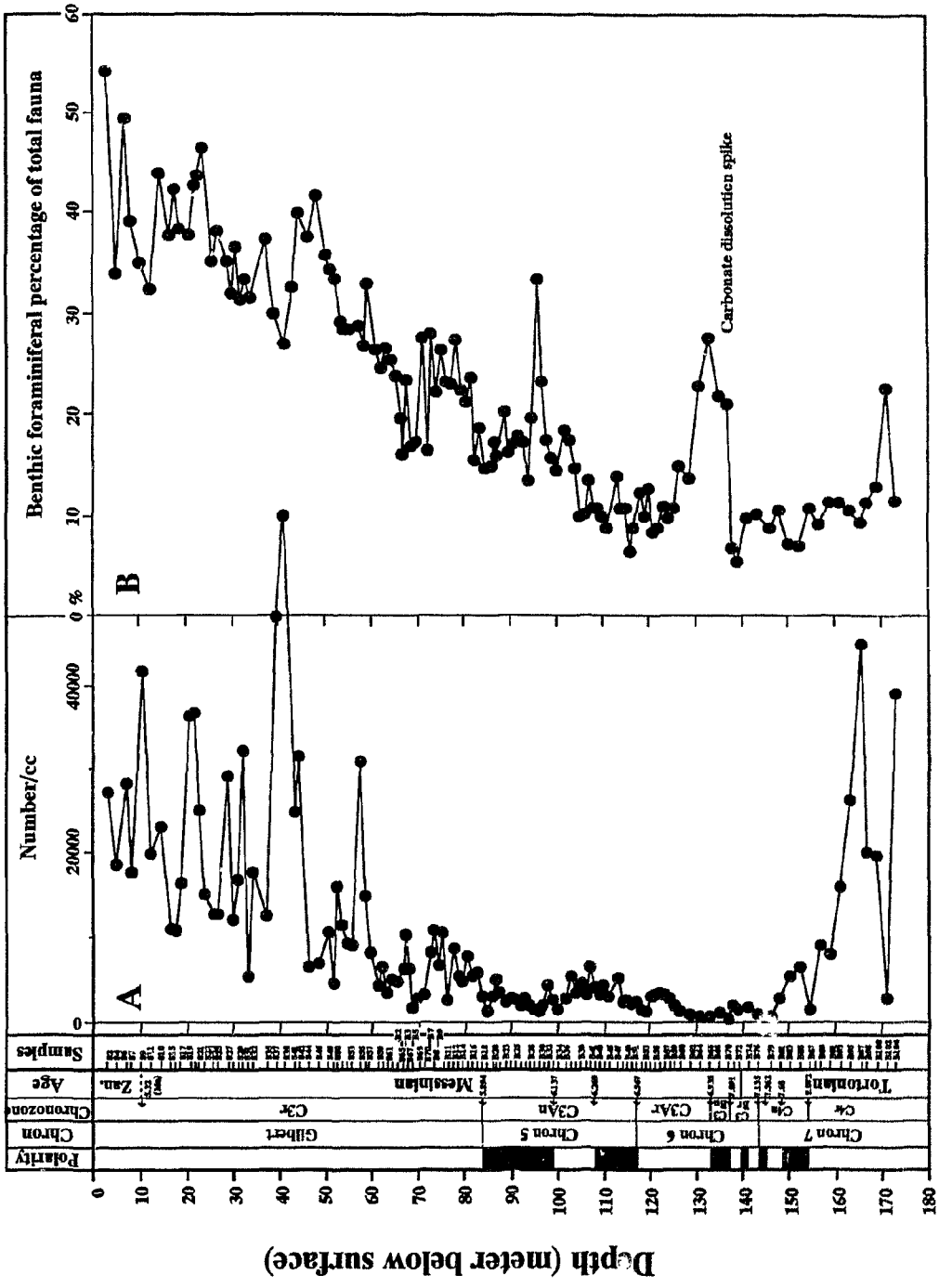
Depth (meter below surface)
Polarity
Chron
Chronozone
Age
Samples
Chron 7
Chron 6
Chron 5
Gilbert
C4
C3Ar
C3An
C3r
Messinian
Tortonian
Zan.
Number/cc
0
20000
40000
A
Benthic foraminiferal percentage of total fauna
0 %
10
20
30
40
50
60
B
Carbonate dissolution spike

dissolution because less resistant planktonic foraminifera are easier to dissolve in carbonate-undersaturated deep water.

Table 3-1 lists benthic foraminiferal assemblages for the different stages of the Messinian. Detailed information on distribution of dominant and geologically or ecologically significant benthic species are given in Figs. 3-1 to 3-4, Table 3-1, and in Appendix A. As indicated in the figures, the Messinian section in this borehole is dominated by *Globocassidulina subglobosa, Cassidulina reniforme, Cibicidoides* spp, *Trifarina angulosa, Gavelinopsis praegeri, Eponides weddellensis, Bolivina albatrossi* and others. The benthic foraminiferal data show that there is a major faunal change in Chron 5, although some species, such as *Discorbinella bertheloti, Bulimina mexicana/costata, Gavelinopsis praegeri,* and *Planulina ariminensis*, show no significant changes. A high peak (up to 15%) of *Bolivinita pseudothalmanni* is recorded in the lower Gilbert (lower C3r).

3.1.2. Oxygen stable isotopes

Oxygen stable isotopic data used here are from Hodell et al. (1994). As shown Fig. 3-5A, $\delta^{18}O$ values from the base of the section to 148m are about +0.8‰. There is a brief depletion that averages about 0.3‰ in the interval between 148–140m just below the Messinian/Tortonian boundary. $\delta^{18}O$ values are enriched by ~ 0.4‰ immediately across the Messinian/Tortonian boundary, varying from +1.0 to 1.4‰ with average of about 1.2‰, indicated by both unsmoothed and 3–point running average curves. In general, these values remain consistently high in the interval from 140m to 53m, reaching a maximum (1.8‰) between 60 and 70m. Hodell et al. (1994) determined that glacial/interglacial cycles are superimposed upon the overall high mean values of the $\delta^{18}O$ signal. Glacial values commonly reach 1.3‰, while interglacial values average about 0.8‰. The isotopic values are depleted to 0.6–1.0‰ on average in the interval from 53m to the top of the section, with minimum values about 0.3 to 0.4‰. This is quite different from those in deep ocean,

Fig. 3-2. Relative abundance of *Globocassidulina subglobosa, Epistominella exigua, Eponides weddellensis* and *Bolivina albatrossi* in Salé core, northwestern Morocco.

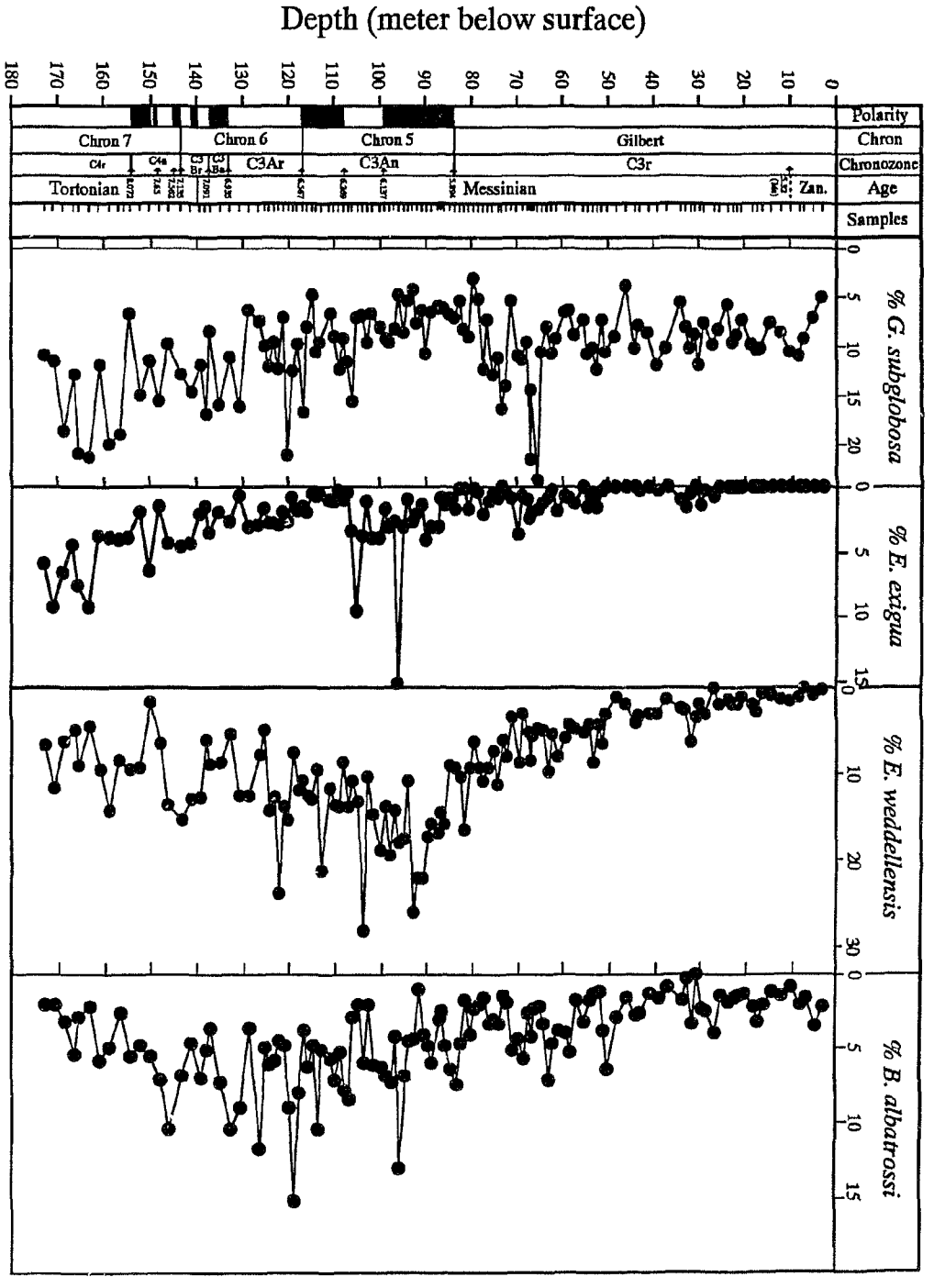
Depth (meter below surface)
Polarity
Chron
Chronozone
Age
Samples
Chron 7
Chron 6
Chron 5
Gilbert
C4r
C4n
C3 Br
C3 Bn
C3Ar
C3An
C3r
Tortonian
Messinian
Zan.
% G. subglobosa
% E. exigua
% E. weddellensis
% B. albatrossi

Fig. 3-3. Relative abundance of *Cibicidoides mundulus+pachyderma, Bulimina aculeata, Trifarina angulosa,* and *Bolivina lowmani* in Salé core, northwestern Morocco.

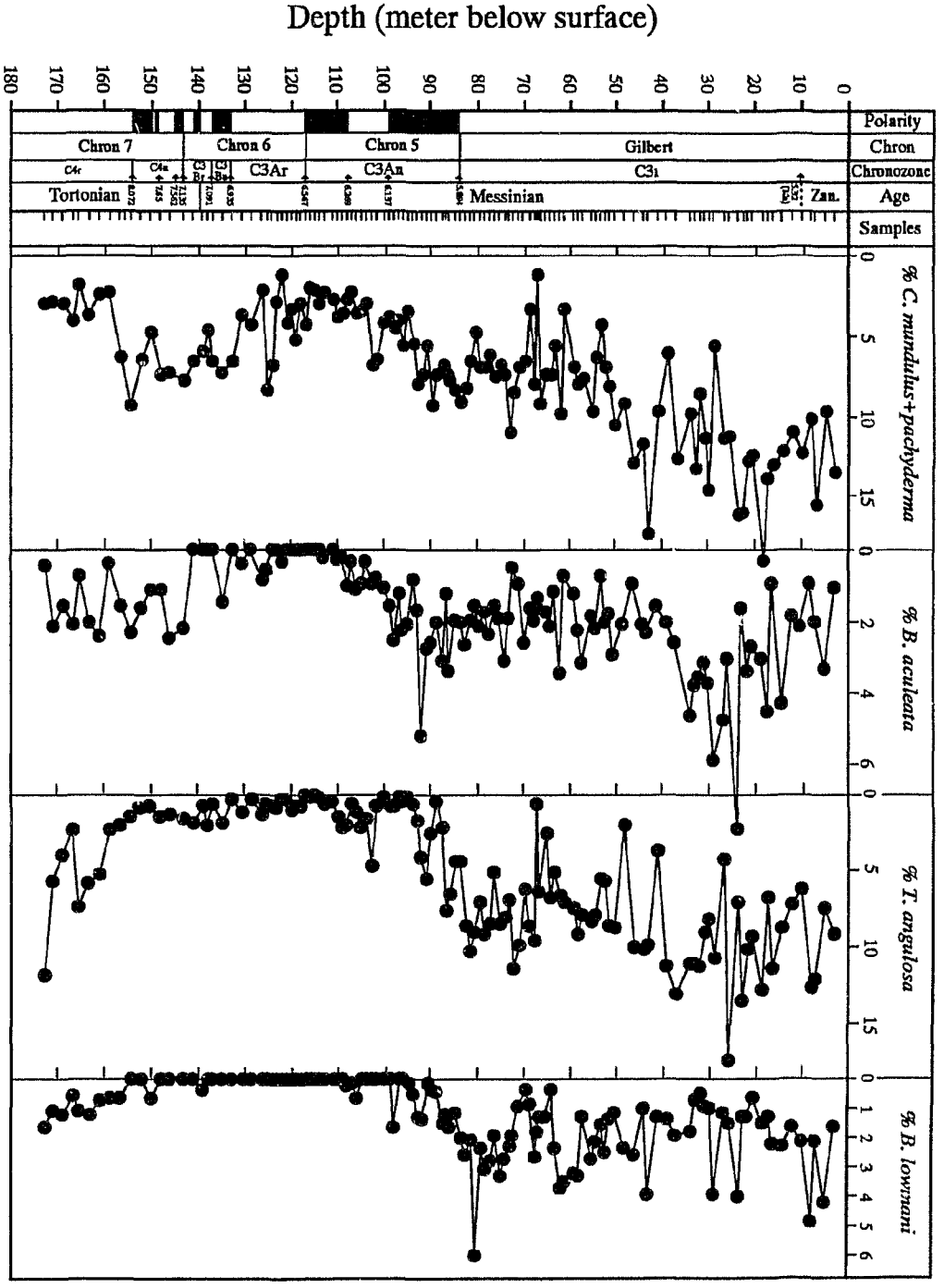
Depth (meter below surface)
180
170
160
150
140
130
120
110
100
90
80
70
60
50
40
30
20
10
0
Polarity
Chron 7
Chron 6
Chron 5
Gilbert
Chron
C4r
C4n
C3r
C3n
C3Ar
C3An
C3
Chronozone
Tortonian
Messinian
Zan.
Age
Samples
% C. mundulus+pachyderma
% B. aculeata
% T. anguiosa
% B. lowmani

Fig. 3-4. Relative abundance of *Eponides?* sp. A, *Oridorsalis umbonatus*, *Pleurostomella* spp. *Fursenkoina pontoni,* and *Heronallenia crosbyi* in Salé core, northwestern Morocco

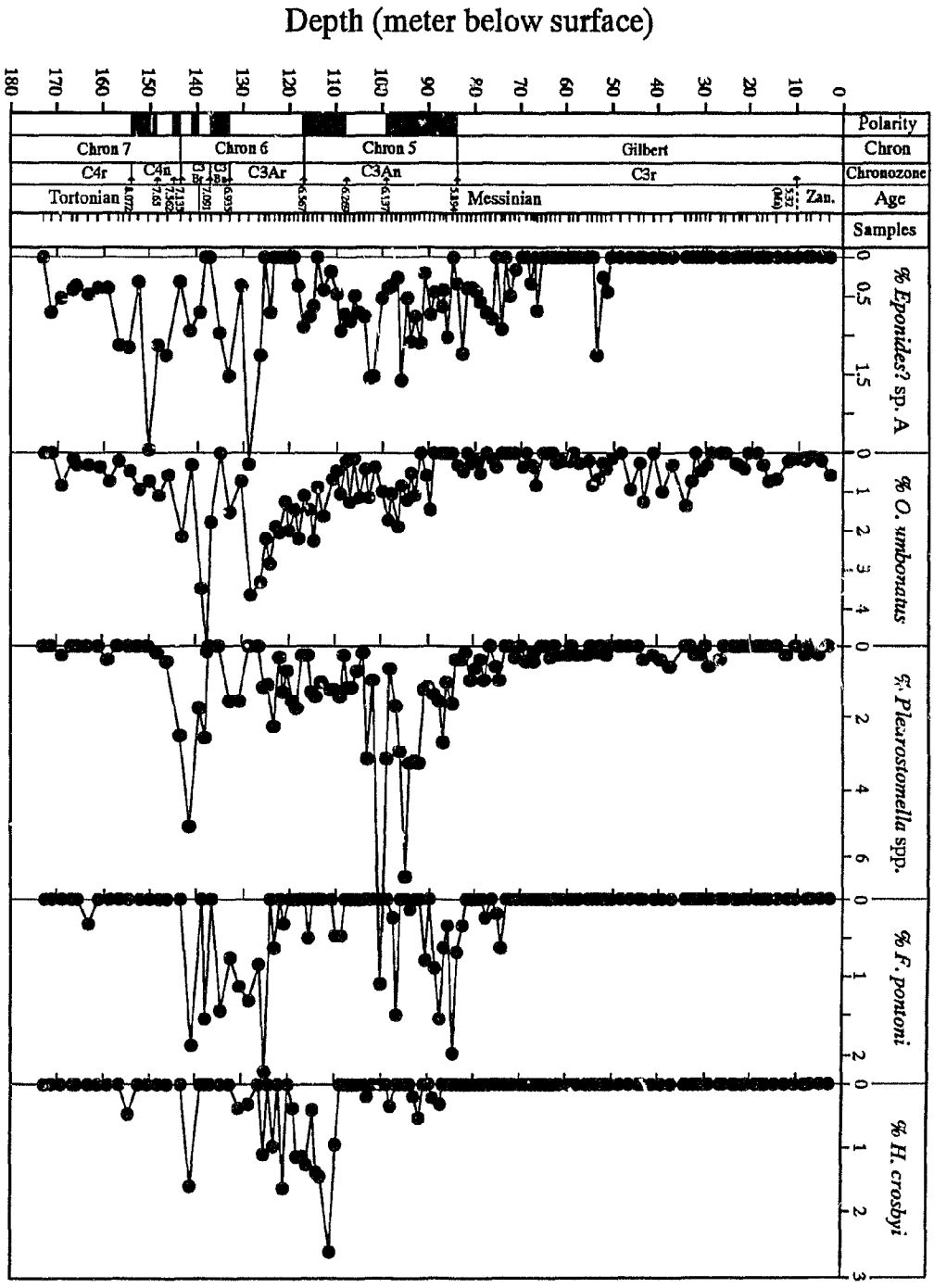
Depth (meter below surface)
180
170
160
150
140
130
120
110
100
90
80
70
60
50
40
30
20
10
0
Polarity
Chron 7
Chron 6
Chron 5
Gilbert
Chron
C4r
C4n
C3Br
C3Ar
C3An
C3r
Chronozone
Tortonian
Messinian
Zan.
Age
Samples
% Eponides? sp. A
% O. umbonatus
% Pleurostomella spp.
% F. pontoni
% H. crosbyi

Table 3-1. Benthic foraminiferal assemblages in the different stages of the Messinian, Salé Borehole, Morocco.

Late Messinian (5.9-5.32 Ma)	*G. subglobosa* 10-15%; *C. reniforme* ~5%; *E. exigua* 0-1%; *C. mundulus+pachyderma* 10-15%; *T. angulosa* ~10%; *B. lowmani* 1-5%; *G. praegeri* 5-10%; *Rosalina* 1%; *B. dialata* ~3%.
"Middle" Messinian (6.2-5.9 Ma)	*G. subglobosa* 5-10%; *C. reniforme* ~5%; *C. mundulus+pachyderma* <10%; *T. angulosa* 0-10%; *G. praegeri* <5%; *E. weddellensis* 10-25%; *U. peregrina* <2%; *E. exigua* up to 15%.
Early Messinian (7.12-6.2Ma)	*G. subglobosa* 10-20%; *E. weddellensis* 10-15%; *E. exigua* 2-10%; *C. mundulus+pachyderma* <10%; *B. albatrossi* 5-10%; *U. peregrina* 10%; *O. umbonatus* 2-4%; *H. crosbyi* 2%; *Gyroidina* spp. 5-10%.

Fig. 3-5. Stable isotopes of Salé borehole, northwestern Morocco. A: oxygen-18, and B: carbon-13. Data are from Hodell et al., 1994.

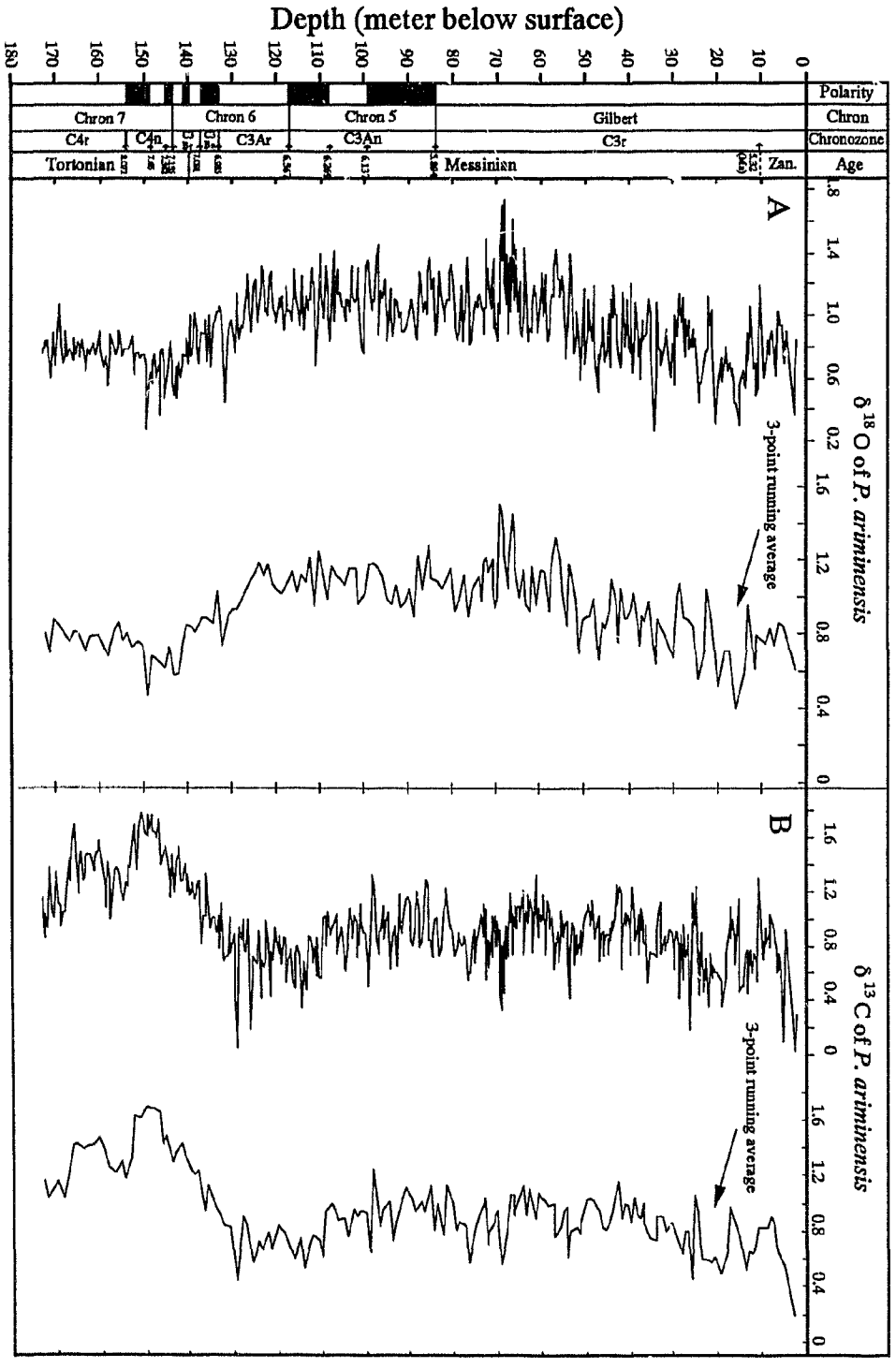
Depth (meter below surface)
180
170
160
150
140
130
120
110
100
90
80
70
60
50
40
30
20
10
0
Polarity
Chron 7
Chron 6
Chron 5
Gilbert
Chron
C4r
C4n
C3Ar
C3An
C3r
Chronozone
Tortonian
Messinian
Zan.
Age
A
B
δ 18O of P. ariminensis
δ 13C of P. ariminensis
3-point running average
3-point running average

e.g., DSDP Hole 552A where such a distinct depletion was not recognized (Keigwin, 1987). I consider that it may have been related to local temperature increase caused by tectonic uplifting of Morocco during the late Messinian.

3.1.3. Carbon stable isotopes

As with oxygen stable isotopes, the carbon stable isotopic data are also provided by Hodell et al. (1994). As given in Fig. 3-5B, higher $\delta^{13}C$ values (about 1.3‰ in average) occur in the interval between 175m and 140m during the uppermost Tortonian. However, two distinct fluctuations are determined in this interval. The maximum spike (greater than 1.6‰) is seen in the interval between 145m and 150m in Subchron C4n. A major decrease by 1.0‰ (minimum ca. 0.0‰) occurs above 140m near the Messinian/Tortonian boundary, which is known as global Chron 6 $\delta^{13}C$ shift. Values of $\delta^{13}C$ remain permanently low throughout the Salé borehole. However, secondary fluctuations occur frequently. From 110m to ~30m, $\delta^{13}C$ values are slightly enriched by 0.2‰. The values deplete again above 30m, with minimum values of about 0.0‰.

3.2. DSDP Hole 552A

3.2.1. Distribution of Benthic Foraminifera of DSDP Hole 552A

71 samples from the interval of 87.5 m to 163.55 m subbottom (msb) were quantitatively analyzed for benthic foraminifera greater than 63μm. This yields an average sampling interval of 1.07 msb (meters in subbottom) per sample. About 70 species have been identified in these samples. As shown in Fig. 3-6, benthic foraminiferal abundance is high during the Tortonian, usually over 4,000 per cc sample. It consistently decreases throughout the Messinian. Two major decreases are recognized in the late Messinian and early Pliocene, where abundances drop below 1000 per cc. In comparison with planktonic foraminifera, benthic foraminifera are extremely low (less than 3%) in percentage of total foraminiferal abundance (Fig. 3-6). During the late Messinian and early Pliocene, benthic

faunas are distinctly reduced (less than 2%).

In general, the benthic foraminiferal assemblage is dominated by *Globocassidulina subglobosa, Epistominella exigua, Eponides weddellensis, Bolivina cf. pygmaea,* and *Eponides tumidulus.* These species make up 50-60% in relative abundance. *G. subglobosa* is about 10% higher in the Messinian and Tortonian than in the Pliocene. *Nuttallides umbonifera* occurs in low percentage in the early Messinian, Tortonian, and the upper part of planktonic foraminiferal Zone PL-1 (lower Pliocene). It is almost absent in the upper Messinian and lower part of Zone PL-1. Detailed information on distribution of benthic foraminiferal species is given in Figs. 3-6 to 3-8 and Appendix B.

3.2.2. Oxygen stable isotopes

Oxygen isotopes were measured both from benthic foraminifera *(Planulina wuellerstorfi)* and surface dweller *Globigerina bulloides* by Keigwin et al. (1987) and Keigwin (1987). In this study, I re-plotted the latter data in Figs. 3-9 and 3-10, together with a smoothed 3-point running average curve. As shown in the figures, oxygen isotopes from benthic and planktonic foraminifera generally exhibit a similar pattern. However a major difference occurs in the earliest Messinian (145-150 msb), where the benthic isotopic values increase, while the planktonic values decrease; planktonic foraminifera indicate a major increase (~1.7‰) in the interval between 135 and 145 m subbottom, while the benthic values remain approximately the same as in the preceding interval. Two important isotope maximum incursions indicating global glaciations both in benthic and planktonic foraminiferal shells were recognized in the upper Messinian with a duration of ca. 15,000 years at 106 m and 119m subbottom, respectively. More specifically, the occurrence of the lower $\delta^{18}O$ maximum from benthic foraminifera is at 118.82 msb, while that from planktonic foraminifera is at 119.15 msb, suggesting a delay of ~10,000 years (see Keigwin et al., 1987; Keigwin, 1987; and Chapter 4 for more details).

3.2.3. Carbon Stable Isotope:

$\delta^{13}C$ data from benthic *(Planulina wuellerstorfi)* and planktonic foraminifera (*Globigerina bulloides*) provided by Keigwin et al. (1987) and Keigwin (1987) are re-plotted in Figs. 3-9 and 3-10. It is clear that the carbon isotopes from both benthic and planktonic foraminifera show a distinct shift from high values to low values ~148 msb, immediately above the Messinian/Tortonian boundary. The average decline in $\delta^{13}C$ values constantly continue to the top of the Messinian interval, although a number of secondary order fluctuations have occurred (Figs. 3-9 and 3-10). A tendency towards increased $\delta^{13}C$ values occurred near the Pliocene/Messinian boundary at this site (see Keigwin et al., 1987; Keigwin, 1987 for more details).

3.3. DSDP Hole 608

3.3.1. Distribution of benthic foraminifera

61 samples for the interval from 105.3 msb to 219.7 msb were quantitatively analyzed for benthic foraminifera greater than 63μm, yielding an average spacing of 1.87 m. Note that within the Messinian, the sampling spacing is about 1.3 m per sample with stratigraphic resolution of ~50 kyrs. About 70 species have been identified (Appendix C).

Total benthic foraminiferal abundance is similar to that in DSDP Hole 552A, varying from 200 to 500 per cc. A few peaks over 600 per cc occur in Cores 14, 17, 20. The abundance of benthic foraminifera reaches a minimum in Core 18. This is caused by carbonate dissolution as indicated by high planktonic foraminiferal fragments and suddenly increased benthic foraminifera relative to the planktonic foraminifera (i.e., B/P ratios), where both of them climax (Fig. 3-11). The planktonic foraminiferal fragments decrease dramatically in the Pliocene immediately across the Messinian/Pliocene boundary.

Generally speaking, the benthic faunas are dominated by *Globocassidulina subglobosa, Epistominella exigua,* and *Eponides weddellensis* (Fig. 3-12). Secondary important species include *Oridorsalis umbonatus, Eponides tumidulus, Gyroidi*[illegible]*p.,*

Fig. 3-6. Distribution of benthic foraminiferal abundance and relative abundance of *Epistominella exigua* and *Globocassidulina subglobosa.*

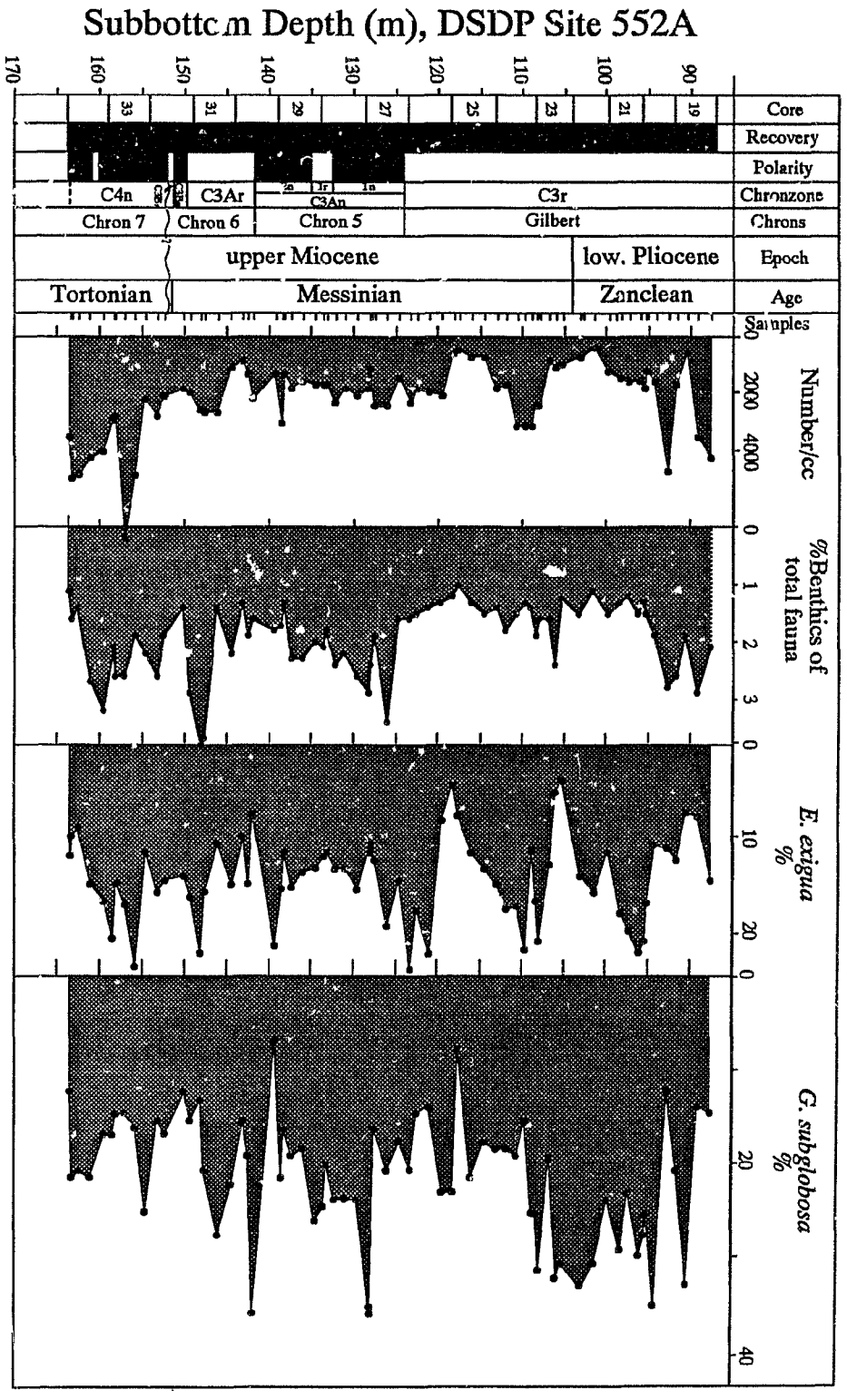
Subbottom Depth (m), DSDP Site 552A
170
160
150
140
130
120
110
100
90
33
31
29
27
25
23
21
19
Core
Recovery
Polarity
C4n
C3Ar
C3An
C3r
Chronzone
Chron 7
Chron 6
Chron 5
Gilbert
Chrons
upper Miocene
low. Pliocene
Epoch
Tortonian
Messinian
Zanclean
Age
Samples
Number/cc
0
2000
4000
%Benthics of total fauna
0
1
2
3
E. exigua %
0
10
20
G. subglobosa %
0
20
40

Fig. 3-7. Relative abundance of *Eponides tumidulus, Bolivina pygmaea, Eponides weddellensis, Gyroidina spp., Uvigerina peregrina* and *Nonionella* spp.

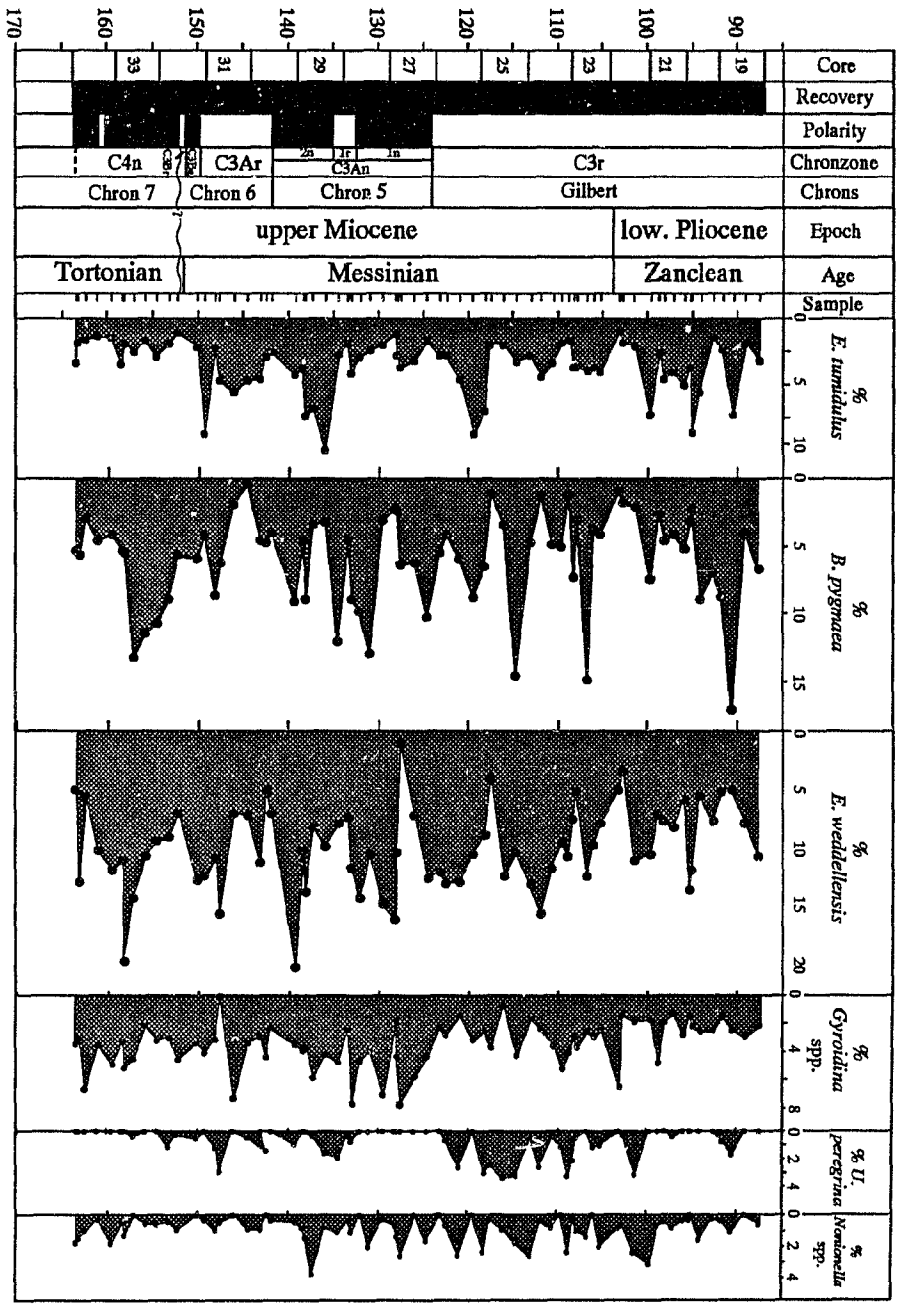
Subbottom Depth (m), DSDP Site 552A
170
160
150
140
130
120
110
100
90
33
31
29
27
25
23
21
19
Core
Recovery
Polarity
C4n
C3Ar
C3An
C3r
Chronzone
Chron 7
Chron 6
Chron 5
Gilbert
Chrons
upper Miocene
low. Pliocene
Epoch
Tortonian
Messinian
Zanclean
Age
Sample
% E. tumidulus
% B. pygmaea
% E. weddellensis
% Gyroidina spp.
% U. peregrina
% Nonionella spp.

Fig. 3-8. Relative abundance of *Nuttallides umbonifera, Trifarina angulosa, Ehrenbergina trigona, Bolivina pseudopunctata, Melonis barleeanum, Stilostomella antillea,* and *Bolivina inflata.*

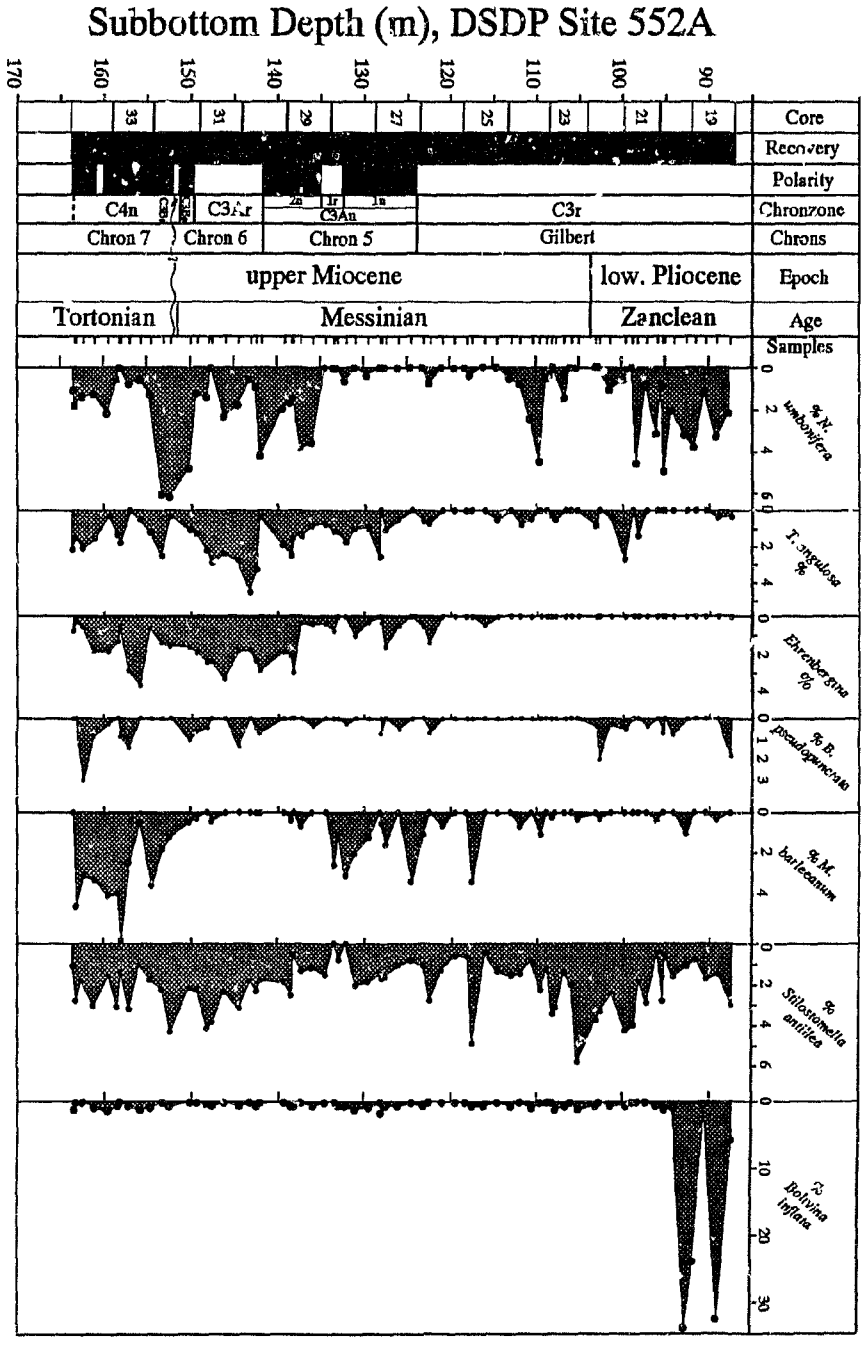
Subbottom Depth (m), DSDP Site 552A
170
160
150
140
130
120
110
100
90
33
31
29
27
25
23
21
19
Core
Recovery
Polarity
C4n
C3Ar
C3An
C3r
Chronzone
Chron 7
Chron 6
Chron 5
Gilbert
Chrons
upper Miocene
low. Pliocene
Epoch
Tortonian
Messinian
Zanclean
Age
Samples
% N. umbonifera
T. angulosa %
Ehrenbergina %
% B. pseudopunctata
% M. barleeanum
% Stilostomella antillea
% Bolivina inflata

Fig. 3-9. Oxygen and carbon stable isotopes of *Planulina wuellerstorfi* (benthic foraminifera), DSDP Hole 552A (Data are from Keigwin, 1987).

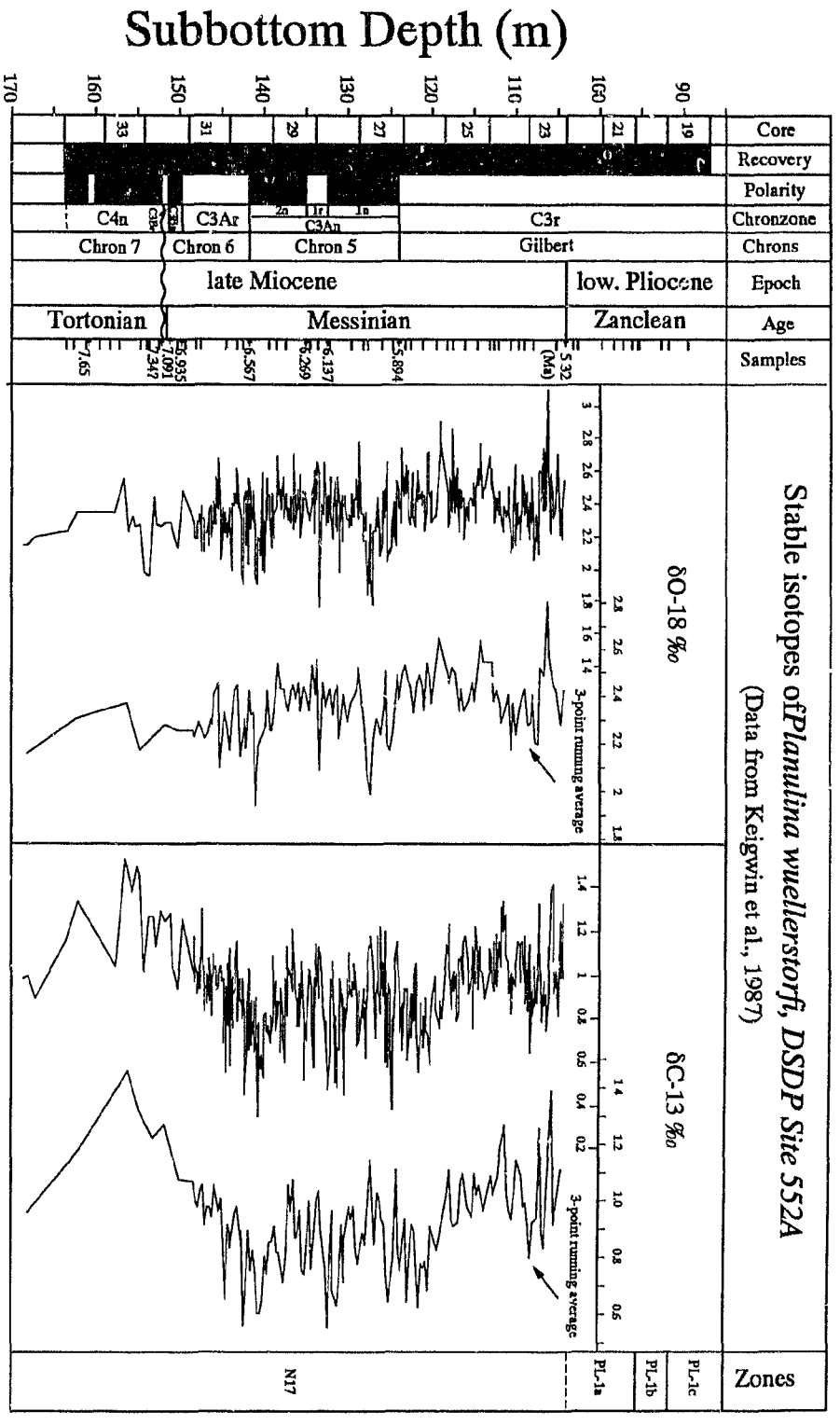
Subbottom Depth (m)
170
160
150
140
130
120
110
100
90
Core
Recovery
Polarity
Chronzone
C4n
C3Ar
C3An
C3r
Chrons
Chron 7
Chron 6
Chron 5
Gilbert
Epoch
late Miocene
low. Pliocene
Age
Tortonian
Messinian
Zanclean
Samples
7.65
7.341
7.091
6.935
6.567
6.269
6.137
5.894
5.32
(Ma)
δO-18 ‰
3-point running average
δC-13 ‰
3-point running average
Zones
N17
PL-1a
PL-1b
PL-1c
Stable isotopes of *Planulina wuellerstorfi*, DSDP Site 552A
(Data from Keigwin et al., 1987)

Fig. 3-10. Oxygen and carbon stable isotopes of *Globigerina bulloides* (planktonic foraminifera), DSDP Hole 552A (Data are from Keigwin, 1987).

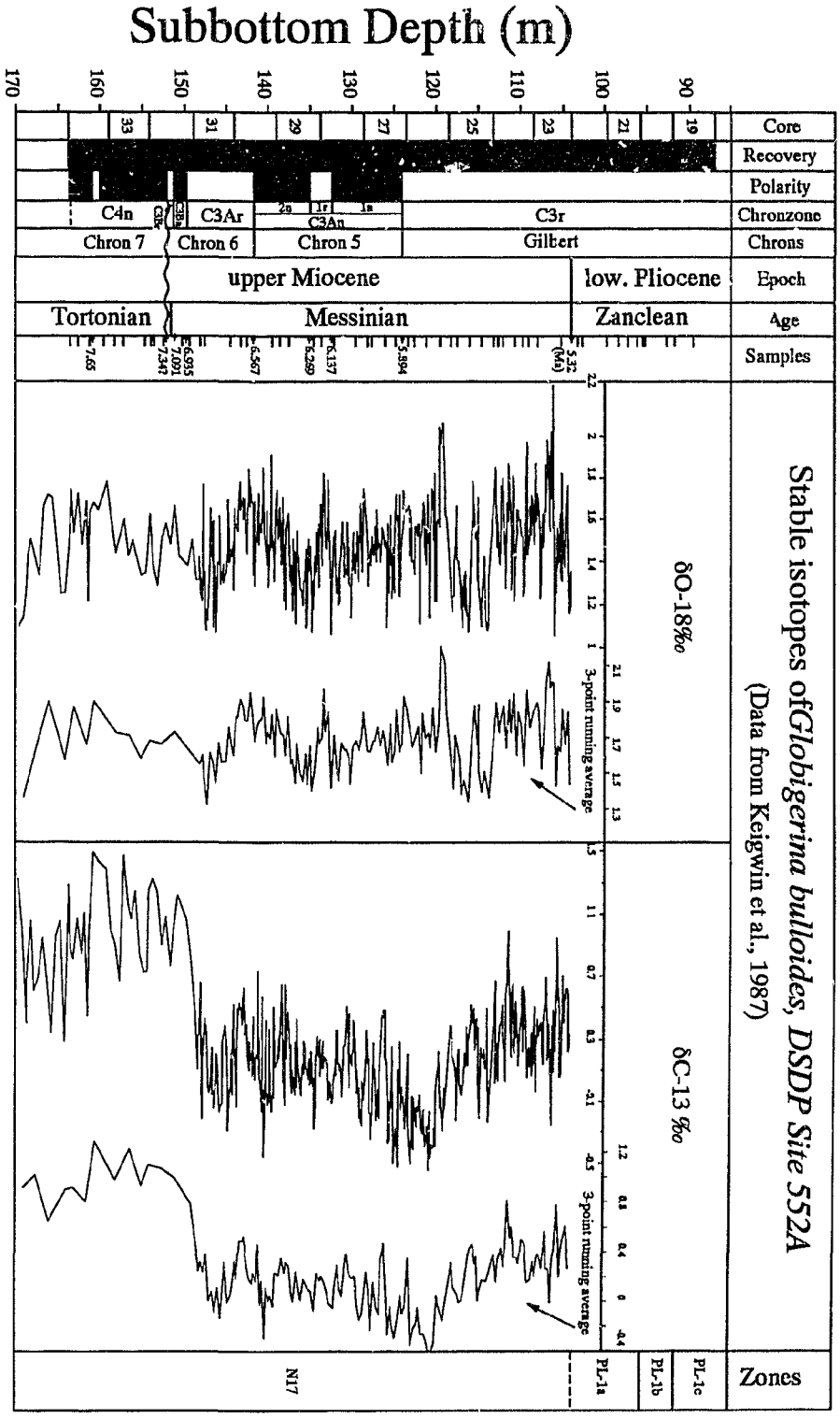
Subbottom Depth (m)
170
160
150
140
130
120
110
100
90
Core
Recovery
Polarity
Chronzone
C4n
C3Ar
C3An
C3r
Chrons
Chron 7
Chron 6
Chron 5
Gilbert
Epoch
upper Miocene
low. Pliocene
Age
Tortonian
Messinian
Zanclean
Samples
7.65
7.091
7.341
6.567
6.137
5.894
5.32 (Ma)
δO-18‰
3-point running average
δC-13 ‰
3-point running average
Zones
N17
PL-1a
PL-1b
PL-1c
Stable isotopes of Globigerina bulloides, DSDP Site 552A
(Data from Keigwin et al., 1987)

Fig. 3-11. Benthic foraminiferal abundance, percentage of planktonic foraminiferal fragments in total planktonic foraminifera, and percentage of benthic foraminifera of total fauna, DSDP Site 608.

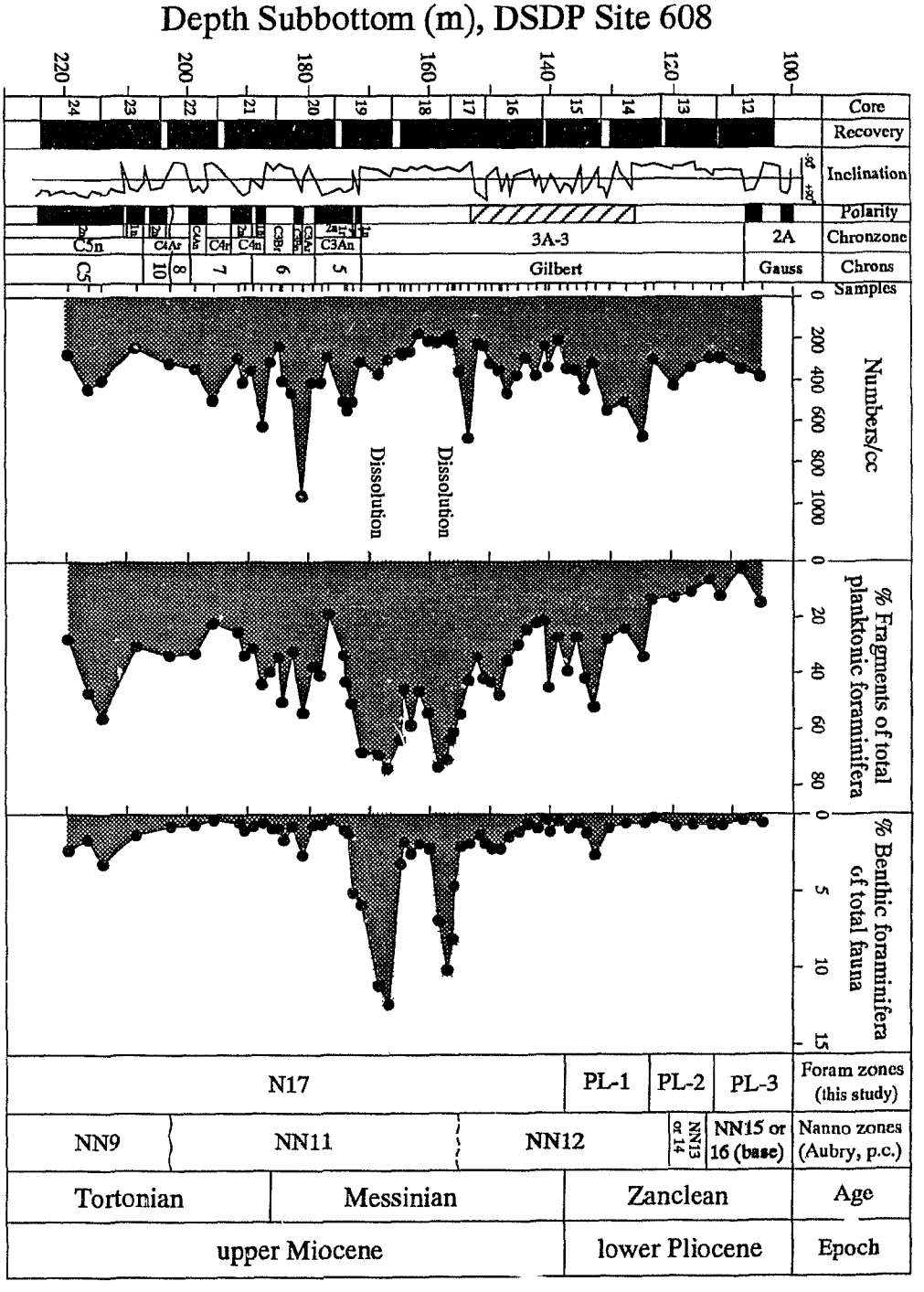
Depth Subbottom (m), DSDP Site 608
220
200
180
160
140
120
100
Core
Recovery
Inclination
Polarity
Chronzone
Chrons
3A-3
2A
Gilbert
Gauss
Samples
Numbers/cc
Dissolution
Dissolution
% Fragments of total planktonic foraminifera
% Benthic foraminifera of total fauna
N17
PL-1
PL-2
PL-3
Foram zones (this study)
NN9
NN11
NN12
NN13 or 14
NN15 or 16 (base)
Nanno zones (Aubry, p.c.)
Tortonian
Messinian
Zanclean
Age
upper Miocene
lower Pliocene
Epoch

Fig. 3-12. Relative abundance of *Epistominella exigua, Nuttallides umbonifera, Eponides weddellensis* and *Globocassidulina subglobosa*, DSDP Site 608.

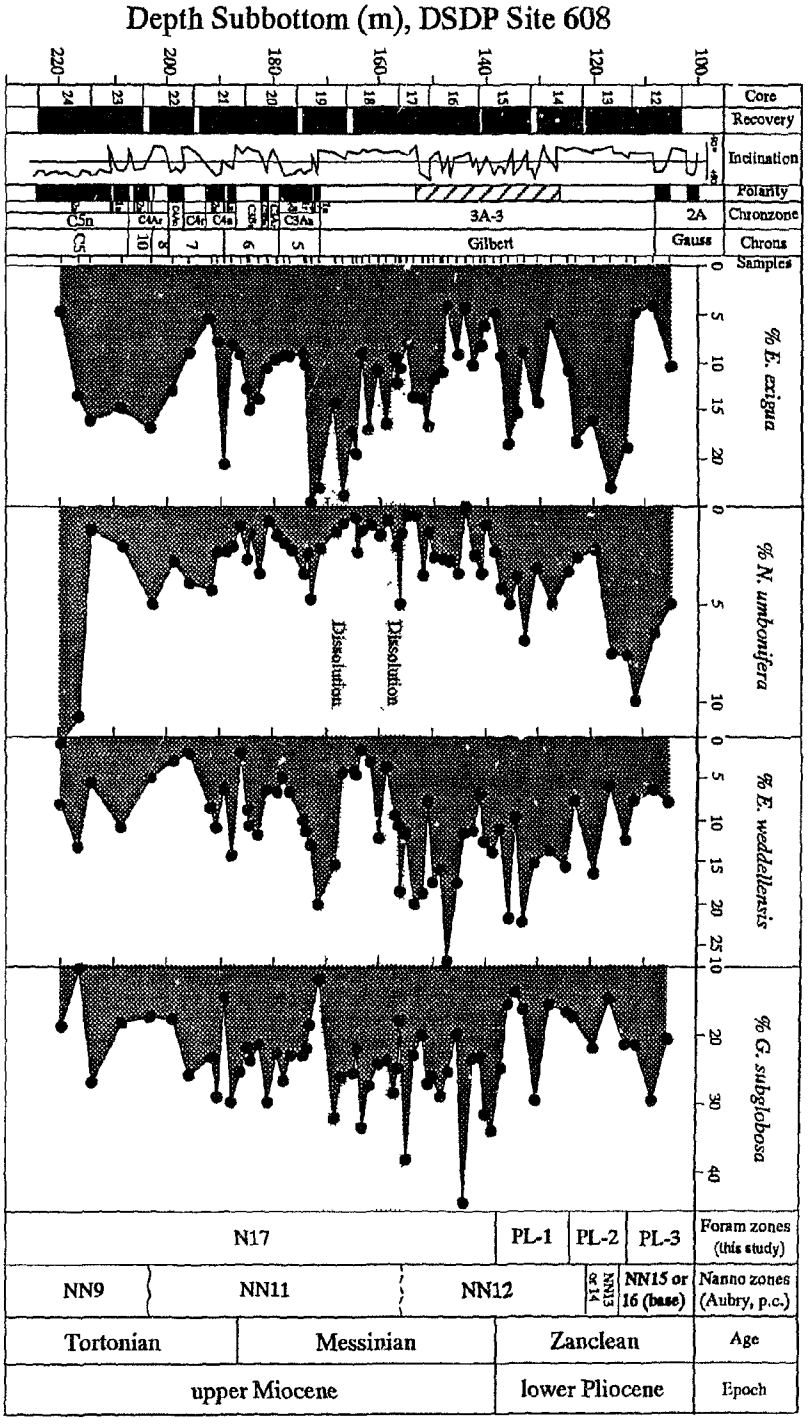
Depth Subbottom (m), DSDP Site 608
220
200
180
160
140
120
100
Core
Recovery
Inclination
Polarity
Chronzone
Chrons
Samples
3A-3
2A
Gilbert
Gauss
% E. exigua
% N. umbonifera
% E. weddellensis
% G. subglobosa
Dissolution
Dissolution
N17
PL-1
PL-2
PL-3
Foram zones (this study)
NN9
NN11
NN12
NN15 or 16 (base)
Nanno zones (Aubry, p.c.)
Tortonian
Messinian
Zanclean
Age
upper Miocene
lower Pliocene
Epoch

Fig. 3-13. Relative abundance of *Oridorsalis umbonatus, Cassidulina reniforme*, and *Eponides tumidulus*, DSDP Site 608.

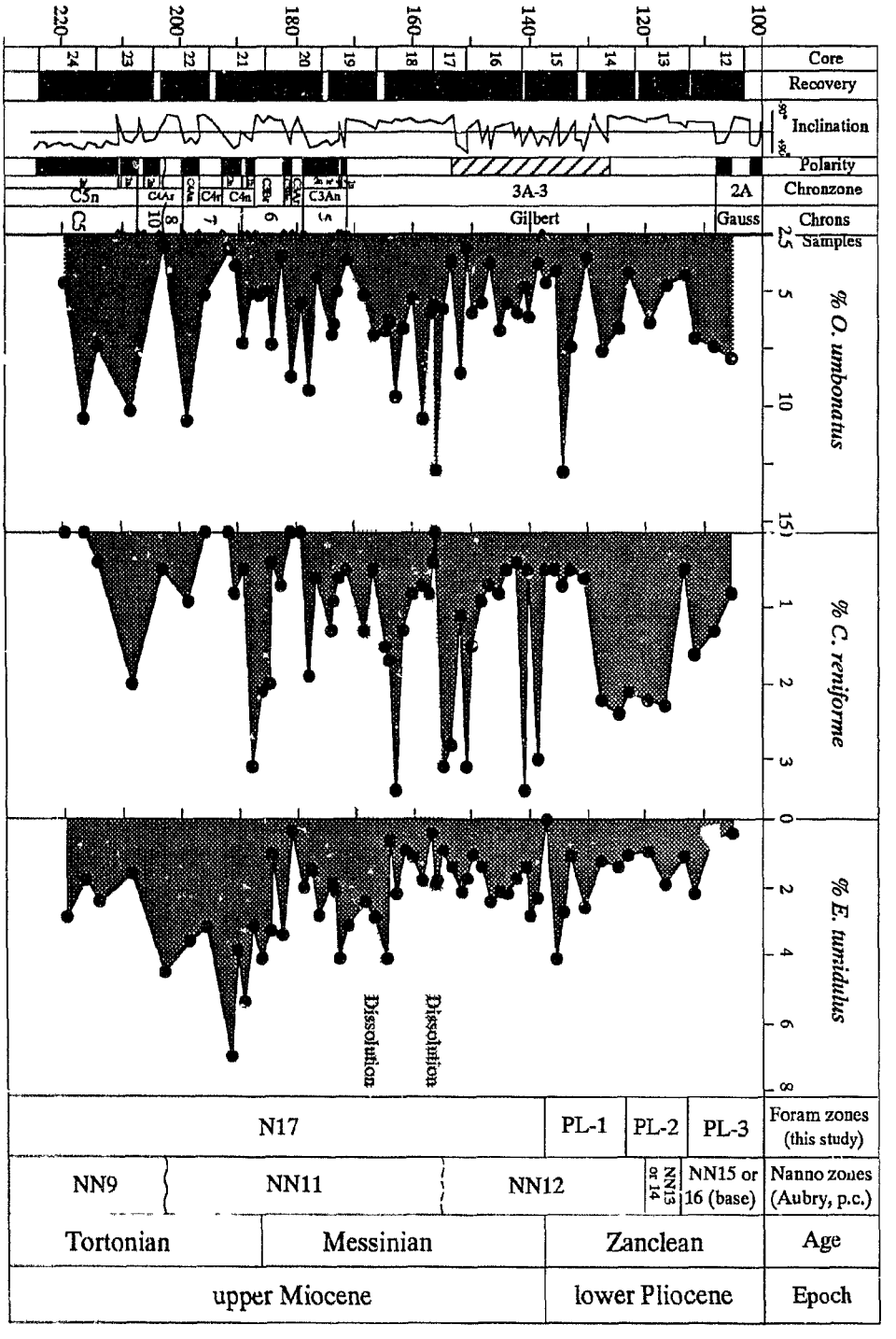
Depth Subbottom (m), DSDP Site 608
220
200
180
160
140
120
100
Core
Recovery
Inclination
Polarity
Chronzone
Chrons
Samples
3A-3
2A
Gilbert
Gauss
% O. umbonatus
% C. reniforme
% E. tumidulus
Dissolution
Dissolution
N17
PL-1
PL-2
PL-3
Foram zones (this study)
NN9
NN11
NN12
NN13 or 14
NN15 or 16 (base)
Nanno zones (Aubry, p.c.)
Tortonian
Messinian
Zanclean
Age
upper Miocene
lower Pliocene
Epoch

Fig. 3-14. Relative abundance of *Pullenia quinqueloba*, *Gyroidina* spp., and *Melonis barleeanum*, DSDP Site 608.

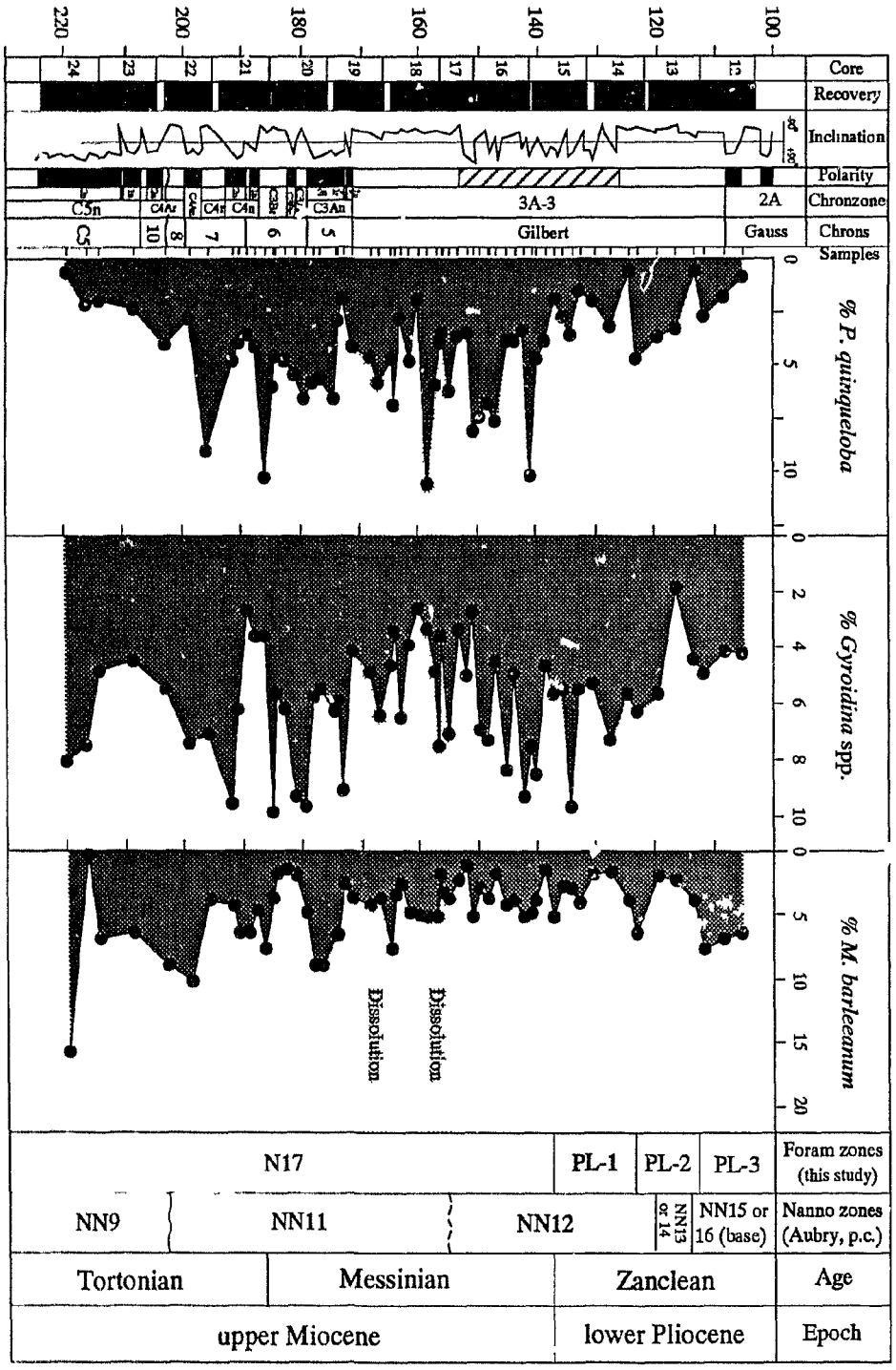
Depth Subbottom (m), DSDP Site 608
220
200
180
160
140
120
100
Core
Recovery
Inclination
Polarity
Chronzone
Chrons
Samples
C5n
C4Ar
C4n
C3Ar
C3An
3A-3
2A
Gilbert
Gauss
% P. quinqueloba
% Gyroidina spp.
% M. barleeanum
Dissolution
Dissolution
N17
PL-1
PL-2
PL-3
Foram zones (this study)
NN9
NN11
NN12
NN13 or 14
NN15 or 16 (base)
Nanno zones (Aubry, p.c.)
Tortonian
Messinian
Zanclean
Age
upper Miocene
lower Pliocene
Epoch

Pullenia quinqueloba ,Melonis barleeanum, etc. (Figs. 3-13 and 3-14). *E. exigua* reaches three major peaks in Cores 13 and 14, 17-19, and 22-24, where *E. weddellensis* is lowered in its relative abundance. *G. subglobosa* is relatively high from Cores 15 to 20 within the Messinian section. *Nuttallides umbonifera* is relatively low (> 5%) from Cores 15 to 21, reaching a minimum in Core 18 where carbonate dissolution has taken place.

3.3.2. Oxygen stable isotopes

All stable isotopic data from this site are given in Appendix D and illustrated in Figs 3-15 & 3-16 Oxygen stable isotopes in benthic foraminifera (*P. wuellerstorfi)* show a permanent enrichment (~2.3‰ in average) from the upper part of Core 22 to Core 12 (fig. 3-15). In this interval, five $\delta^{18}O$ incursions, which reach about 2.6‰, occur in Core 22, Core 19, Core 17, Core 15 and Core 14. A major $\delta^{18}O$ depletion occurs in cores 23 and 24, which reaches ~1.8‰.

In planktonic foraminifera (*G. bulloides*, solid line), the $\delta^{18}O$ pattern is rather different from that in benthic foraminiferal $\delta^{18}O$ (Fig. 3-16). No major depletion is recorded in cores 23 and 24, and no significant variations are observed below Core 21. Similar to $\delta^{18}O$ in benthic foraminifera, two major planktonic foraminiferal $\delta^{18}O$ enrichments occur in Core 15 (but it is stratigraphically slightly higher than the peak in benthic foraminiferal $\delta^{18}O$) and Core 17. In Core 19, an enriched $\delta^{18}O$ peak is recorded although it is not as clear as that recorded in benthic $\delta^{18}O$. It is considered to have been related to the absence of *G. bulloides* resulting from the carbonate dissolution in this interval. $\delta^{18}O$ in *O. universa* (broken line) shows a major depletion in the dissolution interval from Core 17 to Core 19 (see Chapter 4 for a discussion on the depletion).

3.3.3. Carbon stable isotopes

All $\delta^{13}C$ data from DSDP Site 608 are provided in Appendix D, and shown in figs 3-15 & 3-16. $\delta^{13}C$ of *P. wuellerstorfi* varies greatly, particularly below Core 17. In the

Fig. 3-15. Oxygen and carbon stable isotopes of *Planulina wuellerstorfi* (benthic foraminifera), DSDP Site 608.

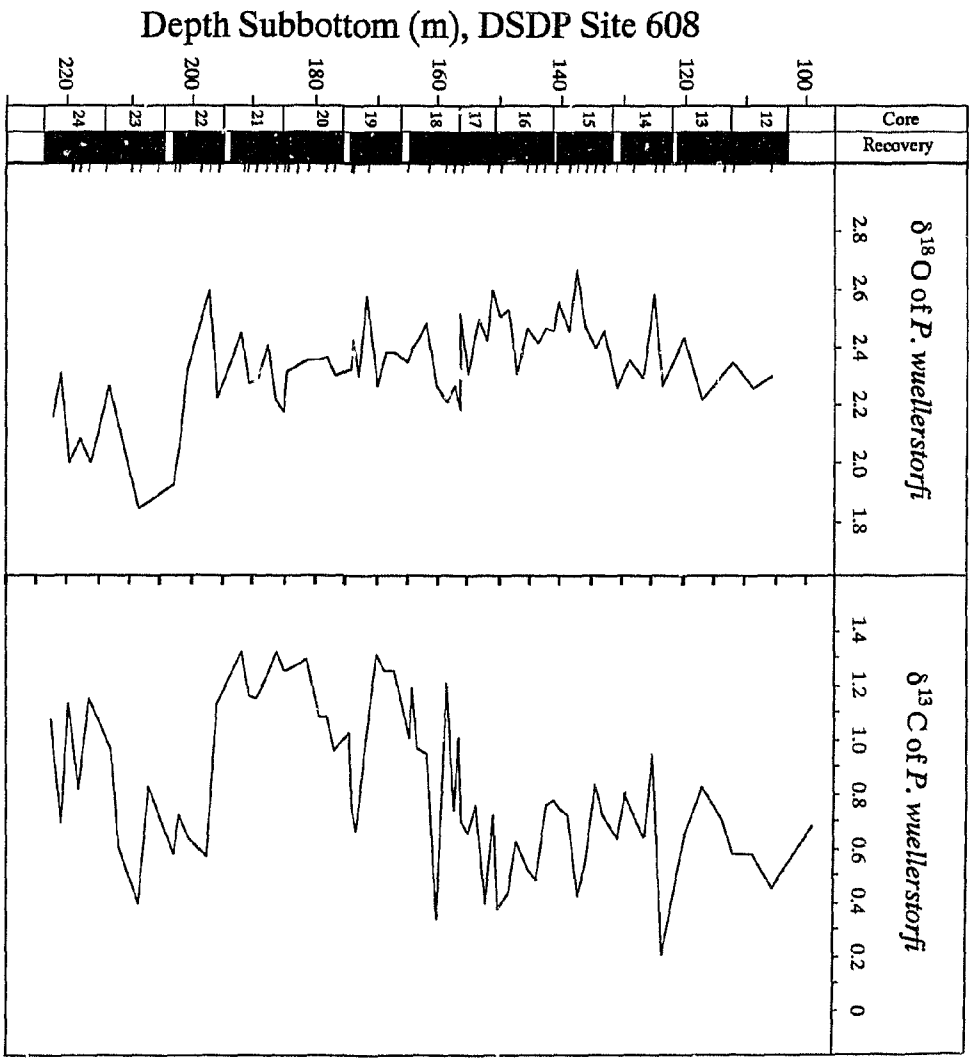
Depth Subbottom (m), DSDP Site 608
220
200
180
160
140
120
100
24
23
22
21
20
19
18
17
16
15
14
13
12
Core
Recovery
δ18O of P. wuellerstorfi
2.8
2.6
2.4
2.2
2.0
1.8
δ13C of P. wuellerstorfi
1.4
1.2
1.0
0.8
0.6
0.4
0.2
0

Fig. 3-16. Oxygen and carbon stable isotopes of *Globigerina bulloides and Orbulina universa* (planktonic foraminifera; solid lines = *G. bulloides*; broken lines = *O. universa*), DSDP Site 608.

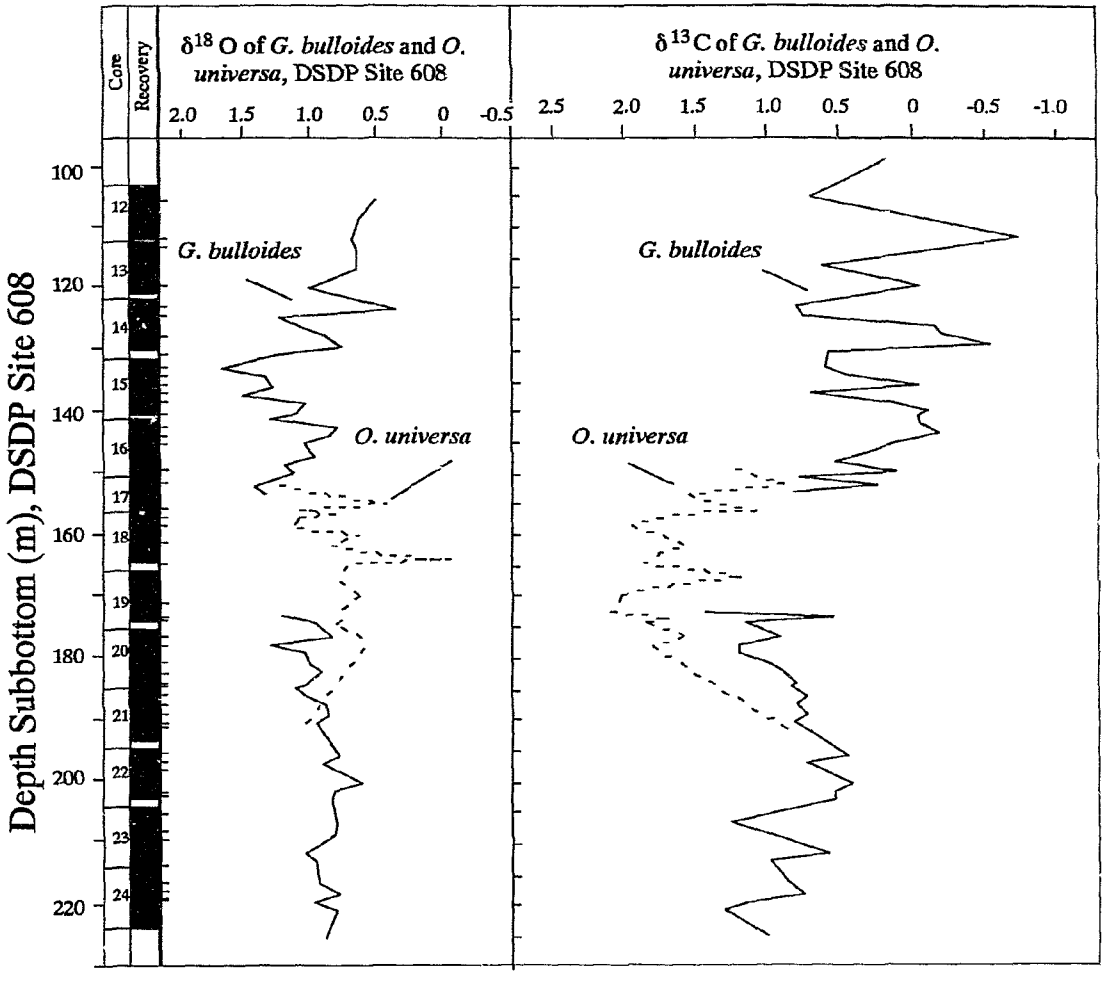
Core
Recovery
δ18 O of G. bulloides and O. universa, DSDP Site 608
2.0 1.5 1.0 0.5 0 -0.5
δ13C of G. bulloides and O. universa, DSDP Site 608
2.5 2.0 1.5 1.0 0.5 0 -0.5 -1.0
G. bulloides
O. universa
G. bulloides
O. universa
Depth Subbottom (m), DSDP Site 608
100
120
140
160
180
200
220
12
13
14
15
16
17
18
19
20
21
22
23
24

interval from Core 24 to Core 18, three enriched incursions are recognized. They occur in Core 24 (1.1‰), Cores 21 and 20 (1.3‰), and Cores 19 and 18 (1.3‰), respectively. A constant depletion above Core 17 with values of ~0.6‰ is observed.

Planktonic foraminiferal $\delta^{13}C$ shows a similar trend to the benthic $\delta^{13}C$, except the interval between 175m and 195 msb (cores 21 and 20) where $\delta^{13}C$ of *G. bulloides* (solid line) does not show significant increase although it trends to increase. However, $\delta^{13}C$ of *O. universa* (broken line) indicates a rapid increase at Core 20. In general, both planktonic and benthic foraminiferal $\delta^{13}C$ exhibit two depletion shifts within the interval from 160 to 195 msb. These two shifts will be discussed in great detail in Chapter 4.

3.4 DSDP Hole 547A

3.4.1. Distribution of benthic Foraminifera

37 samples in this hole have been analyzed, with a sampling space of 0.6-0.8 m. Over 90 species have been identified (see Figs. 3-17, 3-18, and Appendix F). As seen in Fig. 3-17, benthic foraminiferal abundance is low from Cores 5-9, less than 1000 per cc, while in Cores 3 and 4, it is over 1000 per cc. Planktonic foraminiferal fragments are relatively low in this hole, usually less than 5% of total planktonic foraminiferal tests. Two spikes over 5% occur in Cores 5 and 8 (Fig. 3-17). In comparison with DSDP Holes 552A and 608, benthic foraminifera are extremely high relative to planktonic fauna in the interval from Cores 5 to 8, making up 20 to 40% in total foraminiferal fauna (Fig. 3-17). This obviously indicates high carbonate dissolution rates in this interval. From Cores 5 to 9, the benthic foraminiferal fauna is dominated by *G. subglobosa* (20-30%), *E. exigua* (~20%), *E. weddellensis* (~20%), and *N. umbonifera* (10-15%). In Cores 3 and 4, the fauna is dominated by *Bolivina inflata, Bolivinita pseudothalmanni* and *Bolivina* spp., making up ~50% of total benthic fauna. These species are relatively common in bathyal environments (see Chapter 6). Therefore it may indicate that downslope transportation may have taken place at this time. The downslope transportation may also have occurred in Cores 5 and 6

Fig. 3-17. Distribution of benthic foraminifera, *Globocassidulina subglobosa, Nuttallides umbonifera, Epistominella exigua*, and *Eponides weddellensis*, DSDP Hole 547A. H1, H2, and H3 are hiatuses.

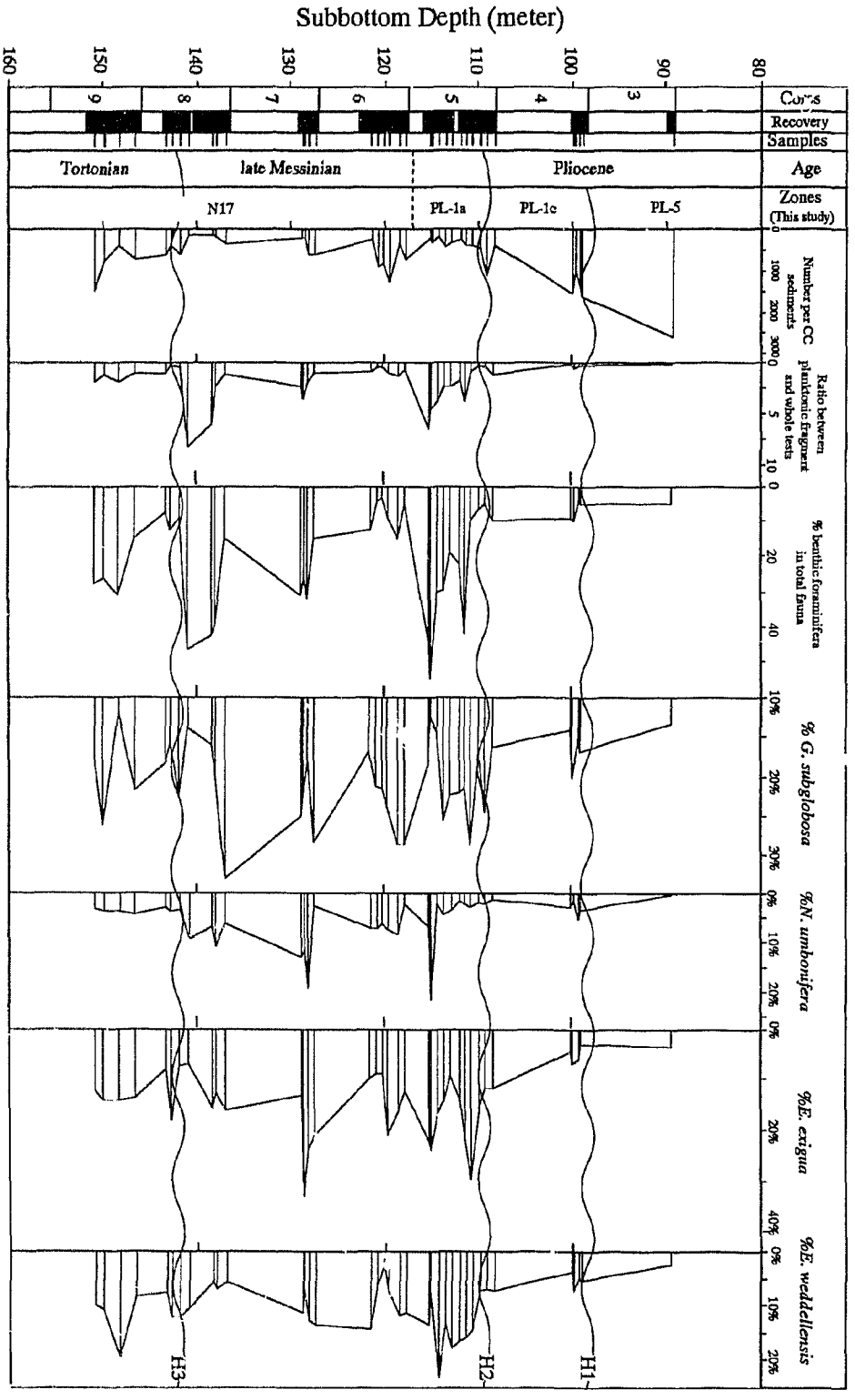
Subbottom Depth (meter)
160
150
140
130
120
110
100
90
80
Cores
Recovery
Samples
Tortonian
late Messinian
Pliocene
Age
N17
PL-1a
PL-1c
PL-5
Zones (This study)
Number per CC sediments
Ratio between planktonic fragment and whole tests
% benthic foraminifera in total fauna
% G. subglobosa
%N. umbonifera
%E. exigua
%E. weddellensis
H3
H2
H1

Fig. 3-18. Relative abundance of benthic foraminifera, *Bolivina pygmaea, B. pseudothalmanni, B. inflata, B. pseudoplicata, Trifarina angulosa, Pullenia bulloides, Oridorsalis umbonatus, Sphaeroidina bulloides, Cibicidoides* spp., *Planulina wuellerstorfi, Stilostomella* spp., *Gyroidina* spp., and *Uvigerina peregrina*, DSDP Hole 547A. H1, H2, and H3 are hiatuses.

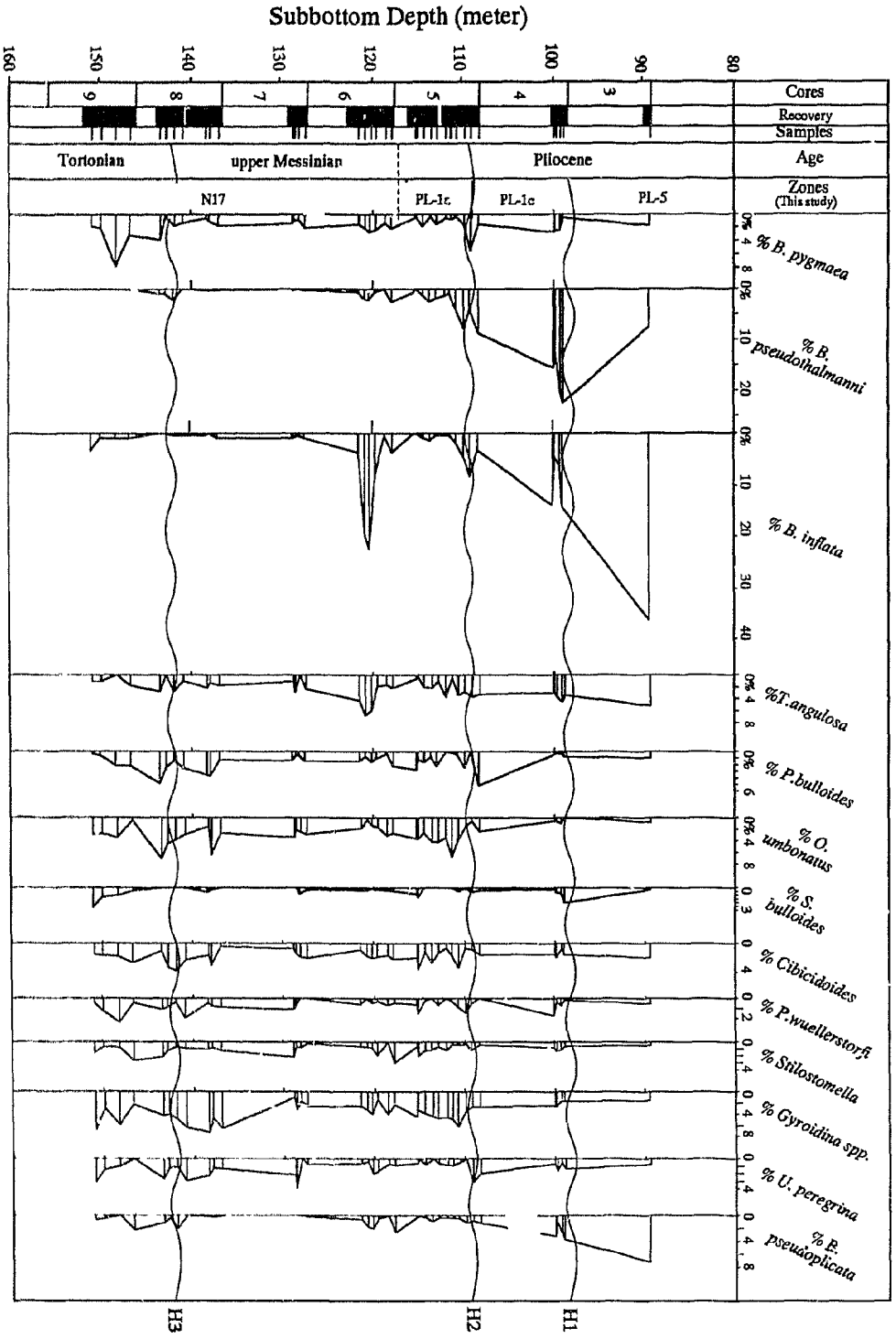
Subbottom Depth (meter)
160
150
140
130
120
110
100
90
80
Cores
Recovery
Samples
Tortonian
upper Messinian
Pliocene
Age
N17
PL-1c
PL-1c
PL-5
Zones
(This study)
% B. pygmaea
% B. pseudothalmanni
% B. inflata
%T.angulosa
% P.bulloides
% O. umbonatus
% S. bulloides
% Cibicidoides
% P.wuellerstorfi
% Stilostomella
% Gyroidina spp.
% U. peregrina
% B. pseudoplicata
H3
H2
H1

as indicated by low relative abundance of these two species. Other deep-water species are constantly low in relative abundance (Fig. 3-18).

3.5. ODP Site 646B

3.5.1. Distribution of benthic foraminifera and other flora

Ninety samples from Cores 40-80 (389-789m subbottom depth (msb)) were studied for benthic foraminifera. Over one hundred species have been identified (Appendix G). As seen in Fig. 3-19, the total number of benthic foraminifera per cc are rather consistent throughout the hole, but increase slightly downwards. During the Tortonian these numbers are particularly low.

As indicated in Fig. 3-19, the Messinian interval from Cores 45X to 77X is dominated by agglutinated foraminifera, while calcareous foraminifera dominate the intervals of Pliocene and Tortonian. Benthic/planktonic foraminiferal ratios are high in the Messinian section, except for some particular levels (Fig. 3-19). They are relatively low during the Pliocene and Tortonian. Nevertheless, both calcareous/agglutinated and benthic/planktonic ratios exhibit high amplitudes of variations.

Three poorly-preserved, small-sized, brown-colored marsh-type agglutinated benthic foraminiferal species, i.e., *Trochammina* cf. *squamata, Ammotium* sp. A, and *Miliammina fusca* are encountered in this hole. *Ammotium* sp. A occurs in most samples from Cores 42X-1 to 65X-CC, with the highest peak (15%) at Core 57X-3. It is rare below Core 65 (Fig. 3-21). *Miliammina fusca* is found in Sample 63X-CC, 10-14cm. These forms are well known to inhabit in marsh or coastal environments today (e.g. Scott and Medioli, 1980). *Trochammina* cf. *squamata* varies episodically in abundance from 0 to 100% (Fig. 3-19) with high amplitudes of variation. These forms are concentrated in nine levels throughout the hole, which are separated by corresponding numbers of deep-water foraminiferal layers accompanied with relatively low proportion of shallow water fauna (Fig. 3-19), suggesting nine turbidite cycles. They occur in Cores 77X-74X Cores 74-

Fig. 3-19. Distribution of benthic foraminifera from ODP Hole 646B. The column to the right shows cyclic turbidites marked by marsh benthic foraminifera and other shallow water sediment components, interbedded with deep water benthic foraminifera.

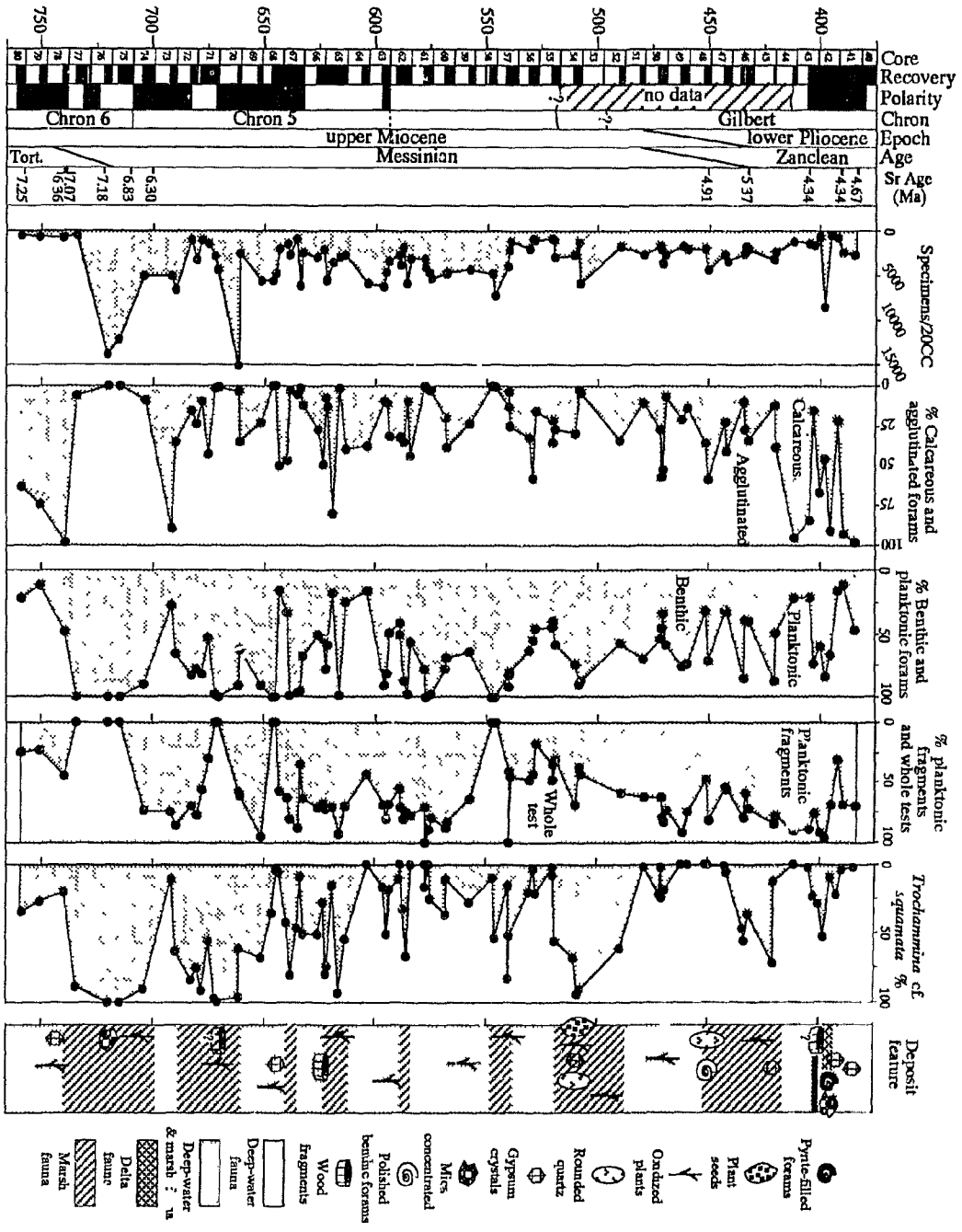
Depth (meters subbottom)
750
700
650
600
550
500
450
400
Core
Recovery
Polarity
Chron
Epoch
Age
Sr Age (Ma)
no data
Chron 6
Chron 5
Gilbert
upper Miocene
lower Pliocene
Tort.
Messinian
Zanclean
7.25
7.07
6.96
7.18
6.83
6.30
4.91
5.37
4.34
4.67
4.34
Specimens/20CC
0
500
1000
1500
% Calcareous and agglutinated forams
Calcareous
Agglutinated
0
25
50
75
100
% Benthic and planktonic forams
Benthic
Planktonic
0
50
100
% planktonic fragments and whole tests
Planktonic fragments
Whole test
0
50
100
Trochammina cf. squamata %
0
50
100
Deposit feature
Pyrite-filled forams
Plant seeds
Oxidized plants
Rounded quartz
Gypsum crystals
Mica concentrated
Polished benthic forams
Wood fragments
Deep-water fauna
Deep-water & marsh fauna
Delta fauna
Marsh fauna

Fig. 3-20. Relative abundance of agglutinated benthic foraminifera, *Trochammina* sp. A, *Rhizammina* spp., *Ammotium* sp. A, *Psammosphaera* spp., *Lagenammina* spp. and *Cornuspirella diffusa*, from ODP Hole 646B.

Depth (meters subbottom)

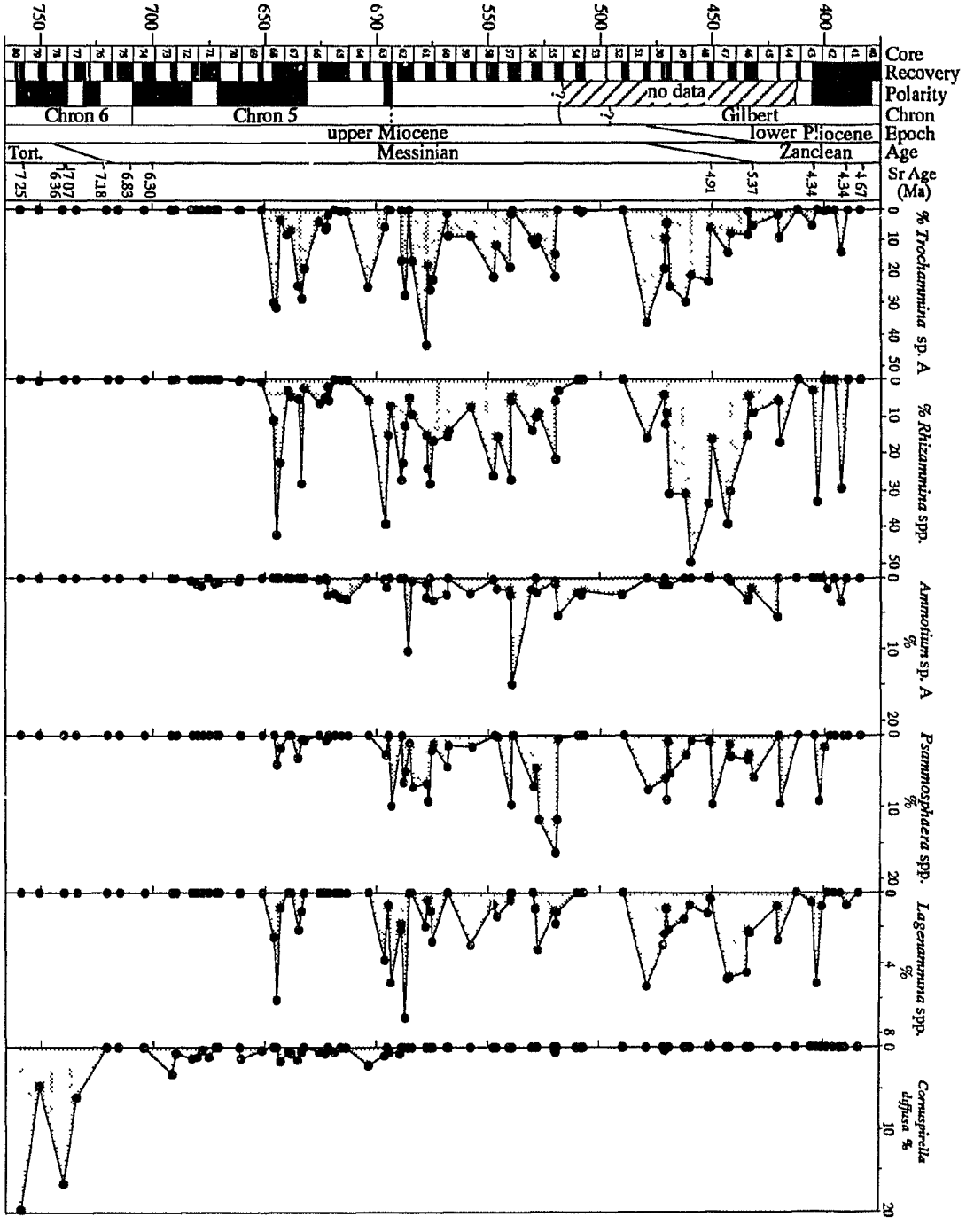

Fig. 3-21. Relative abundance of deep water calcareous benthic foraminifera, *Oridorsalis umbonatus, Nuttallides umbonifera, Epistominella exigua, Eponides weddellensis, Nonionids,* and *Gyroidina* spp., from ODP Hole 646B.

Depth (meters subbottom)

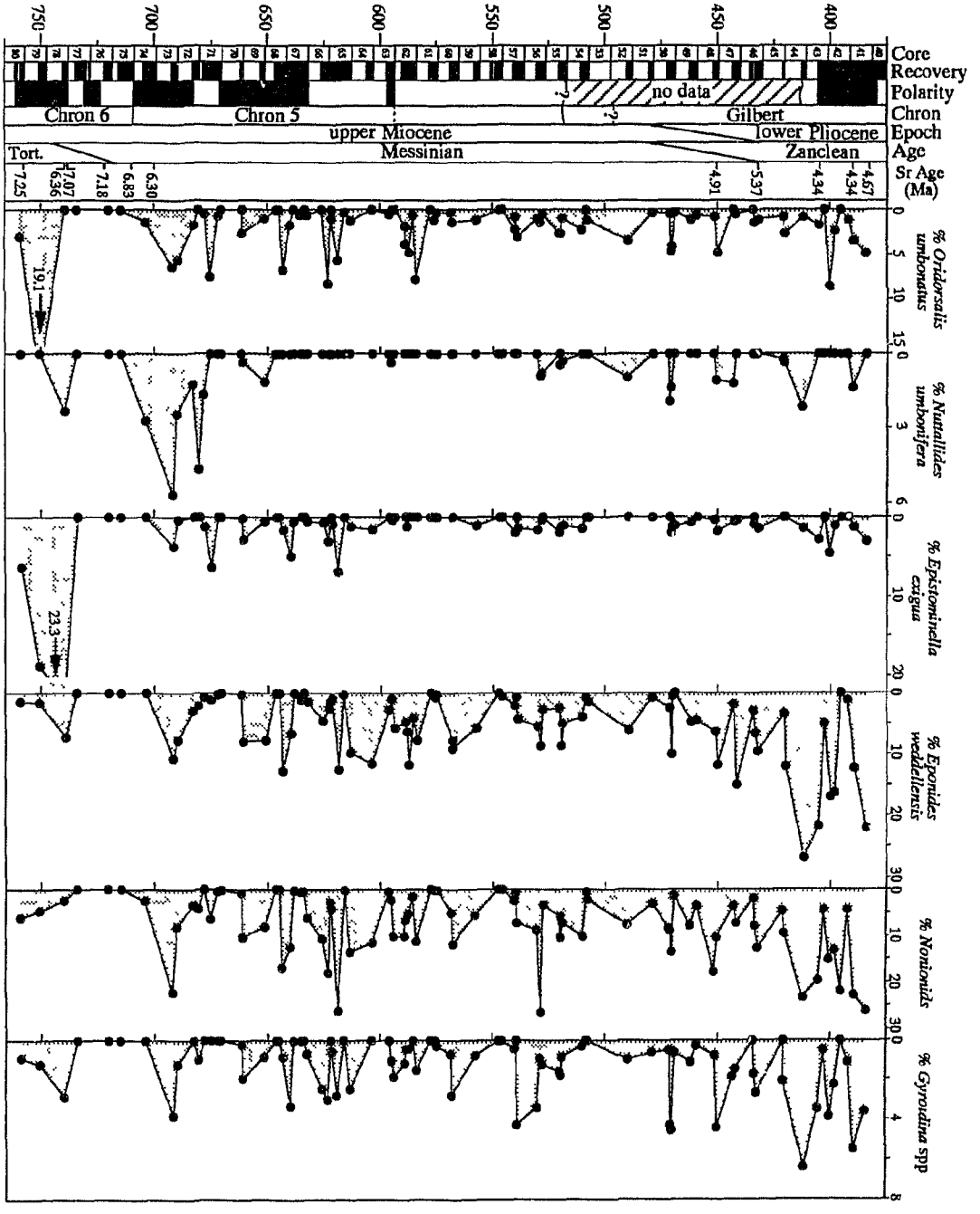

Fig. 3-22. Relative abundance of deep water calcareous benthic foraminifera, *Eponides tumidulus, Globobulimina auriculata, Melonis pompiloides, Pullenia bulloides, P. quinqueloba*, and *Melonis barleeanum*, from ODP Site 646B.

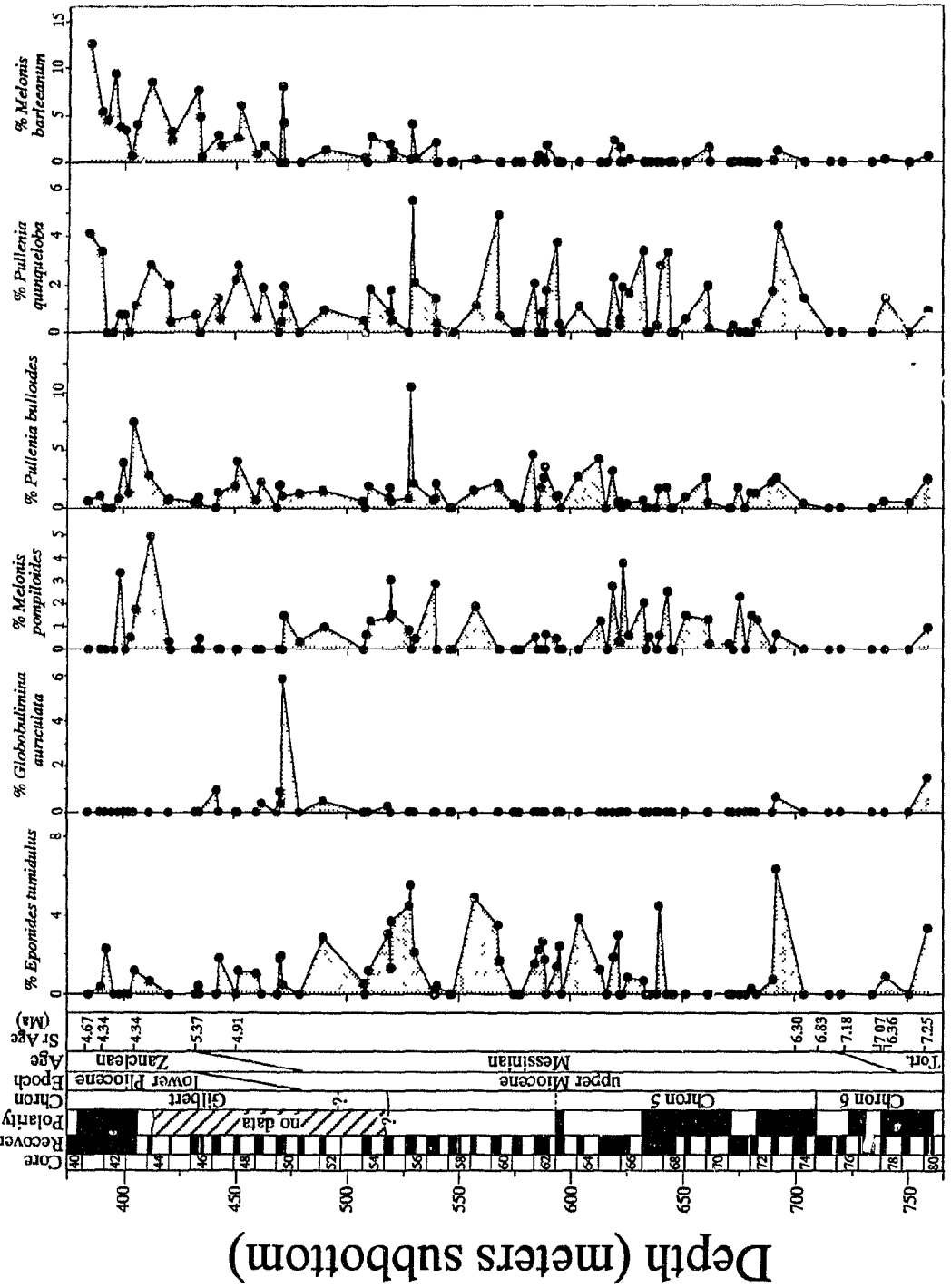
% Melonis barleeanum
% Pullenia quinqueloba
% Pullenia bulloides
% Melonis pompiloides
% Globobulimina auriculata
% Eponides tumidulus
Sr Age (Ma)
Age
Epoch
Chron
Polarity
Recovery
Core
Zanclean
Messinian
Tort.
lower Pliocene
upper Miocene
Gilbert
Chron 5
Chron 6
no data
4.67
4.34
4.34
5.37
4.91
6.30
6.83
7.18
7.07
6.36
7.25
Depth (meters subbottom)

72X, Core 67X Core 65X, Core 62X, Core 57X, Cores 52X-55X Cores 45X-48X, Cores 42X-43X, respectively. In these turbidite layers, plant seeds, oxidized plant fragments, rounded quartz, highly polished benthic foraminiferal shells, wood fragments, pyrite-filled foraminiferal shells, highly concentrated mica, and gypsum crystals, which indicate the origin as shallow water, are also commonly observed (see discussion section for details).

Deep-water coarse agglutinated foraminifera, for example, *Rhizammina* spp., *Psammosphaera* spp., *Lagenammina* spp., are found commonly from Cores 42X-7 to 51X-1, from 55X-2 to 63X-CC, and from 65X-7 to 68X-4. These coarse foraminifera are not present or extremely rare down to Core 80X-2 from Core 69X-1 (Fig. 3-21). Other deep-water agglutinated foraminifera, such as *Martinottiella communis, Cyclammina cancellata,* and *Recurvoides* spp. occur sporadically in this Hole.

The greatest abundance of deep-water calcareous foraminifera occurs in the Tortonian and early Pliocene (below Core 77X, and above Core 43X). Calcareous foraminifera are dominated by Nonionids (including *Pullenia bulloides, P. quinqueloba, Melonis barleeanum*) ranging from 0 to 30%) (Fig. 3-22), *Eponides weddellensis* (0-25%), *Oridorsalis umbonatus* (0 to 10%), *Eponides tumidulus* (0-7%), and *Gyroidina* spp. (0-5%), with considerable amplitudes of variation. *Epistominella exigua* and *Nuttallides umbonifera* are extremely low in abundance, usually less than 2% in the Messinian section. I found a spike (~3-6%) of *N. umbonifera* near seismic reflector R3 in the interval between 680.48 and 703.8 msb (Cores 72X-1 to 74X-4) similar to that of Kaminski et al. (1989; ~20-80%), but much lower in percentage. This probably resulted from the different size ranges of benthic foraminifera performed in this study (>63 m) and Kaminski et al.'s study (>150 m). The fraction of >150 m could eliminate a large number of small-sized benthic foraminifera that comprise the major component (~80%) of total benthic community. *E. exigua* reaches a peak of 23.3% in the Tortonian (Fig. 3-20). As mentioned above, these bathyal calcareous foraminifera act to separate the *Trochammina* cf. *squamata*-concentrated layers in the Messinian section. *Melonis barleeanum,* a typical form in glacial sediments in

Table 3-2. Sr measurements and age estimates for the Tortonian/Messinian and Messinian/Pliocene boundaries in cores from Site 646B. All data listed below were analyzed by Drs. Miller and Liu at Rutgers University, NJ, USA. The Age equations are after Farrell et al. (1995).

Core	Sr87/83	Error ±	Age (Ma)	Age error	Comments
646B, 41-2	0.709058	0.000008	4.67	0.68	Age=59941.95-(Sr87/86X84530.85(Sr=0.709080-0.709056)
646B, 41-6	0.709062	0.000005	4.34	0.42	Ibid.
646B, 43cc	0.709062	0.000005	4.34	0.42	Ibid.
646B, 46-3	0.709033	0.000007	5.37	0.15	Age=15640.06-(Sr87/86)X22050.72(Sr=0.709056-0.708955)
646B, 48-2	0.709054	0.000007	4.91	0.15	Ibid.
646B, 74-1	0.708991	0.000008	6.3	0.18	Ibid
646B, 75-2	0.708967	0.000008	6.83	0.18	Ibid.
646B, 76cc	0.708951	0.000008	7.18	0.18	Ibid.
646B, 78-2	0.708956	0.000044	7.07	0.97	Ibid.
646B, 78cc	0.708988	0.000007	6.36	0.15	Ibid
646B, 80-1	0.708948	0.000007	7.25	0.15	Ibid.

lower bathyal DSDP sites in northern Atlantic (Murray, 1984) and in the Norwegian-Greenland Sea (Talwani et al., 1976), is common from Cores 41X-2 to 50X-3. It is low in percentage in Cores 53-55, and almost absent from Cores 56-80 (Fig. 3-22). Another calcareous deep-water species, *Cornuspirella diffusa* is found up to ~20% in Tortonian section, but absent in the upper Messinian (Fig. 3-20).

3.5.2. Sr stable isotopes

11 samples have been measured for strontium isotopes ($^{87}Sr/^{86}Sr$) to determine the Tortonian/Messinian and Messinian/Pliocene boundaries, and presented in Table 3-2 (See Chapter 4 for more details).

CHAPTER 4

INTEGRATED BIO-, MAGNETO-, AND STABLE ISOTOPE STRATIGRAPHY OF THE MESSINIAN

4.1. Stratigraphy

4.1.1. Salé Briquetterie Borehole, Morocco

4.1.1.1. Biostratigraphy

Planktonic foraminiferal biostratigraphy of this borehole was previously reported by Hodell et al. (1994) and Benson et al. (1995), and several important datums for Messinian planktonic foraminiferal bio–events have been identified in this borehole. In the course of the present benthic foraminiferal study (Chapter 3), I realized that some important biodatums are slightly different from those of Hodell et al.(1994), probably as a result of increased sampling resolution and examining of smaller size fractions or because of low abundance of specimens. In this study, I have examined 90 samples from the Salé borehole (one sample per 2 meters in average). My observations of planktonic foraminifera, together with those from Hodell et al. (1994; marked with asterisks) are plotted in Fig. 4-1, and some critical bioevents and their age estimates are shown in Table 4-1.

Between 135m and 150m, I identified several important bioevents: 1) FO *Globorotalia conomiozea*. My specimens of *Gt. conomiozea* recovered in Sample B72 are typical conic form with 4 chambers in the last whorl and flat dorsal side, with raised dorsal sutures; 2) The coiling change of *Globorotalia menardii* from dextral to sinistral occurred in Sample B72 at the T/M boundary, which was not reported by Hodell et al. (1994). It is interesting that this coiling change is juxtaposed with the FO of *Gt. conomiozea*. Hodell et al. (1994), however, observed another important coiling change of *Globorotalia menardii* from sinistral to dextral at 148.15 m (sample B81), representing the latest Tortonian Stage, which is equivalent to PF–Event 1 of Sierro et al. (1993), who suggested a southward

Fig. 4-1. Planktonic foraminiferal stratigraphic ranges of Salé borehole, Morocco. Arrows indicate changes of coiling direction. X indicates single fossil occurrences. Magnetostratigraphic data and absolute age are from Hodell et al., 1994. T and reversed T are the first and last occurrences of planktonic faunas. D and S represents right and left coiling, respectively. Bioevents with asterisks are from Hodell et al., 1994.

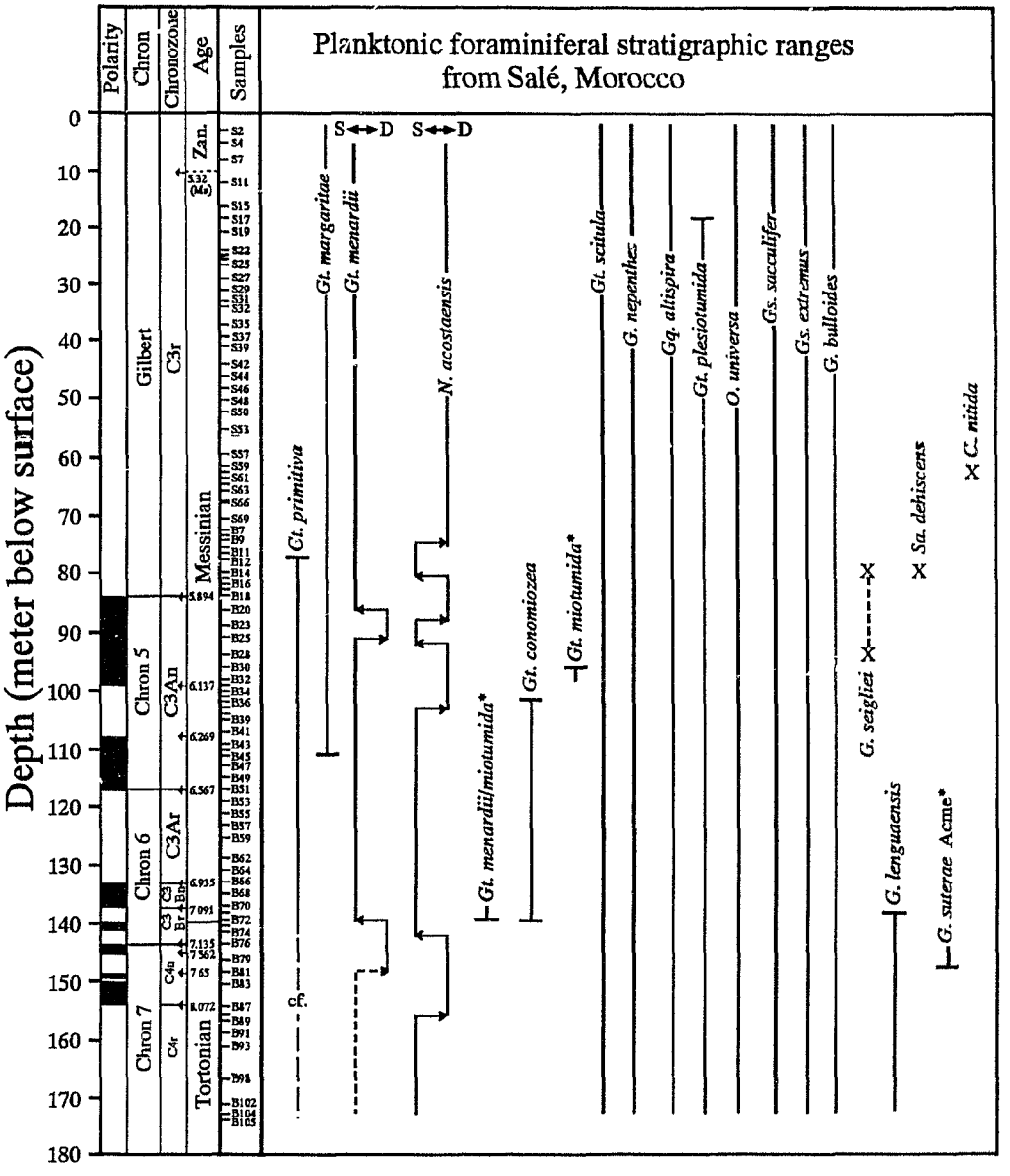
Depth (meter below surface)
Polarity
Chron
Chronozone
Age
Samples
Planktonic foraminiferal stratigraphic ranges
from Salé, Morocco
Chron 7
Chron 6
Chron 5
Gilbert
C3r
C3An
C3Ar
C3
C3r
C3n
C4r
C4n
Tortonian
Messinian
Zan.
Gt. primitiva
Gt. margaritae
Gt. menardii
Gt. menardii/miotumida*
Gt. conomiozea
Gt. miotumida*
N. acostaensis
Gt. scitula
G. nepenthes
Gq. altispira
Gt. plesiotumida
O. universa
Gs. saccullifer
Gs. extremus
G. bulloides
G. seiglieі
G. lenguaensis
Sa. dehiscens
G. suterae Acme*
C. nitida
S↔D
S↔D

Table 4-1. Paleomagnetic and biological stratigraphic events from Salé borehole, Morocco. Age estimates are calibrated to the new time scale by Berggren et al. (1995). Paleomagnetic data are from Hodell et al.(1994).

Sample	Events	Depth (M)	Age estimates (Ma)
B19	C3r base	84.65	5.894
B33	C3An.1r top	98.95	6.137
B36	LO *Gt. conomiozea*	101.75	5.32
B37	FO *Neogloboquadrina* S/D	102.85	6.2
B43	C3An.1r base	108.9	6.269
B45	FO *Gt. margaritae*	110.95	6.0
B51	C3Ar top	116.85	6.567
B66	C3Ar base	132.75	6.935
B70	C3Br top	136.95	7.091
B72	FO *Gt. conomiozea*	139.05	7.12
B72	LO *Gt. lenguaensis*	139.05	6.0
B74	FO *Neogloboquadrina* D/S	141.15	6.8
B76	C3Br base	143.3	7.34
B78	C4n.1r top	145.25	7.562
B81	*Gt. menardii* D/S	148.15	7.4

retreat of the form in the North Atlantic; 3) A major turnover of *Gt. menardii/Gt. miotumida* occurred at 138.0 m (B71), which was also reported by Hodell et al. (1994) at the same level, indicating a major climate change from subtropical to temperate. This turnover has also been observed in other regions, e.g., the northeast Atlantic and Mediterranean Sea (Sierro, 1985; Benson and Rakic–El Bied, 1991a, b; Sierro et al., 1993); 4) A coiling change of *Neogloboquadrina acostaensis* from dextral to sinistral occurs at a level of 141.15 m (Sample B74). This coiling shift is also observed at DSDP/ODP sites in the North Atlantic Ocean, e.g., 552A, 646B (see below). Another coiling change of the taxon from sinistral to dextral is identified in Sample B88 during the late Tortonian; 5) The last occurrence (LO) of *Globorotalia lenguaensis* is found in Sample B70 (136.95 m), just above the T/M boundary; and 6) Hodell et al. (1994) reported that an acme of *Globorotalia suterae* is present in Subchron C4n.1n at ~7.5 Ma in Salé borehole, slightly younger than its FO (7.8 Ma; Berggren et al., 1995). This acme may allow stratigraphic correlation between the Italian stratotype sequence and those in the Atlantic.

During the Chronozone C3r (the lower Gilbert) ranging from 84 m to the top of the borehole, no significant bioevents have occurred. This is called the biostratigraphic "quiet zone" (see Benson et al., 1991a; Hodell et al., 1994), except for the LO of *Globorotalia plesiotumida* at a level of 18.54 m (Sample S17).

No deposition breaks have been detected in this borehole as shown in Fig. 4-2. However, sedimentation rate during the latest Tortonian is rather slow, about 14 m per million years in average (= 1.4 cm/k.y.). During the lower Messinian (7.12 to 5.894 Ma), sedimentation rates greatly increase, with an average of 44.4 m/m.y. (4.44 cm/k.y.). In the upper Messinian, the sedimentation rate reaches 130 m/m.y., suggesting the shallowing of the location resulting from the uplifting of Morocco.

Fig. 4-2. Depth-age plot of Salé borehole, Morocco. Paleomagnetic and stable isotopic data are from Hodell et al., 1994. Vertical arrows indicate early occurrences and horizontal arrows indicates late occurrences.

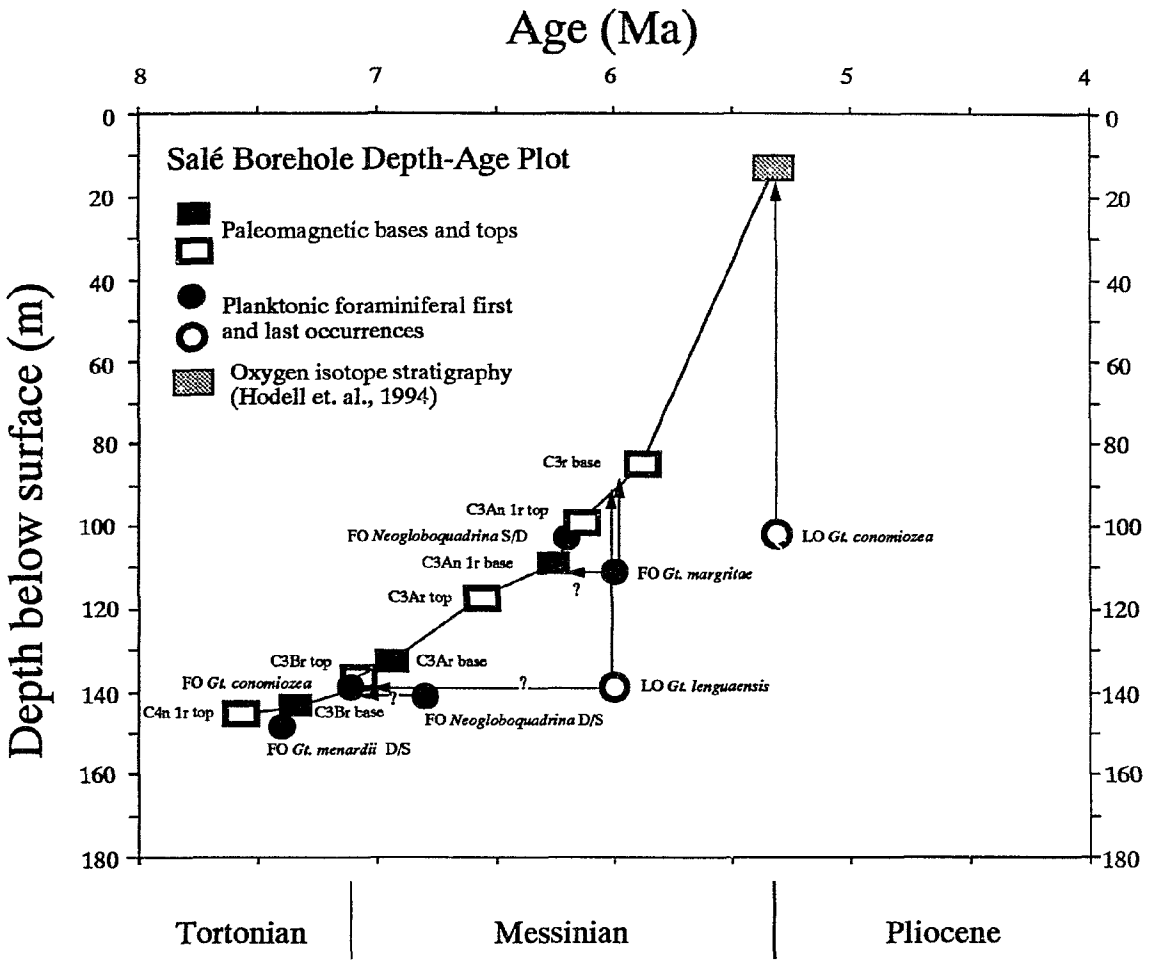
Age (Ma)
8
7
6
5
4
Depth below surface (m)
0
20
40
60
80
100
120
140
160
180
Salé Borehole Depth-Age Plot
Paleomagnetic bases and tops
Planktonic foraminiferal first and last occurrences
Oxygen isotope stratigraphy (Hodell et. al., 1994)
C3r base
C3An 1r top
FO Neogloboquadrina S/D
C3An 1r base
C3Ar top
C3Br top
C3Ar base
FO Gt. conomiozea
C4n 1r top
C3Br base
FO Gt. menardii D/S
FO Neogloboquadrina D/S
FO Gt. margritae
LO Gt. conomiozea
LO Gt. lenguaensis
?
Tortonian
Messinian
Pliocene

4.1.1.2.Stable Isotope Stratigraphy

Oxygen Stable Isotopes: Detailed oxygen isotope stages in the Salé borehole were numbered by Hodell et al. (1994). TG22 was the oldest oxygen isotope stage in the lower part of reversed subchron of the Gilbert (Chronozone C3r) at ~5.75 Ma, which was also recognized by Shackleton et al. (1995) in the eastern equatorial Pacific Ocean. "TG" signifies the time interval from the lowermost part of Subchronozone Thvera to the base of the Gilbert (equivalent to Chronozone C3r). The oxygen isotope records at Leg 138, Site 846 from the Pacific Ocean between TG22 and Subchronozone C3An.1n were not recognizable for the stage nomenclature due to the low–amplitude variation, and no stage has been identified below C3An.1n by Shackleton et al. (1995). Hodell et al. (1994) extended oxygen isotope stratigraphy of the Salé borehole starting from TG22 down to the upper Tortonian, following the extension of stage numbering scheme of Shackleton et al. (1995) from ODP Site 846 in the eastern equatorial Pacific.

In B series samples, the oxygen isotope record exhibits distinct evidence of 41–kyr (obliquity) cyc' , during Chronozones C3An and C3Ar. Hodell et al. (1994) identified 34 stages (i.e., C3An.δ^{18}O.1 to C3An.δ^{18}O.34) in Chronozone C3An from 6.567 to 5.894 Ma, with a duration of 673,000 years, and 18 stages (e.g., C3Ar.δ^{18}O.1 to C3Ar.δ^{18}O.18) in C3Ar from 6.935 to 6.567 Ma, with a duration of 368,000 years (Hodell et al., 1994). In addition, they also recognized 14 oxygen isotope stages (from TG21–TG34) in Thvera–C3r interval.

The S series samples provide a relatively poor signature of the oxygen isotope record (Hodell et al., 1994). Above stage TG20, only two distinct glacial stages, i.e., TG14 and TG12, were recognized. TG stages from 1 to 9 are difficult to determine because of low–amplitude variation. The oxygen isotope curve between TG14 and TG20 in the Salé borehole shows 7 stages, while in the eastern equatorial Pacific Ocean, only 5 stages were identified (Shackleton et al., 1995). T stages in Subchronozone Thvera were not well defined due to poor magneto– and bio–stratigraphic control (Hodell et al., 1994), and

probably confused by extremely high sedimentation rates in this interval. Nevertheless, Hodell et al. (1994) distinguished 4 distinct glacial stages, namely TG 12, TG14, TG20 and TG22 in S series interval. TG22 was also identified in B series samples and in DSDP Hole 522A, and thus it is considered to be an extremely useful isotope event in global stratigraphic correlation.

Carbon Stable Isotopes: In the Salé borehole, the most distinct ^{13}C event useful for Messinian stratigraphy, is the dramatic decrease in the isotope value just above the Tortonian/Messinian boundary at ~140 m (Chronozone C3Bn, =7.1 Ma). This decrease has been determined elsewhere in the world ocean, and is termed "the Carbon–13 Shift". In Salé, the decreased $\delta^{13}C$ values continue to the top of the section, although a number of fluctuations occurred throughout this section (see Hodell et al. 1994 for more detail).

4.1.1.3. Magnetostratigraphy

As in stable isotopes, magnetostratigraphic study of the Salé borehole was also done by Hodell et al. (1994). Their study reveals that the polarity patterns from the B series samples are complete from C3r (the lower Gilbert) down to the top of C4n, and thus can be correlated to the GPTS of Cande and Kent (1995) and of Berggren et al. (1995). The Chronozone C3r/C3An boundary was placed at 84.35 m (5.894 Ma); C3An/C3Ar at 117.7 m (6.567 Ma); C3Ar/C3Bn at 133.5 m (6.935 Ma); the C3Bn/C3Br at 138.25 m (7.091 Ma); and C3Br/C4n at 145.49 m (7.375 Ma).

The entire magnetic record in the S series samples is poor relative to that of the B series core. The reversed polarity below 40 m in the S series is attributed to C3r (the lowermost Gilbert), whereas the polarities in the interval above 40 m are not possible to explain, including the Subchronozone Thvera, the oldest normal polarity of the Chron Gilbert, because of either weak magnetization or unstable behavior of thermal demagnetization (Hodell et al., 1994).

4.1.1.4. Boundary placement

Based on these observations, I place the Tortonian/Messinian (T/M) boundary at 139.05m (sample B72), defined by the FO of *Globorotalia conomiozea* juxtaposed with D/S coiling change of *Globorotalia menardii* at the top of Chronozone C3Br, with an age estimate of 7.12 Ma calibrated to the GPTS of Berggren et al. (1995). It is 0.8 m below the C3Bn/C3Br boundary at 138.25 m, and 2.35 m lower than that of Hodell et al. (1994) who located the boundary at 136.7 m within Chronozone C3Bn based on their observation of the FO of *Globorotalia conomiozea*. The FO of *Globorotalia conomiozea* is used to define the Tortonian/Messinian boundary in the Atlantic and Mediterranean regions (Channell et al., 1990a; Krijgsman et al., 1994; Berggren et al., 1995).

The Messinian/Pliocene (M/P) boundary is difficult to determine directly because of the absence and uncertainty of geological and biological events in this interval. Hodell et al. (1994) suggested that the boundary may be extrapolated based only on the absence of the lower Pliocene species *Gt. puncticulata* in the Salé core because it may indicate that the sediments are older than Pliocene age. In this study, I provide the LO of *Gt. plesiotumida* as secondary supporting evidence, despite the uncertainty of the stratigraphic importance of the LO of *Gt. plesiotumida* at 18.54 m (Sample S17). As observed that boreholes E68–138 and E66–73 in the Gulf of M.. .o (Zhang et al., 1993), this taxon last occurred in the upper Miocene slightly older than M/P boundary. I therefore suggest a placement of the M/P boundary on the top of the Salé section between S series samples S7 and S11 at ~10 m below surface with the LO of the species. This is, to some extent, in agreement with Hodell et al. (1994), who suggested that the top of the Salé section is older than the FO of *Globorotalia puncticulata*.

4.1.2. DSDP Site 552A

4.1.2.1. Biostratigraphy

Planktonic foraminiferal biostratigraphy in this hole was initially studied by Huddlestun (1984) in low resolution during the Deep Sea Drilling Project Leg 81, based only on core catchers, and no diagnostic bioevents defining the Messinian Stage were reported. In this study, I examined 56 samples from cores 19 to 34, yielding an average of 3.5 samples per core for first and last occurrences of diagnostic planktonic foraminiferal taxa. As shown in Figs. 4-3 and 4-4, a possible small hiatus has been recognized by cutting off the Subchronozones C3Br.1n to C3Br.2n (duration 0.1–0.2 m.y) in the lower part of Core 32 at ~7.34 Ma (the uppermost Tortonian) as shown by calcareous nannofossils (Keigwin et al., 1987). However, planktonic foraminiferal biostratigraphic events fail to support the hiatus because of the absence of diagnostic zonal markers in such a short interval. In the entire section from cores 19 to middle 32, no hiatuses are present, except for possible reworking in cores 19 and 20, which is suggested by middle Miocene planktonic foraminifera, such as *Globorotalia mayeri,* and *Globorotalia praefohsi.*

The sedimentation rates as seen in Fig. 4-4 appear to be consistent for the most part of the Messinian despite a rapid increase in the lower part of Gilbert (C3r), but during the early Pliocene the sedimentation rates are relatively slow.

Several important bioevents and their age estimates, based on Berggren et al.'s (1995) new time scale, are plotted in Fig. 4-3 and listed in Table 4-2, and described as follows:

1) *Globorotalia conomiozea* s.s. first occurs at 150.16 m subbottom (msb; Sample 32–2, 16–20cm) at the top of Chronozone C3Br, nearly at the same level as observed in the Salé borehole. *Gt. conomiozea* is a conic form, with 4 chambers in the last whorl, flat dorsal side and raised sutures on the dorsal, which was not reported in this hole by Huddlestun (1984). The LO of *Gt. conomiozea* occurs at a level of 137.33 msb (sample 29–3, 83–87cm) near the top of Subchronozone C3An.1n, in contrast to the Salé borehole where the LO is in the middle of C3An.

2) A coiling direction change of *Neogloboquadrina acostaensis* occurred at 154.62 msb (Sample 33–1, 112–116cm) in the upper part of Chronozone C4n, below the T/M boundary.

3) In Hole 552A no coiling changes of *Neogloboquadrina* were determined in Chronozone C3An as recognized in Salé borehole and DSDP Hole 609 (Hooper and Weaver, 1987). However, I have determined two coiling changes below the Messinian/Pliocene boundary, and three in the interval between the upper PL–1a and PL–1b of Pliocene planktonic foraminiferal zones (Fig. 4-3).

4) A lineage of *Globorotalia margaritae* has been distinguished in Hole 552A. The FO of the species is found at 137.33 msb (Sample 29–3, 87–89cm) within Subchronozone C3An.2n, while a similar form which does not have a well developed keel in the first few chambers in the last whorl, called *Gt.* cf. *margaritae*, first occurred in sample 31–4, 11–15cm at a level of 148.11 msb. *Gt. primitiva,* ancestral to *Gt. margaritae,* last occurs in sample 28-CC, 8–12cm at 133.5 msb. These bioevents provic useful information for stratigraphic correlation between basins.

5) *Globoquadrina dehiscens* last occurs at 152.4 msb (sample 32–3, 94–98cm) immediately below the Tortonian/Messinian boundary. This species was found to last occur in Core 34-CC (Huddlestun, 1984).

6) The LO of *Globorotalia lenguaensis* is identified at 154.62 msb (sample 33–1, 112– 116cm) below the T/M boundary in this hole. It was reported in Sample 33-CC by Huddlestun (1984). As in the Salé core, it displays a distinct diachrony because the LO falls far away from the line of correlation (LOC) (Fig. 4-4).

7) *Gt. puncticulata* first occurs at 95.35 msb (Sample 20-CC, 4–8cm), where it was also reported by Huddlestun (1984). The FO of *Gt. crassaformis* occurred at 91.00 msb (19-CC, 10– 14cm), which is different from the level reported by previous study of Huddlestun (1984) who found the FO at 67.0 msb (Sample 14-CC). These two FOs mark the Pliocene planktonic foraminiferal subzones PL–1a/PL–1b and PL–1b/PL–1c

Table 4-2. Paleomagnetic, oxygen stable isotopic, and biological stratigraphic events from DSDP Hole 552A. Age estimates are calibrated to the new time scale by Berggren et al. (1995). Age estimates with asterisks are calibrated to the new time scale of Berggren et al. (1995) in this study. Paleomagnetic data are from Keigwin et al., 1987. Oxygen isotopic age estimates are from Shackleton et al., 1995.

Sample	Events	Depth (M)	Age estimates (Ma)
19cc, 10-14	FO *Gt. crassaformis*	91.00	4.3*
27-1, 4-8	FO *Gt. puncticulata*	95.35	4.6*
	TG14	107.0	5.55
	TG22	119.0	5.75
27-2, 049	C3r base	124.44	5.894
28-3, 075	C3An.1r top	132.25	6.137
29-1, 099	C3An.1r base	134.49	6.269
29-3, 83-87	FO *Gt. margaritae*	137.33	6.0
30-3, 074	C3Ar top	141.98	6.567
32-1, 144	C3Ar base	149.94	6.935
32-2, 16-20	FO *Gt. conomiozea*	150.16	7.12
32-2, 144	C3Br top	151.44	7.091
32-3, 051	C3Br base	152.01	7.34
32-3, 94-98	LO *Gq. dehiscens*	152.4	5.8
33-1, 112-116	LO *Gt. lenguaensis*	154.62	6.0
34-2, 098	C4n.1r base	160.98	7.65

Fig. 4-3. Planktonic foraminiferal stratigraphic ranges and zones of DSDP Hole 552A. Magnetostratigraphic and stable isotope data are from Keigwin (1987). "R" represents rare occurrence, and "F" indicates few occurrence in abundance. * indicates interval reworked or contaminated. Age estimates are from Berggren et al. (1995).

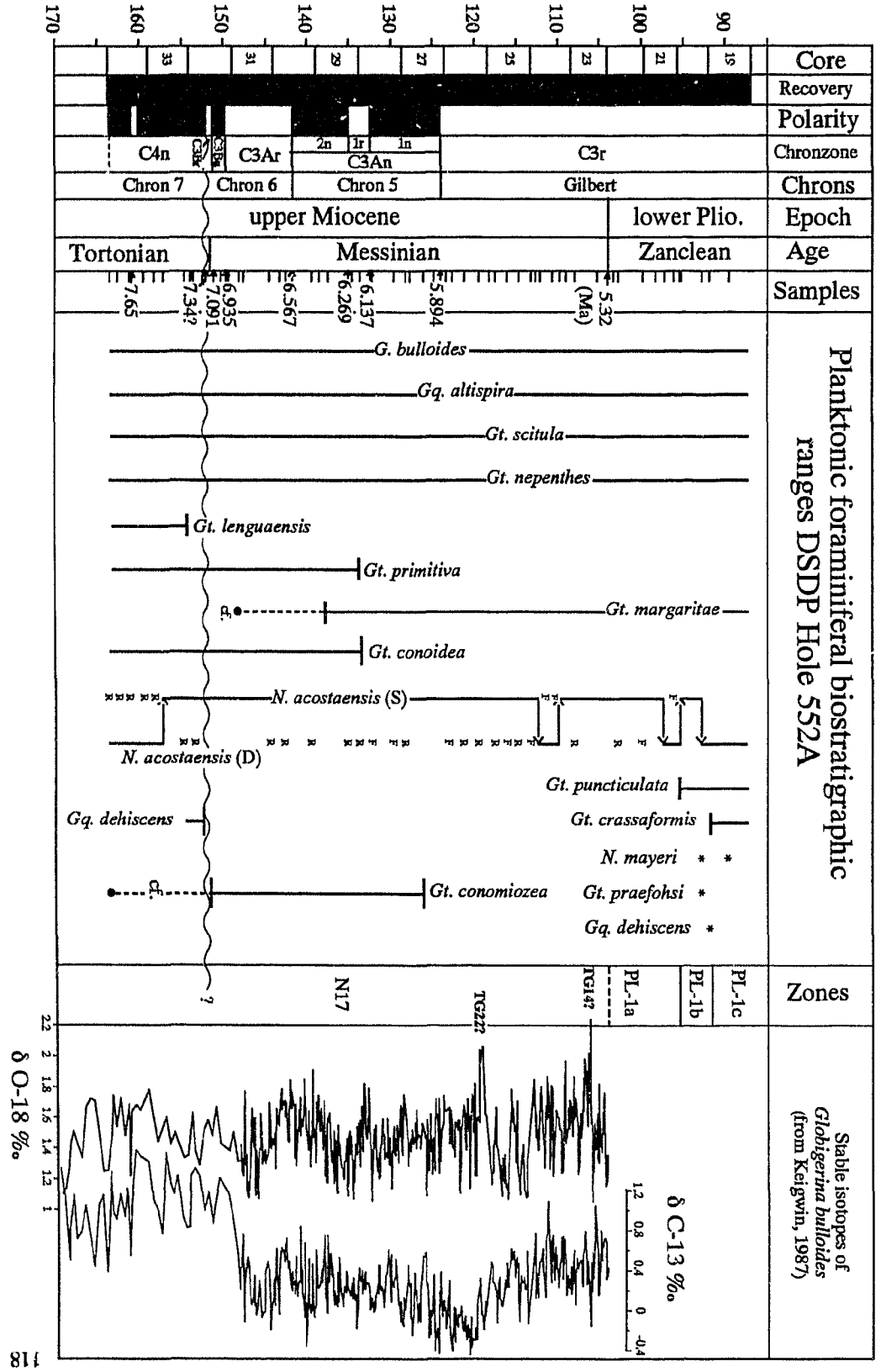
Subbottom Depth (m)
170
160
150
140
130
120
110
100
90
Core
Recovery
Polarity
Chronzone
C4n
C3Bn
C3Br
C3Ar
2n
1r
1n
C3An
C3r
Chrons
Chron 7
Chron 6
Chron 5
Gilbert
Epoch
upper Miocene
lower Plio.
Age
Tortonian
Messinian
Zanclean
Samples
7.65
7.34?
7.091
6.935
6.567
6.269
6.137
5.894
5.32
(Ma)
Planktonic foraminiferal biostratigraphic ranges DSDP Hole 552A
G. bulloides
Gq. altispira
Gt. scitula
Gt. nepenthes
Gt. lenguaensis
Gt. primitiva
cf.
Gt. margaritae
Gt. conoidea
N. acostaensis (S)
N. acostaensis (D)
Gt. puncticulata
Gt. crassaformis
N. mayeri
Gt. praefohsi
Gq. dehiscens
Gq. dehiscens
cf.
Gt. conomiozea
Zones
?
N17
TG22?
TG14?
PL-1a
PL-1b
PL-1c
δ O-18 ‰
δ C-13 ‰
Stable isotopes of Globigerina bulloides (from Keigwin, 1987)

Fig. 4-4. Depth-age plot of DSDP Hole 552A. Paleomagnetic and stable isotopic data are from Keigwin, 1987.

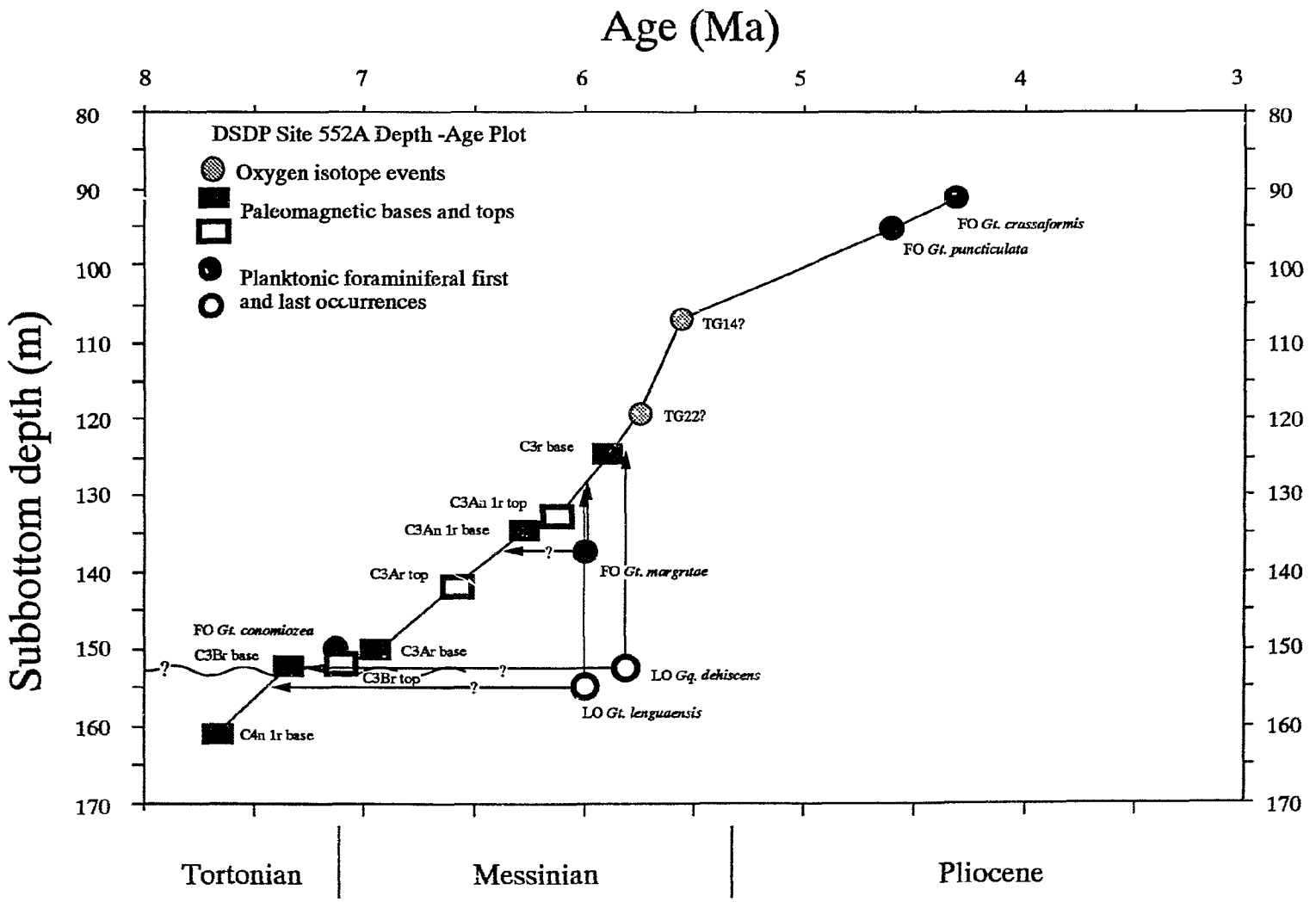
Age (Ma)
8
7
6
5
4
3
DSDP Site 552A Depth -Age Plot
Oxygen isotope events
Paleomagnetic bases and tops
Planktonic foraminiferal first and last occurrences
Subbottom depth (m)
80
90
100
110
120
130
140
150
160
170
FO Gt. crassaformis
FO Gt. puncticulata
TG14?
TG22?
C3r base
C3An 1r top
C3An 1r base
C3Ar top
FO Gt. margritae
FO Gt. conomiozea
C3Br base
C3Ar base
C3Br top
LO Gq. dehiscens
LO Gt. lenguaensis
C4n 1r base
Tortonian
Messinian
Pliocene

boundaries, respectively, based on the time scale of Berggren et al. (1985).
In the interval between cores 21 and 26, no critical planktonic foraminiferal bioevents have been recognized. This interval may be equivalent to the "quiet zone" determined in the Salé core by Benson et al.(1991b), and Hodell et al. (1994).

4.1.2.2. Stable isotopic stratigraphy

Oxygen Isotopes: Oxygen isotope data from the surface dweller *Globigerina bulloides* provided by Keigwin (1987), are plotted against biostratigraphic data (Fig. 4-3) for correlation. I have attempted to establish oxygen isotope stages associated with 41–kyrs obliquity cycles for the Hole 552A as recorded in Salé borehole. With the exception of Chronozone C3An in which I have tentatively determined 34 stages (C3An.^{18}O.1–34; Fig. 4-5), it is difficult to determine the stages in Chronozones C3r, C3Ar and C3Bn based on the smoothed oxygen isotope curve of three running point average with new timescale of Berggren et al. (1995), probably because of relatively low sedimentation rates in these intervals. I thus consider that the 41–kyrs quasi– periodicity of Earth's obliquity observed at this site (Keigwin, 1987) may only be applied to the interval of C3An, rather than the entire Messinian sequence. The 41–kyrs quasi–periodicity was not evident in benthic foraminiferal (*Planulina wuellerstorfi*) isotope records provided by Keigwin et al. (1987).

In addition, two important oxygen isotope maxima indicating global glaciations both in benthic and planktonic foraminiferal tests were recognized in the upper Messinian with a duration of ca. 15,000 years. It is interesting that the occurrence of the lower ^{18}O maximum from benthic foraminifera is at 118.82 msb, while that from planktonic foraminifera is at 119.15 msb, suggesting a delay of ~10,000 years. The delay of the δ^{18}O maximum occurrence in benthic foraminifera is considered to have occurred within 41–kyrs cycles, and thus I suggest that it may not critically affect the age placement. The time difference of the oxygen isotope maximum between the benthic and planktonic may result from ice volume variation and temperature fluctuation in deep water and surface water

realms. Therefore, I attribute these two isotope events to the stages TG22 (5.75 Ma) and TG14? (5.55 Ma) in Chronozone C3r based on the age estimates as interpolated from Shackleton et al.(1995) in the eastern equatorial Pacific Ocean. TG14 is characterized by ^{18}O enrichment, and also indicating a possible glaciation, as reported in the eastern Pacific (Shackleton et al., 1995) and in Morocco (Hodell et al., 1994). These two chemo–events were calibrated to 5.2 and 4.8 Ma respectively in previous study (Keigwin, 1987) using the GPTS of Berggren et al. (1985).

Carbon Stable Isotopes: As in the Salé borehole, a $\delta^{13}C$ shift is observed in the upper part of Chronozone C3Bn at ~148 msb, immediately above the Tortonian/Messinian boundary. The decreased $\delta^{13}C$ values continue to the top of the Messinian interval, although a number of secondary order of fluctuations have occurred (see Keigwin, 1987 for more details). The tendency of increasing in $\delta^{13}C$ values occurs near the Pliocene/Messinian boundary at this site.

4.1.2.3. Magnetostratigraphy

Magnetostratigraphy at this site was carried out by Keigwin et al. (1987) (Fig. 4-3). As shown in the figure, magnetochronozones from C4n to C3An were well recovered in the interval from cores 26 to 34 (below ~120 msb), with the exception of some minor subchronozones, namely C3Br.1n to C3Br.2n (a duration of 0.1–0.2 m.y), which were cut off by a small hiatus in the uppermost Tortonian. Chronozone C3An ranges from 125.49 msb (Core 27–2, 094cm) to 141.28 msb (Core 30–3, 048cm); C3Ar ranges from 141.28 msb to 150.25 msb (Core 32–2, 025cm); C3Bn is only about 1 meter thick, ranging from 150.25 msb to 151.26 msb (Core 32–2, 126cm); and C3Br and C4n representing the Tortonian spans from 151.26 msb to 164.47 msb (Core 35–1, 97cm). No reliable magnetostratigraphy was acquired from Core 13 to 25, because of coring disturbance and generally very weak magnetizations ($< 2 \times 10^{-5}$ A/m) (Keigwin et al., 1987).

Fig. 4-5. Oxygen isotopic stratigraphy of the planktonic foraminifera, *Globigerina bulloides*, DSDP Hole 552A. The interpretation of the isotopic stages are based on the nomenclature of Shackleton et al., 1995. Odd numbers corresponds to interglaciation, while even ones indicate glaciations. 34 stage are identified in Chron C3An, which are consistent with those recognized in Salé borehole, Morocco. In other chrons, i.e., C3r, C3Ar, and C4n, the isotopic stages are difficult to identify.

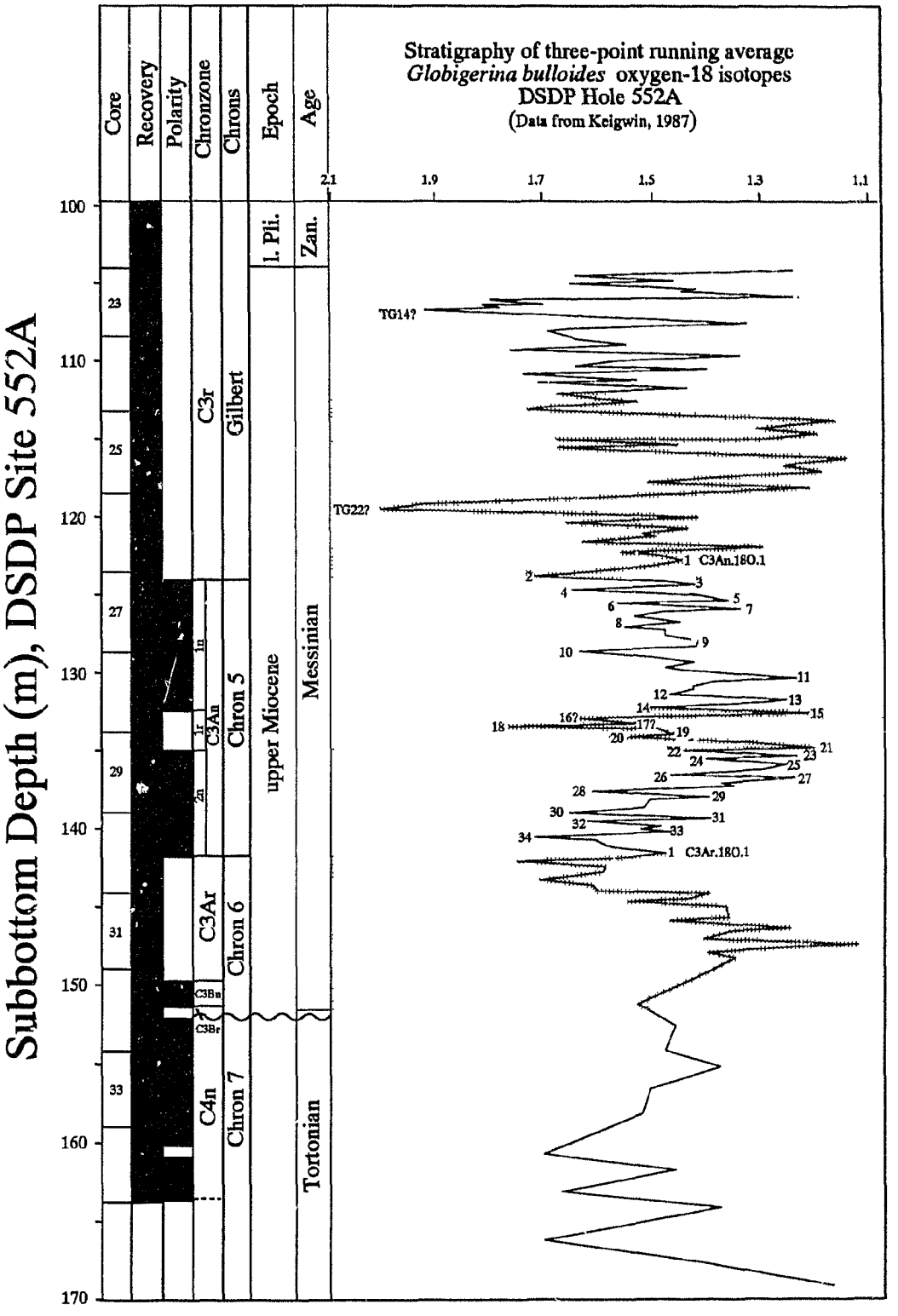
Subbottom Depth (m), DSDP Site 552A
Stratigraphy of three-point running average
Globigerina bulloides oxygen-18 isotopes
DSDP Hole 552A
(Data from Keigwin, 1987)
Core
Recovery
Polarity
Chronzone
Chrons
Epoch
Age
2.1
1.9
1.7
1.5
1.3
1.1
100
110
120
130
140
150
160
170
23
25
27
29
31
33
C3r
C4n
C3Ar
C3Bn
C3Br
1n
1r
C3An
2n
Gilbert
Chron 5
Chron 6
Chron 7
l. Pli.
upper Miocene
Zan.
Messinian
Tortonian
TG14?
TG22?
1 C3An.18O.1
1 C3Ar.18O.1

4.1.2.4. Boundary placement

The Tortonian/Messinian boundary is placed at 150.16 msb at the top of Chronozone C3Br with the FO of *Globorotalia conomiozea* s.s. at this site. It is supported by a number of secondary supportives, such as the $\delta^{13}C$ shift, ^{18}O enrichment, and D/S coiling direction change of *Neogloboquadrina acostaensis* near the boundary. The *Globorotalia* shift from *menardii* to *miotumida* observed in Salé core has not been determined in this hole by either Huddlestun (1984) or in this study, probably due to lack of these taxa.

The Pliocene/Messinian boundary is rather difficult to determine because no definite bio–, magneto–, and chemo–events have occurred in this "quiet zone" interval. However, a relevant age estimate of the boundary may be interpolated through several pieces of indirect evidence: 1) The FO of *Gt. puncticulata.* This event occurs in the lower Pliocene in temperate area (Berggren, 1977; Keller, 1978; 1979a–c) and was used to define the PL–1a and PL–1b boundary, while the FO of *G. crassaformis* denotes the PL–1b/PL–1c boundary (Berggren, 1977; Berggren et al., 1985), although it is absent, rare or delayed in most low–latitude regions (Keigwin, 1982; Thunell, 1981; Srinivasan and Chaturvedi, 1992; Berggren et al., 1995). In spite of the current thought that the FOs of the two species may be simultaneous in (sub)tropical regions (Berggren et al., 1995), I recognized that *Gt. puncticulata* occurred prior to *Gt. crassaformis* (Fig. 4-3), which may provide the validity to separate the subzones of the lowermost Pliocene Zone PL–1. A similar observation was also reported at this site by Huddlestun (1984). In this study I tentatively calibrate these events to 4.3 Ma for *Gt. crassaformis* and 4.6 Ma for *Gt. puncticulata* based on the GPTS of Berggren et al. (1995). In this case, I consider that the first occurrence of *Gt. puncticulata* denotes the lower Pliocene at this site, and that the M/P boundary must be below this level; 2) TG14 oxygen isotope stage at 106 msb. This was estimated to be 4.8 Ma (Keigwin, 1987), and now it is calibrated to ~ 5.55 Ma using the GPTS of Berggren et al. (1995), below the M/P boundary (Shackleton et al., 1995); 3) By using my age–depth

plot (Fig. 4-2), I interpolate the M/P boundary at 103 msb between the FO of *Gt. puncticulata* and TG14 isotope stage. This boundary assignment is in agreement with Keigwin (1987), who suggested that this oxygen–18 isotope enrichment reflects continental glaciation and sea-level lowering which contributes to the isolation of the Mediterranean Sea from the Atlantic Ocean and the salinity crisis of the Mediterranean region during the Messinian. He further suggested that this interpretation is consistent with magnetostratigraphy, biostratigraphy and isotope stratigraphy at Site 397 and land work in the Mediterranean region (Keigwin, 1987).

4.1.3. DSDP Site 608

4.1.3.1. Planktonic foraminiferal biostratigraphy

Planktonic foraminifera: Planktonic foraminiferal biostratigraphy for the Messinian interval of this hole was studied by Weaver (1987) using core catcher samples and hence low resolution. In my study, 4 samples from each core were examined from Cores 24 to 14 for biostratigraphic study. Only one sample was examined from Core 12 because it was out of my biostratigraphic and paleoceanographic scopes. Some major differences of critical and diagnostic planktonic foraminiferal FO and LO bioevents, such as *Gt. conomiozea, Gt. margaritae, Gt. suterae, Gt. puncticulata, Gt. crassaformis,* have been recognized between the studies of Weaver (1987) and mine. For example, I found the FO of *Gt. conomiozea* in Sample 29-CC, 6-10 (184.9 msb), while Weaver (1987) detected it in Sample 19-CC (174.2 msb). A small hiatus (0.6 m.y.) suggested by nannofossils is present in the upper Tortonian at ~205 msb within Chronozone C4Ar, which cut off the entire nannofossil zone NN10 equivalent to Chrons 9 and 10 partium. No other hiatus has been detected in the Messinian and lower Pliocene sections based on my integrated bio–, magneto– and isotope stratigraphy, although my age–depth plot (Fig. 4-8) suggests that the sedimentation rates from the uppermost Tortonian to middle Messinian are relatively low (only about 11.5 m

Fig. 4-6. Late Miocene and Pliocene planktonic foraminiferal biostratigraphy of DSDP Site 608. Paleomagnetic data are from Clement and Robinson (1983) and re-interpreted in this study. Back-slash bar in polarity column indicates low intensity of paleomagnetics. Sr dating is from Miller et al., 1991.

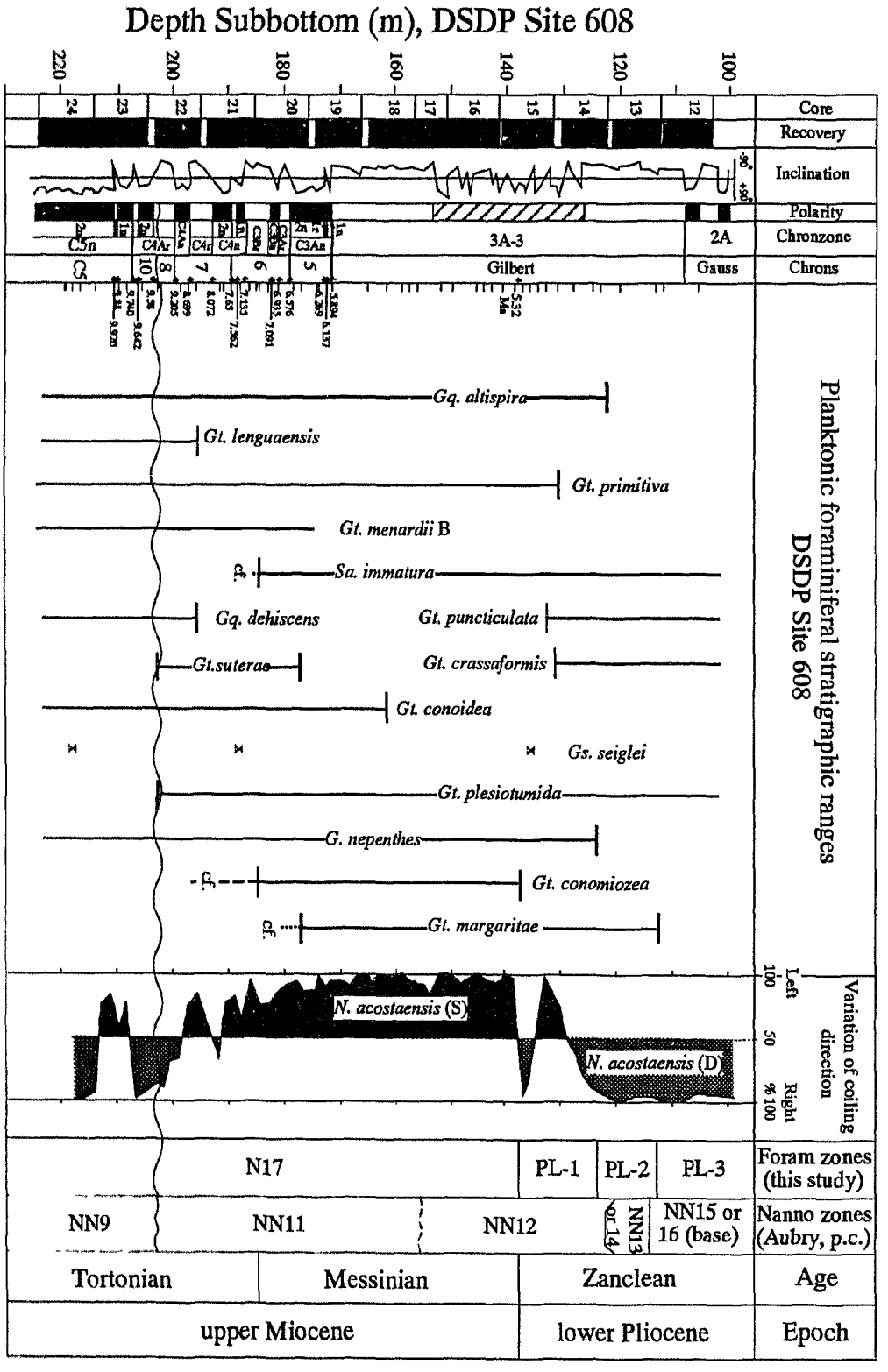
Depth Subbottom (m), DSDP Site 608
220
200
180
160
140
120
100
Core
Recovery
Inclination
Polarity
Chronzone
Chrons
3A-3
2A
Gilbert
Gauss
Gq. altispira
Gt. lenguaensis
Gt. primitiva
Gt. menardii B
Sa. immatura
Gq. dehiscens
Gt. puncticulata
Gt.suteras
Gt. crassaformis
Gt. conoidea
Gs. seiglei
Gt. plesiotumida
G. nepenthes
Gt. conomiozea
Gt. margaritae
Planktonic foraminiferal stratigraphic ranges
DSDP Site 608
N. acostaensis (S)
N. acostaensis (D)
Left
Right
Variation of coiling direction
N17
PL-1
PL-2
PL-3
Foram zones (this study)
NN9
NN11
NN12
NN13
NN15 or 16 (base)
Nanno zones (Aubry, p.c.)
Tortonian
Messinian
Zanclean
Age
upper Miocene
lower Pliocene
Epoch

Table 4-3. Paleomagnetic and biological stratigraphic events from DSDP Hole 608. Age estimates are calibrated to the new time scale by Berggren et al. (1995). Age estimates with asterisks are calibrated to the new time scale of Berggren et al. (1995) in this study. Paleomagnetic data are from Clement and Robinson (1987).

Sample	Events	Depth (M)	Age estimates (Ma)
14-2, 90-94	LO *G. nepenthes*	124.60	4.18
14cc, 10-14	FO *Gt. crassaformis*	130.44	4.3*
15-1,100-104	FO *Gt. puncticulata*	132.80	4.6*
15-5, 80-84	LO *Gt. conomiozea/ miotumida*	138.60	5.32
19-4, 25	C3r base	170.09	5.894
19cc, 10-14	FO *Gt. margaritae*	174.19	6.0
20-5, 25	C3Ar base	181.96	6.935
20cc, 6-10	FO *Gt. conomiozea*	184.88	7.12
21-3, 25	C3Ar base	188.56	8.699
22-1, 90-94	LO *Gq. dehiscens*	195.80	5.8
22-1, 90-94	LO *Gt. lenguaensis*	195.80	6.0
22-4, 24	C4Ar top	199.66	9.205
22cc, 6-10	FO *Gt. suterae*	202.90	7.8
22cc, 6-10	FO *Gt. plesiotumida*	202.90	8.3
23-3, 98	C5 top	208.49	9.74

per million years). Sedimentation rates were increased in the upper Messinian within the lower reversed Gilbert (C3r).

My biostratigraphic results with some species double checked by Dr. W.A. Berggren at Woods Hole Oceanographic Institution, MA, USA, are plotted in Fig. 4-6, and age estimates calibrated to the GPTS of Berggren et al. (1995) are listed in Table 4-3. The following bioevents for the Messinian in this hole are considered to be the most important:

1) Typical 4–chambered *Gt. conomiozea* first occurred in Sample 20-CC, 6–10 at 184.88 msb within paleomagnetic Chronozone C3Br, and last occurred in sample 15–5, 80–84 at a depth of 138.60 msb. I caution that the 4 chambered forms from Cores 17 to 15 differ from *Gt. conomiozea* s.s. found in Core 20 by having smaller size and thinner test, which I call *Gt. conomiozea/miotumida* plexus. It is evident that the LO of *Gt. conomiozea* plexus at this site is considerably higher than the LOs found in other holes examined in this study. It is indeed rather difficult to determine as to whether or not it is diachronous based on planktonic foraminifera alone. However, I consider that the LO of *Gt. conomiozea* plexus at this site may be the real last occurrence, because of the following four observations: 1) It last occurred in the middle part of the Gilbert, rather than in Chronozone C3An as observed in DSDP Hole 552A and Moroccan Salé borehole; 2) It seems to be correlative with oxygen isotope stage TG14? (see Fig. 4-9), which appeared below the Messinian/Pliocene boundary; 3) It occurred near the S/D coiling shift of *N. acostaensis* between oxygen isotope stages TG14 and TG22 as identified in Hole 552A; and 4) It is overlain by Pliocene taxa *Gt. puncticulata* and *Gt. crassaformis* which first occurred at 132.80 and 130.44 msb, respectively.

2) As in Hole 552A, the Messinian interval is dominated by sinistrally coiled *N. acostaensis* (Fig. 4-6 and Table 4-4). A coiling shift from dextral to sinistral occurs at a level of 195.8 msb at the base of C4n, which is probably equivalent to that in Hole 552A (top C4n); the other four coiling changes are observed below Chronozone C4n (from C5 to

Table 4-4. Coiling direction changes of *Neogloboquadrina acostaensis* during latest Miocene and early Pliocene at Site 608.

Samples	Depth (m)	% sinistral form
11-4, 80-84	98.7	4.2
12-2, 80-84	105.3	8
12-4, 80-84	108.3	0
12-6, 120-124	111.7	0
13-1, 80-84	113.4	4.3
13-3, 90-94	116.5	4.8
13-5, 90-94	119.5	0
14-1, 80-84	123	7.4
14-2, 90-94	124.6	12.2
14-3, 90-94	126.1	22.4
14-4, 90-94	127.6	37.5
14-5, 80-84	129	50
14cc, 10-14	130.44	73.3
15-1, 100-104	132.8	97.1
15-2, 90-94	134.2	64.2
15-3, 80-84	135.6	18.6
15-4, 80-84	137.1	5.9
15-5, 80-84	138.6	95.7
15-6, 80-84	140.1	100
15cc, 10-14	140.83	95
16-1, 80-84	142.2	92.9
16-2, 90-94	143.8	95.1
16-3, 80-84	145.2	100
16-4, 110-114	147	95.6
16-5, 90-94	148.3	93
16-6, 90-94	149.8	97.7
16cc, 10-14	150.86	100
17-1, 90-94	151.9	100
17-2, 90-94	153.4	83.3
17-3, 90-94	154.9	91.2
17-4, 60-64	156.1	92.4
17cc, 10-14	156.43	94.1
18-1, 60-64	157.1	93.3
18-2, 60-64	158.6	100
18-3, 62-66	160.12	97.4
18-4, 68-72	161.68	97.2
18-5, 64-68	163.14	98.8
18-6, 20-24	164.2	93.2
18cc, 6-10	164.73	98.2
19-1, 80-84	166.9	98.1
19-2, 80-84	168.4	90.2
19-3, 80-84	169.9	93.8
19-4, 80-84	171.4	94.2
19-5, 80-84	172.9	89.8
19-6,14-16	173.74	98.6
19cc, 10-14	174.19	87.8
20-1, 102-106	176.72	86.4
20-2, 80-84	178	93.6
20-3, 60-64	179.3	91.5
20-4, 80-84	181	86.2
20-5, 104-108	182.74	76.7
20-6, 110-104	184.3	75
20cc, 6-10	184.88	82.4
21-1, 90-94	186.2	94.4
21-2, 90-94	187.7	64
21-3, 90-94	189.2	82
21-4, 80-84	190.6	77
21-5, 60-64	191.9	39
22-1, 90-94	195.8	84.4
22-2, 90-94	197.3	75
22-3, 90-94	198.8	34
22-4, 100-104	200.4	31.1
22-5, 80-84	201.7	11.6
22cc, 6-10	202.9	15
23-1, 90-94	205.4	7
23-2, 90-94	206.9	2.1
23-3, 100-104	208.5	76.2
23-4, 81-85	209.81	58
23-5, 100-104	211.5	83.5
23-6, 104-108	213.04	75.5
23cc, 10-14	214.12	7
24-2, 80-84	216.4	1.1
24-3, 110-114	218.2	1

C4r). In the Pliocene, two are recognized; planktonic foraminiferal Zones PL–3, PL–2 and PL–1 partium are dominated by dextrally coiled *N. acostaensis* (Fig. 4-6).

3) *Globoquadrina dehiscens* last occurred at 195.8 msb (sample 22–1, 90–94) below the Tortonian/Messinian boundary, juxtaposed with the LO of *Gt. lenguaensis*. The LO of the species was calibrated to 5.8 Ma below the Tortonian/Messinian boundary based on the last occurrences in the Pacific (Berggren et al., 1995). As illustrated in Fig. 4-8, these two LOs are far below the LOC, suggesting a pronounced diachrony.

4) The FO of *Globorotalia margaritae* has been distinguished at 174.2 msb (sample 19-CC, 10–14), within Subchronozone C3An.2n as observed in Hole 552A. A similar form which is not well keeled on the first few chambers in the last whorl, called *Gt.* cf. *margaritae*, first occurs immediately above the T/M boundary.

5) The presence of *Gt. margaritae* and *Gt. primitiva* (also called *cibaoensis)* at 137.1 msb (sample 15–4, 80–84) indicates Zone PL–1a in the revised zonal biostratigraphy of Berggren et al. (1995), suggesting an age older than ~4.5 Ma (Berggren et al., pers. comm.).

6) *Gt. puncticulata* first occurs at 132.8 msb (sample 15–1, 100–104), while *Gt. crassaformis* first occurred at 130.44 msb (14-CC, 10–14), only about ~ 2 meter above the former. I have not made further subdivisions for Zone PL–1 here, although it is possible to do so with these biodatums; and

7) *Globorotalia suterae* first occurs in sample 22-CC, 6–10 at 202.9 msb in C4Ar (~9.5 Ma), about 2 m.y. older than that in Salé borehole where it occurs in Subchron C4n.1n (~7.5 Ma). Comparing with the age estimate of Berggren et al. (7.8 Ma; 1995), a distinct diachrony (~1.7 m.y.) is present here.

Nannofossils: Nannofossil biostratigraphy in this hole was initially studied by Takayama and Sato (1987), and additional study followed by Gardner (1992). The nannofossil biostratigraphic schemes provided in these two studies are quite different for the Messinian boundaries. The Messinian/Pliocene boundary was placed between Samples

17-CC and 17–3, 46–47 by Takayama and Sato (1987), and at Sample 14–6, 46–47 (129.86 msb) by Gardner (1992), respectively. Both assignments of the boundary were based on the presence of the LO of *Discoaster quinqueramus* they identified. This problem remains unsolved as I have no unwashed material available for further investigation of nannofossils in this study.

The T/M boundary was placed at the same level at 164.7 msb (Sample 18-CC) by both Takayama and Sato (1987) and Gardner (1992), defined by the FOs of *Amaurolithus delicatus* and *A. primus*. This level is contradictory to the T/M boundary suggested by the first occurrence of *Globorotalia conomiozea* (184.88 msb), used to define the T/M boundary by planktonic foraminiferal means (see below).

Due to the difficulty of the placement of boundaries, the nannofossil data from Takayama and Sato (1987) have been re–interpreted by M.-P Aubry (pers. comm., 1994) based on the most recent concept of nannofossil zonation attributes for this study. With particular caution, Aubry interprets the section quite differently from Takayama and Sato (1987). First of all, she places a short hiatus at the NN11/NN12 zonal boundary, or slightly below (Fig. 4-7). I consider that this hiatus may be caused by intense carbonate dissolution which occurred in this interval. Another hiatus cutting off the entire Zone NN10 is recognized in the upper Tortonian by both Takayama and Sato (1987) and Aubry (pers. comm.). Thus the Zones NN11 and NN9 are unconformable based on the FO of *Discoaster quinqueramus*. However this hiatus was not reported by Gardner (1992). Second, she extends the Zone NN12 up to the top of Core 14 using the FO of *Ceratolithus rugosus*, rather than using the FO of *Discoaster asymmetricus* because it has been shown to be quite unreliable, yielding a thick Zone NN12 from Core 17–14. This assignment allows us to interpolate the T/M boundary in lower NN12 by using the definition of the Messinian/Pliocene boundary proposed by Berggren et al. (1995). The interval between the LO of *C. rugosus* and the LO of *Amaurolithus delicatus* could represent an undifferentiated

Fig. 4-7. Late Miocene and Pliocene nannofossil biostratigraphy of DSDP Site 608. Paleomagnetic data are from Clement and Robinson, 1983 and re-interpreted in this study. Back-slash bar in polarity column indicates low intensity of paleomagnetics. Nannofossil data are from Takayama and Sato, 1983. Left column biozonations are re-interpreted by Aubry (pers. comm., 1994) for this study, and right column zonations are given by Takayama and Sato, 1983. Shaded bars on left of the figure correspond to the zonal patterns on right.

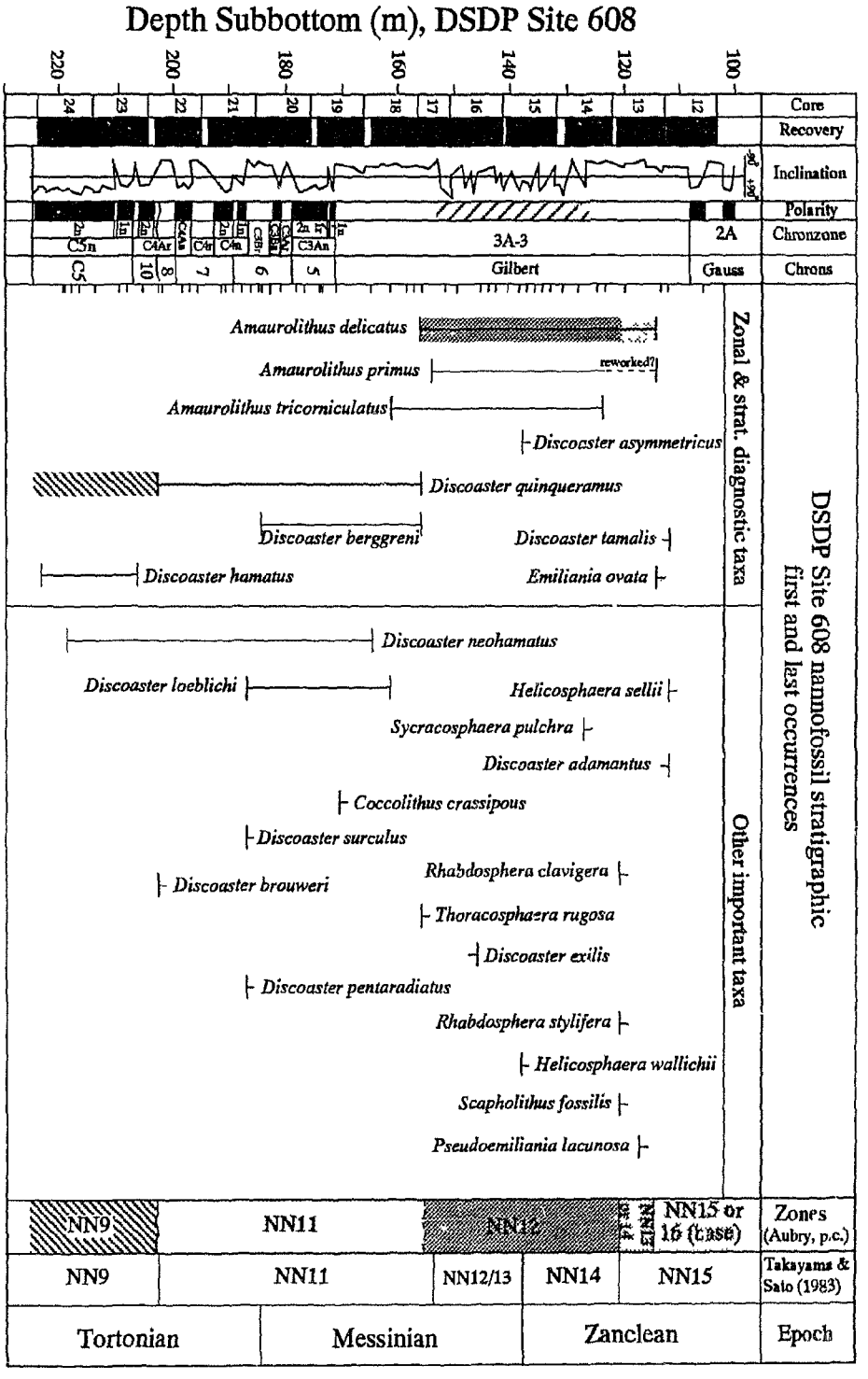
Depth Subbottom (m), DSDP Site 608
220
200
180
160
140
120
100
Core
Recovery
Inclination
Polarity
Chronzone
Chrons
C5n
C4Ar
C4n
C3n
3A-3
2A
C5
Gilbert
Gauss
Amaurolithus delicatus
Amaurolithus primus
reworked?
Amaurolithus tricorniculatus
Discoaster asymmetricus
Discoaster quinqueramus
Discoaster berggreni
Discoaster tamalis
Discoaster hamatus
Emiliania ovata
Zonal & strat. diagnostic taxa
Discoaster neohamatus
Discoaster loeblichi
Helicosphaera sellii
Sycracosphaera pulchra
Discoaster adamantus
Coccolithus crassipous
Discoaster surculus
Rhabdosphera clavigera
Discoaster brouweri
Thoracosphaera rugosa
Discoaster exilis
Discoaster pentaradiatus
Rhabdosphera stylifera
Helicosphaera wallichii
Scapholithus fossilis
Pseudoemiliania lacunosa
Other important taxa
DSDP Site 608 nannofossil stratigraphic
first and last occurrences
NN9
NN11
NN12
NN13
NN14
NN15 or 16 (base)
Zones (Aubry, p.c.)
NN9
NN11
NN12/13
NN14
NN15
Takayama & Sato (1983)
Tortonian
Messinian
Zanclean
Epoch

Fig. 4-8. Depth-age plot of DSDP Hole 608. Paleomagnetic data from Clement and Robinson, 1983 are reinterpreted in this study.

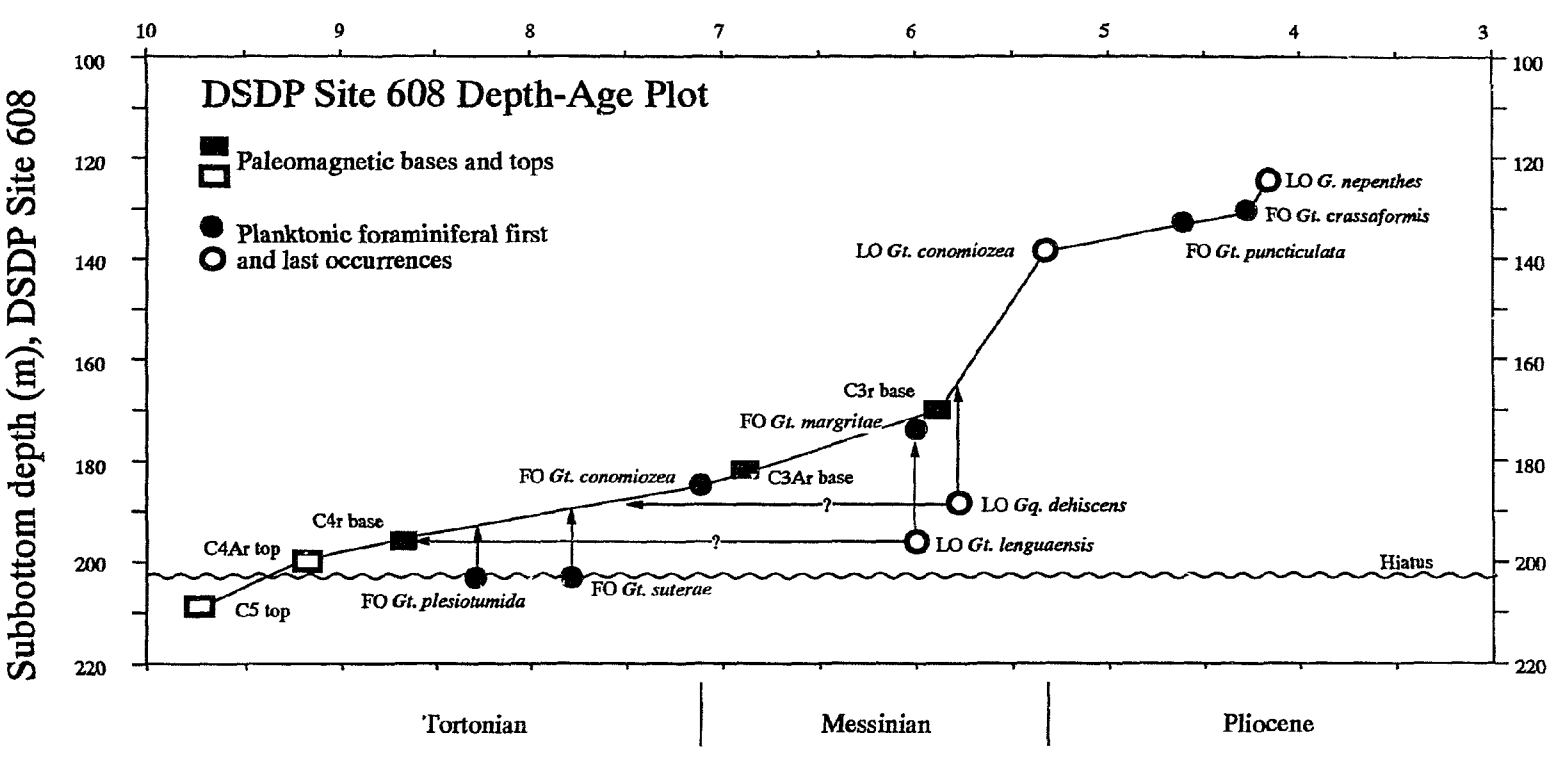
Age (Ma)
10
9
8
7
6
5
4
3
DSDP Site 608 Depth-Age Plot
Paleomagnetic bases and tops
Planktonic foraminiferal first and last occurrences
Subbottom depth (m), DSDP Site 608
100
120
140
160
180
200
220
LO G. nepenthes
FO Gt. crassaformis
LO Gt. conomiozea
FO Gt. puncticulata
C3r base
FO Gt. margritae
FO Gt. conomiozea
C3Ar base
LO Gq. dehiscens
C4r base
C4Ar top
LO Gt. lenguaensis
Hiatus
C5 top
FO Gt. plesiotumida
FO Gt. suterae
Tortonian
Messinian
Pliocene

Fig. 4-9. Oxygen and carbon stable isotopic stratigraphy of the benthic foraminifera (*Planulina wuellerstorfi*) of DSDP Site 608. See Fig. 4-7 for detailed explanations.

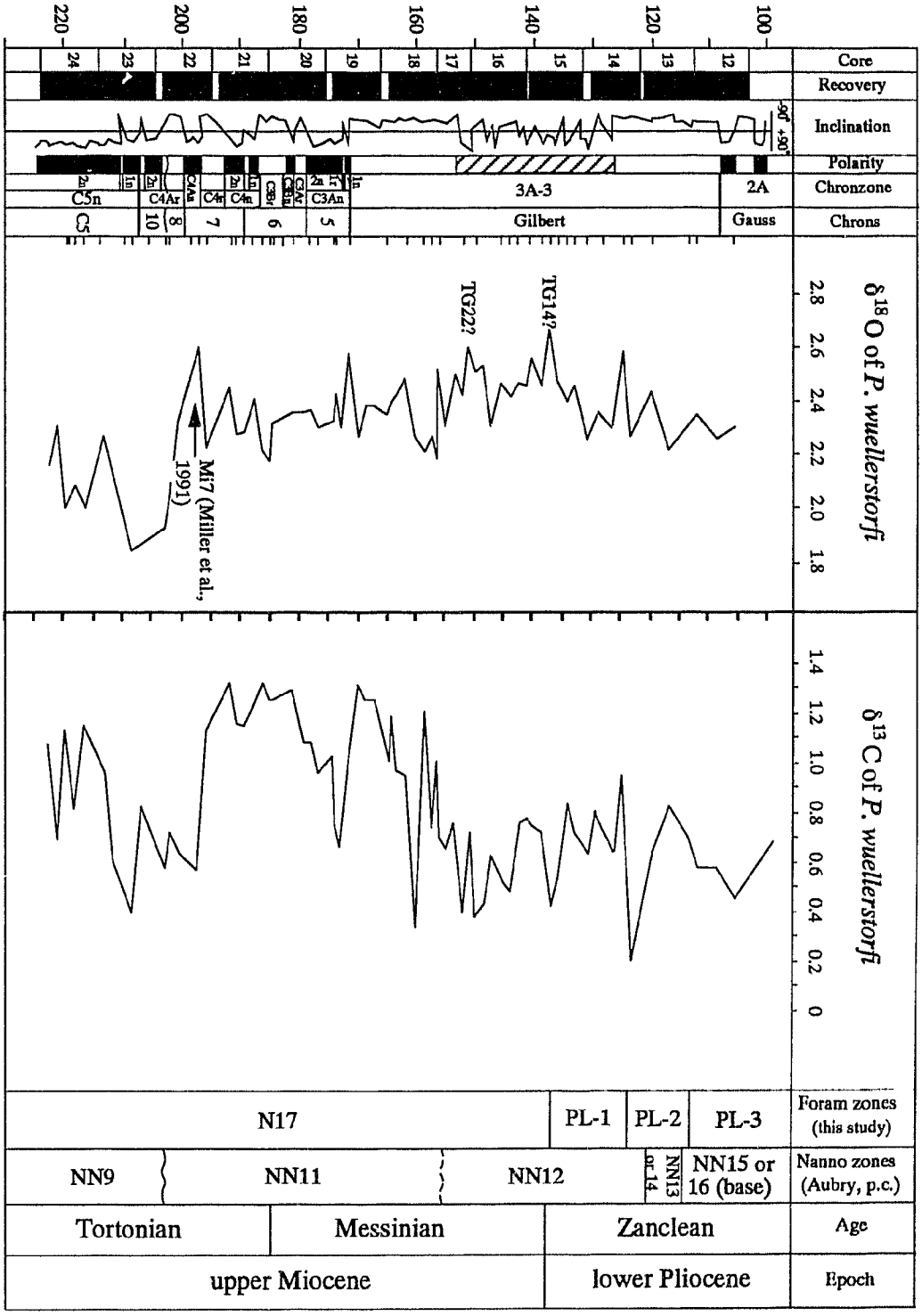
Depth Subbottom (m), DSDP Site 608
220
200
180
160
140
120
100
Core
Recovery
Inclination
-90°
+90°
Polarity
Chronzone
Chrons
C5n
C5
C4Ar
3A-3
2A
Gilbert
Gauss
TG22?
TG14?
M17 (Miller et al., 1991)
δ18O of P. wuellerstorfi
δ13C of P. wuellerstorfi
Foram zones (this study)
N17
PL-1
PL-2
PL-3
Nanno zones (Aubry, p.c.)
NN9
NN11
NN12
NN13 or 14
NN15 or 16 (base)
Age
Tortonian
Messinian
Zanclean
Epoch
upper Miocene
lower Pliocene

Zone NN13/14. Another undifferentiated Zone NN15/NN16 is suggested in Cores 13 and 12 by Aubry (pers. comm., 1993).

4.1.3.2. Stable isotopic stratigraphy

Oxygen stable isotopes: A significant depletion of oxygen stable isotope in benthic foraminifera (Fig. 4-10) is recognized in the interval from Chronozones C5 to the middle part of C4A (Cores 23, 24, and lower 22); this event was also determined by Miller et al., 1991. A major $\delta^{18}O$ enrichment is identified at 200.4 msb, probably indicating ice volume increase during the late Tortonian. Miller et al. (1991) defined this shift as Mi7 (Miocene Isotope Stage 7), a late Miocene $\delta^{18}O$ stage. In general, $\delta^{18}O$ values exhibit a tendency of increase during the Messinian (from 185 to 135.6 msb).I identify 3 $\delta^{18}O$ enrichments in this interval at 171.4, 148.3, and 137.1 msb, respectively. These three events are probably equivalent to C3An.18O.2, TG22? and TG14? as observed in Salé borehole (Hodell et al. (1994), and in the North Atlantic Ocean (Keigwin et al., 1987). The oxygen isotope values become depleted in ^{18}O by about 0.2‰ immediately above the Messinian/Pliocene boundary.

Planktonic foraminiferal oxygen isotopic data (*G. bulloides*, solid line; Fig. 4-10) display no pronounced $\delta^{18}O$ depletion in the late Tortonian and no Stage Mi7 as recognized in benthic foraminifera. My data show that a general $\delta^{18}O$ enrichment starts near the Tortonian/Messinian boundary. Two distinct $\delta^{18}O$ enrichments are observed in planktonic foraminifera within the Messinian, and they may be equivalent to TG22? and TG14?. I caution that Stage TG14? of the planktonic foraminifera seems to have a longer duration, which continues up across the Messinian/Pliocene boundary. Analogous to the benthic foraminifera, planktonic foraminiferal $\delta^{18}O$ depleted rapidly above the Messinian/Pliocene boundary, indicating ice volume reduction and paleoclimate warming. It should be mentioned that a significant $\delta^{18}O$ depletion both from planktonic (*Orbulina*, dash line; Fig.

Fig. 4-10. Oxygen and carbon stable isotopic stratigraphy of the planktonic foraminifera (*Globigerina bulloides* and *Orbulina universa*), DSDP Site 608. Solid lines represent *Globigerina bulloides* and dot lines represent *Orbulina universa.* Proper overlap between the two species is considered. See Fig. 4-7 for more details.

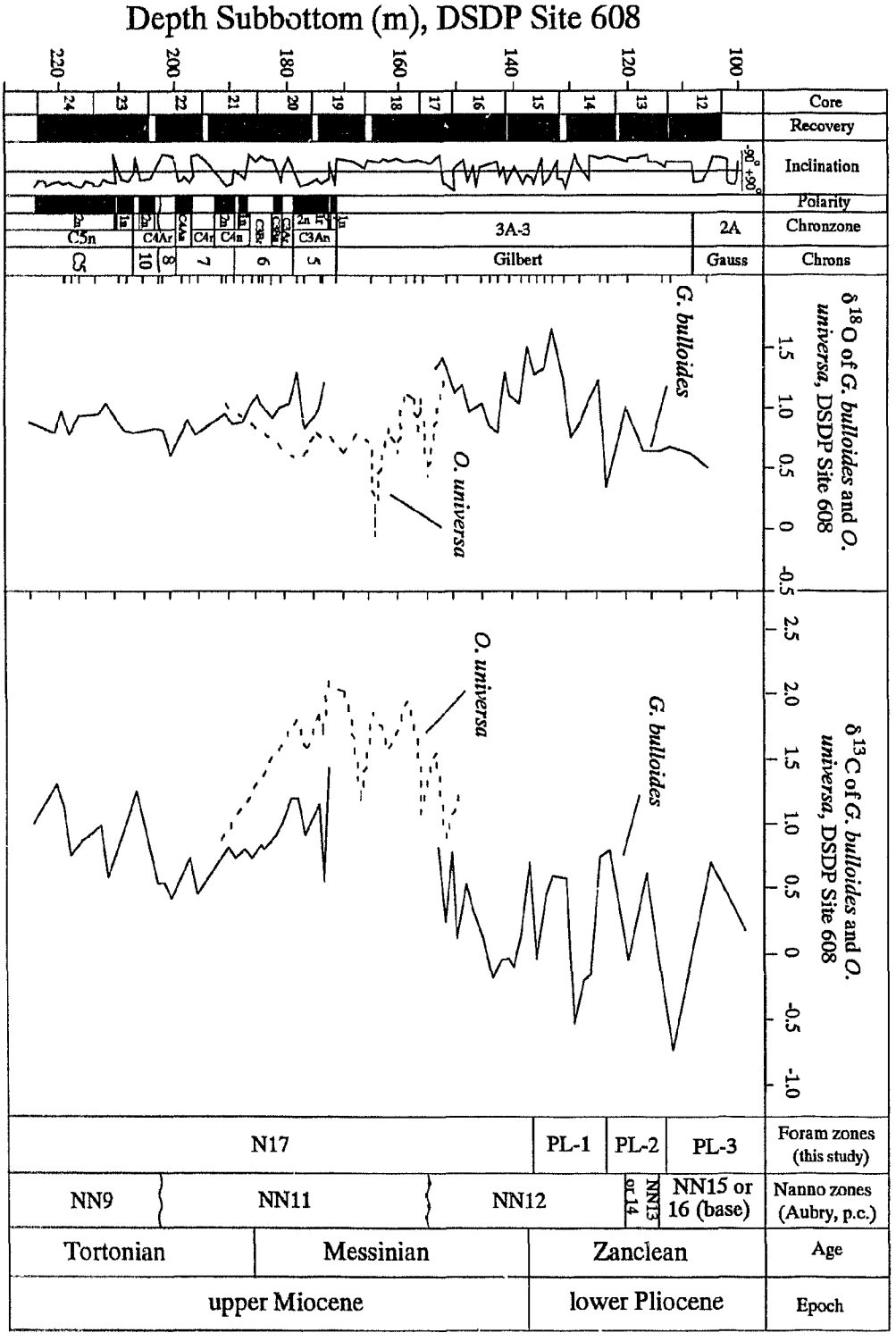
Depth Subbottom (m), DSDP Site 608
220
200
180
160
140
120
100
Core
Recovery
Inclination
-90°
+90°
Polarity
Chronzone
Chrons
C5n
C4Ar
C4n
C3Bn
C3An
3A-3
2A
Gilbert
Gauss
G. bulloides
O. universa
δ 18O of G. bulloides and O. universa, DSDP Site 608
1.5
1.0
0.5
0
-0.5
O. universa
G. bulloides
δ 13C of G. bulloides and O. universa, DSDP Site 608
2.5
2.0
1.5
1.0
0.5
0
-0.5
-1.0
N17
PL-1
PL-2
PL-3
Foram zones (this study)
NN9
NN11
NN12
NN13 or 14
NN15 or 16 (base)
Nanno zones (Aubry, p.c.)
Tortonian
Messinian
Zanclean
Age
upper Miocene
lower Pliocene
Epoch

4-10) and benthic foraminifera (Fig. 4-9) in the lower part (reversed) of the Gilbert could also be associated with strong carbonate dissolution in this interval.

Carbon Stable Isotopes: At Site 608, both benthic and planktonic foraminiferal $\delta^{13}C$ signals are characterized by high amplitude fluctuations in the selected section of this study. Three distinct $\delta^{13}C$ depleted shifts from benthic foraminifera have been observed in Cores 23, 20, and 18, respectively (Fig. 4-9). The former one occurred in the late Tortonian and the later two occurred in Messinian time. Similar shifts are also identified in planktonic foraminifera (Fig. 4-10), although the late Tortonian shift in Core 22 is not as clear as that in the benthic foraminifera. It is well known that during the Messinian only one major $\delta^{13}C$ shift has been recorded elsewhere in the world ocean immediately above the Tortonian/Messinian boundary. It is unique for Site 608 to have two major shifts. In comparison with my benthic foraminiferal study, I realize that the rapid $\delta^{13}C$ increasing in Cores 19 and 18 matches an intense carbonate dissolution interval indicated by high planktonic foraminiferal fragments, high benthic/planktonic ratios and low abundance of benthic foraminifera (see Chapter 7). This phenomenon suggests that the $\delta^{13}C$ increase may have been caused by carbonate dissolution, and the shift in Core 18 may not be real. If the assumption is correct, then the shift in Core 20 could be real. I prefer the latter because the FO of *Gt. conomiozea* occurred in Core 20, which is considered to be most reliable marker of the Tortonian/Messinian boundary in the North Atlantic.

4.1.3.3. Magnetostratigraphy

The magnetostratigraphy was initially studied by DSDP drilling staffs Clement and Robinson (1987), and the results below Core 20, equivalent to the late Tortonian, were re-interpreted by Miller et al. (1991). More detailed magnetostratigraphic interpretation for the Messinian and lower Pliocene section was given by Gardner (1992). The latter interpretation was quite different from the initial study by Clement and Robinson (1987). According to Gardner (1992), Chronozone C3B marking the lowermost Messinian seems

to be missing. The interval from Core 14 to 16 contains magnetizations below the noise level of the cryogenic magnetometer, therefore, magnetostratigraphic zones are difficult to interpret.

In this study I have re-interpreted the magnetostratigraphy based on the previous studies and the most recent progress on geochronology (Berggren et al., 1995). My interpretation indicates that magnetostratigraphic records are complete, and no sedimentation breaks are present from the uppermost Tortonian to the lower Pliocene except for a possible small hiatus present within Chronozone C4Ar (Fig. 4-6). This interpretation is consistent with my planktonic foraminiferal and stable isotope stratigraphic studies.

4.1.3.4. Placement of Boundaries

As mentioned above, the Messinian/Pliocene boundary positions reported by Takayama and Sato (1987) and by Gardner (1992) are contradictory based on the nannofossil studies. The LO of *Discoaster quinqueramus* identified by Takayama and Sato is much lower than the LO of *Gt. conomiozea/miotumida* plexus, while that reported by Gardner (1992) is even higher than the FOs of *Gt. puncticulata* and *Gt. crassaformis*. Thus I suggest that the LO of *D. quinqueramus* appears to be unreliable in this hole. In this case, I present my observation, mainly relying upon my planktonic foraminiferal and stable isotope studies. Based on the LO of *Gt. conomiozea/miotumida* plexus that last occurred at the end of the Messinian, marking the Messinian/Pliocene boundary (Berggren, 1977; Berggren et al., 1995; Berggren, pers. comm.). and the remarkable $\delta^{18}O$ enrichment (TG14?), I would place the M/P boundary at 138.6 msb within Core 15. The TG14 $\delta^{18}O$ enrichment is considered to be associated with latest Messinian climate deterioration and Mediterranean Salinity Crisis as observed in Hole 552A by Keigwin (1987). In addition, the S/D coiling shift of *N. acostaensis* between oxygen isotope stages TG14? and TG22? and overlying Pliocene taxa *Gt. puncticulata* and *Gt. crassaformis* first occurred above the

LO of *Gt. conomiozea/miotumida* can also be indirect supportives of my placement of the M/P boundary.

As mentioned above, the placement of the T/M boundary becomes rather difficult, because of the contradictory nannofossil (Takayama and Sato, 1987; Gardner, 1992) and planktonic foraminiferal data (this study), as well as the double $\delta^{13}C$ shifts in the interval between Cores 18 and 20. Two boundaries are suggested by biostratigraphic data: Nannofossils suggest the boundary at the base of Core 18, while planktonic foraminifera suggest it at the base of Core 20. Interestingly, each boundary meets a major $\delta^{13}C$ shift. However I realize that the shift in Core 18 seems to be artifact because: 1) It falls completely within an intense carbonate dissolution interval. As reported by Berger (1970) and Berger et al. (1975), planktonic foraminifera dwell in surface oceanic water when they are young, and gradually migrate down to the depth as they grow. As a result, the early stages of the shells are depleted in oxygen–18 and enriched in carbon–13, while the later stage receives more oxygen–18 and less carbon–13 due to the change of water masses with depth. Based on this observation, I assume that the carbonate dissolution could remove outer layers (or whorls) of foraminifera, either completely or partially, which could result in an altered signal since the deeper water ^{18}O and ^{13}C would be removed. It is also observed in the same interval in benthic foraminifera (Fig. 4-9), where smaller sized *Planulina wuellerstorfi* and *Cibicidoides* (>150μm) are used for stable isotope measurements; and 2) Image processing using laser light distinctly shows that the planktonic foraminiferal shell (*Protentelloides dalhousiei* Zhang and Scott, 1995) bears a great number of micro–perforations in each single perforation (Kuang and Cada, submitted). These micro– perforations are not visible either in light microscope or scanning electronic microscope, because they are blocked by clay, mud or dust, but they are visible by removal of the fine particles with a specialized mathematic filter (Kuang and Cada, submitted). I speculate that these micro–perforations may play an important role in deep marine carbonate dissolution, and therefore effect the stable isotopic composition. If so,

then the carbon–13 shift in Core 19 and 18 may be an artifact, and the real shift must be in Core 20. Interestingly, this speculation agrees with the FO of *Globorotalia conomiozea* and magnetostratigraphic data, (i.e., Chronozone C3Br). The FO of *Globorotalia conomiozea* falls within C3Br where the T/M boundary was proposed (Berggren et al., 1995). I, therefore, rely upon my investigation of planktonic foraminifera and place the T/M boundary at 184.88 msb, rather than that of nannofossils. Of course, further investigation for nannofossils may be needed.

4.1.4. DSDP Site 547A

4.1.4.1. Planktonic foraminiferal biostratigraphy

No detailed planktonic foraminiferal or nannofossil biostratigraphy for the late Miocene and early Pliocene was reported by scientists during DSDP drilling of Leg 79, but was briefly mentioned by Winterer and Hinz (1984) and Hinz et al. (1984) in DSDP initial results. They reported that the uppermost Miocene rests unconformably on the middle Miocene. In this study, 37 samples from Cores 4 to 9 have been analyzed for planktonic foraminiferal biostratigraphy, about 4–6 samples per core. My biostratigraphic results are plotted in Fig. 4-11, and age estimates are listed in Table 4-5, which forms an age-depth plot (Fig. 4-12) of the hole. No magnetostratigraphy or stable isotope stratigraphy were carried out for this interval during the DSDP drilling or in this study. The late Miocene–early Pliocene section was extremely condensed and interrupted by several sedimentation gaps, resulting from carbonate dissolution and possible deep water erosion (see Discussion).

The FO of *Gt. plesiotumida* is observed at 149.9 msb (Sample 9–3, 90–94 cm). It is consistent with the others identified at other sites in this study. *Gt. lenguaensis* last occurred at 136.9 msb (Sample 8–1, 120–124 cm).

I have identified a number of important planktonic foraminiferal bioevents in Core 8. *Gt. conomiozea* is recorded in the interval from the middle Core 8 to the top of Core 6

(Fig. 4-11), bracketing the Messinian Stage. In Cores 8–6, several FOs of other species, such as *Globorotalia pseudomiocenica, Globorotalia crassula, Globorotalia* cf. *exilis, Sphaeroidinella immatura* are recognized. A single specimen of *Gq. dehiscens,* which occurred with a Cretaceous species *Globotruncana* in sample 6–1, 30–34 cm (117.8 msb), is considered to have been reworked.

In Cores 3 through 5, faunal components are composed of Pliocene microfossils. Those fossils allow us to denote convincing biostratigraphic assignments for the Pliocene.

Based on these results, I place the Tortonian/Messinian and Messinian/Pliocene boundaries at 141.80 msb and 117.80 msb respectively marked by the FO and LO of *Gt. conomiozea.* The juxtaposition of the FO of *Gt. conomiozea,* the FO of *Gt. margaritae,* and the LO of *Gt. suterae* at 141.8 msb (Sample 8–4, 80–84cm) indicates that the lower Messinian section and probably the uppermost Tortonian section are missing (see below for more discussion). The Messinian/Pliocene boundary is dashed because I have no other means to support as to whether or not the LO of *Gt. conomiozea* is true. According to the present study, the LO of *Gt. conomiozea* is usually diachronous in this area (refer to Salé borehole and DSDP Site 552A). However, the attribution of Messinian section is secure because *Gt. conomiozea* always occurs within the Messinian as so far I have ascertained. Sporadic Pliocene deposits are recognized in the upper section of the hole, which are interrupted by two hiatuses.

4.1.4.2. The hiatuses

Three hiatuses are recognized (Figs. 4-11 and 4-12). A distinct hiatus (H3) is present at the Tortonian/Messinian boundary. This hiatus is suggested by the juxtaposition of the FO of *Gt. conomiozea,* the FO of *Gt. margaritae,* and the LO of *Gt. suterae* at 141.8 msb (Sample 8–4, 80–84cm) and may cut off the lower Messinian section and probably the uppermost Tortonian. As discussed above, the FO of *Gt. conomiozea* occurred within paleomagnetic Chronozone C3B (age estimate 7.12 Ma), while the FO of *Gt. margaritae*

Fig. 4-11. Planktonic foraminiferal biostratigraphy of DSDP Hole 547A. Age estimates are from Berggren et al., 1995. S and D indicate coiling direction changes of *Neogloboquadrina acostaensis*. Reversed T and T represent first and last occurrences, respectively. H indicates hiatus. * represents reworked specimens.

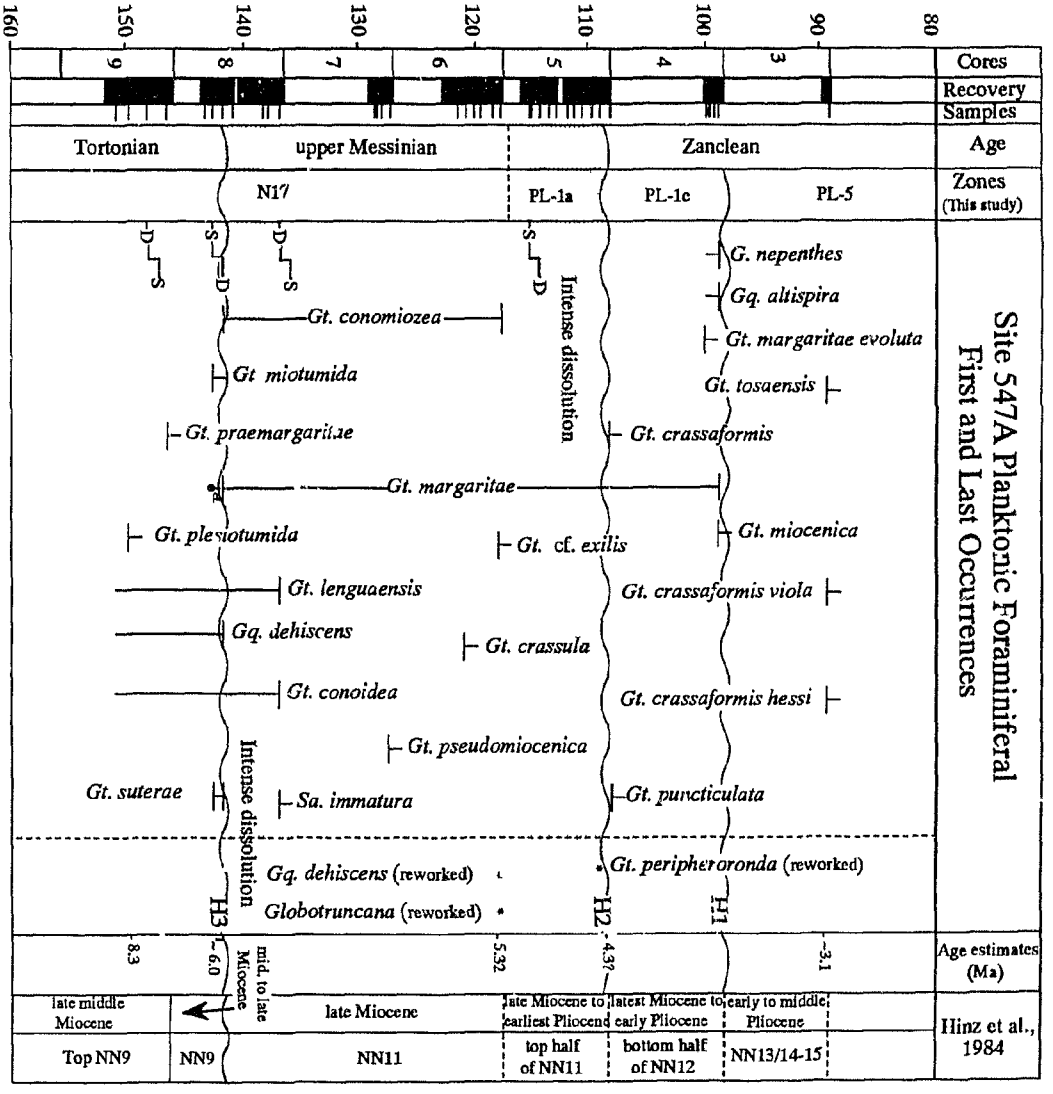
Subbottom Depth (meter)
160
150
140
130
120
110
100
90
80
9
8
7
6
5
4
3
Cores
Recovery
Samples
Tortonian
upper Messinian
Zanclean
Age
N17
PL-1a
PL-1c
PL-5
Zones
(This study)
Site 547A Planktonic Foraminiferal
First and Last Occurrences
G. nepenthes
Gq. altispira
Gt. margaritae evoluta
Gt. tosaensis
Gt. crassaformis
Gt. conomiozea
Gt miotumida
Gt. praemargaritae
Intense dissolution
Gt. margaritae
Gt. plesiotumida
Gt. cf. exilis
Gt. miocenica
Gt. lenguaensis
Gt. crassaformis viola
Gq. dehiscens
Gt. crassula
Gt. conoidea
Gt. crassaformis hessi
Gt. pseudomiocenica
Gt. suterae
Sa. immatura
Gt. puncticulata
Intense dissolution
Gq. dehiscens (reworked)
Gt. peripheroronda (reworked)
Globotruncana (reworked)
H3
H2
H1
8.3
6.0
5.32
4.37
3.1
Age estimates
(Ma)
late middle Miocene
mid. to late Miocene
late Miocene
late Miocene to earliest Pliocene
latest Miocene to early Pliocene
early to middle Pliocene
Hinz et al., 1984
Top NN9
NN9
NN11
top half of NN11
bottom half of NN12
NN13/14-15

Fig. 4-12. Depth-age plot of DSDP Hole 547A. No paleomagenetic data are available at this site (See Table 4-5 for more details).

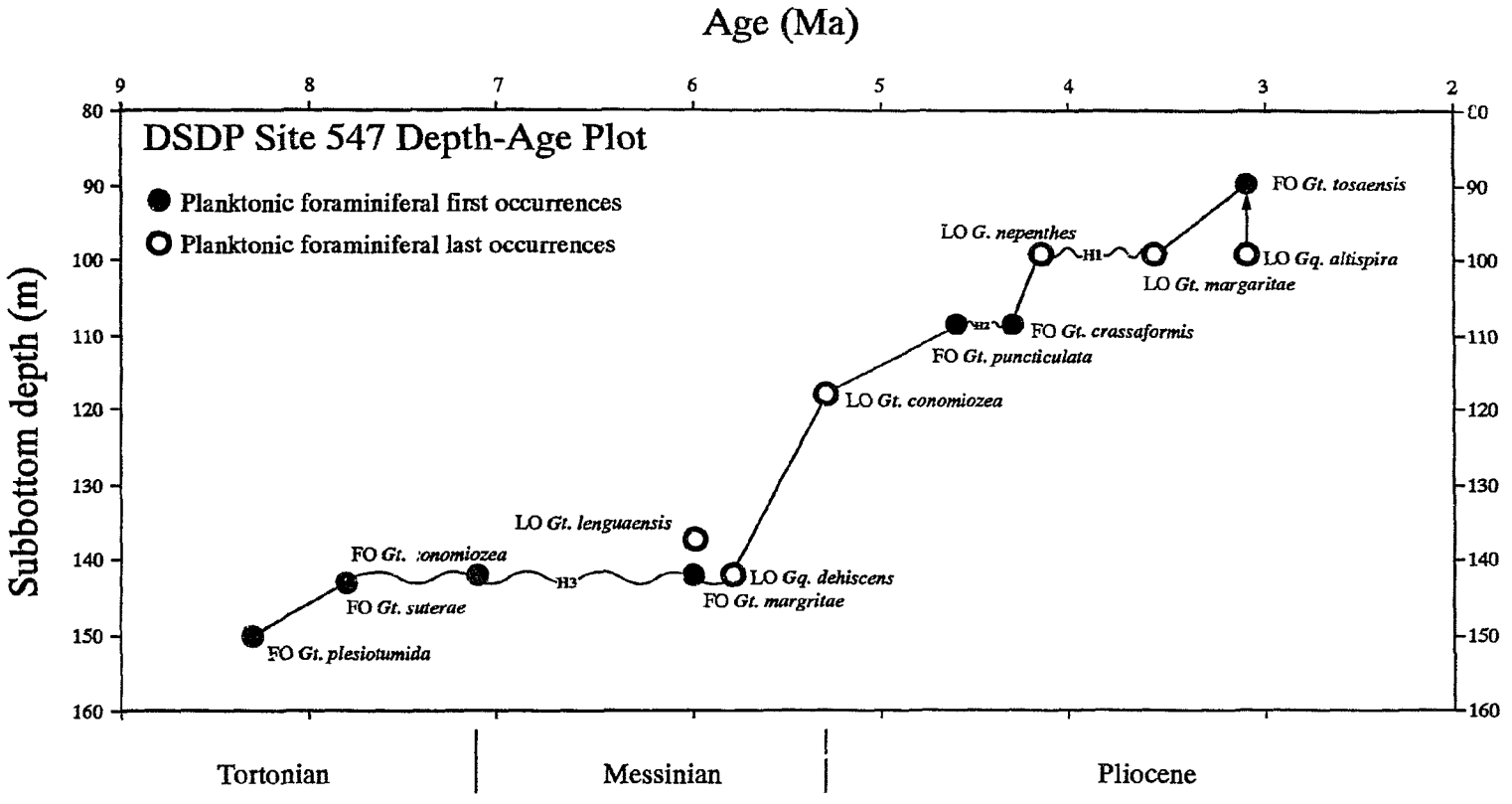
Age (Ma)
9
8
7
6
5
4
3
2
DSDP Site 547 Depth-Age Plot
Planktonic foraminiferal first occurrences
Planktonic foraminiferal last occurrences
Subbottom depth (m)
80
90
100
110
120
130
140
150
160
FO Gt. tosaensis
LO G. nepenthes
H1
LO Gq. altispira
LO Gt. margaritae
H2
FO Gt. crassaformis
FO Gt. puncticulata
LO Gt. conomiozea
LO Gt. lenguaensis
FO Gt. conomiozea
H3
LO Gq. dehiscens
FO Gt. margritae
FO Gt. suterae
FO Gt. plesiotumida
Tortonian
Messinian
Pliocene

Table 4-5. Biological stratigraphic events from DSDP Hole 547A. Age estimates were calibrated to the new time scale by Berggren et al. (1995). Age estimates with asterisks are calibrated to the new time scale of Berggren et al. (1995) in this study. Age estimates with two asterisks are from Berggren et al., 1985 without calibration to the new time scale of Berggren et al. (1995) as this has not been changed in the new time scale.

Sample	Events	Depth (M)	Age estimates (Ma)
3-1, 45-49	FO *Gt. tosaensis*	89.43	3.11**
4-1, 45-49	LO *Gq. altispira*	98.95	43.09
4-1, 45-49	LO *Gt. margaritae*	98.95	3.58
4-1, 45-49	LO *G. nepenthes*	98.95	4.18
5-1, 31-35	FO *Gt. crassaformis*	108.31	4.3*
5-1, 31-35	FO *Gt. puncticulata*	108.31	4.6*
6-1, 30-34	LO *Gt. conomiozea*	117.80	5.32
8-1, 40-44	LO *Gt. lenguaensis*	136.90	6.0
8-4, 80-84	FO *Gt. margaritae*	141.80	6.0
8-4, 80-84	FO *Gt. conomiozea*	141.80	7.12
8-4, 80-84	LO *Gq. dehiscens*	141.80	5.8
8-5, 20-24	FO *Gt. suterae*	142.70	7.8
9-3, 90-94	FO *Gt. plesiotumida*	149.90	8.3

(6.0 Ma by Berggren et al., 1995; my datums indicates an age of ca. 6.3 Ma in this study) and the LO of *Gt. suterae* (~6.4 Ma, this study) occurred within Chronozone C3An (~6.4 Ma) in Holes 608, 552A, and Salé borehole. I emphasize that the FOs of *Gt. margaritae* in Holes 608, 552A and Salé consistently occurred in Chronozone C3An at 6.3 Ma, about 0.3 m.y. older than that given by Berggren et al. (1995). If I use the age estimate of *Gt. margaritae* given by Berggren et al. (1995), then the duration of the hiatus is at least 1.12 m.y.(Fig. 4-12); if using the age estimate given in this study, then the duration is about 0.82 m.y. These data suggest that the lower Messinian is missing at Site 547A. The upper Tortonian section bracketed by the FO of *Globorotalia plesiotumida* (8.3 Ma, Berggren et al., 1995) at 149.9 msb (Sample 9–3, 90– 94cm) and the FO of *Gt. conomiozea* is thin, only about 6.3 m thick (actual recovery) in over 1 million years. It seems to indicate that the section may be either partially missing or extremely condensed.

A possible short hiatus (H2) in the early Pliocene is suggested by the juxtaposition of the FOs of *Gt. puncticulata* and *Gt. crassaformis*, with a duration of 0.1 m.y., indicating that the Subzone PL–1b is probably missing. Although the FOs of *Gt. puncticulata* and *Gt. crassaformis* may not be reliable for global correlation due to the absence and delay in low latitudes (*fide* Berggren et al., 1995), these two datums in temperate areas appear to be suitable for regional stratigraphic correlation.

Hiatus 1 (H1) is identified by the juxtaposition of the LO of *Globigerina nepenthes,* the LO of *Gt. margaritae,* and the LO of *Globoquadrina altispira*, which have been calibrated to 4.18 Ma, 3.58 Ma, and 3.09 Ma, respectively as zonal markers of PL1–b/PL2, PL2/PL3, and PL4/PL5 boundaries (Berggren et al., 1995). Hence, it is clear that the hiatus cut out at least three entire zones, i.e., PL2–PL4, with a duration of 1.09 m.y. I attribute these hiatuses to deep water production in the abyssal plain during the early Messinian and early Pliocene.

4.1.5. ODP Site 646B

4.1.5.1. Biostratigraphy

The Miocene–Pliocene biostratigraphy was studied by shipboard scientists at ODP Leg 105 (Knüttel et al., 1985; Aksu and Kaminski, 1989), and no further subdivision for the Messinian was given. I re–examined the first and last occurrences (FO and LO) of planktonic foraminifera from Cores 80 to 41 to determine the Tortonian/Messinian and Messinian/Pliocene boundaries. The dominant planktonic foraminiferal taxa at this location are *Neogloboquadrina atlantica, N. pachyderma, Globigerina bulloides and Globorotalia scitula*. These taxa yield poor stratigraphic resolution for the Messinian and earliest Pliocene intervals due to their long life spans. *Globorotalia conomiozea*, the critical marker for the Tortonian/Messinian boundary currently proposed by Berggren et al. (1995) is not present. However I have determined a major coiling change of *Neogloboquadrina* from dextral to sinistral at 734.10 msb (Sample 77X–5, 20–24), followed by a long interval of sinistral *Neogloboquadrina* usually up to Messinian/Pliocene boundary as seen at Holes 552A and 608. The first occurrence of the coiling change occurs slightly below the Tortonian/Messinian boundary within the paleomagnetic Chronozone C4n (upper Tortonian) in North Atlantic Ocean (DSDP Holes 552A, and 608, and Salé Borehole), although it could be slightly diachronous. Thus it may be important to consider it as a secondary criteria for the T/M boundary when the other markers are not available (Fig. 4-13).

Aksu and Kaminski (1989) reported that the FO of *Globorotalia margaritae* occurred in Sample 53X-CC (506.90 msb) and the LO in Sample 39X–5, 11–13 (368.12 msb); the FO of *Globorotalia puncticulata* in Sample 41X–2, 26–30cm (383.08 msb), and the LO in sample 36X–1, 82–87cm (331.95 msb) (Fig. 4-13). Unfortunately, I was unable to find these two taxa, possibly because of either low diversity or smaller–sized samples used in this study. These two taxa are useful in determining the upper section of the Messinian and early Pliocene.

Fig. 4-13. Stable isotopic, magneto- and biostratigraphy, ODP Hole 646B. Magnetostratigraphy is re-interpreted after Clement et al., 1989; nannofossil data are from Knüttel et al., 1989; oxygen and carbon stable isotopes are after Aksu and Hillaire-Marcel, 1989; T and reversed T represent last and first occurrences of fauna and flora; Sr age estimates are conducted by Drs. Miller and Liu at Rutgers University. D and S represent right and left coiling.

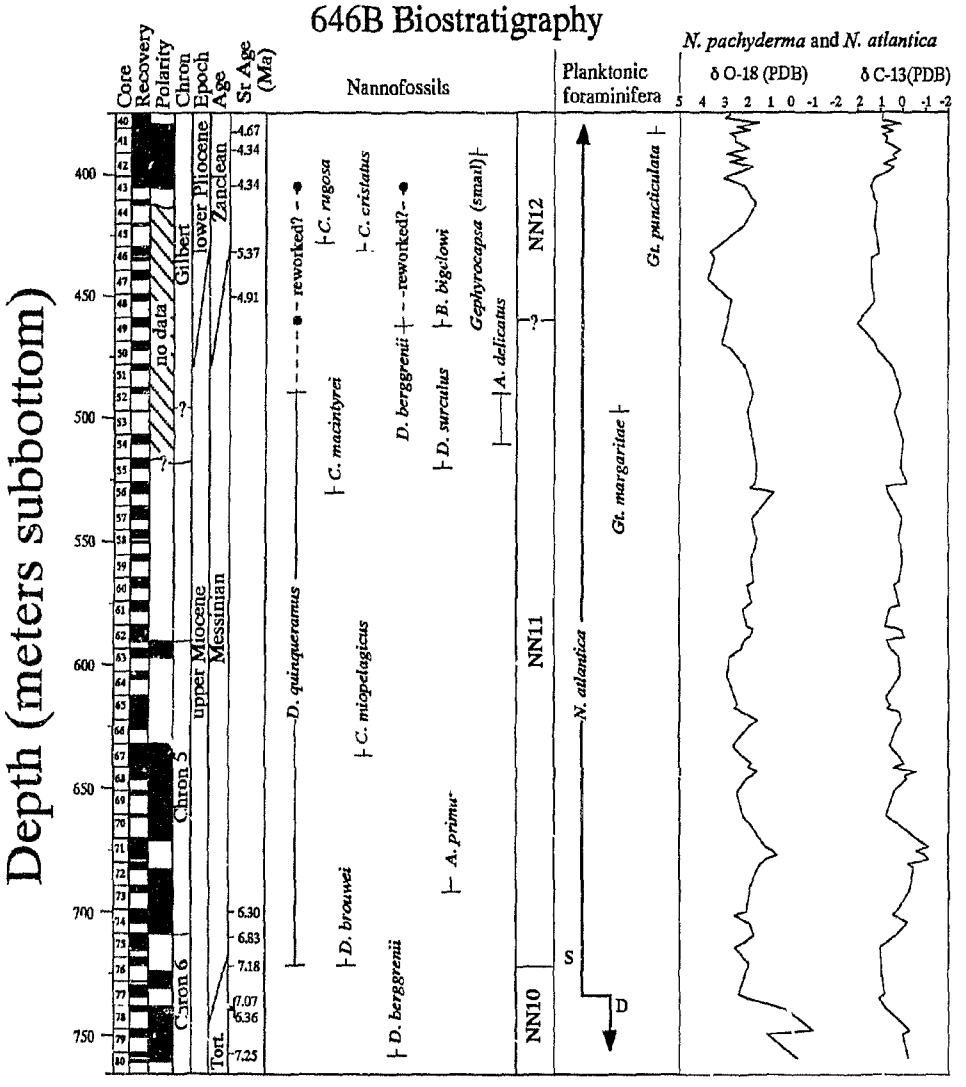
646B Biostratigraphy
Depth (meters subbottom)
Core
Recovery
Polarity
Chron
Epoch
Age
Sr Age (Ma)
Nannofossils
Planktonic foraminifera
N. pachyderma and N. atlantica
δ O-18 (PDB)
δ C-13(PDB)
Gilbert
lower Pliocene
Zanclean
upper Miocene
Messinian
Tort.
Chron 5
Chron 6
no data
D. quinqueramus
reworked?
C. rugosa
C. macintyrei
C. tricorniculatus
C. miopelagicus
D. bergrenii
D. brouwei
A. primus
D. surculus
B. bigelowi
Gephyrocapsa (small)
A. delicatus
NN12
NN11
NN10
N. atlantica
Gt. margaritae
Gt. puncticulata
S
D

Nannofossil biostratigraphy was studied by Knüttel et al. (1989), and the data are plotted here in support of my biostratigraphic interpretation (Fig. 4-13). The interval from Cores 80X to 76X was designated as nannofossil Zone NN10 by Knüttel et al. (1989), which was based on the FO of *D. berggrenii* at Core 80X and the FO of *Discoaster quinqueramus* at 721.44 msb (76X-CC). However, I caution that the FO of *Discoaster quinqueramus* may not be the real first occurrence because *Discoaster berggrenii* first occurred at a level of about 760 msb (Sample 80X-CC; Knüttel et al., 1989). According to Perch–Nielsen (1985), Bukry (1973, 1975), and Martini (1971), the FO of both *D. quinqueramus* and *D. berggrenii* marks the base of NN11. Under these circumstances, I would tentatively place the NN10/NN11 boundary in Sample 80X-CC at 760 msb.

From Cores 53 to 41, no certain nannofossil zonal assignments were made by Knüttel et al. (1989). They tentatively placed the NN11/NN12 boundary at 497.2 msb (Sample 53X-CC) using the LO of *D. quinqueramus* and NN12/NN13/14 boundary at 435.1 msb (Sample 46X-CC) indicated by a single occurrence of *Ceratolithus acutus*. The interval from Core 46 to 41X–4, 43–45 cm was tentatively attributed to an undifferentiated Zone NN13/14 based on the FO of *Ceratolithus rugosus* at Sample 46X–2, 25–27 cm. However, I realize that *D. berggren* tends rather consistently up to 49X-CC, which has much higher occurrence than *D. quinqueramus*. According to Perch–Nielsen (1985), *D. berggrenii* goes out at the end of NN11a before the extinction of *D. quinqueramus*. Concerning these observations, I would suggest that the NN11/NN12 boundary may be up to 462 msb (Sample 49X-CC), which is about 35 m higher than the boundary assignment given by Knüttel et al. (1989). Furthermore, these two species were also identified in Core 43X, although they were explained as reworking (Knüttel et al., 1989). In any case this interval seems to be extremely difficult to give definite zonal boundaries because of paucity of nannofossils, downslope transportation, and possibly down caved sediments in the poorly recovered section. Hence integrated chronology must be considered when zones are being constructed.

4.1.5.2. Stable isotopic stratigraphy

Although the ($^{87}Sr/^{86}Sr$) values are relatively disordered, the values in the lower section between 757.8 and 699.7 msb still show somewhat constant increase upwards at an average rate of 7.4 x 10^{-6}/10m, which is similar to that from the Niue section in the Pacific (8.5 X 10^{-6}/10m; Aharon et al., 1993). Two samples (78X-CC, 26–30 and 78X–2, 16–20) within the section exhibit values higher than the adjacent samples. My age estimates are calculated from the $^{87}Sr/^{86}Sr$ range of 7.25 Ma (Sample 80X–1, 80–84) to 6.30 Ma (74X–1, 70–74). Sample 76X-CC was dated at 7.18 Ma, very close to the age of Tortonian/Messinian boundary (7.12 Ma) based on the new time scale of Berggren et al. (1995).

$^{87}Sr/^{86}Sr$ ratios from the interval between 450.9 and 384.1 msb (Core 48X–2 to 41X–2) exhibit alternative changes (Table 3-1). These values vary from 0.709033 to 0.709062, with general increase upwards, yielding ages ranging from 5.37 (with error ±0.15 Ma) to 4.34 Ma (with error ±0.42 Ma). In Sample 41X–2, 130–134, Sr exhibits a value of 0.709058 ±0.000008. These disordered orientations of Sr values are considered to be caused either by sample contamination or by down–slope mass transportation, but I prefer to attribute it to the latter. In any case, a full consideration of all chronological tools must be used, and I should not completely rest upon the Sr data (Dr. Liu at Rutgers University, pers. comm.).

Carbon and oxygen isotopes: Stable isotopes were analyzed by Aksu and Hillaire–Marcel (1989) using *N. atlantica* for entire Messinian section chosen in this study. As shown in Fig. 4-13, a distinct decrease in $\delta^{13}C$ occurred in Core 75 at level of 709.15 msb, a decreasing from -0.7 to -1.4‰. This shift is probably correlative with those from Hole 552A, the Morocco borehole, and other oceans where a global $\delta^{13}C$ shift is recognized (Keigwin, 1987; Hodell et al., 1986). The light values continue up to the top of Core 50X without significant fluctuations, followed by a relative increase of $\delta^{13}C$ at 471.5 msb.

For oxygen stable isotopes, three intervals of major $\delta^{18}O$ events were obtained from the Messinian section: 1) $\delta^{18}O$ enrichment shift increased by about 2‰ at 730 msb (Core 77X). It appears to be related to the coiling shift of *N. atlantica* at 734 msb. Aksu and Hillaire–Marcel (1989) suggested that the increase may represent a late Miocene cooling in the surface waters in the Labrador Sea, with little or no long–term continental ice storage. I attribute this enrichment to the global cooling at the beginning of the Messinian as observed elsewhere in the world ocean (e.g., Keigwin 1987; Hodell et al., 1986; Hodell et al., 1994); 2) In the interval from 471 to 421 msb (Cores 50X to 45X) there is an enrichment of about 2‰ which may be associated with the latest Miocene glaciation found in Hole 552A and Morocco at 5.6 Ma, as interpreted by Aksu and Hillaire–Marcel (1989); and 3) There is a $\delta^{18}O$ decrease of about 2‰ above 421 msb (Core 45). I attribute this shift to the global warming across the Messinian/Pliocene boundary.

4.1.5.3. Magnetostratigraphy

The magnetostratigraphic data used here are from Clement et al. (1989). The polarity interpretations are based on the inclination data alone by Clement et al. (1989). I must caution that the magnetic polarities may not be reliable without the support of other stratigraphic means because of the cyclic turbidite features in this hole during the Messinian (Chapter 5, this thesis). Here I re–interpreted the polarities based on currently available strontium dating (Fig. 4-13). The polarity sequence from 620 to 700 msb was correlated with Chronozone C4 to the top of Chronozone C4An. Chronozone C3A (Chron 5) was considered to be missing (Clement et al., 1989). My Sr dating indicates that the sequence from Core 62 to 80 belongs to Chronozone C3, including Chrons 5 and 6, equivalent to the lower Messinian and the uppermost Tortonian.

4.1.5.4. Boundary Placement

Neither the Tortonian/Messinian nor the Messinian/Pliocene boundaries can be easily assigned because of the downslope transportation during the Messinian Stage (See Chapter 5, this thesis). To provide a better solution, I place the T/M boundary between Core 75X and 78X within Chron 6. This placement may be supported by the following observations: 1) $^{87}Sr/^{86}Sr$ age estimate ranges from 7.07 to 7.18 Ma in Cores 77X and 76X; 2) Chron 6 $\delta^{13}C$ shift at Core 75X. As seen elsewhere, Chron 6 $\delta^{13}C$ shift is not situated exactly at the T/M boundary, but slightly above it (see DSDP Hole 552A and Moroccan Salé borehole, this study); 3) $\delta^{18}O$ enrichment in Core 77X; 4) *Neogloboquadrina* coiling change from the dextral to sinistral, which occurs immediately below the T/M boundary as seen in Hole 552, Hole 608 and Moroccan Salé borehole; and 5) The FO of *D. berggrenii* occurred in Core 76X, which is obviously delayed (Fig. 4-14; Table 4-6) as a result of down-slope transportation (Chapter 5, this thesis). The FO of *Globorotalia conomiozea* marking the base of the Messinian is absent at this location. I consider that the assignment of the T/M boundary for this hole is relatively solid, and consistent with the other placement of the T/M boundaries in other holes in this study.

The Messinian/Pliocene is tentatively suggested between Cores 46X and 50X in C3r (lower Gilbert reverse) based on the following observations: 1) The LO of *D. berggrenii* in Sample 49X-CC. It must be mentioned that this event may stratigraphically yield a lower M/P boundary relative to that of *D. quinqueramus,* because the former is a zonal marker separating Subzones NN11a and NN11b (Perch–Nielsen, 1985); 2) The Sr age of 5.37 Ma (Sample 46X–3, 30–4 cm) with a value of 0.709033±0.0000007. McKenzie et al. (1988) reported a mean $^{87}Sr/^{86}Sr$ value of 0.708995±0.00002 derived from 5 samples at the M/P boundary of the Capo Rossello stratotype, which is significantly different from that given by Farrell et al. (1995). Farrell et al. reported a $^{87}Sr/^{86}Sr$ ratio value of about 0.70904 at the M/P boundary from ODP Site 758 in the Indian Ocean by

Fig. 4-14. Depth-age plot of ODP Site 646B. Age estimates are from Berggren et al.[1995] and Benson et al. (in press) (see Table 2 for details).

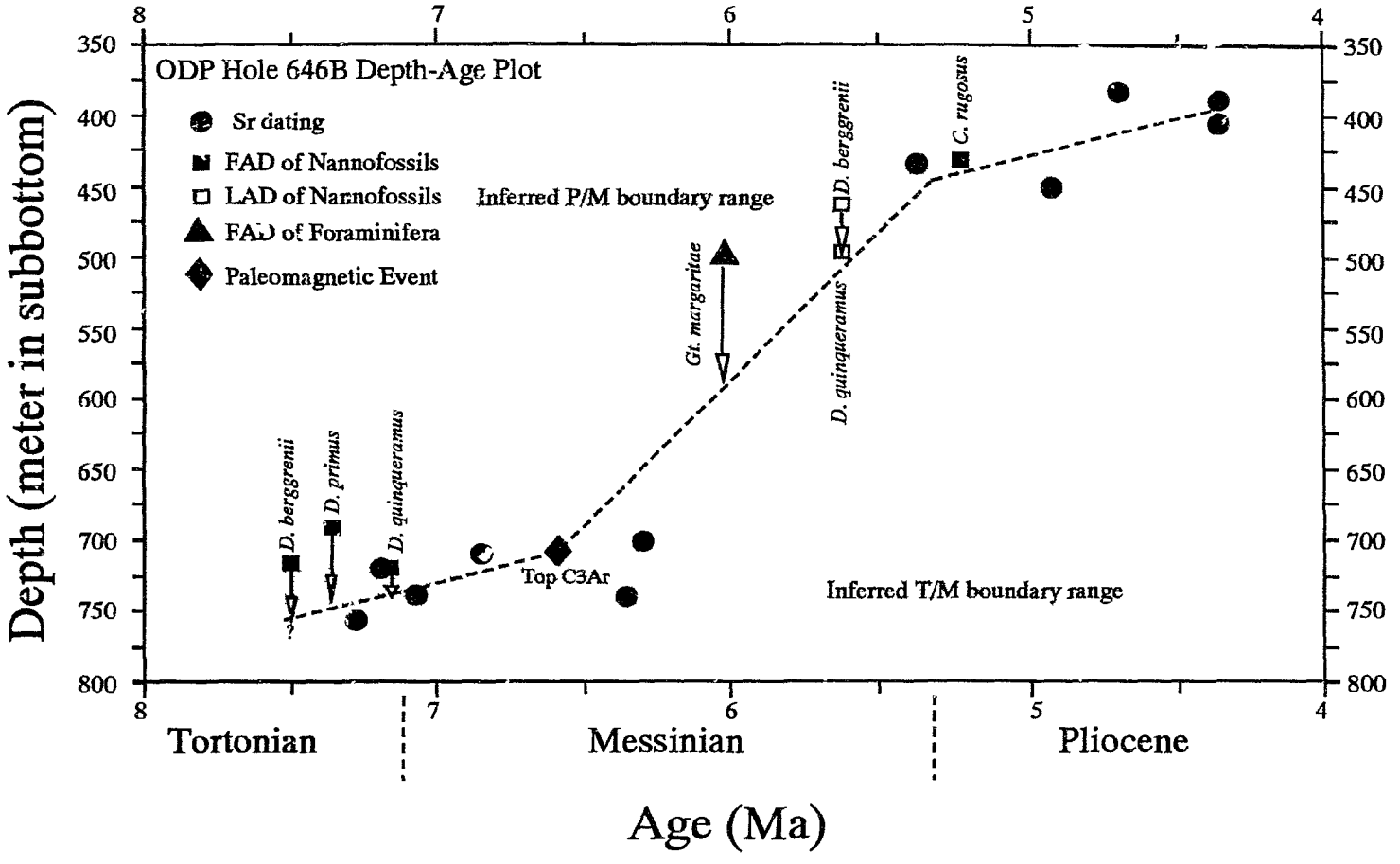
ODP Hole 646B Depth-Age Plot
Sr dating
FAD of Nannofossils
LAD of Nannofossils
FAD of Foraminifera
Paleomagnetic Event
Inferred P/M boundary range
Inferred T/M boundary range
D. berggrenii
D. primus
D. quinqueramus
Top C3Ar
Gt. margaritae
D. quinqueramus
D. berggrenii
C. rugosus
Depth (meter in subbottom)
Age (Ma)
Tortonian
Messinian
Pliocene
8
7
6
5
4
350
400
450
500
550
600
650
700
750
800

Table 4-6. Age estimates of nannofossils from Berggren et al. (1995) and Benson et al. (in press) and strontium stable isotopes.

Events	Species	Core	Depth (msb)	Age (Ma)	References
	Sr	646B, 41X-2	384.1	4.67	
	Sr	646B, 41X-6	389.5	4.34	
	Sr	646B, 43X-CC	405.1	4.34	
FO	*C. rugosus*	646B, 46X-2	431.6	5.23	Berggren et al., 1995
	Sr	646B, 46X-3	433.1	5.37	
	Sr	646B, 48X-2	450.9	4.91	
LO	*D. berggrenii*	646B, 49X-CC	461.9	5.6	Berggren et al., 1995
FO	*Gt. margaritae*	646B, 52X-CC	497	6	Berggren et al., 1995
LO	*D. quinqueramus*	646B, 53X-CC	497.2	5.6	Berggren et al., 1995
FO	*D. primus*	646B, 73X-CC	692	7.35	Benson et al., in press
	Sr	646B, 74X-1	699.7	6.3	
Top	C3Ar	646B, 75X	708.6	6.567	Berggren et al., 1995
	Sr	646B, 75X-2	711.1	6.83	
FO	*D. quinqueramus*	646B, 76X-CC	721.4	7.15	Benson et al., in press
	Sr	646B, 76X-CC	721.4	7.18	
	Sr	646B, 78-2	739.2	7.07	
	Sr	646B, 78X-CC	739.8	6.36	
	Sr	646B, 80X-1	757.8	7.25	
FO	*D. berggrenii*	646B, 80X-CC	716	7.48	Benson et al., in press

using the new time scale of Berggren et al. (1995). My $^{87}Sr/^{86}Sr$ is obviously similiar to that of Farrell et al. (1995). Strict attention must be adhered to when the Sr age estimates are undertaken as constraints of the boundary because of the poor results obtained from this interval; 3) the interpolation of the age of the FO of *G. margaritae* (6.0 Ma of Berggren et al., 1995) at 506.9 msb and FO of *G. puncticulata* (4.6 Ma of Berggren et al., 1995) at 383.08 msb; and 4) $\delta^{18}O$ depletion above Core 45X and $\delta^{18}O$ enrichment in the interval from Core 47X to 46X. These isotope events are basically identical to those observed in Holes 552A and 608, and other locations in the world ocean (Hodell et al., 1986). My boundary assignment is higher than those of Knüttel et al., 1989 and Baldauf et al., 1989, who placed the M/P boundary in Core 53X and 52X, respectively.

4.2. Discussion

4.2.1. Diachroneity and Synchroneity of Planktonic Foraminifera

As discussed previously, DSDP/ODP Sites 552A, 608, 646B and Salé Moroccan borehole yield ideal planktonic foraminiferal biostratigraphy, magnetostratigraphy and stable isotope stratigraphy for the early Messinian section, except for the Messinian section in which poor paleomagnetic records were obtained. This provides a base line for assessment of future biostratigraphic study, and allows tentative evaluation of the degree of diachrony and synchrony of the planktonic foraminifera in the North Atlantic Ocean. Some important planktonic foraminiferal events are critical in determining the Messinian boundaries; my planktonic foraminiferal datums calibrated to the new geomagnetic polarity time scale (GPTS), using Berggren et al. (1995), are plotted in Fig. 4-15, with deep-water site arrangement from north to south to facilitate comparison.

Globoquadrina dehiscens, a morphologically diagnostic species occurs in three DSDP holes, i.e., 547, 608 and 552A. It is not identified in Salé borehole, which may imply that *Gq. dehiscens* has an earlier extinction than those in other sites. According to the calibration given by Berggren et al. (1995) the LO of *Gq. dehiscens* has age estimate of 5.8

Fig. 4-15. Diachrony and synchrony of selected late Miocene and early Pliocene planktonic foraminiferal taxa from DSDP Holes 552A, 608, 547A and Salé borehole of Morocco.

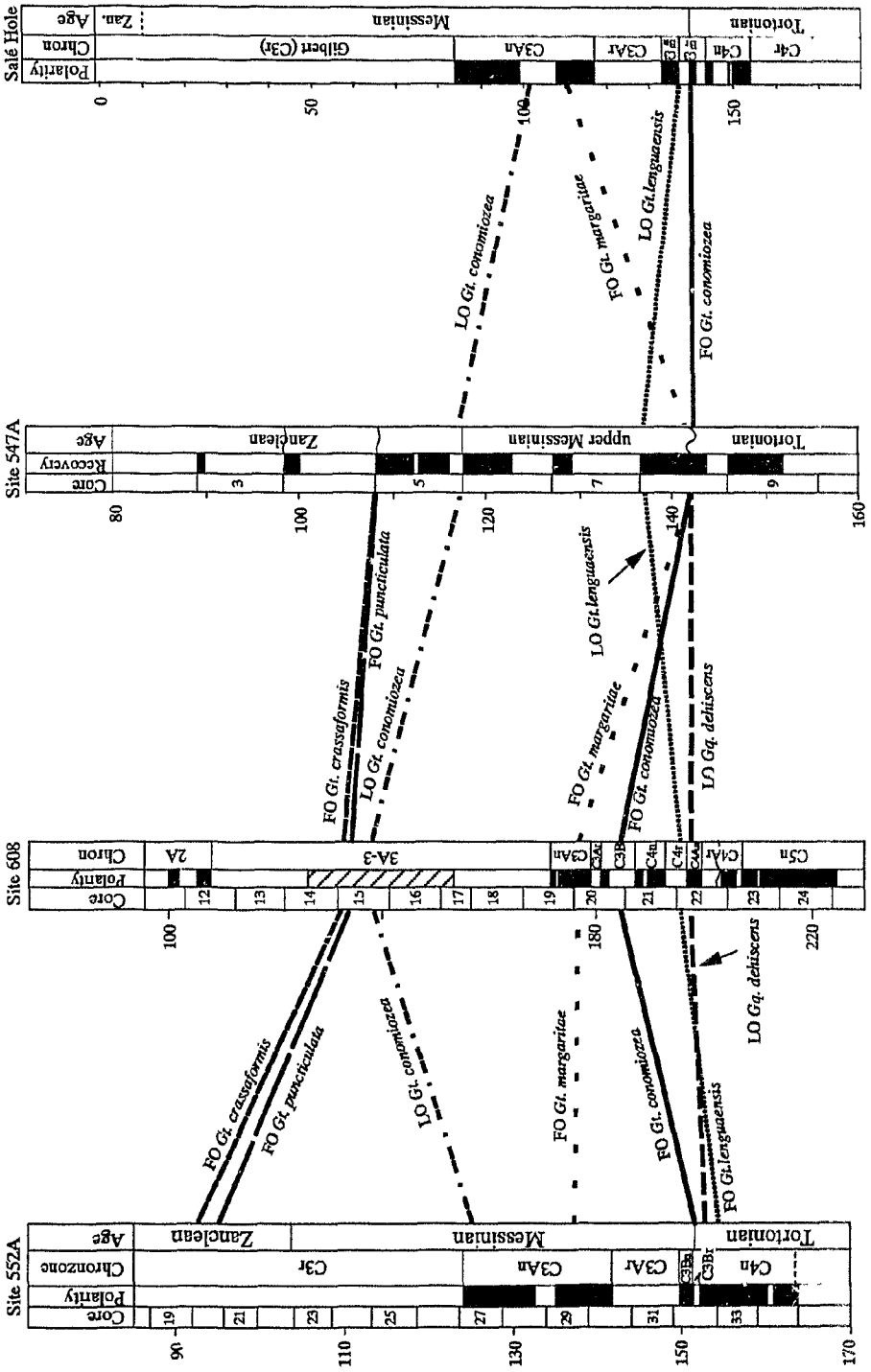
Site 552A
Core
Polarity
Chronzone
Age
Zanclean
Messinian
Tortonian
C3r
C3An
C3Ar
C3Bn
C3Br
C4n
FO Gt. crassaformis
FO Gt. puncticulata
LO Gt. conomiozea
FO Gt. margaritae
FO Gt. conomiozea
LO Gq. dehiscens
FO Gt.lenguaensis
Site 608
Core
Polarity
Chron
2A
3A-3
C3An
C3Bn
C4n
C4r
C4Ar
C5n
C5r
FO Gt. crassaformis
FO Gt. puncticulata
LO Gt. conomiozea
FO Gt. conomiozea
FO Gt. margaritae
LO Gt.lenguaensis
LO Gq. dehiscens
Site 547A
Core
Recovery
Age
Zanclean
upper Messinian
Tortonian
LO Gt. conomiozea
FO Gt. margaritae
LO Gt.lenguaensis
FO Gt. conomiozea
Salé Hole
Polarity
Chron
Age
Zan.
Messinian
Tortonian
Gilbert (C3r)
C3An
C3Ar
C3Bn
C3Br
C4n
C4r

Ma near the top of Chronozone C3An, below the Messinian/Pliocene boundary based on the last occurrences in the Pacific (Berggren et al., 1995), and in the South Atlantic (Rio Grande Rise) (Berggren, 1977, 1983). In my material, the LO of the species may be calibrated to C4Ar, with age estimate of 8.6 Ma. As indicated in Figs. 4-3 and 4-4, the LO is far below the LOC, suggesting a remarkable diachrony. However at Sites 547A and 552A, the LOs are obviously truncated by hiatuses (Fig. 4-15). No age for the LO in Hole 547A can be estimated due to a relatively large hiatus that cuts off the interval from the uppermost Tortonian and lower Messinian.

Globorotalia lenguaensis occurs in four boreholes but not at ODP Site 646B. This species has received attention for late Miocene stratigraphic purposes because of its diagnostic morphology and geographically widespread distribution. The LO of the species was calibrated to the top of Chronozone C4An in Hole 519 (South Atlantic) by Poore et al. (1983). However, the most recent studies have calibrated it to the lower part of Subchronozone C3An.1n, yielding an age estimate of 6.0 Ma in ODP Hole 840 (Tongan Platform) (Chaproniere et al., 1994) and ODP Hole 806B in Ontong–Java Plateau equatorial west Pacific (*fide* Berggren et al., 1995), as well as Rio Grande Rise (Berggren, 1977). In Gulf of Mexico boreholes E66–73 and E68–136, the LO of *Gt. lenguaensis* is juxtaposed with the FO of *Gt. plesiotumida* within nannofossil Zone NN10 (Zhang et al., 1993; Aubry, 1993). In comparison with the age estimate given by Berggren et al. (1995), the LO found in my three locations is far below the LOC (Figs. 4-2, 4-4, 4-8 and 4-15) and below the FO of *Gt. margaritae*, while in Hole 547A it is found in the late Messinian above the FO of *Gt. margaritae*, showing a noticeable diachrony. In addition I also realized that the LO of this species in my material occurs in different chronozones, for instance, in C3Br in Salé borehole, C4n in Hole 552A, and C4r in Hole 608. At ODP Site 840 in the Pacific Ocean, this LO is found within the upper Chronozone C3An.1n (Chaproniere et al., 1994). However, Kennett and Srinivasan (1983) reported that it occurs in planktonic foraminiferal Zone 17A, which is similar to my observation. Nevertheless, my observation in this study

yields similar agreement with the identification of Zhang et al. (1993) in Gulf of Mexico and the observation in South Atlantic by Poore et al. (1983, 1984), where it was calibrated to C4ANy (~8.7 Ma). Although the LO may not be considered as a helpful bioevent in stratigraphic assignment due to possible diachrony (Fig. 4-2), it may provide a secondary criterion in determining the Messinian Stage.

Globorotalia conomiozea first occurs constantly in the middle Chronozone C3Br at my locations, except for the DSDP Hole 552A where it first occurs at the top of C3Br. As mentioned previously, Krijgsman et al. (1994) calibrated the FO of the species to Chronozone C3Br.1r in Crete of the Eastern Mediterranean with an astrochronologic age estimate of 7.1 Ma. The age of the FO adopted by Berggren et al. (1995) is 7.12 Ma, which is basically identical to the age estimate of Krijgsman et al. (1994). In terms of the occurrences of *Gt. conomiozea* in the North Atlantic and the Mediterranean region, I suggest that the FOs of the species are synchronous and can be used as critical markers of the T/M boundary, although the significance of global correlation is uncertain due to the delayed occurrence (6.05 Ma) in the southwest Pacific Ocean as reported by Roberts et al. (1994), and South Pacific Ocean reported by Hodell and Kennett (1986). However, Berggren has cautioned that the forms from the North Atlantic and South Pacific are probably not identical in morphology (pers comm., 1993). In addition, the LO of *Gt. conomiozea* is obviously diachronous as shown in Fig. 4-15. It ranges from the middle Chronozone C3An (Salé borehole) to the middle Gilbert (e.g., Site 608). I do not find other similar extinctions of *Gt. conomiozea* in DSDP Holes 552A and 608. The extinction in Salé borehole is about 0.23 m.y. earlier than that in Hole 552A, while in Hole 608 the LO is at the M/P boundary. *Gt. conomiozea* in Salé disappeared about 0.23 m.y. earlier than that in Hole 552A. Therefore, in stratigraphic point of view, it cannot be considered as a useful stratigraphic bioevent.

Globorotalia margaritae s.l. includes several subspecies i.e., *Gt. margaritae primitiva, Gt. praemargaritae, Gt. margaritae margaritae,* and *Gt. margaritae evoluta.* The

detailed *Gt. margaritae* phylogenetic lineage was discussed by Benson et al. (in press) and Cita (1973). This species was originally described from the upper Miocene, Las Hernandez, a local equivalent of Cubagua Formation, Venezuela (Bolli and Bermúdez, 1965). In this paper I will discuss the *Gt. margaritae margaritae (Gt. margaritae* s.s.) since this is considered to be the most important component in *margaritae* group in Messinian stratigraphic study. *Gt. margaritae* s.s. in my DSDP Hole 552A, 608 and Salé borehole first consistently occurs in Chronozone C3An.2n (Fig. 4-15), which coincides with that in ODP Hole 840 of Tong Platform (Chaproniere et al., 1994). No distinct diachrony has been detected. In Hole 547A, it is truncated by a hiatus which occurred in the lower Messinian, and thus certain attribution of age is not known (Fig. 4-15). The FO was also reported to occur in C3An.1r by Benson et al. (in preparation) in Bou Regreg, Morocco, which is slightly higher than my records. In the Mediterranean Sea, the FO of *Gt. margaritae* s.s. occurs in the lowermost part of the Gilbert reversal at DSDP Site 132, corresponding to the upper part of *Ceratolithus tricorniculatus* zone (Cita, 1973, 1976), and its total range zone was attributed to the lowermost Pliocene known as the Trubi Formation (Cita, 1975). Similarly, Langereis and Hilgen (1991) reported that the FO of the species in the Mediterranean Sea is immediately above the base of Zanclean in the middle of Thvera at 4.93 Ma. It is evident that the FO of the species shows a remarkable diachrony between the Mediterranean and open Atlantic Ocean. The lack of the species in the upper Messinian in the Mediterranean Sea could be related either to the limited Atlantic inflow into the Mediterranean basin or to the extremely constrained paleoenvironment during the Mediterranean Salinity Crisis, which probably has led to the salinity crisis in the Mediterranean. In addition, my records suggest that the FO of *Gt. margaritae* may serve as a zonal marker to define the middle C3An in the North Atlantic Ocean, and that the most recent calibration of the FO of the species to the middle of C3An.1r (~6.2 Ma) given by Berggren et al. (1995) is reasonable for the North Atlantic Ocean.

At my locations, I recognize that the FO of *Gt. puncticulata* is slightly earlier than that of *Gt. crassaformis*, in agreement with its original phylogenetic pattern (Fig. 4-15). I have not observed the first occurrence of *Gt. crassaformis* prior to *Gt. puncticulata,* or simultaneous first occurrences as reported by various workers (e.g., Keigwin, 1982; Thunell, 1981; Keller, 1978; Weaver and Clement, 1987; Scott, 1982; Hornibrook et al., 1989). I, therefore, suggest that this may serve as an important zonal bioevent in separating the subzones of the lowermost Pliocene Zone PL–1 in my study area, even if it is not global.

4.3. Summary

Four DSDP/ODP Holes (552A, 646B, 608, and 547A) from the North Atlantic Ocean and one land borehole from Morocco were studied for integrated bio-, magneto-, and stable isotope Messinian stratigraphic study with high resolution sampling. In general, my results show that the Tortonian/Messinian boundaries in all holes are well controlled with bio, magneto- and stable isotopic events, while the M/P boundary is relatively difficult to determine based on any single mean of chronological dating. Major conclusions are given as follows:

1) In Salé Borehole, Morocco, the Tortonian/Messinian boundary is located at 139.05 m (sample B72), mainly defined by the FO of *Globorotalia conomiozea*, with an age estimate of 7.12 Ma. The Pliocene/Messinian boundary is interpolated between S series samples S7 and S11 at ~10 m below surface just above the LO of *Gt. plesiotumida* . This is in agreement with that given by Hodell et al. (1994).

2) In DSDP Hole 552A, the Tortonian/Messinian boundary is defined on the FO of *Globorotalia conomiozea* s.s. at 150.16 msb in Chronozone C3Br. The Pliocene/Messinian boundary is interpolated based on several pieces of indirect evidence, namely 1) The FO of *Gt. puncticulata,* 2) TG14 oxygen isotope stage at 106 msb, and 3) Using my age– depth plot (Fig. 3).

3) In DSDP Hole 608, the Messinian/Pliocene boundary is placed at 138.6 msb within Core 15, mainly relying upon the LO of *Gt. conomiozea/miotumida* plexus and the marked $\delta^{18}O$ enrichment (TG14?). The Tortonian/Messinian boundary is placed at the FO of *Gt. conomiozea* within Core 20 at 184.88 msb. A small hiatus may be present within the Messinian (between Cores 18 and 17) as suggested by nannofossils, where a strong carbonate dissolution has taken place.

4) In DSDP Hole 547A, the condensed Messinian section is bracketed by the FO and LO of *Gt. conomiozea,* ranging from the middle of Core 8 to the top of Core 6. Three hiatuses are identified in this hole, one in the Messinian, which separates the upper Messinian from the upper Tortonian; and two in the Pliocene.

5) Neither the Tortonian/Messinian nor the Messinian/Pliocene boundaries in ODP Hole 646B can be easily assigned because of rare foraminifera markers and the downslope transportation during the Messinian Stage. The Tortonian/Messinian boundary is placed between Core 75X and 78, using $^{87}Sr/^{86}Sr$ age estimate, Chron 6 $\delta^{13}C$ shift at Core 75X, $\delta^{18}O$ enrichment in Core 77X, *Neogloboquadrina* coiling change from the dextral to sinistral, and the FO of *D. berggrenii* occurred in Core 76X.

The Messinian/Pliocene boundary is tentatively suggested between Cores 46X and 50X, based on the following observations: 1) The LO of *D. berggrenii* in Sample 49X-CC, 2) The Sr age of 5.37 Ma, 3) The interpolation of the FO of *G. margaritae* at 506.9 msb and FO of *G. puncticulata* at 383.08 msb; and 4) $\delta^{18}O$ depletion above Core 45X and $\delta^{18}O$ enrichment.

Diachrony and synchrony of some important Messinian planktonic foraminifera from these Atlantic DSDP/ODP holes and Salé borehole, such as the LO of *Gq. dehiscens* , the LO of *Gt. lenguaensis*, the FO and LO of Gt. *conomiozea* , the FO of *Gt. margaritae* s.s., the FO of *Gt. puncticulata* , and the FO of *Gt. crassaformis* are discussed for understanding some of the paleoceanographic changes. This stratigraphy now permits us to compare intra-Mediterranean paleoceanographic changes with those in the open Atlantic

Ocean to determine what effect the Mediterranean salinity crisis had on deep-water paleoceanography during the Messinian Stage.

CHAPTER 5

MESSINIAN DEEP-WATER TURBIDITES AND GLACIOEUSTATIC SEA-LEVEL CHANGES IN THE NORTH ATLANTIC: LINKAGE TO THE MEDITERRANEAN SALINITY CRISIS

5.1. Deep-water turbidite deposits

Deep water turbidites are characterized by marsh foraminifera and terrigenous deposits, and occur in 9 discrete layers throughout the Messinian and lower part of Pliocene at Site 646B (Fig. 5-1).

Pliocene turbidite cycle 1 (PTL 1) includes 5 samples (42X-1, 100-104 cm through 43X-2, 50-54 cm; 392 to 402.7 msb. Benthic foraminifera are relatively rare, dominated by small *Trochammina* cf. *squamata*, which ranges from 20% up to 53% of the total fauna. Calcareous foraminifera are small, thin-shelled, and filled with pyrite. This layer is composed of abundant mica, and very fine, grey silts or clay, with gypsum crystals. The sediments represent typical deltaic deposits formed in an organic-rich environment. A few deep-water species are present, (e.g., *Eponides weddellensis, Melonis barleeanum; Epistominella exigua*) at low percentages. These may have been mixed with the shallow water forms during the down-slope transport.

Layer 2 (i.e., Messinian turbidite cycle MTL 1) includes 7 samples (45X-CC, 20-24 cm to 48X-1, 110-114 cm; 420.7 to 450.2 msb). This layer is dominated *T.* cf. *squamata* (up to 55%) and *Ammotium* sp. A (up to ~5%). Oxidized plant fragments are common. Some highly rounded and polished quartz grains (>1 mm in diameter) and benthic foraminiferal shells occur at the base of the layer. All these indicate transport from a shallow organic rich paleoenvironment. *Eponides weddellensis and Melonis barleeanum* are found in low percentages in this interval.

Layer 3 (MTL 2) contains 5 samples (52X-CC, 20-24 cm to 55X-2, 80-84 cm; 489.62 to 518.8 msb). This interval is dominated by *Trochammina* cf. *squamata* (70% to 95%), and about 2% *Ammotium* sp. A. Calcareous foraminifera occur at less than 1%. In Sample 54X-1, 140-144 cm, we also found an oxidized, but well preserved plant seed (plate 1, fig. 17) and quartz grains (>1 mm in diameter). Oxidized grass/wood fragments are highly concentrated; these materials originated in a shallow water, organic rich paleoenvironment.

Layer 4 (MTL 3) includes 4 samples (57X-3, 40-44 cm, 57X-4, 22-26 cm, 57X-CC, 20-24, and 58X-1, 50-54 cm; 539.2 to 546 msb). This layer is dominated by *T.* cf. *squamata* (~51% in average and maximum 83.6%), with a deep-water agglutinated form *Rhizammina* spp. (varying from 4% to 27%) and a few deep-water calcareous benthic foraminifera such as *Eponides weddellensis* and *Melonis barleeanum.*

Layer 5 (MTL 4; 62X-2, 50-54 cm to 62X-3, 80-84 cm; 585.6 to 587.4 msb). *T.* cf. *squamata* is 66.8% in Sample 62X-2, 50-54 cm and 27.3% in sample 62X-3, 80-84 cm. *Ammotium* sp. A reaches 10% in the former sample. Deep-water agglutinated and calcareous species include *Rhizammina* spp., *Psammosphaera* spp., *Lagenammina* spp., *Eponides weddellensis, Melonis barleeanum, Eponides tumidulus*, etc. Oxidized plant fragments are present.

Layer 6 (MTL 5) occupies in entire Core 65X (613.3 to 622.05 msb), and is characterized by marsh foraminifera, *T.* cf. *squamata* and *Ammotium* sp. A, with a maximum value of ~94%, with rare calcareous benthic foraminifera such as *Eponides weddellensis, Melonis* spp., *Oridorsalis umbonatus, Eponides tumidulus, Epistominella exigua, Gyroidina soldani* etc. Oxidized plant fragments are common, and a large wood fragment (>1 cm long) occurs at the base of the layer.

Layer 7 (MTL 6) occurs in 3 samples in the lower part of Core 67X (67X-3, 40-44 cm, 67X-5, 50-54 cm, and 67X-6, 50-54 cm; from 635.2 msb to 639.8 msb). It is dominated by *T.* cf. *squamata* varying from 41 to 81%. *Rhizammina* spp. is rare (4% on average). A

deep-water *Trochammina* sp. is common (from 7-24%), and calcareous benthic foraminifera are rare. Oxidized plant fragments and gypsum crystals are present.

Layer 8 (MTL 7), from 661.55 msb to 682.71 msb, spans more than two cores (70X-CC, 20-24 cm to 72X-CC, 6-10 cm). Faunas are dominated by *T.* cf. *squamata*, with a maximum of 99%. *Ammotium* sp. A is rare, less than 1%. Wood fragments, oxidized grass/plant fragments and plant fruit (plate 1, fig. 16) are identified in this interval.

Layer 9 (MTL 8), from 703.8 msb to 734.1 msb, (Cores 74X to 77X). This layer is dominated by *T.* cf. *squamata*, which varies from 90% to 100%. Mica and oxidized grass/plant fragments are highly concentrated. Calcareous benthic and planktonic foraminifera are extremely rare.

Turbidites are usually recognized by graded bedding, sediment components, and tractional structures. Typical turbidite sequences are known as Bouma sequences, which consist of 5 divisions, A, B, C, D, and E, as function of grain size change from coarse (bottom) to fine (top). However, in the most cases, a complete Bouma sequence is not recorded, especially in distal sequences. From the micropaleontological point of view, all our turbidite layers are characterized by a well stratified two-layer structure, a mixed faunal layer below, with a marsh faunal layer capping the sequence (see Chapter 3), thus suggesting a turbidite origin with the various turbidite packages separated by hemipelagic sediments that have a strictly deep-water fauna. The deep-water faunal layer has *Eponides weddellensis, Melonis* spp., *Gyroidina soldani, Uvigerina* spp., *Globocassidulina subglobosa, Pullenia bulloides* etc., with extremely rare shallow water components; the mixed layer contains mainly deep-water fauna as given above, with lesser amounts of shallow water agglutinated forms such as *T.* cf. *squamata* and *Ammotium* sp. A., which may vary from 10% to 50%; and the marsh faunal assemblage is dominated by *T.* cf. *squamata* and *Ammotium* sp. A (60% to 100%). These repeated three-layer packages throughout the hole strongly suggest turbidite origin for the mixed and marsh foraminiferal layers. We suggest that the deep-water faunal layer is formed during high sea-level periods,

and the latter two are formed by down slope transportation from the subaerially exposed continental shelf edge off southwest Greenland, where the marsh foraminifera dwelled (Fig. 5-1). Chaotic lithological textures in the interval bracketed by reflectors R2 and R3/4 (lithological Unit 3, now known as an equivalent to the Messinian) were confirmed by acoustic signals of multichannel seismic reflections reported by Arthur et al. (1989; fig. 9 of p. 967), suggesting the presence of turbidites during Messinian time.

It is difficult to determine exactly how many turbidite flows in each layer based on the homogenous sedimentary structure, log data, faunal compositions, and the poor core recovery. The turbidite layers vary considerably in thickness (recovered thicknesses ranging from 1 m to 12 m). As distal phases of turbidites, their thicknesses suggest that each layer certainly contains numerous turbidite flows that formed during lower sea-level stands.

In ODP Site 646B, the typical Bouma sequence does not exist, because the sediment components are relatively homogenous, and mainly composed of clay (Srivastava et al., 1989a, pt. 1, p. 488, fig. 54; Srivastava et al., 1989b). In the layer 2, coarser sediments such as polished quartz grains and rounded, large shallow-water benthic foraminiferal shells occur at the base of the layer, while finer components at the top, indicating fining upwards. Younger turbidites (early Pliocene) at this site have parallel- and cross laminated siliciclastic silts, but those are attributed to traction transportation by vigorous bottom currents (contour currents) in the vicinity of Eirik Ridge (Hiscott et al., 1989).

Significant changes at Site 646 in texture of the Messinian section were observed and considered to be related to an intensification of deep-water currents (Cremer, 1989). Similar conclusions on the association with active deep-water circulation were also suggested by Kaminski et al. (1989) based on the presence of epibenthic suspension-feeders, *Rhizammina*, which strongly dominated in lithological Unit 3 (equivalent to the Messinian) at this site. Wolf (1991) also interpreted changes in benthic foraminifera from this site in terms of fluctuations in the intensity and composition of the Denmark Strait

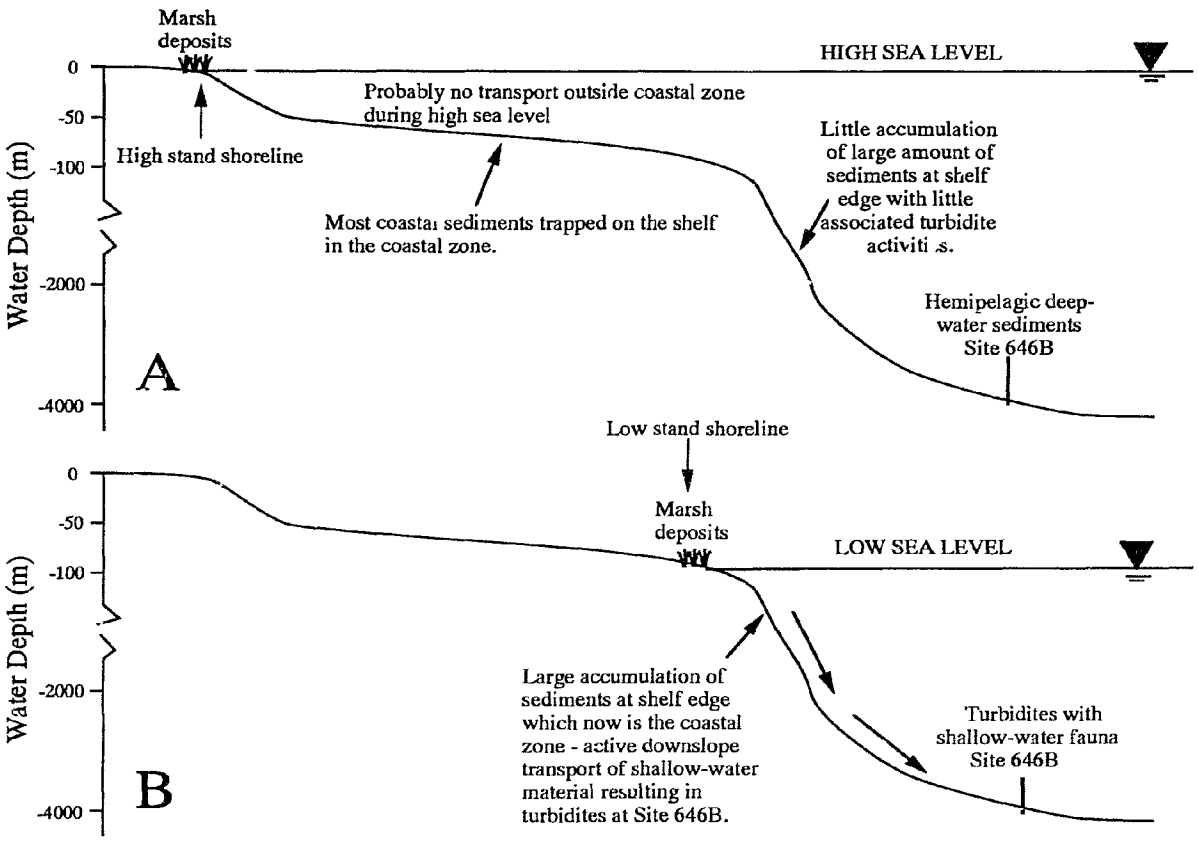

Fig. 5-1. Schematic diagram of southern Greenland margin with both high and low sea-level stands and suggested sediment mechanisms for deep-sea turbidites at ODP Site 646B. A=high sea-level stand, and B=low sea-level stand.

Overflow. Suspension feeding communities require gentle bottom currents to bring them food, and they may be common in the area of contour currents (Schröder, 1986). However, when currents are too strong, these epifaunal tubular forms will be the first to be transported (Kaminski et al., 1988a). Concentrations of these forms (*Rhizammina*) also occur in laminated fine grained turbidites (Kaminski et al., 1988a). Our benthic foraminiferal data show that *Rhizammina* is concentrated in mixed faunal layers, rather than in deep-water faunal layers which presumably formed in relatively stable environments during high sea-level stands. Scott et al. (1989) saw similar sequences in the Quaternary of Baffin Bay (site surveys for ODP Leg 105, Site 645), where there were turbidite layers, hemipelagic and then a layer of sediments with only *Rhizammina algaeformis* linings - this sequence repeated several times. The turbidites did not have marsh foraminifera however because the Quaternary turbidites were fed by glacial debris, not slumping of coastal deposits as we see at Site 646B in the Messinian. Thus we suggest the *Rhizammina* assemblage to be more likely an association with some down-slope sediment transportation controlled by sea-level fluctuations through the submarine channel in the southwest of Greenland (Arthur et al., 1989). This transportation may provide sufficient food for the suspension feeders. We speculate that at Site 646B, the deep-water circulation may play a less important role in the occurrence of *Rhizammina* - the tubular forms which appear to characterize disturbed sites, but display a poor ability to quickly recolonise substrate (Kaminski et al., 1988b).

5.2. Correlation between turbidite layers and glacioeustatic sea-level fluctuations

Maybe one of the most important aspects of the turbidites at Site 646B is their origin and the implication for sea level during the late Miocene. The foraminifera occurring in these turbidite layers are salt marsh foraminifera which have been demonstrated to have an extremely narrow range vertically (±10 cm) with respect to sea level, and thus provide the

most accurate means of relocating ancient sea level when found "in situ" (Scott and Medioli, 1978, 1980, 1986). During high stands of sea level, carbon (and sediments) are trapped on the continental shelves and the coastal zone is remote to the shelf edge (Fig. 5-1) if we assume a continental margin configuration for Greenland during the Messinian is similar to the present. Hence to have marginal marine foraminiferal fauna in turbidites, sea level must have been 80-100 m lower to expose the shelf edge, to allow salt marsh formation near the edge (Scott and Medioli, 1986). If sea level fluctuated between the present shoreline and the outer shelf as it does now off southern Greenland, then the presence of the marsh foraminifera in deep-sea turbidites during sea-level low stands suggests the amplitude of sea-level change to have been about 80-100 m. Although clearly the sea level was not at the present Quaternary shoreline in the Miocene, it is reasonable to assume there was a continental shelf in the Miocene with a similar morphology (i.e., wide platform) which when emerged rapidly would have had coastal deposits at the edge of the shelf with an 80-100 m sea-level lowering. This is why we think these data provide such an accurate measure of sea-level amplitude. In a similar setting in the Indian Ocean (ODP Leg 116, Site 717), there were many terrestrial plant fragments and some shallow water foraminifera, but never as many as at Site 646B (Scott and Leger, 1990) because sea level was probably not at the shelf edge at that location.

To understand the cause of the deep-water turbidite layers at Site 646B, we compare them with the oxygen isotopes of *Globigerina bulloides*, a surface water dweller, from DSDP Site 552A where a complete, high-resolution oxygen isotope record for the Messinian interval has been obtained (Keigwin, 1987). A smoothed $\delta^{18}O$ curve from the curve with three-point running average is plotted in Fig. 5-2 against the turbidite layers from ODP Site 646B. This smoothed curve displays nine major episodes of $\delta^{18}O$ enrichment (Fig. 5-2), which may correspond to the deep-water turbidite layers. Positive $\delta^{18}O$ excursions are proxies of cooling and sea-level lowering resulting from increase in

Fig. 5-2. Correlation between the deep-water turbidite layers in Site 646B and oxygen stable isotope enrichment excursions in DSDP Site 552A. Oxygen stable isotopes from *Globigerina bulloides* were done by Keigwin (1987). Smoothed $\delta^{18}O$ cycles were obtained from three-point running average curve given by Keigwin (1987). MTL = Messinian turbidite layers. See figure 2 for legends of lithologic section, ODP Site 646B.

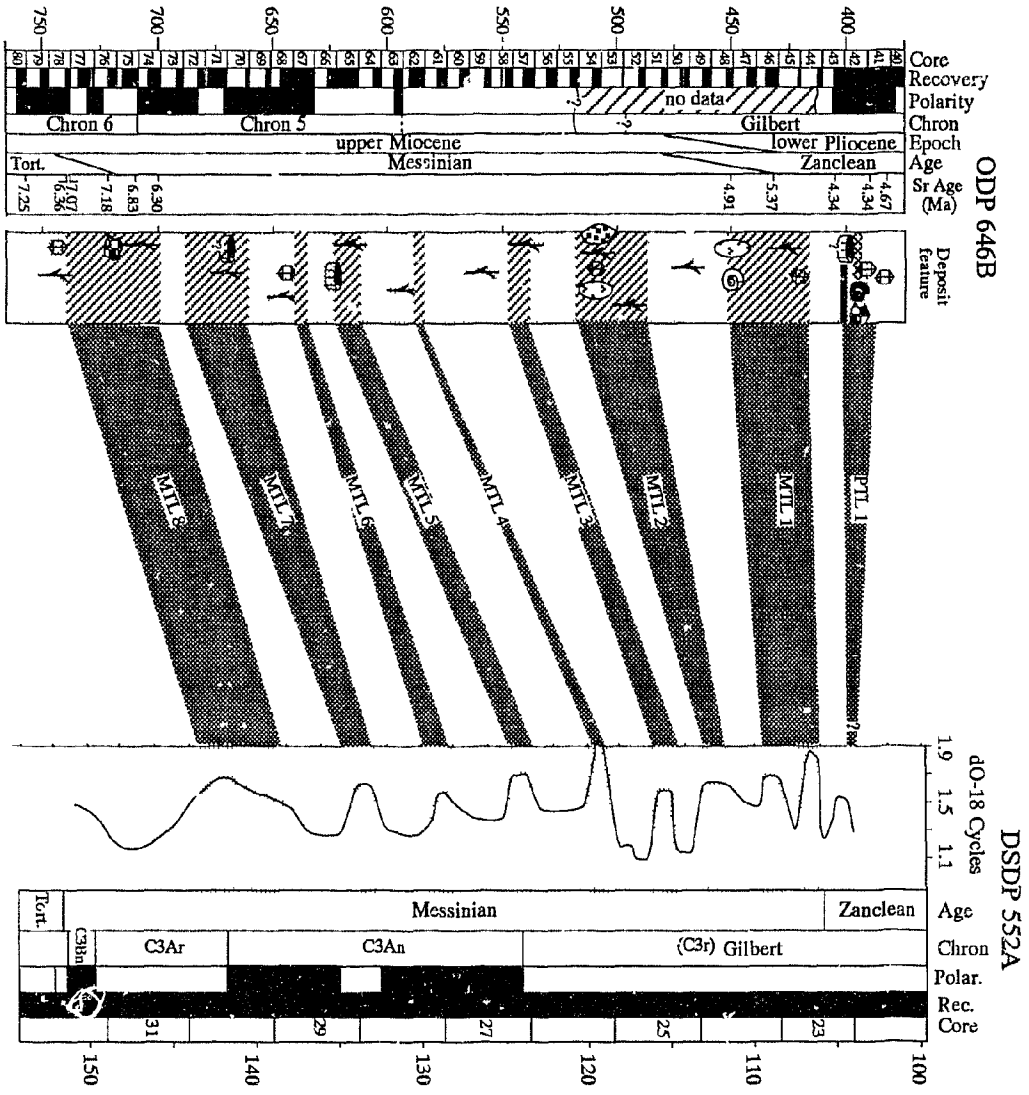
Depth (meters subbottom)
Core
Recovery
Polarity
Chron
Epoch
Age
Sr Age (Ma)
Deposit feature
ODP 646B
no data
Chron 6
Chron 5
Gilbert
upper Miocene
lower Pliocene
Tort.
Messinian
Zanclean
MTL 8
MTL 7
MTL 6
MTL 5
MTL 4
MTL 3
MTL 2
MTL 1
PTL 1
dO-18 Cycles
DSDP 552A
Tort.
Messinian
Zanclean
Age
C3Ar
C3An
(C3r) Gilbert
Chron
Polar.
Rec.
Core
Subbottom Depth (m) Site 552A

the size of polar ice caps, which is in concert with the turbidite origin of an exposed Greenland shelf.

Using the late Quaternary $\delta^{18}O$ sea level calibration (0.11‰ $\delta^{18}O$ per 10 m of sea-level change (Fairbanks and Matthews, 1978; Miller et al., 1987), Keigwin (1987) suggested that a 0.6‰ benthic foraminiferal positive shift oxygen isotopes may correspond to 55 m sea-level lowering in the latest Miocene. He noted that this is a minimum estimate, because the unsmoothed $\delta^{18}O$ data show a 0.75 amplitude for the 5.55 Ma glacial event (4.8 Ma event of Keigwin, 1987), which would yield 68 m sea-level lowering. The amplitudes of other enriched benthic $\delta^{18}O$ peaks at Site 552A vary from 4-5.5‰ (Keigwin, 1987), suggesting 36-50 m sea-level lowerings. Similar estimates of late Miocene global sea-level lowering (40-70 m) were derived in southern Spain (Berggren and Haq, 1976), New Zealand (Kennett, 1967b; Roberts et al., 1994), Australia (Carter, 1978), Pacific islands (Adams et al., 1979), Atlantic coastal plain of North America (Adams et al., 1977), Mediterranean region (Hsü et al., 1973a, b; Cita and Ryan, 1979; McKenzie et al., 1979; Müller and Hsü, 1987; Kastens and Mascle, 1990). Aharon et al. (1993) suggest a sea-level change of 10 m amplitude at the beginning of the Messinian, terminating in a large sea-level fall of at least 30 m near the Miocene/Pliocene boundary for Niue (South Pacific Ocean), rather different from these mentioned above. We consider that the amplitudes in Niue may have been coupled with co-variation of tectonic uplifting and glacioeustatic fluctuations because Niue is located in active tectonic region (Cole and Lew , 1981; Lincoln and Schlanger, 1987). This, however, remains uncertain because limited available tectonic data from this area (Dubois et al., 1975) suggest a recent (Holocene) uplifting. Much evidence on ice volume growth at this time has been discovered worldwide both from land and ocean (Mercer and Sutter, 1982; Shackleton and Kennett, 1975; Loutit and Kennett, 1979; Keigwin, 1987; Hayes et al., 1975; Denton and Armstrong, 1969; Bandy et al., 1969; McDougall et al., 1976; Clark et al., 1980; ODP Leg 151 Shipboard Scientists,

1994; Hodell et al., 1986; Hodell et al., 1994b; Kemp et al., 1975; Ciesielski et al., 1982; Pomar and Ward, 1994).

Based on the marsh foraminifera at Site 646B, we suggest a substantially greater sea-level lowering from Site 646B data (80-100m), which is more of a direct measurement based on certain assumptions (see Fig. 5-1). The sea-level changes during the Messinian, unlike in any other periods of the Cenozoic, may have been controlled not only by ice volume changes, but also by the repeated Mediterranean desiccation cycles. Atlantic water refilling into the Mediterranean Sea with an amount of 3.614×10^{15} m^3 could yield a global instantaneous sea-level lowering of about 10 m, according to the calculation of Hsü et al. (1977) and Müller and Mueller (1991), while a water transfer from the Mediterranean to global ocean area of 3.6×10^{14} m^2 could cause about 10 m sea-level rise, and would be incorporated into the sea-level changes if a complete Mediterranean desiccation had taken place. Based on these considerations, we suggest that 80 m global sea-level lowering at least at 5.55 and 5.75 Ma is quite reasonable. It is obvious that there is an about 30 m difference in amplitude of sea-level changes between the estimates from marsh foraminifera at Site 646 and from $\delta^{18}O$ values at Site 552. The difference may be attributed to: 1) underestimate of amplitudes of Messinian $\delta^{18}O$ sea-level lowering because of water vapor evaporated from the Mediterranean Sea with lower $\delta^{18}O$ returning to the open ocean. This would result in a lower $\delta^{18}O$ value in the open ocean, and possibly the cancellation of part of the ice volume signal; 2) tectonic difference from region to region; and 3) increasing area and altitude of growing ice sheets which lead to lower mean ice sheet $\delta^{18}O$ values (*Miller et al.,* 1987). In this paper, we cannot assess the exact amplitudes of the global sea-level fluctuations during the Messinian, but only those off Greenland. Sea-level fluctuations show great differences between regions, even in the Holocene (Pirazzoli, 1991).

Accurate chronology of the deep-water turbidites cannot be determined directly from our intra-Messinian stratigraphic data of ODP Site 646. The paleomagnetic data are not sufficiently reliable for precise dating because this interval proved less than satisfactory for

magnetostratigraphic study due to poor recovery and drilling disturbance (Clement et al., 1989). However, if we assume the turbidites formed during climatic lowering of sea level, chronology of the turbidites can be suggested from our DSDP Site 552 depth-age plot (Fig. 5-3), which indicates the climatic cycles from the smoothed $\delta^{18}O$ curve climax at 6.59, 6.22, 6.01, 5.89, 5.75, 5.7, 5.65, 5.60, 5.55, and 4.6 Ma, respectively, coeval with climate cooling (ice-volume) intervals. It should be pointed out that our calibrations cannot be correlated with 100k eccentricity from Site 552A given by Beaufort and Aubry (1990). Because of the poor age control for the lower Gilbert paleomagnetic chron, we prefer the age estimates derived from the age-depth plot, rather than time series analysis. The nine oxygen excursions and deep-water turbidite layers could be coeval with eight unconformities in the Niue coral atoll east of Tonga Trench, South Pacific (Aharon et al, 1993), which were formed during low sea-level stands during Messinian time. However, it is rather difficult to make detailed correlation between Site 646B turbidite layers and sea-level cycles from Niue of the Pacific Ocean (Aharon et al., 1993) because they used 6.2 Ma as the Tortonian/Messinian boundary (Berggren et al., 1985) and had poor stratigraphic control. At Site 646B, PTL 1 may be related to the early Pliocene glaciation at 4.6 Ma (Burckle, 1995).

5.3. Turbidite layers and sea-level changes linked to the Messinian Salinity Crisis (5.9-5.32 Ma)

The Messinian sequence in the Mediterranean Basin is basically composed of five major successions, i.e.: Tripoli marine formation, *Caliza Tosca* shallow-water deposits, Lower Evaporite, Upper Evaporite, and a thin layer of *Lago Mare* deposits (fresh/brackish water deposits) that capped the sequence. Hsü et al. (1973a, b), in their early work, claimed that to form a thickness of 2,000-3,000 m evaporites in the Mediterranean Sea, at least 11-13 inundations would be required if all salts were deposited in the center of the Mediterranean basin; or up to 100 inundations would be necessary if the salts were deposited evenly on

Fig. 5-3. Chronology of episodic climatic cycles from DSDP Site 552A established mainly for tentative age estimates of Messinian turbidite layers at Site 646B. The depth-age plot is originally from Chapter 4 of this thesis. MOIE = Messinian oxygen isotope enrichment. Paleomagnetic and oxygen stable isotope data are from Keigwin (1987).

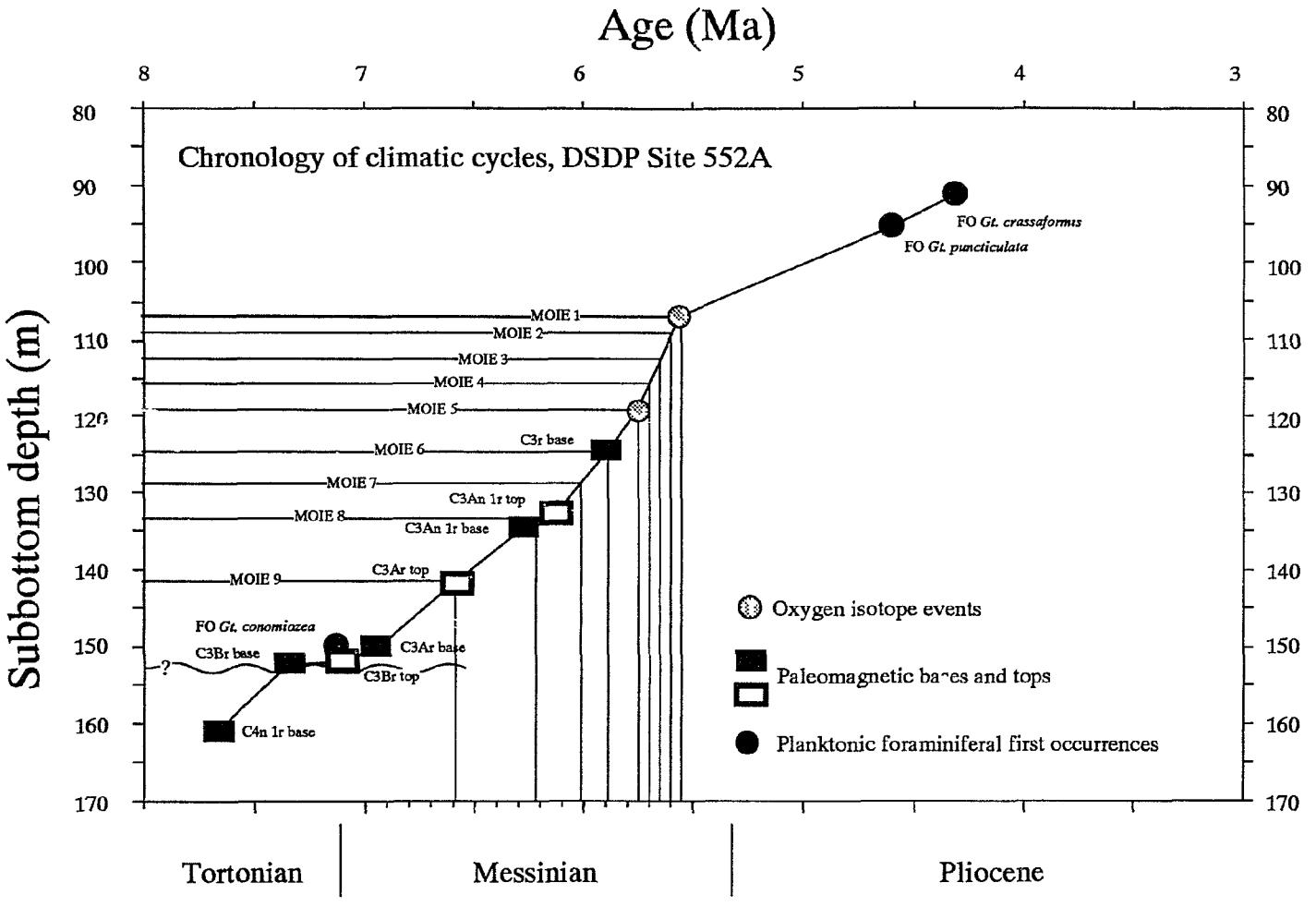
Age (Ma)
8
7
6
5
4
3
Chronology of climatic cycles, DSDP Site 552A
Subbottom depth (m)
80
90
100
110
120
130
140
150
160
170
FO Gt. crassaformis
FO Gt. puncticulata
MOIE 1
MOIE 2
MOIE 3
MOIE 4
MOIE 5
MOIE 6
MOIE 7
MOIE 8
MOIE 9
C3r base
C3An 1r top
C3An 1r base
C3Ar top
C3Ar base
C3Br top
C3Br base
FO Gt. conomiozea
C4n 1r base
?
Oxygen isotope events
Paleomagnetic bases and tops
Planktonic foraminiferal first occurrences
Tortonian
Messinian
Pliocene

the basin floor. Benson and Rakic-El Bied (1991) suggested 7-8 inundations, which is even less than Hsü 's later suggestion (8-10 inundations; fide Benson and Rakic-El Bied (1991)). These speculations greatly stimulated scientists to find connections between the isotope records in deep-sea marine sediments and the Mediterranean Messinian Salinity Crisis. So far, these have not been easily proven. Some authors remarked that two oxygen isotopic enrichment events may have corresponded to the Salinity Crisis; one in the youngest Chron 5 and the other in the earliest Gilbert, which have been linked to the formation of the Lower and Upper Evaporites in the Mediterranean Basin. (McKenzie and Oberhänsli, 1985; Hodell et al., 1986; Cita and McKenzie, 1986; Müller and Hsü, 1987; Keigwin, 1987; Chapter 7 of this thesis). Recently, the Messinian Salinity Crisis was correlated to eustatic changes indicated by eight unconformities from Niue coral atoll, South Pacific Ocean (Aharon et al., 1993), but this requires further age re-calibration for each unconformity.

Six oxygen enrichment excursions in the interval between 5.9 and 5.32 Ma are recognized (Fig. 5-2), indicating more frequent climatic changes at this time than during the early Messinian (from 7.12 to 5.8 Ma). This interval is equivalent to the Messinian Salinity Crisis, caused by either limited Atlantic inflow or isolation of the Mediterranean from the Atlantic Ocean near 5.9 Ma suggested by Berggren et al. (1995) (Note: Gautier et al. (1994) suggest a slightly later time, *i.e.,* 5.8 Ma). The sea-level lowerings that led to the turbidite formation might also have contributed to the repeated isolation of the Mediterranean Basin during the late Messinian, although there are not as many as 11-13 inundations (Hsü et al., 1973a, b), or 7-8 suggested by Benson and Rakic-El Bied (1991). We cannot expect the exact number of inundations in the Mediterranean to be recorded in deep water turbidites suggested by Hsü et al. (1973a, b) or by Benson and Rakic-El Bied (1991), because of complicated geological/hydrological processes of deep-water turbidites, and poor preservation and/or core recovery at Site 646B where part of the turbidite record could have been missing or not sampled.

5.4. Summary

Our benthic foraminiferal data clearly indicate that eight layers (MTL 1-8) of deep-water turbidites during the Messinian and one in the early Pliocene (PTL 1) formed at Site 646B (water depth 3461.3 m). These deep-water turbidite layers are characterized by high contents of agglutinated marsh benthic foraminifera (e.g., *Trochammina* cf. *squamata*, *Ammotium* sp. A, *Miliammina fusca*), rounded quartz, polished thick-shelled benthic foraminifera, wood fragments, plant seeds, fruits, and highly concentrated mica, and are interbedded with sediments containing hemipelagic deep-water benthic faunas. These turbidites may be attributed to the distal turbidite facies because of the relatively homogenous clay components. A chronology for these deep-water turbidites have been tentatively correlated to the heavy $\delta^{18}O$ excursions at DSDP Site 552. The turbidite layers are dated at 6.59, 6.22, 6.01, 5.89, 5.75, 5.70, 5.65, 5.60, 5.55, and 4.6 Ma. The turbidites originated from intertidal deposits as indicated by their foraminiferal content, and they are the best direct measurement to define the amplitudes of sea-level lowering of 80-100 m during the Messinian. Sea-level falls could have been caused by increased polar ice volume, or/and by water transfer between the Mediterranean Sea and the Atlantic Ocean in the Messinian.

Our evidence suggests that the six deep-water turbidite layers during the late Messinian from ODP Site 646B and oxygen isotope excursions from DSDP Site 552A may be correlated to the Mediterranean Lower and Upper evaporites, which might have formed if sea level lowered sufficiently to isolate partially or totally the Mediterranean Basin. The most profound climate changes occurred at 5.75 and 5.55 Ma, when the major bodies of the Lower and Upper evaporites were formed. It is evident that the formation of Mediterranean evaporites has had a close affiliation with severe climate fluctuation during the Messinian.

CHAPTER 6

PALEOCEANOGRAPHY, PALEOTECTONISM AND GLACIOEUSTATIC SEA-LEVEL: BENTHIC FORAMINIFERAL AND STABLE ISOTOPIC EVIDENCE FROM NORTHWESTERN MOROCCO

6.1. Paleoecology, Paleobathymetry and Chron 5 Events

To discuss the water exchange between the Mediterranean and the Atlantic, it is essential to understand the paleo-bathymetric variations in Morocco throughout the Messinian. This section provides relative paleobathymetric estimates based on benthic foraminifera in Salé core although it is well understood that most deep-water benthic species are associated with water mass changes. Table 6-1 lists some important benthic foraminifera from living and dead fauna off northwest Africa (Lutze, 1980), off Portugal (Seiler, 1975), the Gulf of Mexico (Phleger, 1951), as well as the northeastern Gulf of Mexico (Katz and Miller, 1993) for a comparison of depth habitats. The benthic foraminifera from the Gulf of Mexico (Phleger, 1951), together with the others, form a primary base for estimates of paleobathymetry of the Miocene–Pliocene benthic foraminifera in the Guadalquivir Basin, southwest Spain (Berggren and Haq, 1976; Berggren et al., 1976; and Van Couvering et al., 1976). The benthic foraminifera from northwest Africa and Portugal may provide the best comparison relative to those from other areas because of its close geographic location and the size fraction (>63μm), which is the same as used in this study. However it is somewhat difficult for the comparison because of the difference of species compositions between the late Miocene and the Recent. This difference is probably due to different climate, water mass patterns, or possible evolutionary turnovers of benthic foraminifera during these two time intervals.

To make better estimates of the paleobathymetry, five groupings of the Salé benthic faunas are given based on the living foraminiferal depth ranges of Lutze (1980) in

Table 6-1. Comparison of water depth ranges of major bathyal benthic foraminifera from world continental slopes. L=living, D=dead, mx=maximum. 63μm size fraction are used by Lutze (1980), Phleger (1951), and Seiler (1975); 150μm is used by Katz and Miller, 1993. Depths are in meters. Note that most species in the table have different depth ranges from place to place, which may indicate a close association with water masses, rather than with water depth alone.

Table 6-1

	NW Africa (Lutze, 1980)		Gulf of Mexico (Phleger, 1951)		NE Gulf of Mexico (Katz and Miller, 1993)	Off K. Sines, Portugal (Seiler, 1975)	
	L	D	L	D	D	L	D
G. subglobosa	100–800 mx 500	100–300 mx 500–700	100–1000	80–2000 mx=1300	600–1500 mx ~600	150–4000 mx ~600	150–4000
C. reniforme	60–3000 mx ~2000	100–2000 mx 500–700					
Rosalina	100		200–400	200–600		150	
E. exigua	500–3500	700–4000		200–1400			
C. oblongus	20–500 mx 40		30–120 mx 70–100	30–200			
C mundulus					mx 600–700		
A beccarii			20–50				
G. prageri	200–400						
O. umbonatus	1000–4000	1000–3000		90–500			
D. bertheloti				30–200			
Gyroidina spp.					500–1500	400–4000	150–4000
P. bulloides					500–1500	900–	500–1700
B. mex/costata	1300–3000	1000–3000		200–1700	upper bathyal		
U. mexicana				100–600	upper bathyal		
U. peregrina	800–3000 mx 1700	100–3000 mx 500–800	100–1500	100–1600 mx 300–1300		150–2000	150–2000
T. angulosa	64–800	100–1500				400–600	400–1700
B. lowmani			15–1000	40–1200 mx 600–700			
B pseuoplicata	500–4000 mx 200–300	100–3000 mx 300					400–4000
B albatrossi			~1000	300–1300 mx 600–1000			
B alazaensis	300–1300	1000–3000		200–1300		900	900–2000
T bradyi	500–1300	200–700				400–600	400–1700
C. lobatulus	60–500						
small *Bolivina*		60–1000 (>10%)					

northwest Africa and of Seiler (1975) in Portugal:

Group 1 (water depth <100m) includes *Ammonia beccarii and Rosalina sp.*, which are rare in abundance. Other shelf species reported in NW Africa (Lutze, 1980, p. 60), such as *Elphidium advenum, E. cripsum, Trochammina advena, Bulimina marginata, Patellina corrugata, Uvigerina bononiensis*, etc., are not seen in Salé samples. Diversity of the shelf fauna is very low in the Salé section relative to that reported by Lutze (1980). I consider that *Ammonia beccarii and Rosalina sp.* in the Salé section could be related to down–slope transportation from shelf to slope;

Group 2 (20–500m) contains species such as *Gavelinopsis praegeri, Cibicides lobatulus, Cancris sp.A Trifarina angulosa, Bolivina pseudoplicata, Cassidulina laevigata,* numerous small bolivinids etc. This group becomes common both in abundance and diversity in upper section of the sale core;

Group 3 (500–1,000m) includes *Planulina ariminensis, Trifarina bradyi, Uvigerina hispida, Bulimina aculeata,and* small bolivinids;

Group 4 (500–3,000m) comprises *Uvigerina peregrina, Epistominella exigua, Bulimina mexicana, Sphaeroidina bulloides, Oridorsalis umbonatus, Cibicidoides mundulus, Bulimina alazaensis, and Eponides polius.* Some species in this group may extend down to 3,000m in lower proportion. This group together with Group 3 dominates throughout the Salé section; and

Group 5 is represented by *Globocassidulina subglobosa* and *Cassidulina reniforme*, which has a broad depth range from 20m to 3,000m off northwest Africa.

Other dominant or major species in the Salé section, such as *Bolivina lowmani* and *Discorbinella bertheloti,* are considered to be upper bathyal species, while *B. albatrossi* is commonly observed in middle bathyal zone (600–1,000m). These determinations are based on occurrences in the Gulf of Mexico reported by Phleger (1951) and Katz and Miller (1993) (Table 6-1) although there is no direct comparison with those off northwest Africa.

Living species dwelling below 1000m off northwest Africa are not often observed in the Salé section (see Lutze, 1980, p. 64 and 65).

In addition, planktonic/benthic (P/B) foraminiferal ratios can be considered as an indicator of paleodepth or proximity to the open oceans, as they are a function of open water conditions (Murray, 1973, Murray, 1976, Wang et al., 1988). The higher values indicate greater depth, and lower ones suggest shallower environment or less open ocean influence. In the Gulf of Mexico, Celtic Sea, Persian Gulf, and Andaman Sea, planktonic foraminifera make up between 40–70% in outer shelf, and >70% on slope (Murray, 1976). In the Guadalquivir Basin, SW Spain, P/B ratios were 5:1 and 10:1 in the bathyal zone (Berggren and Haq, 1976).

Based on these criteria, I subdivide the benthic foraminifera of the Salé section into three major stages reflecting significant changes of paleobathymetry during the upper Tortonian and Messinian:

Stage 1 (interval between 163m and 173m; equivalent to paleomagnetic Subchronozone C4r; upper Tortonian): This stage is considered to be the upper bathyal, probably shallower than 500m. It is characterized by high total number of benthic foraminifera (20,000–40,000 specimens per cc) and high percentage of benthic fauna (Fig. 3-1). Benthic foraminifera are dominated by cassidulinids (20–40%), *Trifarina angulosa* (5–10%), and small bolivinids (18–27%). The base of the borehole is suggested to be littoral (R.H. Benson, pers. comm., 1995).

Stage 2 (interval between 163–90m from the uppermost Tortonian to early late Messinian; C4n to Subchronozone C3An.1n; = upper Chron 5): It is suggested to be a middle bathyal environment with a paleodepth of 600–800m, indicating sudden subsidence of Morocco during the early Messinian. The benthic fauna is characterized by Groups 3–5 and some other deeper water species, e. g., *Eponides weddellensis* (18%), *Bolivina albatrossi* (~10%), *Stilostomella* spp., *Heronallenia crosbyi, Bolivina* cf. *pygmaea, Cibicidoides bradyi, Karreriella bradyi* mainly occur in this interval, while shallow–water

species are extremely rare. *Bolivina inflata*, dominant in Pliocene sediments in Hole 547A (present water depth 3,938m), is common (10–20%) in this interval (see Chapter 3). Down–slope transportation may have occasionally occurred, and is recognized by the presence of shallow water species. Abundance of the benthic foraminifera is low (<5000 per cc) and planktonic foraminifera make up 80-90%, indicating a middle bathyal paleoenvironment. Paleodepth estimates is about 600–1000m in Guadalquivir Basin, Spain (Berggren and Haq, 1976). The paleodepth estimates of 600–800m at Bou Regreg (Gharb Basin) in Morocco were based on changes in light sensitive ocular tubercles of ostracodes and benthic foraminifera (Benson et al., 1991). Benson et al. (1991) further suggested that the Salé section, farther downslope into the Gharb Basin, to be probably about 100m deeper; this estimate is in agreemen with mine.

Stage 3 (90m to the top of the section; equivalent to the uppermost Subchronozone C3An.1n and C3r). This stage is characterized by fauna Group 2 and other upper bathyal species, such as *Bolivina lowmani,* and *Epistominella* cf. *takayanagii.* Abundance of the benthic foraminifera and benthic/planktonic foraminiferal ratios increase significantly, although frequent oscillations have occurred. Deeper water species are sharply decreased or disappear, while shallow water species, such as *Rosalina spp., Sigmavirgulina spp., Ammonia beccarii, Bolivina dialata, Elphidium spp.,* and *Florilus spp.,* occur more frequently than in Stage 2. But it does not exhibit a typical outshelf benthic foraminiferal characters. At the top of the section, planktonic foraminifera make up over 50%, and according to the recent distribution of planktonic foraminifera, percentages less than 70% usually occur on the outer shelf (Murray, 1976; Wang et al., 1988). In the Messinian deposits in Guadalquivir Basin, SW Spain, upper bathyal deposits (~200m) contain 30% planktonic foraminifera (Berggren and Haq, 1976). If this is applicable to Moroccan Messinian deposits, 50% planktonic values may suggest the upper limit of the paleodepths for the Salé section possibly deeper than 200m, although it may be associated with the width of continental shelf. In any case, all these data suggest an upper bathyal environment

durir.g the late Messinian. I suggest that the paleodepths vary from 300–500m in this stage. This upper limit is higher than that of Buzas who suggests 600–800m for the whole section (*fide* Benson, personal written communication). It appears that Morocco was uplifted abruptly after being deep for about 2 million years.

This benthic faunal turnover, along with a number of coiling changes of *Neogloboquadrina acostaensis* and extinction of *Globorotalia conomiozea* during C3An (Chron 5) (see Chapter 4, this thesis) in this borehole is probably caused by the rapid tectonic uplifting. It not only caused the disconnection between the Mediterranean Sea and open ocean, but also the Mediterranean sea–water evaporation and local/regional climate warming as revealed by oxygen isotopes (Hodell et al., 1994) and by megafloras in Mediterranean region (Gregor, 1995) (see below for more details).

6.2. Paleotectonism

The principle of the method to calculate the vertical movement was provided by Bandy and Arnal (1976), and can be achieved by determining the interrelation of water depth changes and sediment thickness from one stage to the next. Four types of bathymetric changes associated with paleotectonism and their calculations were described by Bandy and Arnal (1960): 1) If the depth of the water is indicated by facies at the end of the preceding stage, the amount of deepening is added to the sedimentary thickness to obtain the total subsidence; 2) If no change of the depth (facies) occurs between the end of the stage and the end of the preceding stage, the amount of subsidence is the same as the thickness of the section; 3) If the depth indicated by the facies at the end of one stage is less than the depth suggested at the end of the preceding stage, the amount of shoaling is then subtracted from the sedimentary thickness to obtain the subsidence figure; and 4) If, in the last case, the amount of shoaling indicated is in excess of the sedimentary thickness, the excess of shoaling represents the approximate uplift. The paleotectonism for the Salé section can be calculated using this simple method.

Table 6-2. Estimates of paleotectonism of the Salé section in Morocco during the late Tortonian and Messinian, using the method of Bandy and Arnal (1960). A net subsidence of ~310m is estimated for the interval between 173 and 163m during the late Tortonian. A net uplift of ~273m is estimated during the early Messinian between 163m and 99m. Another net uplift of 287m is calculated between 99m and 3m. Depth (m) refers to the stratigraphic level to the base of the Salé section; Thickness (m) refers to the thickness between two stratigraphic levels in the Salé section; Depth (m) in middle column (Bathymetry column) refers to the estimated water depths in meters indicated by benthic foraminiferal bathymetric ranges in the Salé section.

Table 6-2

Stratigraphic thickness			Bathymetry		Paleotectonism	
Samples	Depth (m)	Thickness (m)	Depth (m)	Shoaling (–) Deepening (+)	Uplifting (+ in m.)	Subsidence (– in m.)
S2	3		~400			
		87		~200 (–)	~ +287	
B25	99		~600			
		73		~200 (–)	~ +273	
B95	163		~ 800			
		10		~300 (+)		~ –310
B104	173		~500			

Table 6–2 shows the estimates of paleotectonic vertical movement in Salé, Morocco during the late Tortonian and Messinian. A significant increase in water depth suggests a net subsidence of about 310m during the late Tortonian. A total net uplift of about 560m has occurred during the period of ~0.7 m.y. from 6 Ma to 5.32 Ma, indicating a rapid tectonic uplifting. According to the benthic foraminiferal records, northeastern Morocco become land and never subsided below sea level after ~5 Ma (the earliest Pliocene).

The Rifian Corridor in Morocco and Betic Passage in Spain were probably the only paleo– channels to have linked the Mediterranean Sea and the open ocean during the Messinian Stage, and were recognized as the basis of the "twin–channel" model of (Benson et al., 1991). However, the benthic foraminifera from the Guadalquivir Basin reveal that the paleotectonism in that area is somewhat different from that in Morocco. In SW Spain, paleotectonism may have been more complicated. The current revision of the stratigraphy of the Andalusian stratotype in western Guadalquivir Basin (Sierro et al., 1993; Benson and Rakic–El Bied, 1991b) is based on the stratigraphic framework by Berggren and Haq (1976), Berggren et al. (1976), and Van Couvering et al. (1976). It shows that within the Messinian, the Betic passage in SW Spain underwent deepening (latest Tortonian and early Messinian) ⇒ shoaling ("early late Messinian", i.e., "*Caliza Tosca* deposits") ⇒ deepening (late Messinian; Green Marl deposits), while the Rifian Corridor in northern Morocco underwent deepening (latest Tortonian and early Messinian) ⇒ shoaling (early late Messinian) ⇒ further shoaling (late Messinian). It is evident that the pattern of bathymetric changes in SW Spain is different from that in Morocco during the early late Messinian. The distinct "re–subsidence" that occurred in SW Spain after the *Caliza Tosca* is not observed in the Rifian Corridor in Morocco.

The *Caliza Tosca* deposits were reportedly as shallow as 30m, suggesting a neritic paleoenvironment (Berggren and Haq, 1976; Benson et al., in press), and they were considered to have been predominantly associated with the global sea–level lowering (Berggren and Haq, 1976). Stratigraphically, the *Caliza Tosca* was attributed to the latest

Messinian, and the Green Marl above the *Caliza Tosca* was considered to be Pliocene in age (Berggren and Haq, 1976). But these are now recognized as the early late and latest Messinian deposits, respectively. Therefore there are no Pliocene deposits recovered in the Andalusian stratotype (Sierro et al., 1987; Sierro et al., 1993; Benson and Rakic– El Bied, 1991b), probably not even reaching up to the Miocene/Pliocene boundary (Benson et al., in press). Benson and Rakic–El Bied (1991b) further suggested that the *Caliza Tosca* may be about the time of the paleomagnetic reversal between the Chron 5 and Gilbert Chron, with an age of ~5.4 Ma (new time scale 5.75 Ma). If this is correct, the neritic *Caliza Tosca* most Shallow water deposits likely reflect global glacioeustatic sea–level change, because it coincides with global cooling at this time as indicated by ^{18}O isotopes at DSDP/ODP Sites 552, 608, 646. It is also in agreement with $\delta^{18}O$ isotopic signal (Hodell et al., 1994) and benthic foraminiferal signal (see below for details) in the Salé borehole, although no neritic deposits are determined at this time. The absence of neritic deposits in the Salé section and Bou Regreg section (Benson and Rakic–El Bied, 1991b; Benson et al., 1991; Benson et al., in press) in Morocco may be attributed to the greater paleodepth (~400–500m). Even if the glacioeustatic change has caused about 100m sea–level lowering at this time, the paleodepth still remained about 300–400m in Morocco. However it may be reduced to 30–50m in the Guadalquivir Basin, SW Spain because of much shallower paleodepth (150–200m estimated by Berggren and Haq, 1976). It is noted that the 100m sea–level lowering appears to be reasonable at this particular time, and it agrees with the estimates of sea–level lowering based on the shallow–water–originated turbidites recorded at ODP Site 646 (Chapter 5, this thesis). In any case, the origin of the *Caliza Tosca* deposits should be attributed to both glacioeustatic sea–level changes and tectonic uplifting because the Guadalquivir Basin commenced uplift before the *Caliza Tosca*. Therefore I suggest that the glacioeustatic sea–level change was superimposed upon the major background of paleotectonism.

6.3. Circulation systems in the Rifian Corridor during the Messinian

Most recently, a number of detailed studies in oxygen and carbon isotopes and ostracodes from the Rifian Corridor, Morocco have made great progress in Messinian paleoceanography (Hodell et al., 1989; Benson et al., 1991; Benson and Rakic–El Bied, 1991a; Benson et al., in press; Benson and Rakic–El Bied, 1991b; Benson et al., 1995; Hodell et al., 1994). This work formed a basis of a two-stage model to interpret the Mediterranean Salinity Crisis. It is possible that the stable isotopes alone may provide ambiguous interpretation of paleoceanography without detailed faunal and ecological studies. Some previous benthic foraminiferal studies in Moroccan area (e.g., Thomas Ehrendorfer at Woods Hole Oceanographic Institution, unpublished data) were based on relatively lower resolution sampling and a larger size fraction, and thus provided limited ecological information for understanding the paleoceanography and water exchange systems of the Messinian. Benthic foraminifera with high resolution sampling in this study provide more detail in evaluating the paleoceanography in the Mediterranean region. In other words, my benthic foraminiferal data clearly show three different stages of circulation evolution throughout the Messinian, which may in turn suggest important paleoclimatic changes and some details of the Messinian salinity crisis in the Mediterranean basin. As a hypothesis, I propose a three-stage model for the evolution of circulation in the Rifian Corridor region based on the following observations:

6.3.1. Stage 1 - PMOW leaking and anti-estuarine circulation during the early Messinian (7.12-6.2 Ma)

A high peak of *Uvigerina peregrina* (average ~ 10%) is documented in the interval between 105m (sample B39) and 139m (Sample B72) in the Salé borehole during the early Messinian, but its paleoceanographic significance is still debatable because of the confusion of the ecological interpretation of this fauna. As it is known, *U. peregrina* could be associated with various ecological factors, such as low oxygen content, high organic

carbon content, water temperature etc. Several major possible factors regarding the distribution of the fauna are reviewed as follows:

1) Association with depth: Costate *Uvigerina peregrina* have been recognized as a shallow infauna morphotype (0–2cm) (Corliss and Chen, 1988; Corliss, 1991). This species was considered the indicator of water depths (Phleger, 1942; Phleger and Parker, 1951; Bandy, 1960; Pflum and Frerichs, 1976), but studies from different regions of the world ocean show different depth habitats. But in general, it ranges from 500m to 3,000m in water depth, probably with high abundance at ~2,000m as observed in northeast US continental margin (Miller and Lohmann, 1982; Phleger, 1942; Cushman, 1918–1931), South Atlantic Ocean (Lohmann, 1978), and northwest African continental margin (Lutze, 1980). It is well documented that the oxygen levels at these depths are usually low.

2) Association with temperature: Some previous studies suggested that *U. peregrina* is restricted to temperature from about 3–4^{o}C, and used it to indicate warm bottom water during the Pleistocene glaciations in the North Atlantic Ocean (Streeter, 1973; Schnitker, 1974). On the contrary, this species is reportedly associated with lower temperature (< 3^{o}C; Lohmann, 1978) in the South Atlantic Ocean. It is obvious that the relationship between the species and temperature is not clear. Miller and Lohmann (1982) concluded that the correlation between *U. peregrina* and temperature is not consistent from region to region, similar to its correlation with water depth.

3) Association with low oxygen and organic carbon: It is widely documented that the abundant *U. peregrina* is closely associated with low dissolved oxygen in the overlying water (<5 ml/l) (Lohmann, 1978). Similar reports were also from bathyal zones below 2,000m in the North and South Atlantic Oceans (Streeter and Shackleton, 1979; Schnitker, 1979, 1980). Living *U. peregrina* (7.7%) climaxes at 996m (Station 8060A) off Cape Sines, Portugal (Seiler, 1975), where the water is mixed with the Mediterranean outflow water (MOW) characterized with high temperature, high salinity, and low oxygen (Gieskes et al., 1970; Gorshkov, 1974; Fuglister, 1960). It is not recorded below 1730m (Seiler,

1975), where the water is not distinctly affected by MOW. off west Africa *U. peregrina* is abundant from 700m to 2,000m off Senegal and Gambia (Haake, 1980), and from 500m–1,500m off Bojador and Dakar (Lutze, 1980), where the oxygen content is low (< 4ml/l) (Lutze, 1980), but it does not show a clear correlation with oxygen content less than 2ml/l. Schnitker also suggests that *U. peregrina* is low or absent when oxygen content is extremely low (2ml/l-1ml/l) (pers. comm., 1995). In the Gulf of Mexico, *U. peregrina* is abundant in the oxygen minimum zone on continental slope (Pflum and Frerichs, 1976), supporting the correlation between the oxygen content in the water column and *U. peregrina* in surface sediments. The low oxygen characteristics of *U. peregrina* allow Streeter and Shackleton (1979) to recognize the reduction or cessation of the North Atlantic Deep Water (NADW) at times of *U. peregrina* peaks during the last glaciation. On the United States continental slope *U. peregrina* is noted to have a close coincidence with organic carbon, not of low oxygen (Miller and Lohmann, 1982). Low oxygen values in the water column are often associated with high organic carbon in the substrate, but sometimes it may not be necessary (Miller and Lohmann, 1982). It is also true that O_2 in the sediments could be low, but not in the water column.

The presence of *U. peregrina* in the Rifian Corridor area (e.g., in Salé, Bou Regreg and Ain el Beida cores), together with psychrospheric ostracodes, formed a basis for Hodell et al. (1989), Benson et al. (1991), Hodell et al. (1994), and Benson et al. (in press) to propose a current reversal model which suggests that strong Atlantic water inflows into the paleo–Mediterranean Sea via the Rifian Corridor during the early Messinian (Chron 6 to the top of Chron 5). This inflow is suggested to have replaced the warm, saline PMOW, and thus called "current reversal" (Hodell et al., 1989), or called "siphon event" (Benson et al., 1991). The siphon event has also led to the formation of a horizontal loop circulation between the Mediterranean Sea and North Atlantic Ocean caused by Coriolis force during the early Messinian (Benson et al., 1991). In other words, no outflow entered the Atlantic Ocean only through the siphon, but through the Betic passage

in southern Spain at that time. The reversal system was considered because *U. peregrina* was found to be common in Pleistocene sediments of the Atlantic Ocean (Schnitker, 1980; Streeter and Shackleton, 1979), and therefore a typical North Atlantic Deep Water benthic fauna for the Messinian. My anti-estuarine circulation model does not agree with this previous interpretation for the following reasons:

1) *U. peregrina*, together with other costate uvigerinids is rare (< 1%), at least in the eastern North Atlantic where Atlantic water dominates (Chapter 3, this thesis; Thomas, 1986; Murray et al., 1986; Murray, 1984) during the Miocene, although it has been found to be abundant during the Pleistocene glaciations (Schnitker, 1980; Streeter and Shackleton, 1979; Murray et al., 1984). Benson and Rakic–El Bied (1991a) noted that it is common in the Mediterranean region. This suggests that *U. peregrina* in the Salé borehole and other locations in the Rifian Corridor may have no close association with the Atlantic fauna during Messinian time, but it may have been associated with the Mediterranean fauna itself as a low oxygen indicator.

2) *U. peregrina* is considered to be an indicator of glaciation, rather than of NADW. It is abundant in oxygen isotope Stage 2 in the Labrador Sea and elsewhere (Scott et al., 1989 (ODP leg 105)) in the Quaternary. As mentioned above, Streeter and Shackleton (1979) used it as an indicator of reduction or cessation of NADW resulting from stagnation of oceans during the last glaciation, rather than of NADW production.

3) *U. peregrina* climaxes above 1,000m in present water depth off the Cape Sines, Portugal, where is under the influence of MOW, suggesting a possible association with low oxygen environment, although it occurs sporadically (Seiler, 1980). Therefore *U. peregrina* peaks in the Salé borehole and from the other locations in Rifian Corridor, Morocco are most likely related to the low oxygen. It is noted here that the low oxygen in Morocco may be associated with three factors: 1) world–wide high surface paleoproductivity as observed along the modern continental slopes of the world; 2) low oxygen paleo–Mediterranean outflow water (PMOW); and 3) local high paleoproductivity

Fig. 6-1. A comparison of benthic foraminiferal assemblages from the Salé borehole, Morocco (this thesis), Portugal (Seiler, 1975), and NW Africa (Lutze, 1980).

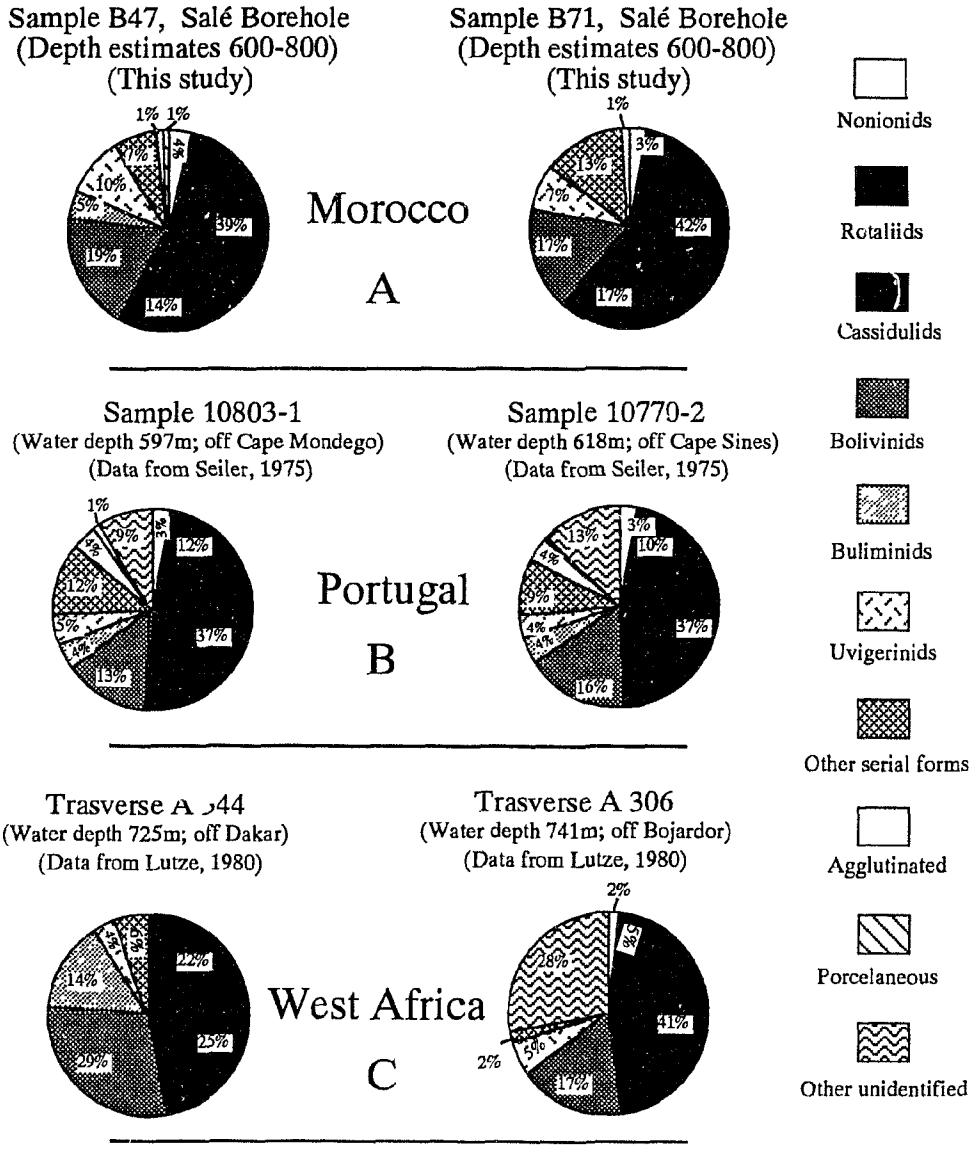
Sample B47, Salé Borehole
(Depth estimates 600-800)
(This study)
1% 1%
4%
39%
14%
19%
5%
10%
7%
Morocco
A
Sample B71, Salé Borehole
(Depth estimates 600-800)
(This study)
1%
3%
42%
17%
17%
7%
13%
Nonionids
Rotaliids
Cassidulids
Bolivinids
Buliminids
Uvigerinids
Other serial forms
Agglutinated
Porcelaneous
Other unidentified
Sample 10803-1
(Water depth 597m; off Cape Mondego)
(Data from Seiler, 1975)
1%
3%
12%
37%
13%
5%
12%
4%
9%
4%
Portugal
B
Sample 10770-2
(Water depth 618m; off Cape Sines)
(Data from Seiler, 1975)
3%
10%
37%
16%
4%
4%
9%
4%
13%
Trasverse A 344
(Water depth 725m; off Dakar)
(Data from Lutze, 1980)
22%
25%
29%
14%
4%
4%
West Africa
C
Trasverse A 306
(Water depth 741m; off Bojardor)
(Data from Lutze, 1980)
2%
41%
17%
2%
5%
28%

caused by mixing of warm, saline MOW and cold Atlantic water near the outlet of MOW on Atlantic side, which may produce high organic carbon at the same time. I suggest that PMOW may have been the major cause of the sudden increase of *U. peregrina* during the early Messinian.

4) Benthic foraminiferal assemblages from Salé borehole, off Portugal, and off west Africa (Fig. 6-1) show major differences in their species composition. As seen in the figure, both in Portugal and west Africa, the major components are cassidulinids (~40% in total faunas), while in the Salé borehole, it makes up only ~15%. It is well documented that cassidulinids are one of the dominant groups in the northeast Atlantic, which makes up 20–40% throughout the Messinian (DSDP Holes 608, 552A and 547A, this thesis). This suggests that the assemblages off Portugal and west Africa may have closer affinities to the Atlantic fauna than the assemblages in the Salé borehole.

5) The typical NADW indicator, *Epistominella exigua* decreases and approaches 0% near the top of the *U. peregrina* interval. This species makes up 10–20% at DSDP Site 608, >20% at DSDP Site 547A, and 15–20% at DSDP Site 552A. It strongly indicates that the water in this interval at Salé borehole may be associated with PMOW, rather than a pure NADW.

6) Some deep and cold water indicators sharply decrease in this interval, e.g., *Cassidulina reniforme, Bulimina aculeata, Cibicidoides mundulus* (Figs. 3-2, 3-3).

7) A carbonate dissolution peak is determined at about 130m as indicated by an abrupt decrease of planktonic foraminiferal tests (Fig. 3-1). This is most likely associated with PMOW since PMOW could increase $CaCO_3$ dissolution (Thunell et al., 1987; Ryan, 1973).

8) $\delta^{13}C$ isotopes in the *U. peregrina* interval are more depleted than those in overlying Messinian sediments. Averaged $\delta^{13}C$ values are about 0.5‰ with minimum depleted values of ~0.0‰, while they are about 0.9‰ in average in overlying Messinian deposits (fig. 6 of Hodell et al., 1994). It suggests that the *U. peregrina* interval may have

been affected by low oxygen, high salinity PMOW, which caused about 2–3‰ $\delta^{13}C$ local decrease that was superimposed on the permanent global carbon–13 shift above the Tortonian/Messinian boundary. Such a local $\delta^{13}C$ depletion is not clear in open ocean (e.g., DSDP Hole 552A, Keigwin, 1987).

9) A continuous enrichment of $\delta^{18}O$ (up to middle C3An) in the *U. peregrina* interval is also considered to have been associated with high salinity PMOW. The $\delta^{18}O$ values in this interval are about 0.1‰ heavier than those in overlying interval. As $\delta^{13}C$ isotopes mentioned above, this enrichment signal was not clearly recorded in DSDP Hole 552A (Keigwin, 1987) or in the Pacific Ocean (Hodell et al., 1986), and thus probably reflects a local variation of $\delta^{18}O$ isotopes that is superimposed on the global cooling as recorded elsewhere in the world (see Chapter 6 for details). As an alternate interpretation, Hodell et al. (1994) suggested that the increase in $\delta^{18}O$ values during the late Miocene represents, at least in part, an increase in global ice that lowered sea level and contributed to the establishment of the negative water budget in the Mediterranean. In the Mediterranean Sea, similar heavy oxygen isotope ratios were obtained both from dolomite samples (Pierre and Rouchey, 1990) and planktonic foraminifera (ODP Site 654; Glacon et al., 1990) during the early Messinian in the Tyrrhenian Sea (the Mediterranean), suggesting substantial evaporation (Pierre and Rouchey, 1990).

10) Thomas Ehrendorfer (unpublished reports) observed that the costate uvigerinids acme comes in a little earlier than the occurrence of the psychrospheric ostracods assemblage. He attributed the *Uvigerina* increase to the same environmental changes that favored the development of psychrospheric ostracodes. Unfortunately, the relationship between uvigerinids and psychrospheric ostracod fauna in the Salé section is not clear because quantitative studies of ostracodes are not available at this time. In any case, it is suggested that the costate *Uvigerina* acme may be interpreted as a main effect of PMOW during the early Messinian, while the psychrospheric ostracodes may indicate a current reversal after the peak of *U. peregrina* (see below for details).

11) At ODP Site 654 in the Tyrrhenian Sea, the first lithologic sign of the impending salinity crisis is the abrupt appearance of dark colored laminated, dolomitic, organic–rich sediments (lithologic Unit III) containing radiolarians, sponge spicules, and diatoms. High concentrations of organic carbon, abundant pyrite, and lack of burrowing suggest an anoxic environment during the early Messinian (Kastens and Mascle, 1990), indicating a stratified basin (Robertson et al., 1990). This unit is considered to be equivalent to the Tripoli Formation exposed in Sicily (Borsetti et al., 1990), which has similar sedimentary history (McKenzie et al., 1979).

12) A similar high peak of *U. peregrina* is also found in the same interval in the Betic Passage in the southern Spain (Sierro, pers. comm., 1995; Hilgen, pers. comm., 1995). It is difficult for the "current reversal model" (Benson et al., 1991; Hodell et al., 1989) to interpret the presence of the species in southern Spain, because their model requires the absence of *U. peregrina* in southern Spain.

It is apparent that my detailed benthic foraminiferal study, together with stable isotopes, strongly suggests PMOW leaking out through the Rifian Corridor at depth, while inflow of less saline, cool Atlantic water spilled into the paleo–Mediterranean basin at surface, reflecting a negative water balance. This allows a reconstruction of an anti-estuarine circulation system in this area for the interval from 7.12 Ma to 6.2 Ma marked by the *U. peregrina* peak (Fig. 6-2A). It strongly supports the deep-basin, deep-water evaporation hypothesis of van Couvering et al. (1976) and of Weijermars (1988). My model suggests that the paleo– Mediterranean Basin during the early Messinian probably was equivalent to an euxinic environment where the bottom water became stagnant and poorly oxygenated below sill depth, with low nutrients and unproductive features. An anti-estuarine system reflects an arid climate, and is characterized by a negative water balance (namely evaporation exceeds runoff and precipitation). This stage may be considered to be a precondition of the Mediterranean salinity crisis.

Fig. 6-2. Paleotectonism and three stage water circulation systems in Rifian Corridor during the Messinian. Stage A shows an anti-estuarine circulation system from 7.12–6.2 Ma; stage B indicates upwelled Atlantic inflow running into the Mediterranean Sea and cessation of PMOW from 6.2 to 5.9 Ma. Severe restriction to the Mediterranean Sea from the open ocean was mainly caused by tectonic uplifting at this time; Stage C shows that the Mediterranean Sea was completely separated from the Atlantic Ocean from 5.9 to 5.32 Ma, causing the Messinian Salinity Crisis in the Mediterranean Basin.

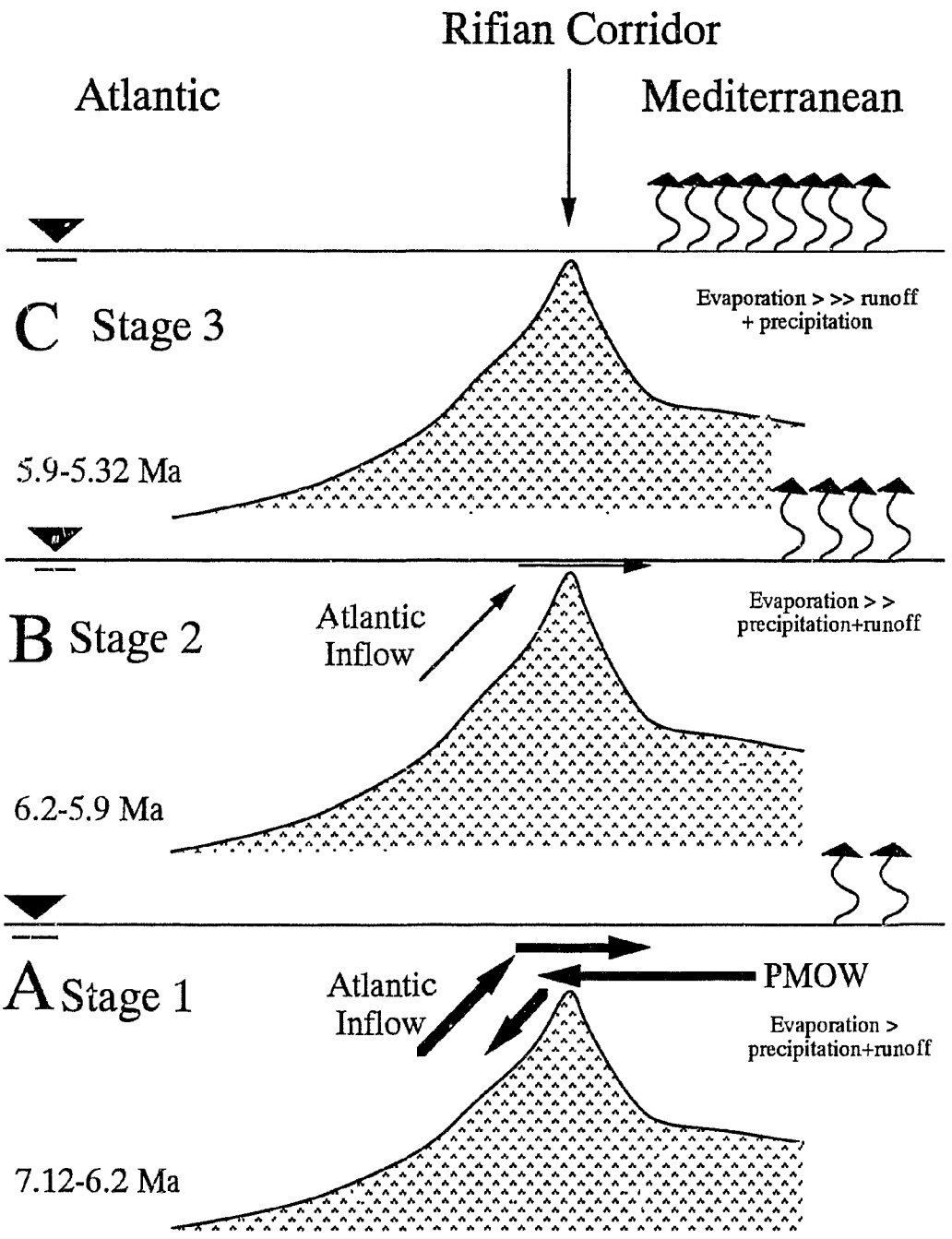
Rifian Corridor
Atlantic
Mediterranean
C Stage 3
Evaporation > >> runoff
+ precipitation
5.9-5.32 Ma
B Stage 2
Atlantic
Inflow
Evaporation > >
precipitation+runoff
6.2-5.9 Ma
A Stage 1
Atlantic
Inflow
PMOW
Evaporation >
precipitation+runoff
7.12-6.2 Ma

As mentioned above Benson et al. (1991) proposed a "Twin–channel flow model", which suggests a spill of all PMOW through the Betic Passage, north of Alicante, Spain, pushed by Coriolis force, and Atlantic inflow through the Rifian. I believe, that in a view of large scale circulation, this is correct. However, the size of the "island" situated between the Rifian Corridor and Betic Passage and the width of the Betic Passage may have been important factors to control the Coriolis–force–driven Mediterranean circulation (Van Couvering, pers. comm., 1993). The "island" today is measured about 1,000 km in width from Rabat of Morocco to Alicante of Spain (Benson et al., 1991) with a length of about 200 km. This island may have been larger during the Messinian than today, because the possible tectonic compression is not considered here. It is believed that the "island" was probably large enough to deflect PMOW toward Morocco and then go southward as observed today (see fig. 9 of Benson et al., 1991). One of the best modern counterparts is Sardinia (~300 km long) or Corsica (~210 km long) island, which deflect the Mediterranean current in the Tyrrhenian Sea to south along the eastern coast of the Sardinia (refer to fig. 9 of Benson et al., 1991). I believe that an analogous current deflected by the "Rifian–Betic island" could have existed in the Alboran basin, which could have been pushed out through the Rifian Corridor by Coriolis force during the early Messinian, even though it may not have been as strong as the one via the Betic Passage.

It must be noted that the benthic foraminiferal assemblage in the Salé section of Morocco in the *U. peregrina* interval contains some of Atlantic deep water species with low percentage as well, for example, *Gyroidina* spp., *Stilostomella, Heronallenia crosbyi, Oridorsalis umbonatus*, as well as psychrospheric ostracodes, indicating a mixture of Atlantic inflow and Mediterranean outflow waters.

6.3.2. Stage 2 - Current reversal - Atlantic infill (6.2–5.9 Ma)

A short period with a duration of 0.3 million years (C3An.1r and 1n from 106m–87m; sample B40–B22) of current reversal occurred just after the PMOW leaking and

before the dramatic Moroccan uplift marked by benthic foraminifera in the Rifian Corridor (Fig. 6-2B). The reversal duration (about 0.3 m.y.) is shorter than that of Hodell et al. (1989), Benson et al. (1991); Benson and Rakic–El Bied (1991a) who suggested ~1.22 m.y. This reversed current is characterized by a peak of the typical NADW indicators, *Epistominella exigua* and *Eponides weddellensis* (>20%), abrupt decrease of *U. peregrina,* and sudden re–increases of *Cibicidoides mundulus* and *Bulimina aculeata* and 0.1‰ decrease of $\delta^{18}O$ values (Hodell et al., 1994). All these clearly indicate the domination of NADW and the cessation of PMOW. *E. exigua* makes up about 5%, with a maximum of 15.21% that is almost as high as in abyssal North Atlantic controlled by NADW during the Messinian as seen at DSDP Site 552A (this thesis). A number of other deep water species are also recorded, for example, *Pleurostomella* spp., *Eponides?* sp. A, *Bolivina inflata, Bolivina* cf. *pygmaea,* and psychrospheric ostracodes (such as *Agrenocythere pliocenica, Oblitacythereis mediterranean*) (Hodell et al., 1989; Benson et al., 1991; Benson Rakic–El Bied, 1991a and 1991b; Benson et al., in press; Hodell et al., 1994). This is equivalent to the top of current reversal proposed by Hodell et al. (1989); Benson et al. (1991).

This reversed current reflects a strong negative water balance in the Mediterranean Basin caused by strong evaporation, and marks the onset of the Mediterranean salinity crisis. At this time, the paleoclimates in the Mediterranean region became unstable. Strong evaporation may also have stimulated water stratifications in the circum–Mediterranean region. Oxygen isotopic records from benthic (*Planulina ariminensis*) and planktonic (*Globigerinoides obliquus*) foraminifera display clearly opposite variations in this period in the Ain El Beida core, Morocco (Hodell et al., 1989). In addition, the extinction of conoid *Globorotalia conomiozea* and a series of coiling direction changes of *Neogloboquadrina acostaensis* suggest significant surface water temperature variations associated with PMOW in Chronozone C3An.1r and 1n in Morocco (see Chapter 4 for more details), although the coiling direction changes of *N. acostaensis* were interpreted as a possible association with orbital forcing (Benson et al., in press). One single coiling direction change of *N.*

acostaensis at DSDP Site 397 was reported in the lower part of Chron 5.2n (Cita and Ryan, 1979), which is obviously earlier than from those observed in Chron 5.1r and 1n (= C3An.1r and 1n) in the Rifian Corridor, again indicating a local coiling variation.

This interval is probably equivalent to the *Calcare di Base* underlain by the Tripoli diatomites in Sicily, because the top of the Tripoli Formation occurs near a coiling direction change of *N. acostaensis* (Sierro et al., 1993). McKenzie et al. (1979/1980) and Pedley and Grasso (1993) reported that *Calcare di Base* is characterized by an evaporitic limestone facies that heralds the onset of evaporite deposition. In the Salé core, Hodell et al. (1989; 1994) and Benson and Rakic–el Bied (1991a) suggested that the onset of deposition of the lower evaporites probably began in C3An.1n based on a series of coiling changes of *N. acostaensis*. It is interesting that no gypsum was reported in Subchronozone C3An.1n (e.g., Kastens, 1992). The balatino–type (namely, cyclic) gypsum at ODP Site 654 was assigned to C3r (Channell et al, 1990). Gautier et al. (1994) suggested that the evaporite deposition did not begin in the Mediterranean until early Subchronozone C3r at ~5.7, and the entire salinity crisis was limited to Chronozone C3r between 5.7 and 5.3 Ma, although this appears to be associated with a hiatus between the Tripoli Formation and *Calcare di Base*. This information suggests that this interval is characterized by the reversed current and represents a more restricted Mediterranean environment that led to the formation of salinity crisis limestone in the Mediterranean region rather than the interval of *U. peregrina*. However, it does not rule out the possibility that some gypsum or gypsum–associated deposits formed in the Mediterranean region because of the late phase of euxinic paleoenvironment and local paleoenvironmental/geographic constraints around paleo–Mediterranean margins at this time.

6.3.3. Stage 3 - Closing of the Mediterranean Sea (5.9–5.32 Ma) and the Salinity Crisis

The present benthic foraminiferal study clearly shows that dramatic tectonic changes (compression and uplifting) beginning at the top of C3An.1n, suggest the severe constraints for water exchange between the Mediterranean Basin and the Atlantic Ocean just after the reversed current in upper Chronozone C3An (Fig. 6-2C). Within C3r, the abundance of benthic foraminifera, B/P ratios, increase of shallow water faunas, and progressively depleted $\delta^{18}O$ clearly mark the gradual tectonic uplifting. As mentioned earlier, the progressively depleted $\delta^{18}O$ (Hodell et al., 1994) is interpreted as a local temperature increase caused by constant Mediterranean evaporation. It is evident that the isolation is the most important geological event during the Messinian and the major cause of the formation of a giant evaporitic salt in the Mediterranean Basin (Hsü, 1973; Hsü et al, 1973a; Hsü et al., 1973b; Hsü, 1987).

As briefly mentioned above, the most recent study (Gautier et al., 1994) suggests that the Mediterranean Salinity Crisis began at about 5.7 Ma in the lowermost of Gilbert reversal (or C3r) in the Sorbas section (Andalusia, SW Spain, and in the Sicilian sections (Caltanissetta Basins). My benthic foraminiferal data may not be suitable to constrain the exact time when the open ocean and Mediterranean Sea were separated during the Messinian because of its upper bathyal environmental characteristics throughout the late Messinian and the formation of major body of evaporite salts. However, the rapid changes and turnover of benthic foraminifera at the uppermost Chron 5 and earliest Gilbert (= C3r) in the Salé section (Figs. 3-1, 3-3, 3-7, 3-8) resulting from the Moroccan tectonic compression and uplifting, may provide critical information to support the suggestion of Hodell et al. (1989), Hodell et al. (1994), and Benson and Rakic–El Bied (1991a) that the Mediterranean Salinity Crisis and the formation of the Mediterranean evaporites began within Subchronozone C3An.1n at ~ 5.9 Ma. This estimate based on Salé benthic foraminifera is slightly earlier (~0.1–0.2 m.y.) than the age proposed by Gautier et al. (1994).

6.4. Paleoclimatic/sea-level fluctuations

Many of the global paleoclimatic changes in the late Messinian have been reviewed in Chapter 5. Detailed paleoclimatic study of the Salé core was carried out by Hodell et al. (1994) based on oxygen stable isotopes with a range of $\delta^{18}O$ values of 0.5 to 0.6‰. Their isotopic signals have shown distinct glacial–interglacial changes driven by insolation resulting from orbital obliquity changes at each ~41–kyrs. The $\delta^{18}O$ signals were partly controlled by changes of continental ice volume that were responding to insolation fluctuations at high latitudes. Hodell et al. (1994) also reported that the oxygen isotopes in the Salé core are associated with the waxing and waning of icesheets identical to the orbital obliquity cycles.

Precessional forcing was not verified from the carbonate data of the Salé section probably as a result of low sampling resolution (Hodell et al., 1994). Precessional forcing was determined in the Bou Regreg Messinian section at Ain el Beida near Rabat, Morocco (Benson et al., 1995), and in Pliocene and Pleistocene sediments in the Mediterranean (Hilgen, 1987, 1991a, b; 1993).

Carbonate cyclicities in the Salé core, however, are reportedly dominated by the eccentricity cycles with periodicity of 100 kyrs for the interval from C3An to C3Ar (5.894 to 6.935 Ma) (Hodell et al., 1994). Seven Milankovitch eccentricity cycles (100 kyrs) in the upper section from 5.894 to 5.32 Ma, that are considered to have been relatively shallow water environment, are determined based on the time series analysis using carbonate data of Hodell et al. (1994) in this study (Fig. 6-3). These cycles also co-vary with the $\delta^{18}O$ positive excursions, smoothed P/B ratio curve, and percent *B. lowmani*. Therefore I suggest that the P/B ratio and *B. lowmani* cycles and $\delta^{18}O$ positive excursions in this core may have been associated with eccentricity forcing. The major $\delta^{18}O$ enrichments in Fig. 6-4 indicate that seven glaciations or climate coolings may have occurred in this interval, which have caused corresponding sea-level lowerings as labeled

Fig. 6-3. Power spectrum analysis for oxygen-18 (top), planktonic/benthic ratios (middle), and carbonate (bottom) signals during Chronozone C3r (=lower reversal of the Gilbert with a duration of 5.894 and 5.32 Ma). The distinct peak corresponds to the Milankovitch cycles of eccentricity (100 kyrs). The oxygen-18 and carbonate data are from Hodell et al. (1994).

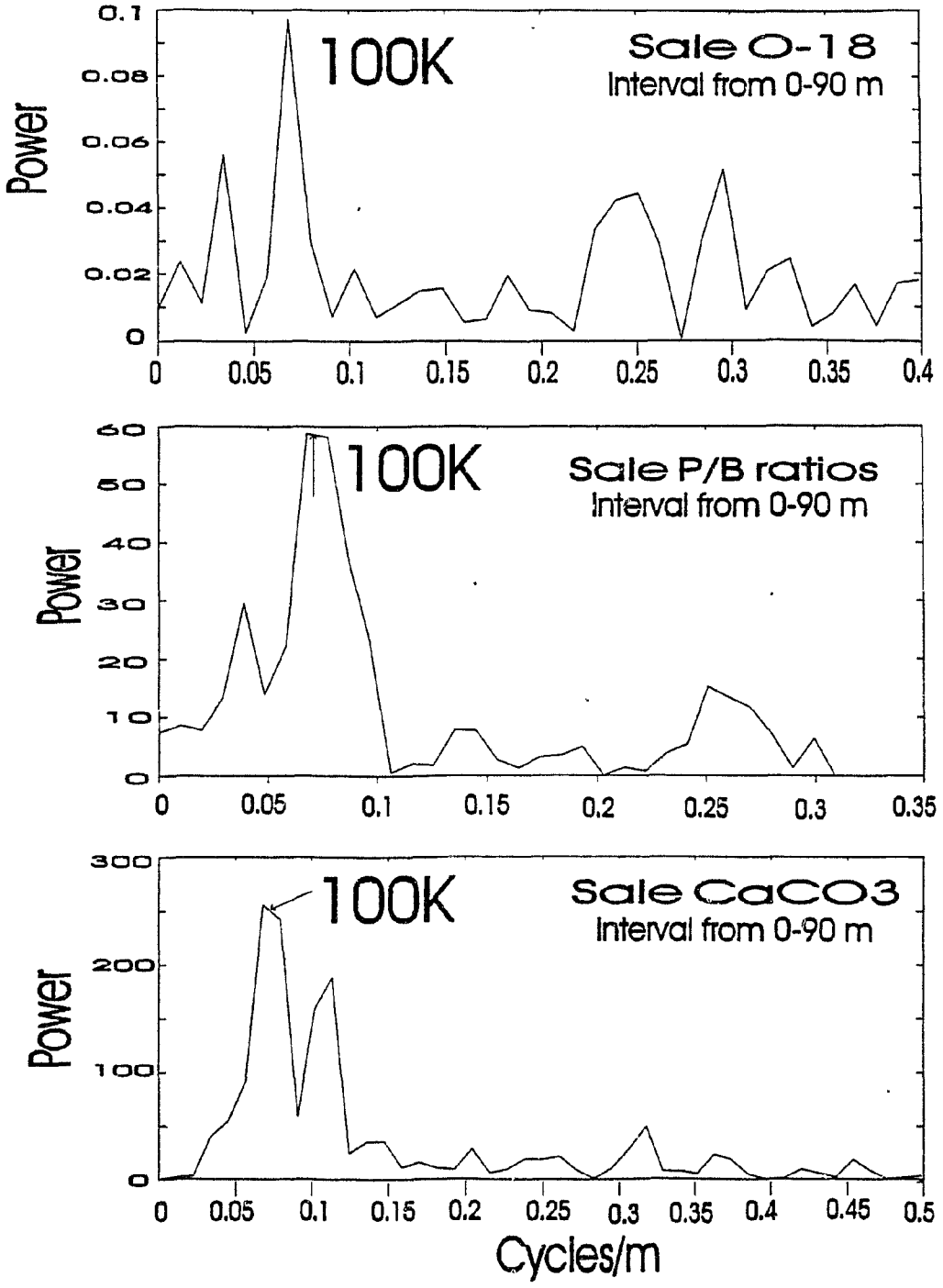
100K
Sale O-18
Interval from 0-90 m
Power
0.1
0.08
0.06
0.04
0.02
0
0
0.05
0.1
0.15
0.2
0.25
0.3
0.35
0.4
100K
Sale P/B ratios
Interval from 0-90 m
Power
60
50
40
30
20
10
0
0
0.05
0.1
0.15
0.2
0.25
0.3
0.35
100K
Sale CaCO3
Interval from 0-90 m
Power
300
200
100
0
0
0.05
0.1
0.15
0.2
0.25
0.3
0.35
0.4
0.45
0.5
Cycles/m

Fig. 6-4. Detailed view of Stage 3 in Salé core. During this stage (~5.9–5.32 Ma), 7 sea–level lowerings are recognized using P/B ratios, $CaCO_3$, $\delta^{18}O$ and *Bolivina lowmani*. The sea–level cycles are coinciding with eccentricity forcing according to the time series analysis. These sea–level fluctuations has played as an "automatic choke" to control the infilling of Atlantic water to the Mediterranean Basin. SLL = sea–level lowering. 3 point running average oxygen-18 curve is from Fig. 3-10.

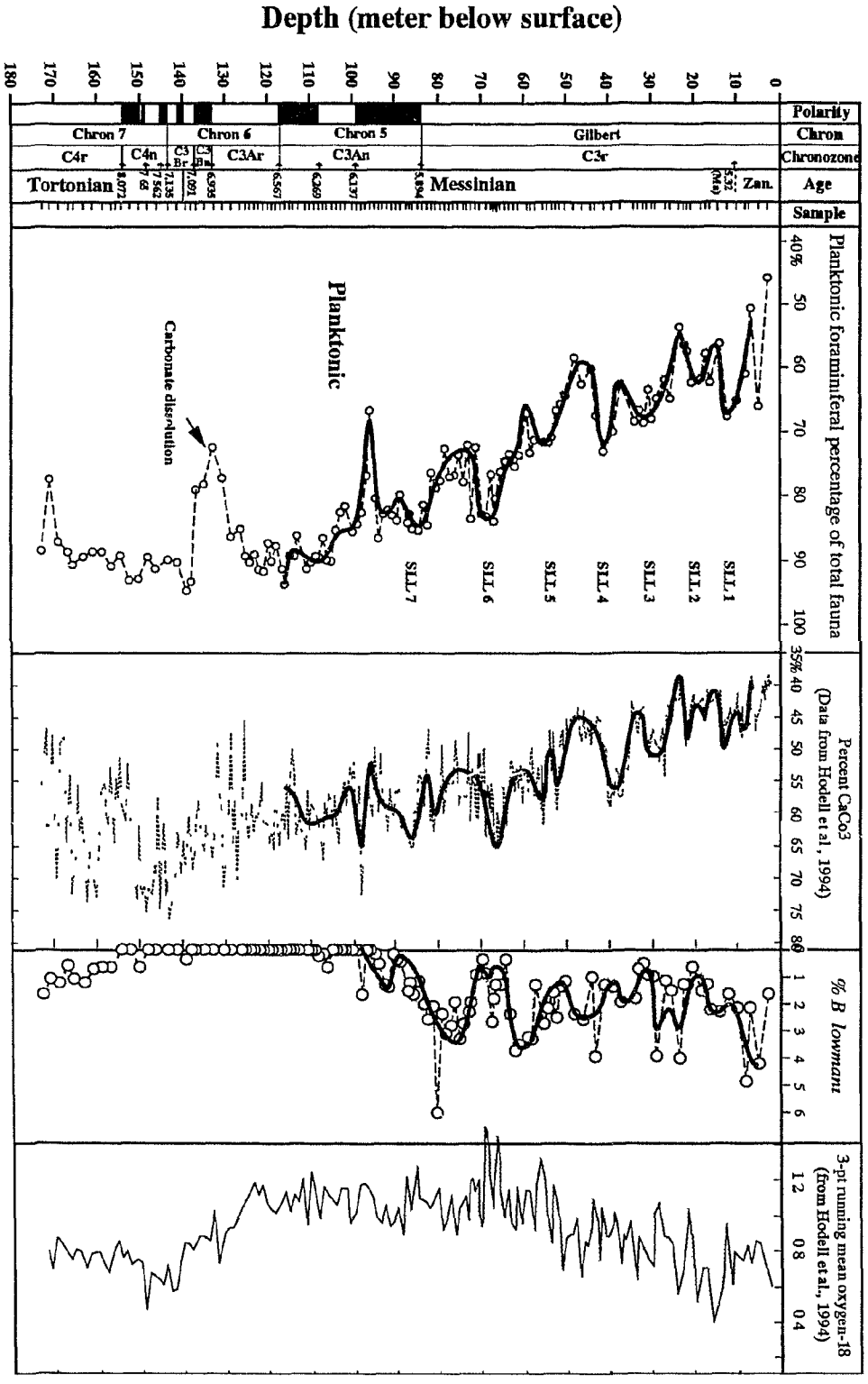
Depth (meter below surface)
Polarity
Chron
Chronozone
Age
Sample
Chron 7
Chron 6
Chron 5
Gilbert
C4r
C4n
C3 Br
C3 An
C3Ar
C3An
C3r
Tortonian
Messinian
Zan.
Carbonate dissolution
Planktonic
SLL7
SLL6
SLL5
SLL4
SLL3
SLL2
SLL1
Planktonic foraminiferal percentage of total fauna
Percent CaCo3 (Data from Hodell et al., 1994)
% B lowmani
3-pt running mean oxygen-18 (from Hodell et al., 1994)

in the figure (SLL 1-7). *Bolivina lowmani* is considered to be a depth–dependent species, which decreases in abundance when sea–level drops. Fig. 6-4 clearly shows that these sea–level fluctuations are superimposed on the signals resulting from rapid tectonic uplifting. No major sea–level changes as indicated by indistinct variations of P/B ratios and CaCO3, as well as the absence of shallow water benthic foraminiferal fluctuations, can be recognized below C3An.1n because this interval remains deeper (600–800m). Similar sea–level changes are observed with turbidite cycles in ODP Hole 646B and $\delta^{18}O$ fluctuations in DSDP Hole 552A (this thesis), although only six cycles are determined in the same time interval. The increases of planktonic foraminifera and $CaCO_3$ during the sea–level lowerings or glaciations recorded in the Salé core are not well understood because it cannot be explained with sea–level fluctuations. In the most ideal case, planktonic foraminifera and $CaCO_3$ would decrease, while benthic foraminifera would increase in abundance when water depth became shallower. I tentatively interpret that these increases of planktonic faunas and $CaCO_3$ may have been associated with increased surface productivity resulting from upwellings during the glaciations. It is well known that during glaciations, winds on land became more intense. When winds blow away from the land, offshore flow of water may be produced, causing water loss near shore or sea–level fall. As a result, the lost near–shore water would be replaced by upwelled nutrient–rich deep water that could cause oceanic surface blooms. The association between surface productivity and dramatic climatic change has been recently recognized in the Indian Ocean (Siesser, 1995). In addition, DeMenocal (1995) reported that during the late Miocene, the eolian deposits were found in marine sediments off west Africa, which supports the presence of intensified winds on African continent at this time. Furthermore, the terrestrial influx that contains high iron (Martin, 1990) may have greatly increased Fe content in oceanic water column, which could stimulate the oceanic surface productivity during glaciations (Martin, 1990). This paleoproductivity increase during the glacials is also supported by Sarnthein et al. (1987),

who suggested that the paleoproductivity increased from interglacial to glacial delimiting clear 100 kyr cycles.

As observed in $\delta^{18}O$ isotopes at Atlantic DSDP Sites 552A, DSDP 608 and Salé core (Keigwin, 1987, Hodell et al., 1994; this thesis), and in the Pacific ODP Site 846 (Shackleton et al., 1995), the benthic foraminifera in the Salé core strongly support major glaciation at 5.75 Ma (new time scale of Berggren et al., 1995) labeled as SLL 6 (Fig. 6-4). At this time, cassidulinids, *Trifarina angulosa, Bolivina lowmani, Melonis* spp., and *Bolivinita pseudothalmanni* are reduced, while some shallow water species (*Bolivina dialata* and *Gavelinopsis praegeri* are) increased. These suggest water depth has been decreased suddenly. It is suggested to be equivalent to the *Caliza Tosca* deposits in Spain, indicating ~100m sea–level lowering at this time.

In addition, a warm, tropical planktonic foraminiferal assemblage, characterized by *Globorotalia menardii* and *Globigerinoides* spp., has been displaced by a temperate fauna dominated by conoid *Globorotalia* group *(G. miotumida, conomiozea,* etc.) at the beginning of the Messinian (e.g., Sierro, 1985), indicating a climate cooling, although there may be a major diachroneity between the Pacific Ocean and the Mediterranean region (Roberts et al., 1994). This is supported by the global $\delta^{18}O$ enrichment at the beginning of the Messinian.

6.5. Possible cause of the Messinian Salinity Crisis in the Mediterranean Basin

It is documented that the Messinian deposits in the Mediterranean region, both sea and land, are basically composed of the following major sequences, i.e., Tripoli marine formation, *Calcare di Base,* cyclic lower and upper evaporites, and a thin layer of *Lago Mare* deposits - fresh/brackish water deposits that capped the sequence. *Calcare di Base* marks a rapid change from a bathyal environment of hemipelagic sedimentation to a shallow, or subaerial environment of carbonate deposition and diagenesis (see Hsü et al.,

1978). The Lower Evaporite sequence is overlain unconformably by the Upper Evaporites of gypsum and marls. *Lago Mare* deposits are fresh/brackish water deposits, formed in the Mediterranean Basin at the end of the Messinian. The latter three layers were considered to have been formed in a repeatedly desiccated Mediterranean deep basin resulting from the complete isolations of the Mediterranean Sea from the Atlantic Ocean (Hsü et al., 1973a, b). Hsü et al. (1973a, b) claimed that to form a volume of 2,000-3,000 m evaporites in the Mediterranean Sea, 11 interludes of infill from the Atlantic Ocean during the later Messinian would be required if all salts deposited in the center of the Mediterranean Basin (Hsü et al., 1973a, p. 1215; Hsü et al., 1978, p. 1070) (note that Benson and Rakic-El Bied (1991a) suggested 7-8 interludes of infilling). The speculation of Hsü et al. (1973a) on the repeated infilling greatly stimulated scientists to find connections between the Mediterranean Basin and open ocean. Much work was targeted to southern Spain and Northern Morocco (e.g., Berggren and Haq, 1976; Berggren et al., 1976; Van Couvering et al., 1976; Benson and Rakic-El Bied, 1991b; Benson and Rakic-El Bied, 1991a; Benson et al., in press; Benson et al., 1991; Hodell et al., 1989; Hodell et al., 1994; Cita and Ryan, 1978) to seek possible associations between the Mediterranean and Atlantic Ocean because these areas were expected to be the only conduits for water exchange during the Messinian although the Eastern Mediterranean may have been connected to the Indian Ocean for some time (Hsü et al., 1978). The evidence both from Spain and Morocco shows that the Messinian Salinity Crisis may have been controlled by both tectonic movements in southern Spain and northern Morocco and glacioeustatic sea-level changes (e.g., Hsü et al., 1973; Benson and Rakic-El Bied, 1991a), but the corresponding numbers of the repeated infilling resulting from the sea-level changes as suggested by either Hsü et al. (1973) and Hsü et al. (1978), and Benson and Rakic-El Bied (1991a) were not substantiated. However, in abyssal Atlantic basins outside the Mediterranean Sea, two major oxygen isotopic enrichment events in the youngest Chron 5 and in the earliest Gilbert (Hodell et al., 1986; Cita and McKenzie, 1986; Müller and Hsü, 1987; Keigwin, 1987), respectively, were found, which

were considered to have been associated with the Salinity Crisis. Most recently, Aharon et al. (1993) reported that the Messinian Salinity Crisis was linked to glacioeustatic sea-level changes indicated by eight unconformites from Niue coral atoll, South Pacific Ocean, but these appear to lack fine timing control (Benson, pers. comm., 1995).

As discussed above foraminiferal and oxygen isotopic data from the Salé core provide critical information for the evaluation of the Mediterranean Salinity Crisis during the late Messinian from ~5.9 to 5.32 Ma. These results strongly suggest: 1) A dramatic tectonic uplifting during late Chronozone C3An and gradual uplifting throughout Subchronozone C3r (=lower Gilbert). Possibly, a complete isolation of the Mediterranean Basin from the Atlantic Ocean may have taken place at the end of the Messinian or the earliest Pliocene; 2) Glacioeustatic sea-level changes driven by eccentricity forcing in each 100 kyrs during the late Messinian (5.9-5.32 Ma).

It is clear that the tectonic uplifting in Morocco plays a major role in the circulation restriction and final isolation from the Atlantic Ocean, while the eustatic sea-level changes superimposed on the tectonic background, serve as an "automatic choke" that controls the Atlantic infilling to the Mediterranean Basin and results in cyclic evaporitic deposits (e.g., Hsü, 1973). Seven glacioeustatic sea-level fluctuations recorded in the Salé core coincide well with the 7-8 Atlantic inundations into the Mediterranean Sea given by Benson and Rakic-El Bied (1991a), but is lower than the estimate of Hsü et al. (1973a, b, 1978). In Hole 646B, 6 deep-water turbidite cycles are determined in the same interval of time.

Once again, the amplitudes of the sea-level fluctuations at Salé are difficult to estimate based on the foraminiferal data. However, the most distinct sea-level lowering occurred at 5.75 Ma may have reached ~100 m. This estimate rests on the observation of *Caliza Tosca* deposits (shelly calcarenite at the top of the Andalusian stratotype) at Camonia in southwest Spain (Berggren and Haq, 1976), deep-water turbidites that originated near the coast, south of Greenland (Chapter 5), and oxygen isotope values at Salé (Hodell et al., 1994), and in the North Atlantic (Keigwin, 1987; also see Chapter 5, this thesis).

6.6. Summary

1) Water depth in northeastern Morocco increased significantly during the late Tortonian and early Messinian, suggesting a net subsidence of about 310m; a total net uplift of about 560m occurred from 6 Ma to 5.32 Ma (~0.8 m.y.), indicating a rapid tectonic uplifting; the northeastern Morocco has become a land and has never subsided again below sea level after ~5 Ma (the earliest Pliocene).

2) Three major circulation stages associated with tectonic changes in the Rifian Corridor area are determined:

Stage 1 - PMOW leaking and anti-estuarine circulation during the early Messinian (7.12–6.2 Ma). This stage is supported by evidence observed both in deep oceanic and the Mediterranean Basin. It indicates a pre-condition of the Messinian Salinity Crisis in the Mediterranean Basin.

Stage 2 - Atlantic inflow (6.2–5.9 Ma): This reversed current is characterized by a peak of the typical NADW species, abrupt decrease of *U. peregrina,* decrease of ^{18}O values, and psychrospheric ostracodes, reflecting a strong negative water balance in the Mediterranean Basin due to strong evaporation, and the onset of the Mediterranean Salinity Crisis. Both Stages 1 and 2 are considered to be deep-basin, deep-water paleoenvironments.

Stage 3 - Closing of the Mediterranean Sea (5.9–5.32 Ma) and Salinity Crisis: Morocco underwent a rapid tectonic changes (compression and uplifting) beginning at the top of C3An.1n, which suggests the severe constraints for water exchange between the Mediterranean Basin from the Atlantic Ocean just after the reversed current in upper Chronozone C3An. It is considered to have been the major cause of the formation of giant evaporitic salts in the Mediterranean Basin. The Mediterranean Salinity Crisis and the formation of the Mediterranean evaporites began within Subchronozone C3An.1n at ~ 5.9 Ma, which is slightly earlier (~0.1–0.2 m.y.) than the age proposed before.

3) The present foraminiferal and oxygen isotopic data from the Salé core strongly suggest that the Messinian Salinity Crisis in the Mediterranean Basin was associated with dramatic tectonic uplifting of Morocco during late Chronozone C3An and glacioeustatic sea-level changes driven by eccentricity forcing in each 100 kyrs during the late Messinian (5.9-5.32 Ma). Similar numbers of glacioeustatic sea-level cycles in the same time interval are also recorded in deep water turbidites in the North Atlantic Ocean (ODP Site 646B). I suggest that the tectonic uplifting in Morocco may have played a major role in the circulation restriction and final isolation from the Atlantic Ocean, while eustatic sea-level changes have been superimposed on the tectonic background, and served as an "automatic choke" that controlled the Atlantic infilling to the Mediterranean Basin and resulting in cyclic evaporitic deposits (e.g., Hsü, 1973).

CHAPTER 7

ATLANTIC DEEP WATER CIRCULATION PATTERNS: CAUSES AND EFFECTS

7.1. Benthic foraminifera as indicators of deep–water circulation

The importance of deep sea benthic foraminifera for determination of deep ocean circulation has been studied intensively in the last 30 years. Most deep-sea benthic foraminifera are sensitive to the physiochemical properties of the water masses in the world oceans and thus are used as indicators of deep–water circulation (e.g., Murray et al., 1986; Murray, 1987; Murray, 1984; Schnitker, 1980; Schnitker, 1986; Schnitker, 1974; Miller and Fairbanks, 1985; Miller et al., 1987; Miller and Tucholke, 1983; Miller and Katz, 1987; Streeter and Shackleton, 1979; Streeter, 1973; Streeter et al., 1982; Lohmann, 1978; Hodell et al., 1985; Corliss, 1982; Zahn et al., 1987; Hermelin, 1986).

Using statistical analysis based on the Quaternary foraminiferal counts of Phleger et al. (1953), together with other Lamont–Doherty data, Streeter (1973) was able to recognize three major benthic foraminiferal biofacies in the North Atlantic Ocean which have been associated with deep–water masses characterized by different temperature and salinity by Worthington and Wright (1970). This study shows that the faunal Group I characterized by *Nuttallides umbonifera* is closely related to the Antarctic Bottom Water (AABW); Group II dominated by *Planulina wuellerstorfi* and *Epistominella exigua* occurs in the samples under the influence of North Atlantic Deep Water (NADW); and Group III dominated by *Uvigerina peregrina* occurs in the area largely influenced by warm and saline Mediterranean Outflow Water (MOW). On the other hand, Schnitker (1986) suggested that *U. peregrina* has been linked to glacial bottom water at about 18,000 years BP and that Atlantic bottom water must have been warm in temperature (4°C) and low in oxygen content at this time, indicating a stagnation of the North Atlantic Ocean in agreement with Streeter (1973, 1976,

1977). In addition, Schnitker (1974) also reported that in the Western North Atlantic Basin, the *Epistominella exigua* fauna occurs in areas overlain by Norwegian Sea Overflow Water that triggers NADW and approximately within 1.9°C potential temperature contour; and the *Nuttallides umbonifera* fauna is best developed within 1.4°C potential temperature contour of AABW. In the area between 40°N and 50°N (potential temperature from 1.4°C to 1.9°C) exactly where the two bottom waters mingle, the two benthic foraminiferal faunas are no longer distinguishable (Schnitker, 1974). This may indicate the northern limit of AABW. Ten years later Weston and Murray (1983) and Murray et al. (1986) recognized different water masses in the northeastern Atlantic Ocean, namely, AABW, NADW, and NEADW (Northeast Atlantic Deep Water) from the Miocene to Recent based on analogous benthic foraminiferal species.

More recent studies, however, indicate that some species such as *Epistominella exigua* and *Eponides weddellensis*, are associated with photosynthetically produced organic material, called "phytodetritus" (Gooday, 1988; Gooday and Lambshead, 1989; Gooday et al., 1990; Gooday, 1993; Smart et al., 1993). Phytodetritus consists of phyloplankton and zooplankton remains, bound together in a gelatinous matrix to form aggregates up to about one centimeter thick. These originate in the euphotic zone during the spring bloom, and settle over a period of weeks through the water column to form a patchy deposit of light fluffy material on the ocean floor (Smart et al., 1993). Phytodetritus is well documented at bathyal and abyssal depths in the northeastern Atlantic today (Gooday and Turley, 1990), and is considered as an ephemeral food source for above–mentioned opportunists and, therefore, might control their population dynamics (Gooday and Lambshead, 1989; Gooday and Turley, 1990).

In DSDP holes 608 and 552A, available benthic foraminiferal and $\delta^{13}C$ data both from planktonic and benthic faunas make a possible comparison to determine the relationship between the surface paleoproductivity and benthic production on the ocean floor. Theoretically, high $^{13}C_{planktonic}$ values suggest high ocean surface productivity,

because photosynthesis takes up ^{12}C in water. Another approach to determine the surface productivity to use the difference ($\Delta\delta^{13}C$) between $^{13}C_{planktonic}$ and $^{13}C_{benthic}$ ($^{13}C_{P-B}$). The reason is that ^{13}C in oceanic surface water would be enriched because of the uptake of ^{12}C by plants during the photosynthesis on ocean surface, while on the ocean floor ^{13}C would be depleted through the release of ^{12}C resulting from the decay organisms from ocean surface. Therefore the difference between $\delta^{13}C_P$ and $\delta^{13}C_B$ can be used as an indicator of surface productivity and organic carbon flux from ocean surface to the bottom (Sarnthein and Winn, 1990).

In comparison with carbon stable isotopes from a surface dweller *Globigerina bulloides*, no clear relationship between the benthic faunas and paleoproductivity has been clearly determined in DSDP holes 608 and 552A (Figs. 7–1 and 7–3). The major peaks of *E. exigua* and *E. weddellensis* in the figures are characterized by widely varied $\delta^{13}C$ values. Particularly in DSDP Hole 552A, most peaks of *E. exigua* are associated with $\delta^{13}C$ depletion, rather than increases (note that depleted $\delta^{13}C$ suggests low productivity, and vice versa). The strongest evidence for the argument are the two peaks of *E. exigua* in the intervals of 109–114 msb and 121– 126 msb in Hole 552A, respectively. As shown in Fig. 7–3, the upper peak corresponds to the high $\delta^{13}C$ values up to +0.8‰, while the lower peak corresponds to the extremely depleted $\delta^{13}C$ (down to –0.4‰) that indicate extremely low surface productivity. In addition, other spikes with single sample at Site 608, however, co–vary with $\delta^{13}C$ (Fig. 7–1), indicating a possible association with paleoproductivity because Site 608 is geographically close to the area of present–day phytodetritus production in the northeastern Atlantic (Gooday and Turley, 1990). Smart et al. (1994) reported that in the North Atlantic, the percentage of *E. exigua* shows relatively modest fluctuations ranging from 5–18% during the Miocene, while in the northern margin of the Bay of Biscay in the area of present–day phytodetritus production it varies greatly from 0 to ~40%. The results in this study obviously show a similarity to the former

Fig. 7-1. Correlation between benthic foraminifera (*Epistominella exigua* and *Eponides weddellensis*) and oxygen-18 and carbon-13 data in surface dwellers (*Globigerina bulloides* and *Orbulina universa*) at DSDP Site 608. It shows no clear relationship between benthic foraminifera and surface productivity as indicated by carbon-13.

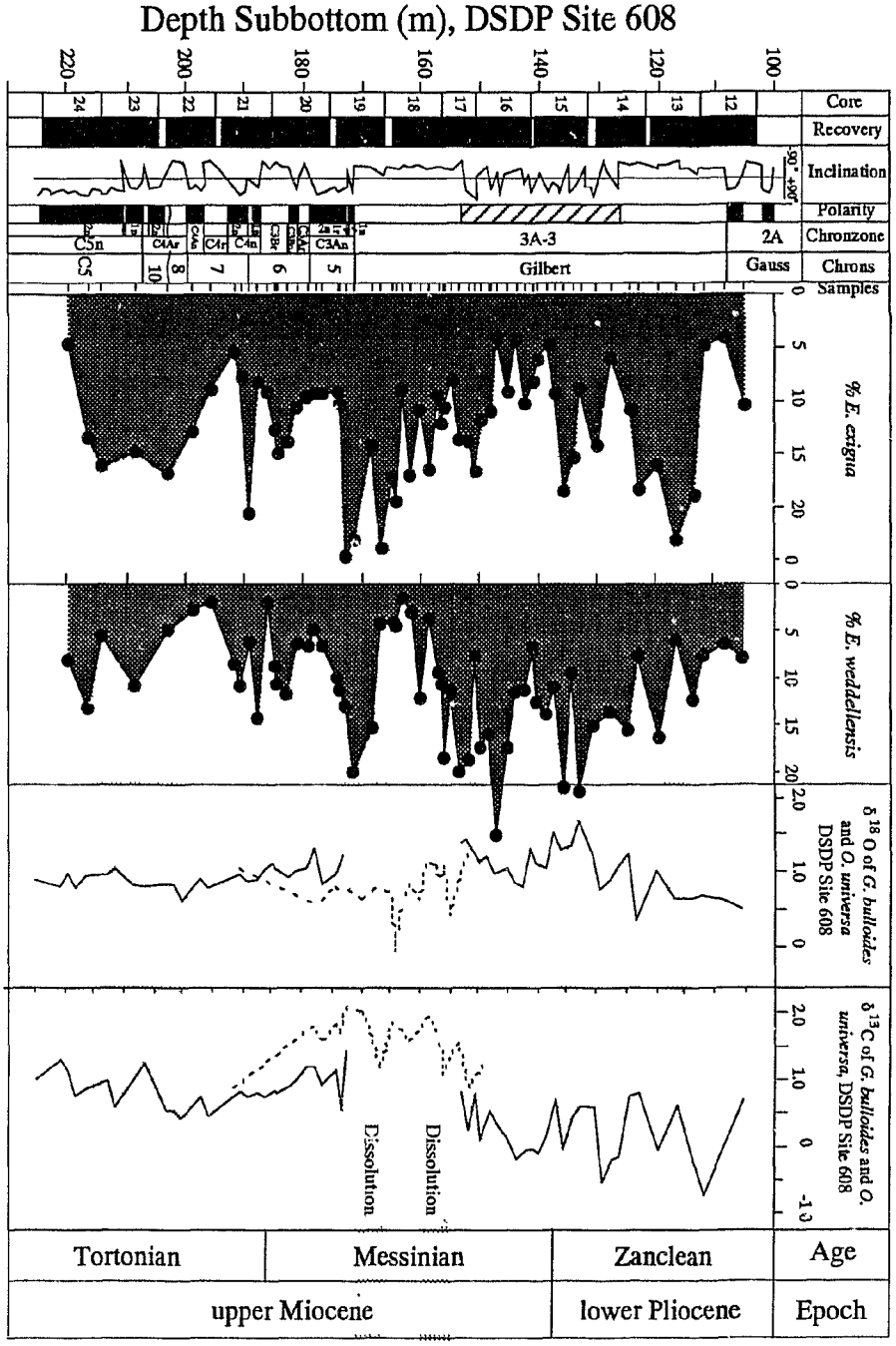
Depth Subbottom (m), DSDP Site 608
220
200
180
160
140
120
100
Core
Recovery
Inclination
-90° +90°
Polarity
Chronzone
Chrons
Samples
C5n
C5
C5r
C5An
C5Ar
C5Cn
C5Cr
C5Dn
C5Dr
C5En
C5Er
C3r
C4n
C4r
C3Br
C3An
3A-3
Gilbert
2A
Gauss
24
23
22
21
20
19
18
17
16
15
14
13
12
10
8
7
6
5
% E. exigua
% E. weddellensis
δ 18O of G. bulloides and O. universa DSDP Site 608
δ 13C of G. bulloides and O. universa, DSDP Site 608
Dissolution
Dissolution
Tortonian
Messinian
Zanclean
Age
upper Miocene
lower Pliocene
Epoch

Fig. 7-2. Messinian deep-water changes at DSDP Site 608. Note that AABW as indicated by its proxy *(Nuttallides umbonifera)* decreased during the Messinian Stage, particularly, the onset of Messinian Salinity Crisis, and the North Atlantic Ocean may have been more sluggish during the Salinity Crisis than the early Messinian and early Pliocene as suggested by *Uvigerina*.

Depth Subbottom (m), DSDP Site 608

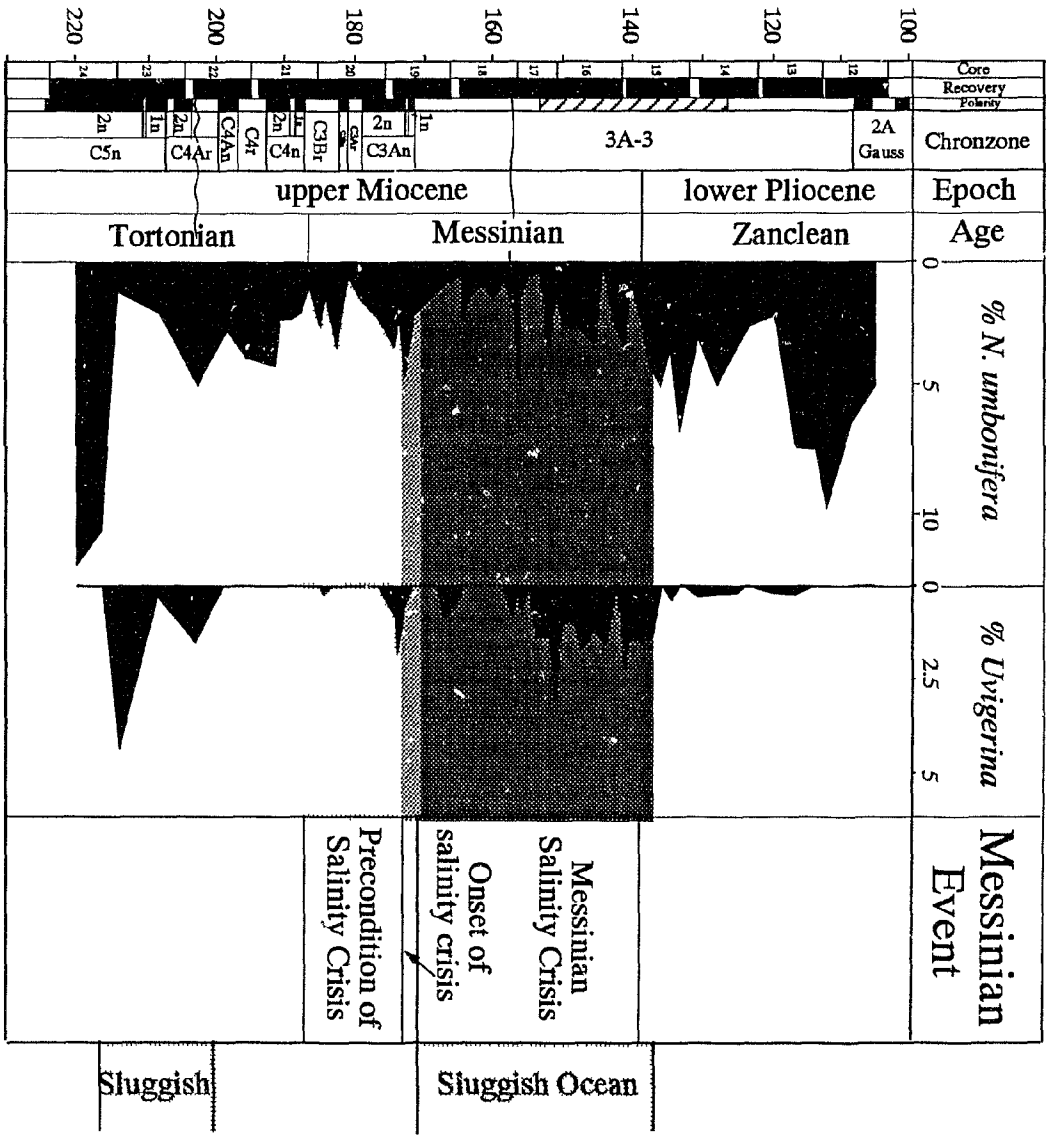

Fig. 7-3. Correlation between benthic foraminifera (*Epistominella exigua* and *Eponides weddellensis*) and oxygen-18 and carbon-13 data in surface dwellers (*Globigerina bulloides* and *Orbulina universa*) at DSDP Hole 552A. It shows no clear relationship between benthic foraminifera and surface productivity as indicated by carbon-13, except in the interval from 105 and 110m. Generally, *E. exigua* peaks are correlated well with enriched excursions of oxygen-18 in *G. bulloides* shells.

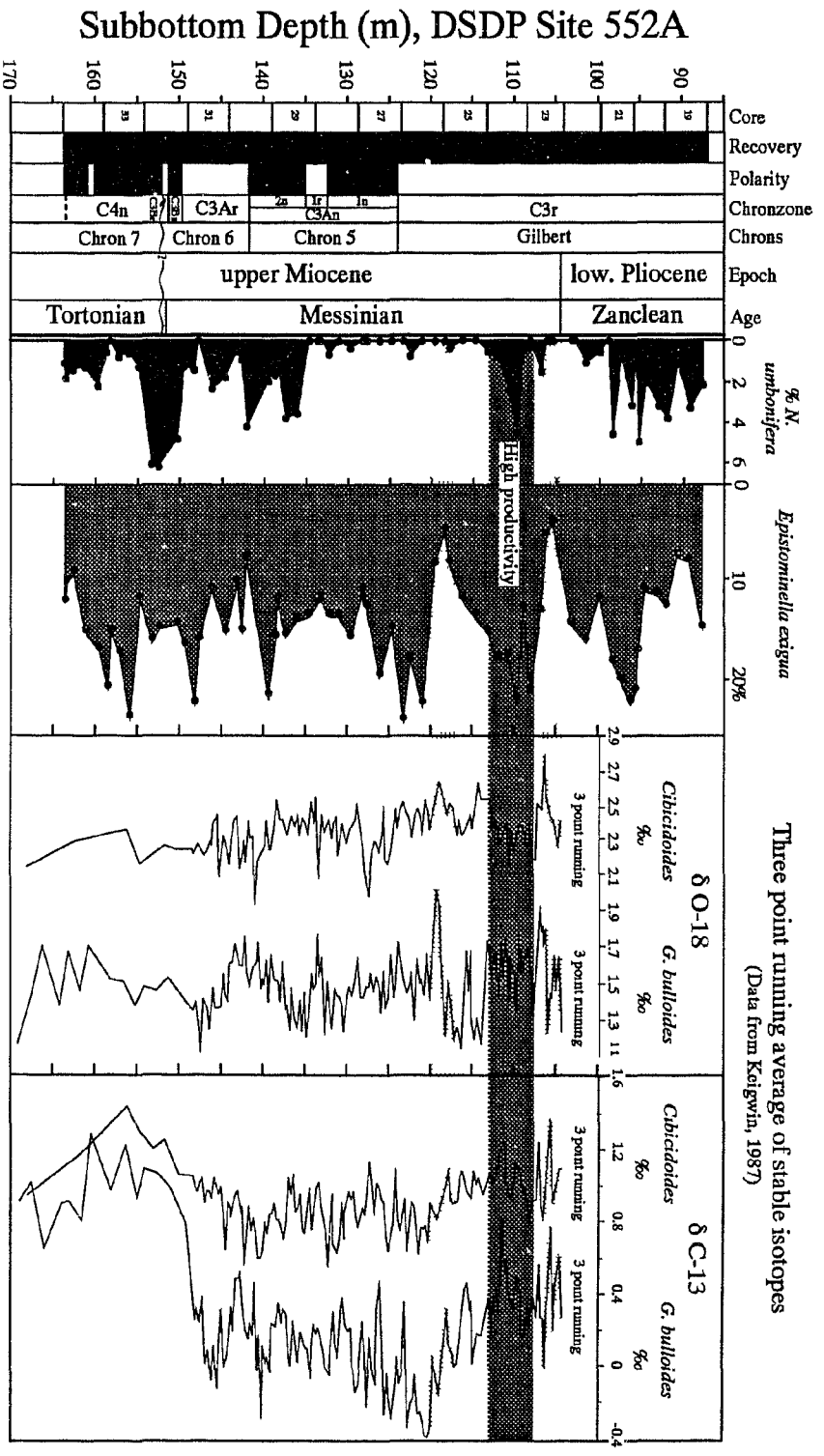
Subbottom Depth (m), DSDP Site 552A
170
160
150
140
130
120
110
100
90
Core
Recovery
Polarity
Chronzone
Chrons
Epoch
Age
C4n
C3Ar
C3An
C3r
Chron 7
Chron 6
Chron 5
Gilbert
upper Miocene
low. Pliocene
Tortonian
Messinian
Zanclean
% N. umbonifera
Epistominella exigua
High productivity
δ O-18
Cibicidoides ‰
G. bulloides ‰
δ C-13
3 point running
Three point running average of stable isotopes
(Data from Keigwin, 1987)

Fig. 7-4. Correlation between benthic foraminifera (*Epistominell xigua* and *Eponides weddellensis*) and $\Delta\delta^{13}C$ at DSDP Hole 552A, showing the relation between benthic fauna and surface productivity.

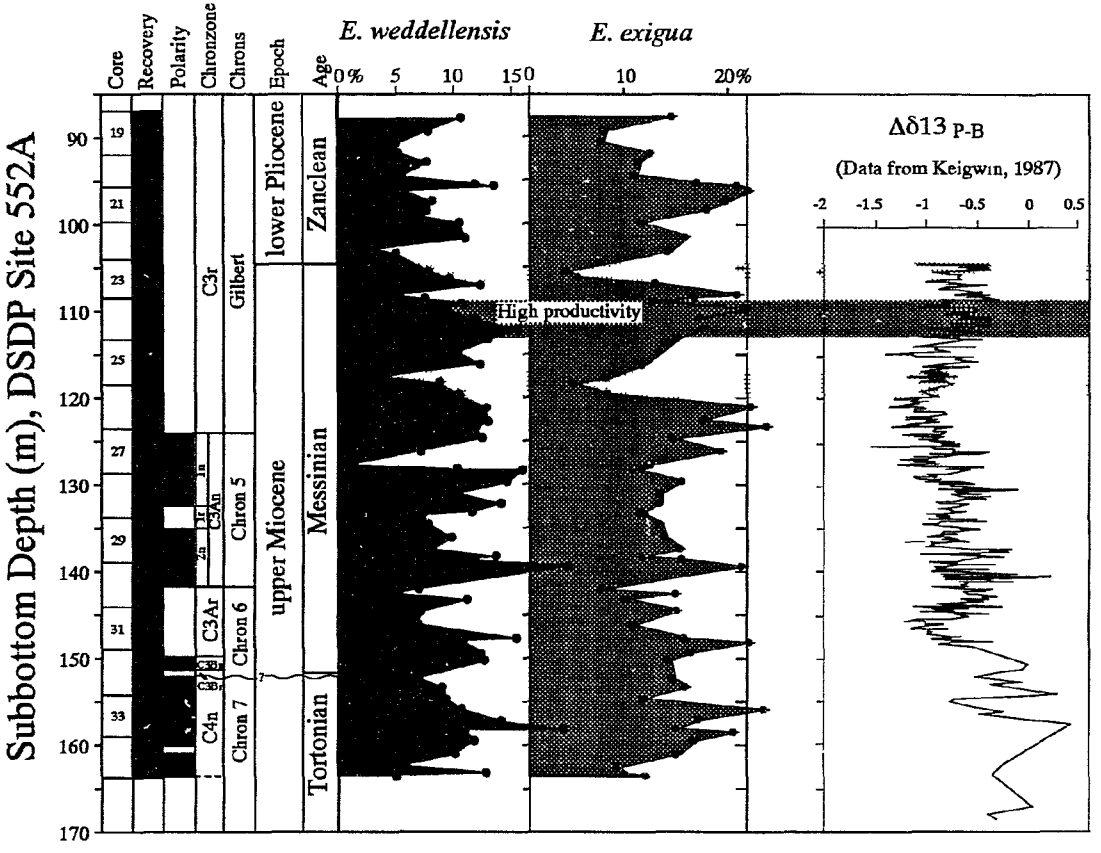
Subbottom Depth (m), DSDP Site 552A
Core
Recovery
Polarity
Chronzone
Chrons
Epoch
Age
E. weddellensis
E. exigua
0%
5
10
15
10
20%
Δδ13 P-B
(Data from Keigwin, 1987)
-2
-1.5
-1
-0.5
0
0.5
High productivity
C3r
Gilbert
C3An
Chron 5
C3Ar
Chron 6
C4n
Chron 7
lower Pliocene
upper Miocene
Zanclean
Messinian
Tortonian
90
100
110
120
130
140
150
160
170
19
21
23
25
27
29
31
33

observation. Based on these observations, I suggest that *E. exigua* at Sites 552A and 608 is essentially associated with deep–water masses. Paleoproductivity, however, may have played an important role in certain intervals, for example, the interval from 108 to 113 msb (Core 24, Hole 552A; see below for more details), where $\delta^{13}C$ values are extremely high (Fig. 7–3). In the remainder of the cores, paleoproductivity at both sites appears to be less significant although relatively long–term correlation may have occurred in the interval between 144–148m as reflected by $\Delta\delta^{13}C$ ($\delta^{13}C_{planktonic} - \delta^{13}C_{benthic}$) at Site 552 (Fig. 7–4). It, however, may have opportunistically superimposed upon the background of influence of water masses.

7.2. Temporal and spatial deep–water distribution in the North Atlantic

DSDP Site 552 from North Atlantic deep water region provides an ideal location for the view of paleoceanographic changes during the Messinian due to its location exactly under the path of NADW.

7.2.1. The Tortonian

Benthic foraminifera and stable isotopes at DSDP Sites 608 and 552A exhibit clear changes of deep–water circulation during the Tortonian. In the earliest Tortonian at about 10.3 Ma (=216–220 msb, Core 24; new time scale) at Site 608, a brief, relatively strong AABW invasion characterized by higher *N. umbonifera* (>10%), lower *Epistominella exigua*, relatively high $\delta^{18}O$ of benthic foraminifera (*Planulina wuellerstorfi*) and relatively low $\delta^{13}C$ to the northeastern Atlantic Basin is recognized (Fig. 7–2). It may be difficult to determine with low sample resolution because it has a duration of only ~0.1 Ma. This strong invasion is followed immediately after a strong NCW (Northern Component Water; analogous to NADW) production determined in the interval of 220–230 msb at Site 608 based on the large $\delta^{13}C$ difference between the North Atlantic (Site 608) and the Southern Ocean (Sites 360 and 704) by Wright et al. (1991).

During the rest of the latest Tortonian (216–186 msb at Site 608; 165–152 msb at Site 552), AABW was still present in the eastern basin as indicated by relatively high percentage of *N. umbonifera* although it may have been much reduced. Correspondingly, Wright et al. (1991) reported that NADW shows a sharp reduction in the Southern Ocean because of the decreased $\delta^{13}C$ difference between the Pacific and Southern Ocean (Wright et al., 1991). Wright et al. (1991) speculate that the reduction of NADW could allow AABW to fill most of the deep North Atlantic Ocean. This AABW invasion cannot be determined at DSDP Site 547, because of the presence of an unconformity (i.e., H3; see Chapter 4 for details) that probably cut off the latest Tortonian and the early Messinian.

7.2.2. The Messinian

A comparison with Salé Messinian section shows that three major paleoceanographic stages at Site 552 coincide well with the precondition of Messinian Crisis, the onset of Messinian Salinity Crisis and the Messinian Salinity Crisis observed in Salé borehole, Morocco (also see Chapter 6). A Similar three stages can also be distinguished at Site 608 (Fig. 7–2). However, it must be noted that Site 608 would not record as much information on paleoceanographic events as in Hole 552A, because this site rests too far from the axes of NADW and PMOW.

Stage 1 (7.12–6.2 Ma): Stage 1 stratigraphically ranges from C3Br to the top of the lower normal polarity of C3An within the time interval from 7.12–6.2 Ma according to the new time scale given by Berggren et al. (1995). It is equivalent to the Tripoli Formation, a sequence with alternating diatomites and claystones (McKenzie et al., 1979) in the Mediterranean Sea. This interval is suggested as "pre–condition of Messinian Salinity Crisis" (see Chapter 6 for details). Deposits of the Tripoli Formation indicate a restricted paleo–Mediterranean in this period.

In this stage, several minor oscillations alternate between NADW and AABW as indicated by *E. exigua* and *N. umbonifera* during the early Messinian (Figs. 7–3 and 7–6)

Fig. 7-5. Deep-water circulation model during the early Messinian (7.12 to 6.2 Ma) in the North Atlantic Ocean.

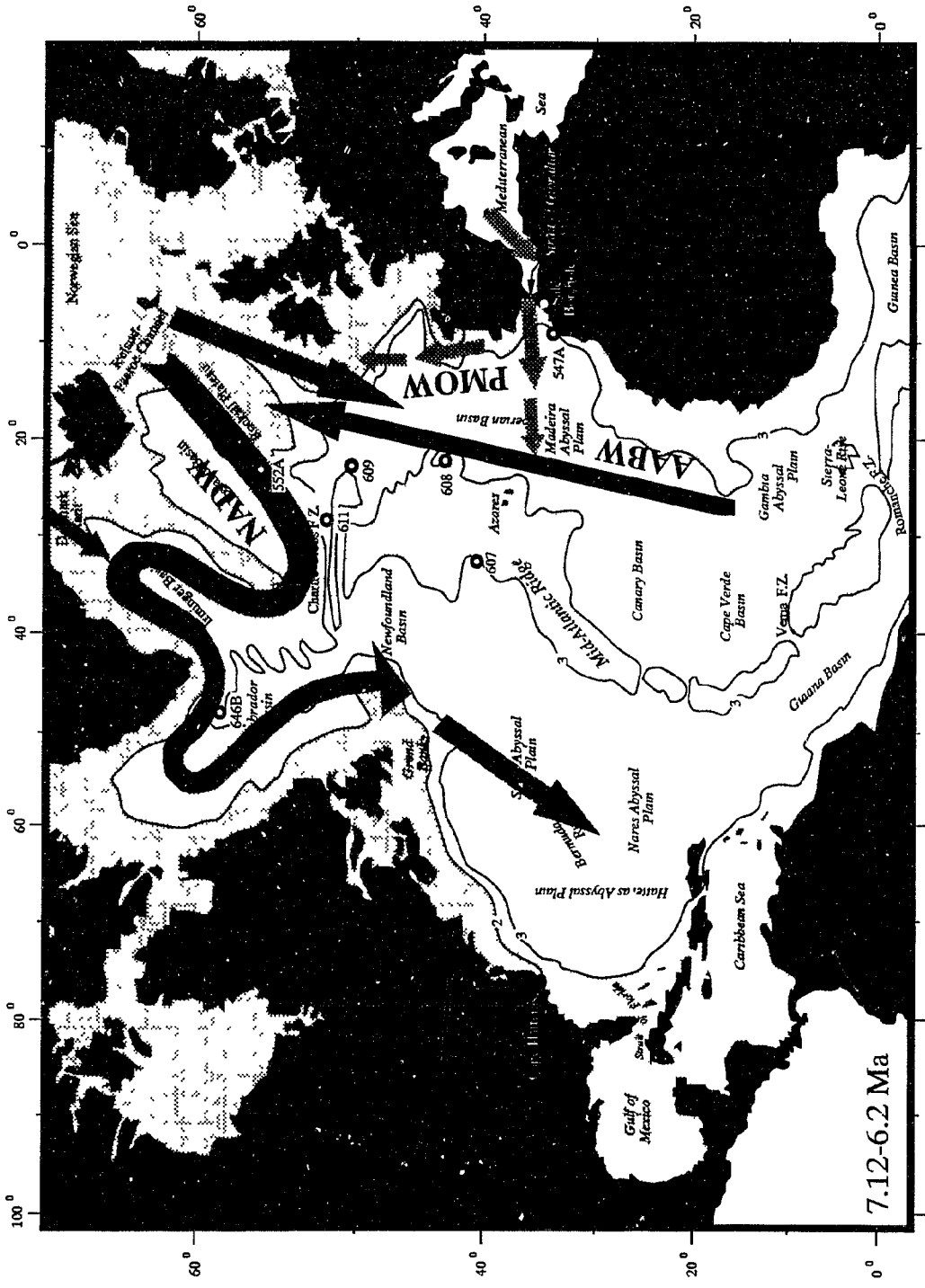
7.12-6.2 Ma
PMOW
AABW
NADW
Norwegian Sea
Mediterranean Sea
Iceland Faroe Channel
Labrador Sea
Newfoundland Basin
Azores
Canary Basin
Cape Verde Basin
Gambia Abyssal Plain
Sierra Leone Rise
Guinea Basin
Mid-Atlantic Ridge
Vema F.Z.
Guiana Basin
Hatteras Abyssal Plain
Nares Abyssal Plain
Caribbean Sea
Gulf of Mexico
Grand Banks
Bermuda Rise
Romanche F.Z.
552A
609
608
607
611
646B
547A

Fig. 7-6. Correlation between oceanic Site 552 and inland Salé borehole. It shows that: 1) during the early Messinian, the North Atlantic had relatively good ventilation indicated by relatively high *N. umbonifera* at Site 552, in part associated with outgoing PMOW indicated by *U. peregrina* in Salé core; 2) AABW retreated southward during the Onset of Salinity Crisis indicated by the absence of *N. umbonifera* at Site 552; 3) The North Atlantic was stagnant during the Salinity Crisis as indicated by *U. peregrina* at Site 552. Lower and Upper Evaporites were formed in the Mediterranean Basin when both NADW and AABW ware significantly reduced, coeval with glaciations at 7.75 and 5.55 Ma. A brief return of NADW and AABW occurred at ~5.6 Ma, which is linked to the major unconformity as a result of the "Mediterranean transgression". This unconformity separates the Lower Evaporite from the Upper Evaporite.

Fig. 7-5. Deep-water circulation model during the early Messinian (7.12 to 6.2 Ma) in the North Atlantic Ocean.

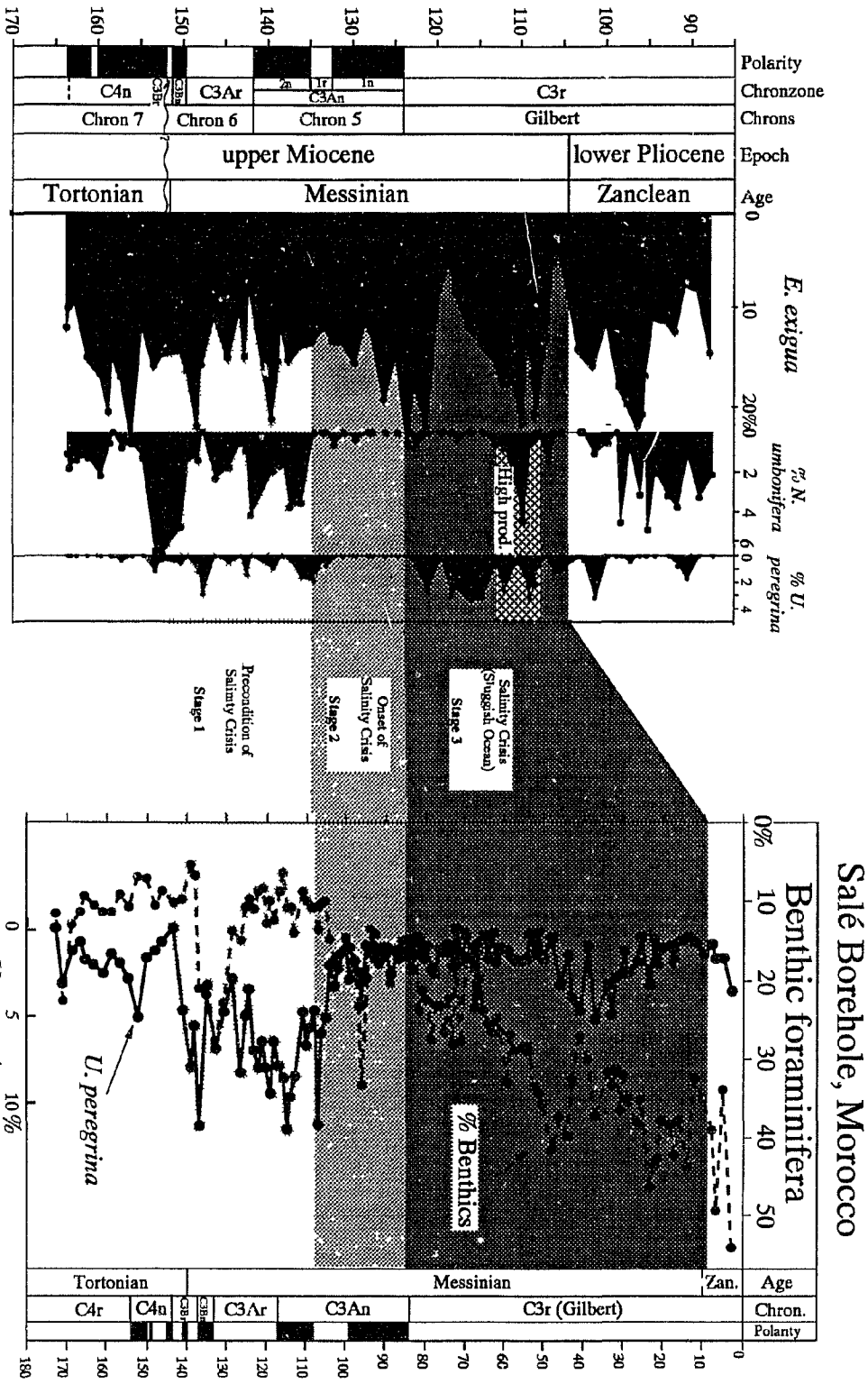

Salé Borehole, Morocco

Fig. 7-7. Deep-water circulation model during the onset of the Messinian Salinity Crisis (6.2-5.9 Ma) in the North Atlantic Ocean.

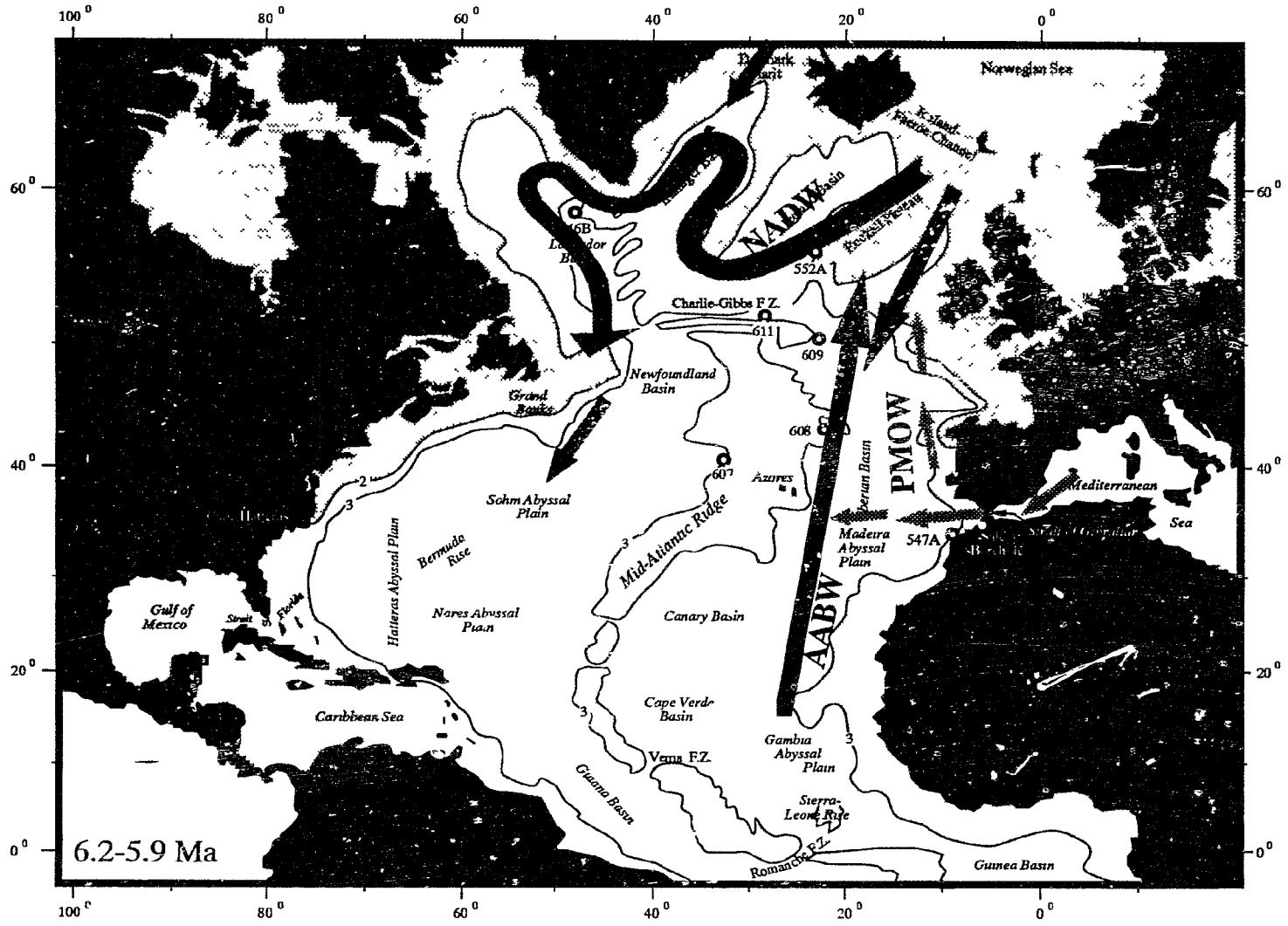
100°
80°
60°
40°
20°
0°
60°
40°
20°
0°
Norwegian Sea
NADW
Basin
552A
Charlie-Gibbs F.Z.
611
609
608
607
Newfoundland Basin
Grand Banks
Azores
PMOW
Iberian Basin
Mediterranean Sea
Sohm Abyssal Plain
Bermuda Rise
Hatteras Abyssal Plain
Mid-Atlantic Ridge
Madeira Abyssal Plain
547A
AABW
Gulf of Mexico
Florida Strait
Nares Abyssal Plain
Canary Basin
Caribbean Sea
Cape Verde Basin
Gambia Abyssal Plain
Vema F.Z.
Guiana Basin
Sierra-Leone Rise
Romanche F.Z.
Guinea Basin
6.2-5.9 Ma

which may suggest unstable climatic changes. Fig. 7–5 shows a general distribution of deep–water circulation during the early Messinian in the North Atlantic based on the benthic foraminifera. In the Southern Ocean, ODP Site 704 is dominated by NCW as shown by higher $\delta^{13}C$ values during the early Messinian (Wright et al., 1991). The alternations between NADW and AABW were not reported based on stable isotopes by (Wright et al., 1991). At Site 608, Wright et al. (1991) also reported a major NCW flux between 7.8 and 7.0 Ma (187–170 msb interval), which is calibrated to 7.2 to 5.9 Ma in this study (see Chapter 4), indicating early Messinian age. Therefore, the NCW flux determined by Wright et al. (1991) is consistent with my observation based on benthic foraminifera at Sites 552 and 608. DSDP Site 238 in the Pacific Ocean is characterized by the absence of *Uvigerina* (Vincent et al., 1980), and at Site 547 in the Madeira abyssal plain off the northwestern Africa the lower Messinian was missing, suggesting the intensification of deep water circulation. It is obvious that the evidence from all the different oceans accounts for relatively good basin to basin ventilation at this time.

In comparison with the distribution of *N. umbonifera* during the latest Tortonian, the paleoenvironment in this stage appears to have been similar to that of the latest Tortonian. AABW at this time was also reported to reach ~50°N in the eastern Atlantic Basin (DSDP Site 608) by Murray et al. (1987) based on benthic foraminiferal studies using >125μm size fraction of sediments, although it may have been little more sluggish during the early Messinian as reflected by the presence of *U. peregrina* (Fig. 7–6).

Stage 2 (6.2–5.9 Ma): Stage 2 is represented by the interval from the bottom of C3An.1r to the top of C3An.1n (6.2–5.9 Ma). It is interpreted to be equivalent to *Calcare di Base* underlain by the Tripoli Formation in Sicily, Mediterranean Sea. In this stage, AABW has been significantly reduced at Site 552 as suggested by the absence of *N. umbonifera* (Figs. 7–6 and 7–7), probably indicating relatively poor basin to basin ventilation relative to Stage 1.

Fig. 7-8. Deep-water circulation model during the beginning of the Messinian Salinity Crisis (5.9-5.78 Ma) in the North Atlantic Ocean.

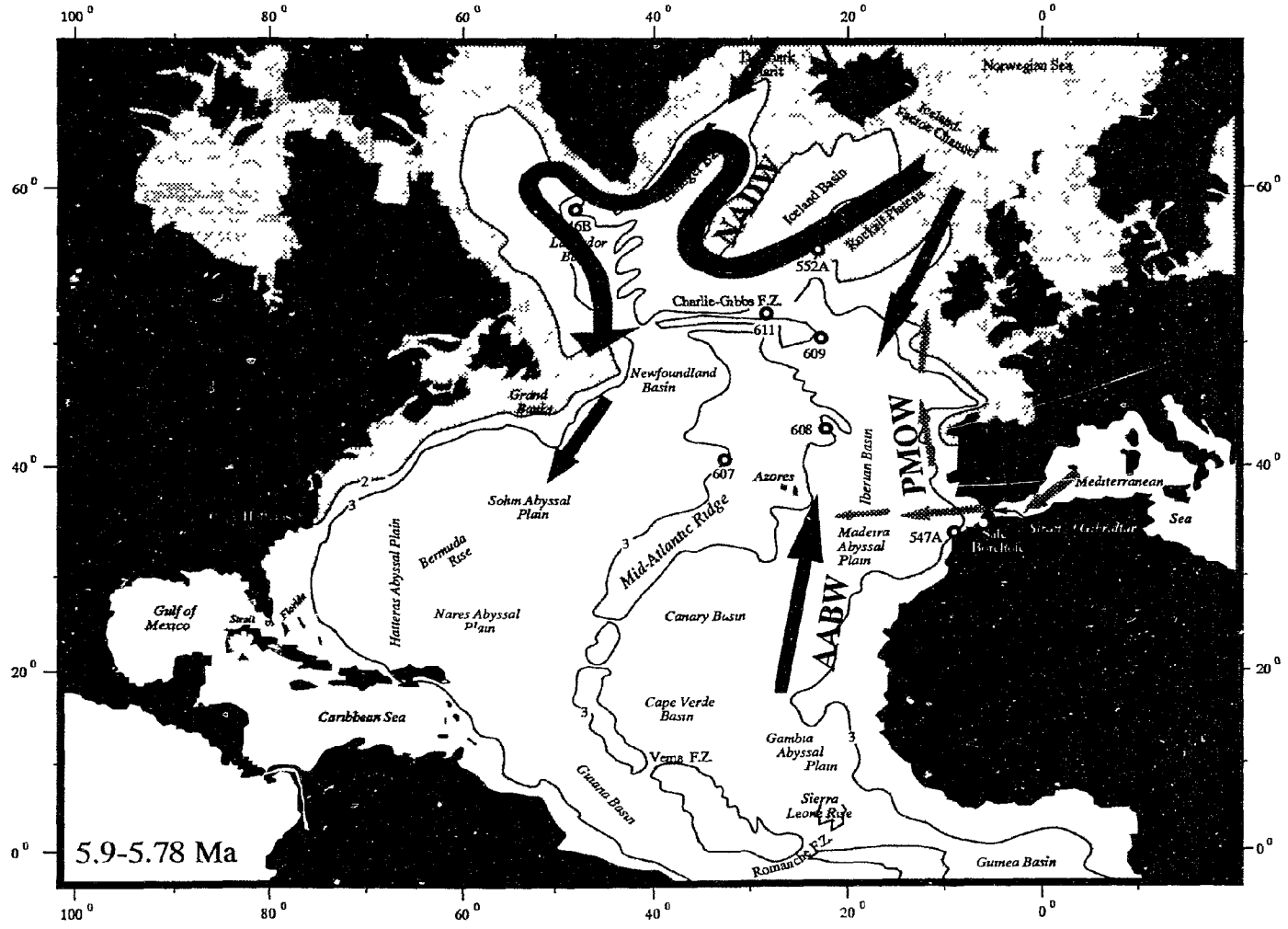
100°
80°
60°
40°
20°
0°
60°
40°
20°
0°
Norwegian Sea
Iceland Basin
Rockall Plateau
NADW
552A
6B
Charlie-Gibbs F.Z.
611
609
608
607
Newfoundland Basin
Grand Banks
Azores
Iberian Basin
PMOW
Mediterranean Sea
Sohm Abyssal Plain
Bermuda Rise
Hatteras Abyssal Plain
Mid-Atlantic Ridge
Madeira Abyssal Plain
547A
Gulf of Mexico
Florida Straits
Nares Abyssal Plain
Canary Basin
AABW
Caribbean Sea
Cape Verde Basin
Vema F.Z.
Gambia Abyssal Plain
Guiana Basin
Sierra Leone Rise
Romanche F.Z.
Guinea Basin
5.9-5.78 Ma

Fig. 7-9. Deep-water circulation model at 5.75 Ma (late Messinian) in the North Atlantic Ocean.

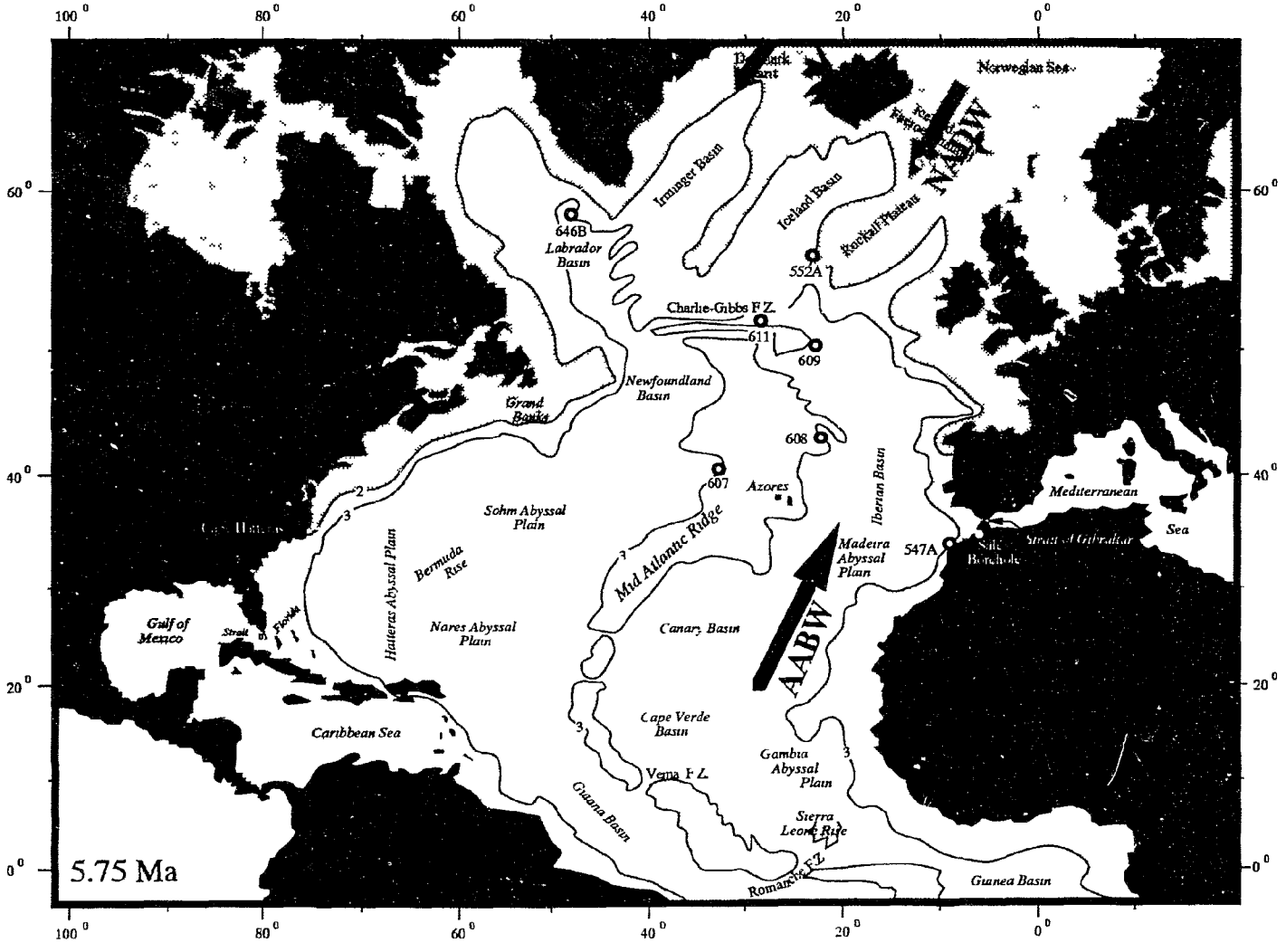
100°
80°
60°
40°
20°
0°
60°
40°
20°
0°
Norwegian Sea
NADW
Irminger Basin
Iceland Basin
Rockall Plateau
646B
Labrador Basin
552A
Charlie-Gibbs F.Z.
611
609
Newfoundland Basin
Grand Banks
608
607
Azores
Sohm Abyssal Plain
Mid Atlantic Ridge
Iberian Basin
Mediterranean Sea
Strait of Gibraltar
547A
Madeira Abyssal Plain
AABW
Bermuda Rise
Hatteras Abyssal Plain
Nares Abyssal Plain
Canary Basin
Gulf of Mexico
Florida Strait
Caribbean Sea
Cape Verde Basin
Gambia Abyssal Plain
Vema F.Z.
Guiana Basin
Sierra Leone Rise
Romanche F.Z.
Guinea Basin
5.75 Ma

Stage 3 (5.9–5.32 Ma). This stage, equivalent to the latest Messinian is characterized by great oscillations of deep–water circulation. From 5.9 to 5.8 Ma a major AABW reduction has occurred as reflected by absence of *N. umbonifera* (Fig. 7–8), coinciding with the low occurrence of *N. umbonifera* at ODP sites 747, 751, 748 in the Kerguelen Plateau of the Southern Ocean (Mackensen, 1992). The North Atlantic Ocean appears to have been essentially characterized by NADW. At DSDP Site 609, Murray (1987) reported a similarity of deep–water circulation pattern (p. 979, fig. 18) to that of this study. In the Southern Ocean, Mackensen (1992) reported that a NADW–like water mass once bathed the Southern Ocean at this time. These studies are in agreement with the observation of this study. But their studies were based on low sampling resolution, and thus little detail on the deep–water circulation was given for the interval with frequent climatic changes. Moreover, stable isotopes given by Wright et al. (1991) show no major NCW occurred in this interval.

From 5.78 to 5.32 Ma, the present study shows that two major NADW reductions indicated by low abundance of *E. exigua* have occurred at 5.75 Ma and 5.55 Ma, respectively at Site 552 (Figs. 7–9 and 7–11). NADW is determined at Site 552 before 7.8 Ma and at ~5.6 Ma (Fig. 7–10). At DSDP Site 547 off northwestern Africa, this interval contains high percentage of *E. exigua* (average >20%) and *N. umbonifera* (average >10%), indicating a mixture of NADW and AABW waters (see Fig. 3–22). My study also shows that AABW may have been absent except for a brief return at 5.6 Ma at Site 552 (Fig. 7–6) and at Site 608 (Fig. 7–2).

7.2.3. The early Pliocene

During the early Pliocene, the North Atlantic Ocean appears to be characterized by a mixture of NADW and AABW waters at sites 608 and 552, although alternating oscillations among the two water masses may have occurred at this time (Figs. 7–2, 7–3, 7–6). This is in agreement with the observation of Murray (1987), who determined that

Fig. 7-10. Deep-water circulation model at ~5.60 Ma (the late Messinian) in the North Atlantic Ocean.

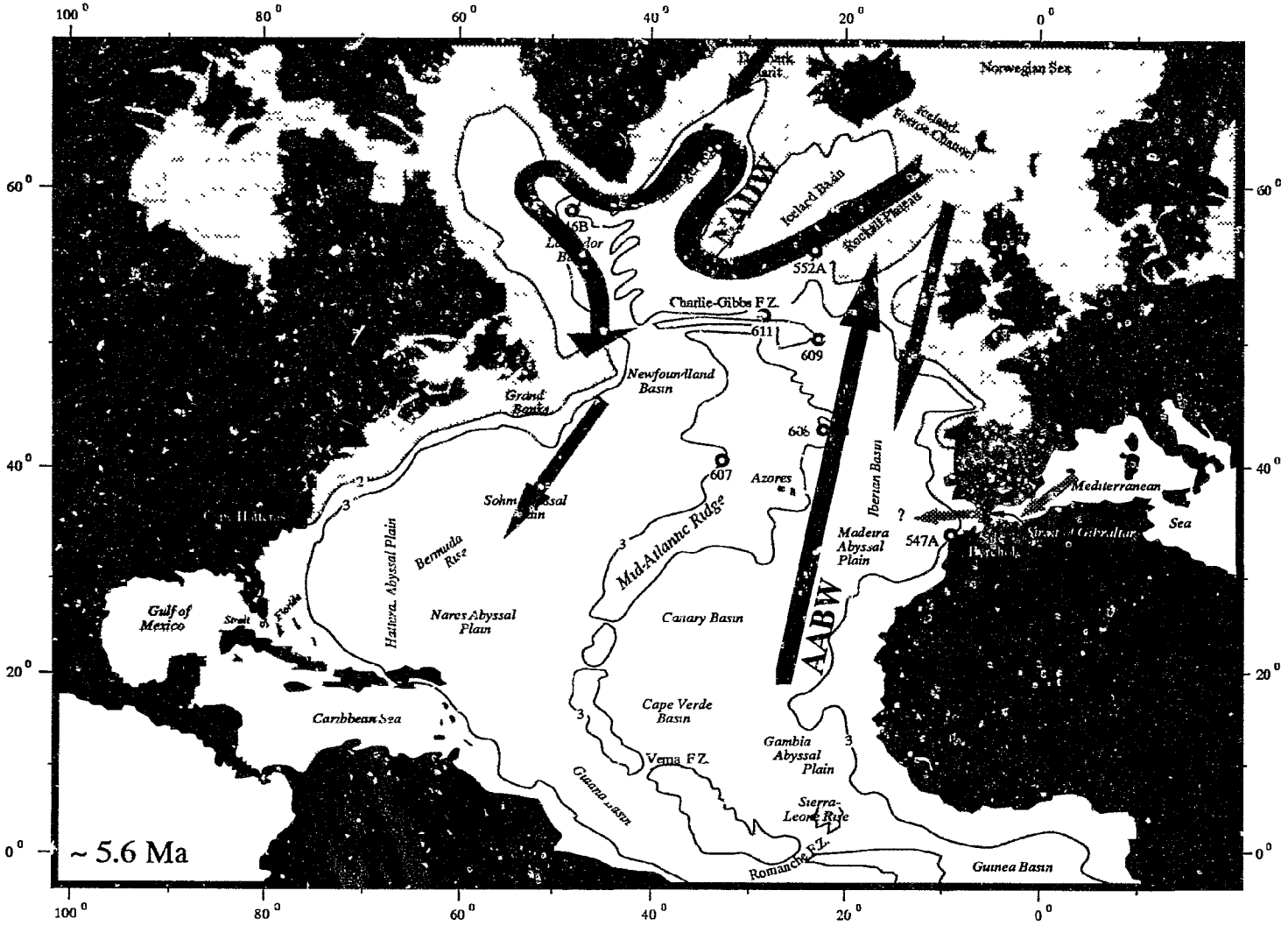
100°
80°
60°
40°
20°
0°
60°
40°
20°
0°
Norwegian Sea
Iceland-Faeroe Channel
Iceland Basin
Rockall Plateau
NADW
552A
Charlie-Gibbs F.Z.
611
609
608
607
Azores
Newfoundland Basin
Grand Banks
Iberian Basin
Mediterranean Sea
Strait of Gibraltar
547A
Madeira Abyssal Plain
Mid-Atlantic Ridge
Bermuda Rise
Hatteras Abyssal Plain
Nares Abyssal Plain
Canary Basin
Gulf of Mexico
Florida Straits
Caribbean Sea
Cape Verde Basin
Vema F.Z.
Gambia Abyssal Plain
Sierra Leone Rise
Romanche F.Z.
Guinea Basin
AABW
~ 5.6 Ma

Fig. 7-11. Deep-water circulation model at ~5.55 Ma (the latest Messinian) in the North Atlantic Ocean.

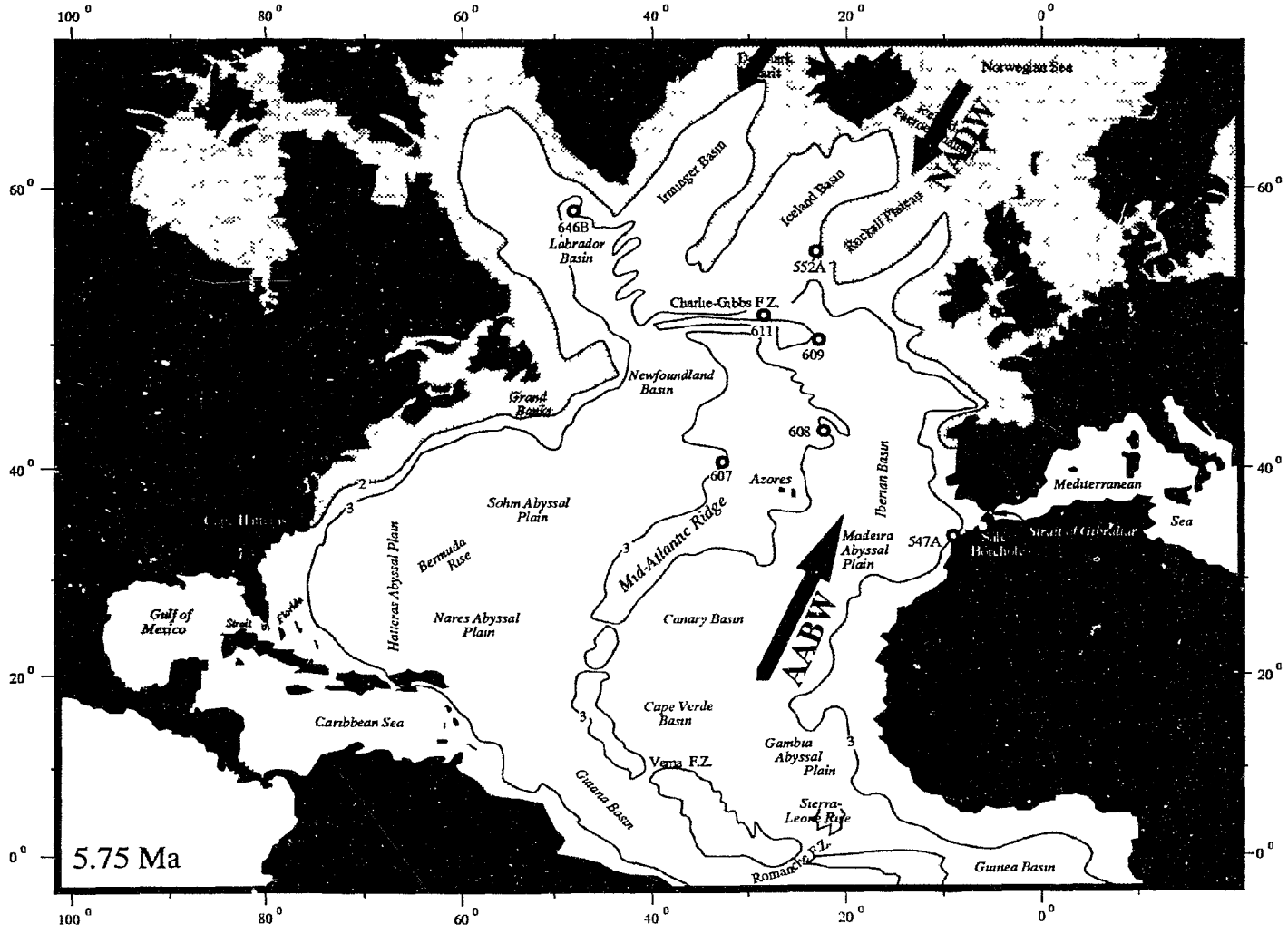
100°
80°
60°
40°
20°
0°
60°
40°
20°
0°
Norwegian Sea
NADW
Iceland Basin
Reykjanes Ridge
Irminger Basin
646B
Labrador Basin
552A
Charlie-Gibbs F.Z.
611
609
Newfoundland Basin
Grand Banks
608
607
Azores
Iberian Basin
Mediterranean Sea
Sohm Abyssal Plain
Mid-Atlantic Ridge
Madeira Abyssal Plain
547A
Bermuda Rise
Hatteras Abyssal Plain
Gulf of Mexico
Florida Straits
Nares Abyssal Plain
Canary Basin
AABW
Caribbean Sea
Cape Verde Basin
Gambia Abyssal Plain
Vema F.Z.
Guiana Basin
Sierra-Leone Rise
Romanche F.Z.
Guinea Basin
5.75 Ma

Fig. 7-11. Deep-water circulation model at ~5.55 Ma (the latest Messinian) in the North Atlantic Ocean.

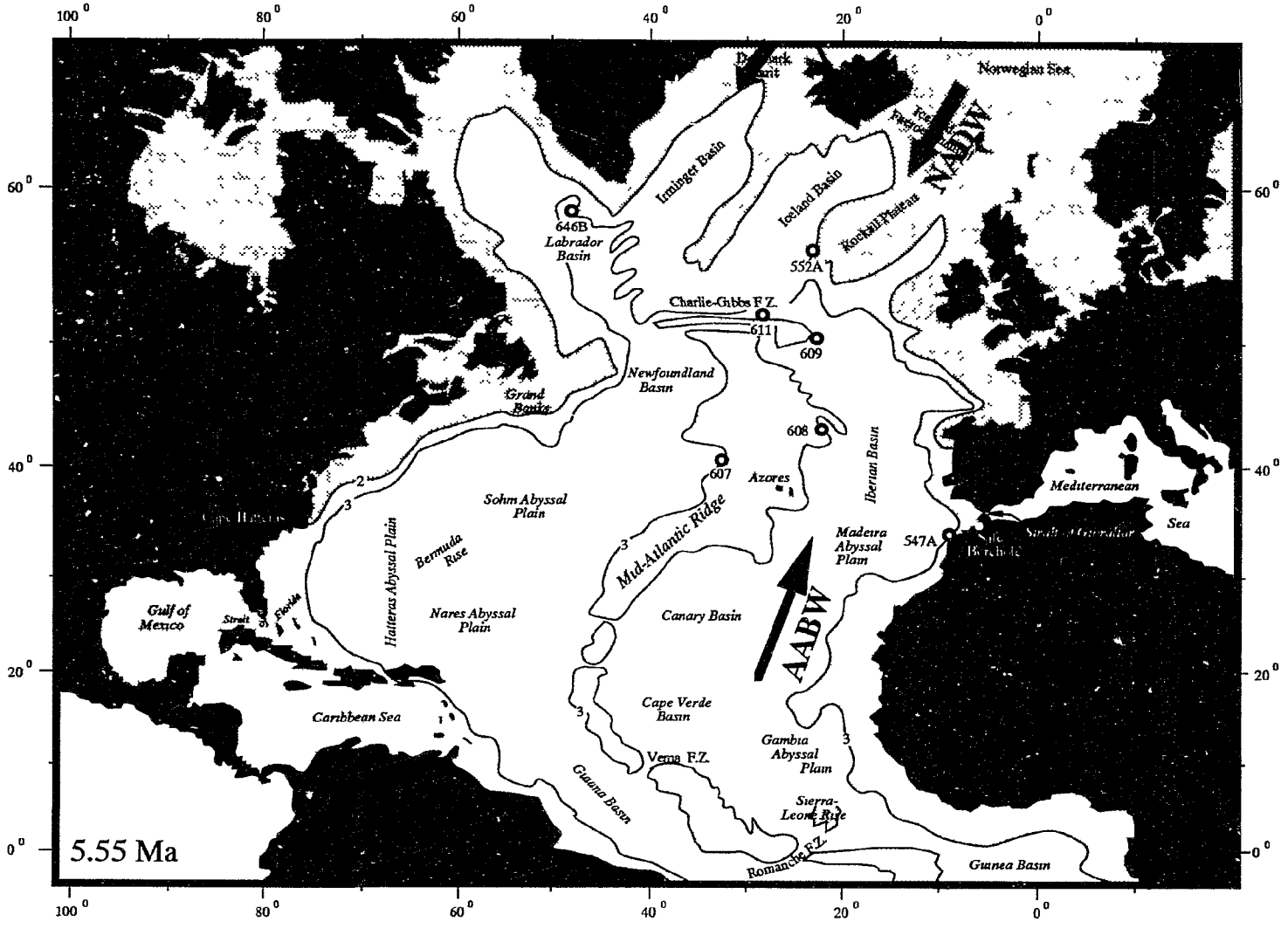
100°
80°
60°
40°
20°
0°
60°
40°
20°
0°
Norwegian Sea
NADW
Irminger Basin
Iceland Basin
Rockall Plateau
646B
Labrador Basin
552A
Charlie-Gibbs F.Z.
611
609
Newfoundland Basin
Grand Banks
608
607
Azores
Iberian Basin
Mediterranean Sea
Sohm Abyssal Plain
Cape Hatteras
Bermuda Rise
Mid-Atlantic Ridge
Madeira Abyssal Plain
547A
Halteras Abyssal Plain
Gulf of Mexico
Florida Strait
Nares Abyssal Plain
Canary Basin
AABW
Caribbean Sea
Cape Verde Basin
Gambia Abyssal Plain
Vema F.Z.
Guyana Basin
Sierra-Leone Rise
Romanche F.Z.
Guinea Basin
5.55 Ma

AABW has reached as far as 53°N, north of DSDP Site 611 during the early Pliocene (nannofossil zone NN13). A gradual decrease in the relative abundance of *N. umbonifera* from Site 608 to Site 552 shows that AABW may have decreased from south to north, while NADW does not show such a north–south trend. At Site 547, no clear NADW or AABW are distinguished from the benthic foraminiferal distribution, because both signals of *E. exigua* and *N. umbonifera* are extremely diluted by sudden increase of *Bolivina inflata* and *Bolivina pseudothalmanni* (see Fig. 3–23; Site 547A). A similar increase is also observed at Site 552 in the early Pliocene. The significance of the sudden increase is not clear at present, probably because of high productivity in ocean surface, or downslope transportation, or low oxygen content in bottom water caused by sluggish circulation, as reported by various workers (Harman, 1964; Cita and Podenzani, 1980; Van der Zwaan, 1980; Sen Gupta et al., 1981; Casey et al., 1981; Thomas, 1986; Thomas, 1987a, b).

7.3. Messinian deep–water circulation – possible cause and effect

7.3.1. Climate fluctuations as a major cause of deep–water circulation

During the beginning of the early Messinian, a cooling period was determined by oxygen stable isotopes from planktonic foraminiferal tests at Site 519 (*O. universa*) in the South Atlantic Ocean (McKenzie and Oberhänsli, 1985) and at Site 608 (*Globigerina bulloides*) (Fig. 7–1), but at Site 552 a marked decrease in planktonic foraminiferal oxygen isotopes has occurred, indicating a significant difference from Sites 519 and 608. It is interesting that such a decrease is not recorded in benthic foraminiferal (*P. wuellerstorfi*) oxygen isotopes at the same site (Fig. 7–3). The difference between the sites is not understood. It may be expressed as a local event, rather than a global one. I tentatively propose four interpretations for the difference: 1) This decreased signal could result from low sampling resolution for Sites 519 and 608; 2) .To some degree, it could have been related to PMOW changes. It is clear that density surface of today's MOW moves up to between 200 and 100 m below sea surface when it moves northward (Barry Ruddick, pers.

comm., 1995), and it could warm up the uppermost layer of water; 3) The signal could have been associated with warm paleo– Gulf Stream that flowed over the site during the Messinian; or 4) It could be a combination of 2 and 3. I prefer the last interpretation, because I speculate that PMOW alone may not have been strong enough to change oxygen isotopic values so significantly.

During the late Messinian two major NADW reductions occur at 5.75 Ma and 5.55 Ma, respectively, as indicated by sudden decrease of *E. exigua* (Fig. 7–3). These two events are coeval with major AABW reductions and major enrichments of $\delta^{18}O$ known as major glacials in the late Miocene (Keigwin, 1987) (Figs. 7–3 and 7–5). These two glacials could have caused significant sea–level lowerings and southward movement of the Polar Front in the Northern Hemisphere. It was reported that the Polar Front moved to the south of 45^0N during the Last Glacial, resulting in the cessation of NADW (Ruddiman and McIntyre, 1977). I speculate that the NADW reductions during the late Messinian may have had a similar origin in association with the Polar Front that moved southward, and further caused the Norwegian–Greenland seas to be stagnant or shut–down production of NADW. Although both glacials are brief, only about 10,000 yrs each in duration (Keigwin, 1987), they appear to have had profound influence on the deep–water circulation. As seen in Fig. 7–3, NADW reduced dramatically when glaciations started, and came back gradually with the onset of deglaciation. In addition, sea–level lowerings caused by glaciations could have separated the Mediterranean Sea from the Atlantic Ocean, and further created the Lower and Upper evaporites in the Mediterranean Basin at this time.

A significant increase of *E. exigua* occurs between the two major reductions of NADW in Core 24, indicating a brief return of NADW during the interglacial. It is also supported by high $\delta^{13}C_B$ values which reach over 1.2‰, indicating a younger deep–water incursion. Atlantic inflow water into the Mediterranean Basin at this time was also recorded in Salé borehole, in which several deep–water benthic foraminiferal species (such as *Oridorsalis umbonatus, Stilostomella* spp.) increased in abundance. According to the

variations of planktonic foraminifera, $CaCO_3$ and stable oxygen isotopes at Salé, Morocco, this inflow may have occurred between SLL 4 and SLL 3 (Fig. 6–4), with a duration of about 10,000–20,000 years. The return of NADW, together with sea–level fluctuation could have caused an inundation into the Messinian Mediterranean Basin, yielding a major unconformity that separates the Lower Evaporite from the Upper Evaporite as observed in the Mediterranean Basin (Hsü et al, 1973a). Moreover, it is possible that a small amount of PMOW may have occurred as well, as indicated by increased low oxygen species *U. peregrina*, suggesting a water exchange between the Atlantic and the Mediterranean.

It must be mentioned that the increase of *E. exigua* observed at Site 552 may have also been associated with increased surface oceanic productivity because of high $\delta^{13}C$ (values 0.4– 0.8‰) of the planktonic *G. bulloides* (Fig. 7–3). It is known that $\Delta\delta^{13}C$ generally indicates surface productivity (Sarnthein and Winn, 1990; Ellen Thomas, pers. comm., 1995). However, at Site 552, $\delta^{13}C$ at this time does not reflect the surface productivity because this site has received younger NADW that contains high $\delta^{13}C$ (Fig. 7–3). It is clear that caution must be taken into account when we use $\delta^{13}C$ as an indicator of surface productivity. It may be used only for a steady state ocean. In addition, an increased NADW flux may also be a possible contribution since it was recognized in the Southern Ocean as a "major NCW flux" which occurred during the "interglacial" interval (Wright et al., 1991). Hence, it appears to be little doubt that the major peak of *E. exigua* may have been associated with both high paleoproductivity and NADW flux.

At Site 608 (present water depth 3511 m) and Site 547 (water depth 3948 m), a strong carbonate dissolution took place exactly in this interval (see Fig. 3–16). It is not completely understood at the moment, but probably because of two reasons: 1) It may have been associated with the Messinian Salinity Crisis when the major body of evaporites (i.e., the Lower Evaporites) formed in the Mediterranean Basin. This is observed at Site 552 because it is located at shallower water depth (2311 m). The formation of Mediterranean evaporites could turn the world ocean less alkaline and raise the lysocline and carbonate

compensation depths, resulting in stronger deep–sea carbonate dissolution (Ryan, 1973); 2) It may have been related to the climatic changes that could have lowered sea level as suggested by $\delta^{18}O$ enrichments in this interval at Sites 552, 608 and Salé borehole (see Figs. 3–20, 7–3, and 3–10).

7.3.2. Association with the Messinian Salinity Crisis

The basin to basin ventilation system during the early Messinian (Stage 1) is also suggested to have been in part associated with less PMOW entering the Norwegian–Greenland seas and producing less deep–water overflows across the Faeroe–Scotland sill back to the North Atlantic Ocean. Evidence for the PMOW flux to the North Atlantic through the Betic Passage in southern Spain and Rifian Corridor in Morocco (Benson and Rakic–El Bied, 1991a; McKenzie and Oberhänsli, 1985; Chapter 6) is strong at this time. It is understood that NADW would have increased and AABW would have decreased when more PMOW filled the Norwegian–Greenland seas, and vice versa. It is speculated that the spatial contribution of PMOW during the early Messinian may be similar to the modern MOW that spreads partially northward and enters the Norwegian–Greenland seas (Reid, 1979; Open University, 1989; Barry Ruddick, pers. comm., 1995).

During the onset of Messinian Salinity Crisis, three major coiling direction changes of *Neogloboquadrina acostaensis* within paleomagnetic Chron 5 in Salé borehole are observed. The first S/D coiling change in this interval occurred at 102.85 m (Sample B37) in Subchronozone C3An.1r (Fig. 4-1); the first D/S change occurs at 90.8 m (Sample B25; middle C3An.1n); and the second S/D change at 86.65 m (Sample B21; top of C3An.1n). I have not determined any major changes in DSDP/ODP Holes 552A, 608 and 646B. Hole 547A near the Strait of Gibraltar shows only one D/S change occurs in the late Miocene, but this hole stratigraphically is far beyond control due to carbonate dissolution and a hiatus within the Messinian section (Fig. 4–11). In Holes 552A, 608 and 646B, Chron 5 section is dominated by sinistral *Neogloboquadrina*. However, two major S/D coiling changes that

are reported in DSDP Site 609 in open Atlantic by Hooper and Weaver (1987), Sites 611, 607 and in the Mediterranean region (Hilgen, pers. comm., 1995; Sierro, pers. comm., 1995) are identical to those in the Salé borehole; one is in C3An.1r (middle Chron 5), and another in C3An.1n (top of Chron 5). In the Pacific Ocean, such coiling changes are not well documented, although some minor changes of *Neogloboquadrina pachyderma* (maximum ~20%) were reported in the Blind River section, New Zealand, and DSDP Site 281 by Loutit (1981) and Roberts et al. (1994). I suggest that the pattern of the coiling shift in the Blind River section and DSDP Hole 281 appears to be different from those around the Mediterranean region, because 1) The D:S ratio is only ~1:4 in the Pacific, while the coiling direction is almost completely shifted from sinistral to dextral or from dextral to sinistral in the Mediterranean region; 2) The coiling change in the Pacific is from dextral to sinistral in C3An.1r, while in the Mediterranean region it is from sinistral to dextral; and 3) There is only one shift recorded in Chron 5 in the Pacific, while three (i.e. S/D, D/S and S/D) around the Mediterranean region. In addition, Keigwin and Shackleton (1980) observed sinistral *N. acostaensis* just above the $\delta^{13}C$ shift followed by the FO of *Pulleniatina primalis* in the Pacific Ocean, but did not report the S/D and D/S shifts in Chron 5. At Site 397 off western Africa, there is one S/D change at Chron 6/5 boundary (Mazzei et al., 1979), which is much lower than the first change at the middle of Chron 5 in Salé core.

The major synchronous coiling changes observed in this study and reported by Hooper and Weaver (1987) are most likely restricted to the Mediterranean region and particular part of the northeastern Atlantic Ocean. If this is true, then these changes may indicate unstable local/regional paleoenvironments, and may be associated with the paleo–Mediterranean water mass production entering the northeastern Atlantic Ocean during the early phase of the Mediterranean Salinity Crisis. Here, I tentatively re–construct the paleo–Mediterranean outflow water (PMOW) history in the North Atlantic (Fig. 7–12) based on the regional coiling change. It is expected that the warm, saline PMOW could cause coiling

Fig. 12. Paleo-Mediterranean Outflow re-construction in the North Atlantic Ocean during the middle and upper Chron 5 (=C3An.1r and 1n).

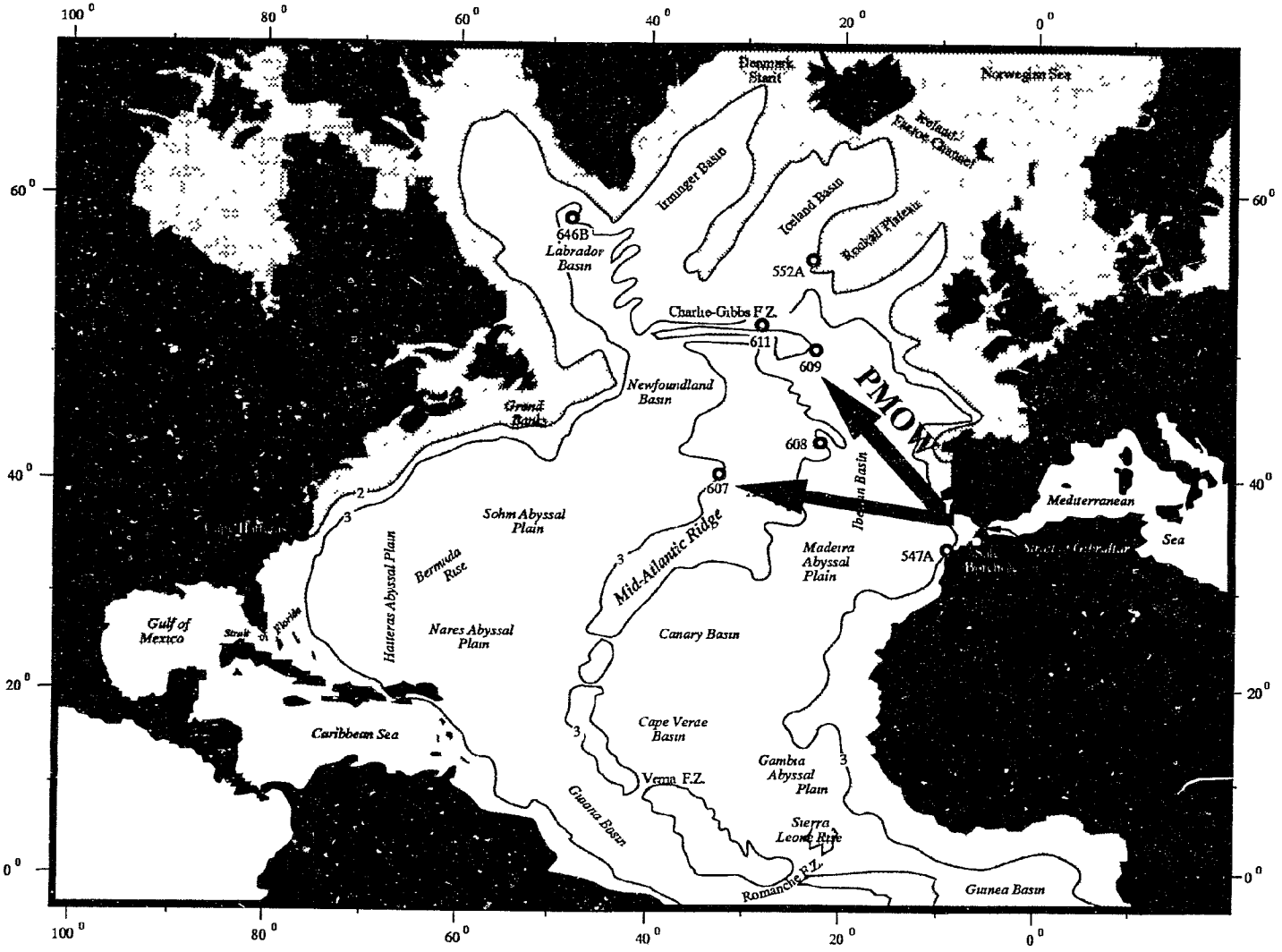
100°
80°
60°
40°
20°
0°
60°
40°
20°
0°
Denmark Strait
Norwegian Sea
Iceland Faeroe Channel
Irminger Basin
Iceland Basin
Reykjanes Plateau
646B
Labrador Basin
552A
Charlie-Gibbs F.Z.
611
609
PMOW
Newfoundland Basin
Grand Banks
608
607
Iberian Basin
Mediterranean Sea
Sohm Abyssal Plain
Mid-Atlantic Ridge
Madeira Abyssal Plain
547A
Bermuda Rise
Hatteras Abyssal Plain
Gulf of Mexico
Straits of Florida
Nares Abyssal Plain
Canary Basin
Caribbean Sea
Cape Verde Basin
Gambia Abyssal Plain
Vema F.Z.
Guiana Basin
Sierra Leone Rise
Romanche F.Z.
Guinea Basin

direction change of *Neogloboquadrina pachyderma/acostaensis* from sinistral to dextral in C3An.1r because of the temperature increase of upper layer oceanic water affected by "hot" PMOW and regional temperature increase. The modern MOW is currently reported in the Labrador Sea (Mudie, pers. comm., 1995) and the Norwegian Sea (Reid, 1979). MOW enters the Labrador Sea probably across the Charlie-Gibbs Fracture Zone over Site 609 and Site 611, and enters the Norwegian Sea through the Iceland–Faeroe Ridge. In addition, Messinian oxygen isotopic study shows a distinct warming at ~120m ($\delta^{18}O$ Stage C3An.18O.17; Hodell et al., 1994; p. 847, fig. 10) where the first S/D exactly occurred in C3An.1r, juxtaposed with the first S/D change. The early extinction of *Gt. conomiozea* at the same level may also have been associated with the regional temperature increase that killed the temperate fauna. We suggest that this marked $\delta^{18}O$ depletion in Salé borehole may reflect a local climatic warming, because this warming peak is not recognized in other regions, such as in the Blind River section and Hole 281, as indicated by planktonic foraminifera (i.e., *N. pachyderma* and *Globigerina bulloides*) at this time (Loutit, 1981). In fact, Loutit's work (1981) suggests a climate cooling. Such a cooling is also detected in DSDP Holes 552A (Fig. 7–3) and 608 (Fig. 3–20) in C3An.1r. Based on these observations, we may conclude that the period of middle C3An.1r may represent a global climate cooling, but local warming may have occurred in some particular areas associated with the warm PMOW activities and the onset of the Mediterranean Salinity Crisis.

Tectonic evidence shows that there was a channel present in northern Morocco and southern Spain, to allow water circulation exchange between the North Atlantic and Mediterranean Sea during Chron 5. These two channels were called the "twin channel" (Benson et al., 1991a). Benson et al. (1991a) further suggested that the paleo–Mediterranean outflow water entered the North Atlantic via the Betic Passage in Spain and inflow came into the Mediterranean Sea across the Rifian Channel (also called the "siphon" by Benson et al., 1991a) in Morocco during Chron 5. Benthic foraminiferal studies both in Spain (Berggren et al., 1976; Berggren and Haq, 1976) and Morocco indicated a conduit in

each place as well. It is evident that our interpretation is in agreement with that of Cita and Ryan (1979), rather than that of Hooper and Weaver (1987) who suggested the effect by global glacial cycles based on *Neogloboquadrina pachyderma* distribution, rather than by the Mediterranean salinity crisis. We assume that if these changes had been caused by global glacial cycles as speculated by Hooper and Weaver (1987), then the S/D coiling change in C3An.1r should be determined in all the oceans, but this appears not to be the case.

Another alternate interpretation is that these regional/local coiling changes could have been related to the changing strength of the gyre rotation with the oscillation caused by earth orbital forcing (Benson and Rakic–El Bied, 1991a; Benson, pers. comm.). However the available data appear to support an association with PMOW because the locations containing Chron 5 coiling changes are on the route of PMOW, and these events are restricted to the Mediterranean region (Hodell et al., 1994). Thus I, prefer the former interpretation. Obviously, further study for this issue may be required to prove my interpretation.

There are two other coiling changes in the lowermost C3r at 80.55 m (D/S; Sample B15), and 76.3 m (S/D; Sample B11), respectively, immediately above Chron 5. Above the last S/D shift at 76.3 m, dextrally coiled *N. acostaensis* extends dominantly up to the top of the section. It does not agree with Hodell et al.'s (1994) observation that the sinistral form dominates for the remainder of the core record above 82.6 m. These frequent coiling changes are also considered to be associated with unstable paleoenvironment during the Mediterranean Salinity Crisis.

In this circumstance, I would prefer to link the deep–water production in Chron 5 and lowermost C3r to the quasiperiodic coiling changes that may have been controlled by PMOW although these PMOW fluctuations have not been recorded in benthic foraminifera in Salé core.

The Mediterranean Salinity Crisis during the latest Messinian has been widely believed to cause a series of paleoceanographic changes. For example, cessation of deep–water formation could have occurred in the northern hemisphere (Blanc and Duplessy, 1982; Murray, 1987; McKenzie and Oberhänsli, 1985) because MOW no longer entered the Norwegian–Greenland seas as a result of isolation of the Mediterranean Sea from the Atlantic Ocean, and 6% reduction of global oceanic alkalinity (Ryan, 1973) because of the extraction of a great volume of salts in the Mediterranean from open ocean.

As seen at Sites 552 and 608, a relatively long–term reduction of AABW as reflected by *U. umbonifera* (a proxy of AABW) in the entire interval of the late Messinian from 6.2 (C3An.1r) to 5.55 Ma cannot be simply explained by climate pulses. In fact, this reduction coincides extremely well with the Messinian Salinity Crisis and onset of the crisis, except for a brief return of AABW near the Messinian/Pliocene boundary at 5.6 Ma. I interpret that this long–term AABW reduction must have been linked to the Messinian Salinity Crisis although the great climate fluctuations (two brief glaciations) have caused two major reductions of NADW at 5.75 and 5.55 Ma. It is evident that since the onset of the salinity crisis at Subchronozones C3An.1r and 1n (6.2 to 5.894 Ma), PMOW may have been greatly constrained because of the uplift of Morocco. The limited PMOW that drained into the North Atlantic Ocean via Betic Passage of southern Spain may not have been strong enough to enter the Norwegian–Greenland seas to produce NADW to spill over the Iceland–Faeroe Ridge and Denmark Strait. As a consequence, the ocean lost a dynamic feature and became sluggish. This is strongly supported by a major increase of *U. peregrina* within the interval of Messinian Salinity Crisis (5.9–5.32 Ma) both at Site 552 and Site 608 (Figs. 7–2, 3 and 5). It is also supported by a similar spike of *Uvigerina peregrina* reported at DSDP Site 238 in the Indian Ocean (Vincent et al., 1980). The increase of the species, therefore, is counted as a global event. As discussed in Chapter 6, *U. peregrina* apparently is an indicator of low oxygen water masses (also Streeter and

Shackleton, 1979). Its increase in this interval may suggest that the global ocean was under relatively poor basin to basin ventilation during the Messinian Salinity Crisis.

7.4. Summary

The present deep-water benthic foraminiferal and stable isotopic studies show that:

1) A comparison of benthic foraminifera with $\delta^{13}C_p$ and $\Delta\delta^{13}C_{P\text{-}B}$ suggests that the production of *Epistominella exigua* and *Eponides weddellensis* may not be necessarily related to the oceanic surface productivity during the Messinian. Instead, they are associated with deep-water masses, and thus may be used as indicators of deep-water masses.

2) During the Messinian, three major paleoceanographic stages recognized in deep sea cores.

Stage 1 (7.12–6.2 Ma): Stage 1 is equivalent to the "pre–condition of Messinian Salinity Crisis" as in Salé borehole. It has several minor oscillations alternate between NADW and AABW, which may suggest unstable climatic changes.

Stage 2 (6.2–5.9 Ma): Stage 2 is equivalent to *Calcare di Base* underlain by the Tripoli Formation in Sicily. In this stage, AABW has been significantly reduced at Site 552, probably indicating relatively poor basin to basin ventilation relative to Stage 1.

Stage 3 (5.9–5.32 Ma). This stage is equivalent to the Messinian Salinity Crisis, characterized by great oscillations of deep–water circulation. A major AABW reduction has taken place in this stage. From 5.8 to 5.32 Ma, two major NADW reductions occurred at 5.75 Ma and 5.55 Ma, respectively.

3) Climate fluctuations are the major cause of the changes in of deep–water circulation. During the late Messinian the two major NADW reductions at 5.75 Ma and 5.55 Ma are coeval with major enrichments of $\delta^{18}O$ known as major glacials in the late Miocene. These two glacials could also have caused significant sea–level lowerings and southward movement of the Polar Front in the Northern Hemisphere.

Brief returns of NADW and AABW have taken place at ~5.6 Ma (interglacial), with a duration of about 10,000–20,000 years. The return of NADW, together with sea–level fluctuation could have caused an inundation into the Messinian Mediterranean Basin as recorded in Salé borehole, yielding a major unconformity that separates the Lower Evaporite from the Upper Evaporite as observed in the Mediterranean Basin. In addition, it is possible that a small amount of PMOW may have occurred as well, as indicated by increased low oxygen species *U. peregrina*, suggesting a water exchange between the Atlantic and the Mediterranean at this time.

4) The formation of deep-water circulation is also associated with the Messinian Salinity Crisis. The relative dynamic basin to basin ventilation system during the early Messinian (Stage 1) has been in part associated with less PMOW.

During the onset of Messinian Salinity Crisis, coiling direction changes of *Neogloboquadrina acostaensis* in Salé borehole, DSDP sites 609, 611, 607 and in the Mediterranean region indicate an unstable local/regional paleoenvironments, and may be associated with the paleo–Mediterranean water mass production entering the northeastern Atlantic Ocean during the early phase of the Mediterranean Salinity Crisis.

The Messinian Salinity Crisis has caused the world ocean to be sluggish. The relatively long–term reduction of AABW and pulse variations of NADW in the interval from 6.2 (C3An.1r) to 5.32 Ma is linked to the Messinian Salinity Crisis because it coincides extremely well with the Salinity Crisis and onset of the crisis. It is also supported by the global increase of *U. peregrina* in this interval, which suggests that the global ocean was under relatively poor basin to basin ventilation at this time.

CHAPTER 8

CONCLUSIONS

This multi-disciplinary study leads to the following major conclusions:

8.1. Stratigraphy

To obtain detailed time control for the Messinian paleoceanographic study, four DSDP/ODP Holes (552A, 646B, 608, and 547A) from the North Atlantic Ocean and one land borehole from Morocco were analyzed for integrated bio-, magneto-, and stable isotope Messinian stratigraphic study with sampling interval. These results indicate:

a) In Salé Borehole, Morocco, the Tortonian/Messinian boundary is located at 139.05 m (sample B72), defined by the FO of *Globorotalia conomiozea*, with an age estimate of 7.12 Ma (C3Br). The Pliocene/Messinian boundary is interpolated between S series samples S7 and S11 at ~10 m just above the LO of *Gt. plesiotumida* .

b) In DSDP Hole 552A, the Tortonian/Messinian boundary is defined by the FO of *Globorotalia conomiozea* s.s. at 150.16 msb in Chronozone C3Br. The Pliocene/Messinian boundary is based on indirect evidence, namely 1) The FO of *Gt. puncticulata,* 2) TG14 oxygen isotope stage at 106 msb, and 3) Using our age– depth plot.

c) In DSDP Hole 608, the Messinian/Pliocene boundary is placed at 138.6 msb within Core 15, mainly relying upon the LO of *Gt. conomiozea/miotumida* plexus and the marked $\delta^{18}O$ enrichment (TG14?). The Tortonian/Messinian boundary is placed with the FO Gt. *conomiozea* within Core 20 at 184.88 msb. A small hiatus may be present within the Messinian (between Cores 18 and 17) as suggested by nannofossils, where a strong carbonate dissolution has taken place.

d) In DSDP Hole 547A, a condensed Messinian section is bracketed by the FO and LO of *Gt. conomiozea,* ranging from the middle of Core 8 to the top of Core 6. Three

hiatuses are identified in this hole, one in the Messinian, which separates the upper Messinian from the upper Tortonian; and two in the Pliocene.

e) Neither the Tortonian/Messinian nor the Messinian/Pliocene boundaries in ODP Hole 646B can be easily assigned because of downslope transportation during the Messinian Stage. The Tortonian/Messinian boundary is placed between Cores 75X and 78X, using $^{87}Sr/^{86}Sr$ age estimate, Chron 6 $\delta^{13}C$ shift at Core 75X, $\delta^{18}O$ enrichment in Core 77X, *Neogloboquadrina* coiling change from the dextral to sinistral, and the FO of *D. berggrenii* in Core 76X.

The Messinian/Pliocene boundary is tentatively placed between Cores 46X and 50X, based on the following observations: 1) the LO of *D. berggrenii* in Sample 49X-CC, 2) a Sr age of 5.37 Ma, 3) the interpolation of the FO of *G. margaritae* at 506.9 msb and FO of *G. puncticulata* at 383.08 msb; and 4) $\delta^{18}O$ depletion above Core 45X and $\delta^{18}O$ enrichment.

Diachrony and synchrony of some important Messinian planktonic foraminifera from these Atlantic DSDP/ODP holes and Salé borehole, such as the LO of *Gq. dehiscens*, the LO of *Gt. lenguaensis*, the FO and LO of Gt. *conomiozea*, the FO of *Gt. margaritae* s.s., the FO of *Gt. puncticulata*, and the FO of *Gt. crassaformis* are discussed for understanding some of the paleoceanographic changes. This stratigraphy permits us to compare intra-Mediterranean paleoceanographic changes with those in the open Atlantic Ocean to determine what effect the Mediterranean salinity crisis had on deep-water paleoceanography during the Messinian Stage.

8.2. Glacioeustatic sea-level and paleoclimatic fluctuations

During the Messinian Salinity Crisis, frequent sea-level and climate fluctuations are recorded by deep-water turbidites (ODP Hole 646B), foraminifera (Salé borehole, Morocco), and oxygen stable isotopes (DSDP 552 and Salé borehole). Eight deep-water turbidite cycles in Hole 646B can be correlated well with the same number of oxygen

isotopic enrichments in Hole 552A, indicating that they may have been caused by sea-level lowerings. Marsh agglutinated benthic foraminifera in deep-water turbidites suggest that sea level may have been lowered about 80-100 m. At Salé, faunal, carbonate and isotopic cycles coincide with eccentricity cycles (100 kyrs).

8.3. Uplifting of Morocco

a) Water depth in northeastern Morocco increased significantly during the late Tortonian and early Messinian, suggesting a net subsidence of about 310m; a total net uplift of about 560m occurred from 6 Ma to 5.32 Ma (~0.8 m.y.), indicating a rapid tectonic uplifting; the northeastern Morocco became a land and never subsided again below sea level after ~5 Ma (the earliest Pliocene).

8.4. Water exchange in the Rifian Corridor during the Messinian.

Uplift of Morocco caused three major circulation changes: a) Stage 1 - PMOW leaking and anti-estuarine circulation during the early Messinian (7.12–6.2 Ma): This stage is strongly supported by a number of observations both in the deep oceanic and in the Mediterranean Basin. It indicates a pre-condition of the Messinian Salinity Crisis in the Mediterranean Basin.

b) Stage 2 - Current reversal (6.2–5.9 Ma): This reversed current is characterized by a peak of the typical NADW species, an abrupt decrease of *U. peregrina,* decrease of ^{18}O values, and psychrospheric ostracodes, reflecting a strong negative water balance in the Mediterranean Basin caused by strong evaporation, and the onset of the Mediterranean Salinity Crisis. Both Stages 1 and 2 are considered to be deep-basin, deep-water paleoenvironments.

c) Stage 3 - Closing of the Mediterranean Sea (5.9–5.32 Ma) and Salinity Crisis: Morocco underwent a rapid tectonic changes (compression and uplifting) beginning at the top of C3An.1n, which suggests the severe constraints for water exchange between the

Mediterranean Basin from the Atlantic Ocean just after the reversed current in upper Chronozone C3An. It is considered to have been the major cause of the formation of giant evaporitic salts in the Mediterranean Basin. The Mediterranean Salinity Crisis and the formation of the Mediterranean evaporites began within Subchronozone C3An.1 at ~ 5.9 Ma, which is slightly earlier (~0.1–0.2 m.y.) than the age proposed before.

8.5. The cause of the Messinian Salinity Crisis:

Foraminiferal and oxygen isotopic data from the Salé core strongly suggest that the tectonic uplifting in Morocco may have played a major role in the circulation restriction and final isolation from the Atlantic Ocean. Eustatic sea-level changes superimposed on the tectonic background, served as an "automatic choke" that controlled the Atlantic infilling to the Mediterranean Basin and resulted in cyclic evaporitic deposits.

8.6. Distribution of deep-water masses

a) A comparison of benthic foraminifera with $^{13}C_p$ and $\Delta\delta^{13}C_{P\text{-}B}$ suggests that the production of *Epistominella exigua* and *Eponides weddellensis* may not be necessarily related to oceanic surface productivity during the Messinian. Instead, they are associated with deep-water masses, and thus may be used as indicators of deep-water masses.

b) During the Messinian, three major paleoceanographic stages are recognized in deep sea cores.

Stage 1 (7.12–6.2 Ma): Stage 1 is equivalent to the "pre–condition of Messinian Salinity Crisis" as in Salé borehole. It has several minor oscillations that alternate between NADW and AABW, which may suggest unstable climatic changes.

Stage 2 (6.2–5.9 Ma): Stage 2 is equivalent to *Calcare di Base* underlain by the Tripoli Formation in Sicily. In this stage, AABW has been significantly reduced at Site 552, probably indicating relatively poor basin to basin ventilation relative to Stage 1.

Stage 3 (5.9–5.32 Ma). This stage is equivalent to the Messinian Salinity Crisis, characterized by great oscillations of deep–water circulation. A major AABW reduction has taken place from in this stage. From 5.8 to 5.32 Ma, two major NADW reductions occurred at 5.75 Ma and 5.55 Ma, respectively.

8.7. The cause of deep-water circulation changes

a) Climate fluctuations are the major cause of the production and changes in deep–water circulation. During the late Messinian the two major NADW reductions at 5.75 Ma and 5.55 Ma are coeval with major enrichments of $\delta^{18}O$ known as major glacials in the late Miocene. These two glacials could have also caused significant sea–level lowerings and southward movement of the Polar Front in the Northern Hemisphere.

Brief returns of NADW and AABW have taken place at ~5.6 Ma (interglacial), with a duration of about 10,000–20,000 years. The return of NADW, together with sea–level fluctuation could have caused an inundation into the Messinian Mediterranean Basin as recorded in Salé borehole, yielding a major unconformity that separates the Lower Evaporite from the Upper Evaporite as observed in the Mediterranean Basin. In addition, it is possible that a small amount of PMOW may have occurred as well, as indicated by increased low oxygen species *U. peregrina*, suggesting a water exchange between the Atlantic and the Mediterranean at this time.

b) A change of deep-water circulation is also associated with the Messinian Salinity Crisis. The relative dynamic basin to basin ventilation system during the early Messinian (Stage 1) has been in part associated with less PMOW.

During the onset of the Messinian Salinity Crisis, coiling direction changes of *Neogloboquadrina acostaensis* in the Salé borehole, DSDP sites 609, 611, 607 and in the Mediterranean region indicate an unstable local/regional paleoenvironments, and may be associated with the paleo–Mediterranean water mass production entering the northeastern Atlantic Ocean during the early phase of the Mediterranean Salinity Crisis.

The Messinian Salinity Crisis caused the world ocean to become sluggish. The relatively long–term reduction of AABW and pulse variations of NADW in the interval from 6.2 (C3An.1r) to 5.32 Ma is linked to the Messinian Salinity Crisis, because it coincides extremely well with the Salinity Crisis and onset of the crisis. It is also supported by the global increase of *U. peregrina* in this interval, which suggests that the global ocean was under relatively poor basin to basin ventilation at this time.

ABBREVIATED SYSTEMATIC TAXONOMY FOR BENTHIC FORAMINIFERA

***Ammonia beccarii* (Linné)**

Nautilus beccarii Linné, 1758, p. 710.

Ammonia beccarii (Linné), Loeblich and Tappan, 1988, p. 664, pl. 767, figs. 1-7.

***Ammotium* sp. A** (Pl. 9, Figs. 10-12)

***Amphicoryna scalaris* (Batsch)**

Nautilus scalaris Batsch, 1791, pl. 2, fig. 4.

Amphicoryna scalaris (Batsch), Loeblich and Tappan, 1988, p. 410, pl. 450, figs. 11-14.

***Anomalina colligera* Chapman and Parr** (Pl. 1, Fig. 22)

Anomalina colligera Chapman and Parr, 1937, p. 117, pl. 9, fig. 26.

Anomalina colligera Chapman and Parr, Wang et al., 1988, p. 177, pl. 32, fig. 11.

***Anomalinoides flinti* Cushman** (Pl. 8, Fig. 8)

Anomalinoides flinti Cushman.

Anomalinoides flinti Cushman, Berggren and Haq, 1976, p.108, pl. 2, figs. 14-15.

***Astrononion echolsi* Kennett**

Astrononion echolsi, Kennett, 1967b, p. 134-135. pl. 11, figs. 7, 8.

***Bigenerina irregularis* Phleger and Parker**

Bigenerina irregularis Phleger and Parker, 1951, p. 4, pl. 1, figs. 16-21.

***Bolivina albatrossi* Cushman** (Pl. 2, Fig. 18; Pl. 5, Fig. 4; Pl. 6, Fig. 26)

Bolivina albatrossi Cushman, 1922, pt. 3, p. 31, pl. 6, fig. 4.

***Bolivina byramensis* Cushman**

Bolivina byramensis Cushman, 1937, p. 69, pl. 8, figs. 18, 20.

***Bolivina catanensis* Seguenza**

Bolivina catanensis Seguenza, 1862, p. 113, 125, pl. 2, fig. 3.

Bolivina catanensis Seguenza, Wright, 1978, p. 710, pl. 1, fig. 16, 17.

***Bolivina dilatata* Reuss** (Pl. 3, Fig. 3)

Bolivina dilatata Reuss, 1850, p. 381, pl. 48, fig. 5.

Bolivina dilatata Reuss, Van Der Zwan, 1982, p. 139, pl. 1, figs. 3-5.

***Bolivina inflata* Heron-Allen and Earland** (Pl. 2, Figs. 7, 9)

Bolivina inflata Heron-Allen and Earland, 1913.

Bolivina inflata Heron-Allen and Earland, McLaughlin and Sen Gupta, 1994, p. 87, pl. 2, fig. 3.

Bolivina inflata–pseudoplicata transition form (Pl. 2, Fig. 11, 12)

***Bolivina lowmani* Phleger and Parker** (Pl. 3, Fig. 1)

Bolivina lowmani Phleger and Parker, 1951, p. 13, pl. 6, figs. 20, 21.

***Bolivina multicostata* Cushman**

Bolivina margariata Cushman var. *multicostata* Cushman, 1930, p. 46, pl. 8, figs. 13, 14.

***Bolivina pseudoplicata* Heron-Allen and Earland**

Bolivina pseudoplicata Heron-Allen and Earland, 1930, p. 81, pl. 3, figs. 36-40.

***Bolivina pseudopunctata* Höglund** (Pl. 3, Fig. 2)

Bolivina pseudopunctata Höglund, 1947, p. 273, pl. 24, fig. 5, pl. 32, figs. 23, 24.

***Bolivina pygmaea* Brady** (Pl. 6, Figs. 23-25)

Bolivina pygmaea Brady, 1881, p. 406.

Bolivina pygmaea Brady, Barker, 1966, p. 108, pl. 52, figs. 5, 6.

Bolivina pygmaea Brady, Hermelin and Scott, 1985, p. 24, pl. 2, fig. 15.

Bolivina* cf. *pygmaea (Pl. 3, Fig. 4)

Bolivina reticulata Hantken (Pl. 2, Fig. 20)

Bolivina reticulata Hantken, 1875, p. 65, pl. 15, fig. 6.

Bolivina reticulata Hantken, Brady 1884, p. 426, pl. 53, figs. 28, 29.

***Bolivina simplex* Phleger and Parker** (Pl. 2, Fig. 19)

Bolivina simplex Phleger and Parker, 1951, pt. 2, p. 14, pl. 7, fig. 4-6.

***Bolivina spathulata* (Williamson)** (Pl. 2, Fig. 17)

Textularia variabilis Williamson var. *spathulata* Williamson, 1858, p. 76, pl. 6, figs. 164.

Bolivina spathulata (Williamson), Phleger and Parker, 1951, p. 14, pl. 20, fig. 15.

***Bolivina subaenariensis* (Cushman)**

Bolivina subaenariensis Cushman, 1922, p. 46, pl. 7, fig. 6.

***Bolivina subspinescens* Cushman** (Pl. 2, Fig. 21)

Bolivina subspinescens Cushman, 1922, p. 48, pl. 7, fig. 5.

***Bolivina suteri* Cushman and Renz**

Bolivina suteri Cushman and Renz, 1941, p. 18, pl. 3, fig. 9.

***Bolivinita pseudothalmanni* Boltovskoy and Giussani de Khan** (Pl. 2, Figs. 13-16)

Bolivinita pseudothalmanni Boltovskoy and Giussani de Khan, 1981.

Abditodentrix pseudothalmanni (Boltovskoy and Giussani de Khan), Loeblich and Tappan, 1988, p. 503, pl. 554, fig. 1-5.

Bolivinita suturornata Zhang, 1988, p. 149, pl. 11, figs. 1, 2. In Wang et al., 1988.

***Bolivinita truncata* (Phleger)**

Loxostomum truncatum Phleger, 1951, p. 17, pl. 7, figs. 15-19.

Bolivinita truncata (Phleger), Collins et al., in press.

***Bulimina aculeata* d'Orbigny** (Pl. 3, Fig. 9)

Bulimina aculeata d'Orbigny, 1826, p. 269, no. 7.

Bulimina aculeata d'Orbigny, Wang et al., 1988, p. 151, pl. 11, fig. 5.

***Bulimina alazaensis* Cushman** (Pl. 5, Fig. 5; Pl. 6, Fig. 15)

Bulimina alazaensis Cushman, 1927a, p. 161, pl. 25, fig. 4.

***Bulimina elongata* d'Orbigny**

Bulimina elongata d'Orbigny, 1846, p. 187, pl. 11, figs. 19, 20.

Bulimina elongata d'Orbigny, Cimerman and Langer, 1991, p. 62, pl. 64, figs. 3-8.

***Bulimina mexicana* Cushman** (Pl. 3, Figs. 11, 12; Pl. 6, Fig. 16)

Bulimina striata r. *mexicana* Cushman, 1922, pt. 3, p. 95, pl. 21, fig. 2.

***Bulimina ovata* Brady**

Bulimina ovata Brady, 1884, p. 400, 401, pl. 50, fig. 13.

***Bulimina tessellata* (Phleger and Parker)**

Virgulina tessellata Phleger and Parker, 1951, p. 19, pl. 9, figs. 15, 16.

***Cancris oblongus* (Williamson)** (Pl. 1, Fig. 23)

Rotalina oblonga Williamson, 1858, p. 51, pl. 4, figs. 98-100.

Cancris oblongus (Williamson), Berggren and Hag, 1976, p. 103, pl. 1, fig. 15.

***Cassidulina laevigata* d'Orbigny** (Pl. 1, Fig. 5)

Cassidulina laevigata d'Orbigny, 1826, p. 282, pl. 15, figs. 4, 5.

***Cassidulina reniforme* Norvang** (Pl. 1, Fig. 4; Pl. 5, Fig. 11)

Cassidulina crassa var. *reniforme* Norvang, 1945, p. 41, text figs. 6c-h.

***Cassidulinoides tenuis* Phleger and Parker** (Pl. 1, Fig. 10)

Cassidulinoides tenuis Phleger and Parker, 1951, p. 27, pl. 14, figs. 15-17.

***Cibicides lobatulus* (Walker and Jacob)** (Pl. 4, Fig. 5)

Nautilus lobatulus Walker and Jacob in Kanmacher, 1798, p. 642, pl. 14, fig. 36.

Truncatulina lobatula (Walker and Jacob), Brady, 1884, p. 660, pl. 92, fig. 10; pl. 93, fig. 1, 4, 5.

Cibicides lobatulus (Walker and Jacob), Wang et al., 1988, p. 162, pl. 15, figs. 12-14.

***Cibicidoides bradyi* (Trauth)** (Pl. 7, Fig. 1)

Truncatulina bradyi Trauth, 1918, with figures of Brady (1884, pl. 95, figs. 5) and Egger (1893, pl. 16, figs. 22, 23, 30, 54-56).

Cibicidoides bradyi (Trauth), van Morkhoven et al., 1986, p. 100-102, pl. 30, figs. 1-2.

***Cibicidoides crebbsi* Hedberg** (Pl. 4, Fig. 3)

Eponides crebbsi Hedberg, 1937, p. 679, pl. 92, fig. 1.

***Cibicidoides dutemplei* (d'Orbigny)** (Pl. 4, Fig. 4)

Rotalina dutemplei d'Orbigny, p. 157, pl. 8, figs. 19-20.

Heterolepa dutemplei (d'Orbigny), Wang et al., 1988, p. 178, pl. 13, figs. 9, 10.

Cibicidoides dutemplei (d'Orbigny), Van Morkhoven et al, 1986, p. 112-115, pl. 35, figs. 1-2

***Cibicidoides mundulus* (Brady, Parker and Jones)** (Pl. 4, Fig. 10; Pl. 7, Figs. 9, 11)

Truncatulina mundula Brady, Parker and Jones, 1890, p. 228.

Cibicidoides mundulus (Brady, Parker and Jones), van Morkhoven et al., 1986, p. 65-67, pl. 21, fig. 1a-c.

***Cibicidoides pachyderma* (Rzehak)** (Pl. 4, Fig. 2)

Truncatulina pachyderma Rzehak, 1886, p. 87, pl. 1, fig. 5.

Cibicidoides pachyderma (Rzehak), van Morkhoven et al., 1986, p. 68-71, pl. 22, fig. 1.

***Cibicidoides walli* (Bandy)**

Cibicidoides walli Bandy, 1949, p. 95, pl. 15, fig. 50.

***Cornuspirella diffusa* (Heron-Allen and Earland)** (Pl. 9, Fig. 4)

Cornuspira diffusa Heron-Allen and Earland, 1913, p. 272.

Cornuspirella diffusa (Heron-Allen and Earland), Loeblich and Tappan, 1988, p. 310, 311, pl. 323, fig. 1.

***Cyclammina cancellata* Brady**

Cyclammina cancellata Brady, 1884, p. 351, pl. 37, figs. 8-16.

***Cylindroclavulina bradyi* (Cushman)**

Clavulina bradyi Cushman, 1911, p. 73.

Cylindroclavulina bradyi (Cushman), Loeblich and Tappan, 1988, p. 182, pl. 201, fig. 7-13.

***Dentalina communis* d'Orbigny** (Pl. 2, Fig. 2)

Nodosaria (Dentalina) communis d'Orbigny, 1826, p. 254, no. 35.

Dentalina communis d'Orbigny, Wang et al., 1988, p. 137, pl. 17, fig. 11.

***Discorbinella bertheloti* (d'Orbigny)** (Pl. 4, Figs. 1, 6)

Rosalina bertheloti d'Orbigny, 1893, in Barker-Webb and Berthelot, p. 135, pl. 1, figs. 28-30 (*Berthelotiana* on explanation of plates).

Discorbis bertheloti (d'Orbigny), Phleger and Parker, 1951, p. 20, pl. 10, figs. 1, 2.

Discorbinella bertheloti (d'Orbigny),Berggren and Hag, 1976, p. 110, pl. 6, figs. 9, 10.

***Eggerella bradyi* (Cushman)**

Verneuilina bradyi Cushman, 1911, p. 54, pl. 6, fig. 4.

Eggerella bradyi (Cushman), Phleger and Parker, 1951, p. 6, pl. 3, figs. 1, 2.

***Ehrenbergina trigona* Goës** (Pl. 6, Fig. 17)

Ehrenbergina serrada var.*trigona* Goës, 1896, p. 49.

Ehrenbergina trigona Goës, Phleger and Parker, 1951, p. 28, pl. 15, fig. 1.

***Entosolenia duplicata* (Sidebottom)** (Pl. 6, Fig. 5)

Lagena auriculata Brady var. *duplicata* Sidebottom, 1912, p. 42, pl. 20, figs. 23.

Entosolenia duplicata (Sidebottom), Boltovskoy and Giussani de Kahn, 1990, p. 373, pl. 1, fig. 4.

***Epistominella exigua* (Brady)** (Pl. 1, Figs. 27-29; Pl. 5, Fig. 17; Pl. 9, Fig. 19)

Pulvinulina exigua Brady, 1884, p. 696, pl. 103, figs. 13, 14.

Pseudoparrella exigua (Brady), Phleger and Parker, 1951, p. 28, pl. 15, figs. 6, 7.

Epistominella exigua (Brady), Hermelin and Scott, 1985, p. 208, pl. 4, fig. 6.

***Epistominella takayanagii* Iwasa** (Pl. 1, Figs. 26, 30)

Epistominella takayanagii Iwasa, 1955, p. 16, 17, text figs. 4a-c.

***Eponides polius* (Phleger and Parker)** (Pl. 7, Fig. 5)

Eponides polius Phleger and Parker, 1951, p. 11, figs. 1, 2.

***Eponides tumidulus* (Brady)** (Pl. 1, Figs. 19, 21; Pl. 7, Figs. 16, 18)

Truncatulina tumidula Brady, 1884, p. 666, pl. 95, figs. 8a-d.

Eponides tumidulus (Brady), Phleger and Parker, 1951, p. 21, 23, pl. 11, figs. 7, 8.

***Eponides weddellensis* Earland** (Pl. 1, Figs. 16-18; Pl. 5, Fig. 18; Pl. 7, Fig. 17;)

Eponides weddellensis Earland, 1936, p. 57, pl. 1, figs. 65-67.

***Eponides* sp. A.** (Pl. 4, Fig. 9)

***Fissurina acuta* (Reuss)** (Pl. 6, Fig. 6)

Lagena acuta Reuss, 1858, p.434; Brady, 1884, p. 474, pl. 59, fig. 6.

Fissurina acuta (Reuss), Brady, 1884, p. 474, pl. 59, fig. 6.

***Fissurina laevigata* Reuss** (Pl. 3, Fig. 18)

Fissurina laevigata Reuss, 1849, p. 366, pl. 46, fig. 1; Brady, 1884, p. 473, pl. 114, fig. 8.

Fissurina laevigata Reuss, Brady, 1884, p. 473, pl. 114, fig. 8.

***Fissurina annectens* (Burrows and Holand)** (Pl. 6, Fig. 7)

Lagena annectens Burrows and Holand, 1895, p. 203, pl. 7, fig. 11.

Fissurina annectens (Burrows and Holand), Boltovskoy and Giussani de Khan, p. 372.

***Fursenkoina fusiformis* (Williamson)** (Pl. 6, Fig. 8)

Bulimina pupoides d'Orbigny var. *fusiformis* Williamson, 1858, p. 64, pl. 5, figs. 129.

Fursenkoina fusiformis (Williamson), Hermelin and Scott, 1985, p. 210, pl. 4, fig. 14.

***Gavelinopsis praegeri* (Heron-Allen and Earland)** (Pl. 1, Figs. 14, 15)

Discorbina praegeri Heron-Allen and Earland, 1913, p. 122.

Gavelinopsis praegeri (Heron-Allen and Earland), Loeblich and Tappan, 1988, p. 560, pl. 608, fig. 6-12.

***Glandiculina* sp.A.** (Pl. 6, Fig. 20)

***Globobulimina auriculata* (Bailey)** (Pl. 3, Fig. 13)

Bulimina auriculata Bailey, 1851, p. 12, pl. 1, figs. 25-27.

Globobulimina auriculata (Bailey), Thomas et al., 1990, P. 227, pl. 6, figs. 3, 4.

***Globobulimina* ? sp.A.** (Pl. 6, Fig. 18)

***Globobulimina* ? sp.B.** (Pl. 6, Fig. 19)

***Globocassidulina subglobosa* (Brady)** (Pl. 8, Figs. 1, 2; Pl. 5, Fig. 12; Pl. 9, Fig. 7)

Cassidulina subglobosa Brady, 1881, p. 60.

Cassidulina subglobosa Brady, Phleger and Parker, 1951, p. 27, pl. 14, figs. 11-13.

Globocassidulina subglobosa (Brady), Wang et al., 1988, p. 173, pl. 30, figs. 1, 2.

Gyroidina neosoldanii Brotzen (Pl. 1, Fig. 13)

Gyroidina neosoldanii Brotzen, 1936, p. 158.

***Gyroidina soldanii* (d'Orbigny)**

Rotalina soldanii d'Orbigny, 1826, p. 278, fig. 36.

Gyroidina soldanii (d'Orbigny), Hermelin and Scott, 1985, p. 210, pl. 5, figs. 6, 8.

***Heronallenia crosbyi* McCulloch** (Pl. 7, Figs. 7, 12)

Heronallenia crosbyi McCulloch, 1977.

Heronallenia crosbyi McCulloch, Loeblich and Tappan, 1988, p. 569, pl. 623, figs. 13-15.

***Hoeglundina elegans* (d'Orbigny)** (Pl. 1, Fig. 11)

Rotalia elegans d'Orbigny, 1826, p. 276, no. 54.

Hoeglundina elegans (d'Orbigny), Wang, 1988, p. 145, pl. 20, figs. 2-4.

***Hopkinsina pacifica* Cushman**

Hopkinsina pacifica Cushman, 1933, p. 86, pl. 8, fig. 16.

Hopkinsina pacifica Cushman, Wang et al., 1988, p. 135, pl. 30, fig. 3.

***Karreriella bradyi* (Cushman)** (Pl. 8, Fig. 11)

Gaudryina bradyi Cushman, 1911, p. 67, fig. 107.

Karreriella bradyi (Cushman), Thomas et al., 1990, p. 227, pl. 3, fig. 17.

***Lagena distoma* Parker and Jones** (Pl. 6, Fig. 2)

Lagena distoma Parker and Jones, 1864; after Brady, 1884, p. 461, pl. 58, figs. 11-15.

***Lagena elegantissima* (Bornemann)** (Pl. 6, Fig. 3)

Ovulina eleganitssima Bornemann, 1855, p. 1126, pl. 12, fig. 1.

Lagena elegantissima (Bornemann), Boltovskoy and Giussani de Khan, 1990, p. 391, pl. 4, fig. 1.

***Lagena formosa* Schwager** (Pl. 6, Fig. 4)

Lagena formosa Schwager, 1866, p. 206, pl. 4, fig. 9, pl. 7, fig. 1.

***Lagena gracilis* Williamson** (Pl. 6, Fig. 1)

Lagena gracilis Williamson, in Brady, 1884, p. 464, pl. 58, figs. 19, 22-24.

***Laticarinina pauperata* (Parker and Jones)** (Pl. 8, Fig. 9)

Pulvinulina repanda (Fichtel and Moll) var. *menardii* (d'Orbigny) subvar. *pauperata* Parker and Jones, 1865, p. 395.

Laticarinina pauperata (Parker and Jones), Loeblich and Tappan, 1988, p. 578, pl. 631, figs. 1-4.

***Lenticulina peregrina* (Schwager)** (Pl. 1, Fig. 1)

Cristellaria peregrina Schwager, p. 245, pl. 7, fig. 89.

Lenticulina peregrina (Schwager), Van Morkhoven et al., 1986, p. 92-94, pl. 27, figs. 1, 2.

Loxostomum cf. normale (Pl. 3, Fig. 5)

***Martinottiella communis* (d'Orbigny)** (Pl. 4, Fig. 11)

Clavulina communis d'Orbigny, 1826, p. 268.

Martinottiella communis (d'Orbigny), Loeblich and Tappan, 1988, p. 171, pl. 190, figs. 3-4.

***Melonis affinis* (Reuss)** (Pl. 1, Fig. 6; Pl. 7; Fig. 15)

Nonion affinis Reuss, 1851, p. 72, pl. 5, fig. 32.

Melonis affinis (Reuss), Hayward and Buzas, 1979, p. 65, pl. 129, fig. 256.

***Melonis barleeanum* (Williamson)** (Pl. 8, Fig. 6)

Nonionina barleeana Williamson, 1858, p. 32, pl. 4, figs. 68, 69.

Melonis barleeanum (Williamson), Wang et al., 1988, p. 179, pl. 12, fig. 4.

***Melonis pompilioides* (Fichtel and Moll)** (Pl. 1, Figs. 7, 9; Pl. 9, Fig. 2)

Nautilus pompilioides Fichtel and Moll, 1798, p. 31, pl. 2, figs. a-c.

Melonis pompilioides (Fichtel and Moll), Hermelin and Scott, 1985, p. 212, pl. 6, fig. 5.

***Miliammina fusca* (Brady)** (Pl. 9, Figs. 13, 14)

Quinqueloculina fusca Brady, 1870, p. 47, pl. 11, figs. 2, 3.

Miliammina fusca (Brady), Scott et al., 1991, p. 386, pl. 1, fig. 4.

***Nonionella miocenica* Cushman**

Nonionella miocenica Cushman, 1926, p. 64.

Nonionella miocenica Cushman, Loeblich and Tappan, 1988, p. 617, pl. 689, figs. 18-21.

***Nonionella turigida* (Williamson)**

Rotalina turigida Williamson, 1858, p. 50, pl. 4, figs. 95-97.

Nonionella turigida (Williamson),Thomas et al., 1990, p. 227.

***Nonionella* sp. A.** (Pl. 5, Fig. 8)

***Nonionella* sp.B.** (Pl. 5, Fig. 9)

***Nuttallides umbonifera* (Cushman)** (Pl. 7, Figs. 8. 9; Pl. 9, Fig. 3)

Pulvinulinella umbonifera Cushman, 1933, p. 90, pl. 9, figs. 9a-c.

Nuttallides umbonifera (Cushman), Hermelin and Scott, 1985, p. 214, pl. 5, figs. 11, 13.

Oolina *hexagona* (Williamson) (Pl. 5, Fig. 1)

Entosolenia squamosa (Montagu) var. *hexagona* Williamson, 1848, - Williamson, 1858, p. 13, pl. 1, fig. 32.

Oolina *hexagona* (Williamson),Ujiie, 1990, p. 22, pl. 7, fig. 4.

***Oridorsalis umbonatus* (Reuss)** (Pl. 2, Fig. 2)

Rotalina umbonata Reuss, 1851, p. 75, pl. 5, figs. 35a-c.

Oridorsalis umbonatus (Reuss), Hermelin and Scott, 1985, p. 214, pl. 5, fig. 10.

***Osangularia culter* (Parker and Jones)** (Pl. 8, Fig. 10)

Osangularia (Planorbulina) farcta (Fichtel and Moll) var. *ungeriana* (d'Orbigny) subvar. *culter* Parker and Jones 1865, p. 382, 421, pl. 19, fig. 1.

***Astrononion umbilicatulum* (Uchio)** (Pl. 8, Fig. 4)

Astrononion umbilicatulum Uchio, 1951, p. 36, tf. 1, pl. 1, figs. 5 - 8.

***Pacinonion* sp. A.** (Pl. 8, Fig 5)

***Planulina ariminensis* d'Orbigny** (Pl. 4, Figs. 7, 8)

Planulina ariminensis d'Orbigny, 1826, p. 280, pl. 14, figs. 1-3.

***Planulina rugosa* (Phleger and Parker)**

Cibicides rugosa Phleger and Parker, 1951, p. 31, pl. 17, fig. 5-6.

Planulina rugosa (Phleger and Parker),Var Morkhoven, 1986, p. 45-47, pl. 13, figs. 1-2.

***Planulina wuellerstorfi* (Schwager)** (Pl. 5, Figs. 14, 15; Pl. 7, Fig. 13; Pl. 9, Fig. 5)

Anomalina wuellerstorfi Schwager, 1866, p. 258, pl. 7, figs. 105, 107.

Planulina wuellerstorfi (Schwager), van Morkhoven et al., 1986, pp. 48-50, pl. 14, figs. 1-2.

***Pleurostomella alternans* Schwager** (Pl. 6, Fig. 12)

Pleurostomella alternans Schwager, 1866, p. 238, pl. 6, figs. 79 - 80.

***Pleurostomella obtusa* Berthelin** (Pl. 6, Fig. 11)

Pleurostomella obtusa Berthelin, 1880, pl. 1, fig. 9.

***Pleurostomella* ? sp. A.** (Pl. 6, Fig. 9)

***Pleurostomella* ? sp. A.** (Pl. 6, Fig. 9)

***Praeglobobulimina?* sp. A..** (Pl. 6, Fig. 21)

***Pullenia bulloides* (d'Orbigny)** (Pl. 8, Fig. 7)

Nonionina bulloides d'Orbigny, 1826, p. 293.

Nonionina bulloides d'Orbigny, 1846, p. 107, pl. 5, figs. 9, 10.

Pullenia bulloides (d'Orbigny), Wang et al., 1988, p. 176, pl. 12, figs. 6, 7.

***Pullenia quinqueloba* (Reuss)** (Pl. 8, Fig. 3)

Nonionina quinqueloba (Reuss), 1851, p. 71, pl. 5, fig. 31.

Pullenia quinqueloba (Reuss), Ujiie, 1990, p. 43, pl. 24, figs. 1-5.

***Pullenia subcarinata* (d'Orbigny)** (Pl. 5, Fig. 10)

Nonionina subcarinata d'Orbigny, 1839a, p. 28, pl. 5, figs. 23, 24.

Pullenia subcarinata (d'Orbigny), Hermelin and Scott, 1985, p. 216, pl. 5, figs. 5-9.

***Pyrgo murrhyna* (Schwager)** (Pl. 9, Fig. 6)

Biloculina murrhyna Schwager, 1866, p. 203, pl. 4, figs. 15a-c.

Pyrgo murrhyna (Schwager), Ujiie, 1990, p. 16, pl. 4, figs. 3-5.

***Pyrulina augusta* (Egger)** (Pl. 2, Fig. 1)

Polymorphina (Globulina) angusta Egger, 1857, p. 290, pl. 13, figs. 13-15.

Pyrulina augusta (Egger), Ujiie, 1990, p. 21, pl. 6, figs. 10, 11.

***Quinqueloculina seminulum* (Linné)**

Serpula seminulum Linné, 1758, p. 786.

Quinqueloculina seminulum (Linné),Renz, 1948, p. 156, pl. 3, fig. 1.

***Rectuvigerina compressa* (Cushman)** (Pl. 5, Figs, 2, 3)

Uvigerina compressa Cushman, 1926.

Rectuvigerina compressa (Cushman), Murray, 1984, p. 532, pl. 3, fig. 16.

***Rectuvigerina multicostata* (Cushman and Jarvis)** (Pl. 2, Fig. 6; Pl. 6, Fig. 14)

Siphogenerina multicostata Cushman and Jarvis, 1929, p. 14, pl. 3, fig. 6.

Rectuvigerina multicostata (Cushman and Jarvis),Van Morkhoven et al., 1986, p. 115-117, pl. 36, figs. 1-4.

***Ressella spinulosa* (Reuss)**

Verneuilina spinulosa Reuss, 1850, p. 374, fig. 12.

Ressella spinulosa (Reuss), Cimerman and Langer, 1991, p. 63, pl. 66, figs. 5-8.

***Rhizammina* sp. A.** (Pl. 9, Fig. 15)

***Robertinoides charlottensis* (Cushman)**

Cassidulina charlottensis Cushman, 1925, p. 41, pl. 6, figs. 6, 7.

Robertinoides charlottensis (Cushman), Loeblich and Tappan, 1988, p. 452, pl. 483, figs. 5-14.

***Rosalina* sp. A.** (Pl. 1, Fig. 24)

***Seabrookia earlandi* Wright** (Pl. 1, Fig. 2)

Seabrookia earlandi Wright, 1891.

Seabrookia earlandi Wright, Boltovskoy and Ocampo, 1993, p. 144, pl. 5, fig. 8.

***Sigmavirgulina* sp. A.** (Pl. 3, Fig. 6)

***Sigmoilina tenuis* (Czjzek)** (Pl. 4, Fig. 12)

Quinqueloculina tenuis Czjzek, 1848, p. 149, pl. 13, figs. 31-34.

Sigmoilina tenuis (Czjzek), Phleger and Parker, 1951, p. 8, pl. 4, figs. 3-5.

***Sigmoilopsis schlumbergeri* (Silvestri)**

Sigmoilina schlumbergeri Silvestri, 1904, p. 267, 269.

Sigmoilopsis schlumbergeri (Silvestri), Loeblich and Tappan, 1988, p. 350, pl. 356, figs. 8-13.

***Siphonina tenuicarinata* Cushman** (Pl. 1, Fig. 3)

Siphonina tenuicarinata Cushman, 1927; after Murray, 1984, p. 532, pl. 3, figs. 5 - 7.

***Siphotextularia catenata* (Cushman)** (Pl. 8, Fig. 12)

Textularia catenata Cushman, 1911, p. 23, figs. 39, 40.

Siphotextularia catenata (Cushman), Murray, 1984, p. 532, pl. 3, figs. 8, 9.

***Siphotextularia rolshauseni* Phleger and Parker** (Pl. 5, Fig. 7)

Siphotextularia rolshauseni Phleger and Parker, 1951, p. 4, pl. 1, figs. 23, 24a, b.

***Sphaeroidina bulloides* d'Orbigny** (Pl. 1, Fig. 12)

Sphaeroidina bulloides d'Orbigny, 1826, p. 267, no. 1.

Sphaeroidina bulloides d'Orbigny, Loeblich and Tappan, 1988, p. 564, pl. 617, figs. 1-6.

***Stilostomella antillea* (Cushman)** (Pl. 6, Fig. 13)

Nodosaria antillea Cushman, 1923, p. 91.

Orthomorphia antillea (Cushman), Boltovskoy, 1988, p. 381, pl. 1, figs, C, D.

Stilostomella antillea (Cushman), Hayward and Buzas, 1979, p. 75, pl. 28, fig. 339.

***Stilostomella hispida* (d'Orbigny)** (Pl. 2, Fig. 5)

Nodosarina hispida d'Orbigny, 1846, p. 35, pl. 1, figs. 24, 25.

***Stilostomella subspinosa* (Cushman)** (Pl. 5, Fig. 6)

Ellipsonodosaria subspinosa Cushman, 1943, p. 92, pl. 16, figs. 6, 7.

Stilostomella subspinosa (Cushman), Boltovskoy, 1978, p. 170, pl. 7, figs. 24-28.

***Tosaia hanzawai* Takayanagi** (Pl. 7, Fig. 20)

Tosaia hanzawai Takayanagi, 1953, p. 30, pl. 40, fig. 7.

***Trifarina angulosa* (Williamson)** (Pl. 3, Fig. 7)

Uvigerina angulosa Williamson, 1858, p. 67.

Angulogerina angulosa (Williamson), Loeblich and Tappan, 1988, p. 525, pl. 574, figs. 5-9.

Trifarina angulosa (Williamson), Wang et al., 1988, p. 155, pl. 12, figs. 9, 10.

***Trifarina bradyi* Cushman** (Pl. 3, Fig. 8)

Trifarina bradyi Cushman, 1923, p. 99, pl. 22, figs. 3 - 9.

***Trochammina* cf. *squamata* Jones and Parker** (Pl. 9, Figs. 8, 9)

Trochammina squamata Jones and Parker, 1860, p. 304.

Trochammina squamata Jones and Parker, 1865, p. 407, pl. 15, fig. 30.

Trochammina squamata Jones and Parker, Wang et al., 1988, p. 123, pl. 11, fig. 14.

***Uvigerina canariensis* d'Orbigny**

Uvigerina canariensis d'Orbigny, 1839a (*fide* Ellis and Messina, 1940, *et seq.*). - Brady, 1884, p. 573, pl. 74, figs. 1-3.

***Uvigerina hispida* Schwager**

Uvigerina hispida Schwager, 1866, p. 249, pl. 7, fig. 95.

***Uvigerina peregrina* Cushman** (Pl. 3, Figs. 14, 15)

Uvigerina peregrina Cushman, 1923, p. 166, pl. 42, figs. 7-10.

***Uvigerina proboscidea* Schwager** (Pl. 6, Fig. 22; Pl. 3, Fig. 16)

Uvigerina proboscidea Schwager, 1866, p. 7, pl. 7, fig. 96.

***Uvigerina schwageri* Brady**

Uvigerina schwageri Brady, 1884, p. 575, pl. 74, figs. 8-10.

***Valvulineria laevigata* Phleger and Parker** (Pl. 1, Fig. 25)

Valvulineria laevigata Phleger and Parker, 1951, p. 28, pl. 13, figs. 11, 12.

***Virgulina pontoni* (Cushman)** (Pl. 2, Figs. 3, 4)

Virgulina pontoni Cushman, 1932, p. 17, pl. 3, fig. 7.

Vulvulina spinosa **Cushman**

Vulvulina spinosa Cushman, 1927, p. 111, pl. 23, fig. 1.

ABBREVIATED SYSTEMATIC TAXONOMY
PLANKTONIC FORAMINIFERA

***Candeina nitida* d'Orbigny**

Candeina nitida d'Orbigny, 1839b, p. 108, pl. 2, figs. 27, 28.

Candeina nitida d'Orbigny, Bolli and Saunders, 1985, p. 191, figs. 19, 1-2.

***Globigerina bulloides* d'Orbigny**

Globigerina bulloides d'Orbigny, 1826, p. 277, Mod. no 17 (juvenile), Mod. no. 76 (adult).

Globigerina bulloides d'Orbigny, Wang et al., 1988, p. 39, pl. 7, figs. 1-5.

***Globigerina nepenthes* Todd** (Pl. 8, Fig. 20)

Globigerina nepenthes Todd, 1957, p. 301, pl. 78, fig. 7.

***Globigerinoides conglobatus* (Brady)**

Globigerinoides conglobatus Brady, 1879, p. 286, pl. 80, figs. 1-3,.

***Globigerinoides extremus* Bolli and Bermúdez** (Pl. 8, Fig. 16)

Globigerinoides obliquus Bolli subsp. *extremus* Bolli and Bermúdez, 1965, p. 139, pl. 1, figs. 10-12.

***Globigerinoides seigliei* Bermúdez and Bolli**

Globigerinoides rubra (d'Orbigny) *subsp. seigliei* Bermúdez and Bolli, 1969, p. 164, pl. 8, figs. 10-12.

***Globigerinoides sacculifer* (Brady)**

Globigerinoides trilobus sacculifer Brady, 1877, p. 535, no figures.

Globigerinoides sacculifer (Brady), Wang et al., 1988, p. 42, pl. 6, figs. 1-12.

***Globoquadrina altispira* (Cushman and Jarvis)**

Globoquadrina altispira Cushman and Jarvis, 1936, P. 5, pl. 1, figs. 13, 14.

***Globorotalia conoidea* Walters** (Pl. 8, Fig. 15)

Globorotalia miozea conoidea Walters, 1965, p. 124, fig. 8, I-M,

***Globorotalia conomiozea* Kennett** (Pl. 4, Fig. 14)

Globorotalia conomiozea Kennett, 1966, p. 235, text-figs. 10a-c.

***Globorotalia crassaformis* (Galloway and Wissler)** (Pl. 8, Fig. 19)

Globorotalia crassaformis (Galloway and Wissler), 1927, p. 41, pl. 7, fig. 12.

***Globorotalia crassaformis hessi* Bolli and Premoli Silva**

Globorotalia hessi Bolli and Premoli Silva, 1973 (=*Globorotalia crassaformis* 'B' Bolli, 1970, p. 580, pl. 4, figs. 13, 15, 16)

Globorotalia crassaformis hessi Bolli and Premoli Silva, Bolli and Saunders, 1985, p. 233, figs. 36. 3-5

***Globorotalia crassaformis viola* Blow**

Globorotalia (Globorotalia) crassula viola Blow, 1969, p. 397, pl. 5, figs. 4-6.

Globorotalia crassaformis viola Blow, Bolli and Saunders, 1985, p. 234, fig. 36. 1.

***Globorotalia crassula* Cushman, Stewart and Stewart**

Globorotalia crassula Cushman, Stewart and Stewart, 1930, p. 77, pl. 7, fig. 1.

***Globorotalia fohsi peripheroronda* Blow and Banner**

Globorotalia (Turborotalia) peripheroronda Blow and Banner, 1966, p. 294, pl. 1, figs. 1a-c.

Globorotalia fohsi peripheroronda Blow and Banner, Bolli and Saunders, 1985, p. 213, figs. 29.5, 13.

***Globorotalia lenguaensis* Bolli**

Globorotalia lenguaensis Bolli, 1957, p. 120, pl. 29, figs. 5a-c.

***Globorotalia margaritae* Bolli and Bermudez** (Pl. 8, Fig. 17)

Globorotalia margaritae Bolli and Bermudez, 1965, p. 132, pl. 1, figs. 16-18.

***Globorotalia mayeri* Cushman and Ellisor**

Globorotalia mayeri Cushman and Ellisor, 1939, p. 11, pl. 2, figs. 4a-c.

***Globorotalia mediterranea* Catalano and Sprovieri** (Pl. 8, Fig. 21)

Globorotalia miocenica mediterranea Catalano and Sprovieri, 1969, p. 522, pl. 2, figs. 6.

Globorotalia mediterranea Catalano and Sprovieri, Iaccarino, 1985, p. 307, fig. 6.2.

***Globorotalia menardii* B Bolli**

Globorotalia menardii B Bolli, 1970, p. 582, pl. 5, figs. 5-7.

***Globorotalia miocenica* Palmer**

Globorotalia menardii (d'Orbigny) var. *miocenica* Palmer, 1945, p. 70, pl. 1, figs. 10a-c.

Globorotalia miocenica Palmer, Bolli and Saunders, 1985, p. 230, figs. 33.2, 35.4-8.

***Globorotalia miotumida* Jenkins**

Globorotalia menardii miotumida Jenkins, 1960, p. 362, pl. 4, figs. 9a-c.

Globorotalia miotumida Jenkins, Jenkins, 1985, p. 278, figs. 7-12-13.

***Globorotalia plesiotumida* Blow and Banner**

Globorotalia tumida plesiotumida Blow and Banner, in Banner and Blow, 1965, p. 1353, figs. 2.

Globorotalia plesiotumida Blow and Banner, Bolli and Saunders, 1985, p. 227, fig. 33.5.

***Globorotalia praemargaritae* Catalano and Sprovieri**

Globorotalia praemargaritae Catalano and Sprovieri, 1969, p. 523, 524, pl. 1, fig. 5; pl. 3, fig. 5, tf. 4.

***Globorotalia pseudomiocenica* Bolli and Bermúdez**

Globorotalia pseudomiocenica Bolli and Bermúdez, 1965, p. 140, 141, pl. 1, figs. 13-15.

***Globorotalia pseudomiocenica* Bolli and Bermúdez**

Globorotalia pseudomiocenica Bolli and Bermúdez, 1965, p. 140, pl. 1, figs. 13-15.

***Globorotalia puncticulata* (Deshayes)**

Globigerina puncticulata Deshayes, 1832, p. 170; figures in Fornasini, 1899, p. 210, text-fig. 5.

Globorotalia puncticulata (Deshayes), Iaccarino, 1985, p. 308, fig. 6.12.

***Globorotalia scitula* (Brady)**

Pulvinulina scitula Brady, 1882, p. 716.

Globorotalia scitula (Brady), Bolli and Saunders, 1985, p. 219, figs. 30.26-29.

***Globorotalia suterae* Catalano and Sprovieri**

Globorotalia suterae Catalano and Sprovieri, 1971, p. 241, pl. 1, figs. 1a-c.

***Globorotalia tosaensis* Takayanagi and Saito**

Globorotalia tosaensis Takayanagi and Saito, 1962, p. 81, pl. 28, figs. 11a-c.

***Neogloboquadrina acostaensis* Blow** (Pl. 4, Fig. 15; Pl. 8. Figs. 13, 14)

Globorotalia acostaensis Blow, 1959, p. 208, pl. 17, figs. 106a-c.

***Neogloboquadrina atlantica* Berggren**

Globigerina atlantica Berggren, 1972, pl. 2, figs. 5-8.

Neogloboquadrina atlantica Berggren, Miller et al., 1991, p. 37.

***Orbulina universa* d'Orbigny**

Orbulina universa d'Orbigny, 1839b, p. 2, pl. 1, fig. 1.

Orbulina universa d'Orbigny, Bolli and Saunders, 1985, p. 201, figs. 23.1, 24.2.

***Sphaeroidinella dehiscens* (Parker and Jones)**

Sphaeroidina bulloides d'Orbigny var. *dehiscens* Parker and Jones, 1865, p. 369, pl. 19, figs. 5.

Sphaeroidinella dehiscens (Parker and Jones), Wang et al., 1988, p. 44, pl. 5, figs. 7-9.

***Sphaeroidinella immaturus* Cushman** (Pl. 4, Fig. 13)

Sphaeroidinella immaturus Cushman, 1919, p. 40, pl. 14, fig. 2.

***Sphaeroidinellopsis seminulina* (Schwager)**

Sphaeroidinellopsis seminulina Schwager, 1866, p. 256, pl. 7, fig. 112.

Sphaeroidinellopsis seminulina (Schwager), Kennett and Srinivasan, 1983, p. 206, pl. 51, figs. 6-8.

PLATE ILLUSTRATIONS OF FORAMINIFERA FROM MOROCCO AND NORTH ATLANTIC OCEAN

Plate 1

(Benthic foraminifera from Salé, northwestern Morocco)

1) *Lenticulina peregrina,* side view, Sample S70, Salé Borehole.

2) *Seabrookia earlandi,* side view, Sample B16, Salé Borehole.

3) *Siphonina tenuicarinata,* side view, Sample S70, Salé Borehole.

4) *Cassidulina reniforme,* side view, Sample S6, Salé Borehole.

5) *Cassidulina laevigata,* side view, Sample S2, Salé Borehole.

6) *Melonis affinis,* side view, Sample S16, Salé Borehole.

7, 9) *Melonis pompilioides,* side view, Sample S23, Salé Borehole.

8)*Astrononion umbilicatulum,* side view, Sample S6, Salé Borehole.

10) *Cassidulinoides tenuis,* side view, Sample Site S2, Salé Borehole.

11) *Hoeglundina elegans,* ventral view, Sample S23, Salé Borehole.

12) *Sphaeroidina bulloides,* side view, Sample S6, Salé Borehole.

13) *Gyroidina neosoldanii,* side view, Sample S67, Salé Borehole.

14, 15) *Gavelinopsis praegeri,* ventral and dorsal views, Sample S67, Salé Borehole.

16–18) *Eponides weddellensis,* ventral, dorsal and ventral views, Samples B16, B16 and S67, Salé Borehole.

19–21) *Eponides tumidulus,* ventral, dorsal and ventral views, Samples B51, B47, and B51, Salé Borehole.

22) *Anomalina colligera,* ventral view, Sample S2, Salé Borehole.

23) *Cancris oblongus,* ventral view, Sample S67, Salé Borehole.

24) *Rosalina* sp. A., ventral view, Sample S70, Salé Borehole.

25) *Valvulineria laevigata,* dorsal view, Sample B66, Salé Borehole.

26, 30) *Epistominella* cf. *takanayagii,* ventral views, Sample S2, Salé Borehole.

27–29) *Epistominella exigua,* ventral, dorsal and ventral views, Samples B83, B83 and S67

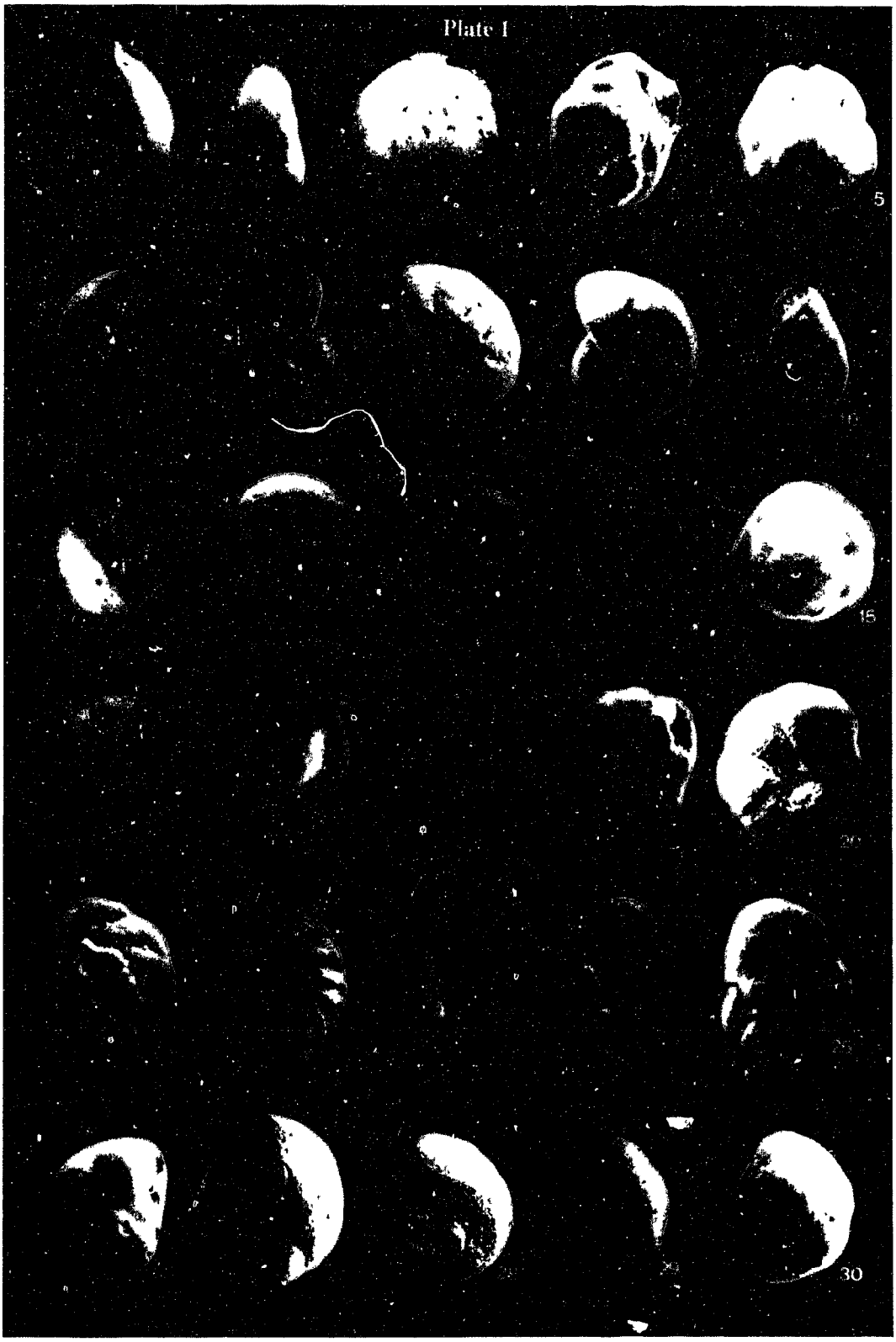
Plate I
5
15
30

Plate 2

(Benthic foraminifera from Salé borehole)

1) *Pyrulina augusta,* side view, Sample B52, Salé Borehole.

2) *Dentalina communis,* side view, Sample S67, Salé Borehole.

3, 4) *Virgulina pontoni,* side view, Samples B57 and B50, Salé Borehole.

5) *Stilostomella hispida,* side view, Sample S70, Salé Borehole.

6) *Rectuvigerina multicostata,* side view, Sample S6, Salé Borehole.

7–9) *Bolivina inflata,* side views, Samples B14, B14, and S67, Salé Borehole.

10, 11) *Bolivina inflata–pseudoplicata* transition form, side views, Samples B16 and B14, Salé Borehole.

12, 13) *Bolivina pseudoplicata,* Side views, Samples B16 and S67, Salé Borehole.

14–16) *Bolivinita pseudothalmanni,* side views, Samples S67, S70, B14, S70, Salé Borehole.

17) *Bolivina spathulata,* side view, Sample B87, Salé Borehole.

18) *Bolivina albatrossi,* side view, Sample S67, Salé Borehole.

19) *Bolivina simplex,* side view, Sample B14, Salé Borehole.

20) *Bolivina reticulata,* side view, Sample S70, Salé Borehole.

21) *Bolivina subspinescens,* side view, Sample S70, Salé Borehole.

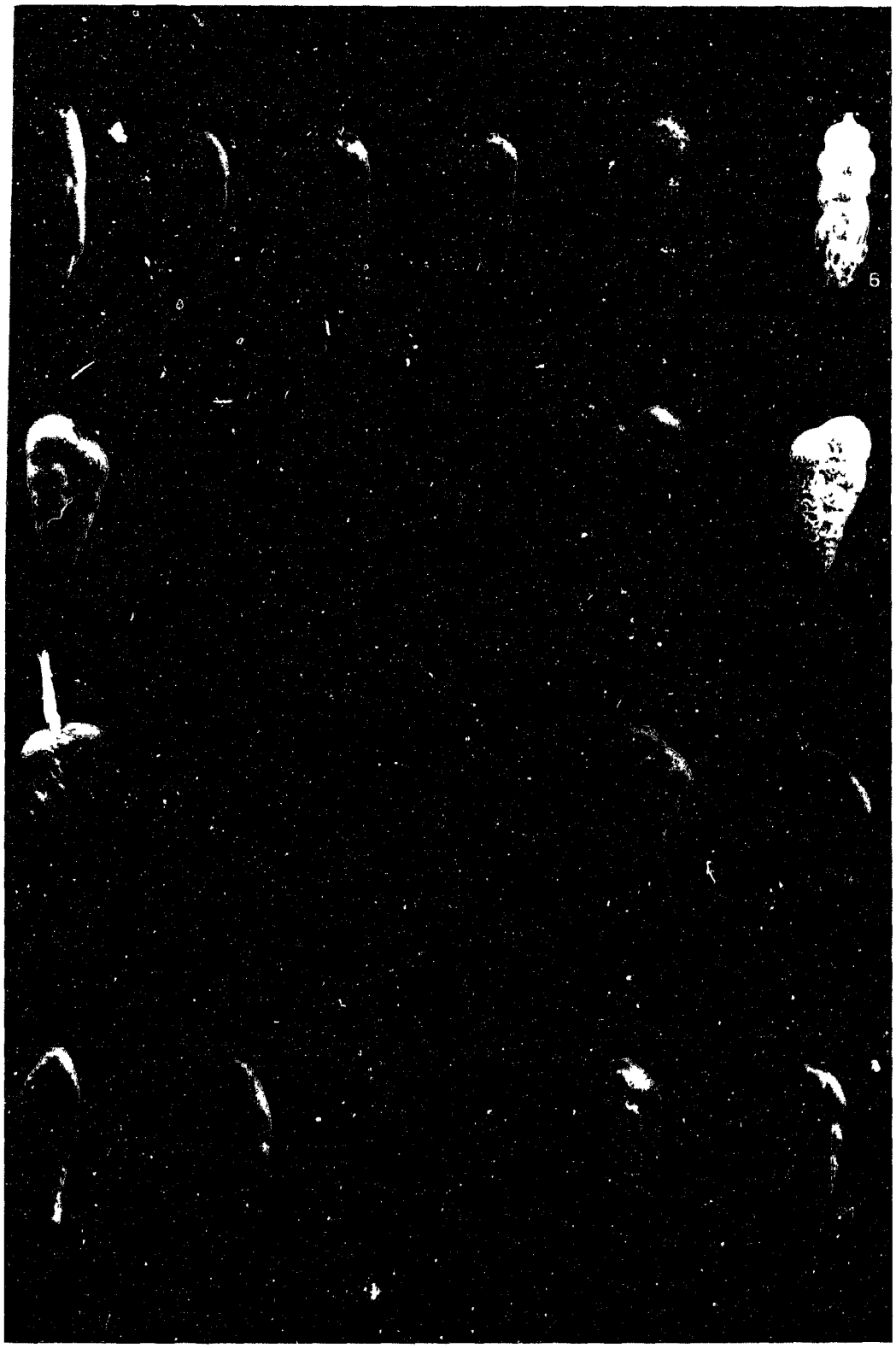
6

Plate 3

(Benthic foraminifera from Salé borehole)

1) *Bolivina lowmani,* side view, Sample S70, Salé Borehole.

2) *Bolivina pseudopunctata,* side view, Sample S2, Salé Borehole.

3) *Bolivina dilatata,* side view, Sample S67, Salé Borehole.

4) *Bolivina* cf. *pygmaea,* side view, Sample B87, Salé Borehole.

5) *Loxostomum cf. normale,* side view, Sample S6, Salé Borehole.

6) *Sigmavirgulina* sp. A, side view, Sample S60, Salé Borehole.

7) *Trifarina angulosa,* side view, Sample B14, Salé Borehole.

8) *Trifarina bradyi,* side view, Sample S2, Salé Borehole.

9) *Bulimina aculeata,* side view, Sample S6, Salé Borehole.

10-12) *Bulimina mexicana,* side views. Sample B16, B14 and S6, Salé Borehole.

13) *Globobulimina auriculata,* side view, Sample S2, Salé Borehole.

14, 15) *Uvigerina peregrina,* side view, Samples S70, and S2, Salé Borehole.

16) *Uvigerina. proboscidea,* side view, Sample B57, Salé Borehole.

17) *Uvigerina bradyi,* side view, Sample S2, Salé Borehole.

18) *Fissurina laevigata,* side view, Sample S70, Salé Borehole.

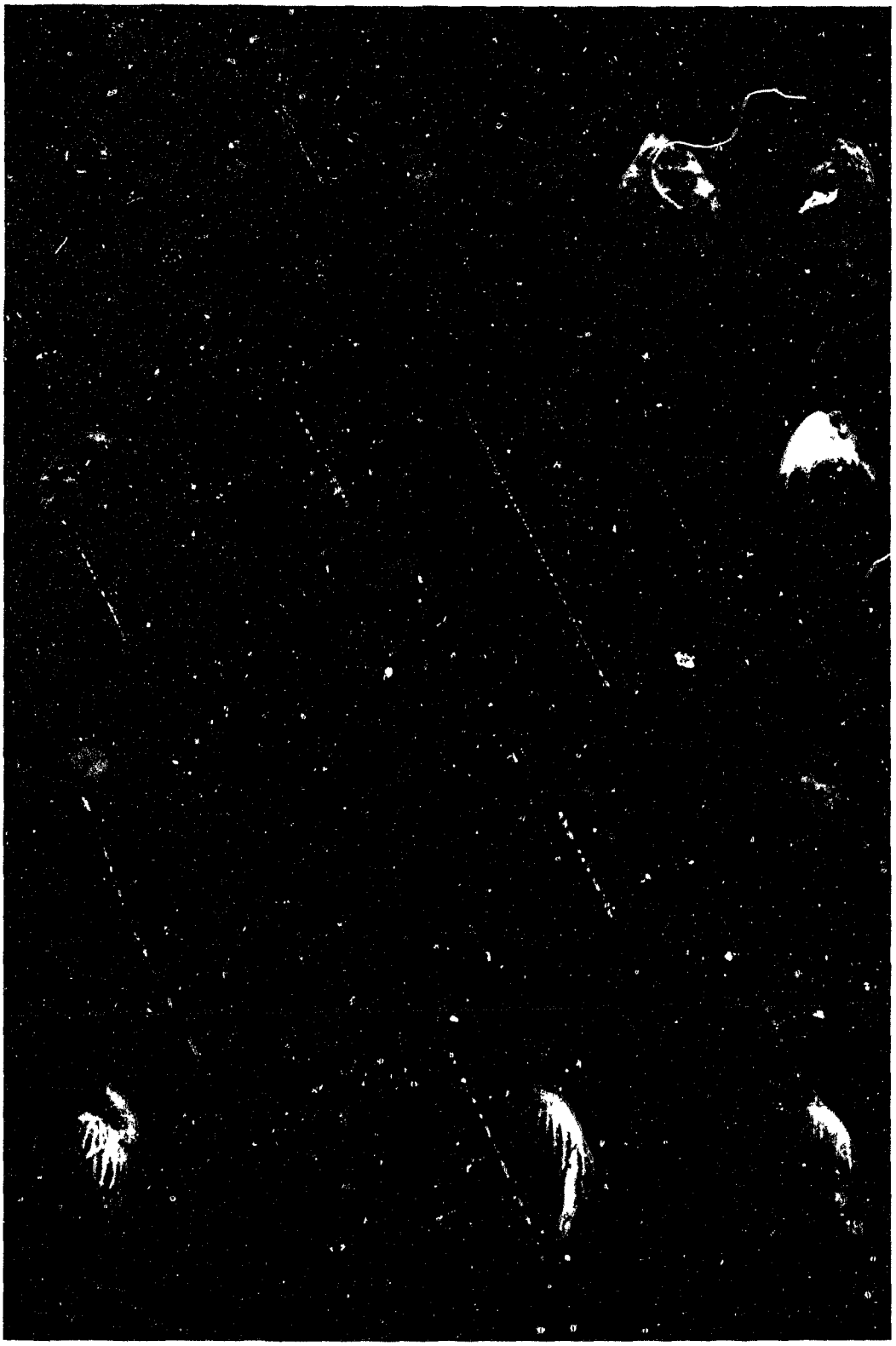

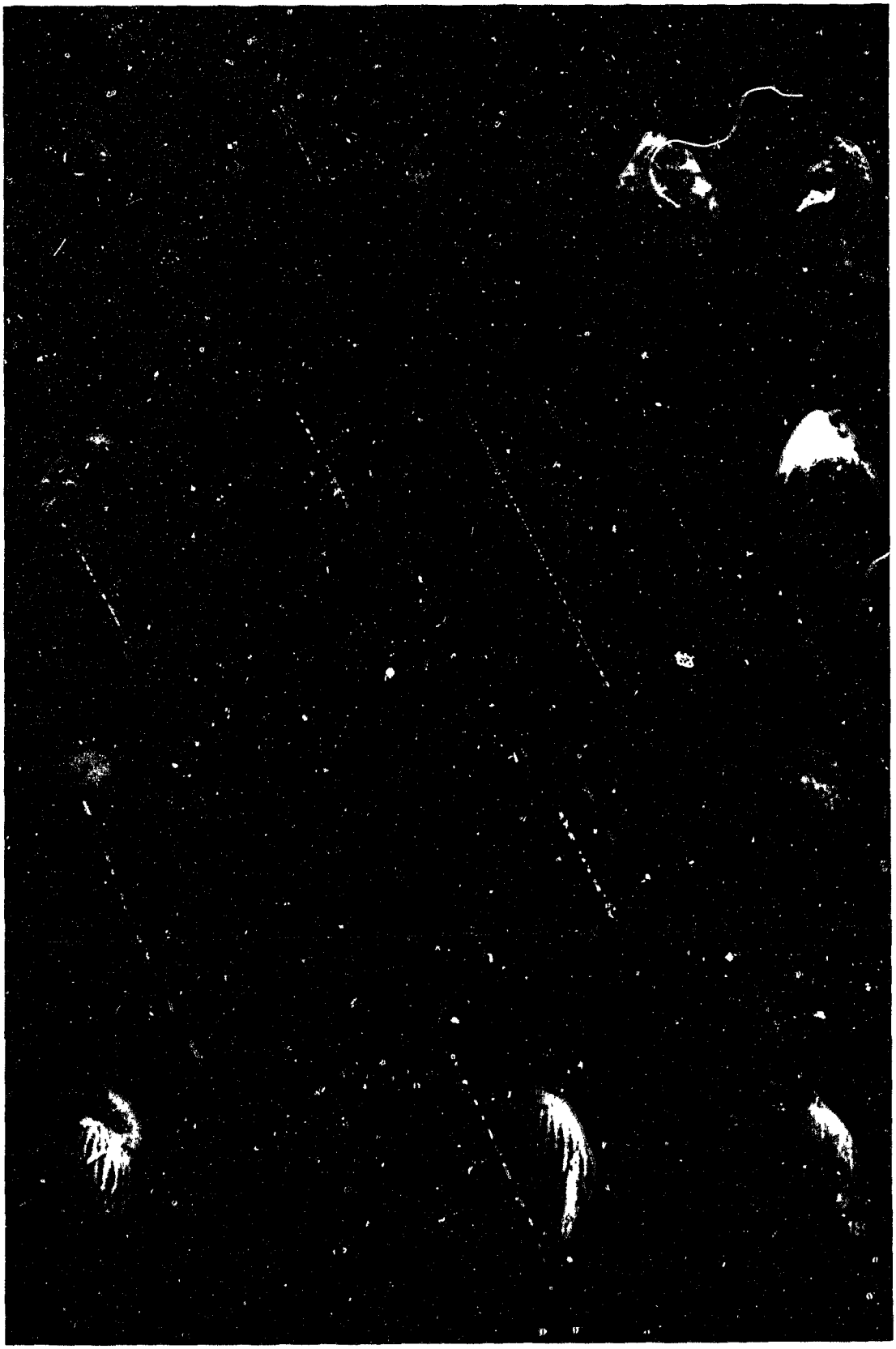

Plate 4

(Benthic and planktonic foraminifera from Salé borehole)

1, 6) *Discorbinella bertheloti,* dorsal and ventral views, Sample S2, Salé Borehole.

2) *Cibicidoides pachyderma,* ventral view, Sample S6, Salé Borehole.

3) *Cibicidoides crebbsi* , ventral view, Sample S23, Salé Borehole.

4) *Cibicidoides dutemplei,* ventral view, Sample S6, Salé Borehole.

5) *Cibicides lobatulus,* ventral view, Sample S23, Salé Borehole.

7, 8) *Planulina ariminensis,* dorsal and ventral views, Samples S6 and S70, Salé Borehole.

9) *Eponides* sp. A, ventral view, Sample B14, Salé Borehole.

10) *Cibicidoides mundulus,* ventral view, Sample B52, Salé Borehole.

11) *Martinottiella communis,* side view, Sample S70, Salé Borehole.

12) *Sigmoilina tenuis,* side view, Sample S70, Salé Borehole.

13) *Sphaeroidinella immatura,* dorsal view, Sample S60, Salé Borehole.

14) *Globorotalia conomiozea,* ventral view, Sample B71, Salé Borehole.

15) *Neogloboquadrina acostaensis, ventral view, Sample* S6, Salé Borehole.

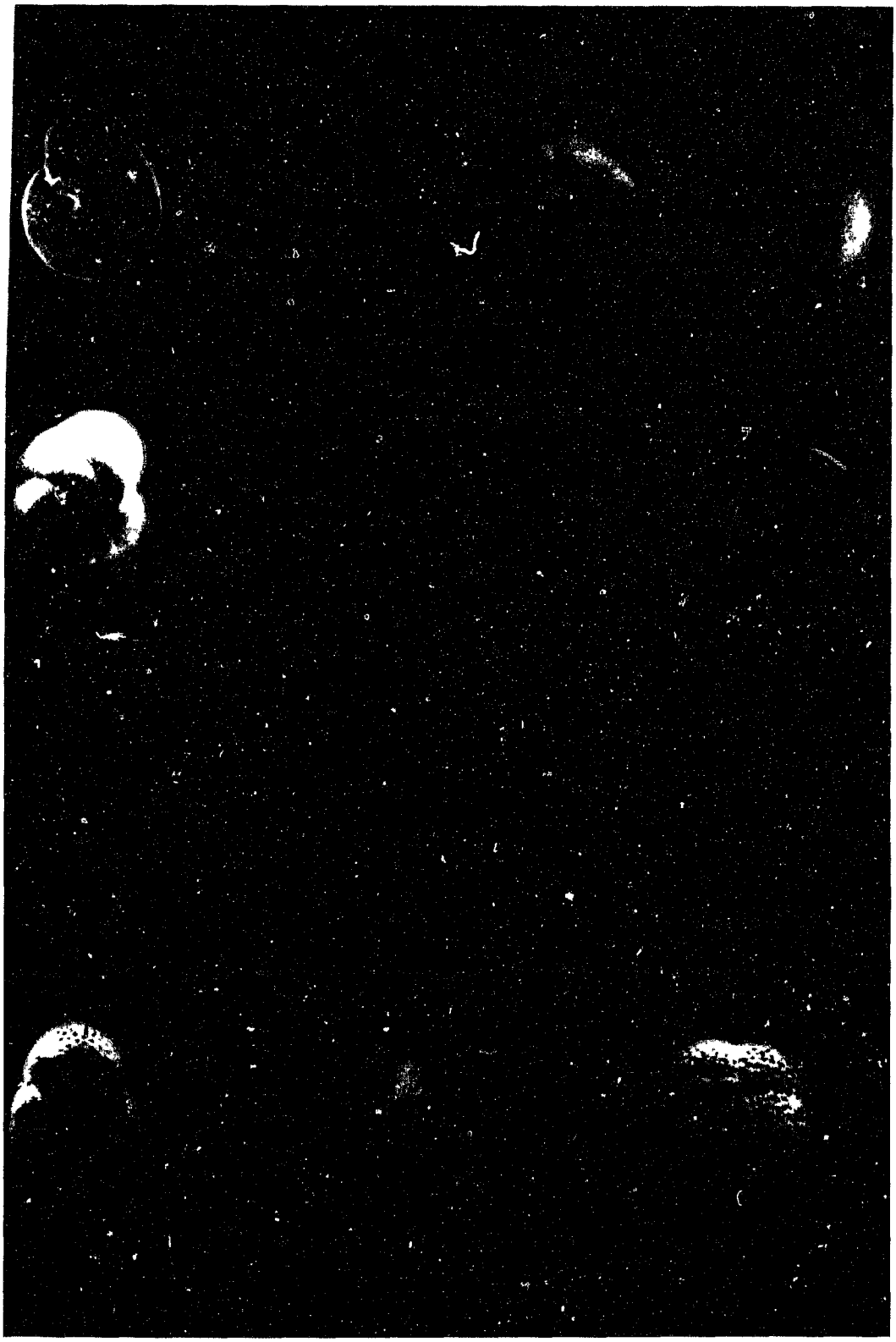

Plate 5

(Benthic foraminifera from DSDP Hole 552A)

1) *Oolina hexagona,* side view, Sample Hole 552A, 34–3, 102–106 cm.

2, 3) *Rectuvigerina compressa,* side views, Sample Site 552A, 20–1,70–74 cm; 24–3, 83–87 cm.

4) *Bolivina albatrossi,* side view, Sample Hole 552A, 31–4, 11–15 cm.

5) *Bulimina alazaensis,* side view, Sample Hole 552A, 19–1, 50–54 cm.

6) *Stilostomella subspinosa,* side view, Sample Hole 552A, 28–1, 105–109 cm.

7) *Siphotextularia rolhauseri,* side view, Sample Hole 552A, 29–3, 83–87 cm.

8) *Nonionella* sp. A, side view, Sample Hole 552A, 34–3, 102–106 cm.

9) *Nonionella sp.B,* side view, Sample Hole 552A, 28–2, 104–108 cm.

10) *Pullenia subcarinata,* side view, Sample Hole 552A, 31–4, 11–15 cm.

11) *Cassidulina reniforme,* apertural view, Sample Hole 552A, 19–1, 50–54 cm.

12) *Globocassidulina subglobosa,* apertural view, Sample Hole 552A, 30–3, 100–104 cm.

13) *Gyroidina soldanii,* ventral view, Sample Hole 552A, 31–4, 11–15 cm.

14, 15) *Planulina wuellerstorfi,* ventral and dorsal views, Samples Hole 552A, 34–3, 102–106 cm, and 28–2, 104–108 cm.

16) *Eponides polius,* ventral view, Sample Hole 552A, 29–3, 83–87 cm.

17) *Epistominella exigua,* ventral view, Sample, Hole 552A, 29–3, 83–87 cm.

18) *Eponides weddellensis,* dorsal view, Sample Hole 552A, 29–3, 83–87 cm.

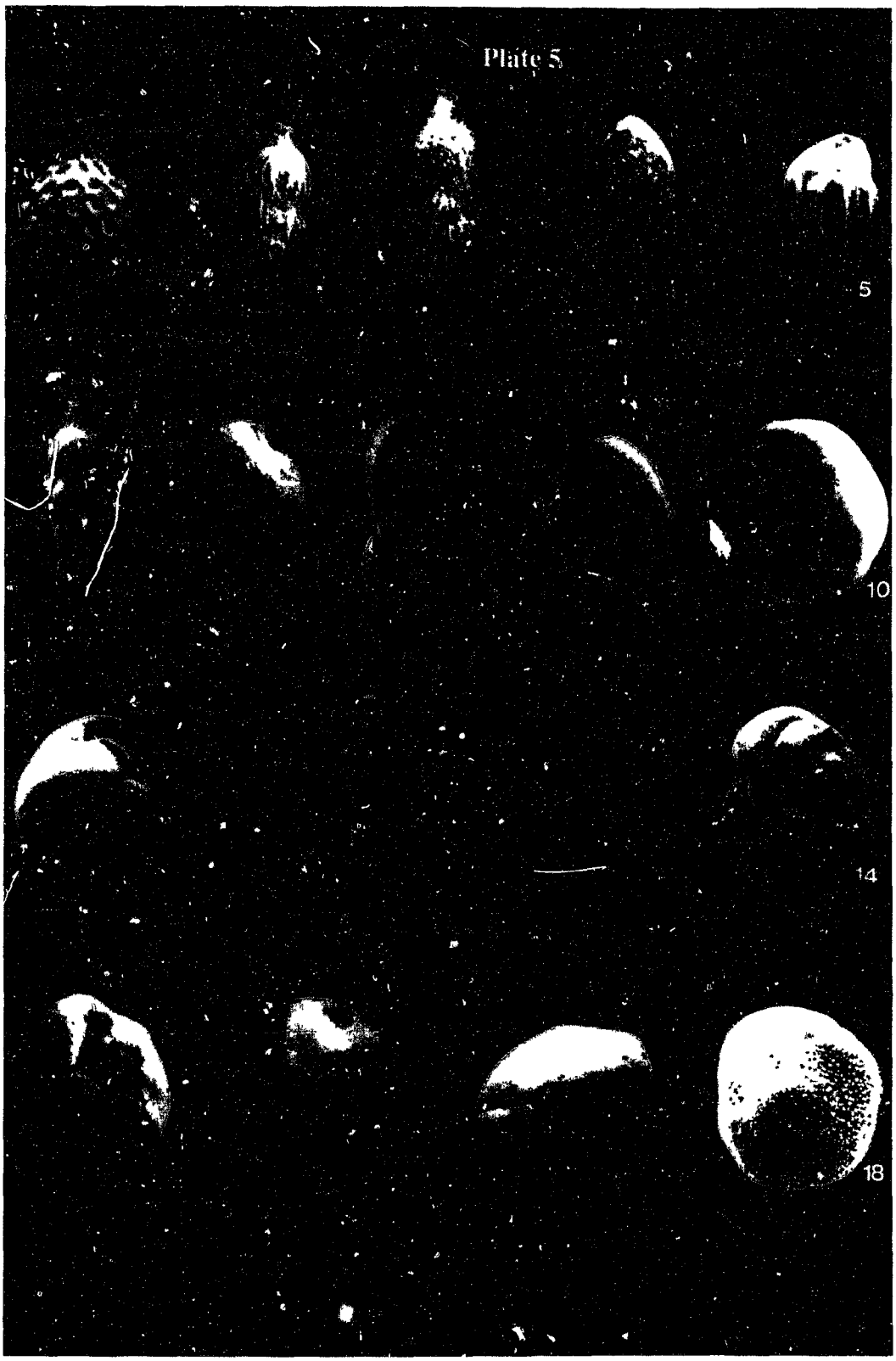
Plate 5
5
10
14
18

Plate 6

(Benthic foraminifera from DSDP Holes 608 and 547A)

1) *Lagena gracilis,* 1962, side view, Sample Site 608, 19-CC, 10–14 cm.

2) *Lagena distoma,* side view, Sample Site 608, 12–2, 80–84 cm.

3) *Lagena elegantissima,* side view, Sample Site 608, 20–3, 60–64 cm.

4) *Lagena formosa,* side view, Site 608, 13–1, 80–84 cm.

5) *Entosolenia duplicata,* side view, Sample Site 608, 13–1, 80–84 cm.

6) *Fissurina acuta,* side view, Sample Site 608, 12–4, 80–84 cm.

7) *Fissurina annectens* , side view, Sample Site 608, 12–4, 80–84 cm.

8) *Fursenkoina fusiformis,* side view, Sample Site 608, 12–4, 80–84 cm.

9) *Pleurostomella* ? sp. A, side view, Sample Site 608, 12–2, 80–84 cm.

10) *Pleurostomella* ? sp. A. side view, Sample Site 608, 12–12, 102–104 cm.

11) *Pleurostomella obtusa,* side view, Sample Site 608, 20–1, 102–106 cm.

12) *Pleurostomella alternans,* side view, Sample Site 608, 12–4, 80–84 cm.

13) *Stilostomella antillea,* side view, Sample Hole 547A, 31–4, 11–15 cm.

14) *Rectuvigerina multicostata,* side view, Sample Hole 547A, 8-CC, 2–6 cm.

15) *Bulimina alazaensis,* side view, Sample Site 608, 13–1, 80–84 cm.

16) *Bulimina mexicana,* side view, Sample Hole 547A, 8–4, 80–84 cm.

17) *Ehrenbergina trigona,* side view, Sample Hole 547A, 8-CC, 2–6 cm.

18) *Globobulimina* ? sp.A, side view, Sample Site 608, 19-CC, 10–14 cm.

19) *Globobulimina* ? sp.B, side view, Sample Site 608, 12–6, 120–124 cm.

20) *Glandiculina* sp.A, side view, Sample Site 608, 20–1, 102–104 cm.

21) *Praeglobobulimina?* sp.A., side view, Sample, Site 547A, 8–4, 80–84 cm.

22) *Uvigerina proboscidea,* side view, Sample Site 547A, 8–4, 80–84 cm.

23–25) *Bolivina pygmaea,* side views, Sample Site 608, 20–1, 102–106 cm (23), Site 608, 12–6, 120– 124 cm (24), and Hole 547A, 8–4, 80–84 cm (25).

26) *Bolivina albatrossi, side view,* Sample Site S67 of Salé Borehole, Morocco.

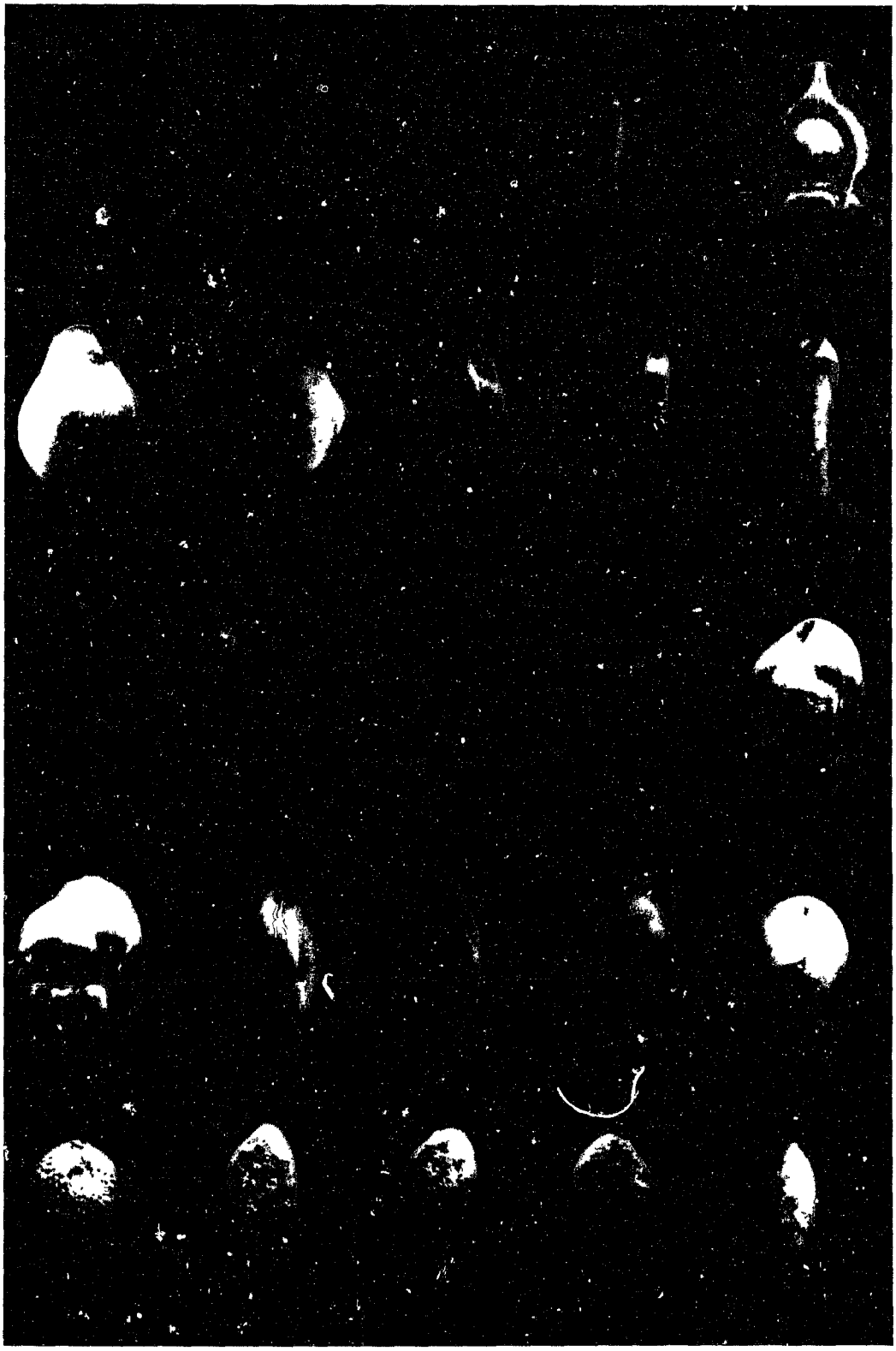

Plate 7

(Benthic foraminifera from DSDP Holes 608 and 547A)

1) *Cibicidoides bradyi*, ventral view, Sample Site 608, 20–6, 110–114 cm.

2, 14) *Oridorsalis umbonatus*, ventral view, Samples Site 608, 20–6, 110–114 cm; and 20–1, 102–106 cm.

3, 4,6) *Gyroidina soldanii*, ventral edge and ventral views, Samples Site 608, 13–1, 80–84 cm; 4, 12–6, 120–124 cm; 552A, 13–4, 11–15 cm.

5) *Eponides polius*, ventral view, Sample Site 608, 12–6, 120 124 cm.

7, 12) *Heronallenia crosbyi*, ventral and dorsal view, Samples Site 608, 20–2, 80–84 cm; and 20–3, 60–64 cm.

8, 10) *Nuttallides umbonifera*, ventral views, Samples Site 608, 20–3, 60–64 cm; and 12–6, 120–124 cm.

9, 11) *Cibicidoides mundulus*, dorsal and ventral views, Samples Site 608, 12–6, 120–124 cm; and 12–4, 80–84 cm.

13) *Planulina wuellerstorfi*, side view, Sample Site 608, 19–6, 14–18 cm.

15) *Melonis affinis*, side view, Sample Site 547A, 8–4, 80–84 cm.

16, 18) *Eponides tumidulus*, ventral views, Sample Site 608, 19–6, 14–18 cm; and 12–6, 120–124 cm.

17) *Eponides weddellensis*, dorsal view, Sample Site 608, 19–6, 14–18 cm.

19) *Epistominella exigua*, ventral view, Site 608, 20–1, 102–104 cm.

20) *Tosaia hanzawai*, side view, Site 608, 12–4, 80–84 cm.

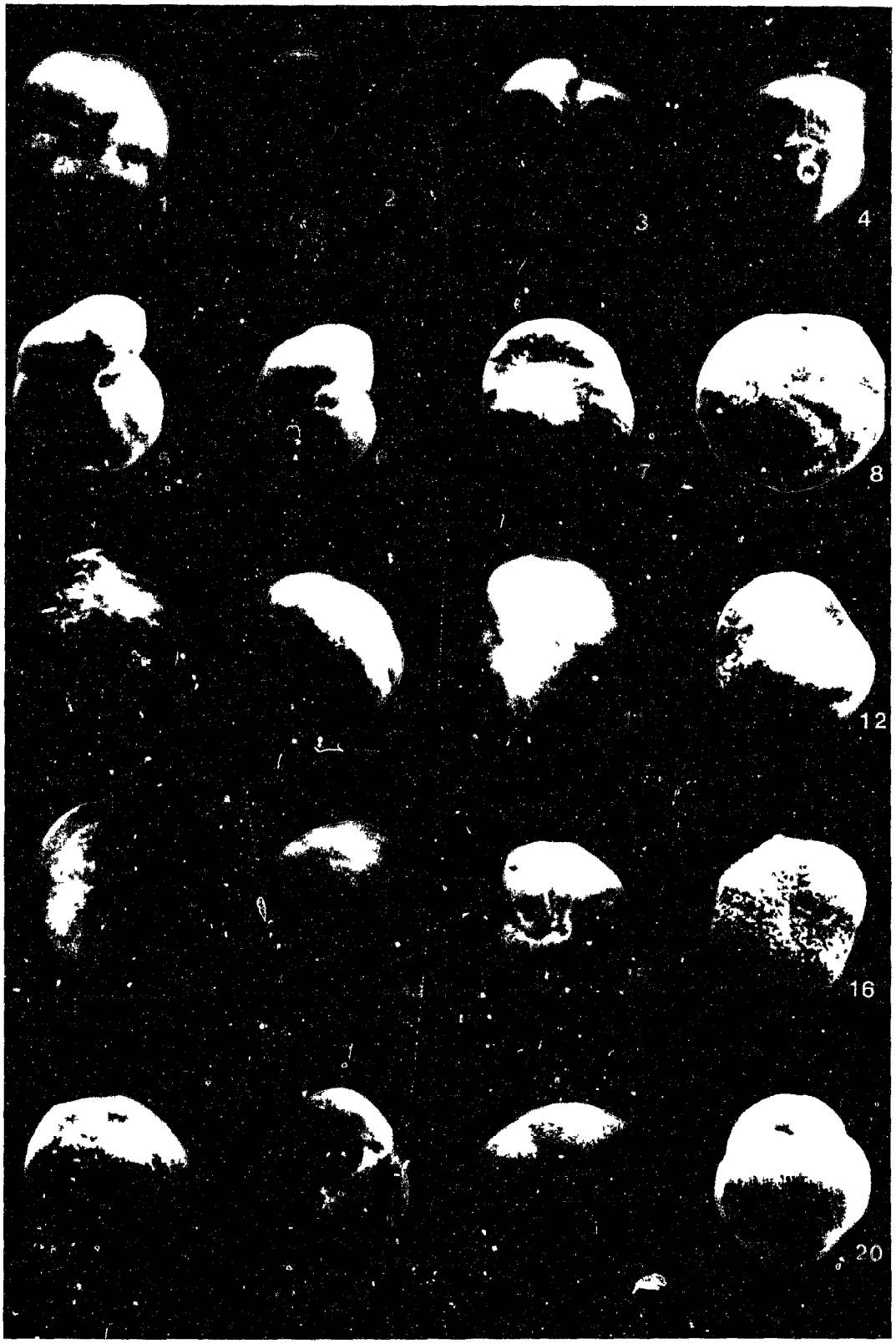
1
2
3
4
8
12
16
20

Plate 8

(Benthic and planktonic foraminifera from DSDP Holes 608 and 547A)

1, 2) *Globocassidulina subglobosa* , side view, Sample Hole 547A, 5-CC, 4–8 cm.

3) *Pullenia quinqueloba,* side view, Sample Site 608, 20–1, 102–106 cm.

4) *Astrononion umbilicatulum,* side view, Sample Site 608, 12–6, 120–124 cm.

5) *Pacinonion* sp. A., side view, Sample Site 608, 12–4, 80–84 cm.

6) *Melonis barleeanum,* side view, Sample Site 608, 12–2, 80–84 cm.

7) *Pullenia bulloides,* side view, Sample Site 608, 12–2, 80–84 cm.

8) *Anomalinoides flinti,* ventral view, Sample Hole 547A, 8–4, 80–84 cm.

9) *Laticarinina pauperata* , ventral view, Sample Site 608, 13–1, 80–84 cm.

10) *Osangularia culter,* ventral view, Sample Hole 547A, 8–4, 80–84 cm.

11) *Karreriella bradyi* , side view, Sample Hole 547A, 8–4, 80–84 cm.

12) *Siphotextularia catenata* , side view, Sample Site 608, 12–6, 120–124 cm.

13, 14) *Neogloboquadrina acostaensis,* ventral view, Sample Site 608, 15–2, 90–94 cm.

15) *Globorotalia conoidea,* ventral view, Sample Site 608, 21–5,60–64 cm.

16) *Globigerinoides extremus,* umbilical view, Sample Site 608, 15–2, 90–94 cm.

17, 18) *Globorotalia margaritae,* dorsal and ventral views, Sample Site 608, 13–1, 80–84 cm.

19) *Globorotalia crassaformis,* ventral view, Sample Site 608, 13–1, 80–84 cm.

20) *Globigerina nepenthes,* ventral view, Sample Site 608, 20–6, 110–114 cm.

21) *Globorotalia mediterranea,* ventral view, Sample Site 334, 5–4, 76–78 cm.

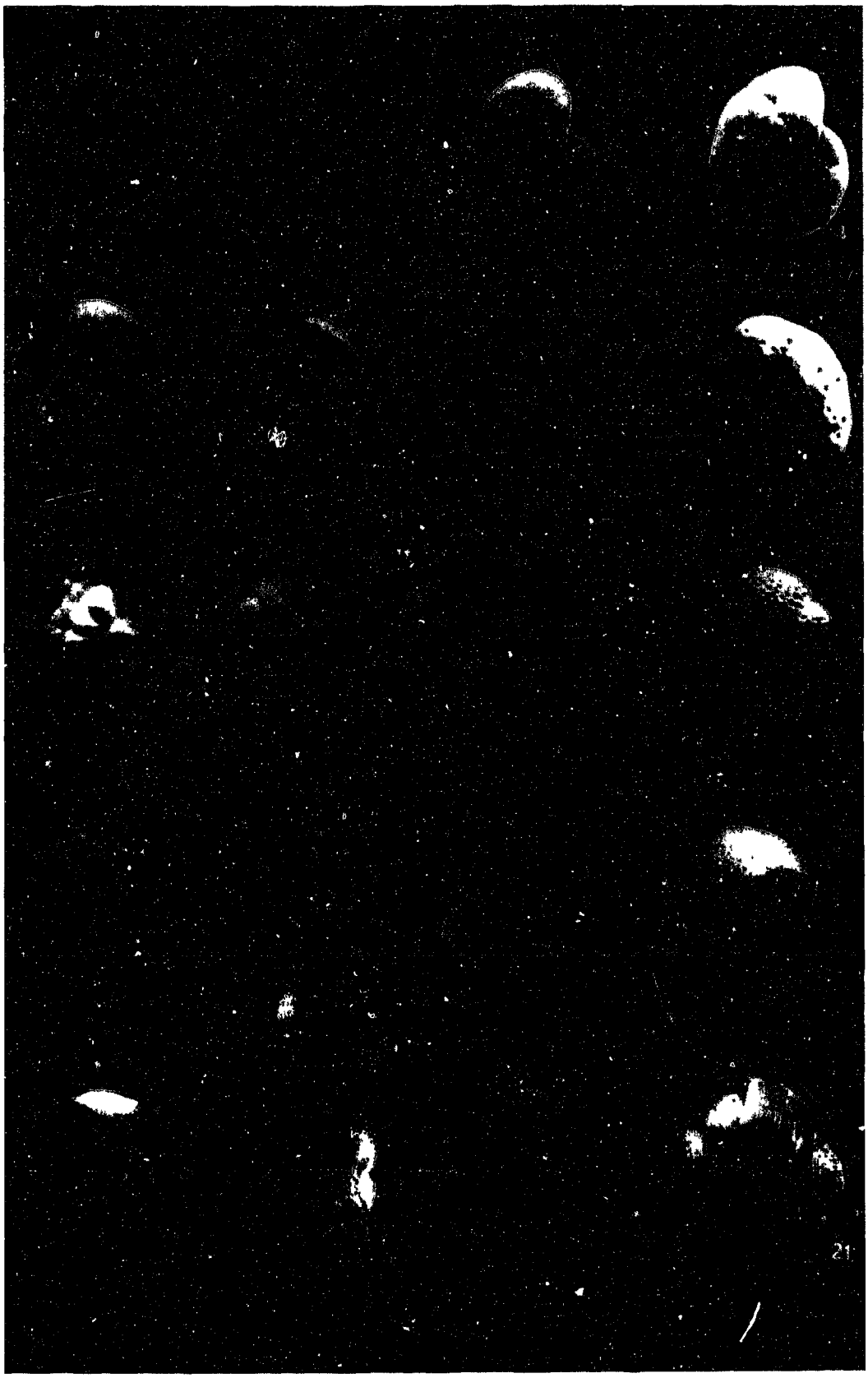
21

Plate 9

(Benthic and planktonic foraminifera from ODP Hole 646B)

1) *Neogloboquadrina atlantica*, ventral view, from Site 646B, Core 44X-CC, 30-34 cm.

2) *Melonis pompilioides*, side view, from Site 646B, Core 44X-CC, 30-34 cm.

3) *Nuttallides umbonifera*, ventral view, from Site 646B, Core 44X-CC, 30-34 cm.

4) *Cornuspirella diffusa*, side view, from Site 646B, Core 78X-CC, 26-30 cm.

5) *Planulina wuellerstorfi*, ventral view, from Site 646B, Core 44X-CC, 30-34 cm.

6) *Pyrgo murrhyna*, side view, from Site 646B, Core 44X-CC, 30-34 cm.

7) *Globocassidulina subglobosa*, ventral view, from Site 646B, Core 44X-CC, 30-34 cm.

8, 9) *Trochammina* cf. *squamata*, ventral views, 8 from Site 646B, Core 69X-1, 40-44 cm, 9 from Site 646B, Core 75X-CC, 10-14 cm.

10-12) *Ammotium* sp. A, side views, all from Site 646B, Core 76X-2, 50-54 cm.

13, 14) *Miliammina fusca*, side views, 13 from Site 646B, Core 69X-1, 40-44 cm, 14 from Site 646B, Core 76X-1, 100-104 cm.

15) *Rhizammina* sp. A. side view, from Core 78X-CC, 26-30 cm.

16) Plant fruit, from Core 71X-1, 5054 cm.

17) Plant seed, from Core 54X-1, 140-144 cm.

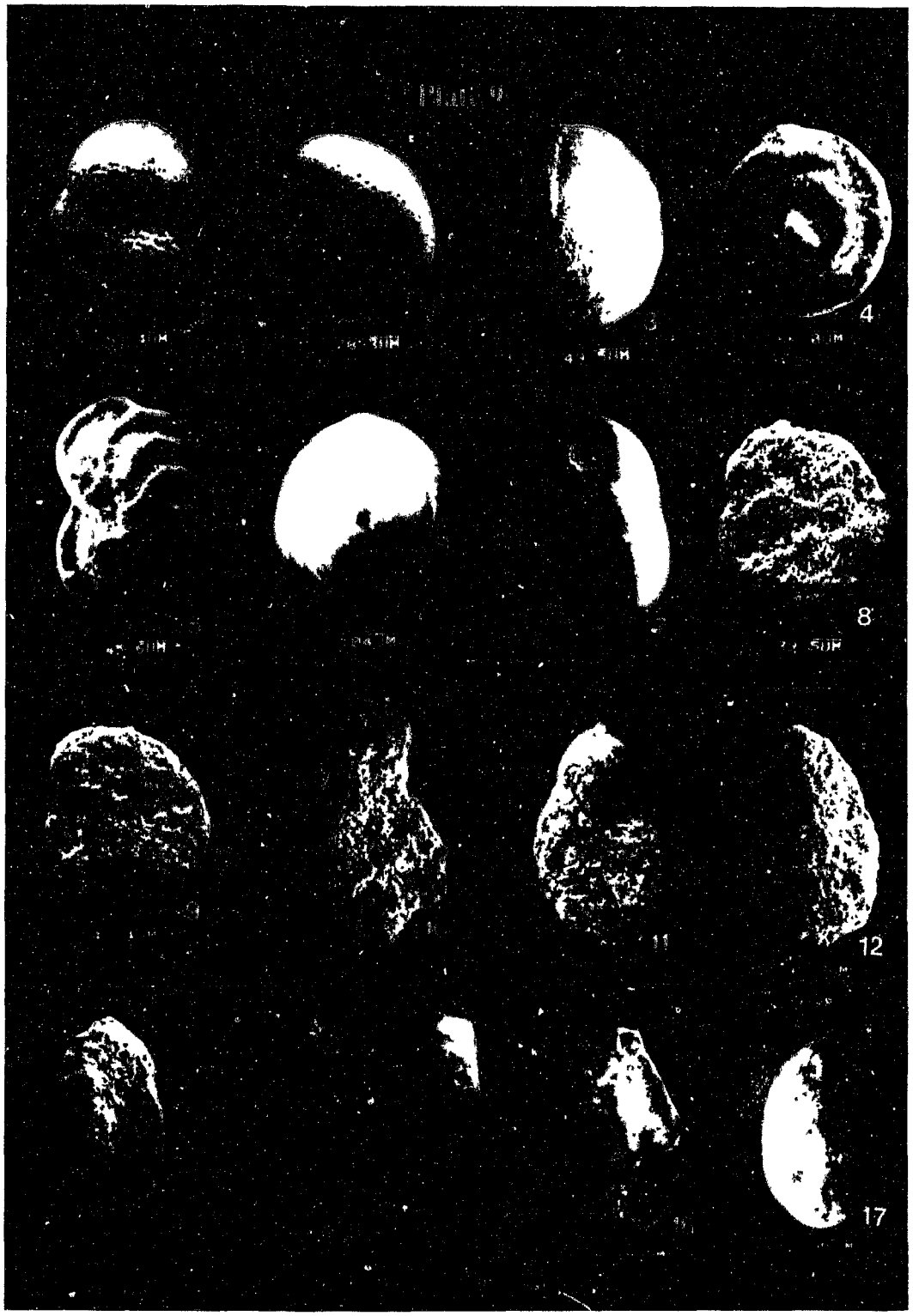
4
8
12
17

Appendix A

Table of benthic foraminifera from Salé Borehole, northwestern Morocco.

Salé, Morocco Samples	S2	S4	S6	S7	S9	S11	S13	S15	S16	S17	S19	S20	S21	S22	S24	S25	S27
Depth (m below surface)	2.99	5.05	7.17	8.21	10.29	12.31	14.38	16.42	17.49	18.54	20.63	21.73	22.71	23.74	25.74	26.77	28.94
Split	2048	2048	2048	2048	4096	2048	2048	1024	1024	2048	4096	4096	4096	2048	2048	2048	4096
No. picked	671	452	689	434	510	484	563	538	310	399	442	447	305	371	196	255	357
No. in per cc sediments	27162	18513	28221	17776	41779	19824	23060	11018	10772	16343	36208	36618	24985	15196	12779	12738	29245
% benthic forams in total	54.2	34	49.3	39.1	34.9	32.4	43.8	37.7	42.3	38.3	37.6	42.7	43.7	46.4	35.1	38.1	35.2
Nonion spp.	0	0	0	0	0.59	1.24	0	1.49	1.61	0.75	0.9	2.24	0	0	3.06	0	0
Nonionella turgida	0.89	0	0	0	0	0	0	0	0	0	0	0	0	0	0	0	0
N. miocenica	1.34	0.22	0	0	0	0	0	0	0	0	0	0	0	0	0	0	0
N. sp. A	0	0.66	0	0	0	0	0	0.19	0	0	0.23	0	0	0	0	0	0
Melonis pompilioides	0.45	0.88	0	0.23	0	0	0.18	0.93	0.65	0	0	2.46	0.33	2.16	2.04	0	0.28
M. barleeanum/affinis	3.58	1.77	3.05	1.38	5.29	5.17	2.84	2.42	3.23	3.01	2.49	1.79	2.3	0.81	1.02	2.35	0
Pullenia bulloides	0.6	0	0.73	0	0.39	0.41	1.42	0	0	1	0.9	0.45	0.33	0.81	1.02	0	0.28
P. quinqueloba	0	0.44	0	0.46	0.78	0.21	0	0.37	0.32	0	0	0	0	0	0	0	1.12
Astrononion echolsi	0.15	0	0	0	0	0	0	0	0	0	0	0	0	0	0	0	0
A. umbilicatulum	0	0.22	1.89	1.84	0.39	0.21	0.18	1.49	1.29	0	1.13	0.45	0	0.81	0	0	0
Elphidium sp.	0	0.44	0.44	0.23	0	0	0.18	0.74	0	0.25	0.23	0	0.66	0	1.02	0	0.28
Florilus sp.	0	0.22	0.58	0.46	0	0.83	0.36	0.37	0	0	0	0.22	0.33	0.54	1.53	1.57	1.96
Anomalina colligera	0	0	0	0	0	0	0	0	0	0	0	0	0	0	0	0	0
Sphaeroidina bulloides	1.19	2.21	0.73	0.46	0.98	0.62	0.18	0.93	0.97	0	0.45	0.45	0 66	1.08	1.02	2.35	0.28
Oridorsalis umbonatus	0.6	0.22	0.15	0.23	0.2	0.21	0.71	0.74	0.32	0	0	0.45	0.33	0.27	0	0	0
Rosalina sp.	0	0.88	0	0	0.2	0.41	0	0.37	0	0.25	0	0.22	0	0	1.53	0.78	0
Discorbinella bertheloti	4 23	2.43	3.19	1.61	1.76	1.65	2.49	2.79	3.23	3.01	2.71	2.01	4.26	2.7	6.63	1.57	1.12
Discorbinella sp.	0.3	0.22	0.44	0.46	0.39	0.21	0	0	0	0	0.45	0.45	0	0.54	0	0	1.12
Heronallenia crosbyi	0	0	0	0	0	0	0	0	0	0	0	0	0	0	0	0	0
Planulina ariminensis	0	0	0.44	0.23	0.59	0.83	0.36	0.37	0.32	0.5	0	0	0	0.27	0.51	0.39	0.56
Planulina wuellerstorfi	0	0	0	0	0	0	0	0	0	0	0	0	0	0	0	0	0
Cibicides lobatulus	0	0	0	0	0	0	0	0	0	0	0	0	0	0	0.53	0	0
Cibicidoides bradyi	0.6	0.22	0	0	0	0.21	0	0.19	0	0.75	0	0.45	0	0 91	0	0.39	0.28
C. walli	0	0.22	0	0	0	0	0	0	0	0	0	0	0	0	0	0	0
C. mundulus	6.11	8.85	12.9	9.67	11.76	10.33	12.08	13.01	13.87	18.05	11.31	12.53	15.08	12.39	9.69	10.59	4.76
C. pachyderma	7.45	0.88	2.61	0.46	0.59	0.62	0 17	0	0	1	1.13	0.22	0.98	3.77	1.53	0.73	0.84
C. mundulus+pachyderma	13.56	9.73	15.51	10.13	12.35	10.95	12.25	13.01	13.87	19.05	12.44	12.75	16.06	16.16	11.22	11.32	5.6
C. bradyi	0	0	0	0	0	0	0	0	0	0	0	0	0	0	0	0	0
C. crebbsi	0.6	0.5	0.58	0.23	0.58	0.21	0.35	0	0.97	0	0.22	0.22	0	0	0.53	0	0
C. dutemplei	0.1	0.7	0.15	0	0	0	0.17	0	0	0	0	0	0.33	0	0	0	0
Gavelinopsis praegeri	5.37	9.73	9	5.07	10	9.92	11.37	9 29	6.45	10.53	10.41	6.49	8.52	5.66	4.08	11.76	4.76
Epistominella exigua	0	0	0	0	0	0	0	0	0	0	0	0	0	0	0	0.78	0.28
E. takanayagii	1.94	1.99	1.89	2.53	2.73	3.31	1 78	2.79	0 65	1	5.2	1.57	3.61	1.35	2.55	2.35	2.24
Gyroidina slodaniii	6.56	3.54	4.06	2.76	4.71	3 51	4.09	4.46	1 29	2.01	7.01	3.36	1.97	3.5	1.53	2.35	2.52
Eponides polius	0.15	0.22	0	0	0	0	0	0	0	0	0	0	0	0	0	0	0
E. tumidulus	0	0.22	0	0	0	0	0	0	0	0	0	0	0	0	0	0	0
E. weddellensis	0 3	0.88	0	1.15	1.96	1.23	0 89	0.56	2.9	2.01	1.13	2.01	1.97	1.35	2.04	0	3.08

Salé, Morocco Samples	S28	S29	S30	S31	S32	S35	S37	S39	S41	S42	S44	S46	S48	S49	S50	S51	S52
Depth (m below surface)	29.94	30.99	32.06	33.1	34.16	37.22	39.15	41.12	43.23	44.16	46 22	48.29	50.44	51.44	52.35	53.39	54.39
Split	2048	2048	4096	512	2048	1024	4098	4096	2048	2048	512	512	512	256	1024	512	512
No. picked	295	413	393	263	215	307	294	382	305	385	310	337	517	441	92	559	457
No. in per cc sediments	12083	16916	32194	5386	17612	12574	48168	62586	24903	31539	6348	6901	10588	4515	16056	11448	9359
% benthic forams in total	32	36.4	31.4	33.4	31.6	37.3	30	27	32.5	39.9	37.5	41.7	35.8	34.3	33.4	29.1	28.4
Nonion spp.	0	0	0	0	0	0	0	0	0	1.82	1.61	0	0.39	2.04	0.26	0.72	0.44
Nonionella turgida	0	0	0	0	0	0	0	0	0	0	0	0	0	0	0	0	0
N. miocenica	0	0	0	0	0	0	0	0	0	0	0	0	0	0	0	0	0
N. sp. A	0.3	0	0	0	0	0	0	0.26	0	0	0	0.89	0	0	0	0	0
Melonis pompilioides	0	0 24	0	1.14	0	0.33	0.34	0	0	0	0	0	0	0	0	0	0
M. barleeanum/affinis	1.02	1.45	1.78	1.14	2.33	2.61	1.7	2.09	1.64	2.08	3.87	1.19	2	1.36	1.53	0.54	2.63
Pullenia bulloides	0	0.48	0.76	0	0.47	0	0.68	0.52	0	0	0	0.3	0.39	0	1.02	0	0.22
P. quinqueloba	0	0.24	0.51	0	1.4	0.33	0	0.52	0	0	0	0.59	0.39	0.45	1.28	0.54	0.44
Astrononion echolsi	0	0	0	0	0	0	0	0	0	0	0	0	0	0	0	0	0
A. umbilicatulum	0	0.73	0.76	2.28	0	0.98	0 68	1.05	0	0	0	0.89	0.58	1.59	0	0.54	0.88
Elphidium sp.	0.68	0	0	0	0	0.33	0	0	0	0.26	0	0.3	0	0	0	0	0
Florilus sp.	0	0.24	0.51	0	0	0	0	0	0.33	0.52	0	0	0	0	0.51	0.92	0.44
Anomalina colligera	0	0	0	0	0	0	0	0	0	0	0	0.3	0	0	0	0	0
Sphaeroidina bulloides	0.68	0.97	0	0.76	0.47	1.3	1.36	1.57	0.33	0.26	1.61	1.78	0.19	0.91	0.51	0.36	0.44
Oridorsalis umbonatus	0.34	0.48	0	0.76	1.4	0.33	1.02	0	1.31	0.26	0.97	0	0.19	0.45	0.26	0.72	0.88
Rosalina sp.	0	0	0.25	0.76	0.47	0.33	0.68	0	0	0	0.97	0	0.77	0.23	0	0.36	0.22
Discorbinella bertheloti	2.71	4.12	3.05	3 8	3.26	1.63	4.08	4.19	2.95	2.34	4.19	1.19	2.51	2.04	3.57	1.43	1.31
Discorbinella sp.	0	0.97	0.51	0	0	0	0.68	0.79	0	0.26	0	0.3	0	0.91	1.02	1.97	1.09
Heronallenia crosbyi	0	0	0	0	0	0	0	0	0	0	0	0	0	0	0	0	0
Planulina ariminensis	0	0.24	0.25	0.38	2.33	0.65	1.36	0	1.97	0.26	1.61	0	0.19	0	0.26	0.36	1.09
Planulina wuellerstorfi	0	0	0	0	0	0	0	0	0	0	0	0	0.39	0	0	0	0
Cibicides lobatulus	0	0	0	0	0	0	0	0	0	0	0	0	0	0	0	0	0
Cibicidoides bradyi	0	0.48	0	0.38	0	0	0.34	0.52	0	0.26	0.32	0	0	0.45	0.26	0.18	0.44
C. walli	0	0	0	0	0	0	0	0	0	0	0	0	0	0	0	0	0
C. mundulus	11.86	10.17	8.4	11.41	7.41	10.1	6.12	6.54	16.72	11.69	11.61	8.01	10.25	7.26	6.63	3.76	6.35
C. pachyderma	2.71	1.2	0.25	1.9	2.33	2.61	0	3.14	0.64	0	1.29	1.18	0.26	0.91	0.26	0.54	0
C. mundulus+pachyderma	14.57	11.37	8.65	13.31	9.74	12.71	6.12	3	17.36	11.69	12.9	9.19	10.51	8.17	6.89	4.3	6.35
C. bradyi	0	0	0	0	0	0	0		0	0	0	0	0	0	0	0	0
C. crebbsi	0	0.24	0	0	0.46	0	0	6	0	0	0.32	0	0	0	0	0.18	0
C. dutemplei	0	0	0	1.9	0	0.32	0.34	0	0	0	0	0	0	0	0	0	0
Gavelinopsis praegeri	8.47	9.2	6.62	4.56	6.98	6.51	4.76	6.02	3.93	7.79	4.19	7.12	7.54	5.44	8.16	7.51	8.53
Epistominella exigua	1.35	0	0.51	1.52	0.93	0	0.34	0	0.32	0	0	0	0	0.23	1.53	0.71	1.53
E. takanayagii	1.69	1.69	1.02	1.14	0.93	0.33	0.68	0	0.32	0.26	0.32	0.3	0	0	0.51	2.86	1.31
Gyroidina slodanii	2.37	3.63	3.31	2.66	3.72	2.93	3.74	3.66	2.3	4.42	3.23	5.04	1.35	5.44	3.83	6.08	3.28
Eponides polius	0	0	0	0	0	0	0	0	0	0	0	0	0	0	0	0	0
E. tumidulus	0	0	0	0	0	0	0	0	0	0	0	0	0	0	0	0	0
E. weddellensis	2.03	3.39	6.36	2.66	2.33	1.3	3.06	3.14	3.28	4.16	1.94	1.19	3.09	6.58	4.34	8.59	4.38

Salé, Morocco Samples	S53	S55	S56	S57	S59	S60	S61	S62	S63	B2	S65	B3	S67	B5	S70	B7	B8
Depth (m below surface)	55.46	57.38	58.46	59.36	61.14	62.19	63.25	64.25	65.29	66.67	67.01	67.67	68.67	69.7	71.15	72.4	73.15
Split	512	2048	1024	512	256	512	256	512	512	512	512	512	64	256	128	1024	1024
No. picked	436	378	361	402	426	318	337	236	229	299	501	301	666	273	616	201	263
No. in per cc sediments	8929	30965	14786	8232	4362	6512	3450	4833	4689	6123	10260	6164	1704	2795	3153	8232	10772
% benthic forams in total	28.3	28.8	26.8	33	26.3	24.5	26.6	25.4	23.8	19.7	16	23.5	16.9	17.3	27.5	16.5	27.9
Nonion spp.	0.23	1.59	1.66	0.25	1.17	0	0	0	1.75	0.43	1	1.66	0	2.93	0	0	0.38
Nonionella turgida	0	0	0	0	0	0	0	0	0	0	1	0	0	0	0.32	0	0
N. miocenica	0	0	0	0	0	0	0	0	0	0	0	0	0	0	0	0	0
N. sp.A	0.23	0.79	0	0	0.47	0.31	0	0	0	0	0.4	0	0.3	0	0.49	0	0.38
Melonis pompilioides	0	0	0	0	0	0	0	0	0	0	0	0.33	0	0	0	0.5	0
M. barlecanum/affinis	0.92	0.53	1.94	1.74	2.58	1.89	2.37	2.97	1.31	2.18	0.4	1.66	0	1.1	0.49	1	1.9
Pullenia bulloides	0.23	0.26	0	0	0	0.31	0.3	0.42	0.44	0.87	0.2	0.33	0	0.33	0	0	0
P. quinqueloba	0.46	0.26	0.28	0.48	0.94	0	0	1.27	0.44	0.43	0.6	0.33	0.15	0	0.65	0	0
Astrononion echolsi	0	0	0.28	0.25	0	0	0	0	0	0	0	0	0	0	0	0	0
A. umbilicatulum	0	0.26	0.28	0.25	1.87	0	0	0	0.87	1.33	0.8	0.33	0.6	0.74	0.65	1.99	0.38
Elphidium sp.	0	0.79	0	0	0	0	0.3	0.42	0	0	0	0.33	0	0	0	0.5	0
Florilus sp.	0.46	0.26	0	0.25	0	0.63	0	0.85	0	0	0	0.33	0	0.37	0	0.5	0
Anomalina colligera	0	0	0.28	0.25	0	0.31	0	0	0	0	0	0	0.75	0.37	0.97	0	0
Sphaeroidina bulloides	0.46	0	0	0.5	0.23	1.26	0.3	1.27	1.31	1	0.8	1	2.55	0.73	2.27	0	1.52
Oridorsalis umbonatus	0.23	0.26	0	0.25	0.23	0.31	0	0	0	0.87	0.4	0.33	0	0.37	0	0	0
Rosalina sp.	0	0.26	0	0.25	0	0	0	0.42	1.31	0.33	0	0.33	0	1.1	0	0	0
Discorbinella bertheloti	4.36	2.65	3.88	2.74	3.05	1.89	3.56	1.27	3.06	0.87	2.79	2.33	3.45	1.83	2.76	3.48	3.8
Discorbinella sp.	1.15	0	0.28	0.5	0.94	0	0.89	1.27	0.44	0	0.2	1.66	0	1.83	0.32	0.5	0.38
Heronallenia crosbyi	0	0	0	0	0	0	0	0	0	0	0	0	0	0	0	0	0
Planulina ariminensis	0.46	0.26	0	1	0.23	1.26	0.3	0.42	0.44	0	1.4	0.33	1.95	0.37	0.81	0	0.76
Planulina wuellerstorfi	0	0	0	0	0	0	0	0	0	0	0	0	0	0	0	0	0
Cibicides lobatulus	0	0	0	0	0	0	0	0	0	0	0	0	0	0	0	0	0
Cibicidoides bradyi	0	0.26	0.28	0.5	0.7	0.31	0.3	0.42	0.44	0	0.2	0.67	0.15	0	0	0.5	0
C. walli	0	0	0	0	0	0	0	0	0	0	0	0	0	0	0	0	0
C. mundulus	9.17	7.41	7.76	6.97	2.82	9.75	4.75	6.99	7.42	8.36	1.2	5.98	3.3	5.13	6.49	7.96	11.03
C. pachyderma	0.46	0.26	0.28	0	0.46	0	0.89	0.44	0	0.87	0	1.99	0	1.47	0.49	0.49	0
C. mundulus+pachyderma	9.63	7.67	8.04	6.97	3.28	9.75	5.64	7.43	7.42	9.23	1.2	7.97	3.3	6.6	6.98	8.45	11.03
C. bradyi	0	0	0	0	0	0	0	0	0	0	0	0	0	0	0	0	0
C. crebbsi	0	0	0	0	0	0	0	0	0	0	0	0	0	0	0	0	0
C. dutemplei	0.23	0	0	0	0	0	0	0	0	0	0	0	0	0	0	0	0
Gavelinopsis praegeri	6.42	6.08	7.76	6.97	4.46	7.23	9.2	9.32	6.55	11.37	4.79	5.64	13.06	8.42	9.42	4.48	5.32
Epistominella exigua	0	1.32	0.83	0.75	1.88	0.31	0.89	1.27	1.75	2.01	2.4	1	0.75	3.66	0.81	0.5	0
E. takanayagii	1.1	1.32	1.11	0.5	0.7	0.63	0.89	0.42	0	0	0	0	0.15	0	0	0	0
Gyroidina slodanii	3.9	3.17	1.66	2.74	6.81	1.89	0.89	3.39	2.18	3.34	2	2.66	1.65	2.2	2.76	2.99	2.28
Eponides polius	0	0	0	0	0	0	0	0	0	0	0	0	0	0	0	0	0
E. tumidulus	0	0	0	0	0	0	0	0	0	0	0	0	0	0	0	0	0
E. weddellensis	5.28	4.76	4.43	5.97	7.98	5.35	9.79	5.08	4.8	5.68	8.38	5.31	3.15	8.79	3.57	7.96	6.08

Salé, Morocco Samples	B9	B10	B11	B12	B13	B14	B15	B16	B17	B18	B19	B20	B21	B22	B23	B24	B25
Depth (m below surface)	74 15	75 2	76 3	77 4	78.5	79 5	80 55	81 55	82.55	83 6	84 65	85 9	86 65	87 25	88 75	89 8	90 8
Split	512	512	128	512	256	256	256	256	256	256	128	256	256	256	128	256	128
No picked	325	518	506	423	523	465	753	516	573	297	252	295	487	324	449	270	512
No in per cc sediments	6656	10608	2590	8662	5354	4760	7710	5282	5866	3040	1290	3020	4986	3317	2298	2764	2621
% benthic forams in total	22.2	26 4	23 2	23 1	27 3	22.4	21 3	23 7	15 5	18 7	14 7	14 8	17 2	15 8	20 3	16 2	17
Nonion spp	0 62	0 19	0	0 71	0.57	0	0 4	0 78	1 75	2.02	1 98	2 37	2.46	2.16	1 34	2 96	0 98
Nonionella turgida	0	0	0	0	0	0	0	0	0	0	0	0	0	0	0	0	0
N miocenica	0	0	0	0	0	0	0	0	0	0	0	0	0	0	0	0	0
N sp A	0	0	0	0	0	0	0	0	0	0	0	0	0	0	0	0	0 2
Melonis pompilioides	0	0	0 2	0	0	0	0	0	0	0	0	0	0	0	0	0	0
M barleeanum/affinis	1 23	1.54	0 99	1 42	1 34	0 86	0 27	0 19	0	0	0 79	1 02	1 03	1 23	0 9	1 85	1 11
Pullenia bulloides	0 31	0 19	0 2	0	0	0 22	0 13	0 58	0 17	1 01	0 4	0.34	0 62	0 62	0 45	0 37	0 59
P quinqueloba	0 31	0 19	0 4	0 47	0 19	0 43	0	0 78	0 35	1 01	1 19	0.34	0 21	0	0 45	0	0 78
Astrononion echolsi	0	0	0	0	0 57	0 22	0	0	0 35	0	0	0	0	0	0	0	0
A umbilicatulum	0 62	0	1 19	0	0 38	1 08	0 93	0	0 52	0	0	0.34	0	0 93	0 67	1 17	0 98
Elphidium sp	0 31	0	0 2	0	0 38	0	0	0	0	0.34	0	0	0 21	0	0	0	0
Florilus sp	0	0 19	0 59	0	0 38	0 22	0 4	0 97	0	0	0	0	0 21	0	0 22	0	0
Anomalina colligera	0 31	0	0 2	0	0	0	0	0	0 17	1 01	0 79	0	0	0 31	0	0	0
Sphaeroidina bulloides	2.15	0 39	0 59	0 47	0	1 29	0 27	1 36	0 35	1 01	1 59	0 34	1 64	0 62	0 89	1 48	1 17
Oridorsalis umbonatus	0	0 39	0 2	0	0.57	0 22	0 27	0	0 52	0 34	0	0	0	0	0	1 48	0 59
Rosalina sp	0 62	0 97	0 59	0 24	0 19	0 86	0 27	0	0	0	0	0	0	0 62	0 22	0	0
Discorbinella bertheloti	4 62	2 12	1 58	2.6	2.49	2.58	2 66	1 74	1 92	2.36	3 17	2 03	5 95	2.16	4 9	2 22	1 76
Discorbinella sp	0 62	0 58	0	0 24	0.57	0	0 53	0 19	0 35	0	0	0 34	0 41	0	0	0	0 2
Heronallena crosbyi	0	0	0	0	0	0	0	0	0	0	0	0	0	0 31	0 22	0	0
Planulina ariminensis	0 62	1 16	0.59	0 71	0 96	2.8	0 8	0 78	1 4	0 67	1 59	1 69	1 64	0 31	1 56	1 11	0 78
Planulina wuellerstorfi	0	0	0	0	0	0	0	0	0	0	0	0	0	0	0	0	0
Cibicides lobatulus	0	0	0	0	0	0	0	0	0	0	0	0	0	0	0	0	0
Cibicidoides bradyi	0	0 19	0 2	0 24	0 19	0 43	0 27	0	0 17	0	0 79	0 34	0 21	0 62	0	0	0
C walli	0	0	0	0	0	0	0	0	0	0	0	0	0	0	0	0	0
C mundulus	6 15	6 56	6 72	5 2	5 93	5 59	4 52	4 45	6 63	8 08	3 97	5 76	4 31	6 79	5 79	8 52	5 27
C pachyderma	1 23	0 19	0 79	0 95	0 96	1 29	0 27	2 13	1 57	1 01	4 37	2 03	3 08	0	1.56	0 74	0 39
C mundulus+pachyderma	7.38	6 75	7 51	6 15	6 89	6 88	4 79	6 58	8 2	9 09	8 34	7 79	7 39	6 79	7 35	9 26	5 66
C bradyi	0	0	0	0	0	0	0	0	0	0	0	0	0	0	0	0	0
C crebbsi	0	0	0	0	0	0	0	0	0	0 67	0	0	0	0	0	0	0
C dutemplei	0 31	0	0	0	0	0	0	0	0	0	0	0	0	0	0	0	0
Gavelinopsis praegeri	4 62	2 7	5 93	4 02	5 93	7 53	5 84	4 84	3 66	2.36	3 17	2 71	4 31	3 7	2.9	3 33	4 3
Epistominella exigua	0 92	0 58	1 18	2.13	0 38	0 22	1 73	0 19	0 17	1 68	0 79	1 36	0 82	3 09	3 13	4 07	1 36
E. takanayagi	0	0	0 19	0	0	0	0 13	0	0	1 68	0	1 36	0 62	0 93	0	0	0
Gyroidina slodani	4 31	3 67	4 15	3 55	2.1	3 23	2 79	1 94	2.62	4 04	2.38	2 71	2.26	3 09	0 22	3 7	1 56
Eponides polius	0	0	0	0	0	0	0	0	0	0	0	0	0	0	0	0	0
E. tumidulus	0	0	0	0	0	0	0	0	0	0	0	0	0	0	0	0	0
E. weddellensis	11 38	7 34	9 29	10 87	9.37	6 24	9 43	16 47	10 47	9 43	9 13	15 93	14 58	16 98	15 81	17 41	22.07

Salé, Morocco Samples	B26	B27	B28	B29	B30	B31	B32	B33	B34	B36	B37	B38	B39	B40	B41	B42	B43
Depth (m below surface)	91.9	92.9	93.9	94.85	96.1	96.85	97.95	98.95	100.05	101.75	102.85	103.9	105	106.1	107	108	108.9
Split	128	128	64	64	64	64	128	128	64	128	256	128	256	128	256	256	128
No. picked	367	528	742	572	447	737	832	516	580	530	516	671	430	618	626	406	634
No. in per cc sediments	1879	2703	1899	1464	1144	1886	4259	2641	1484	2713	5273	3435	4403	3164	6410	4157	3246
% benthic forams in total	17.9	17.3	13.5	19.6	33.3	23.2	17.5	15.7	14.4	18.5	17.4	14.7	10	10.1	13.5	10.8	10.7
Nonion spp.	1.09	1.33	1.89	0.87	1.57	2.71	2.16	0.69	2.41	6.04	3.29	4.02	3.72	3.56	6.87	5.67	1.26
Nonionella turgida	0	0	0	0	0	0	0	0	0	0	0	0	0	0	0	0	0
N. miocenica	0	0	0	0	0	0	0	0	0	0	0	0	0	0	0	0	0
N. sp.A	0	0	0	0	0.89	0.14	0.12	0	0.52	1.32	0.58	0	0.23	0.49	0.16	0.99	0
Melonis pompilioides	0	0	0	0.87	0	0.27	0	0	0	0	0	0	0	0	0	0	0.16
M. barleeanum/affinis	1.91	1.7	0	0	0.67	0	1.67	0.78	2.24	1.51	1.94	0.45	1.16	0.97	0.32	0.49	1.74
Pullenia bulloides	0.27	0.19	0.54	0.35	0.22	0	0.24	0.58	0.34	0.57	0.78	0.3	0.23	0.81	0.32	1.48	1.26
P. quinqueloba	0.54	0	0.67	0.35	0.22	0.27	0.12	0.39	0.17	0.38	0.19	0	0	0.16	0	0.99	0.47
Astrononion echolsi	0	0	0	0	0 22	0.14	0	0	0.34	0.57	0.78	0	1.63	1.13	1.12	0	0
A. umbilicatulum	0.27	0.57	0.67	0.52	1.78	0.41	1.08	0.39	0.34	0.19	1.36	0.6	0.23	0.49	1.12	0.74	0.95
Elphidium sp.	0	0	0.13	0	0	0	0	0	0	0	0	0	0	0	0	0	0
Florilus sp.	0	1.14	0	0	0	0	0	0	0	0	0	0	0	0	0	0	0
Anomalina colligera	0	0	0.54	0	0.22	0.14	0	0	0.52	0	0	0	0.23	0	0	0	0
Sphaeroidina bulloides	1.36	1.7	0.67	0.87	0.45	0.54	2.4	1.16	1.38	1.32	0.78	1.04	0.47	1.13	0.32	1.97	1.58
Oridorsalis umbonatus	0	1.14	0.54	1.22	0 89	1.9	1.08	1.74	1.03	0.38	1.16	0.45	1.16	0.16	1.28	0.25	1.1
Rosalina sp.	0	0.57	0	1.4	0	0	0.12	0.19	0.52	0	0	0.15	0	0	0.32	0	0
Discorbinella bertheloti	1.91	3.79	1.62	1.92	3.8	2.04	1.8	2.71	2.93	1.89	2.91	1.79	0.7	3.07	0.8	1.72	2 52
Discorbinella sp.	0	0.19	0	0	0	0	0	0	0	0	0.19	0.3	0	0	0	1.72	0
Heronallenia crosbyi	0.54	0.19	0	0	0	0	0.36	0	0	0	0.19	0	0	0	0	0	0
Planulina ariminensis	1.63	1.52	0.81	1.4	2.46	0.81	1.32	1.16	0.52	1.51	1.16	0.75	0.93	1.13	0.64	1.48	1.26
Planulina wuellerstorfi	0	0	0	0	0	0	0	0	0	0	0	0	0	0	0	0	0
Cibicides lobatulus	0	0	0	0	0	0	0	0	0	0	0	0	0	0	0	0	0
Cibicidoides bradyi	0	0	0.27	0	0	0.14	0	0	0.17	0	0	0	0	0.16	0	0	0
C. walli	0	0	0	0	0	0	0	0	0	0	0	0	0	0	0	0	0
C. mundulus	6.81	6.25	4.85	2.75	4.47	4.07	3 61	3.87	4.14	6.42	6.78	2.98	3.49	3.4	2.24	2.71	3.31
C. pachyderma	0.54	1.7	0.67	0.7	1.12	0	0.96	0	0	0	0	0	0	0.16	0	0	0.32
C. mundulus+pachyderma	7.35	7.95	5.52	3.45	5.59	4.07	4.57	3.87	4.14	6.42	6.78	2.98	3.49	3.56	2.24	2.71	3 63
C. bradyi	0	0	0	0	0	0	0	0	0	0	0	0	0	0	0	0	0
C. crebbsi	0.27	0	0.13	0.17	0	0	0	0	0	0	0.19	0.45	0	0	0	0	0
C. dutemplei	0.54	0	0	0	0	0	0	0	0	0	0	0	0	0	0	0	0
Gavelinopsis praegeri	4.63	4.73	2.43	2.62	2.01	2.17	3 85	8.33	4.48	2.64	6.98	2.68	2.33	5.18	3.67	5.17	5.99
Epistominella exigua	2.18	2.65	0.94	3.1	15.21	2.71	3.13	1.74	3.97	3.96	1.16	3.87	9.53	3.39	0.48	0.99	0.32
E. takanayagii	0	0.38	0.13	0	0	0.54	0	0	1.38	0.94	0	0	0	0	0	0	0
Gyroidina slodanii	2.18	1.52	2.16	0.7	1.12	1.09	1 32	1.94	0.86	9.62	2.33	1.64	2.56	1.29	1.6	1.72	2.37
Eponides polius	0	0	0	0	0	0	0	0	0	0	0	0	0	0	0	0	0
E. tumidulus	0	0	0	0	0	0	0	0	0	0	0	0	0	0	0	0	0
E. weddellensis	22.07	26.14	10.78	17.66	17.96	14 25	19.47	13.95	18.79	14.72	10.47	28.32	13.26	10.84	13.9	8.62	13.88

Salé, Morocco Samples	B44	B45	B47	B48	B49	B50	B51	B52	B53	B54	B55	B56	B57	B58	B59	B60	B62*
Depth (m below surface)	109 9	110 9	112.95	113 95	114 85	115 85	116 85	118	119 09	120 1	121 1	122.1	123 15	124 2	125 25	126 35	128 55
Split	256	128	256	128	128	128	128	64	128	256	256	256	256	128	256	128	64
No picked	419	575	492	435	481	396	445	536	264	299	309	335	313	560	180	240	303
No in per cc sediments	4290	2944	5038	2227	2462	2027	2278	1372	1351	3061	3164	3430	3205	2867	1843	1228	775
% benthic forams in total	9 9	8 8	13 8	10 8	10 8	6 4	8 8	12 2	9 9	12.7	8 4	8 8	10 9	9 8	10 8	14 9	13 7
Nonion spp	3 1	2.43	1 62	1 38	2.29	0	0 9	1 68	0	0	2.26	0 6	0	0 71	3 33	0	0 99
Nonionella turgida	0	0	0	0	0	0	0	0	0	0	0	0	0	0	0	0	0
N miocenica	0	0	0	0	0	0	0	0	0	0	0	0	0	0	0	0	0
N sp. A	0 24	0 52	0 71	0 69	0 21	0 76	0 67	0	0 76	0 67	0	0 67	0 96	0 71	0	0	1 32
Melonis pompilioides	0	0	0	0	0	0	0	0	0	0	0	0	0	0	0	0	0
M barleeanum/affinis	1 19	1 04	0 41	0	0 76	0 76	0 67	0 19	0 38	0.33	0 64	0 6	0 64	0	1 11	0 83	0 66
Pullenia bulloides	0 72	1 39	0 2	0 23	0 42	1 01	0	1 87	0 38	0 33	0	0	0	0 71	0 56	0 83	0 33
P quinqueloba	0	0.52	0	0	0 21	1 26	0 45	0 56	1 52	1	0 65	0.6	0	1 07	0	0 83	0 33
Astrononion echolsi	0.24	1.39	0	0	0 42	0 25	0 45	0	0	0	0	0	0	0	0	0	0
A umbilicatulum	0 72	0	1 22	0 46	0	0	0 45	0	1 52	0 33	2.59	2 69	2.88	0	0	0	0
Elphidium sp.	0 24	0	0	0	0	0	0	0	0	0	0	0	0	0	0	0	0
Florilus sp	0	0	0	0	0	0	0	0	0	0	0	0	0	0	0	0	0
Anomalina colligera	0 72	0 87	0	0 23	0 42	0 76	0 45	1 12	2.27	1 34	0	3 58	0 64	1 43	4 44	2.92	3 96
Sphaeroidina bulloides	1 19	1 57	2 24	1 15	2.29	2.53	1 57	1 68	2.27	2.34	1 29	0 9	3 51	1 07	2.22	0 83	0 33
Oridorsalis umbonatus	0 48	0 7	1 63	0 92	2.29	1 52	1 12	2.24	1 52	2.01	1 29	2 09	1 92	2.86	2.22	3 33	3 63
Rosalina sp.	0	0	0	0	0	0	0	0	0	0	0	0	0	0	0	0	0
Discorbinella berthelotti	3 34	1 74	2 24	3 91	6 24	1 26	2 7	2.61	2.01	2.01	3 24	1 79	1 27	2.86	4 44	2 1	2 97
Discorbinella sp.	0	1 74	0	0	0	0	0	0 55	3 79	1 67	0 97	0 6	2.56	1 07	1 11	0	0 33
Heronallenia crosbyi	0 95	2 61	1 42	1 38	0 42	1 26	1 12	1 12	0 38	0	1 62	0	0 96	0	1 11	0	0 33
Planulina arimunensis	1 43	1 91	0	1 84	0 62	0 25	1.35	1 12	2.27	1 67	0 65	0 3	0 96	1 43	0	0 42	0 66
Planulina wuellerstorfi	0	0	0	0	0	0 25	0 22	0	0	0	0	0	0	0	0	0	0
Cibicides lobatulus	0	0	0	0	0	0	0	0	0	0	0	0	0	0	0	0	0
Cibicidoides bradyi	0	0	0	0	0 21	0	0 22	0	0 76	0 67	0.32	0	0	0	0	0 42	0
C walli	0	0	0	0	0	0	0	0	0	0	0	0	0	0	0	0	0
C mundulus	3 82	2 78	2 24	2.99	2.08	1 77	4 26	2.99	5 3	3 01	3.24	1 19	2.59	6 79	7 22	2 08	3 63
C pachyderma	0	0	0	0	0	0 25	0	0	0	0 33	0 97	0	0 32	0	1 11	0	0 66
C mundulus+pachyderma	3.82	2 78	2 24	2.99	2.08	2.02	4 26	2.99	5 3	3 34	4 21	1 19	2.91	6 79	8 33	2 08	4 29
C bradyi	0	0	0	0	0	0	0 22	0	0	0	0	0	0	0	0	0	0
C crebbsi	0 24	0 34	0	0 46	0	0	0	0	0	0	0	0	0	0	0	0	0
C dutemplei	0	0	0	0	0	0	0	0	0	0	0	0	0	0	0	0	0
Gavelinopsis praegeri	3 1	5 22	2 64	5 29	7 48	5 56	5 84	4 66	3 79	3 34	5 83	4 18	3 83	1 79	3 89	6 25	4 95
Epistominella exigua	1 2	1 04	0 61	0 69	0 62	2.02	1 57	1 87	0 8	2.67	1 94	2 98	2.87	2.86	1 67	2 92	3 13
E. takanayagii	0	0	0	0	0	0	0	0	0	0	0	0	0	0	0	0	0
Gyroidina slodani	0 72	1 91	3 66	3 68	5 2	3 54	0 67	2.61	0 38	3 01	2.27	5 67	4 79	2.5	7 78	9 58	11 22
Eponides polius	0	0	0	0	0	0	0	0 19	0	0	0	0	0	0	0	0	0
E. tumidulus	0	0	0	0	0	0	0	0	0	0	0	0	0	0	0	0	0
E. weddellensis	1	11 65	21 34	9 66	13 1	12.63	10 79	11 94	7.58	15 38	13 92	23 88	12.78	14 29	5	7 92	12.5

Salé, Morocco Samples	B64*	B66*	B68*	B70*	B71	B72	B74	B76	B79	B81	B83	B85	B87	B89	B91	B93	B95
Depth (m below surface)	130.6	132.75	134.9	136.95	138	139.05	141.15	143.3	146.25	148.15	150.15	152.25	154.45	156.65	158.85	161.05	163.25
Split	64	64	128	64	256	128	128	64	32	128	256	512	64	512	250	512	1024
No. picked	269	261	207	167	195	287	317	322	480	531	529	313	610	442	770	783	645
No. in per cc sediments	688	668	1059	427	1996	1469	1623	824	616	2718	5416	6410	1561	9052	7884	16035	26419
% benthic forams in total	22.8	27.5	21.8	21.1	6.8	5.3	9.7	10.2	8.7	10.6	7.2	6.9	10.7	9.1	11.3	11.3	10.5
Nonion spp.	1.12	1.15	2.42	0	0	2.79	4.1	2.48	0	1.32	4.54	2.88	1.31	1.81	1.95	1.4	2.33
Nonionella turgida	0.37	0	0	0	0	0	0	0	0	0	0	0	0	0	0	0	0
N. miocenica	0	0	0	0	0	0	0	0	0	0	0	0	0	0	0	0	0
N. sp. A	0.37	0	0	0	1.03	0.35	0.32	0	0	0.19	0	0	0	0	0.26	0.26	0
Melonis pompilioides	0	0	0	0	0	0	0	0	0	0	0	0	0	0	0	0	0
M. barleeanum/affinis	0.37	1.53	0.48	1.2	0.51	0.35	0	0.31	0.21	0.38	1.33	0.32	0.66	0.23	0.65	1.15	0
Pullenia bulloides	0.37	1.53	0.48	1.2	0.51	0	0.63	0.62	0.83	0.19	1.13	0.64	1.8	0.68	0.65	2.43	0.47
P. quinqueloba	0.74	0.38	0	0	0.51	0.35	0	0	0.42	0.38	0.57	0.32	0.98	0.23	0.26	0.26	0.78
Astrononion echolsi	0	0	0.97	0	0	0.7	0	0	0	0	0	0	0	0.23	0	0	0
A. umbilicatulum	0	0.77	0	0	1.03	0	1.26	1.55	1.46	3.95	4.54	1.92	0.66	1.13	0.52	0.26	0.78
Elphidium sp.	0	0	0	0	0	0	0	0	0	0	0	0	0	0	0	0	0
Florilus sp.	0	0	0.97	0	0	0	0	0	0	0	0	0	0	0	0	0	0
Anomalina colligera	3.35	1.92	0	0.6	0	0.35	0.32	0	0.42	0	0	0.64	0.16	0.23	0	0	0
Sphaeroidina bulloides	0.74	6.13	2.9	0	1.54	0.7	0.63	2.17	1.46	0.19	0.19	0.96	4.26	3.17	0.78	0.89	1.71
Oridorsalis umbonatus	0.74	1.53	0	1.8	5.13	3.48	0.32	2.17	0.62	1.13	0.76	0.96	0.49	0.23	0.78	0.38	0.34
Rosalina sp.	0	0	0	0	0.51	0	0	0	0	0	0.19	0.32	0.16	0	0	0	0
Discorbinella bertheloti	1.5	2.68	4.83	2.99	6.15	4.51	1.26	4.97	2.29	2.82	4.54	0.64	2.13	2.26	3.51	2.81	2.79
Discorbinella sp.	0.37	0	0	0	6.15	0	0	0	0	0	0.18	0	0	0	0	0.25	0
Heronallenia crosbyi	0.37	0	0	0	0	0	1.58	0	0	0	0	0	0.49	0	0	0	0
Planulina ariminensis	1.12	1.15	0.48	1.2	1.03	2.79	1.26	0.93	1.25	2.26	0.95	3.19	1.15	0.9	0.39	1.28	0.31
Planulina wuellerstorfi	0	0	0	0	0	0	0	0	0	0	0	0.32	0	0	0	0	0
Cibicides lobatulus	0	0	0	0	0	0	0	0	0	0	0	0	0.49	0.22	0	0	0
Cibicidoides bradyi	0	0	0	0.6	0	0	0.32	0	0	0.19	0.19	0	0.16	0.45	0	0	0.47
C. walli	0	0	0	0	0	0	0	0	0	0	0	0	0	0	0	0	0
C. mundulus	3.72	4.98	6.28	6.59	4.62	5.92	6.62	7.45	6.67	7.16	4.54	6.39	8.85	6.33	2.21	1.01	3.1
C. pachyderma	0	1.53	0.97	0	0	0	0	0.31	0.62	0.19	0.19	0	0.49	0	0	1.4	0.62
C. mundulus+pachyderma	3.72	6.51	7.25	6.59	4.62	5.92	6.62	7.76	7.29	7.35	4.73	6.39	9.34	6.33	2.21	2.41	3.72
C. bradyi	0	0	0	0	0	0	0	0	0	0	0	0	0	0	0	0	0
C. crebbsi	0	0	0	0	0	0	0	0	0	0	0	0	0	0.22	0	0	0
C. dutemplei	0	0	0	0	0	0	0	0	0	0	0	0	0	0.22	0	0	0
Gavelinopsis praegeri	3.35	4.98	6.28	4.19	3.08	2.09	0.95	0.62	0.62	6.42	2.84	4.79	2.79	4.52	1.56	3.83	4.65
Epistominella exigua	0.74	2.68	1.93	3.59	1.54	2.09	4.42	4.66	4.38	1.56	6.43	1.91	3.93	4.07	3.9	3.83	9.3
E. takanayagii	0	0.38	0	0	0	0	0	0	0	0	0.18	0	0	0	0	0.89	0
Gyroidina slodanii	8.17	6.51	2.42	7.19	2.56	2.09	4.1	2.48	4.38	3.01	4.91	5.43	4.43	2.71	1.95	4.34	4.34
Eponides polius	0	0	0	0	0	0	0	0	0.21	0.19	0	0	0	0	0	0	0.16
E. tumidulus	0	0	0	0	0	0	0	0	0	0	0	0	0	0	0	0	0
E. weddellensis	12.63	5.36	8.7	8.98	6.15	12.89	12.93	15.52	13.75	6.59	1.7	9.26	9.51	8.37	14.42	9.58	4.65

Salé, Morocco Samples	B97	B98	B100	B102	B104
Depth (m below surface)	165.6	166.7	168.9	171	172.85
Split	4096	1024	512	256	8196
No. picked	274	488	957	280	238
No. in per cc sediments	44892	19988	19599	2867	39012
% benthic forams in total	9.3	11.3	12.9	22.6	11.5
Nonion spp.	0	1.02	0.52	0	0
Nonioncila turgida	0	0	0	0	0
N. miocenica	0	0	0	0	0
N. sp. A	0	0	0	0.36	0
Melonis pompilioides	0	0	0.21	0	0
M. barleeanum/affinis	1.09	1.23	0	0.71	0.84
Pullenia bulloides	1.46	1.02	1.04	0.36	0.42
P. quinqueloba	0.36	0.41	0	0.36	0.42
Astrononion echolsi	0	0	0	0	0
A. umbilicatulum	0.36	0.82	0.21	0	0.42
Elphidium sp.	0	0	0	0	0
Florilus sp.	0	0	0	0	0
Anomalina colligera	0	0	0	0	0
Sphaeroidina bulloides	1.46	0.61	1.25	1.79	1.26
Oridorsalis umbonatus	0.36	0.2	0.84	0	0
Rosalina sp.	0	0	0	0	0.84
Discorbinella bertheloti	5.11	2.87	2.93	4.29	5.04
Discorbinella sp.	0	0	0.21	0	0
Heronallenia crosbyi	0	0	0	0	0
Planulina ariminensis	0.73	1.23	0.31	0.36	0
Planulina wuellerstorfi	0	0	0	0	0
Cibicides lobatulus	0	0	0	0	0
Cibicidoides bradyi	0	1.02	0	1.07	0.42
C. walli	0	0	0	0	0
C. mundulus	1.46	4.1	2.61	2.86	2.94
C. pachyderma	0.36	0	0.31	0	0
C. mundulus+pachyderma	1.82	4.1	2.92	2.86	2.94
C. bradyi	0	0	0	0	0
C. crebbsi	0	0	0	0	0
C. dutemplei	0	0	0	0	0
Gavelinopsis praegeri	6.2	4.92	4.49	3.2	6.3
Epistominella exigua	7.66	4.51	6.58	9.29	5.88
E. takanayagii	0	0	0	0	0
Gyroidina slodanii	0.73	3.07	6.58	3.57	4.2
Eponides polius	0	0	0	0	0
E. tumidulus	0	0	0	0	0
E. weddellensis	9.12	4.92	6.37	11.79	6.72

Salé, Morocco Samples	S2	S4	S6	S7	S9	S11	S13	S15	S16	S17	S19	S20	S21	S22	S24	S25	S27
E.? sp.A	0	0	0	0	0	0	0	0	0	0	0	0	0	0	0	0	0
Hanzawaia sp.	0	0	0	0	0	0	0	0	0	0	0	0	0	0	0	0	0
Neoeponides sp.	0	0	0	0	0	0	0	0	0	0	0	0	0	0	0	0	0
Ammonia becarrii	0.6	0	0.44	0.69	0	0	0	0	0	0	0	0	0	0	0	0	0
Valvulireria laevigata	0	0	0	0	0.2	0	0	0	0	0.5	0.45	0	0	0.54	1.53	1.96	0
Cancris oblongus	0.6	1.99	0.73	0	0.2	0	0.36	0	2.58	0	0.23	0	0	0.27	0	0	0
Hoeglundina elegans	0	0	0	0.46	0	0.41	0	0	0	0	0	0	0	0	0	0	0
Siphonina tenuicarinata	0	0	0	0	0.2	0	0	0	0	0	0	0	0	0	0	0	0
Globocassidulina subglobosa	4.9	7.08	9.14	10.83	10.58	8.67	7.63	10.04	10.32	9.77	7 24	8.72	9.51	5.66	8.16	9.8	7.56
Cassidulina laevigata	5.07	0.44	1.16	2.53	0	2.68	1.42	1.3	0	0	0	1.78	0	1.08	1.02	0.78	0
C. reniforme	3.6	3.76	1.74	4.5	3.14	8.05	9.24	2.97	5.16	4.01	4.75	5.14	5.57	3.5	2.55	4.7	6.16
Trifarina angulosa	9.09	7.52	12.05	12.67	6 27	7.23	8.7	11.34	6.77	12.78	9.28	10.07	13.44	7.01	17.35	4.31	10.64
T. bradyi	1.19	0.88	0	1.84	0.59	0.83	0.36	0.37	0.65	0.5	0.9	0.45	3.93	2.43	1.53	0.78	0.56
Reussella spinulosa	0	0	0.15	0	0	0.21	0	0	0	0	0	0	0	0	0.51	0	0
Ehrenbergina trigona	0.45	0	0	0	0	0	0	0	0	0	0	0	0	0	0	0	0
Tosaia hanzawai	0	0	0	0	0	0.83	0.53	0	0	0	0.23	0.67	0.33	0	0	0	0
Fursenkoina fusiformis	0.3	0.22	0	0.23	0	1.03	0.18	0	0.32	0.25	0.45	0.22	0	0.27	0	0	0.84
Virgulina pontoni	0	0	0	0	0	0	0	0	0	0	0	0	0	0	0	0	0
Pyrulina augusta	0	0	0	0	0	0	0	0	0	0	0	0	0	0	0	0	0
Bulimina aculeata	1.04	3.32	2.03	0.92	2.16	1.86	4.26	0 93	4 52	3.01	2.71	3.36	1.64	7.82	3.06	4.71	5.88
B. mexicana	3.13	1.81	0	0	0.78	0.42	1.24	0.93	1 29	0 5	0	1.12	1.31	1.34	0	1.17	0
B. alazaensis	0.89	0	0.15	0.46	0.59	0.21	0.18	0.19	1 29	0 5	1.36	0	0	1.35	0	1.18	0.28
Globobulimina auriculata	0	0.44	0	0	0	0.42	0	0	0	0	0 22	0	0	0	0	0	0
Uvigerina peregrina	3.58	1.77	1.74	0.92	1.57	0.83	0.53	0.74	1 94	1	1.13	2 01	0.66	3.23	0 51	1.96	2.52
U. proboscidea	0	0	0	0	0	0	0	0	0	0	0	0.22	0	0	0	0	0.28
U. schwageri	0.45	0	0.29	0	0.2	0.21	0.18	0	0	0	0	0	0	0	0	0	0
U. spp.	0	0	0.29	0	0.58	0.21	0.53	0	0	0	0	0	0	0	0	0	0
Rectuvigerina multicostata	0.3	0.66	0.58	0	0.2	0	0	0	0	0	0	0	0	1.35	0	0	0.56
Amphicoryna scalaris	0	0	0	0	0	0	0	0	0	0	0	0	0	0	0	0	0
Frondicularia sp.	0	0	0	0	0 2	0	0	0	0 32	0	0	0	0	0	0	0	0
Pleurostomella spp.	0	0.22	0	0 23	0	0.21	0	0	0	0	0	0	0	0	0	0.39	0.56
Stilostomella antillea	0.89	0.22	0.43	0 46	1.18	0.62	0.71	0 56	0	0	0.22	0.22	0.98	0.54	1.53	0.78	3.92
S. hispida	0	0.89	0.29	0	0	0	0	0	0	0	0	0	0	0 27	0	0	0
S. spp.	0	0	0	0	0	0	0	0	0	0	0	0	0	0	0	0	0
Dentalina communis	0	0	0	0	0.2	0	0	0	0	0	0	0 22	0	0	0.51	0	0.28
D. sp.	0	0	0	0	0	0	0	0	0	0	0	0	0	0	0	0	0
Lenticulina spp.	0.75	1.33	0.29	0 46	0.59	0 62	0.89	0 37	0 65	0.75	0 23	0.22	0	1.62	1.53	1.57	0.28
Fissurina. spp.	0.6	0.44	1.02	1.61	0.39	0.41	0	0 56	0 65	0 75	0 68	0 89	0 33	0.27	0.51	0	0.56
Lagena spp.	0	0.22	0.15	0	0.2	0	0 18	0 19	0	0 25	0 23	0 45	0	0 27	1 02	0 39	0
Bolivina inflata	0.45	3.76	0.73	3.23	3.73	4 75	0 36	3 53	3 23	1.5	4 3	2 46	2 95	4.04	4 08	11.76	2.8
B. pseudoplicata	1.34	1.99	2.76	5 76	1.96	2.89	2 49	5.2	2 58	1 5	2 71	3 30	1.31	1 35	2.55	1.57	6.44
B. cf. pygmaea	0	0	0	0	0	0	0	0	0 32	0 25	0	0	0	0	0	0	0.28

Salé, Morocco Samples	S28	S29	S30	S31	S32	S35	S37	S39	S41	S42	S44	S46	S48	S49	S50	S51	S52
E.? sp. A	0	0	0	0	0	0	0	0	0	0	0	0	0	0 45	0.26	1.25	0
Hanzawaia sp.	0	0	0.51	0	0	0	0	0	0	0	0	0	0	0	0	0	0
Neoeponides sp	0	0	0	0	0	0	0	0	0	0	0	0	0	0	0	0 17	0
Ammonia becarii	0	0	0	0	0	0	0	0	0	0	0	0	0	0	0	0 18	0
Valvulineria laevigata	1.02	0.24	0	0.76	0 93	0 33	0.34	0	0 66	0	0 65	0.59	0 58	0 45	0.51	0 36	0.44
Cancris oblongus	0	0	0	0	0	0	0	0	0 33	0 52	0.32	0	0 19	0 45	0 26	0 18	0 44
Hoeglundina elegans	0	0	0	0	0	0	0	0	0	0	0	0	0	0	0	0	0
Siphonina tenuicarinata	0.34	0 48	0	1 52	0 93	0	0 34	1 31	0 66	0 52	1 29	0 3	0	0 23	0 26	0 18	1 09
Globocassidulina subglobosa	11 86	8 71	10 04	7 98	5 5	10 1	11 9	8 64	7 87	10 13	3 87	8 9	10 44	7 25	12.24	10 19	10 72
Cassidulina laevigata	0	2.42	0 51	0	0	1 63	0.34	0	0 66	2.08	2 56	6.53	1 74	4 08	2.29	0.89	1.97
C. reniformis	7.79	3 63	2 79	1.52	0 46	1 95	2.72	3.4	5 25	1 81	3.54	1.48	3 09	2.49	4 08	1 7	2 62
Trifarina angulosa	8.14	8.96	11.2	11 03	11.16	13.03	11.22	3 66	9 84	10.13	10	2.08	8.7	8 62	5 61	5.55	7 88
T. bradyi	1 69	1.69	0.51	0 76	1 4	0	2 04	2.09	0	1 04	0	0 3	0 97	0	0	0.36	0
Reussella spinulosa	0	0 24	0	0	0	0	0	0	0	0	0	0 3	0	0 23	0	0	0
Ehrenbergina trigona	0	0	0	0	0	0	0	0	0	0	0	0	0	0	0	0	0
Tosaia hanzawai	0	0	0	0	0	0	0	0	0 33	0 52	0 65	0.59	1 74	0 45	0.51	0.72	3.94
Fursenkoina fusiformis	0	0 48	0 25	0	0	0	0	0	0	0	0	0	0	0	0	0	0
Virgulina pontoni	0	0	0	0	0	0	0	0	0	0	0	0	0	0	0	0	0
Pyrulina augusta	0	0	0	0	0	0	0	0	0	0	0	0	0	0	0	0	0
Bulimina aculeata	3 73	3 15	3.56	3 8	4 65	2.61	2 04	1 57	2.3	2.08	0 97	2 08	2.9	1 81	2.04	0 72	2 19
B. mexicana	0	0.48	0 25	0	0 46	0 32	1.02	2.09	0 98	0 26	1 29	1.48	0 19	0 45	0.51	0 36	0 44
B. alazaensis	1.02	0 48	0 25	1.14	0.93	0 33	0	1.57	0 66	0	0	0	0 19	0	0	0.54	0
Globobulimina auriculata	0	0	0	0	0	0	0	0	0	0	0	0	0	0	0	0	0
Uvigerina peregrina	1.36	2 66	2.8	4.94	3 26	5 21	1.02	4 71	3 93	1.56	3 23	0.59	1 74	0 23	1.53	0.36	1.75
U proboscidea	0	0	0	0	0	0	0	0	0	0	0	0	0	0	0	0	0
U schwageri	0	0	0	0	0	0	0	0	0	0	0	0	0	0	0	0	0
U. spp	0	0.24	0	0	1.4	0	1.02	0	0	0	0	0	0	0	0	0 18	0
Rectuvigerina multicostata	0	0	0	0	0	0	0	0	0	0	0	0	0	0	0	0	0
Amphicoryna scalaris	0	0	0	0	0	0	0	0	0	0	0	0	0	0	0	0	0
Frondicularia sp	0	0	0	0	0	0	0	0	0	0	0	0	0	0	0	0	0
Pleurostomella spp	0	0 24	0 25	0	0	0 56	0 34	0 26	0.33	0	0	0	0	0 23	0	0 18	0
Stilostomella antillea	1 69	0 24	1 27	0 38	1 4	0 98	0 34	0 26	0	0	0 32	0	0 19	0	0 26	0	0 44
S hispida	0	0	0	0	0	0	0	0	0	0	0	0	0	0	0	0	0
S. spp	0	0	0	0	0	0	0	0	0	0	0	0	0	0	0	0	0
Dentalina communis	0 34	0	0	0	0	0	0	0	0	0	0.32	0	0	0	0	0 36	0
D sp	0.34	0	0	0	0	0	0	0	0	0	0	0	0	0	0	0	0
Lenticulina spp	0 34	0 97	0	0 38	0 47	1 63	1 36	0 26	0 98	0 78	0 65	0.59	0 19	0	1 02	0 36	0 44
Fissurina. spp.	0.34	0.48	0 51	0 38	0.93	1 3	0 68	0 26	0	0 52	0 65	0.59	0 58	0 45	0	0 36	0.44
Lagena spp	0	0 24	0	0	0 47	0	1 02	0 52	0 98	0	0	0	0 19	0 23	0	0 36	0
Bolivina inflata	1 69	3 87	4 83	3 04	2.33	3 91	4 76	4 45	10 16	9 61	8.39	21 07	9 67	10.2	6 89	13 95	3 5
B. pseudoplicata	2.37	2 91	3 31	4.56	4 65	2.61	5.78	7 33	3 28	3 64	3.87	1.19	0 97	0 68	1.28	0 54	1 09
B cf pygmaea	0	0	0	0	0	0	0 34	0	0	0	0	0	0	0	0	0	0

Salé, Morocco Samples	S53	S55	S56	S57	S59	S60	S61	S62	S63	B2	S65	B3	S67	B5	S70	B7	B8
E.? sp.A	0	0	0	0	0	0	0	0	0	0.67	0	0.33	0	0	0.16	0.5	0
Hanzawaia sp.	0	0	0	0	0	0	0	0	0	0	0	0	0	0	0.32	0	0
Neoeponides sp.	0	0	0	0	0	0	0	0	0	0	0	0	0	0	0	0	0
Ammonia becarrii	0	0	0	0	0	0	0	0	0	0	0	0	0.15	0	0	0	0.38
Valvulineria laevigata	0.46	1.06	0.28	0.75	0	0.31	0	0.42	0	0.87	1	0.33	0.15	1.46	0.49	1	0.76
Cancris oblongus	0	0	0.55	0	0.47	0.63	0.3	0.42	0.44	0.87	0	0	0.45	0.37	0	0	0.76
Hoeglundina elegans	0	0	0	0	0	0	0	0	0	0	0	0	0	0	0	0	0
Siphonina tenuicarinata	0.23	0.26	0.55	0	0.47	0.63	1.78	0	0	0	0.8	1	0.6	0	0.16	0	0
Globocassidulina subglobosa	7.34	8.73	6.37	6.47	9.15	10.69	8.01	10.59	23.58	14.38	21.56	9.63	11.26	10.98	5.36	13.93	16.35
Cassidulina laevigata	1.15	1.85	1.1	0.75	0.47	0	0	0.42	2.62	0.43	1.2	0	0	0	1.62	0.49	0.76
C. reniforme	3.21	1.85	1.93	2.48	0.93	5.03	2.97	2.97	0	0.87	3.39	0.67	1.5	1.1	2.27	6.46	3.42
Trifarina angulosa	8.26	7.94	9.14	7.46	7.04	6.6	5.04	6.78	2.62	6.35	0.6	9.63	8.56	6.23	9.9	11.44	6.84
T. bradyi	0.69	0	0.28	0.25	0	0	0.3	0.42	0	0	0.4	0.33	1.2	1.1	0.65	0.5	0.76
Reussella spinulosa	0	0	0	0	0	0	0	0.42	0	0	0	0	0	0	0	0	0
Ehrenbergina trigona	0	0	0	0	0	0	0	0	0	0	0	0	0	0	0	0	0
Tosaia hanzawai	0.46	1.32	1.66	1.49	1.88	1.57	1.78	1.27	0.87	1.67	0.8	1	1.5	2.93	0.65	1	0.38
Fursenkoina fusiformis	0	0	0	0	0	0	0	0	0	0	0	0	0.3	0.37	0	0	0
Virgulina pontoni	0	0	0	0	0	0	0	0	0	0	0	0	0	0	0	0	0
Pyrulina augusta	0	0	0	0	0	0	0	0	0	0	0	0	0	0	0	0	0
Bulimina aculeata	1.83	3.17	2.22	1.24	0.7	3.46	1.19	2.12	1.75	1.33	1.6	1.94	1.65	2.56	0.97	0.5	1.9
B. mexicana	0.46	0.79	0.28	0.75	1.4	0	1.19	0	1.75	0.86	0.6	0	0.15	0	0.49	1.49	0
B. alazaensis	0	0	0	0	0	0	0	0	0.87	0	0	0	0.15	0.37	0	1	0
Globobulimina auriculata	0	0	0	0	0	0	0	0	0	0	0	0	0	0	0	0	0
Uvigerina peregrina	1.83	1.85	1.66	1.24	1.17	1.89	0.3	1.69	0.44	0.87	3.79	1	1.65	0.37	1.79	0	2.28
U. proboscidea	0	0	0	0	0	0	0	0.42	0	0	0	0	0	0	0	0	0
U. schwageri	0	0	0	0	0	0	0	0	0	0	0	0	0	0	0	0	0
U. spp.	0.92	0	0	0	0	0.31	0	0	0	0	1.2	0	0	0	0	0	0
Rectuvigerina multicostata	0	0	0	0	0	0	0	0	0	0	0	0	0	0	0	0	0
Amphicoryna scalaris	0	0	0	0	0	0	0	0	0	0	0	0	0	0	0	0	0
Frondicularia sp.	0	0	0	0	0	0	0	0	0	0	0	0	0	0	0	0	0.38
Pleurostomella spp.	0.23	0.26	0	0.25	0.23	0	0.3	0	0	0.43	0.2	0.33	0.45	0	0.32	0	0
Stilostomella antillea	0.23	0.79	0.83	0.25	0.23	0.31	0.3	0.85	0	0	0.4	0	0.45	0	0.16	0	0
S. hispida	0	0	0	0	0.23	0	0	0	0	0	0	0.33	0	0.37	0	0	0
S. spp.	0	0	0.28	0	0	0	0	0	0	0	0.4	0	0	0	0.16	0	0
Dentalina communis	0	0	0	0	0	0	0.3	0.42	0.87	0.33	0	0.33	0.15	0.37	0	0	0.38
D. sp.	0	0	0	0	0	0	0	0	0	0	0	0.33	0	0	0	0	0
Lenticulina spp.	0.23	0	0.28	0.75	0	0.31	0	0	0	0.43	0.8	1	0.9	0.73	0	0.5	0.38
Fissurina. spp.	0.46	0.53	0	0.5	0.7	0.31	0.3	0	1.75	0.87	0.8	2.66	1.05	0.73	1.3	0.5	0.38
Lagena spp.	0.46	0	0.55	0.75	0	0.31	0.59	0.42	0	0.43	0	0	0.6	0.73	0.16	0	0.38
Bolivina inflata	6.42	3.96	2.77	6.47	7.51	3.46	6.82	2.12	2.62	6.35	3.59	7.64	8.56	5.49	7.79	9.95	5.7
B. pseudoplicata	1.38	1.59	0.28	2.24	0.23	3.77	2.08	0.85	4.37	1.33	0.59	1.99	0	1.83	1.62	3.48	0.38
B. cf. pygmaea	0	0	0	0	0	0	0	0	0	0	0	0	0	0	0	0	0.38

Salé, Morocco Samples	B9	B10	B11	B12	B13	B14	B15	B16	B17	B18	B19	B20	B21	B22	B23	B24	B25
E.? sp.A	0.92	0	0.79	0.71	0.57	0.43	0.4	0.39	1.22	0.34	0	1.02	0.41	0.62	0.45	0.74	0.2
Hanzawaia sp.	0	0	0	0	0	0	0	0	0	0	0	0	0	0	0	0	0
Neoeponides sp.	0	0	0	0	0	0	0	0	0	0	0	0	0	0	0	0	0
Ammonia becarrii	0	0	0	0	0	0	0	0	0	0	0	0	0	0	0	0	0
Valvulineria laevigata	0	0.77	0.79	0	0	0.65	0.66	0.39	0.7	0.67	0	1.36	0	0	0	0	0
Cancris oblongus	0.31	0.39	0.79	0.24	0.57	0	0.13	0.38	0.17	0	0	0	0	0	0	0	0
Hoeglundina elegans	0	0	0	0	0	0	0	0	0	0	0	0	0	0	0	0	0
Siphonina tenuicarinata	0	0.19	0	0.71	0.57	1.08	0.66	0	0.35	1.35	1.19	0.68	0	0.31	0.89	1.85	0.2
Globocassidulina subglobosa	11.08	12.85	7.31	12.29	5.16	3.01	9.03	8.2	5.24	7.07	6.75	6.1	6.16	5.86	6.46	10.74	6.25
Cassidulina laevigata	0.62	1.16	1.19	0	0	1.94	0.13	0.58	0	0	0	0.34	0.62	0.31	0.22	0.37	0.39
C. reniforme	1.23	5.95	5.14	8.98	12.23	3.87	8.63	14.72	4.71	5.05	1.59	4.41	3.08	3.7	3.79	0.74	4.3
Trifarina angulosa	8	8.49	5.14	8.51	9.18	7.1	9.03	10.27	8.55	4.38	4.37	6.44	7.6	2.16	0.45	2.59	5.47
T. bradyi	0.62	0.19	0	0.95	0	0	0.27	0.19	0.87	0	0.4	0.34	0.41	0.31	0.67	0.37	0.39
Reussella spinulosa	0	0	0.2	0	0	0.22	0	0	0	0	0	0	0	0	0	0	0
Ehrenbergina trigona	0	0	0	0	0.19	0	0	0	0	0	0	0	0	0	0	0	0
Tosaia hanzawai	1.23	1.16	0.4	1.42	1.34	0.65	0.27	0.58	0.17	1.68	1.19	1.02	0.82	0	0.45	1.48	0.98
Fursenkoina fusiformis	0	0	0	0	0	0	0.53	0	0	0	0	0	0	1.54	0	0.37	0
Virgulina pontoni	1.24	0.38	0	0.24	0	0	0	0	0.35	0.67	1.98	0.68	1.03	2.77	1.78	0	0.78
Pyrulina augusta	0	0	0	0	0	0	0	0	0	0	0	0	0	0	0	0	0
Bulimina aculeata	3.08	1.93	1.58	2.36	1.72	2.15	1.59	1.94	2.62	2.02	1.98	3.39	1.73	3.09	2	2.59	2.73
B. mexicana	0	2.32	0.19	0.71	0.76	4.73	0.27	3.08	5.59	0.34	0.39	0	1.23	0.92	1.56	0.37	0.59
B. alazaensis	0	0	0.2	0	0	0	0	1.55	5.24	0.34	0.4	0	0	0	0	0	0.2
Globobulimina auriculata	0	0	0	0	0	0	0	0	0	0	0	0	0	0	0	0	0
Uvigerina peregrina	0.92	1.35	1.19	2.6	2.29	1.08	1.73	0.58	1.4	2.36	1.59	1.36	1.64	1.54	2.67	1.11	1.17
U. proboscidea	0	0	0	0.47	0	0	0.13	0	0	0.34	0	0	0.21	0	0	0	0
U. schwageri	0	0	0	0	0.19	0.22	0.13	0	0	0.34	1.19	0.68	0	0	0	0	0.58
U. spp.	0.62	0	0.2	0	0.19	0	0	0.58	0.7	0.67	0	0.34	0	0.31	0	0	0
Rectuvigerina multicostata	0	0	0	0	0	0	0	0	0	0	0	0	0	0	0	0	0
Amphicoryna scalaris	0	0	0.2	0	0	0	0	0	0	0	0	0	0	0.31	0	0	0
Frondicularia sp.	0.31	0	0	0	0	0	0	0	0	0	0	0	0	0	0	0	0
Pleurostomella spp.	0.92	0.58	0	0.95	0.38	0.65	0.93	0.19	0.34	0.34	1.59	1.02	2.67	1.54	1.33	1.11	1.17
Stilostomella antillea	0	0.39	0.2	0.24	0.38	0.65	0.27	0	1.57	0.34	1.98	1.02	0.21	1.23	2.23	1.48	0.2
S. hispida	0	0	0	0	0	0	0	0	0	0	0	0	0	0	0	0	0
S. spp.	0	0	0.2	0	0	0.22	0	0	0	0.34	0	0	0	0	0	0.37	0.2
Dentalina communis	0	0	0	0	0	0	0	0	0.17	0	0	0.34	0	0.31	0	0	0
D. sp.	0	0	0	0	0	0	0	0	0	0	0	0	0	0	0	0	0
Lenticulina spp.	0.92	0	1.19	0.24	0.96	1.08	0.27	0	0.52	1.68	1.19	1.36	0.82	0.31	0.45	0.37	0.78
Fissurina. spp.	0.62	0.39	0.79	0.24	0.96	1.08	0.13	0.78	0.35	0.34	0.4	0.68	1.23	0.62	0	0	0.39
Lagena spp.	0.62	0	0.2	0	0.19	0.43	0.13	0.19	1.05	0.34	0	0.34	0.41	0	0.22	0	0.2
Bolivina inflata	4.92	7.34	11.46	4.49	9.18	11.18	5.31	2.71	7.33	2.36	8.33	4.07	5.54	7.41	4.23	4.44	7.03
B. pseudoplicata	1.85	0.58	2.37	1.18	0.38	1.08	0.8	1.74	0.87	1.68	0.4	2.71	2.05	1.23	0.22	0.74	1.17
B. cf. pygmaea	0.31	0	0	0.24	0.19	0	1.2	0	0.52	2.36	1.19	1.69	2.46	5.56	2	1.11	2.73

Salé, Morocco Samples	B26	B27	B28	B29	B30	B31	B32	B33	B34	B36	B37	B38	B39	B40	B41	B42	B43
E.? sp. A	1.09	0.76	1.08	0.52	1.57	0.27	0.36	0.39	0.52	1.51	1.55	0.75	0.7	0.49	0.8	0.74	0.95
Hanzawaia sp.	0	0	0	0	0	0	0	0	0	0	0	0	0.93	0	0	0.49	0
Neoeponides sp.	0	0	0	0	0	0	0	0	0	0	0	0	0	0	0	0	0
Ammonia becarrii	0	0	0	0	0	0	0	0	0	0	0.19	0	0	0	0	0	0
Valvulineria laevigata	0	0.38	0.13	0	0.22	0	0.12	0.39	0	0.94	0	0.75	0	0.32	0.48	0.74	0.32
Cancris oblongus	0.54	0	0	1.04	0	0	0	0	0	0	0	0	0	0	0.16	0.98	0
Hoeglundina elegans	0	0	0	0	0	0	0	0	0	0	0	0	0	0	0	0	0
Siphonina tenuicarinata	0	0.76	2.02	0.87	1.12	1.9	0.96	0.39	0.86	1.13	0.97	0.6	0	0.16	0.16	0.49	1.42
Globocassidulina subglobosa	7.62	4.17	5.39	8.57	4.7	8.14	9.62	9.11	8.1	6.6	9.5	6.86	6.98	15.5	11.5	9.11	12.15
Cassidulina laevigata	0	0	1.07	2.97	2.01	3.8	[illegible]	2.33	1.03	0.57	1.16	2.53	0.47	1.78	0	0	0.47
C. reniforme	5.99	4.73	2.96	3.32	2.01	2.17	4.81	3.87	1.21	2.08	4.65	2.98	4.19	2.59	1.12	1.72	1.1
Trifarina angulosa	4.09	1.7	0.67	0.17	0.45	0.14	0.72	0.78	0.17	0.75	4.65	1.64	2.09	1.13	0.64	1.97	2.21
T. bradyi	0.54	0.19	0.4	0.35	0	0.41	0	0.19	0.86	0.19	0	0	0	0	0	0	0
Reussella spinulosa	0	0	0	0	0	0	0	0	0	0	0.19	0	0	0	0	0	0
Ehrenbergina trigona	0	0	0	0	0	0	0	0	0	0	0	0	0	0	0	0	0
Tosaia hanzawai	0.54	0.76	0.4	0.52	0	0.41	1.56	2.33	1.21	0.75	0.19	1.19	1.63	0.97	1.92	2.46	2.05
Fursenkoina fusiformis	0	0	0	0.17	0	0	0	0	0	0	0	0	0.23	0.32	0.16	0	0
Virgulina pontoni	0	0	0.13	0	0	1.49	0.48	0	0	0	0	0	0	0	0	0	0.47
Pyrulina augusta	0	0	0	0	0	0	0	0	0	0	0	0	0	0	0	0	0
Bulimina aculeata	5.18	1.7	0.81	2.1	2.24	1.22	2.52	1.55	1.03	0.75	0.97	0.3	0.93	1.13	0.32	0.99	0.16
B. mexicana	0.54	0.57	0.41	0	0	0.95	0.84	0.19	0.86	1.89	0.78	0.45	2.56	0.16	0.48	0.25	1.89
B. elazaensis	0	0.57	0.13	0	0	0.14	0	0	0	0	0	0	0.23	0	0	0	0
Globobulimina auriculata	0	0	0	0	0	0	0	0	0	0	0	0	0	0	0	0	0
Uvigerina peregrina	1.36	0.38	1.48	1.05	4.47	2.58	1.92	2.91	1.21	1.51	3.29	2.09	5.12	5.99	11.34	4.68	5.68
U. proboscidea	0.54	0	0.13	0	0	0.14	0	0	0	0	1.16	3.73	1.4	1.29	1.28	0.74	1.42
U. schwageri	1.09	1.13	1.62	0.87	0.67	0.27	0.36	0.19	0.69	1.89	0	0	0.47	0.16	0.16	0.49	0
U. spp.	0.27	0.76	0	0.35	0.89	0.14	0.24	0	0.17	0	0	0	0	0	0	0	0
Rectuvigerina multicostata	0	0	0	0	0	0	0	0	0	0	0	0	0	0	0	0	0
Amphicoryna scalaris	0	0	0	0.34	0	0	0	0	0	0	0	0	0	0.16	0	0	0.32
Frondicularia sp.	0	0	0	0	0	0	0	0	0	0	0	0	0	0	0	0	0
Pleurostomella spp.	3.27	3.22	3.23	6.47	2.91	1.63	0.6	3.1	10.34	0.94	3.1	0.15	0.7	1.13	1.12	0.25	1.41
Stilostomella antillea	1.63	0.76	1.75	1.22	1.12	0	1.2	0.19	1.72	0.94	0	0.3	1.4	0.49	0.8	0.49	0.16
S. hispida	0	0	0	0	0.44	0	0	0	0	0	0	0	0	0	0	0	0
S. spp.	0	0	0	0	0	0	0	0	0	0	0	0	0	0	0	0	0
Dentalina communis	0	0	0.13	0	0	0.14	0	0.39	0.52	0.19	0.19	0.15	0.23	0.32	0	0	0.63
D. sp.	0	0	0	0	0	0	0	0	0	0	0	0	0	0	0	0	0
Lenticulina spp.	0.54	1.14	1.08	1.05	0.22	0.68	0.48	0.78	1.9	0.75	1.16	0.3	0.23	0.97	0.48	0.99	1.89
Fissurina. spp.	0.82	0	0.4	0.35	0.22	0.41	0.36	0.78	1.21	0	0.39	0.3	0.23	0.49	0.96	0.74	0.95
Lagena spp.	0	0.76	0.13	0	0.22	0.14	0.24	0	0.69	0.19	0.19	0.15	0.23	0.16	0.16	0.74	0.16
Bolivina inflata	2.72	2.84	28.98	13.81	9.62	30.39	10.94	21.51	9.83	10.38	10.27	11.03	11.4	13.75	15.18	15.76	7.89
B. pseudoplicata	0.82	1.14	2.43	0.7	1.12	0.68	0.96	2.91	1.38	1.51	2.52	2.24	1.86	1.46	2.08	1.48	1.26
B. cf. pygmaea	0	1.14	0.13	1.57	1.12	0	4.09	0.78	1.21	1.7	1.16	3.28	3.26	2.59	1.12	1.72	3.31

Salé, Morocco Samples	B44	B45	B47	B48	B49	B50	B51	B52	B53	B54	B55	B56	B57	B58	B59	B60	B62*
E.? sp. A	0.48	0.17	0.41	0	0.62	0.76	0.9	0.37	0	0	0	0	0	0.71	0	1.25	2.64
Hanzawaia sp.	0	0.52	0	0	0	0.25	1.12	0	0	0	0.97	1.19	1.28	2.86	3.33	2.08	2.64
Neoeponides sp.	0	0	0	0	0	0	0	0	0	0	0	0	0	0	0	0	0
Ammonia becarrii	0	0	0	0	0	0	0	0	0	0	0	0	0	0	0	0	0
Valvulineria laevigata	0.24	0	0	0.69	0.83	0	2.47	0.74	0	1.33	0	0	1.59	0	2.22	1.25	2.97
Cancris oblongus	0	0.34	0.41	0.69	1.44	0	0	0.37	0	0	0.97	1.78	0	0.18	0	0	0
Hoeglundina elegans	0	0	0	0	0	0	0	0	0	0	0	0	0	0	0	0	0
Siphonina tenuicarinata	1.19	0.7	1.02	1.15	0.42	1.01	0.45	1.31	0.76	0.33	2.59	0.6	1.28	1.79	1.11	0.42	1.32
Globocassidulina subglobosa	9.07	6.61	9.55	10.57	4.78	8.08	16.62	9.7	12.5	21.07	7.12	12.24	9.58	12.14	10	7.5	6.27
Cassidulina laevigata	5.97	12.1	4.27	5.29	6.86	1.77	1.34	5.78	6.06	7.02	5.5	4.18	4.47	0	5	0.42	0
C. reniforme	1.43	0.69	1.02	1.15	0.83	2.53	0.67	2.99	0.76	0.67	2.27	0	0.64	1.07	0	1.67	2.31
Trifarina angulosa	1.43	0.52	0.61	0.23	0	0.25	0	0.75	0.76	1	0.32	0.3	0.96	0.71	0.56	1.25	0.33
T. bradyi	0	0.34	0	0	0.21	0.25	0	0	0	0	0	0	0	0	0	0	0
Reussella spinulosa	0	0	0	0	0.21	0	0.22	0	0	0	0	0	0	0	0	0	0
Ehrenbergina trigona	0	0	0	0	0	0	0	1.31	0	0	0	0	0	0	0	0	0
Tosaia hanzawai	0.95	0.17	0.81	0.92	1.87	1.26	1.12	2.05	1.89	1.34	0.97	2.09	2.88	10.36	0	0.42	0.99
Fursenkoina fusiformis	0	0	0.2	0.23	0.42	0	0	0	0	0	0	0	0	0	0	0	0.33
Virgulina pontoni	0.48	0	0	0	0	0.51	0	0	0	0	0.32	0	0.64	0	2.22	0.83	1.32
Pyrulina augusta	0	0	0	0	0	0	0.22	0	0	0	0	0.6	0	0	0	0.83	0
Bulimina aculeata	0.24	0	0.2	0	0	0	0	0	0	0	0	0.3	0	0	0.56	0.83	0
B. mexicana	1.19	1.04	3.86	0	0.42	0	0.22	0.56	0.38	1.34	0.32	0.9	1.28	1.07	0	1.67	0.99
B. alazaensis	3.58	7.13	1.02	3.68	4.78	4.04	0	0	0	0	0	0	0	0.36	0	0	0
Globobulimina auriculata	0	0	0	0	0	0	0	0	0	0	0	0	0	0	0	0	0
Uvigerina peregrina	6.68	4.87	8.54	9.66	11.64	8.59	7.87	6.53	9.47	8.03	6.47	8.06	7.03	3.57	5	8.33	2.97
U. proboscidea	0.95	0	1.02	0	0	0	0	0	1.14	0.33	0.32	0	0.32	0.36	0	0	0
U. schwageri	0.24	1.04	0.41	0.23	0	1.01	0.9	0.74	1.13	0	0	0	0.96	1.07	0	0	0.66
U. spp.	0	0	0.2	0	0	0	0	0	0	0	0.97	0	0	0.18	0	0	0.66
Rectuvigerina multicostata	0	0	0	0	0	0	0	0	0	0	0	0	0	0	0	0	0
Amphicoryna scalaris	0	0.17	0	0	0	0	0.22	0	0	0	0	0	0	0	0	0.42	0
Frondicularia sp.	0	0	0	0	0	0	0	0	0	0	0	0	0.96	0	0	0	0
Pleurostomella spp.	1.19	1.22	1.02	1.38	1.25	0.25	0.22	1.68	1.52	0.67	1.29	0.3	2.23	1.07	1.11	0	0
Stilostomella antillea	2.63	1.04	1.22	0.92	1.25	1.01	0	1.12	0.76	1.67	0.65	0.6	1.28	0.36	1.12	0	0.33
S. hispida	0	0	0	0	0	0	0	0	0	0	0	0	0	0	0.55	0	0.37
S. spp.	0	0	0	0	0	0	0	0	0	0	0	0	0	0	0	0	0
Dentalina communis	0	0.17	0.81	0	2.7	0.25	0	0	0.38	0.33	0	0	0	0.36	0	1.25	0
D. sp.	0	0	0	0	0	0	0.22	0	0	0	0	0	0	0	0	0	0
Lenticulina spp.	2.39	0.7	0.61	0.23	1.04	0.51	1.12	0.56	1.14	0	1.62	0.9	1.28	0.71	2.22	0.42	0.33
Fissurina. spp.	0.72	0.52	0.2	0.23	0.42	0	0.22	0	0	0	0.32	0.6	0.96	1.07	0.56	0.42	0.66
Lagena spp.	0.72	0.17	0.41	0.23	0.21	0.25	1.57	0.37	0.38	0	0.65	0.6	0.32	0.54	0	1.67	1.32
Bolivina inflata	9.31	7.65	2.64	6.9	3.12	7.83	6.97	6.72	5.3	1.34	4.85	1.19	2.56	4.64	2.78	10.83	9.24
B. pseudoplicata	1.19	0	2.64	0.92	1.46	1.01	0.9	1.68	0	1.33	1.62	1.79	1.59	1.11	0.55	0.42	1.32
B. cf. pygmaea	2.63	2.78	2.03	4.14	2.29	2.78	1.8	1.49	1.14	1	2.59	3.28	0.96	0.71	0	0	1.98

Salé, Morocco Samples	B64*	B66*	B68*	B70*	B71	B72	B74	B76	B79	B81	B83	B85	B87	B89	B91	B93	B95
E.? sp. A	0.37	1.53	0.97	0	0	0.7	0.95	0.31	1.25	1.13	2.46	0.32	1.15	1.13	0.39	0.38	0.47
Hanzawaia sp.	1.12	0	0	0	1.03	0.7	0	1.24	0	0	0	0	0	0	0	0	0
Neoeponides sp.	0	0	0	0	0	0	0	0	0	0.19	0	0	0	0	0	0	0
Ammonia becarrii	0	0	0	0	0	0	0	0	0	0	0	0	0	0	0	0	0
Valvulineria laevigata	0	0	0	0	0	0	0	0	0	0.19	1.51	1.6	0	1.13	0.39	0.38	0.16
Cancris oblongus	0	0	0	0	0	0	0	0	0	0	0	0	0.16	0	0	0	0
Hoeglundina elegans	0	0	0	0	0	0	0	0	0	0	0	0	0	0	0	0	0
Siphonina tenuicarinata	1.22	1.92	3.38	2.4	0.51	2.09	1.26	1.24	1.04	0.94	2.29	0.32	2.3	0.68	0.39	0.64	0.47
Globocassidulina subglobosa	15.99	11.11	15.94	8.38	16.92	11.84	14.51	12.73	9.79	15.44	11.53	15.02	6.72	19	20	11.87	21.24
Cassidulina laevigata	0	0.77	0	0	1.03	0.35	0	0	0.21	0.75	2.27	2.24	7.21	2.71	2.34	1.4	1.45
C. reniforme	2.6	0.38	2.9	1.8	0.51	2.09	1.89	3.73	2.29	2.64	5.43	4.15	5.9	8.6	5.97	5.36	3.1
Trifarina angulosa	1.12	0.38	1.93	0.6	2.05	0.7	1.89	1.55	1.25	1.51	0.76	0.96	1.48	2.04	2.34	5.24	5.74
T. bradyi	0	0	0	0	0	0	0	0	0	1.13	0.95	0	0	0	1.17	0	0.31
Reussella spinulosa	0	0	0	0	0	0	0	0	0	0	0	0	0	0	0	0.26	0
Ehrenbergina trigona	0	0	0	2.4	0	0	0	0	0	0	0	0	0	0	0	0	0
Tosaia hanzawai	0	0.38	0	0	0	0.35	0	0.31	1.88	0.38	0	0.96	0.16	0	0	0.51	0.16
Fursenkoina fusiformis	0	0	0	0	0	0	0	0.93	0	0.19	0	0	0	0.68	0.78	0.26	0.31
Virgulina pontoni	1.12	0.77	1.45	0	1.54	0	1.89	0	0	0	0	0	0	0	0	0	0.31
Pyrulina augusta	0	0	0	0	0	0	0	0.31	0	0	0	0	0	0	0	0	0
Bulimina aculeata	0.37	0	1.45	0	0	0	0	2.17	2.5	1.13	1.13	1.6	2.3	1.58	0.39	2.43	2.02
B. mexicana	0.74	0.77	0	1.2	0	0	0.95	0	3.96	0.56	0.95	0.96	0.66	0.23	0.78	0.26	0
B. alazaensis	0	0.77	0	0	0	0.7	0	0.31	4.17	0	0.19	0.32	0.33	0.23	0	0	0.16
Globobulimina auriculata	0	0	0	0	0	0	0	0	0	0	0	0	0	0	0	0	0
Uvigerina peregrina	4.83	6.9	3.38	11.38	5.64	8.01	4.73	0	0.83	1.32	1.7	5.11	2.95	2.04	1.56	2.68	2.17
U. proboscidea	0	0	0	0	1.54	0	0	2.17	0.83	1.69	1.32	0.96	0.49	0.68	2.34	1.4	0.62
U. schwageri	0.37	0	0	2.39	0	0.69	0	0.93	0.42	0.75	0	0.32	0.49	0	0	0	0.47
U. spp.	2.23	0	0	0	0.51	0.69	0	0	0	0	0	0	0	0	0.26	0.13	0
Rectuvigerina multicostata	0	0	0	0	0	0	0	0	0	0	0	0	0	0	0	0	0
Amphicoryna scalaris	0	0.38	0.97	0	0	0	0	0	0	0	0	0	0	0	0	0	0
Frondicularia . sp.	0	0	0	0	0	0	0	0	0.42	0	0	0	0	0	0	0	0
Pleurostomella spp.	1.49	1.5	0	0	2.56	1.74	5.05	2.48	0.42	0.19	0	0	0	0	0.39	0	0
Stilostomella antillea	2.6	2.68	2.41	2.4	1.54	0	0.63	1.24	3.12	0.38	1.32	0	0.33	0.9	0	0	0
S. hispida	0	0	0	0	0	0.7	0	0	0	0	0	0	0	0	0	0	0
S. spp.	0	0	0	0	0	0	0	0	0	0	0	0	0	0.23	0	0	0
Dentalina communis	0.37	0	0.97	0	0	0	0	0	0	0	0	0	0	0	0	0	0
D. sp.	0	0	0	0	0	0	0	0	0	0	0	0	0	0	0	0	0
Lenticulina spp.	0.37	1.15	1.93	0.6	4.62	4.53	1.58	0.31	2.08	0.56	0.57	1.28	0.33	0.68	0.78	0.64	0.93
Fissurina. spp.	0	0	0.48	0	0	0.7	0.32	0	0.42	0.38	0.95	0.96	0.66	0.68	0.78	0.38	0.31
Lagena spp.	1.12	0	0	0	2.05	0.35	1.26	0.31	0	0.19	0.76	0.64	0.66	0.45	0.78	0.26	0.16
Bolivina inflata	0.37	4.21	4.83	0	0.51	1.05	12.3	8.38	2.29	4.71	1.51	0.96	2.13	1.36	2.21	3.83	8.37
B. pseudoplicata	0	0	0	0	2.56	1.74	0.95	0	0.62	5.65	6.43	4.15	2.95	2.71	1.17	2.68	3.26
B. cf. pygmaea	1.11	2.68	1.45	1.8	3.08	1.74	0	1.55	5	1.69	1.89	3.51	2.95	2.49	2.08	1.4	0

Salé, Morocco Samples	B97	B98	B100	B102	B104
E.? sp. A	0.36	0.41	0.52	0.71	0
Hanzawaia sp.	0	0	0.1	1.43	0
Neoeponides sp.	0	0.61	0	0	0
Ammonia becarrii	0	0	0.1	0	0
Valvulineria laevigata	0	0.82	0	0	0.42
Cancris oblongus	0	0	0	0	0.42
Hoeglundina elegans	0	0	0	0	0
Siphonina tenuicarinata	0.36	1.23	0.21	0.71	0
Globocassidulina subglobosa	20.8	12.91	18.6	11.43	10.92
Cassidulina laevigata	0	2.66	1.99	6.07	0
C. reniforme	7.29	7.58	12.33	12.14	9.66
Trifarina angulosa	7.3	2.25	3.97	5.71	11.76
T. bradyi	2.19	0.61	0.52	0	0.84
Reussella spinulosa	0	0	0.52	0	0.42
Ehrenbergina trigona	0	0	0	0	0
Tosaia hanzawai	0	0.41	0	0.71	0
Fursenkoina fusiformis	0	0.41	0.21	0	0
Virgulina pontoni	0	0	0	0	0
Pyrulina augusta	0	0	0	0	0
Bulimina aculeata	0.73	2.05	1.57	2.14	0.42
B. mexicana	2.91	2.46	0.1	1.79	1.68
B. alazaensis	2.92	2.25	0.52	0	1.26
Globobulimina auriculata	0	0	0	0	0
Uvigerina peregrina	1.82	0.82	1.36	3.21	0
U. proboscidea	1.46	1.02	1.36	0	1.68
U. schwageri	0	0	0.2	0	0
U. spp.	0	0.41	0.32	0.36	0
Rectuvigerina multicostata	0	0	0	0	0
Amphicoryna scalaris	0	0	0	0	0
Frondicularia sp.	0	0	0	0	0
Pleurostomella spp.	0	0	0.21	0	0
Stilostomella antillea	0	0	0	0	0
S. hispida	0	0	0.2	0	0
S. spp.	0	0	0	0	0
Dentalina communis	0.36	0	0	0	0.42
D. sp.	0	0	0	0	0
Lenticulina spp.	1.46	1.23	0.84	0.36	0
Fissurina. spp.	0.73	0.41	0.21	0.36	0
Lagena spp.	0	0.61	0	0	0
Bolivina inflata	3.28	2.05	0.21	1.07	0.42
B. pseudoplicata	6.2	3.7	2.09	0	4.2
B. cf. pygmaea	0.36	0.41	0.21	1.07	0.84

Salé, Morocco Samples	S2	S4	S6	S7	S9	S11	S13	S15	S16	S17	S19	S20	S21	S22	S24	S25	S27
B. pseudopunctata	0.15	0	0	0	0	0.21	0	0.19	0	0.25	0.45	0	0	0.27	0	0.78	0
B. lowmani	1.64	4.2	2.18	4.84	2.16	1.65	2.31	2.23	1.29	1.5	0.68	1.34	1.31	4.04	1.53	1.18	3.92
B. albatrossi	2.24	3.54	1.6	2.07	0.98	1.45	1.24	2.04	3.23	2.26	1.36	1.57	1.64	1.89	1.53	3.92	2.52
B. simplex	2.68	2.65	2.47	3.23	3.14	1.03	3.2	0	0.97	2.76	1.81	2.23	0	1.34	1.53	1.18	1.68
B. subspinescens	1.2	0.44	0.73	0.69	1.76	0.41	0.71	1.48	0.97	1	0.45	0.22	1.31	0.54	0.51	0.39	0.56
B. catanensis	1.49	0	0.29	0	0	0.21	0.53	0	0	0	0	0	0	0.26	0	0.72	0
B. dilatata	0.9	0.89	1.74	0.46	1.18	1.44	0.88	0	0.32	2.5	0	0.45	0.33	0.53	4.59	4.7	0
B. cf. dialata	0	0	0	0	0	0	0	0	0	0	0	0	0	0	0	0	0
B. spp.	6.56	1.76	4.78	4.6	3.14	3.5	8.17	3.35	4.19	3	2.04	6.71	4.59	2.15	3.06	7.4	4.76
Bolivinita pseudothalmanni	0.6	1.99	0.15	1.84	1.57	1.03	1.6	1.49	2.9	1	1.13	0.67	1.31	1.35	0	0	2.24
Sigmavirgulina sp. A	1.04	0	1.02	0.23	0.59	0.21	0	0.37	1.29	0	0.23	0.89	0.33	1.08	0.51	1.18	0
Laxostomum cf. normale	1.5	0.44	1.31	1.15	1.18	2.27	1.07	1.67	0.97	1.5	1.36	2.01	0.66	2.43	1.02	3.53	1.4
Seabrookia earlandi	0	0	0	0.69	0	0.62	0	0.56	0	0	0	0	0.33	0	0.51	0	0
Sigmoilopsis schlumbergeri	0	0.66	0	0.23	0	0	0	0	0	0	0.23	0	0	0.27	0	0	0
Textularia spp.	0.45	0.44	0.29	0.92	0.2	0.21	0	0.13	2.26	0.5	1.13	0.22	0	0.27	0.51	0	0.56
Spiroplectammina sp.	0.45	0.88	0.15	0.92	0.59	0	0	0	0.97	0	0	0.22	0	1.08	1.02	0	0
Cylindroclavulina bradyi	0	0	0	0	0	0	0	0	0	0	0	0	0	0	0	0	0
Vulvulina spinosa	0	0	0	0	0	0	0	0	0	0	0	0	0	0	0	0	0
Karreriella bradyi	0	0	0	0	0	0	0	0	0	0	0	0	0	0	0	0	0.28
Eggella bradyi	0	0	0	0	0	0	0	0	0	0	0	0	0	0	0	0	0
Martinottiella communis	0	0	0	0	0	0	0	0	0	0	0	0	0	0	0	0	0
Bigenerina bradyi	0	0	0	0	0	0	0	0	0	0	0	0	0	0	0	0	0
B. irregularis	0	0	0	0	0	0	0	0	0	0	0	0	0	0	0	0	0
Trochammina sp.	0	0	0	0	0	0	0	0	0	0	0	0	0	0	0	0	0
Quinqueloculina spp.	0.3	0.44	0	0.46	0.2	0.62	0	1.3	0.32	0.5	0.45	1.57	0	0	0	0	0.56
Sigmoilina tenuis	0	0.66	0	0	0	0	0	0	0.32	0	0.23	0	0	0	0	0	0.56
Spiroloculina sp.	0	0	0	0	0.2	0	0	0	0	0	0	0	0	0	0	0	0
Pyrgo spp.	0	0	0	0	0	0.21	0	0.19	0	0.25	0.45	0.45	0	0	0	0	0
Unident. porcellaneous forms	0	0.66	0	0.46	0.2	0.83	0	1.49	0 65	0.75	1.36	1.57	0	0	0	0	1.12

Salé, Morocco Samples	S28	S29	S30	S31	S32	S35	S37	S39	S41	S42	S44	S46	S48	S49	S50	S51	S52
B pseudopunctata	0	0 24	0	0	0	0	0	0	0	0	0	0	0	0	0 26	0	0
B. lowmani	1.02	0 97	0 51	0.76	1 83	1 95	1.36	1 31	3 93	1.03	2 58	2.37	1.16	1 36	2.55	1.61	2 19
B. albatrossi	2.37	0	3 31	0 38	1.86	0 98	1.7	1.31	2.62	2.86	1 61	2.97	6 38	3 85	1.28	1.43	1.75
B. simplex	2.03	1.2	4 58	0	0 93	0 65	0	1.05	0 66	0.78	0	0.3	0.19	0 23	0 51	0.36	1.09
B. subspinescens	1.02	0 73	0.51	0.76	0 47	0 33	0 68	0 26	1.31	1 04	0 65	0 89	0	0 91	0.51	0 89	1 09
B. catanensis	0	0	0 24	0	0	0	0	0	0	0	0	0	0	0	0	0	0
B dilatata	4 06	2 91	2.03	1 52	1 4	0	0	4 45	0 65	0.26	0 64	0	0 19	0	0 26	0.36	0
B cf dialata	0	0	0	0	0	0	0	0	0	0	0	0	0	0	0	0	0
B. spp.	4.74	3 63	5 09	6.46	9.76	8 46	0.34	8 11	3.61	6.49	8 71	4 15	2.7	5 2	3.36	3.92	5.03
Bolivinita pseudothalmanni	1.69	1 21	1 27	1.14	0.47	1 3	1.02	1.31	0.33	2.86	3 55	5.34	6 96	7 71	10.71	11.63	9.85
Sigmavirgulina sp A	1.02	0	1 02	1.52	1.4	1 3	0	0 26	0 66	0 26	0	0 89	0	1 13	1 02	0	0 88
Loxostomum cf normale	1.02	1 21	0 76	0.76	0	0	0	0	0 33	0 78	0 32	1 19	1 16	0 91	1 02	0 18	1 09
Seabrookia earlandi	0	0	0	0	0	0	0	0	0	0	0	0	0	0	0	0 18	0
Sigmoilopsis schlumbergeri	0	0	0 25	0 38	0	0	0 68	0 52	0 33	0 26	0	0 3	0 58	0	0	0	0
Textularia spp.	1.02	1.45	2 04	0	1.4	0 65	0 34	0 79	0 66	0 26	0	C	0 77	0 68	0 26	0	0 44
Spiroplectammina sp.	0	0 24	0	1.52	0	0	1.02	0 79	0.98	1 3	3 23	0.89	0.39	0 23	0	0.54	0.44
Cylindroclavulina bradyi	0	0	0	0	0	0	0	0	0	0	0	0	0	0	0	0	0
Vulvulina spinosa	0	0	0	0	0	0	0	0	0	0	0	0	0	0	0	0	0
Karreriella bradyi	0	0	0	0.38	0	0.33	0	0	0	0	0	0	0 19	0 23	0	0 18	0
Eggella bradyi	0	0	0	0	0	0	0	0	0	0	0	0	0	0	0	0	0
Martinottiella communis	0	0	0	0	0	0	0	0	0	0	0	0	0	0	0	0	0
Bigenerina bradyi	0	0	0	0	0	0	0	0	0	0	0	0	0	0	0	0	0
B. irregularis	0	0	0	0	0	0	0	0	0	0	0	0	0	0	0	0	0
Trochammina sp	0	0	0	0	0	0	0	0	0	0	0	0	0	0	0	0	0
Quinqueloculina spp.	0 34	1 45	0 25	0 76	0 47	0 98	0 68	0.26	0	0	0	0	0	0	0 26	0.18	0
Sigmoilina tenuis	0.34	0	0	0 38	0	0	0	0 26	0	0.26	0	0.3	0	0 23	0	0 18	0
Spiroloculina sp	0	0	0	0 38	0	0	0	0	0	0	0	0	0	0	0	0	0
Pyrgo spp	0	0 48	0	0	0	0	0	0	0	0	0	0	0	0	0	0	0
Unident porcellaneous forms	0 34	1 45	0 25	1 52	0 47	0 98	0 68	0 79	0	0	0	0.3	0	0 23	0.26	0.36	0.22

Salé, Morocco Samples	S53	S55	S56	S57	S59	S60	S61	S62	S63	B2	S65	B3	S67	B5	S70	B7	B8
B pseudopunctata	0 23	0	0	0	0	0 31	0 59	0	0	0	0 2	1	0 3	0	0 16	0	0 31
B. lowmani	2.75	1.32	3.32	3.23	3 52	3.77	2.37	0 42	1.31	1.33	1 8	2 66	0.9	0 37	0.97	1 99	2.28
B. albatrossi	3 21	1 85	5.26	3.98	3 76	4.72	7.12	3 39	2.18	2.34	4.29	2 66	5.71	4.39	5.14	1.99	1 52
B. simplex	0 69	0.26	0.83	0.75	0 94	2.52	1.19	2.12	0 87	1	0.4	0 33	0 3	1.47	0 81	1	0.76
B subspinescens	0 46	0 79	1 39	0 75	0 7	0 63	0 3	1 69	0 87	0 87	2 2	0 67	1 5	1 1	1 62	1	1 9
B. catanensis	0	0	0	0 48	0	0	0	0	0	0	0	0	0	0	0	0	0
B. dilatata	0 23	0.53	0 83	1.24	0	0	0 59	0	0	4.68	8.58	1 99	0	0	0.16	0	0
B. cf. dilata	0	0	0	0	0	0	0	0	0	0	0	0	0	0	0	0	0
B spp	3 89	6 61	5 26	8 96	3 05	4 09	3 85	3 81	1 31	7 69	8 78	4 65	5.25	5.13	4.71	5 84	4.56
Bolivinita pseudothalmanni	11.24	16.4	14 13	9 7	13.62	8 18	10 98	11 86	10 48	8 69	4 19	7 64	1 95	3 3	9 09	6 97	6 08
Sigmavirgulina sp A	1 15	0	1 66	1	0 23	0 94	0 3	0	0	0 67	0	0	0	0	0 32	0	0 76
Laxostomum cf. normale	0 23	1.59	1.11	0 25	0 23	0 63	0	0 42	1.75	1.33	0	1	0 15	0.73	0.16	0 5	1 9
Seabrookia earlandi	0	0	0 28	0	0	0	0	0	0	0	0	0	0	0	0.49	0 5	0
Sigmoilopsis schlumbergeri	0	0	0	0 25	0	0	0 3	0	0	0	0	0 66	0 15	0 37	0 32	0	0
Textularia spp.	0 46	0.79	0	0	0 23	0 63	1 19	0	0 44	0	0 2	0 33	0 3	0 37	0	1	0
Spiroplectammina sp	0 69	0	0	0.75	0	0	0 3	0	0	0	0	0	0	0	0	0	0 76
Cylindroclavulina bradyi	0	0	0	0	0	0	0	0	0	0	0	0	0	0	0	0	0
Vulvulina spinosa	0	0	0	0	0	0	0	0	0	0	0	0	0	0	0	0	0
Karreriella bradyi	0	0	0 28	0 25	0	0	0 3	0 42	0	0	0 2	0	0	0	0	0	0
Eggella bradyi	0	0	0	0	0	0	0	0	0	0 67	0	0 33	0	0	0	0	0
Martinottiella communis	0 23	0	0	0	0	0	0	0	0	0	0.2	0	0 15	0	0	0	0
Bigenerina bradyi	0	0	0	0	0	0	0	0	0	0	0	0	0	0	0	0	0
B. irregularis	0	0	0	0	0	0	0	0 42	0	0	0 2	0	0	0	0	0	0
Trochammina sp	0	0	0	0	0	0	0	0	0	0	0	0	0	0	0	0	0
Quinqueloculina spp.	0	0	0	0 5	0	0	0 59	0	0	0 33	0	0 33	0 15	0	0 32	0 5	0 38
Sigmoilina tenuis	0	0	0	0 5	0	0	0	0	0	0	0	1	0 15	1 1	0 49	0	0 38
Spiroloculina sp	0	0 27	0	0	0	0	0	0	0	0	0	0	0	0	0	0	0
Pyrgo spp	0	0	0	0 25	0	0	0	0	0	0	0	0	0	0	0	0	0
Unident porcellaneous forms	0	0 26	0	1 24	0 47	0	0 59	0	0 44	0	0 4	0	0 6	0	0 81	0 5	0 38

Salé, Morocco Samples	B9	B10	B11	B12	B13	B14	B15	B16	B17	B18	B19	B20	B21	B22	B23	B24	B25
B pseudopunctata	0	0	0	0	0	0	0	0 19	0	0	0 39	0	0	0	0	0 37	0
B lowmani	2.77	3 28	1 98	2.84	3 06	2.37	5 9º	2 13	2.62	2.02	1 19	1 69	1 23	1 54	0 45	0 37	0.2
B. albatrossi	3.38	3 09	3 36	1 65	2.1	2.37	4 12	1 74	4 71	7 41	6 35	4 75	2.46	3 09	6 01	4 81	4 1
B simplex	0	0 77	0 99	0 71	1 15	1 94	2 12	0 39	0	0 67	0 4	0	1 23	3 01	0 47	1 48	0 98
B subspinescens	0 31	0 58	0 4	0 24	0 57	0 86	1 06	0 78	0 52	1 01	0	0 34	0	0	0 45	0 37	0
B. catanensis	0	0	0	0	0	0	0	0	0	0	0	0	0	0	0	0	0
B dilatata	1 23	0	0	0	0	0 64	0	0	0	0 67	0 39	0 34	1 43	1 23	0	0	0
B cf dialata	0	0	0	0	0	0	0	0	0	0	0	0	0	0	0	0	0
B. spp	3 38	5 37	2 96	3 78	2.48	2.36	3 58	4 07	6 28	6 06	5 15	5 08	4 34	2.47	6 26	8 89	5 27
Bolivinita pseudothalmanni	5 85	10 81	10 67	7 57	5 54	7 1	6 37	5 04	4 54	6 4	1 98	2 71	5 13	5 25	5 35	1 11	2.54
Sigmavirgulina sp A	0	0.58	0 4	0	0	0	0 13	0.39	0	0	0	0	0	0	0 67	0	0 39
Laxostomum cf normale	0 62	0 77	0 2	0	1 34	1 08	0 4	0 39	0	0	0 79	0 68	0 21	0	1 56	0 74	0 39
Seabrookia earlandi	0.31	0	0 2	0	0	0	0	0	0 17	0	0	0	0	0	0	0	0
Sigmoilopsis schlumbergeri	0	0	0	0	0	0	0	0 58	0 87	0	0 4	0	0	0 31	0 22	0 37	0 2
Textularia spp	0	0 19	0 59	0 24	0 76	0 65	0 13	0 97	0 87	0 67	0 4	0 68	0	0	0	0	0
Spiroplectammina sp	0 92	0 19	0	0	0 19	0	0	0 19	0	0	0 79	0 68	0	0	0	0	0
Cylindroclavulina bradyi	0	0	0	0	0	0	0	0	0	0	0	0	0	0	0	0	0
Vulvulina spinosa	0	0	0	0	0	0	0	0	0	0	0	0	0	0	0	0	0
Karreriella bradyi	0	0	0	0 24	0	0	0	0 39	0	0	0 4	0 34	0	0 62	0 22	0	0
Eggella bradyi	0	0	0	0	0	0	0	0	0	0	0	0	0	0 31	0	0	0
Martinottiella communis	0	0	0	0	0	0	0	0	0	0	0	0	0	0	0	0	0
Bigenerina bradyi	0	0	0	0	0	0	0	0	0	0	0	0	0	0	0	0	0
B. irregularis	0	0	0	0	0	0	0	0	0	0	0	0	0	0	0	0	0
Trochammina sp	0	0	0	0	0	0	0	0	0	0	0	0	0	0	0	0	0
Quinqueloculina spp	0	0	0	0	0 19	0 22	0	0	0 17	0	0 4	0	0 21	0	0	0	0 2
Sigmoilina tenuis	0	0	0	0 24	0	0 65	0 4	0 19	0 17	0	0 79	0 34	0 21	0	0	0	0 2
Spiroloculina sp	0	0	0	0 24	0	0	0	0	0	0	0	0	0	0	0	0	0
Pyrgo spp	0	0	0	0	0	0	0	0	0	0	0	0	0	0	0	0	0
Unident. porcellaneous forms	0	0	0 4	0 47	0 19	0 86	0 27	0 19	0 17	0	1 19	0 34	0 21	0	0	0	0.2

Salé, Morocco Samples	B26	B27	B28	B29	B30	B31	B32	B33	B34	B36	B37	B38	B39	B40	B41	B42	B43
B. pseudopunctata	0	0	0	0	0.22	0.14	0	0	0	0	0	0	0	0	0	0	0
B. lowmani	1.36	1.33	0.54	0.17	0	0	1.68	0	0	0	0	0	0	0.64	0.16	0.25	0
B. albatrossi	1.09	4.36	4.45	6.82	12.97	4.21	7.21	6.78	6.2	5.04	2.13	5.96	2.09	2.91	8.46	7.88	5.21
B. simplex	3.27	1.7	0.94	2.1	1.12	0	0	0	0	1.7	2.71	0	0	0	0.64	0	2.52
B. subspinescens	0.27	0	0.13	0	0.22	0.54	0.12	0.58	0	0.19	0.19	0.15	0	1.13	0.16	0.74	2.21
B. catanensis	0	0	0	0	0	0	0	0	0	0	0	0	0	0	0	0	0
B. dilatata	0.27	0.75	0	0	0	0	0.48	0	0	0.37	0	0	0	0	0	0	0
B. cf. dialata	0	0	0	0	0	0	0	0	0	0	0	0	0	0	0	0	0
B. spp.	2.71	1.33	3.77	2.1	1.79	1.49	0.24	2.13	0.34	0.37	0	0.59	0.7	3.4	1.43	1.23	0.63
Bolivinita pseudothalmanni	1.09	1.33	0.81	0.52	0.67	0.14	0	0	0	0	0	0	0	0.16	0.16	0	0
Sigmavirgulina sp. A	0	0	0	0	0	0	0	0	0	0	0.58	0	0	0	0	0	0
Loxostomum cf. normale	0.27	0.57	0.4	0	0	0.14	0.12	0	0	0	0.78	0.15	0.47	0	0	0	0.63
Seabrookia earlandi	0	0.19	0	0.17	0	0	0	0	0	0	0	0	0	0	0	0	0
Sigmoilopsis schlumbergeri	0	0.38	0	0	0	0	0	0	0.17	0	0.19	0	0.23	0	0.32	0	0.32
Textularia spp.	0.27	0.57	0.4	1.57	0.45	0.27	0.24	0	0	0.19	0.58	0.3	0.47	0.32	0.32	0	0.32
Spiroplectammina sp.	0	0.38	0.27	0.52	0	0	0	0.39	0	0.19	0	0	0.23	0	0	0	0.32
Cylindroclavulina bradyi	0	0	0	0	0	0	0	0	0	0	0	0	0	0	0	0	0
Vulvulina spinosa	0	0	0	0	0	0	0	0	0	0	0	0	0	0	0	0	0
Karreriella bradyi	0	0	0	0	0	0	0	0	0	0	0	0	0	0	0	0	0.16
Eggella bradyi	0	0	0	0	0	0	0	0	0	0	0	0	0	0	0	0	0
Martinottiella communis	0	0	0.13	0	0.22	0.14	0	0	0	0	0	0	0	0.32	0.16	0	0
Bigenerina bradyi	0	0	0	0	0	0	0	0	0	0	0	0	0	0	0	0	0
B. irregularis	0	0.19	0	0	0	0	0	0	0	0	0	0	0	0	0	0.25	0
Trochammina sp.	0	0	0	0	0	0	0.12	0	0	0	0.19	0	0	0	0	0	0
Quinqueloculina spp.	0	0	0	0	0	0	0	0	0	0	0	0	0	0	0	0	0
Sigmoilina tenuis	0	0	0.13	0.35	0	0.54	0	0	0.52	0	0	0	0	0	0.64	0.25	0
Spiroloculina sp.	0	0	0	0	0	0.54	0	0	0	0	0	0	0	0	0	0	0
Pyrgo spp.	0	0	0	0	0	0	0	0	0	0	0	0	0	0	0	0	0
Unident. porcellaneous forms	0	0	0.13	0	0	0.68	0.12	0.58	0.52	0	0	0	0	0.49	0.64	0.25	0.16

Salé, Morocco Samples	B44	B45	B47	B48	B49	B50	B51	B52	B53	B54	B55	B56	B57	B58	B59	B60	B62*
B. pseudopunctata	0	0.34	0.2	0.23	0	0	1.35	1.68	0	0	0	0	0.64	0	0	2.5	0
B. lowmani	0	0	0	0	0	0	0	0	0	0	0	0	0	0	0	0	0
B. albatrossi	7.15	5.73	5.08	10.34	4.78	6.31	3.82	8.02	15.2	9	4.85	4.48	5.75	6.07	5	11.66	3.63
B. simplex	0	0	5.08	0	[illegible]	0	0.45	0	0	0	0	0.29	2.56	2.5	8.33	2.92	0.99
B. subspinescens	0	0.52	1	1.37	0	0.25	0	0.93	0.37	0.33	0 64	0	1.79	1.11	0	0	0
B. catanensis	0	0	0	0	0	0	0	0	0	0	0	0	0	0	0	0	0
B. dilatata	0	0	0	0	0	0	0	0	0	0	0	0	0	0	0	0	0
B. cf. dialata	0	0	0	0	0	0	0	0	0	0	0	0	0	0	0	0	0
B. spp.	0.24	0.52	1.02	1.14	1.76	2.02	7.86	0 56	6.81	5.01	5.15	3.5[illegible]	0.64	0.35	1.11	0	3.63
Bolivinita pseudothalmanni	0	0	0	0	0	0	0	0	0	0	0	0	0	0	0	0	0.33
Sigmavirgulina sp. A	0	0	0	0	0.21	0	0	0	0	0	0	0	0	0	0	0	0
Loxostomum cf. normale	0	0	0	0	0.42	0	0	0	0	0	0	0	0	0	0	0	0
Seabrookia earlandi	0	0	0	0	0	0	0	0	0	0	0 64	0	0	0	0	0	0
Sigmoilopsis schlumbergeri	0	1.22	0.2	0.46	0	0.51	0.22	0.19	1.52	0	0.32	0.3	0.32	0	0	0	0
Textularia spp.	0.48	0.7	0	0.46	0.21	0.76	0	0.75	0	0.67	0	0	0	0.18	0	0	0.66
Spiroplectammina sp.	0	0	0.41	0	0	0	0	0	0	0	0	0	0	0	0	0	0
Cylindroclavulina bradyi	0	0	0	0	0.21	0	0	0	0	0	0	0	0	0	0	0	0
Vulvulina spinosa	0.24	0	0	0	0	0	0	0	0	0	0	0	0	0	0	0	0
Karreriella bradyi	0	0	0.2	0.23	0.21	0.25	0	0	0.38	0	0	0	0.32	0	0	0.42	0
Eggella bradyi	0	0	0.2	0.46	0.21	0	0	0	0.76	0	0.32	0	0	0	0	0	0
Martinottiella communis	0	0	0	0	0	0	0.22	0	0.38	0	0	0	0	0.36	0	0	0
Bigenerina bradyi	0	0	0	0	0	0	0	0	0	0	0	0	0	0	0	0	0
B. irregularis	0	0	0	0	0	0	0	0	0	0	0.32	0	0	0	0	0	0
Trochammina sp.	0	0	0	0	0	0	0	0	0	0	0	0	0	0	0	0	0
Quinqueloculina spp.	0	0	0	0	0	0	0	0	0	0	0	0	0	0	0	[illegible]	0
Sigmoilina tenuis	0	0.52	0.41	0	0.21	0.25	0	0	0.38	0	0.32	0	0	0.18	0	0	0
Spiroloculina sp.	0	0	0	0	0	0	0	0	0	0	0	0	0.32	0	0	0	0
Pyrgo spp.	0	0	0	0	0	0	0	0	0	0	0	0	0	0	0	0	0
Unident. porcellaneous forms	0	0	0.41	0.46	0.21	0.25	0	0	0.38	0	0 97	0	0.64	0	0	0.42	0

Salé, Morocco Samples	B64*	B66*	B68*	B70*	B71	B72	B74	B76	B79	B81	B83	B85	B87	B89	B91	B93	B95
B. pseudopunctata	0	0	0	0	0	0	0	0	0.21	0	0	0	0.16	0	0	0	0
B. lowmani	0	0	0	0	0	0.37	0	0	0	0	0.64	0	0	0.68	0.64	0.76	1.24
B. albatrossi	8.92	10.34	7.24	3.59	5.13	6.96	4.7	6.8	10.41	7.15	5.58	4.79	5.52	2.71	4.94	5.87	2.17
B. simplex	1.11	0.38	0	0.6	0	0	0	0	0	0.56	0	0	0.81	0.68	1.29	2.29	0
B. subspinescens	0	0	0	2.99	0	0	0	0	0.42	0	0.38	1.6	0	0	0	2.17	0.47
B. catanensis	0	0	0	0	0	0	0	0	0	0	0	0	0	0	0	0	0
B. dilatata	0	0	0	0	0	0	0	0	0	0	0	0	0	0	0	0	0
B. cf. dialata	0	0	0	0	2.05	2.43	0.63	0	0.2	0.56	1.11	0.63	3.21	2.03	7.4	4.47	1.86
B. spp.	7.8	1.14	4.34	5.98	5.13	5.2	3.1	4.6	2.08	7.15	4.15	3.83	2.27	5.22	2.21	2.8	2.79
Bolivinita pseudothalmanni	0	0	0	0	0	0	0	0	0	0.56	0	0	0	0	0	0	0
Sigmavirgulina sp. A	0	0	0	0	0	0	0	0	0	0	0.38	0	0	0	0	0	0.31
Loxostomum cf. normale	0	0	0	0	0	0	0.31	0.31	0.41	0.37	0.64	0	0	0	0.13	1.4	0.16
Seabrookia earlandi	0	0	0.48	0	0	0	0.32	0	0	0	0	0	0	0	0	0	0
Sigmoilopsis schlumbergeri	0	0.77	0.48	2.99	0	1.39	0.63	0.31	0.42	0.75	0	0.32	0.16	0	0	0	0
Textularia spp.	0.37	1.15	0.97	0.6	0	0.35	0	0	0	0.38	0.19	0.64	0.16	0	0.52	0.26	0.16
Spiroplectammina sp.	0	0	0	0	0	0	0	0	0	0	0	0	0	0.23	0	0.51	0
Cylindroclavulina bradyi	0	0	0	0	0	0	0	0	0	0	0	0	0	0	0	0	0
Vulvulina spinosa	0	0	0	0	0	0	0	0	0	0	0	0	0	0	0	0	0
Karreriella bradyi	0.37	0	0	0.6	0	0	0.32	0.31	0.42	0	0	0	0	0	0	0	0.16
Eggella bradyi	0.37	0	0.48	0.6	0	0	0.32	0	0.42	0	0	0	0	0	0	0	0
Martinottiella communis	0	0.38	0	0	0	0	0	0	0.42	0	0.19	0	0	0	0	0	0
Bigenerina bradyi	0	0	0	0	0	0	0	0	0	0	0	0	0	0	0	0	0
B. irregularis	0	0.38	0	0	0	0	0	0	0	0	0.19	0	0	0	0	0	0
Trochammina sp.	0	0	0	0	1.03	0	0	0	0	0	0	0	0	0	0	0	0
Quinqueloculina spp.	0	0	0	0	0	0	0	0	0	0	0	0	0	0	0	0	0
Sigmoilina tenuis	0	0	0	0	0	0	0	0	0	0.19	0	0	0	0.23	0	0	0.31
Spiroloculina sp.	0	0	0	0	0	0	0	0	0	0	0	0	0	0	0	0	0
Pyrgo spp.	0	0	0	0	0	0	0	0	0	0	0	0	0	0	0	0	0
Unident. porcellaneous forms	0	0	0	0	0	0	0	0	0	0.19	0	0	0	0	0.13	0	0

Salé, Morocco Samples	B97	B98	B100	B102	B104
B. pseudopunctata	0	0	0.21	0	0
B. lowmani	1.09	0.61	1.25	1.07	1.68
B. albatrossi	2.92	5.32	3.24	2.14	2.1
B. simplex	2.05	0	0.41	0	0.42
B. subspinescens	1.09	0.82	0.31	0.72	1.26
B. catanensis	0	0	0	0	0
B. dilatata	0	0	0	0	0
B. cf. dialata	1.45	0.61	0.52	0	0
B. spp.	4.01	12.09	7.4	10.35	10.5
Bolivinita pseudothalmanni	0	0	0	0	0
Sigmavirgulina sp. A	0.73	0	0.21	0	0
Laxostomum cf. normale	1.09	0.2	0.31	0	0
Seabrookia earlandi	0	0	0	0.36	0
Sigmoilopsis schlumbergeri	0	0	0	0	0
Textularia spp.	0	0	0.1	0	0
Spiroplectammina sp.	0	0	0	0	0.42
Cylindroclavulina bradyi	0	0.2	0	0	0
Vulvulina spinosa	0	0	0	0	0
Karreriella bradyi	0	0	0	0.36	0.42
Eggella bradyi	0	0.2		0	0
Martinottiella communis	0.36	0		0	0
Bigenerina bradyi	0	0	0	0.36	0
B. irregularis	0	0	0	0	0
Trochammina sp.	0	0	0.1	0	0
Quinqueloculina spp.	0	0	0	0	0
Sigmoilina tenuis	0	0	0	0	0
Spiroloculina sp.	0	0	0	0	0
Pyrgo spp.	0	0	0	0	0
Unident. porcellaneous forms	0	0	0.21	0	0

Appendix B

Table of benthic foraminifera from DSDP Hole 552A

Site 552A Cores	19-01	19-02	19-3	19cc	20-1	20-2	20-3	20cc	21-1	21-02	21-3	21cc
Intervals	50-54	60-64	50-54	10-14	70-74	70-74	18-22	4-8	102-106	70-74	20-24	10-14
Depth (m in subbottom)	87.5	89.1	90.5	91.7	92.7	94.2	95.18	95.39	96.02	97.2	98.2	98.8
Number picked	332	278	176	264	377	248	184	286	253	241	220	150
% benthics of total fauna	2.1	2.9	1.9	2.6	2.8	1.9	1.5	1.3	1.5	1.2	1.3	1.4
Number per cc	4249	3558	563	1689	4825	1587	1177	1830	1619	1542	1408	960
Epistominella exigua	14.5	7.9	7.4	12.5	11.1	10.5	16.8	20.6	22.1	19.5	17.7	6.7
Nuttallides umbonifera	2.1	3.2	1.1	3.8	3.2	2	4.9	0.7	3.2	0.8	4.5	0
Eponides pollus	0	1.1	0.6	0	0.5	1.2	0.5	1	0	0	1.4	0.7
E. tumidulus	3	1.8	7.4	2.3	1.3	5.6	8.7	3.5	5.1	4.1	4.5	2.7
E. weddellensis	10.8	7.9	5.1	5.3	7.7	5.6	12	13.6	5.9	8.3	7.7	7.3
E. ? sp. A	0	0	0	0	0	0.4	0	0.7	0	0	0	0.7
Gyroidina soldanii	2.1	2.9	2.3	1.5	2.4	2.4	2.2	1.4	2.8	1.2	1.8	4.7
Heronallenia crosbyi	0.6	0.4	1.1	0	0	0	0.5	0.3	0	0	0	0
Oridorsalis umbonatus	3	1.4	1.1	1.5	1.3	2.8	0.5	0.7	1.6	1.2	2.7	6
Cibicidoides bradyi	0	0	0.6	0	0	0	0	0	0	1.2	0	0
C. mundulus	0	0.7	0	0.4	0	0	1.1	0.3	0.8	0	0	1.3
C. spp.	0	0.7	0.6	0.4	0	0	1.1	0.7	0	1.2	0	1.3
Planulina wuellerstorfi	0	0.4	0	0	0.5	0.4	0	0	0	0	0	0
Osangularia culter	0	0	0	0	0	0	0	0	0	0	0	0
Laticarinina pauperata	0	0	0	0	0	0	0.5	0	0	0	0	0
Valvulineria laevigata	0	0	0	0	0	0.4	0	0	0	0	0	0
Sphaeroidina bulloides	0	0	0.6	0	0	0.8	0	1.4	1.2	1.7	0.9	2
Pullenia bulloides	0.6	1.1	0.6	0.4	0.8	0.8	1.1	2.1	0.8	2.1	1.8	0
P. quinqueloba	1.2	0.4	0	0	0	0.8	0.5	0	0.8	0.4	0.5	0
Nonion sp.	2.7	1.4	0	1.5	0.3	1.2	1.1	2.1	3.2	2.1	1.4	3.3
Melonis pompilioides	0.3	0	0	0	0	0	0	0	0	0	0	0
M. barleeanum/affinis	0	0.4	0	0	1.1	0	0	0	0.4	0	0	0
Nonionella sp. A	0.6	0	1.1	0.4	0.3	1.6	0	0.3	0.4	0.8	0.5	0.7
Astrononion echolsi	0.6	2.2	4	0.4	0.8	0.8	2.2	1.4	2.4	0.8	1.4	2
Anomalina sp.	0	0	0	0	0.3	0	0	0	0	0	0	0
Globocassidulina subglobosa	15.1	13.7	33	20.5	12.7	35.1	25	27.6	29.6	22.8	29.1	40
Cassidulina laevigata	0.6	0	0	0.4	0	0	0	0	0	0.8	0.9	0.7
Rectuvigerina compressa	1.2	0.4	0	0.4	0	0	0.5	1	2.8	0.4	0	1.3
Uvigerina perigrina	0	0	1.7	0.8	0	0	0	0	0	0.4	0	0
U. hispida	0.3	0.4	0	0	0	0	1.6	0	0	0	0	0
Bulimina alazaensis	0.3	0.4	0	0	0.8	0	0	0.7	1.2	0	0	0
B. cf. alazaensis	0.9	0	0	0.4	1.1	1.2	2.2	1.4	1.6	1.2	1.8	1.3
B. mexicana	0.6	0	0	0	0	0.4	0	0	0.4	0	0	0
B. elongata	0	0	0	0	0	0	0	0	0	0	0	0
Globobulimina auriculata	0	0	0	0.4	0	0	0	0	0	1.7	0	0
Bolivina pseudopunctata	1.8	0	0	0	0	0.8	0	0.7	0	0.4	0	0
B. inflata	5.7	32.4	0.6	23.9	34	0.8	1.1	0.3	0.4	0	0	0
B. pygmaea	6.6	4	17	8.7	6.9	8.9	2.2	3.1	5.1	4.1	4.5	2.7
B. subaenariensis	0.9	0.4	0	0.8	0.5	0.4	0	0	0	0	0	0
B. albatrossi	0	0	0	0	0	0	0	0	0	0	0	0
B. lowmani	0	0	0	0	0	0	0	0	0	0	0	0
Bolivinita truncta	0	0	0	0	0	0	0	0	0	0	0	0
Stilostomella antillea	3	1.4	1.7	0.8	1.1	1.6	0.5	2.8	0.4	2.9	1.8	4
S. sp.	0.9	0.7	0	0.4	0	0.8	0	0	0	0	0	0
Pleurostomella spp.	0.6	0	2.3	0.4	0	0.8	0	1.4	1.2	0.4	0.9	0.7
Tosaia hanzawai	2.1	1.1	0.6	1.1	0.3	1.2	2.2	0	1.6	1.2	1.4	2.7
Trifarina angulosa	0.3	0.4	1.1	0	0	0	0	0	0	0	1.4	0
Unidentified triserial forms	0.9	0	1.1	0	0.3	0	0	0	0	0	0.5	0
Ehrenbergina trigona	0	1.4	0	0.8	0	0	0	0	0	0	0	0
Fursenkoina fusiformsis	0.3	0.4	0.6	1.1	0.3	0.8	1.1	0	0	0.8	0.5	0
Lagena spp.	0	0.4	0.6	0.4	0.5	1.6	0.5	0.3	0.4	0	1.4	0.7
Fissurina spp.	1.5	1.4	3.4	0	0.8	1.2	2.7	2.4	1.2	0.8	3.2	1.4
Dentalina communis	0.9	0	0.6	0	0	0	0	0	0	0.4	0	0
Nodosaria sp.	0.3	0	0	0	0	0	0	0	0	0	0	0.7
Quinqueloculina spp.	0	0.7	0	0	0.5	0.8	0	0.7	0	0	0.9	0.7
Pyrgo spp.	0	0	0.6	0	0.3	0.4	0	0	0	0	0	0
Oolina spp.	0	0	0	0.4	0	0	1.6	0	0	0.8	0.9	0.7
Siphonina tenuicarinata	0	0	0	0	0.3	0	0	0	0	0	0	0
Seabrookia earlandi	0	0	0	0	0	0	0.5	0	0	0	0	0
Sigmoilina tenuis	0	0.4	0	0	0	0	0	0	0.4	0.4	0	0
Guttulina sp.	0	0	0	0.4	0	0	0	0	0	0	0	0
Lenticulina spp.	0	0	0	0.4	0	0	0	0	0.4	0.4	0	0
Reussella spinulosa	0	0	0	0	0.5	0	0	0	0	0	0	0
Sigmoilopsis schlumbergeri	0	0	0	0	0	0	0	0	0	0.4	0	0
Siphotextularia rolshauseni	0	0	1.1	0.8	0.3	0	0	0.7	0	0.4	0	0
Vulvulina spinosa	0	0	0	0	0	0.4	0	0	0	0	0	0
Spiroplectammina sp.	0	0	0	0	0	0	0	0	0	0	0	0

Site 552A Cores	22-1	22-2	22-3	22cc	23-1	23-2	23-2	23-3	23cc	24-1	24-1	24-2
Intervals	70-74	91-95	70-74	15-19	123-125	54-58	124-128	94-98	10--12	43-47	112-116	63-67
Depth (m in subbottom)	99.7	101.41	102.7	103.12	105.23	106.04	106.78	107.94	108.32	108.93	109.62	110.63
Number picked	189	289	302	240	292	349	282	193	383	250	178	245
% benthics of total fauna	1.5	1.1	2	1.5	1.24	2.4	1.6	1.6	1.9	1.4	1.3	1.5
Number per cc	1209	393	966	754	934	1116	902	2470	2451	3200	3189	3176
Epistominella exigua	10.6	15.6	3.3	14.2	4.1	5.2	12.8	20.7	16.7	11.2	21.3	17.1
Nuttallides umbonifera	0.5	1	0	0	0	0	1.4	0	0.3	0.4	4.5	2.4
Eponides polius	0.5	0.7	1	0.8	5.5	2	3.2	0	1	2.8	2.2	3.3
E. tumidulus	7.4	2.1	1.7	0.8	4.1	3.7	3.9	3.6	3.7	1.6	1.7	3.3
E. weddellensis	10.6	11.1	3.3	5	7.9	9.7	12.4	5.2	7.6	10.8	9.6	11.8
E. ? sp. A	0	0	0	0	0	0	0	0	0	0	0	0
Gyroidina soldanii	1.6	1.7	1.3	6.2	2.4	2.9	2.5	3.6	2.9	4	5.1	3.3
Heronallenia crosbyi	0	0	0	0	0	0	0	0	0.3	0	0.6	0
Oridorsalis umbonatus	1.6	2.4	1.7	3.3	1.4	4.6	2.1	2.1	1.8	3.6	5.6	1.2
Cibicidoides bradyi	0	0	0.3	0.4	0.3	0.3	0	0	0	0	0	2.4
C. mundulus	0.5	0.3	0.3	0	0	0	0.4	0	0.8	1.6	0	0.4
C. spp.	0.5	0.3	0.7	0.4	0.3	0.3	0.4	0	1	1.6	0	4.1
Planulina wuellerstorfi	0	0.3	0	0.4	0	0	0	0	0	0	0	0
Osangularia culter	0	0	0	0	0	0	0	0	0	0	0	0
Laticarinina pauperata	0	0.3	0	0	0	0	0	0.5	0	0	0	0
Valvulineria laevigata	0	0	0	0	0	0	0	0	0	0	0	0
Sphaeroidina bulloides	2.6	0	0.3	0	0	0.3	1.1	0.5	0.5	0	0	0.4
Pullenia bulloides	0.5	0	1	0.4	0	0.6	1.1	0.5	0.5	0.8	2.2	2
P. quinqueloba	0.5	0.7	2	2.5	1.7	0.6	0	0	0.8	1.2	0.6	0.4
Nonion sp.	0.5	0.7	2.3	0.8	1.7	0	2.1	2.1	2.9	0.8	2.8	4.9
Melonis pompilioides	0	0	0	0	0	0	0	0	0	0	0	0.4
M. barleeanum/affinis	0	0	0.3	0	0.3	0	0	0	0.3	0	1.1	0
Nonionella sp. A	3.2	2.4	0.7	0.8	2.1	0	1.4	1	0.3	2.4	0	0.8
Astrononion echolsi	1.6	1.7	1	2.9	1.7	0.3	0.7	0.5	1	2.4	1.1	1.6
Anomalina sp.	0	0	0	0	0	0	0	0	0	0	0	0
Globocassidulina subglobosa	23.8	30.4	58.6	32.9	30.8	32.4	19.5	31.1	25.6	25.2	15.2	19.6
Cassidulina laevigata	1.6	0.3	1.3	1.2	1	1.7	0	0	1	0.8	0	0
Rectuvigerina compressa	0.5	0.3	0	0	1	2.3	1.1	0	0	0.8	2.8	0.8
Uvigerina perigrina	0	3.1	0.3	0	1	1.1	0	0.5	2.1	3.2	1.1	0.4
U. hispida	0	0	0	0	0	0.3	0	0	0.8	0.4	0	0
Bulimina alazaensis	0	0.3	0.7	0.4	0	0.6	0.4	0.5	1	0.8	0.6	0
B. cf. alazaensis	0	3.8	1.3	0.4	1.7	1.4	1.1	0	1	0.8	3.4	1.2
B. mexicana	0.5	0.3	0	0.4	0.7	0	0	1.6	0.3	0	0	0
B. elongata	0	0	0	0	0	0	0	0	0	0	0	0.4
Globobulimina auriculata	0	1	0	0	0	0.3	0.4	0	0.3	0.8	0	0
Bolivina pseudopunctata	0.5	0.3	2	0.4	0	0	0	0	0	0	0	0
B. inflata	0.5	0.3	0	0.4	1	0	0.4	1	0	0	0	0.8
B. pygmaea	7.4	2.1	1.7	0.8	4.1	3.7	14.9	3.1	7.3	1.2	5.1	4.9
B. subaenariensis	0	0	0	0	0	1.4	0	2.1	1.3	0	0.6	0
B. albatrossi	0	0.3	0	0	0	0	0	0	0	0	0	0
B. lowmani	0	0	0	0	0	0	0	0	0	0	0	0
Bolivinita truncta	0	0	0	0	0	0	0	0	0	0	0	0
Siliostomella antillea	4.2	2.4	3.3	3.8	5.8	2	1.4	3.1	3.4	1.2	2.2	0.8
S. sp.	0	0.3	0	0.8	0.7	0.6	1.1	0	0	1.2	0	0.4
Pleurostomella spp.	0.5	0	0.7	1.2	0.3	0	0	0.5	0	0.8	2.2	0.4
Tosaia hanzawai	2.1	2.1	1.3	2.5	4.5	0.6	1.1	0.5	1	2.8	0	0.4
Trifarina angulosa	2.6	0.3	0	0.8	0	0	0	0.5	0.3	0	0	0.4
Unidentified triserial forms	1.1	0	0	0	0	0	0	0	0	0	0.6	0
Ehrenbergina trigona	1.1	0.3	0	0	0	0	0.7	0	0.3	2.4	0.6	0.8
Fursenkoina fusiformsis	0.5	0.3	0.3	0	1.4	0	0	0	0.3	0	2.2	2
Lagena spp.	1.6	0.7	0.3	0.4	4.1	1.1	0.7	2.1	1.6	0.4	1.1	1.2
Fissurina spp.	3.3	1.4	0.7	3.3	2.7	0.6	0.7	1.6	1.3	2	0.6	1.6
Dentalina communis	0	0	0	0	0	0	0.4	0.5	0	0.4	0.6	0
Nodosaria sp.	0	0	0	0	0	0	0	0	1.3	0	0	0
Quinqueloculina spp.	0	0	0	0	0.3	1.1	0	0	0	0	0	0
Pyrgo spp.	0	0.3	0	0	0	0	0	0	0	0	0	0
Oolina spp.	0	0	0.7	0.8	0	0	0	0.5	0.8	0.4	0	0
Siphonina tenuicarinata	0	0	0	0	0	0	0	0	0	0	0	0
Seabrookia earlandi	1.1	0	0.7	0	1.7	0.9	0.4	0	0	0.8	0	0
Sigmoilina tenuis	1.1	0	0.3	0.8	0.3	0	0	0	0	0	0	0
Guttulina sp.	0	0	0.3	0	0.3	0	0	0	0	0	0	0
Lenticulina spp.	0	0	0	0	0	0	0	0.5	0	0	0	0
Reussella spinulosa	0	0	0	0	0	0	0	0.5	0	0	0	0
Sigmoilopsis schlumbergeri	0	0	0	0	0.3	0	0.4	0	0	0	0	0
Siphotextularia rolshauseni	1.6	0.3	1.3	0.4	1.7	0.6	0.4	0.5	0.5	0.4	1.1	1.6
Vulvulina spinosa	0	0	0	0	0	0	0	0	0	0	0	0
Spiroplectammina sp.	0	0	0	0	0	0	0	0	0	0	0	0

Site 552A Cores	24-3	24cc	25-1	25-2	25-3	25cc	26-1	26-2	26-3	26cc	27-1	27-2
Intervals	36-40	6-10	110-114	106-110	106-110	20-24	104-108	104-108	104-108	6-10	113-117	106-110
Depth (m in subbottom)	111 96	113 06	114 6	116 06	117.56	118 2	119.54	121 04	122 54	123 26	124 63	126 06
Number picked	274	190	219	209	327	168	160	154	145	181	118	195
% benthics of total fauna	1 8	1 4	1.5	1 3	1	1 2	1 3	1 4	1.5	1 6	1 6	3 4
Number per cc	1752	1824	700	668	429	538	2048	1970	1856	2316	1510	2508
Epistominella exigua	17 5	14 7	13 2	11.5	7 7	4 6	8 1	22 1	17.2	23 8	14 4	19
Nuttallides umbonifera	0 7	0.5	0	0	0 3	0	0	0	0 7	0	0	0
Eponides polius	1 5	3.2	0	6 2	3 1	0 6	6 9	2 6	1 4	1 1	1 7	3 1
E tumidulus	4 4	2 6	3 2	1 9	1 8	7 1	8 8	4 5	2.8	2 8	1 7	3 1
E weddellensis	15 7	13 2	10 5	12 4	4	8 9	10 6	13	13 1	12 2	12 7	7 2
E ? sp A	0	0.5	0	0	0 3	0	0	0	0	0	0	0
Gyroidina soldanii	2 2	1 6	4 1	0 5	3 7	2 4	3 1	1 3	2.8	2 2	4 2	5 6
Heronallenia crosbyi	0	0	0	0	0	0	0	0	0	0	0	0
Oridorsalis umbonatus	4 4	2 6	4 1	3 3	5 2	5 4	1 2	2 6	4 1	4 4	3 4	1
Cibicidoides bradyi	0	0	0.5	1	0	0	0	0 6	0	1 7	0	0
C mundulus	0	0	0 9	0	1 2	0 6	0	0	0	0	0	0 5
C spp	0 4	0.5	1 4	1	1 2	1 2	0	0	0	0	0	0 5
Planulina wuellerstorfi	0 7	0	1 4	0.5	0 9	1 8	0	1 3	0	0	1 7	0 5
Osangularia culter	0	0	0	0	0	0	0	0	0	0	0	0
Laticarinina pauperata	0 4	0	0	0	0	0	0	0 6	0	0	0	0
Valvulineria laevigata	0	0	0	0	0	0	0	0	0	0	0	0
Sphaeroidina bulloides	0 7	1 1	0 9	0	1 2	0	0	1 3	0 7	0	0	0
Pullenia bulloides	2 2	0.5	2 3	1 4	0 6	0 6	0	0 6	2.1	1 7	0	2 1
P quinqueloba	0	0	0	1	0 9	0 6	0 6	1 3	0 7	0 6	0	0
Nonion sp.	2 6	4 7	0 9	4 3	0 3	3	2 5	0 6	2.8	2 2	0 8	0 5
Melonis pompilioides	0	0	0	0	0	0	0	0	0	0	0	0
M barleeanum/affinis	0 7	0	0	0	3 4	0	0	0 6	0	1 1	3 4	0
Nonionella sp A	0 4	2 6	1 8	1	0 3	2 4	0	2 6	0 7	0	1 7	0
Astrononion echolsi	0 7	2 1	0 5	1	0 3	0 6	0	0	1 4	0	0	0
Anomalina sp	0	0	0	0	0	0	0	0	0	0	0	0
Globocassidulina subglobosa	18 2	18 4	17 4	21 5	8	23 2	23 1	13 6	14 5	21	17 8	21
Cassidulina laevigata	0 4	0	0	0	0 6	0	0	0	2 8	0	0	0
Rectuvigerina compressa	2.6	0.5	0 9	1 9	0	1 2	2 5	3 9	1 4	0	0	0
Uvigerina peregrina	2.6	0.5	3 2	3 3	2 4	3	0	2 6	0 7	0	0	0
U hispida	0	0.5	0	0	1 2	0	0	0	0	1 7	2 5	1
Bulimina alazaensis	0 4	0	0	0	0 6	0 6	2 5	0	2.1	1 1	0 8	0
B cf alazaensis	1 5	0.5	2 7	1 4	0 9	2 4	0 6	1 9	0 7	1 1	1 7	0 5
B mexicana	0	0.5	0	0	0	0 6	0	0	0	0 6	0 8	0
B elongata	0	0	0	0	0	0	0	0	0	0	0	0
Globobulimina auriculata	0	0	0	0	0 3	0	0	0	0	0 6	0 8	0
Bolivina pseudopunctata	0	0	0	0	0	0	0	0	0 7	0	0	0 5
B inflata	0	0.5	0	0 5	0 3	0	0	0	0	0 6	0	0 5
B pygmaea	1 1	4 7	14 6	3 3	0 9	6 5	8 8	5 8	4 1	5 5	10 2	6 2
B subaenariensis	0 7	0	0	0	0	0	0	0	0	0	0 8	2 6
B albatrossi	0	0	0	0	0	0	0	0	0	0	0	0
B lowmani	0	0	0	0	0	0	0	0	0	0	0	0
Bolivinita truncata	0	0	0	0	0	0	0	0	0	0	0	0
Stilostomella antillea	1 5	1 6	1 4	0 5	4 9	0 6	0 6	1 3	2.8	1 1	0 8	1
S. sp	0 7	0.5	0	1 9	0 6	0 6	1 9	2 6	4 8	0 6	0 8	0
Pleurostomella spp	1 1	1 6	0	0 5	0 6	0	0	0	0 7	0	0 8	0 5
Tosaia hanzawai	0 4	2 1	0 9	1	2.1	0 6	1 2	1 9	1 4	1 1	2 5	1
Trifarina angulosa	0 7	0	0.5	0	0	0	0	0	0 7	0 6	0	0 5
Unidentified triserial forms	0	0	0	0	1 2	0	0	0	0	0 6	0	1 5
Ehrenbergina trigona	0	0	0	0 5	0	0	0	1 9	1 4	0 6	0	0 5
Fursenkoina fusiformsis	0 4	0	1 8	1	0 3	0	1 2	0	0	0	0 8	0
Lagena spp	0 7	1 1	1 4	0 5	1 5	1 2	0 6	0	2.8	0	0 8	0 5
Fissurina spp	3 3	1 1	1 8	1 4	2 1	1 8	3 8	3 9	0 7	0 6	1 7	0 5
Dentalina communis	0	0	0	0	0	0 6	0	0	0	0	0	0
Nodosaria sp	0	0	0	0 5	0 3	0	0	0	0	0	0	0
Quinqueloculina spp	1 1	0	0.5	0	0 6	0	0 6	0	1 4	0	0 8	0 5
Fyrgo spp	0 4	0	0	0	0 6	0	1 2	0	1 4	0	0	0
Oolina spp	0	0	0 9	1 9	0	0 6	0	0 6	0	0	0 8	0 5
Siphonina tenuicarinata	0	0	0	0	0	0	0	0	0	0	0	0
Seabrookia earlandi	0	0	0 9	2 9	0 6	1 2	0	0	0 7	0	0	0 5
Sigmoilina tenuis	0	0	0	0	1 2	0	0	0	0 7	0	0	1
Guttulina sp	0	0	0	0	0	0	0 6	0	0	0	0	0
Lenticulina spp	0 4	0	0	0 5	0 3	0	0	0	0	0	0	0
Reussella spinulosa	0	0	0 5	0	0	0	0	0	0	0	0	0
Sigmoilopsis schlumbergeri	0	0	0 5	0	0	0 6	0	0	0	0 6	0 8	0
Siphotextularia rolshauseni	0 7	1 1	0 5	1	0 6	0	0 6	2 6	1 4	1 1	0 8	0 5
Vulvulina spinosa	0	0	0	0	0	0	0	0	0	0	0	0
Spiroplectammina sp	0	0	0	0	0	0	0	0	0	0	0	0

Site 552A Cores	27-3	27-4	27-4	28-1	28-2	28-3	28-4	28cc	29-1	29-2	29-3	29-4
Intervals	106-110	6-10	18-22	105-109	104-108	65-69	6-10	8-12	104-108	104-108	83-87	23-27
Depth (m in subbottom)	127.56	128.06	128.18	129.55	131.04	132.15	133.06	133.5	134.54	136.04	137.33	138.23
Number picked	188	351	278	323	293	357	269	268	265	251	291	201
% benthics of total fauna	1.9	2.4	2.9	2.6	2.2	2.4	1.8	2.1	2	2.3	2.3	1.3
Number per cc	2406	1123	1779	2067	1875	2284	1721	1715	1726	1606	1862	1286
Epistominella exigua	12.2	11.7	10.8	15.2	13.3	13.2	11.5	11.9	13.2	13.5	15.1	11.4
Nuttallides umbonifera	0	0	0	0.3	0	0.6	0	0	0	3.6	2.8	1.5
Eponides polius	0.5	3.4	1.8	0.6	3.4	1.7	1.9	2.6	1.9	2	0.7	1.5
E. tumidulus	3.7	2.6	1.1	1.9	2.4	2.8	4.1	1.9	2.6	10	6.9	7.5
E. weddellensis	1.1	10.5	16.2	14.9	10.6	14.3	11.9	7.5	7.9	10	8.2	13.9
E. ? sp. A	0	0	0	0	0	0	0	0	0	0	0	0
Gyroidina soldanii	7.4	4.3	1.8	6.8	3.8	4.5	7.4	2.2	4.5	4	5.5	3.5
Heronallenia crosbyi	0	0	0	0	0	0	0	0	0	0	0	0
Oridorsalis umbonatus	3.7	2	1.4	2.8	1.4	2.8	3.3	4.1	2.3	4.4	3.8	4.5
Cibicidoides bradyi	0.5	0.3	0	0.9	1	0	0	0	0	0.4	0	0
C. mundulus	1.1	0.6	0	0	0.3	0.6	0.7	0.7	0.4	0.4	0.7	0.5
C. spp.	2.7	0.9	0	0	0.3	0.6	1.1	1.1	0.4	0.8	0.7	0.5
Planulina wuellerstorfi	0	0	0	0	0.3	0	0.4	0	1.1	0	0	0.5
Osangularia culter	0	0	0	0	0	0	0	0	0	0	0	0
Laticarinina pauperata	0.5	0	0	0	0	0	0	0	0	0.4	0	0
Valvulineria laevigata	0	0	0	0	0	0	0	0	0	0	0	0
Sphaeroidina bulloides	0	0	0	0	0	0	0	0	0	0.4	0	0
Pullenia bulloides	2.7	0	0.4	0	0.7	0.8	0.7	0.7	1.1	0.4	0.7	1
P. quinqueloba	1.1	0	0.4	0.6	0	0.8	0.7	0.7	0.4	0	1.4	2.5
Nonion sp.	2.1	1.7	0.7	0.6	0	0	0.4	0.7	3.4	2.4	1.7	4
Melonis pompilioides	0	0	0	0	0	0	0	0.4	0	0	0	0
M. barleeanum/affinis	1.6	0.6	0	1.2	2	3.1	1.1	2.6	0	0	0.7	0
Nonionella sp. A	2.7	1.4	0.7	0.3	2	0	1.1	0.4	1.1	0.8	3.8	1.5
Astrononion echolsi	0.5	0	2.2	0.9	0	0	0.4	0	1.1	0.4	1.4	1
Anomalina sp.	0.5	0	0.4	0	0	0.3	0	0	0	0	0	0
Globocassidulina subglobosa	16.5	35.9	35.3	23.5	23.9	24.1	20.1	24.3	26	18.7	19.6	15.9
Cassidulina laevigata	0	0	0	0	0	0.3	0	0	0	0.4	0.3	0
Rectuvigerina compressa	0.5	3.4	0	0	0	0	0	0	0.4	1.2	0.3	1
Uvigerina perigrina	0	0	0	0	0	0	0.7	0.4	1.9	1.6	0.3	0
U. hispida	0	0	0	0.9	0	0	3	3	0	0.4	1	0.5
Bulimina alazaensis	2.1	0	0	0	0	0	1.5	0.7	1.1	0.8	0.3	2
B. cf. alazaensis	3.2	1.1	1.4	1.5	2	1.4	1.5	3.4	2.3	1.6	1	0
B. mexicana	0.5	0.3	0	0.3	0.3	0.3	0.4	0	0	0.4	0	0
B. elongata	0	0	0	0	0	0	0	0	0	0	0	0
Globobulimina auriculata	0	0	0	0	0	0.3	0	0	0.4	0	0.3	0.5
Bolivina pseudopunctata	0	0	0.7	0	0	0.3	0	0	0	0.4	0	0
B. inflata	0.5	1.4	0	0.6	1	0.6	0.4	0	0	0.4	0	0.5
B. pygmaea	6.4	2.3	2.2	3.1	13	9.8	8.9	4.5	12.1	3.2	3.4	9
B. subaenariensis	0	0	0	0	0	0	0	0	0	0.8	0	0.5
B. albatrossi	0.5	0	0	0	0	0	0	0	0	0	0	0
B. lowmani	0	0	0	0.3	0	0	0	0	0	0	0	0
Bolivinita truncta	0	0	0	0	0	0.3	0	0	0	0	0	0
Stilostomella antillea	1.6	1.7	1.4	1.9	2	0	0.7	0	1.5	1.2	1.4	0.5
S. sp.	0	0	0	0	0	1.7	1.1	0	0.4	0.4	0.3	0.5
Pleurostomella spp.	0	1.1	1.1	0.9	0.7	0.6	1.5	0.4	0.8	0.8	1	0.5
Tosaia hanzawai	1.1	0.6	0.4	1.5	1	0.3	0	2.2	3	0.4	0.3	2
Trifarina angulosa	1.1	0	2.5	0.9	1	1.7	1.1	1.1	0.8	0.8	1.4	1.5
Unidentified triserial forms	0	1.7	1.4	1.9	0	0	0	0	0	0	0	0
Ehrenbergina trigona	1.6	0.3	0	0.3	1	0	0	0.7	0.4	0.4	0.3	3
Fursenkoina fusiformsis	0	0.3	0	0.3	0	1.7	2.6	0.4	0	0	0	0
Lagena spp.	0.5	0.3	1.8	0.9	1	2	1.9	1.5	0.4	2	0.3	0.5
Fissurina spp.	1.1	2	2.5	0.9	0.7	0.3	1.5	0.7	1.9	0.8	2.4	0.5
Dentalina communis	0	0	0	0	0	0.3	0	0.4	0	0	0	0
Nodosaria sp.	0	0.3	0	0	0	0	0	0.4	0	0	0	0
Quinqueloculina spp.	0	0	0	0	0	0	0	0	0.4	1.2	0	0
Pyrgo spp.	0	0	0	0	0	0	0	0	0	0.4	0	0
Oolina spp.	1.1	0.3	0.7	0.3	0	0.6	0	0	0.4	1.6	1.4	0
Siphonina tenuicarinata	0	0	0	0	0	0	0	0	0	0	0	0
Seabrookia earlandi	0	0	0	0	0	0	0	0.4	0	0.4	0	0
Sigmoilina tenuis	0	0	0	0	0	0.3	0.4	0	0	0.4	0.3	0
Guttulina sp.	0	0	0	0	0	0	0	0	0	0	0	0
Lenticulina spp.	0	0	0	0.3	0	0	0	1.1	0	0	0	0
Reussella spinulosa	0	0	0	0	0	0	0	0	0	0	0	0
Sigmoilopsis schlumbergeri	0.5	0.3	0	0	1	0.6	0	0	0	0	0	0
Siphotextularia rolshauseni	0	2	1.8	2.2	1.4	0.8	0	0	0	1.2	0.7	1
Vulvulina spinosa	0	0	0	0	0	0	0	0	0	0	0	0
Spiroplectammina sp.	0	0	0	0	0	0	0	0	0	0	0	0

Site 552A Cores	29cc	30-1	30-2	30-3	30-4	31-1	31-2	31-3	31-4	32-1	32-2	32-3
Intervals	5-9	84-88	102-106	100-104	16-20	102-106	112-116	111-115	11-15	90-94	16-20	90-94
Depth (m in subbottom)	138.47	139.34	142.02	142.5	143.16	144.52	146.12	147.61	148.11	149.4	150.16	152.4
Number picked	241	212	282	215	222	221	213	209	411	311	188	323
% benthics of total fauna	1.7	1.8	1.6	1.9	1.3	2.2	1.4	3.7	3.8	2.9	1.4	1.9
Number per cc	3084	1356	2240	1376	876	1107	2726	2675	2630	1990	1804	2067
Epistominella exigua	15.4	21.2	7.4	14.9	9.9	14.9	10.8	15.8	22.1	16.1	13.8	14.6
Nuttallides umbonifera	1.7	1.9	4.3	0.9	0.5	1.8	2.3	0	1.5	1.3	4.8	6.2
Eponides polius	1.7	1.4	2.5	0.9	1.4	1.8	4.7	1	3.2	1.3	2.7	2.8
E. tumidulus	3.7	4.2	2.5	2.8	4.5	4.5	5.6	4.8	2.2	8.7	2.1	0.9
E. weddellensis	10.4	20.3	7.1	5.1	11.3	7.2	7	15.8	10.9	12.5	12.8	7.1
E. ? sp. A	0	0	0	0	0	0	0	0	0	0	0	0
Gyroidina soldanii	3.7	3.3	2.1	4.2	2.7	3.2	7	0	2.9	3.9	3.2	4.3
Heronallenia crosbyi	0	0	0	0.5	0	0	0	0	0	0	0.5	0
Oridorsalis umbonatus	2.9	4.7	2.5	5.1	5.4	2.3	1.4	2.4	3.2	2.3	2.7	3.1
Cibicidoides bradyi	0.4	0	1.8	0	0.5	0.5	0	0	0	0	0.5	0.3
C. mundulus	0	0.9	0.4	0	0	0	0	0	0.2	0.6	0.5	0.3
C. spp.	0.4	0.9	2.1	0.5	0.5	0.5	0	0	0.5	1.3	1.1	0.6
Planulina wuellerstorfi	0.4	0	1.1	0	0	0.5	0	0.5	0.7	1	0	0.6
Osangularia culter	0	0	0	0	0	0	0	0	0	0	0	0
Laticarinina pauperata	0	0	0.4	0	0	0	0.5	0	0.5	0	0	0.3
Valvulineria laevigata	0	0	0	0	0	0	0.5	0	0	0	0.5	0
Sphaeroidina bulloides	0.8	1.4	0	0	0	0	0	0	0	0	1.1	0
Pullenia bulloides	2.1	0	0.7	1.4	1.8	1.8	0.5	0	0.7	0.6	3.7	1.5
P. quinqueloba	1.2	0	1.4	2.3	1.8	3.2	0.5	0.5	1	0	0	0.3
Nonion sp.	2.1	1.9	3.9	5.1	3.6	5	3.8	2.9	3.4	6.4	1.6	5
Melonis pompilioides	0	0	0	0	0	0	0	0	0	0	0	0
M. barleeanum/affinis	0.4	0	0	0	0	0	0	0.5	0	0.3	0.5	1.2
Nonionella sp. A	0.8	0.5	0.4	0	0.9	0.9	0	0.5	1	0.3	0	0.9
Astrononion echolsi	2.1	0	0.4	0.9	2.3	0	0.9	0	0.2	0.6	1.6	1.2
Anomalina sp.	0	0	0	0	0	0	0	0	0	0	0.5	0
Globocassidulina subglobosa	21.2	7.1	36.2	19.1	15.3	22.2	27.7	20.6	13.4	15.4	12.8	17.3
Cassidulina laevigata	0	0	0	0	0	0	0	0	0	0	0	0
Rectuvigerina compressa	0.4	1.4	0.7	1.4	0.9	0.5	0	0.5	0.7	1	0	0
Uvigerina perigrina	0	0.9	0	1.4	0	0.5	0	2.9	1.2	0	0.5	0.3
U. hispida	0	0	0	0	2.3	0	0	0	0	0.3	1.1	0
Bulimina alazaensis	1.2	0	0	0	0.5	0	0	0	0	1.3	0.5	0
B. cf. alazaensis	1.2	6.1	0.7	1.9	0.9	0	2.3	1	1.2	1	0	1.9
B. mexicana	0	0	0	0.5	0	0	0	0	0	0.6	0	0
B. elongata	0	0	0	0	0	0	0	0	0	0	0	0
Globobulimina auriculata	0.4	0	0	0	0	0	0	0	0	0	0.5	0
Bolivina pseudopunctata	0	0	0.7	0.5	0	1.4	0	0	0.5	0.6	1.1	0
B. inflata	0.4	0	0	0.5	0	0.5	0	0.5	0.2	0	0	0.3
B. pygmaea	4.6	9	3.9	4.7	4.5	0.5	1.9	6.2	8.5	4.2	5.9	5.6
B. subaenariensis	0.4	0.5	1.4	0	0	0	0.5	0	0.5	0	0.5	1.9
B. albatrossi	0	0	0	0	0	0	0	0	0	0	0	0
B. lowmani	0	0	0	0	0	0	0	0	0	0	0	0
Bolivinita truncta	0	0	0	0	0	0	0	0	0	0	0	0
Stilostomella antillea	2.5	1.9	1.8	2.3	1.8	3.2	2.3	3.8	4.1	2.3	2.1	4.3
S. sp.	0.4	0.9	0.7	0.9	1.8	0.9	0	0.5	0.2	0	3.2	5
Pleurostomella spp.	0	0.9	0.4	1.4	2.3	0.5	1.4	0	0.5	0.6	0	0.9
Tosaia hanzawai	0	0.9	2.5	2.3	2.7	4.1	0.9	1	1.5	0.6	1.6	0.9
Trifarina angulosa	2.5	1.9	0.4	3.3	4.5	2.7	2.3	2.9	2.2	1.3	1.1	0.3
Unidentified triserial forms	0	0	0	0	0.9	0	0	0	0	0	0.5	0.3
Ehrenbergina trigona	2.1	1.9	2.8	2.3	1.8	1.8	3.3	2.4	2.4	1.9	1.6	1.5
Fursenkoina fusiformsis	0	0	0	0	0	1.4	0.5	0.5	1.2	0.3	0	0
Lagena spp.	2.9	0.5	1.1	0	1.4	0.5	1.4	0	1	1	1.1	0.9
Fissurina spp.	2.5	0	1.1	0.9	0.9	0	2.3	1.9	0.7	0.3	2.1	2.5
Dentalina communis	0.4	0	0	0	0	0	0.5	0	0	0	0.5	0
Nodosaria sp.	0.4	0	0	0	0	0.5	0.9	0	0.2	0	0	0
Quinqueloculina spp.	0	0	0	0	0	0	0	0	0.2	0.6	0	0
Pyrgo spp.	0	0	0	0	0	0	0	0	0	0	0	0
Oolina spp.	0.4	0.5	0.7	0.5	0.5	0	0	1.4	0.7	1.6	1.1	0
Siphonina tenuicarinata	0	0	0	0	0	0	0	0	0	0	0	0
Seabrookia earlandi	0	0	0.4	0	0.5	0	0	0	0	0	0	0.3
Sigmoilina tenuis	0	0	0	0.5	0	0	0	0.5	0	0	0	0
Guttulina sp.	0	0	0	0.5	0.5	0.5	0	0.5	0.2	0	0	0
Lenticulina spp.	0	0	0	0.5	0.5	0	0	0	0.2	0	0	0.3
Reussella spinulosa	0	0	0	0	0	0	0	0	0	0	0	0
Sigmoilopsis schlumbergeri	0.4	0	0	0	0	0	0	0	0	0.6	0	0
Siphotextularia rolshauseni	0.4	1.9	0.7	1.9	1.8	0	1.9	0	0	1	0.5	0.9
Vulvulina spinosa	0	0	0	0	0	0	0	0	0	0	0	0
Spiroplectammina sp.	0	0	0	0	0	0	0	0	0.5	0	0	0

Site 552A Cores	32-4	33-1	33-2	33-3	33-4	33cc	34-1	34-2	34-3	34-4	34cc
Intervals	30-34	112-116	90-94	63-67	14-18	10-14	104-108	115-119	102-106	20-24	10-14
Depth (m in subbottom)	153.3	154.62	155.9	157.13	158.14	158.38	159.54	161.15	162.52	163.2	163.55
Number picked	441	168	193	280	223	226	319	331	381	393	279
% benthics of total fauna	2.6	2.2	1.9	2.6	2.6	2.1	3.2	2.7	1.4	1.6	1.1
Number per cc	2822	2150	4940	7168	2856	2892	4083	4236	4876	5030	3568
Epistominella exigua	15.6	11.3	23.3	17.1	14.8	20.4	16.6	14.8	9.2	9.9	11.8
Nuttallides umbonifera	6.1	1.2	0.5	0.7	0	0.4	2.2	1.2	1.3	1.8	1.1
Eponides polius	2.9	0.6	2.6	0.4	2.7	0.9	3.8	2.1	3.4	1.8	2.9
E. tumidulus	1.8	3	1.6	2.5	1.8	3.5	1.3	1.2	1.6	1.8	3.2
E. weddellensis	9.1	9.5	10.9	14.3	19.7	11.1	11.9	10.3	5.5	13	5
E. ? sp. A	0	0	0	0	0	0	0	0	0	0	0
Gyrcidina soldanii	2.7	3	2.1	4.3	4.9	3.1	4.7	3.3	6.6	2.8	3.2
Heronallenia crosbyi	0	0	0	0	0	0	0	0	0	0.5	0
Oridorsalis umbonatus	3.9	1.8	2.6	2.9	1.3	2.7	2.8	3.9	5.8	3.8	9.3
Cibicidoides bradyi	0	0.6	0.5	0	0.9	0.4	0	1.5	0.5	0	3.2
C. mundulus	0.5	0	0	0.7	0	0.9	0.3	0.3	0	0.8	0.4
C. spp.	0.7	0	0.5	0.7	0.9	1.3	0.6	1.8	0	0.3	3.6
Planulina wuellerstorfi	0	0	0	0.7	0	0.9	0	0.6	0.8	2.3	1.1
Osangularia culter	0	0	0	0	0	0	0.6	0	0	0	0
Laticarinina pauperata	0 2	0	0	0.4	0	0	0	0	0	0.5	0.7
Valvulineria laevigata	0	0	0	0	0	0	0	0	0	0	0
Sphaeroidina bulloides	0	0	0	0	0.4	0	0	0	1.3	0	0
Pullenia bulloides	2	2.4	2.6	1.8	2.2	3.1	2.8	1.8	5.5	2.5	6.8
P. quinqueloba	1.4	0	0	0.4	1.3	1.3	2.2	0.6	1.3	2.8	10
Nonion sp.	3.4	2.4	0	0	0.4	0	0	1.8	1	0	0
Melonis pompilioides	0	0	0	0	0	0	0	0	0	0	0
M. barleeanum/affinis	1.8	3.6	0.5	2.5	6.3	4	4.1	3.3	3.1	4.6	0
Nonionella sp. A	0.5	0.6	0.5	0	1.3	0.4	1.9	0.3	1	1.5	1.8
Astrononion echolsi	0.7	3.6	0	6.8	2.7	3.5	1.9	0.3	4.7	1	0
Anomalina sp.	0	0	0	0	0	0	0	0	0	0	0
Globocassidulina subglobosa	15.2	25.6	16.1	14.6	14.8	16.8	16.9	21.5	21	21.6	12.5
Cassidulina laevigata	0	0	0	0	0	0	0	0	0	0	0
Rectuvigerina compressa	2	1.8	2.1	2.5	0.9	0.4	1.9	0	0	0	0
Uvigerina perigrina	1.1	0	0	0.4	0	0	0	0	0	0	0
U. hispida	0.2	0	0	0	0	0	0	0	0	0	0
Bulimina alazaensis	1.1	1.2	0	0.4	0.9	0	0	0	0	0.5	0
B. cf. alazaensis	0.7	1.2	1	0	0	0.9	0.3	0	0	0.3	0
B. mexicana	0.2	0	0	0	0	0	0	0.3	1.3	0.5	0.7
B. elongata	0	0	0	0	0	0	0	0	0.3	0	0
Globobulimina auriculata	0	0	0	0	0	0	0	0	0	0	0
Bolivina pseudopunctata	0	0	0	1.4	0.9	0	0.3	0.9	2.9	0	0
B. inflata	0	0.6	1	0.4	0	0.4	1.3	0.6	0	0	1.1
B. pygmaea	8.8	10.7	11.4	13.2	5.4	5.3	4.1	4.5	2.9	5.6	5.4
B. subaenariensis	0.2	0	0	0.4	0.4	2.7	3.1	0	0.5	0.5	0.4
B. albatrossi	0	0	0	0	0	0	0	0	0	0.5	0
B. lowmani	0	0	0	0	0	0	0	0	0	0	0
Bolivinita truncta	0	0	0	0	0	0	0	0	0	0	0
Stilostomella antillea	2.3	1.8	1	3.2	1.3	3.1	1.6	3	1.8	2.8	1.1
S. sp.	0	0	2.6	0	1.8	3.5	0.6	3.3	2.1	0	3.2
Pleurostomella spp.	0.5	0.6	0.5	0	0	0.4	0	0	1.8	1	3.2
Tosaia hanzawai	0.2	1.2	2 1	0	1.3	0.4	0.6	1 2	0	1	0.7
Trifarina angulosa	2.5	1.2	0.5	0	1.8	1.3	0.3	1.5	2.1	1.5	2.2
Unidentified triserial forms	1.6	0	0	0	0	0	0	0	0	0	0
Ehrenbergina trigona	1.4	0.6	3.6	2.9	0.4	1.3	1.9	1.8	0.5	0.3	0.7
Fursenkoina fusiformsis	1.4	0	2.1	0	0	0	1.3	0.3	0	0.3	0
Lagena spp.	0.9	0.6	0.5	0.7	0.9	0	1.3	0.3	1.6	1.5	0.7
Fissurina spp.	0.7	1.8	1.6	0.7	0.4	0.9	0.6	0.3	1.6	1	0.4
Dentalina communis	0	0	0	0	0.9	0	0	0.9	0.3	0.3	0
Nodosaria sp.	0.7	0	0	0.4	1.8	0.9	0	0	0.3	0.8	0.4
Quinqueloculina spp.	0	0	0	0	0	0	0	0	0	0	0
Pyrgo spp.	0	0	0	0	0	0	0	0	0	0	0
Oolina spp.	0.2	0	0	0	0.4	1.3	0	0	0.3	0	0
Siphonina tenuicarinata	0	0	0	0	0	0	0	0	0	0	0
Seabrookia earlandi	0	0	0	0	0.4	0	0	0	0	0	0
Sigmoilina tenuis	0.5	0	0	0	0	0.4	0	0	0	0	0.4
Guttulina sp.	0.2	0	0	0	0.4	0	0	0	0	0	0
Lenticulina spp.	0.5	0	0.5	0	0	0	0.3	0	0	0	1.1
Reussella spinulosa	0	0	0	0	0	0	0	0	0	0	0
Sigmoilopsis schlumbergeri	0	0	0	0	0	0	0	0.3	0	0	0
Siphotextularia rolshauseni	0	1.8	0	0	0.4	0.9	0 3	0	0.5	0.3	0
Vulvulina spinosa	0	0	0	0	0	0	0	0	0	0	0
Spiroplectammina sp.	0	0	0	0	0	0	0	0.5	0.3	0	0

Appendix C

Table of benthic foraminifera from DSDP Site 608

Site 608 Cores	12-2	12-4	12-6	13-1	13-3	13-5	14-1	14-2	14-4	14cc	15-1	15-2	15-3
Interval	80-84	80-84	120-124	80-84	90-94	90-94	80-84	90-94	90-94	10-14	100-104	90-94	80-84
Depth (m subbottom)	105.3	108.3	111.7	113.4	116.5	119.5	123	124.6	127.6	130.44	132.8	134.2	135.6
Number picked	240	217	183	184	213	267	191	211	317	343	202	280	219
Number per cc	384	347	292	294	341	427	305	675	507	548	323	448	350
% benthics of total fauna	0.6	0.4	0.7	0.7	0.7	0.8	0.3	0.6	0.6	0.9	2.7	1.2	0.6
% fragment of total planktics	15.1	3.1	12.5	6.7	11.3	13.2	13.5	34.4	23.8	28.1	52.5	42.2	27.3
Lenticulina spp.	0	0	0	0	0.5	0	0.5	0	0.3	0.3	0	0	0
Melonis barleeanum/affinis	6.3	6.9	7.7	3.8	2.3	1.9	6.3	3.8	1.6	1.7	4	2.9	2.7
M. pompilioides	0.4	0	0	0	0	0.4	0	0.5	0	0	0.5	0.7	0
Pullenia quinqueloba	0.8	1.8	2.7	0.5	3.3	3.7	4.7	0.5	3.2	2	1.5	3.6	2.7
P. bulloides	5.8	3.2	1.6	2.2	4.7	3.7	4.2	2.4	2.2	2.3	0.5	1.8	1.4
Pullenia sp.	0	0	0.5	0	0	0	0	0	0	0	0	0	0
Nonion sp.	0	0	0.5	0	0	0	0	0.9	0.3	0.6	0	0.7	0
Nonionella sp. A	0.4	0	0	0	0	0	0	0	0	0.6	0	0	1.4
Astrononion echolsi	1.3	0.9	0.5	0.5	1.4	0	2.6	0	0	0	1	0.7	0.5
Anomalina sp.	0	0	0	0	0	0	0	0	0	0	0	0	0
Cibicidoides bradyi	0.8	0	0	0	0	0.4	0	1.4	0	0.3	0	0	0
C. mundulus	0.8	2.3	2.7	1.6	1.9	0.4	6.3	3.8	3.1	1.2	5.4	2.9	0
C. spp.	0	0	0	0.5	0	0	0	0	0	0	0	0.4	0.5
Planulina rugosa	0	0	0	0	0	0	0	0	0	0	0	0	0
Planulina wuellerstorfi	2.1	1.8	2.2	0.5	1.4	1.5	0	0.5	0.9	0.6	0.5	0.7	0.5
Nuttallides umbonifera	5	6.5	9.9	7.6	7.5	2.2	2.6	3.3	5	3.2	6.9	3.6	5
Oridorsalis umbonatus	7.9	7.4	7.1	4.3	4.7	6.4	4.2	6.6	7.6	3.5	7.4	12.9	4.1
Sphaeroidina bulloides	0.4	0.5	1.1	0	0	0.7	0.5	0.9	0	0	0.5	0.4	0
Laticarinina pauperata	0	0	0.5	0	0	0	0	0	0.3	0	0.5	0.4	0
Gyroidina spp.	1.7	3.2	4.9	3.3	1.4	3	6.3	4.7	3.2	4.1	4.5	3.6	4.6
Epistominella exigua	10.4	4.1	4.9	19	23	16.1	18.3	10.9	6	14.3	8.9	15.4	18.6
Eponides polius	2.5	0.9	0	1.1	0.5	2.6	0	0.9	4.1	1.2	1	6.1	0.9
Eponides weddellensis	7.9	6.5	7.7	12.5	6.1	16.5	7.8	15.6	13.6	15.2	22.3	9.6	21.9
E. tumidulus	0.4	0.5	2.2	1.1	1.9	0.9	1	1.4	1.2	2.6	1	2.7	4.1
Eponides? sp. A	0	0	0	0	0	0	0	0	0	0	0	0	0
Heronallenia crosbyi	0	0	0	0	0.5	0.4	1	0	0.6	0	0	0	0.5
Valvulineria laevigata	0	0	0	0	0	0	0	0	0	0	0	0	0
Globobulimina auriculata	0	0.9	0	0	0	0	0.5	0	0.3	0	0	0	0
Bulimina mexicana	0	0	0	0	0	0	0	0	0	0	0	0	0
B. alazaensis	0	0	0	0.5	0	0	0.5	0	0	0.3	0	0	0.5
B. tessellata	0	0	0	0	0	0	0	0	0	0	0	0	0
B. sp.	0	0	0	0	0	0	0	0	0	0	0	0	0
Uvigerina hispida	0	0	0	0	0	0.2	0	0.2	0.4	0.3	0	0.4	0
U. peregrina	0	0	0	0	0	0	0	0	0	0	0	0	0
U. sp.	0	0	0	0	0.4	0	0	0.3	0.3	0	0	0	0
Rectuvigerina compressa	0.4	0	0.5	1.6	0	0	0.5	0	0.6	0	0	0	0
Globocassidulina subglobosa	20.4	29.5	21.4	21.2	14.6	21.7	17.2	16.6	15.5	29.4	16.3	13.6	15.5
G. sp.	0	0	0	0	0	0	0	0	0	0.6	0	0	0
Cassidulina reniforme	0.8	1.3	1.6	0.5	2.3	2.2	2.1	2.4	2.2	0.6	0.5	0.7	0.5
C. ? sp.	0	0	0	0	0.5	0	0	0	0.3	0	0	0.4	0
Cassidulinoides tenuis	0.8	0.5	0	0	0.9	0	1	0.9	0.9	2	2.5	0	0
Trifarina angulosa	0	0	0	0	0	0	0	0	0	0	0	0.4	0
Ehrenbergina trigona	0.8	0	1.1	0	1.9	0.4	0	0	0	0.3	0	0.7	0.9
Bolivina pygmaea	0.4	3.7	1.6	1.6	0.9	0	0	2.4	0	0.3	1	1	0
B. pseudopunctata	0	0.5	1.1	0	0	0.4	0	2.4	4.1	0	1	0.4	0
B. inflata	0	0	0	0	0	0.4	0.5	0.5	0	0	0	0	0
B. sp.	0	0	0	1.6	0	0	0	0	0	0	0	0	0
Hopkinsina pacifica	0	0	0	0	0	0	0	0	0	0	0	0	0
Lagena spp.	1.3	2.8	2.2	1.1	0.9	0.5	2.1	0	0	1.2	2.5	2.1	1.4
Fissurina spp.	2.6	4.6	2.7	2.7	3.8	4.1	1	4.2	3.2	1.4	3	3.2	3.2
Oolina spp.	1.7	0.9	1.1	2.2	3.3	0.9	2.1	2.4	2.2	1.7	0.5	2.7	0.5
Fursenkoina fusiformis	0	0.9	1.1	1.6	1.9	1.2	0.5	0	1.2	0.3	0.3	0	0.5
Unidentified serial form	0	2.3	2.7	1.1	0	0.9	0	2.9	2.5	1.2	0	0.7	2.3
Tosaia hanzawai	1.7	0.9	1.6	0	1.4	1.2	0.5	0.5	2.5	2.3	0.5	1.1	0.9
Nodosaria sp.	0	0	0	0	0	0	0	0	0	0	0	0	0
Stilostomella antillea	0.4	0.5	0	1.1	0.9	1.2	0.5	0.5	1.6	0.3	0.5	0.7	0
Pleurostomella alternans	0	1.4	0.5	0.5	0	0	1	0.5	0	1.2	0.5	1.8	0.9
Dentalina communis	0	0	0	0	0	0	0	0.5	0	0	0	0	0
Amphycoryna scalaris	0	0	0	0	0	0	0	0	0	0	0	0	0
Pyrgo spp.	0.8	0	0.5	0.5	0	0.9	0	0.5	0	0	0	0	0
Pyrulina sp. A	0.8	0	0.5	0	0	1.2	0.5	0	1.2	0.6	0	0.7	0
Quinqueloculina spp.	2.9	1.8	0.5	2.2	3.3	1.2	0.5	0.9	1.6	2	1	0.7	2.3
Sigmoilina tenuis	0	0	0	0	0	0.7	2.1	1.9	0.3	0.3	0.5	0.4	0.5
Martinottiella communis	0	0	0	0	0	0	0	0	0	0	0	0	0
Karreriella bradyi	0	0	0.5	0.5	0.5	0	0	0.5	0	0	0	0	0
Textularia sp.	0	0.5	0	0	0	0	0	0	0	0	0	0	0
Siphotextularia rolshauseni	0	0	2.2	0.5	0.9	0	1	0.9	1.9	0.9	3	0.4	0.9
Vulvulina spinosa	0	0	0	0	0	0	0	0	0	0	0	0	0

Site 608 Cores	15-4	15-5	15-6	15cc	16-1	16-2	16-3	16-4	16-5	16-6	16cc	17-1	17-2
Interval	80-84	80-84	80-84	10-14	80-84	90-94	80-84	110-114	90-94	90-94	10-14	90-94	90-94
Depth (m subbottom)	137.1	138.6	140.1	140.8	142.2	143.8	145.2	147	148.3	149.8	150.86	151.9	153.4
Number picked	215	130	212	147	236	182	239	290	219	204	296	282	214
Number per cc	344	208	339	235	377	291	382	464	350	318	236	225	684
% benthics of total fauna	0.9	0.5	1.1	0.4	0.9	0.7	1.1	1.5	2.2	2.2	1.9	1.4	1.9
% fragment of total planktics	39.4	27.2	45.5	21.6	22.2	24.7	29.6	35.3	47.6	43.2	41.9	34	42.7
Lenticulina spp.	0	0	0	0	0.4	0.5	0	0.3	0	0	0	0	0
Melonis barleeanum/affinis	5.1	1.5	3.8	4.8	5.1	3.8	4.2	1.7	3.7	2.9	5.1	1.1	2.3
M. pompilioides	0.5	0	0.9	0.7	2.1	0	0	0.7	0	1.5	0.7	0	0.5
Pullenia quinqueloba	1.9	3.8	4.7	10.2	3.4	3.8	3.8	7.6	6.8	7.4	8.1	3.5	3.7
P. bulloides	2.8	2.3	0.9	2.7	3	1.6	2.5	3.1	2.7	2	2.4	2.1	4.7
Pullenia sp.	0	0	0	0	0	0	0	0	0	0	0	0	0
Nonion sp.	0.5	0	0	0	0.4	1.1	0.4	0.3	0.9	0	0.5	0.4	0.5
Nonionella sp. A	0	0	0	0	0	0.5	0	1	0	0	0	0	0
Astrononion echolsi	0.5	0.8	0	0	0	0	0.4	0.3	0	0.5	0.7	1.4	0.5
Anomalina sp.	0	0	0	0	0	0	0	0	0	0	0	0	0
Cibicidoides bradyi	0	0	0	0	0	0	0	0.7	0.5	0	0.4	0	0
C. mundulus	1.9	0	1.9	0	0.4	2.2	3.8	1.7	0.5	0.5	0.7	0.4	0.5
C. spp.	0	0	0	0	0	0	0.4	0	0	0	0	0	0.5
Planulina rugosa	0	0	0	0	0	0	0	0	0	0	0	0	0
Planulina wuellerstorfi	0.9	0	0.5	0.7	0	0.5	0.4	0.7	0.9	0	0	0.4	0
Nuttallides umbonifera	4.2	2.3	0.9	3.4	2.5	0	3.4	2.8	2.7	2.6	1.3	3.5	0.5
Oridorsalis umbonatus	4.6	3.8	6.1	4.8	5.9	5.5	6.7	3.8	5.5	5.9	3.1	8.5	3.7
Sphaeroidina bulloides	0	0	0	0	0.8	0	0	0.3	0	0	0	0	0
Laticarinina pauperata	0	0	0	0	0.8	0.5	0	0	0.5	0	0.3	0.4	0
Gyroidina spp.	4.2	3.1	5.7	4.8	5.1	3.8	5.9	2.8	6.4	5.4	2	4.6	2.8
Epistominella exigua	9.3	4.6	6.1	8.2	10.2	4.3	9.2	4.1	11	11.8	16.6	13.8	13.6
Eponides polius	1.4	1.5	2.8	2.7	4.2	1.1	2.5	1.7	0.9	1.5	0.7	0.4	0.5
Eponides weddellensis	11.2	13.8	12.7	6.8	11.4	11.5	17.6	26.9	16	17.6	7.8	18.9	20.1
E. tumidulus	0	2.3	2.8	1.4	1.7	2.2	2.1	2.4	1.4	1	1.7	2.1	1.4
Eponides? sp. A	0	0	0	0	0	0	0	0	0	0	0	0	0
Heronallenia crosbyi	1.9	1.5	0.5	0	0.4	0	0	0	1	0	0	0	0
Valvulineria laevigata	0	0	0	0	0	0	0	0	0	0	0	0	0
Globobulimina auriculata	0.5	0.8	0	0	0	0.5	0.4	0	0	0	0.3	0	0
Bulimina mexicana	0	0	0	0	0	0	0	0	0	0	0	0	0
B. alazaensis	0	0	0.5	0	0	0	0	0	0	0	0	0	0
B. tessellata	0	0	0	0	0	0	0	0	0	0	0	0	0
B. sp.	0	0	0	0	0	0	0	0	0	0	0	0	0
Uvigerina hispida	0.9	1.5	0.9	1.4	0	1.6	0.8	1	0.5	0	3	0.7	0
U. peregrina	0.5	0	0	0.7	0	0	0	0	0	0	0	0	0.5
U. sp.	0	0	0.5	0	0	0	0.4	0.7	0.5	1	0	0.7	0.9
Rectuvigerina compressa	0	0	0	1.4	1.3	0	0	0.3	1	0	0.7	0.7	0
Globocassidulina subglobosa	24.8	33.8	31.6	23.1	23.3	44.5	19.7	25.2	28.8	26	27	19.9	22.9
G. sp.	0	0	0	0	0	0	0	0	0	0	0	0.4	0
Cassidulina reniforme	0.5	3	0.5	3.4	0.4	0.5	0.8	0.7	0.9	1.5	3.1	1.1	2.8
C. ? sp.	0	0	0	0	0	0	0	0	0	0	0	0	0
Cassidulinoides tenuis	0.9	0	0	0	0	0	0.4	0.3	0	0	0.3	0	0
Trifarina angulosa	0	0	0	0	0	0	0	0	0	0	0	0	0.5
Ehrenbergina trigona	0	0	0	0	0	0	0.4	0.3	0	2	1	0.4	0.5
Bolivina pygmaea	1.4	1.5	0.5	0	0	0.5	0	0	1.4	0.5	2.3	3.2	3.7
B. pseudopunctata	0	0	0	0	0	0	0	0	0.9	0.5	0.3	0.4	0.5
B. inflata	0	0	0	0	1.3	0	0	0.3	0	0	0.3	0	0
B. sp.	0	0	0	0.7	0	0	0	0	0	0	0	0	0
Hopkinsina pacifica	0	0	0	0	0	0	0	0	0	0	0	0	0
Lagena spp.	3.7	4.6	1.9	3.4	1.3	1.1	1.2	0.7	0.5	2.5	0.7	0.7	2.8
Fissurina spp.	2.3	1.5	3.8	2.7	2.6	1.1	3.8	2.4	2.7	1.5	2.7	3.5	1.8
Oolina spp.	0.9	0	0.5	2.7	2.1	0	2.1	0.7	0.5	1	1	1.8	0.5
Fursenkoina fusiformis	1.4	1.5	0	0	0	0	0.8	0	0	0	0	0	0
Unidentified serial form	1.9	1.5	0.9	0	2.1	0	0.4	0.3	0	2	1	1.1	0
Tosaia hanzawai	1.4	2.3	2.4	1.4	2.1	2.2	0.8	1.7	0.9	1	1	0.4	1.4
Nodosaria sp.	0	0	0	0	0	0	0	0	0	0	0	0	0
Stilostomella antillea	1.4	1.5	0	2	0.4	0	0.4	0	0	0	0	0.4	0.9
Pleurostomella alternans	2.3	0	0.5	1.4	1.7	0	0.8	0.3	1.4	0	0.7	0.7	0.5
Dentalina communis	0.9	0	0	0	0	0	0	0	0	0	0.7	0	0
Amphycoryna scalaris	0.5	0	0	0	0	0	0	0	0	0	0	0	0
Pyrgo spp.	0	0	0	0	0.4	0	0	0.3	0	0	0	0	0
Pyrulina sp. A	0	0	0	0	0	0	0	0	0	0	0	0	0
Quinqueloculina spp.	3.7	2.3	2.4	2.7	1.3	2.7	2.9	0.3	0.5	0	0	1.4	0.9
Sigmoilina tenuis	0	0	0	0.7	0.4	0.5	0	1	0	0	1	1	0.9
Martinottiella communis	0	0	0	0	0	0	0	0	0.5	0	0	0	0
Karreriella bradyi	0	0	0	0	0	0	0.4	0	0	0	0	0	0
Textularia sp.	0	0	0	1.4	0	0	0	0	0	0	0	0	0
Siphotextularia rolshauseni	1.9	0.8	0.9	0.7	0.8	0.5	0.4	0.7	0.5	0.5	0.4	0.7	2.8
Vulvulina spinosa	0	0	0	0	0	0	0	0	0	0	0	0	0

Site 608 Cores	17-3	17-4	17cc	18-1	18-2	18-3	18-4	18-5	18-6	18cc	19-1	19-2	19-4
Interval	90-94	60-64	10-14	60-64	60-64	62-66	68-72	64-68	20-24	6-10	80-84	80-84	80-84
Depth (m subbottom)	154.9	156.1	156.4	157.1	158.6	160.12	161.68	163.14	164.2	164.73	166.9	168.4	171.4
Number picked	225	281	463	253	273	265	227	324	175	341	377	461	195
Number per cc	360	223	185	202	218	212	181	259	280	273	301	368	312
% benthics of total fauna	2.1	4.7	8.2	10.2	6.9	2.2	1.9	2.6	1.8	3.3	12.4	11.2	5.9
% fragment of total planktics	55.1	61.2	63.6	70.9	73.5	54	46.75	58.4	46.1	63.6	74	68.7	68.2
Lenticulina spp.	0	0.4	0.6	0	0.7	0	0.9	0.3	0	0	0.5	0	0.5
Melonis barlecanum/affinis	3.6	3.2	1.7	5.1	5.1	4.9	4.8	2.5	3.4	7.6	3.7	4.1	3.6
M. pompilioides	0	0.4	0	0.8	0.4	0	0	0.3	1.1	0.9	1.3	0.2	0
Pullenia quinqueloba	6.2	3.5	3.9	5.9	10.5	1.9	4.8	2.8	6.9	4.7	5.8	4.6	4.1
P. bulloides	3.1	2.5	1.7	7.9	3.3	5.7	12.8	7.1	3.4	6.7	3.2	4.1	6.7
Pullenia sp.	0	0	0	0	0	0	0	0	0	0	0	0	0
Nonion sp.	1.8	1.4	1.5	0	0.7	1.1	0.4	0	0.6	0	0	0	
Nonionella sp. A	0	0	0	0	0	0	0	0	0	0	0.3	0	
Astrononion echolsi	1.3	0	0.8	1.2	1.4	0.8	2.2	0.3	0	0.6	0.3	1.1	4.1
Anomalina sp.	0	0	0.2	0.4	0	0	0	0	0	0	0	0	0
Cibicidoides bradyi	0	0	0.2	0	0	0	0	0	0	0	0	0	0
C. mundulus	1.6	1	5.4	5.9	5.4	5.9	2.6	2.2	0	0.3	2.1	0.8	0
C. spp.	0	0	0.2	0	0	0	0	0.3	0	0	0.3	0.2	2
Planulina rugosa	0	0	0	0	0	0.4	0	0	0	0	0	0	0
Planulina wuellerstorfi	0	0	0.8	0	1.5	0.4	0	0.9	1.7	0	0.5	0.7	0
Nuttallides umbonifera	0.5	1.4	5	2	0.7	1.5	0.9	1.2	2.3	0.6	0.8	1.3	2.1
Oridorsalis umbonatus	5.8	12.8	5.6	5.9	10.5	5.3	6.6	9.6	6.3	6.7	6.9	5.2	3.6
Sphaeroidina bulloides	0	0.7	0.4	0	0	0	0	0	0	0.3	0	0	0
Laticarinina pauperata	0.5	0	0	0.8	0.4	0	0.9	0.3	0	0	0	0	0
Gyroidina spp.	4.9	3.2	5.8	2.8	2.2	2.6	3.5	2.8	1.7	2.9	1.6	2.2	4.1
Epistominella exigua	8	10.7	12.1	9.5	16.4	10.9	17	9	19.5	17.3	23.9	14.3	23.1
Eponides polius	2.2	0.4	1.7	2	1.1	0	0.4	3.7	1.7	1.7	4.8	2.6	0
Eponides weddellensis	11.6	18.5	10.8	9.5	3.6	12.1	3.1	1.5	4.6	4.1	4.2	15.4	20
E. tumidulus	0.9	1.8	1.9	0.4	1.8	1.1	0.9	2.2	0.6	4.1	2.9	2.4	3.1
Eponides? sp. A	0	0	0	0	0	0	0	0	0	0	0	0	0
Heronallenia crosbyi	0	0	0.2	0	0	0	0.9	0	0	0	0	0	0.5
Valvulineria laevigata	0	0	0	0	0	0	0	0	0	0	0	0	0
Globobulimina auriculata	0.5	0	0.2	0	1.1	0	0	0	1.1	0	0	0	0
Bulimina mexicana	0	0	0	0	0	0	0	0	0	0	0	0	0
B. alazaensis	0	0	0.2	0	0.4	0	0	0	0	0.3	0	0	0
B. tessellata	0	0	0	0	0	0	0	0	0	0	0	0	0
B. sp.	0	0	0	0	0	0	0	0	0	0	0	0.2	0
Uvigerina hispida	0	0	0	0	0	0	0	0	0	0	0	0	0
U. peregrina	0	0	0	0.4	0	0	0	0	0	0.3	0.5	0	0
U. sp.	0	0.7	0.2	0.4	0	0	0	0	0	0	0.3	0	0
Rectuvigerina compressa	0.9	0	0.2	0	0.4	0.8	0.9	0	0	0.6	1.3	0.4	0
Globocassidulina subglobosa	38.2	17.8	24.6	28.5	23.6	24.2	27.3	33.3	21.8	25.5	26	32.1	11.8
G. sp.	0	0	0	0	0	0	0	0.6	0	0	0	0	0
Cassidulina reniforme	3.1	0	0.4	0.8	0.7	0.8	1.3	3.4	1.7	1.5	0.5	1.3	0.5
C. ? sp.	0	0	0	0	0	0	0	0	0	0.3	0	0	0
Cassidulinoides tenuis	0	0.4	0	0	0	0	0	0	0	0	0	0	0
Trifarina angulosa	0	0	0	0	0	0	0	0	0	0	0	0	0
Ehrenbergina trigona	0.9	0.4	0.4	0.5	1.1	1.9	1.3	1.5	0	1.5	1.1	0.7	1.5
Bolivina pygmaea	0	1.1	0.6	0	0.4	0.8	0.9	1.5	4	2.6	1.1	0.4	0
B. pseudopunctata	0	0	4.5	0.8	0.4	0	0.9	0	0.6	0	0	0.2	0
B. inflata	0	0	0	0	0	0	0	0	0	0	0	0	0
B. sp.	0	0	0	0	0	0	0	0.6	0	0	0	0	0
Hopkinsina pacifica	0	0	0	0	0	0	0	0	0	0	0	0	0
Lagena spp.	1.8	1.4	1	0.8	0.7	0	1.8	1.9	2.2	1.7	0.8	1.1	2.1
Fissurina spp.	0.9	2.1	2.6	1.6	1.8	0.4	1.3	2.8	1.7	1.2	1.6	1.3	1
Oolina spp.	0.5	1.1	0.9	1.6	0.4	1.1	0.9	2.8	2.9	0	0.3	0	1.5
Fursenkoina fusiformis	0	0	0	0	0	0	0.9	0	0	0	0.8	0	0
Unidentified serial form	0	1.4	1.3	1.6	0.4	0.4	0	0	2.9	0.9	0.3	0.6	1
Tosaia hanzawai	0.9	1.4	0.6	0	0.4	1.1	1.3	1.2	0.6	0	0	0.2	0
Nodosaria sp.	0	0	0	0	0	0	0	0	0	0	0	0	0
Stilostomella antillea	0.5	1.1	0.6	0	0	1.5	1.3	1.2	1.1	0.9	1.3	1.1	0.5
Pleurostomella alternans	0	0.7	0.4	0.8	0.7	1.1	0	0	1.1	0.6	0	0.4	1
Dentalina communis	0	0	0	0	0	0	0	0.6	0	0.6	0	0	0
Amphycoryna scalaris	0	0	0	0	0	0	0	0	0	0	0	0	0
Pyrgo spp.	0	0	0.4	0	0	0.4	0	0	0	0	0	0	0
Pyrulina sp. A	0	0	0	0	0	0	0	0	0	0	0.3	0.2	0.5
Quinqueloculina spp.	0	2.5	1.1	1.2	1.1	1.1	1.8	0.6	1.1	2	0	0	0.5
Sigmoilina tenuis	0	0.4	0	0	0	0	0	0.6	0.6	0.3	0	0	0
Martinottiella communis	0	0	0	0	0	0	0	0	0	0	0	0	0
Karreriella bradyi	0	0	0	0	0	0	0	0	0	0	0	0	0
Textularia sp.	0	0.4	0	0	0	0	0	0	0	0	0	0	0
Siphotextularia rolshauseni	0.9	0	0.6	0.4	0.7	0	0	0.9	1.1	0.6	0.8	0.4	0.5
Vulvulina spinosa	0	0	0	0	0	0	0	0	0	0	0	0	0

Site 608 Cores	19-5	19-6	19cc	20-1	20-2	20-3	20-4	20-5	20-6	20cc	21-1	21-2	21-3
Interval	80-84	14-18	10-14	102-106	80-84	60-64	80-84	104-108	110-114	6-10	90-94	90-94	90-94
Depth (m subbottom)	172.9	173.74	174.2	176.72	178	179.3	181	182.74	184.3	184.9	186.2	187.7	189.2
Number picked	316	341	318	180	259	256	298	145	506	360	194	195	222
Number per cc	505	545	508	288	414	409	953	464	404	240	310	624	355
% benthics of total fauna	5.1	1.2	1	0.4	0.7	0.7	2.7	0.8	1.7	0.9	0.9	0.6	0.8
% fragment of total planktics	50.8	43.5	33.9	18.9	40.5	37.5	54.2	32.6	50.6	34.1	39.2	44	31.2
Lenticulina spp.	0.3	0	0.6	0	0.4	0	0	0	0.4	1	0	0	0
Melonis barleeanum/affinis	2.5	6.5	6.6	8.9	8.9	4.7	2	1.4	1.8	3.7	7.7	4.6	6.3
M. pompilioides	0.6	0.9	0	0	0	0	0.3	0.7	0	0	0	0	0
Pullenia quinqueloba	1.9	2.9	6.6	5.6	5.8	6.6	5.4	4.8	4.6	6	10.3	4.1	3.6
P. bulloides	3.2	3.5	4.4	3.9	4.6	4.7	2.7	6.9	6.1	6.3	3.1	5.1	6.3
Pullenia sp.	0	0	0	0	0	0	0	0	0	0	0	0	0
Nonion sp.	0	0	0	0.6	0	0	0.7	0	0	0	1	0	0
Nonionella sp. A	0	0	0	0	0	0	0	0	0.4	0	0	0	0
Astrononion echolsi	1.9	0.9	1.6	0.6	1.5	0.4	0.7	0.7	1.8	0.7	4.6	0.5	0.9
Anomalina sp.	0	0.3	0.9	0.6	0.8	0.8	0.3	0	0	0	0	0	0
Cibicidoides bradyi	0	0	0	0	0	0	0.7	0	0.4	0	0	0	0
C. mundulus	0	0	0	0	0	1.8	1.7	3.4	2	0.3	0.5	1	1.8
C. spp.	0.3	0	0	0	0	0	0	0.7	0.4	1.3	0	1.5	3.6
Planulina rugosa	0	0	0	0	0	0	0	0	0	0	0	0	0
Planulina wuellerstorfi	1	0.3	0.6	1.1	0.8	0.4	1.7	0	1.2	1.7	4.1	1	0
Nuttallides umbonifera	4.7	2.4	3.4	2.2	1.9	1.5	0.7	3.4	1.4	2.7	1	2	2.3
Oridorsalis umbonatus	5	6.5	6.9	4.4	9.3	5.5	8.7	3.4	7.3	5	5.2	5.1	7.2
Sphaeroidina bulloides	0.3	0	0	0	0	0	0.4	0	0	0	0.5	0	0
Laticarinina pauperata	0	0	0	0	0.8	0.4	0	0	0	0.3	0	0	0.9
Gyroidina spp.	4.7	4.1	4.7	2.2	3.1	6.6	7	4.8	4.2	5.6	2.6	3.6	1.8
Epistominella exigua	24.6	10.3	9.1	9.4	9.3	9.8	10.7	13.8	15	12.7	9.2	8.2	20.7
Eponides polius	4.4	1.8	1.6	3.3	2.7	3.1	2.3	1.4	1.4	4.3	1	0	0.9
Eponides weddellensis	13	11.4	10.1	6.7	5	6.6	6.4	11.7	10.7	8.7	2	14.4	6.3
E. tumidulus	4.1	2.1	1.9	2.8	1.5	2	0.3	3.4	1	3.3	4.1	3.1	5.4
Eponides? sp. A	0	0	0	0	0	0	0	0	0	0	0	0	0
Heronallenia crosbyi	0	0.6	0	1.1	0.4	0.8	0	0.7	0.6	0	0.5	0.5	1.8
Valvulineria laevigata	0	0	0	0	0	0	0	0	0.6	0	0	0	0
Globobulimina auriculata	0	0.3	0.6	0	0.8	0	1	0	0.2	0	0.5	0	0.9
Bulimina mexicana	0	0	0	0	0	0	0	0	0	0	0	0	0
B. alazaensis	0	0.3	0.3	0	0	0	0	0	0	0	0	0.5	0
B. tessellata	0	0	0	0	0	0	0	0	0	0	0	0	0
B. sp.	0	0	0	0	0	0	0	0	0	0.3	0	0.5	0
Uvigerina hispida	0	0	0	0	0	0	0	0	0	0	0	0	0
U. peregrina	0	0	0	0	0	0	0	0	0	0	0	0	0
U. sp.	0.6	1.8	0.9	0	0	0	0	0	0.2	0	0	0	0
Rectuvigerina compressa	0.3	0.3	0.3	0.6	0.4	2	1.3	1.4	0.4	0	0	0	0
Globocassidulina subglobosa	18.3	21.7	22.9	22.8	26.6	22.6	29.7	21.4	23.7	21.7	25.3	29.7	14.4
G. sp.	0	0.6	0	0	0	0	0	0	0	0	0	0.5	0
Cassidulina reniforme	0.6	0.9	1.3	0.6	1.9	0	0	0.7	0.4	2	2.1	3.1	0.5
C. ? sp.	0	0	0	0	0	0	0	0	0	0	0	0	0
Cassidulinoides tenuis	0	0	0	0	0	0	0	0	0.4	0	0	0	0
Trifarina angulosa	0	0	0	0	0	0	0	0	0	0	0	0	0
Ehrenbergina trigona	0.6	0.6	0.3	0	0.4	0.8	0.7	0	0.6	0.3	0	0	0
Bolivina pygmaea	1.3	1.5	0.6	0.6	0.8	0.4	1.7	0	1.8	2	1	1	0
B. pseudopunctata	0	1.2	0	0	0	0	0.3	0	2	1	0	0.5	0
B. inflata	0	0	0	0	0	0	0	0.7	0	0	0	0.5	0
B. sp.	0	0.3	0	0	0	0	0.3	0	0	0	0	0	0
Hopkinsina pacifica	0	0	0	0	0	0	0	0	0.8	0	0	0	0
Lagena spp.	0.3	1.2	2.2	1.7	1.9	3.9	0.7	2.1	1.2	1.3	2.6	1.5	1.4
Fissurina spp.	1.3	2.4	2.8	4.4	1.9	3.1	1.7	3.4	1.9	1.7	3.1	2	2.7
Oolina spp.	1.3	1.5	0.6	3.3	1.1	0.8	0	1.4	0.6	1	1	0	0
Fursenkoina fusiformis	0	0.9	0.3	0	0	0	0	0	0.4	0.7	0	0	0.9
Unidentified serial form	0.3	3.2	1.6	2.2	0.4	1.2	0	0	1.2	0.7	0.5	0.5	0.9
Tosaia hanzawai	0	2.1	1.9	1.1	1.9	2	2	2.1	0.4	1	1.5	1	0.9
Nodosaria sp.	0	0	0.6		0.4	0	0	0	0	0	0	0	0
Stilostomella antillea	0.3	0.9	0.6	0.6	0	2	1.7	0.7	0.6	0	1	1.5	0.9
Pleurostomella alternans	0.3	0.9	1.3	1.1	1.9	2.3	1	0.7	1.2	0.3	1.5	1	1.8
Dentalina communis	0	0	0	0	0	0	0	0.7	0.2	0	0	0	0.9
Amphycoryna scalaris	0	0.3	0	0	0	0	0	0	0	0	0	0	0
Pyrgo spp.	0	0	0	0	0	0	0	0	0.2	0	0	0	0
Pyrulina sp. A	0.9	0.6	0	3.9	0.8	0.8	0	0	0.4	0	0	0	0.9
Quinqueloculina spp.	0	0.3	0.6	2.2	0.4	0.8	0.3	0.7	0.6	1.7	1	0.5	1.4
Sigmoilina tenuis	0	1.5	0	0	0	0	1	0	0	0	0.5	0	0
Martinottiella communis	0	0	0	0	0	0	0	0	0	0	0	0	0
Karreriella bradyi	0	0	0	0	0	0	0	0	0	0	0	0	0
Textularia sp.	0.3	0.3	0.3	0	0	0.4	0	0	0	0	0	0	0
Siphotextularia rolshauseni	0.3	0.3	0	1.7	1.1	1.2	0.7	2.8	0.4	0.3	0	0.5	0.9
Vulvulina spinosa	0	0	0	0	0	0	0	0	0	0.3	0	0	0

Site 698 Cores	21-4	21-5	22-1	22-3	22cc	23-3	23cc	24-2	24cc
Interval	80-84	60-64	90-94	90-94	6-10	100-104	10-14	80-84	10-14
Depth (m subbottom)	190 6	191 6	195 8	198 8	202.9	208.5	214 12	216 4	219 7
Number picked	128	187	155	217	202	304	501	277	172
Number per cc	409	299	496	347	323	243	400	443	275
% benthics of total fauna	1	0 6	0 4	0 7	0.8	1 4	3 3	1 7	2 4
% fragment of total planktics	33 6	25 5	22 1	33 3	33 4	30 7	55 8	47 3	27 7
Lenticulina spp	0	1	1 3	0	0	0	0 2	0	0
Melonis barleeanum/affinis	6 3	4 3	3 9	10 1	8 9	6 3	6 9	0 4	15 7
M pompilioides	0	0	0	0	1	0 3	0	0	0
Pullenia quinqueloba	3 9	4 8	9	2.8	4	2.3	2	2 1	0 6
P bulloides	3 1	2 1	5 8	2 8	9 9	5 3	4 8	2 9	8 7
Pullenia sp	0	0	0	0	0	0	0	0	0
Nonion sp	0 8	0	0	0 9	2.5	2 6	0 6	0	0
Nonionella sp A	0	0	0	0	0	0	0 4	0	0
Astrononion echolsi	0	4 8	1 9	4 6	0	0	0	0	0
Anomalina sp	0	0	1 3	0	0	0	0	0 4	0
Cibicidoides bradyi	0 8	0	0 6	0 5	0	0	0	0	0
C mundulus	5 4	0	1 9	0	0	0 7	0 2	3 2	0
C spp	0	0	1 3	2 7	1	1 7	0 2	0	0
Planulina rugosa	0	0	0	0	0	0	0	0	0
Planulina wuellerstorfi	0 8	1 1	1 3	0	1	0 6	1 2	2 5	0 6
Nuttallides umbonifera	2.3	4 3	3 9	2.8	5	2	1 2	10 8	12.2
Oridorsalis umbonatus	3 9	3 2	5 2	10 6	3	10 2	7 4	10 5	4 6
Sphaeroidina bulloides	0	0	0 6	0	0 5	0	0 4	0	0
Laticarinina pauperata	0 8	0	0	0	0	0	0 2	0	0
Gyroidina spp	4 6	5 9	2.6	5 1	2 5	3 9	3 2	6 1	5 2
Epistominella exigua	7 8	5 3	9	12 9	16 8	14 8	16 2	13 4	4 6
Eponides polius	1 6	3 7	4 5	2 3	3	0 6	1 6	1 4	2 9
Eponides weddellensis	10 9	8 6	1 9	2 8	5	10 9	5 6	13 3	8 1
E tumidulus	3 9	7	3 2	3 6	4 5	1 6	2 4	1 8	2 9
Eponides? sp A	0	0	0	0	0	0	0 4	0	0
Heronallenia crosbyi	0	0	0 6	0 5	0	0 3	0 4	0	0 6
Valvulineria laevigata	0	0	0	0	0	0	0	0	0
Globobulimina auriculata	0	1 6	0	0 9	0	0	0	0	0
Bulimina mexicana	0	0	0	0	0	0	0 2	0	0
B alazaensis	0 8	0	0	0	0	0	0 2	0 7	0 6
B tessellata	0	0	0	0	0	0	0 4	0	0
B sp	0	0	0	0	0	0	0	0	0
Uvigerina hispida	0	0	0	0	0	0	0	0	0
U peregrina	0	0	0	0	0	0	0	0	0
U sp	0	0	0	0	1 5	0 3	4 3	0	0
Recluvigerina compressa	0	0	0	0 9	0	0 7	0	9	1 7
Globocassidulina subglobosa	28 9	23 1	25 8	17 5	17 3	18 1	26 7	10 1	18 6
G sp	0	0	0	0	0	0	0	0	0
Cassidulina reniforme	0 8	0	0	0 9	0 5	2	0 4	0	0
C ? sp	0	0	0	0	0	0	0 2	0	0
Cassidulinoides tenuis	0	0	0	0 5	0	0 6	0 6	0 4	0
Trifarina angulosa	0	0	0	0	0	0	0	0	0
Ehrenbergina trigona	0 8	0	0 6	0	0 5	1	0	0	0
Bolivina pygmaea	1 6	0 5	1 3	1 4	2	3	2 2	2 1	1 7
B pseudopunctata	0	0	0	0	0	0	0	0	0
B inflata	0	0	0	0	0	0 6	0	0	0
B sp	0	0	0	0	0	0	0 4	0	0
Hopkinsina pacifica	0	0	0	0	0	0	0	0	0
Lagena spp	1 6	4 2	1 9	1 4	0 5	2 3	0 8	2 1	2 3
Fissurina spp	3 1	2 7	3 2	2 8	3 5	1 3	1	1 4	1 2
Oolina spp	0	0	0 6	1 8	0 5	1 3	0	1 4	0
Fursenkoina fusiformis	0	0	0 6	1 8	0	0	1 3	0	0
Unidentified serial form	0	1 6	1 9	0 5	0 5	0 3	0	0	2 3
Tosaia hanzawai	1 6	3 2	0	0 9	0 5	1	1 6	1 8	0 6
Nodosaria sp	0	0	0	0	0	0	0	0	0
Stilostomella antillea	1 6	0 5	0	1 8	0 5	0 6	1	0	0
Pleurostomella alternans	0	0	0 6	1 4	2 5	0 6	0 7	0	1 2
Dentalina communis	0	0	0	0	0	0	0 4	0	0 6
Amphycoryna scalaris	0	0	0	0	0	0	0	0	0
Pyrgo spp	0	1 1	0	0	0	0	0	0	0
Pyrulina sp A	0	0 5	0	0	0	1	0	0	1 2
Quinqueloculina spp	0	2 2	3 2	0	0	0 3	0 4	0	0
Sigmoilina tenuis	0 8	0	0	0 5	0	0	0	0	0
Martinottiella communis	0	0	0	0	0	0	0	0	0
Karreriella bradyi	0	0	0	0	0	0 3	0	0	0
Textularia sp	0	0	0	0	0	0	0	0	0
Siphotextularia rolshauseri	1 6	0 5	1 9	0 5	0 5	0 6	0 4	0	0 6
Vulvulina spinosa	0	0	0	0	0	0	0	0	0

Appendix D

Benthic foraminiferal oxygen and carbon stable isotopes
from DSDP Site 608

Benthic foraminiferal stable isotopes from DSDP Site 608

Sec.	Core	Interval (cm)	Depth (m)	$\delta^{18}O$ (‰)	$\delta^{13}C$ (‰)	Species
11	4	80-84	98.7	2.21	0.68	wuellerstorfi
12	2	80-84	105.3	2.3	0.46	wuell
12	4	80-84	108.3	2.26	0.58	wuell
12	6	120-124	111.7	2.35	0.58	wuell
13	1	80-84	113.4	2.3	0.7	wuell
13	3	90-94	116.5	2.22	0.83	wuell
13	5	90-94	119.5	2.44	0.65	wuell
14	1	80-84	123	2.27	0.21	wuell
14	2	90-94	124.6	2.59	0.95	wuell&cibs
14	3	90-94	126.1	2.31	0.65	wuell
14	4	90-94	127.6			wuell
14	5	80-84	129	2.35	0.81	wuell
14	cc	10-14	130.44	2.26	0.64	wuell
15	1	100-104	132.8	2.46	0.72	wuell&cibs
15	2	90-94	134.2	2.4	0.84	wuell
15	3	80-84	135.6	2.48	0.54	wuell&cibs
15	4	80-84	137.1	2.67	0.43	wuell&cibs
15	5	80-84	138.6	2.46	0.72	wuell&cibs
15	6	80-84	140.1	2.56	0.75	wuell&cibs
15	cc	10-14	140.83	2.46	0.78	wuell
16	1	80-84	142.2	2.47	0.76	wuell&cibs
16	2	90-94	143.8	2.42	0.48	wuell&cibs
16	3	80-84	145.2	2.47	0.52	wuell&cibs
16	4	110-114	147	2.31	0.63	wuell&cibs
16	5	90-94	148.3	2.54	0.44	wuell&cibs
16	6	90-94	149.8	2.51	0.38	wuell&cibs
16	cc	10-14	150.86	2.6	0.72	wuell
17	1	90-94	151.9	2.43	0.4	wuell&cibs
17	2	90-94	153.4	2.5	0.76	wuell
17	3	90-94	154.9	2.31	0.66	wuell
17	4	60-64	156.1	2.52	0.7	wuell
17	cc	10-14	156.43	2.19	1.01	wuell&cibs
18	1	60-64	157.1	2.27	0.74	wuell&cibs
18	2	60-64	158.6	2.21	1.21	wuell
18	3	62-66	160.12	2.27	0.34	wuell&cibs
18	4	68-72	161.68	2.49	0.95	wuell&cibs
18	5	64-68	163.14	2.43	0.97	wuell&cibs
18	6	20-24	164.2	2.4	1.19	wuell
18	cc	6-10	164.73	2.35	1.01	wuell&cibs
19	1	80-84	166.9	2.39	1.26	wuell&cibs
19	2	80-84	168.4	2.39	1.26	wuell&cibs
19	3	80-84	169.9	2.27	1.31	wuell
19	4	80-84	171.4	2.58	1 02	wuell&cibs
19	5	80-84	172.9	2.3	0.67	wuell
19	6	14-18	173.74	2.43	0.75	wuell&cibs
19	cc	10-14	174.19	2.33	1.03	wuell&cibs
20	1	102-106	176.72	2.3	0.96	wuell&cibs

20	2	80-84	178	2.37	1.09	wuell&cibs
20	3	60-64	179.3	2.36	1.09	wuell
20	4	80-84	181.1	2.36	1.3	wuell
20	6	110-114	184.3	2.32	1.26	wuell
20	cc	6-10	184.88	2.18	1.26	wuell
21	1	90-94	186.2	2.22	1.32	wuell
21	2	90-94	187.[illegible]	2.41	1.23	wuell
21	3	90-94	189.2	2.29	1.15	wuell
21	[illegible]	80-84	190.6	2.28	1.16	wuell
21	5	60-64	191.9	2.45	1.32	wuell&cibs
22	1	90-94	195.8	2.23	1.13	wuell
22	2	90-94	197.3	2.6	0.57	wuell&cibs
22	4	100-104	200.4	2.33	0.64	wuell
22	5	80-84	201.7	2.05	0.72	wuell
22	cc	6-8	202.9	1.93	0.58	wuell
23	2	90-94	206.9	1.87	0.83	wuell
23	3	100-104	208.5	1.85	0.4	wuell
23	5	100-104	211.5	2.11	0.61	wuell
23	6	104-108	213.04	2.27	0.96	wuell
24	2	80-84	216.4	2	1.15	wuell
24	3	110-114	218.2	2.09	0.82	wuell
24	4	110-114	219.7	2	1.13	wuell
24	5	90-94	221	2.31	0.69	wuell
24	6	90-94	222.5	2.16	1.08	wuell

wuell = *Planulina wuellerstorfi*
cibs = *Cibicidoides*

Appendix E

Planktonic foraminiferal oxygen and carbon stable isotopes from DSDP Site 608

Planktonic foraminiferal stable isotopes from DSDP Site 608

Sec.	Core	Interval (cm)	Depth (m)	$\delta^{18}O$ (‰)	$\delta^{13}C$ (‰)	Species
11	4	80-84	98.7	0.85	0.19	bulloides
12	2	80-84	105.3	0.51	0.71	bull
12	4	80-84	108.3	0.62	-0.01	bull
12	c	120-124	111.7	0.68	-0.72	bull
13	1	80-84	113.4	0.65	-0.26	bull
13	3	90-94	116.5	0.65	0.62	bull
13	5	90-94	119.5	1.0	-0.05	bull
14	1	80-84	123	0.35	0.81	bull
14	2	90-94	124.6	1.22	0.75	bull
14	3	90-94	126.1	1.06	-0.14	bull
14	4	90-94	127.6	0.89	-0.2	bull
14	5	80-84	129	0.76	-0.52	bull
14	cc	10~14	130.44	1.24	0.58	bull
15	1	100-104	132.8	1.66	0.61	bull
15	2	90-94	134.2	1.33	0.45	bull
15	3	80-84	135.6	1.28	-0.03	bull
15	4	80-84	137.1	1.5	0.7	bull
15	5	80-84	138.6	1.04	0.13	bull
15	6	80-84	140.1	1.1	-0.1	bull
15	cc	10~14	140.83	1.29	-0.03	bull
16	1	80-84	142.2	0.8	-0.04	orbulina
16	2	90-94	143.8	0.85	-0.18	bull
16	3	80-84	145.2	1.04	0.14	bull
16	4	110-114	147	0.97	0.34	bull
16	5	90-94	148.3	1.2	0.54	bull
16	6	90-94	167	1.12	0.12	bull
16	6	90-94	167	0.67	1.22	orb&bull
16	cc	10~14	150.86	1.24	0.78	bull
17	1	90-94	151.9	1.42	0.25	bull
17	1	90-94	151.9	1.23	0.9	orb
17	2	90-94	153.4	0.79	1.54	orb&bull
17	2	90-94	153.4	1.33	0.82	bull
17	3	90-94	154.9	0.44	1.43	orb
17	4	60-64	156.1	1.08	1.08	orb
17	cc	10~14	156.43	0.82	1.35	orb
18	1	60-64	157.1	1.07	1.6	orb
18	2	60-64	158.6	1.13	1.95	orb
18	3	62-66	160.12	0.64	1.73	orb
18	4	68-72	161.68	0.83	1.57	orb
18	5	64-68	163.14	0.42	1.75	orb
18	6	20-24	164.2	-0.05	1.83	orb
18	cc	6~10	164.73	0.69	1.86	orb
19	1	80-84	166.9	0.8	1.17	orb
19	2	80-89	168.4	0.71	1.62	orb
19	3	80-84	169.9	0.63	2.03	orb
19	5	80-84	172.9	1.21	1.43	bull
19	5	80-84	172.9	0.79	2.09	orb
19	6	14-18	173.74	0.77	1.68	orb

19	6	14-18	173.74	1.01	0.55	bull
19	cc	10~14	174.19	0.96	1.16	bull
19	cc	10~14	174.19	0.81	1.88	orb
20	1	102-106	176.72	0.83	0.92	bull
20	1	102-106	176.72	0.59	1.55	orb
20	2	80-84	178	0.58	1.81	orb
20	2	80-84	178	1.29	1.21	bull
20	3	60-64	179.3	1.04	1.2	bull
20	4	80-84	181.1	1.01	1	bull
20	5	104-108	182.4	0.92	0.9	bull
20	6	110-114	184.4	1.04	0.81	bull
20	cc	6~10	184.88	1.1	0.84	bull
21	1	90-94	186.2	1.02	0.74	bull
21	2	90-94	187.7	0.89	0.8	bull
21	3	90-94	189.2	0.86	0.74	bull
21	4	80-84	190.6	0.96	0.82	bull
21	5	60-64	191.9	1.1	0.88	orb
22	1	90-94	195.8	0.78	0.46	bull
22	2	90-94	197.3	0.9	0.74	bull
22	4	100-104	200.4	0.6	0.42	bull
22	5	80-84	201.7	0.81	0.53	bull
22	cc	6~8	202.9	0.84	0.53	bull
23	2	90-94	206.9	0.79	1.25	bull
23	3	100-104	208.5	0.82	1.02	bull
23	5	100-104	211.5	1.03	0.59	bull
23	6	104-408	213.04	0.96	0.99	bull
24	2	80-84	216.4	0.93	0.87	bull
24	2	80-84	216.4	0.74	1.25	orb
24	3	110-114	218.2	0.78	0.75	bull
24	4	110-114	219.7	0.97	1.14	bull
24	5	90-94	221	0.8	1.3	bull
24	6	90-94	225	0.88	1	bull

bull = *Globigerina bulloides*
orb = *Orbulina*

Appendix F

Table of benthic foraminifera from DSDP Hole 547A

Site 547A Cores	3-1	4-1	4-1	4-1	4cc	5-1	5-1	5-2	5-2	5-3	5-3	5-4	5-4	5-5	5-5	5cc	6-1	6-1
Interval (cm)	43-45	45-49	76-80	130-134	14-14	31-35	120-124	40-44	120-124	40-44	100-104	40-44	110-114	40-44	110-114	4-8	30-34	100-104
Depth (m Subbottom)	89.43	98.95	99.26	99.8	100	108.31	109.2	109.9	110.7	111.4	112	112.9	113.6	114.4	115.1	115.28	117.8	118.5
Number picked	407	505	426	317	479	253	349	287	241	478	327	314	526	487	414	508	230	301
Number/cc	2604	1616	1363	1014	1532	404	1117	459	385	382	261	337	420	194	331	203	736	352
% (fragments/whole tests)	0.22	0.29	0.31	0.58	0.2	1.27	0.51	0.37	0.9	3.8	1.74	2.3	2.4	3.8	4.5	6.5	0.8	1.3
% Benthics of total fauna	5.1	5.3	4.8	10.3	9.1	9.7	5.5	6.8	9.8	41.6	22	19.1	29.2	30.6	54.7	44.3	4.9	14.7
Lenticulina spp.	0.2	0.2	0.2	0.3	0	0	0.3	0	0	0.2	0.6	0	0	0	0.5	0.2	0	0
Nonionella sp. A	0.5	0.2	0.5	0.3	0.2	0.4	0.3	0.3	0.8	0	0	0.3	0.2	0.2	0	0	0	0
Nonion sp.	0	0.6	0.5	0.6	0.2	0	0.3	0.3	0.4	1	0.9	0	1	2.3	0.5	2.8	1.7	1.7
Elphidium ? sp.	0.2	0	0	0	0	0.4	0	0	0	0	0.3	0	0	0	0	0	0	0
Astrononion echolsi	0	0	0.5	0	0.2	0.8	0.3	0	0	0	0	0.3	0.4	0.6	0.5	0.2	0	0
Melonis barleeanum/affinis	0.2	0.6	0.7	1.3	0.8	2	0	1.7	0.8	0.6	2.8	0.6	0	1.2	1.2	1	0.4	1
M. pompilioides	0	0	0.2	0	0	0	0	0	0	0	0	0.3	0	0	0	0	0	0
Pullenia quinqueloba	0.5	0	0	0.9	0.2	1.2	0	1.4	0.8	0	0.3	0.3	0.4	0.2	0.5	0.6	0.4	1.3
P. bulloides	1	0.8	0.5	0.3	0.4	5.1	0	2.4	0.4	0.2	0	2.2	0.8	1.6	1.2	2.8	2.2	0.3
Epistominella exigua	3.7	3	5.9	6.9	4.6	11.9	12	15.7	29.9	22	14.1	9.6	14.4	16.6	23.9	22.2	12.2	16.3
E. ? sp.	1.2	1.6	0	0	0.4	0.4	0.9	0.3	0	0.4	0	0	0	0	0	0	0	0
Eponides polius	0.2	0.2	0.9	0.9	0.6	0.4	0.6	1.4	1.2	1.3	0.9	2.5	1	1.8	1.2	0	0.4	4.3
Eponides weddellensis	2.5	5.3	5.3	7.3	3.8	7.1	6.9	7.3	14.5	15.9	16.5	17.8	13.1	23.2	7	13.6	11.3	12
E. tumidulus	0.2	0.4	0	0	0	0.8	1.1	0	0.8	1.5	1.2	1	1.5	1.6	0.2	0.6	0.4	1.3
Nuttallides umbonifera	0.2	3.4	5.4	1.6	2.7	1.2	2.3	1.7	2.9	2.1	1.5	3.5	4.4	2.3	21.5	6.9	2.2	8.3
Hanzawaia sp.	1	0	0.7	0	0	0.8	0.9	0	0	0	0.3	0	0	0.2	0	0	0	0.3
Oridorsalis umbonatus	0.7	0	0.9	0.6	0.4	2.4	0.6	1.4	3.7	6.7	3.4	4.1	4.2	2.7	3.6	3.5	2.6	3
Cibicidoides bradyi	0	0	0	0	0.6	0	0	0	0	0.2	0	0	0.2	0	0.2	0	0	0.3
Cibicidoides mundulus	2	0	0.7	1.9	0.8	0	0.9	0.3	3.3	1.5	0.6	1.3	2.5	1.2	3.4	2	2.2	1.7
Cibicidoides spp.	2	1.6	0.7	1.9	1.5	1.6	0.9	0.7	3.3	1.7	0.6	1.3	2.7	1.2	3.4	2	2.2	1.7
Anomalina sp.	0.5	0.4	0	0	0	0	0	0	0.4	0	0	0	0.2	0	0	0	0	0
Gyroidina soldanii	1.5	1.8	1.6	2.5	2.3	2.8	2.6	3.5	6.2	5	4.5	4.8	4.4	3.9	3.1	4.3	2.2	4
Gavelinopsis praegeri	1.2	1.4	1.2	2.5	1.7	0.4	0	0	0	0.2	0	0	0.6	0	0.2	0.6	0	0
Valvulineria laevigata	0	0	0	0.3	0	0	0.3	0	0.4	0	0.3	0	0	0	0	0	0.9	0
Osangularia culter	0	0.4	0	0.3	0	0	0	0	0.4	0.2	0	0	0	0	0	0	0.4	0
Hoeglundina elegcns	0	0	0	0	0	0	0	0	0	0	0.3	0	0	0	0	0	0	0
Discorbinella sp.	0	0.4	0.2	0	0.2	0	0	0	0	0	0	0	0	0	0	0	0	0
Heronallenia crosbyi	0	0.2	0	0	0	0	0	0	0	0	0	0	0	0.2	0	0	0	0
Neoeponides sp.	0	0	0.2	0	0	0.4	0.9	1.4	1.2	0.4	1.2	1.3	0	0.2	0	0	0.4	0
Rosalina? sp.	0	0	0	0	0	0.4	0	0	0	0	0	0	0	0	0	0	0	0
Laticarinina pauperata	0	0	0	0	0	0	0	0	0	0	0	0.3	0.4	0	0	0.4	0	0.3
Planulina ariminensis	0	0.2	0	0.6	0	0	0	0	0	0	0	0	0	0	0	0	0	0
Planulina wuellerstorfi	0.5	0.2	0.7	0.3	1.7	0	0.6	1.4	0.8	0.2	0	0.6	0	0.2	1.4	0.6	0.4	0.7
Planulina sp.	0	0.4	0	0	0	0	0	0	0	0	0	0	0	0	0	0	0	0
Sphae. idina bulloides	0.2	2	0.7	0.6	0.2	0.4	0.6	0	0.4	0	0	0	0	0	1.2	0.8	0.4	0.3
Siphonina tenuicarinata	0	0	0	0	0	0	0	0	0	0	0	0	0	0	0	0	0	0
Globocassidulina subglobosa	13.3	16.8	15.5	20.2	14.2	16.2	24.4	17.1	28.6	21.5	22	22.3	25.7	14.4	12.3	18.1	28.7	28.6
Cassidulina reniforme	4.7	2	4.2	4.7	1.5	1.6	3.4	1.4	3.3	2.5	0.3	1	3.2	1	0.5	0.6	0.4	1
Cassidulina laevigata	0	3.2	3.5	2.5	4	0.8	0.6	1	0.8	0.6	0.9	1.3	0.6	0.6	0.2	0	1.7	0.3
Cassidulinoides tenuis	0.2	0.4	0	0	0	0.4	0.9	0.7	1.7	0.4	0	0.3	0.4	0.4	0	0.4	0.4	0.7
Tosaia hanzawai	0.5	0.2	1.4	0.9	0.3	1.6	0.3	3.1	2.5	2.5	0.6	1.6	0.6	0.8	2.4	3.1	3	1
Bolivina lowmani	0.5	1.2	1.4	0.3	2.1	0.8	0.3	0.7	1.2	0	0.9	0.3	1	0.6	0	1	0	0.3
B. pygmaea	1.7	0.6	2.3	2.5	2.7	1.6	5.4	1.7	0.4	0.8	0.6	1.6	0.4	1.8	0.5	0.6	2.2	1.3
B. albatrossi	0.2	0	0	0.6	0.2	0	0.6	0	0	0	0	0.3	0	0.2	0	0.2	0	0

Site 547A Cores	3-1	4-1	4-1	4-1	4cc	5-1	5-1	5-2	5-2	5-3	5-3	5-4	5-4	5-5	5-5	5cc	6-1	6-1
Interval (cm)	43-45	45-49	76-80	130-134	10-14	31-35	120-124	40-44	120-124	40-44	100-104	40-44	110-114	40-44	110-114	4-8	30-34	100-104
B. pseudoplicata	7.1	3.8	2.8	0.9	3.1	1.2	0.9	1	0.4	0.4	0.3	0.3	1	0.4	0	0.2	2.6	0
B. suteri	0	0	0.7	0.3	0	0	0	0	0	0	0	0	0	0	0	0	0	0
B. inflata	36.1	14.5	6.3	4.7	14	3.2	8.3	4.9	1.7	0.6	0.3	0.3	1.3	0.8	0	0.2	3.9	0.7
B. pseudopunctata	0	0	0	0.3	0.2	0	0	0	0	0	0	0	0	0	0	0.2	0	0
B. subaenariensis	0	0	0	0	0	0	0.6	0	0	0	0	0	0.2	0	1.2	0	0	0
B. subspinescens	0	0	0	0	0	0	0	0	0	0	0	0	0.2	0	0	0	0.4	0
B. byramensis	0	0	0	1.9	0.4	0.8	0.3	0.3	0.4	0	0	0	0.4	0	0	0	0.4	0
B. spp.	2	2.4	3.1	1.3	3.8	2	2	2.4	7.1	0.8	3.4	2.2	2.1	1.8	0.7	1.2	1.3	0.3
Bolivinita truncata	7.4	22.4	20.2	12.6	15.7	8.7	4	7.7	4.1	1	1.2	1.9	2.5	1.2	0	0.8	2.6	0
Bolivinids	48.2	42.6	34.5	24.6	41.5	17	21.5	18.1	15.4	3.3	6.4	6.7	7.8	6.6	2.7	4.1	10.9	2.7
Trifarina angulosa	5.2	3.4	4.5	3.8	2.9	3.2	3.7	2.8	3.3	0.4	3.7	1	2.1	2.1	0.2	0.6	2.2	1.7
Trifarina bradyi	0	0	0	0.3	0.8	0	0	0	0	0	0	0	0	0	0	0	0	0.7
Uvigerina spp.	2	1.4	0.5	2.2	0.8	2	3.4	0	1.2	1	0.9	1.6	0.2	0.8	0.2	0.6	0.9	1
Ehrenbergina trigona	0	0.2	0.5	0.6	0.6	2	0.9	3.5	0.4	0.2	0.6	0.6	0	1.8	2.4	1.8	0.9	0
Bulimina alazaensis	0	0	0.7	0	0.6	0	1.4	0.3	0	0	0	0	0	0.6	0	0	0	0.3
B. mexicana	0	0.4	0.7	0.3	0.4	0	0.3	0.7	0.8	0.2	0	0	0	0.4	0	0.4	0	0
B. aculeata	0	0.6	0.5	0	0.2	0	0	0	0	0.2	0	0.3	0	0.2	0	0	0	0
B. ovata	0.7	0.2	0	0	0	0	0	0	0	0	0	0	0	0	0	0	0	0
B. spp.	1.5	1.2	0.7	1.3	1.9	2.8	1.7	0	0	0.2	2.4	0.3	0.2	1	0.2	0	0.9	0.3
Bulimids	2.2	2.6	2.6	1.9	3.1	2.8	3.2	2.4	0.8	1.5	4.6	1	0.2	2.9	0.2	0.8	0.9	0.7
Globobulimina auriculata	0.2	0.2	0	0	0.2	0	0	0	0	0	0.3	0	0.2	0	0.5	0	0	0.3
Reusseela spinulosr.	0	0	0	0	0	0	0	0.7	0	0	0	0	0	0	0	0.2	0	0
Uvigerina hispida	1	0	0	0	0	0	0	0	0.4	0	0	0	0	0	0	0	0	0.3
U. peregrina	0.7	1.4	0.5	1.6	0.6	2	3.2	0	0.4	0.8	0.9	0.6	0	0.8	0	0.6	0.9	0.7
U. canariensis	0	0	0	0.6	0	0	0.3	0	0	0	0	0	0	0	0	0	0	0
Rectuvigerina compressa	0	0	0	0	0	0	0	0	0.4	0.2	0	1	0	0	0	0	0	0
R. sp.	0.2	0	0	0	0	0	0.3	0	0	0	0	0	0	0	0	0	0	0
Dentalina communis	0.2	0	0.2	0	0	0	0	0	0	0	0	0	0.2	0.4	0	0.2	0	0.3
Hopkinsina pacifica	0.2	0	0	0	0	0	0	0	0	0	0	0	0	0	0	0	0	0
Fursenkoina fusiformis	0.5	0	0.2	0	0	0	0	0	0	0	0	0	0	0	0	0	0	0
Guttulina sp.	0	0	0	0	0	0	0	0	0	0	0	0	0	0	0	0	0	0.3
Loxostomum cf. normale	0	0	0	0	0	0	0	0	0	0	0	0	0	0	0	0	0	0
Pleurostomella spp.	0.5	1	0	0.9	0.6	1.2	2.3	0.7	0	1.3	0.9	1.6	0.4	1.4	0.2	0	1.7	0
Stilostomella antillea	0.5	0.6	1.2	1.3	0.8	0.4	1.1	0.3	0.4	0.4	1.2	0.6	1.1	1.2	1.9	0.6	3	0
S. sp.	0	0.4	0.2	0.6	0	0.4	0	0	0.4	0	0.6	0.3	1	0	0	0	0	0
Fissurina spp.	0.2	0.4	0.2	0.3	0.2	0.8	0	1	0	0	0.9	1.3	1.3	1	1.2	0.4	0.4	0.3
Lagena spp.	0	0	0.5	0	0	0	0.3	0	1.2	0.4	1.2	0	0.2	0.4	1.2	0.2	0	0
Oolina spp.	0	0.2	0	0.6	0.6	0.8	0	0.7	0	0	0	1.2	0	0.2	0	0.8	0.4	0.7
Quinqueloculina spp.	0	0	0.2	0	0	0.8	0	1	0.4	0.2	0	1	0.4	0.2	0.2	0	0.9	0.7
Sigmoilina tenuis	0	0	0	0	0	0	0	0	0	0	0	0	0	0	0	0	0	0
Pyrgo spp.	0	0.2	0	0	0	0	0	0	0	0	0	0	0	0	0	0	0.4	0
Nodosaria sp.	0	0	0	0	0	0	0	0	0	0	0	0	0	0	0	0	0.4	0
Textularia sp.	0.2	0	0	0.3	0	0	0	0	0	0	0	0.3	0	0	0	0	0	0
Vulvulina spinosa	0	0	0.2	0	0	0	0	0	0	0	0	0	0	0	0	0.2	0	0
Siphotextularia rolshauseni	0	0.4	0.2	0.3	0.4	2.4	0.3	1.7	0.4	0.4	1.2	1	0.6	0	0.5	1.4	0.4	1.3
Martinottiella communis	0	0	0	0	0	0	0	0	0	0	0	0	0.4	0	0	0	0	0
Eggrella bradyi	0	0	0	0	0	0	0	0	0	0	0	0	0.2	0	0	0	0	0

Site 547A Cores	6~2	6~2	6~3	6~3	7~1	7~1	7~2	7cc	8~1	8~1	8~2	8~3	8~4	8~5	8cc	9~1	9~2	9~3	9~4
Interval (cm)	60-64	120-124	30-34	100-104	40-44	110-114	6~10	2~6	40-44	120-124	90-94	80-84	80-84	20-24	2~6	60-64	70-74	90-94	40-44
Depth (m Subbottom)	119.6	120.2	120.8	121.5	127.4	128.1	128.56	128.8	136.9	137.9	138.3	140.8	141.8	142.7	143.31	146.6	148.2	149.9	150.9
Number picked	378	256	283	329	390	375	286	276	228	402	660	309	291	246	186	226	503	471	459
Number/cc	1257	819	905	263	624	600	228	220	364	160	132	123	608	393	595	723	402	753	1468
% (fragments/whole tests)	1.1	0.43	0.51	0.9	1	1.9	3.5	2.3	1.16	2.4	6	8.2	0.45	0.37	1.1	1.1	1.99	1.26	1.93
% Benthics of total fauna	9.4	3.9	4.7	12.3	15	32.3	26.5	31.5	15.1	39.5	42.3	46.6	9.6	12.2	7.3	14.7	30.9	26.4	28
Lenticulina spp.	0	0.4	0	0	0	0	0	0	0	0	0	0.6	0	0	0	0	0	0.2	0
Nonionella sp. A	0.3	0.4	0.4	0.3	0	0.3	0	0	0	0	0	0	0	0	0	0.4	0.8	0.2	0.7
Nonion sp.	0.8	0.4	0.4	1.2	0.3	1.1	0.3	0.7	0.4	1.5	2.6	3.6	1.4	5.3	3.2	1.3	1.8	4.7	2
Elphidium ? sp.	0	0	0	0	0	0	0	0	0	0	0	0	0	0	0	0	0	0.2	0
Astrononion echolsi	0.5	0.4	0.4	0.3	0.3	0	0	0	0	0	0.2	0	1	0.4	0.5	0.4	0	0.2	0
Melonis barleeanum/affinis	0.3	0	0.4	1.2	0	0.3	0.3	2.9	0	2.5	1.7	1	1.7	1.6	2.2	2.2	1.4	0.4	1.7
M. pompiliodies	0	0	0	0	0	0	0	0	0	0	0	0	0	0.4	2.7	0	0.2	0	0.2
Pullenia quinqueloba	0.3	0.4	0	0.6	0	0.5	2.4	1.1	0	0.5	0.9	1.9	0.7	0	1.6	0	0.4	0	0
P. bulloides	1.1	1.6	0.7	1.5	1.5	0.5	0.7	1.4	1.3	3.7	3.6	2.6	1.4	2.4	4.8	2.2	2.2	0.6	0.4
Epistominella exigua	20.9	9	8.8	10	21	24	32.9	13.4	16.2	12.9	15.5	6.8	7.6	18.3	8.1	13.7	14.1	14.4	12.4
E. ? sp.	0	0	0	0	0	0	0	0	0	0	0	0	0	0	0	0	0	0.6	0.9
Eponides polius	1.9	0.3	0	4	0.8	1.3	1	1.1	1.3	0.2	1.1	1.6	0.7	1.6	2.2	0.9	2.6	0.8	0.9
Eponides weddellensis	7.1	2.3	6.4	14.3	13.3	12.5	7	11.2	5.7	7	5.6	10.4	12	12.2	7.5	8.4	19.5	10.6	9.8
E. tumidulus	0.8	0.8	0.7	1.8	0.5	1.3	1.4	0.4	1.3	0.5	2	1	0.3	1.6	0.5	0	0.6	0.6	0.9
Nuttallides umbonifera	7.4	6.3	7.1	7	2.6	18.9	11.5	13	6.1	10.7	6.8	9.4	3.4	3.7	2.7	4.4	3.6	3.6	3.1
Hanzawaia sp.	0.3	0	0	0	0.3	0	0.3	0	0	0.2	0.2	0	0	0	0.5	0.9	0	0	0
Oridorsalis umbonatus	1.6	1.2	0.4	1.8	2.8	2.4	2.1	3.3	2.6	6.2	1.5	2.9	3.8	4.5	7	0.4	3.4	2.8	2.8
Cibicidoides bradyi	0	0	0	0	0	0	0	0	0	0	0	0	0	0	0.5	0	0	0.2	0
Cibicidoides mundulus	1.9	2	1.8	0.9	2.1	1.9	1.4	0.7	0.4	3	1.7	2.3	3.8	3.3	1.1	2.7	1.8	1.5	1.5
Cibicidoides spp.	1.9	2	1.8	0.9	2.1	1.9	1.4	0.7	0.4	3	1.7	2.3	3.8	3.3	1.1	2.7	1.8	1.7	1.5
Ancnalina sp.	0	0	0	0.6	0	0	0	0	0	0	0	0	0	0	0	0	0.2	0	0
Gyroidina soldanii	1.3	3.9	3.2	2.4	2.6	1.6	3.1	1.1	6.6	4.7	7.3	0.5	4.8	4.1	4.3	2.2	6	3	6.8
Gavelinopsis praegeri	0	0	0	0	0	0.3	0.7	0	0.4	0	0	0	0	0.4	1.1	0	0	0	0.7
Valvulineria laevigata	0	0	0	0	0	0	0	0	0	0	0	0	0.7	0	0	0	0	0	0
Osangularia culter	0	0	0	0	0	0	0	0	0	0	0	0	0	0.8	0	0	0	0	0
Hoeglundina elegans	0	0	0	0	0	0	0	0	0	0	0	0	0	0	0	0	0	0	0
Discorbinella sp.	0	0	0	0	0	0	0.3	0	0	0	0.2	0	0	0	0	0	0.2	0.2	0.2
Heronallenia crosbyi	0	0	0	0	0	0	0	0	0	0	0	0	0	0	0	0.9	0	0	0
Neoeponides sp.	0.8	0.4	1.1	0.9	0.5	0	0.3	0.4	0.9	0.7	0.3	0	0	0	0	0	0.2	0.2	0.4
Rosalina? sp.	0	0	0	0	0	0	0	0	0	0	0	0	0	0	0	0	0	0	0
Laticarinina pauperata	0	0	0	0	0	0	0	0	0	0.2	0.2	0	0	0	0	0	0	0	0
Planulina ariminensis	0	0	0	0	0	0	0	0	0	0	0.5	0	0	0	0	0	0	0	0
Planulina wuellerstorfi	0.3	0.4	0	0.6	0	0	0.7	1.1	0.9	0.7	0.5	1.9	0.3	0.8	1.1	0.4	2.4	1.3	0.4
Planulina sp.	0	0	0	0	0	0	0	0	0	0	0.2	0.3	0.7	0	0	0	0	0	0
Sphaeroidina bulloides	0.3	0	0.4	0.3	0.3	0.8	0	0	0	0.2	0.6	0	0	0	0	0.4	1	1.3	2.6
Siphonina tenuicarinata	0	0	0	0	0	0	0	0.4	0	0	0.2	0	0	0	0	0	0	0	0
Globocassidulina subglobosa	23.5	21.5	21.2	16.7	28.2	17.9	22.4	25	32.9	20.6	16.1	13.9	22.7	15.9	18.3	21.7	11.9	26.1	18.1
Cassidulina reniforme	1.1	2	1.4	0.3	0.8	1.3	1	0.4	0.4	0.2	0.5	0.6	0	0.4	1.6	1.8	1.8	2.1	1.7
Cassidulina laevigata	1.1	0.4	1.1	0.6	0.5	0	0	0.4	0	0.2	0	0	3.1	1.6	1.1	1.3	0.4	0.8	1.3
Cassidulinoides tenuis	0.3	0	0	0.6	0.8	0.3	0	0	0.4	0	0	0	0.3	0.8	0	0	0	0.2	0
Tosaia hanzawai	1.1	0	0.7	1.5	0.5	0	1.7	2.5	0.9	1.2	2.3	3.2	0.3	1.6	1.1	1.8	0.6	0.4	0.4
Bolivina lowmani	1.3	0.8	1.1	2.1	1.3	0.5	1.4	0	0.4	0	0	0.3	0.7	1.2	0	0.4	0	0	0
B. pygmaea	2.4	2.7	2.1	1.5	2.1	0.8	1	1.4	1.8	1	0.6	1.3	1.7	0.4	3.8	3.1	7.8	2.1	1.7
B. albatrossi	0	0.8	0	0	0	0	0	0.4	0	0	0	0	0	0	0	0	0	0	0

Site 547A Cores	6-2	6-2	6-3	6-3	7-1	7-1	7-2	7cc	8-1	8-1	8-2	8-3	8-4	8-5	8cc	9-1	9-2	9-3	9-4
Interval (cm)	60-64	120-124	30-34	100-104	40-44	110-114	6-10	2-6	40-44	120-124	90-94	80-84	80-84	20-24	2-6	60-64	70-74	90-94	40-44
B. pseudoplicata	0.5	2	1.8	0.6	0.3	0	0	0	0	0.2	0.2	0	2.1	0.4	1.1	2.2	0	0.4	0.7
B. suteri	0	0	0	0	0	0	0	0	0	0	0	0	0	0	0	0	0	0	0
B. inflata	7.9	22.3	19.4	4	1	0.3	1	1.1	0.9	0.2	0.5	0.3	0.3	0	0	0.9	0.8	0.8	3.5
B. pseudopunctata	0.3	0	0.4	0	0.3	0	0	0	0	0	0	0	0	0	0	0	0	0	0.2
B. subaenariensis	0	0	0	1.5	0.8	0.3	0.3	1.1	0	0	0	0	1	0.4	1.1	0.4	0.6	0.2	0.2
B. subspinescens	0	0	0	0	0	0	0	0.4	0	0	0	0	0	0	0	0	0	0	0
B. byramensis	0.5	0.4	0	0	0	0	0	0	0.9	0	0.5	0.6	0	0	0	0	0	0	0
B. spp.	0.8	0.4	1.8	1.5	0.8	0	1	0.7	2.2	1.5	1.8	2.9	3.1	1.6	1.6	3.1	1.8	3.4	5.2
Bolivinita truncata	0.5	2.3	1.8	0.6	0.3	0	0.3	0	0.4	0.2	0.3	0	2.1	0.8	1.1	0	0	0	0
Bolivinids	13.8	30.5	26.5	11.2	6.7	1.9	5.2	4.7	6.6	3	3.6	5.5	8.9	4.5	7.5	10.2	10.7	7	11.5
Trifarina angulosa	1.9	5.9	6.7	4.3	2.3	0	2.8	1.1	1.8	1.2	2.1	1	2.7	0	2.7	1.8	0	1.1	1.1
Trifarina bradyi	0	0	0.4	0	0.3	0	0	0	0	0	0.3	0	0.3	0	0.5	0	0	0	0
Uvigerina spp.	3.7	3.1	1.8	0.9	2.3	2.7	8	3.6	2.2	2.7	7.3	4.9	2.1	1.2	3.2	4.9	1.6	2.5	3.5
Ehrenbergina trigona	0.5	0	0	2.1	0	0.3	0	0	0	0.5	1.1	2.3	0	0	0	0	0.4	0	0
Bulimina alazaensis	0.3	0.8	0	1.2	0.3	0	0.3	0.4	0.4	1.7	1.2	1.6	2.7	2	1.5	1.3	1.4	1.3	0.9
B. mexicana	0	0	0	0.6	0.3	0	0	0	0	0	0.3	0	0.7	0	0	0.4	0.2	0.2	0.2
B. aculeata	0	0.4	0.4	0.3	0.5	0	0.3	0	1.3	0.2	0	0	0	0	0	0	0	0.2	0.2
B. ovata	0	0	0	0	0	0	0	0	0	0	0	0	0	0	0	0	0	0	0
B. spp.	0	0	0.4	2.1	1.5	0.3	0.3	1.4	0	0.5	0.3	1.6	0.7	1.2	0	0.4	0.8	1.1	3.5
Buliminids	0.3	1.2	2.5	4.3	2.6	0.5	2.1	2.5	2.6	2.5	2.9	3.2	4.8	3.7	2.7	3.5	3.4	4	5.4
Globobulimina auriculata	0	0	0	0	0	0	0.3	0	0.4	0	0.2	0	0	0	1.1	0.9	0	0	0
Reussella spinulosa	0	0	0	0	0	0	0	0	0	0	0	0	0	0	0	0	0	0	0
Uvigerina hispida	1.3	0.4	0.7	0	0.3	0	2.4	0.7	1.8	0	0	0	0	0	0	0	0	0.2	0.4
U. peregrina	1.6	2	0.4	0.6	0.8	0	3.8	2.2	1.3	1.2	2.3	2.9	1	1.2	2.7	0	1	1.5	3.1
U. canariensis	0	0	0	0	0	0	0	0	0	0	0	0	0	0	0	0	0	0	0
Rectuvigerina compressa	0.8	0.8	0.7	0.3	0.8	0	0	0	0	1	5	1.9	0	0	0	0	0	0	0
R. sp.	0	0	0	0	0	0	0	0	0	0	0	0	0	0	0	0	0	0	0
Dentalina communis	0	0	0	0	0	0.3	0.3	0	0	0.2	0	0.3	0.3	0	0	0	0	0.2	0
Hopkinsina pacifica	0	0	0	0	0	0	0	0	0	0	0	0	0	0	0	0	0	0	0
Fursenkoina fusiformis	0	0.4	0.4	0.3	0	0	1	0	0	0	0.2	1.3	0	0	0	0	0	0	0
Guttulina sp.	0	0	0	0	0	0	0	0	0	0	0	0	0.3	0	0	0	0	0	0
Loxostomum cf. normale	0	0	0	0	0	0	0	0	0	0	0	0	0	0	0	0	0	0	0
Pleurostomella spp.	0	0.4	1.4	0	0.5	0.3	1.4	0.7	0.4	1.2	0.9	0.3	0.7	0.8	0	2.2	1.4	1.1	0.2
Stilostomella antillea	1.9	0.8	0.7	0.6	0.3	0.8	0.7	2.2	1.3	0.7	1.1	1	0.7	1.2	2.2	2.7	0.8	0.6	1.5
S. sp.	0	0	0	0	0.3	0	0.7	0	0	0	0	0.6	0	0	0.5	0.4	0.2	0	0.2
Fissurina spp.	0.5	0	0	0.9	0.5	1.6	0	0.7	0.4	2	1.1	1	0.7	0	1.1	1.3	1	0.6	0.4
Lagena spp.	0	1.2	0.7	0	0	0.3	0	0	0.4	0.7	0.9	0.3	0	0.4	0	0	0.2	0	0.2
Oolina spp.	0	0	0.7	0.6	0.5	0.8	0	0.4	0.4	0.2	0.3	1	1.7	0	0	0.9	0	0	0
Quinqueloculina spp.	0.3	0.4	0	0.6	0.8	0.5	0	0	0	0.2	0.6	0.6	0	0	0	0	0.4	0	0
Sigmoilina tenuis	0	0	0	0	0	0	0	0.4	0	0	0	0	0	0.8	0	0	0.2	0	0.7
Pyrgo spp.	0	0	0	0	0	0	0	0	0	0	0.3	0	0	0	0	0	0	0	0
Nodosaria sp.	0.3	0	0	0	0	0	0	0	0.4	0.2	0	0	0	0.4	0	0	0	0	0
Textularia sp.	0	0	0	0	0	0	0	0	0	0	0	0	0	0	0	0	0	0	0
Vulvulina spinosa	0	0	0	0	0	0	0	0.4	0	0.2	0	0.6	0.3	0	0	0	0		0
Siphotextularia rolshauseni	0	0.8	0	0.9	0.5	0.5	0.7	0.4	0	0	0.9	1	1	0	1.1	0.4	0.2	1.1	0.2
Martinottiella communis	0	0	0	0	0	0	0	0	0	0	0	0	0	0	0	0	0	0	0
Eggrella bradyi	0	0	0	0	0	0	0	0	0	0.2	0.2	0.3	0	0	0	0.4	0	0	0

Appendix G

Table of benthic foraminifera from DSDP Hole 646B

Site 646B Core	41x-2	41x-6	42x-1	42x-3	42x-5	42x-7	43x-2	43xCC	44xCC	45x-1	45xCC	46x-2	46x-4	46xCC	47x-2	47xCC	48x-1	48xCC	49x-1	49xCC
Interval (cm)	130-134	70-74	100-104	116-120	90-94	20-24	50-54	10-14	30-34	20-24	20-24	80-84	20-24	20-24	70-74	10-14	110-114	15-19	60-64	20-24
Depth (m subbottom)	384.1	389.5	392	395.16	397.9	400.2	402.7	405	411.93	420.3	420.71	432.1	433.57	434.07	441.7	442.79	450.2	451.38	459.4	461.97
Number picked	168	293	88	32	268	259	387	174	141	298	404	264	230	312	208	165	273	249	301	269
No./20CC	2688	2344	704	448	8576	518	1548	1392	1128	2384	3232	2112	1840	2496	3328	2640	4368	1992	2048	1614
% calcareous forms of total fauna	98	92.2	21.5	90.6	45.5	66 4	15.8	84.5	95	38.9	11.9	34 1	26.9	9	41.3	22.4	58.6	35.7	13.9	20.4
% benthic forams in total fauna	47.3	11 1	16.1	66.7	83 2	59.5	73.9	21.3	21.8	48 8	87 4	40.5	39 1	85	33.1	32.6	70.9	31.6	73.6	75.4
% Fragments of whole planktonics	70.5	69.1	30.7	68.8	97.2	91.8	76	89 6	90.3	78 1	85	72 7	58.9	79.8	56.4	54.6	82.7	48	74.6	92.3
Lenticulina spp.	0.0	0.0	1.1	0.0	0 0	0 0	0.0	0.0	0.0	0.0	0.0	0.0	0.0	0 0	0.5	0.6	1.1	0.0	0.0	0.0
Nonion spp.	6.5	7.5	0 0	12.5	3.7	5.8	1.8	4.0	2.8	3.0	1.0	3.8	1.7	1.0	1.4	0 0	1.8	4.8	1.3	1.9
Nonionella spp.	2.4	5.5	0.0	0 0	0 7	1.2	0.0	1.1	1.4	0 0	0 0	0 0	0 0	0 0	1 4	0.0	1.8	0.0	0 0	0.0
Astrononion echolsi	0 0	0.0	0 0	0 0	0.0	0 0	0 0	0 0	0 0	0 0	0 0	0 0	0 0	0 0	0 0	0.0	0.0	0.0	0.0	0.0
Astrononion umbilicatulum	0.0	0 0	0 0	0.0	0.0	0 0	0.0	0.0	0.0	0 0	0 0	0 0	0.0	0.0	0.0	0 0	0.0	0.0	0.0	0.0
Elphidium? sp.	0.6	0.0	0.0	0.0	0.0	0 0	0 0	0.0	0.0	0.0	0.0	0.0	0.0	0.0	0.0	0.0	0.7	0.0	0.0	0.0
Pullenia bulloides	0.6	1.0	0 0	0.0	0.7	3.9	1.3	7.5	2.8	0.7	0.7	0.4	0.9	0.3	0.0	1.2	1.8	4 0	0.7	2.2
P. quinqueloba	4.2	3.4	0.0	0.0	0.7	0.8	0 0	1.1	2.8	2.0	0.5	0.8	0 0	0 0	1.4	0 6	2 2	2.8	0.7	1.9
Melonis barleeanum/affinis	12.5	5.5	4.5	9 4	3 7	3.5	0.8	4 0	8 5	3.4	2.5	7.6	4.8	0 6	2.9	1.8	2.6	6.0	1.0	1.9
M. pompilioides	0.0	0 0	0 0	0 0	3 4	0 0	0.5	1.7	5 0	0.3	0 0	0 0	0.4	0.0	0.0	0.0	0.0	0.0	0.0	0.0
Florilus sp.	0.0	0.0	0 0	0.0	0.0	0 0	0 0	0 0	0.0	0.0	0.0	0.0	0.0	0.0	0 0	0.0	1.1	0.0	0.0	0.0
Sphaeroidina bulloides	0.6	2.0	0 0	0.0	0 0	0 0	0.0	0.0	0.0	0.0	0.2	0.4	0 4	0.0	0.5	0 6	0 0	0 0	0.0	0 0
Oridorsalis umbonatus	4.8	3.4	1 1	0.0	2.2	8.5	0 0	1.7	0.7	2.7	0 7	1.1	1.3	0 0	0.5	0.0	4 8	0.8	0 7	1.1
Planulina rugosa	0 0	0 0	0 0	0 0	0 0	0 0	0.0	0 0	0 0	0 0	0 0	0 0	0 0	0 0	0 0	0 0	0.4	0.0	0.0	0.0
Planulina wuellerstorfi	0 0	0.7	1 1	0 0	0 4	0 0	0 0	1 7	2.1	0 7	0 0	0 0	0.4	0.0	0.0	0.0	2.9	0.0	0.0	0.0
Cibicides lobatulus	0 0	0.0	0 0	0.0	0 0	0 0	0 0	0 0	0 0	0.0	0.0	0.0	0.0	0.0	0.0	0.0	0.0	0.0	0.0	0.0
Cibicidoides bradyi	0.0	0.0	0 0	0.0	0.0	0 0	0 0	2.3	0.0	0.0	0.2	0 0	0.0	0.0	0.0	0 0	0 0	0 0	0 0	0 7
C. spp.	1.8	5.8	0 0	0.0	2.2	4 6	0.0	2.3	4.3	0.3	0.2	0 4	0 0	0.3	1.0	0.0	5.5	0 0	0.3	0.4
Rosalina ? sp.	1.8	0.0	0 0	0 0	0 0	0 0	0 0	0 0	0 0	0 0	0 0	0 0	0 0	0 0	0.0	0.0	0.0	0.0	0.0	0.0
Gyroidina soldanii	3.6	5.5	1 1	0 0	2.2	3 9	0.5	3 4	6 4	2.0	0.0	2 7	1.7	0.0	1.4	1.8	4.4	0.8	0.3	1.1
Gavelinopsis praegeri	0.0	0.0	0 0	0.0	0 0	0 0	0 0	0 0	0 0	0.0	0.0	0.0	0 0	0.0	0.0	0.0	0.4	0.0	0.0	0.0
Laticarinina pauperata	0.0	0.7	0 0	0.0	0.0	0.8	0.0	1.1	0.0	0 0	0 0	0 0	0.0	0.0	0.0	0.0	0.0	0 0	0 0	0.0
Valvulineria laevigata	0.0	0.3	0.0	0.0	0 0	0 0	0 0	0.0	0.0	0.0	0 0	0.0	0 0	0 0	0 0	0.6	0 0	2.0	1.3	1.5
Nuttallides umbonifera	0 0	1.4	0 0	0.0	0 0	0 0	0.0	0 0	2.1	0.3	0 2	0 0	0 0	0 0	0 0	1.2	1.1	0.0	0.0	0.0
Hoeglundina elegans	0 0	0.0	0 0	0 0	0 0	2.7	0 3	2.3	0 7	0 0	0 0	0 0	0.0	0.3	0.0	0.0	0 0	0.0	0.0	0.0
Epistominella exigua	3.0	1.4	0 0	0.0	1 1	4 6	0 0	2.9	1.4	0 0	0.0	1.5	0.9	0 0	0.5	0.6	1.8	0.4	0.0	0.7
Eponides polius	3.6	1.4	0 0	0.0	0 0	2.3	0.0	1.7	3.5	0 0	0 0	0.0	0.0	0 0	0.0	0 0	0 0	0 0	0 0	0 0
E. tumidulus	0.0	0.3	2.3	0 0	0 0	0 0	0.0	1.1	0.7	0 0	0.0	0.0	0.4	0 0	0 0	1 8	0 0	1.2	1 0	0 0
E. weddellensis	22.0	12.3	1.1	0.0	16.4	17.0	4 9	21 8	27 0	12 1	3.5	9.5	6.5	2.9	14 9	1.8	11.7	6.4	4.7	4.8
E.? sp. A	0 0	0 0	0 0	0 0	0 0	0 0	0 0	0 0	0 0	0.0	0 0	0 0	0 0	0 0	0 0	0.0	0.0	0 0	0.0	0.0
Discorbinella bertheloti	0.0	0.0	0 0	0 0	0 0	0 0	0 0	0 0	0 0	0 0	0.0	0.0	0 0	0 0	0.0	0.0	0.0	0.0	0.0	1.1
Globocassidulina subglobosa	10.7	15 0	3 4	0.0	2.2	1.9	2.6	2.9	4 3	5.4	1 0	0 8	1.7	0 6	3.8	6.7	3.7	3.6	1 0	0.4
Cassidulina laevigata	1.2	0.0	0 0	6.3	0 0	0 0	0.0	0.0	0.0	0.0	0.2	0 0	0 0	0 0	0.5	0.0	0 0	0 0	0 0	0 0
C. reniforme	11.3	3.1	0 0	0.0	1.5	0 0	0.8	4 6	5.7	3.7	0.0	1.1	0 0	0 0	2 9	0.6	1.1	0 0	0 0	0 0
C. sp.	0.0	0.0	0 0	6.3	0 0	0 0	0.0	0 6	0 0	0 0	0 0	0 0	0 4	0.0	0 0	0 0	0 0	0 0	0.3	0.0
Cassidulinoides tenuis	0 0	0 0	0 0	0 0	0 0	0 0	0 0	0 0	0 0	0 0	0 0	0 0	0 0	0.0	0.0	0.0	0 0	0 0	0.0	0.0
Unidentified rotalids	0 0	1 4	0 0	0 0	0 0	0 0	1 0	1 1	0 7	0.3	0 0	0 4	0.0	0.3	0.5	0.0	1.1	0 0	0.3	0.0
Uvigerina peregrina	1.8	0.0	0 0	0.0	0 0	0 0	0 0	0 0	2.1	0 0	0 0	0 0	1.3	0 0	0 0	0.0	0.0	0 0	0 0	0.0
U. proboscidea	0.0	1.0	0 0	0.0	0 0	0 0	0.0	0.0	2.8	0 0	0.0	0.0	0 0	0 0	0 0	0.0	0 0	0 0	0 0	0 0
U. sp.	0.6	0.3	0 0	0.0	0 0	0 0	0 0	0 0	0 0	0 0	0 0	0.0	0 0	0 0	0 0	0 0	0 4	0 0	0 0	0 0

Site 646B Core	50x-1	50x-2	50x-3	50xCC	51x-1	52xCC	54x-1	54x-1	54x-3	55x-2	55x-3	55xCC	56x-1	56x-2	56xCC	57x-3	57x-4	57xCC	58x-1	58x-2	59xCC
Interval (cm)	62-66	30-34	22-26	30-34	80-84	20-24	60-64	140-144	16-20	80-84	27-31	10-14	110-114	60-64	20-24	40-44	22-26	20-24	50-54	40-44	20-24
Depth (m subbottom)	469 12	470.3	470.87	471.51	478.9	489 62	507.5	508.3	510 06	518.8	519 73	520 03	527 8	528.8	530.3	539.2	539.87	540.22	546	547 4	557 44
Number picked	330	222	258	204	322	209	363	161	334	356	229	191	246	219	238	140	128	140	457	298	268
No./20CC	2640	3552	2064	1632	2576	1672	5808	1288	2672	2848	916	764	984	876	1904	1120	2048	3840	7312	4768	4288
% calcareous forms of total fauna	6.4	52.3	57	27	10.3	34.5	3 7	1.9	29 7	26.8	36	21.9	15.9	58	32.4	25	31	13	0 4	0	23.3
% benthic forams in total fauna	58.9	34.8	45 7	54 4	69.8	57 6	87 1	89	72.8	58	40 1	44.3	45 7	55 4	62.5	80	92	82.5	100	99.3	64 6
% Fragments of whole planktonics	73 4	83.6	80	62.6	62 4	58.8	43.8	37.5	69 1	30.9	48.3	34 4	18.2	42.9	48 7	46	100	41	0	0	64 4
Lenticulina spp.	0 0	0.0	0.0	0.5	0 0	0 0	0 0	0 0	0 0	0 0	0 0	0.5	0 0	0 0	0 0	0.0	0 0	0.0	0 0	0.0	C 0
Nonion spp.	1.5	3.2	1.6	3.9	1 6	2.9	0 6	0 0	2.7	2.2	3.5	2.1	1.2	6 4	3.8	0.0	0 0	0 0	0 0	0.0	0 7
Nonionella spp.	0 0	0 0	0.0	0 0	0 0	0 0	0 0	0 0	0 0	0 0	0 0	0 0	0 0	0 0	0 0	0.0	0 0	0 0	0 0	0.0	0.0
Astrononion echolsi	0 0	0.0	0.0	0 0	0 0	0 0	0 0	0 0	0 0	0 0	0.0	0 0	0.0	0.0	0.0	0.0	0 0	0 0	0 0	0.0	0.0
Astrononion umbilicatulum	0.0	0.0	0.0	0 0	0.0	0 0	0.0	0 0	0 0	0 8	0 0	0.0	0 0	0 0	0 0	0 0	0 0	0 0	0.0	0 0	0 0
Elphidium? sp	0 0	0.0	0 0	0 0	0 0	0 0	0 0	0 0	0 0	0 0	0 0	0 0	0 0	0 0	0 0	0.0	0 0	0 0	0 0	0.0	0.0
Pullenia bulloides	0 0	1.8	1.9	1 0	1.2	1 4	0 6	0 0	1.8	0.8	1 7	0.5	0.8	10.5	2.1	0 7	0.8	2.1	0.0	0 0	1.5
P. quinqueloba	0 0	0.5	1.2	2.0	0 0	1 0	0 6	0 0	1 8	0 8	1 7	0.5	0 0	5.5	2.1	1 4	0 0	0 4	0.0	0 0	1 1
Melonis barleeanum/affinis	0 0	8.1	4.3	0 0	0 0	1 4	0 6	0 0	2.7	2.0	0 4	1 0	0 4	4 1	0 4	2.1	0 0	0.0	0.0	0 0	0 4
M. pompiloides	0 0	0.0	0.0	1.5	0.3	1 0	0.0	0 6	1.2	1 4	3 1	1 6	0.8	0 0	0 4	2.9	0 0	0 0	0.0	0 0	1 9
Florilus sp.	0.0	0.0	0.0	0 0	0.0	0 0	0.0	0 0	0 0	0 0	0.0	0 0	0 0	0 0	0 0	0 0	0 0	0 0	0.0	0 0	0 0
Sphaeroidina bulloides	0.0	1.8	0 0	0.5	0.3	0.5	0 0	0 0	1.2	0.3	0.9	1 0	0 0	0.5	0 4	0.0	0.0	0.0	0 0	0.0	0 0
Oridorsalis umbonatus	0.3	4 1	4 7	0.5	0.3	3.3	1 1	0 0	2.1	0 8	2.6	2.6	0 4	1 4	0.8	2.9	0.8	2.1	0.0	0 0	1 1
Planulina rugosa	0 0	0.0	0.0	0.0	0 0	0 0	0.0	0 0	0 0	0 0	0 0	0 0	0 0	0 0	0 0	0 0	0 0	0 0	0.0	0 0	0 0
Planulina wuellerstorfi	0.0	0.0	0.0	0.0	0.9	0.5	0.0	0 0	0 0	0 0	0.0	0.5	0 0	0.5	0 0	0 0	0 0	.0	0 0	0 0	0 4
Cibicides lobatulus	0 0	0.0	0 0	0 0	0 0	0 0	0 0	0 0	0 0	0 0	0.0	0 0	0 0	0.0	0 0	0 0	0 0	0 0	0 0	0 0	0 0
Cibicidoides bradyi	0 0	0.0	0 4	0.5	0 0	0.5	0 0	0 0	0 0	0 0	0.0	0 0	0 0	0 0	0 8	0 0	0 0	0 0	0 0	0 0	1.5
C. spp.	0.6	0.0	1.9	0 0	0.0	0.5	0.3	0 0	0 6	0 0	1.3	0.5	0 8	0.5	0.8	0 0	0.0	0 0	0 0	0 0	0.4
Rosalina ? sp.	0.0	0.0	0.0	0 0	0.0	0 0	0 0	0 0	0 0	0 0	0.0	0 0	0 0	0.0	0 0	0 0	0.0	0 0	0 0	0 0	0 0
Gyroidina soldanii	0 6	4.5	4.3	0.5	0 6	1 0	0 0	0 0	0.3	0 8	1 7	1.6	1.2	0 9	3 4	4.3	0.0	0 4	0 0	0 0	0 7
Gavelinopsis praegeri	0.0	0.0	0 0	0.0	0.0	0 0	0 0	0 0	0 0	0 0	0.0	0 0	0.0	0 0	0 0	0 0	0.0	0	0 0	0 0	0 0
Laticarinina pauperata	0 0	0.0	0.0	0.0	0.0	0 0	0 0	0 0	0 0	0.0	0.0	0 0	0.0	0 0	0 0	0 7	0.0	0 4	0 0	0 0	0 0
Valvulineria laevigata	0 0	2.3	0.0	0.0	0.3	0 0	0 0	0 0	0 0	0 0	0.0	0.0	0.0	0 0	0 0	0 0	0.0	0 0	0 0	0 0	0 0
Nuttallides umbonifera	0.0	1.4	1.9	0.0	0 0	1 0	0 0	0 0	0 0	0.3	0.4	0.0	0.8	0.9	0 0	0 0	0 0	0 0	0 0	0 0	0 0
Hoeglundina elegans	0 0	0.0	0.0	0.0	0 0	0 0	0 0	0 0	0 0	0.0	0.0	0 0	0.0	0.0	0 0	0 0	0 0	0 0	0 0	0.0	0.0
Epistominella exigua	1.2	1 4	1.9	0.0	0 0	0 0	0 0	0 0	1.5	1 1	1.3	2.1	0 0	0.5	1 7	1 4	0 0	2.1	0 0	0 0	1 1
Eponides polius	0.0	0.0	0.0	0 0	0 0	0.5	0.0	0 0	0 0	0 0	0 0	0 0	0 0	0.0	0 0	0 0	0 0	0 0	0.0	0 0	0 0
E. tumidulus	0.0	1.8	1.9	0.5	0 0	2.9	0.6	0 0	1 2	3 1	1.3	3 7	4.5	5.5	2.1	0 0	0 0	0 4	0 0	0 0	4 9
Eponides weddellensis	0.0	0.5	10 1	2.5	0 6	6.2	1 4	0 6	3.9	5 1	8.7	2.6	2 8	8.7	5.5	4.3	0.8	2.1	0 4	0 0	5 6
E.? sp A	0.0	0.0	0 0	0.0	0 0	0 0	0 0	0 0	0 0	0 0	0 0	0 0	0 0	0.0	0 0	0 0	0 0	0 4	0 0	0 0	0.0
Discorbinella oertheloti	0 0	0 0	0 0	0 0	0 0	0 0	0 0	0 0	0.0	0.3	0 0	0 0	0 0	0.0	0 0	0 0	0 0	^0	0 0	0 0	0 0
Globocassidulina subglobosa	0 0	7 7	5 4	2.5	2.5	2.9	0 0	0 0	2.4	2.0	0.9	0.5	0 0	4 6	1.3	1 4	0 0	2.1	0 0	0 0	1.5
Cassidulina laevigata	0.0	0.0	0 0	0 0	0.0	0 0	0 0	0 0	0 0	0 0	0 4	0.5	0 0	0 0	0 0	0 0	0 0	C 0	0.0	0 0	0 0
C. reniforme	0.3	0 0	0.8	0.5	0 0	0.5	0 0	0 0	0 0	0 6	0 0	0 0	0 0	0 0	0.0	0 0	0 0	0.1	0 0	0 0	0 0
C. sp	0 0	0.9	0 0	0 0	0 0	0 0	0 0	0 0	0 0	0 0	0 0	0 0	0 0	0 0	0.0	0 0	0 0	0 0	0 0	0 0	0 0
Cassidulinoides tenuis	0 0	0 0	0 0	0 0	0 0	0 0	0 0	0 0	0 0	0 0	0 0	0.0	0 0	0 0	0 0	0 0	0 0	0 0	0 0	0 0	0 0
Unidentified rotaliids	0 0	2.3	0 0	0.5	0 0	0 0	0.0	0 0	0 0	0.3	0 0	0.0	0 4	0.9	0 0	0 0	0 0	4.2	0 0	0 0	0 0
Uvigerina peregrina	0 6	1.8	6.2	2.0	0 0	2.4	0.0	0 0	1.2	0 0	0 0	0.0	0 0	4 1	0 0	0 0	0 0	0 0	0.0	0 0	0 0
U proboscidea	0 0	0 0	0 0	0 0	0 0	0 0	0.3	0 0	0.9	0 0	0 0	0.0	0 0	0 0	0.0	0 0	0 0	0 0	0 0	0 0	0.0
U sp.	0 0	0.0	0.8	0 0	0 0	1 0	0.0	0 6	0 0	0.3	0 0	0 0	0 0	0 5	3 4	0 7	0 0	0 0	0 0	0 0	0 0

Site 646B Core	60x-3	60xCC	61x-1	61x-2	61x-3	61xCC	62x-1	62x-2	62x-3	62x-4	62x-5	63x-1	63x-2	63xCC	64x-1	65x-1	65x-3	65x 5	65x-7	65x-CC	66x-1
Interval (cm)	32-36	30-34	80-84	20-24	30-34	30-34	44-48	50-54	80-84	56-60	26-30	60-64	26-30	10-14	80-84	80-84	60-64	40-44	20-24	20-24	90-94
Depth (m subbottom)	567 72	568.2	574.8	575 7	577.3	577 7	584 04	585 6	587 4	588.66	589 09	593.8	594 96	596.26	603 7	613.3	616 1	618.9	621 7	622.05	623 1
Number picked	143	296	327	287	254	374	195	365	227	235	169	215	288	394	182	164	369	218	335	349	268
No./20CC	4576	4736	5232	4592	4064	2992	3120	5840	1816	3760	2704	3340	4608	6304	5824	2624	2952	3488	5376	5584	4144
% calcareous forms of total fauna	38.5	19.9	1.8	2	0.3	0	43.5	9.3	34.8	31.5	32.5	31.2	10.1	8.9	37.9	39 6	1 1	79.8	12 7	7.7	48.9
% benthic forams in total fauna	69.1	77.9	97.3	98 6	99.9	78 2	55 8	97	87 6	49.9	41.5	49 4	81.6	90.2	16 4	25	98 4	17.8	57.9	77 6	54
% Fragments of whole planktomes	84	87.9	80 4	89.2	100	71	77.8	75	80.8	71.2	55.5	68 8	81.2	68 6	43 6	69 6	92.8	71.5	71 7	73	67.7
Lenticulina spp.	0 0	0 0	0 0	0 0	0 0	0 0	0.0	0 0	0 4	0 0	0 0	0 0	0 0	0.0	0.0	0 0	0 0	0 0	0.0	0.0	0 0
Nonion spp.	4.9	2.7	0.0	0 0	0 0	0 0	4 1	0 8	2.2	3.8	1.2	5 1	0 7	0.5	6 6	7.9	0.3	10 1	0.9	1 7	12.3
Nonionella spp	0 0	0 0	0.0	0 0	0 0	0.0	0 0	0 0	0 0	0 4	1.2	0.0	0 0	0 0	1 1	0 0	0 3	5.5	0 6	0 0	0 0
Astrononion echolsi	0.0	0 0	0 0	0 0	0 0	0 0	0.0	0.0	0 0	0 0	0 0	0 0	0 0	0 0	0 0	0 0	0 0	0 0	0 0	0 0	0 0
Astrononion umbilicatulum	0.0	0 0	0 0	0 0	0 0	0 0	0 0	0 0	0 0	0 0	0 0	0.0	0 0	0 0	0 0	0 0	0 0	0 0	0 0	0 0	0.0
Elphidium? sp.	0.0	0 0	0 0	0.0	0 0	0 0	0.0	0 0	0 0	0 0	0 0	0 0	0 0	0 0	0 0	0.0	0 0	0 0	0 0	0 0	0 0
Pullenia bulloides	2.1	1 7	0.3	0.3	0 0	0 0	4 6	0 0	1 8	2.6	3 6	0.9	1 0	0 0	2.7	4.3	0 0	3.2	0.3	0 6	0 0
P quinqueloba	4.9	0 7	0 0	0 0	0 0	0 0	2.1	0 0	0 9	0 0	1.8	3 7	0.3	0 0	1 1	0 0	0 0	2.3	0 6	0.3	1 9
Melonis barleeanum/affinis	0 0	0 0	0 0	0 0	0 0	0 0	0 0	0.8	0 4	0 0	1 8	0 0	0 0	0 0	0 0	0 0	0 0	2.3	1.5	0 0	0.0
M pompiloides	0.0	0 0	0 0	0 0	0 0	0 0	0.5	0 0	0 0	0 0	0 6	0.5	0 0	0.0	0 0	1.2	0 0	2.8	0.3	0.3	3 7
Florilus sp.	0.0	0.0	0 0	0 0	0 0	0 0	0.0	0 0	0 0	0 0	0 0	0 0	0 0	0 0	0.0	0 0	0 0	0 0	0 0	0 0	0.0
Sphaeroidina bulloides	0.7	0 7	0 0	0.0	0 0	0 0	0.0	0.0	0 9	0 4	1 2	0 0	0 0	0 0	0 0	0.0	0 0	0 9	0 6	1 0	0 7
Ondorsalis umbonatus	1 4	0.3	0.3	1 0	0 0	0 0	7 7	0.5	4 8	3.6	1 8	0 0	0 0	0.5	0 0	1.2	0.3	5.5	0 9	0 0	8 2
Planulina rugosa	0.0	0.0	0 0	0 0	0 0	0.0	0 0	0.0	0 0	0 0	0 0	0 0	0 0	0 0	0 0	0 0	0 0	0 0	0 0	0 0	0 0
Planulina wuellerstorfi	0.0	0 0	0.3	0 0	0 0	0 0	0.0	0 0	0 0	0 0	0 0	0 0	0 0	0 0	0 0	0 0	0 0	0 0	0 0	0 0	0.7
Cibicides lobatulus	0.0	0 0	0 0	0 0	0 0	0 0	0 0	0.0	0 0	0 0	0 0	0 0	0 0	0 0	0 0	0 0	0 0	0 0	0 0	0.3	0.0
Cibicadoides bradyi	0 0	0.3	0 0	0 0	0 0	0 0	0.5	0 0	0 0	0 0	0 0	0 0	0 0	0 0	0 0	0 0	0 0	0 0	0 0	0.3	0.0
C. spp.	2.1	0.0	0 0	0 0	0 0	0 0	0 5	0 0	1 3	1 7	0.0	0 9	0.3	0.3	0.0	0 0	0 0	1 4	0 0	0 0	0.0
Rosalina ? sp.	0.0	0 0	0.0	0 0	0 0	0 0	0 0	0.0	0 0	0 0	0 0	0 0	0 0	0 0	0 0	0 0	0 0	0 0	0 0	0 0	0.0
Gyroidina soldanii	2.8	0 7	0 3	0 0	0 0	0 0	1.5	0 0	0 4	0 4	1.2	1 9	1 0	0 0	0 0	2 4	0 0	2.8	0 6	0 0	3 0
Gavelinops.s praegeri	0.0	0 0	0.0	0 0	0 0	0 0	0.0	0 0	0 0	0 0	0 0	0 0	0 0	0 0	0 0	0 0	0 0	0 0	0 0	0 0	0.0
Laticarinina pauperata	0.7	0 0	0 0	0 0	0.0	0.0	0 0	0 0	0 4	0 0	0.0	0.0	0 0	0 0	0 0	0 0	0 0	0 0	0 0	0 0	0 0
Valvulineria laevigata	0 0	0.0	0.0	0 0	0 0	0 0	0.0	0 0	0 0	0 0	0 0	0 0	0 0	0 0	0 0	0 0	0 0	0 0	0 0	0 0	0 0
Nuttallides umbonifera	0.0	0 0	0 0	0 0	0 0	0 0	0 0	0.0	0 0	0 0	0.0	0.0	0.3	0 0	0 0	0 0	0 0	0 0	0 0	0 0	0 0
Hoeglundina elegans	0	0 0	0 0	0.0	0 0	0 0	0.0	0.0	0 0	0 0	0 0	0 0	0 0	0 0	0 0	0 0	0 0	0 0	0 0	0 0	0.0
Epistominella exigua	0 0	0 0	0 0	0 0	0 0	0 0	0 0	0 0	0 0	1 3	0 0	0.0	0.3	0 0	1 6	1.2	0 0	6.9	0.9	0 0	3 0
Eponides polius	0 0	0 0	0 0	0 0	0 0	0.0	0 0	0 0	1 3	0 0	0.0	0.5	0 0	0 0	0 0	0 0	0.0	0 0	0 0	0 0	0 0
E. tumidulus	3.5	1 7	0 0	0 0	0 0	0 0	1.5	2.2	2.6	1 7	0 0	1 4	2.4	0 0	3.8	1.2	0 0	1.8	3 0	0 0	0.0
Eponides weddellensis	9 1	7.8	0 3	0 7	0 0	0 0	7 7	4 1	1 9	6 4	4 7	5 6	1 0	2.8	11.5	9 8	0.3	12 4	0 9	1 4	2.6
E.? sp. A	0 0	0 0	0 0	0 0	0 0	0.0	0 0	0 0	0 0	0 0	0.0	0 0	0 0	0 0	0 0	0 0	0 0	0 0	0 0	0 0	0 4
Discorbinella bertheloti	0.0	0 0	0 0	0 0	0 0	0 0	0.0	0 0	0 0	0 0	0 0	0 0	0 0	0 0	2.2	0 0	0 0	0 0	0 0	0 0	1.5
Globocassidulina subglobosa	4.2	1 0	0.3	0 0	0 4	0.0	5 1	0 0	0.9	2.1	0 0	3.3	0.3	2.3	3.8	3 7	0 0	7.8	0 9	0.3	5 6
Cassidulina laevigata	0 0	0 0	0 0	0.0	0 0	0 0	0.0	0 0	0 0	0 0	0 0	0 0	0 0	0 0	0 0	0 0	0 0	0 0	0 0	0 6	0 0
C. reniforme	0.0	0 0	0 0	0 0	0 0	0 0	0 6	0.0	0 0	0 0	0 0	0.5	0 0	0 0	0 0	0 6	0 0	1 8	0 0	0 6	0 0
C. sp.	1.4	0 0	0.0	0 0	0 0	0.0	0 0	0.3	0 0	0 4	1 8	0.0	0 0	0 0	0 0	0.6	0 0	3 0	0 6	0 0	0 0
Cassidulinoides tenuis	0 0	0 0	0 0	0 0	0 0	0 0	0 0	0 0	0 0	0 0	0.0	0 0	0 0	0 0	0 0	0 0	0 0	0 0	0 0	0.3	0 4
Unidentified rotaliids	0 7	0.3	0 0	0 0	0 0	0 0	0 0	0 3	0 0	0 0	0 0	4.2	1 4	0 0	2.2	0 0	0 0	0 9	0 0	0 0	0 0
Hvigerina peregrina	0.0	0 0	0 0	0.0	0 0	0.0	0 0	0.3	0 4	0 0	0.0	0 0	0 0	0 0	0 0	0 0	0 0	0 0	0 0	0 0	0 0
U proboscidea	0 0	0 0	0.0	0 0	0 0	0 0	0.5	0 0	0 0	0 0	0 0	0 0	0 0	0.0	0 0	0 0	0 0	0 0	0 0	0 0	0 0
U sp.	0 0	0 0	0 0	0 0	0 0	0 0	0 0	0 0	0 0	0 0	1.2	0 0	0 0	0 0	1 1	1 2	0 0	0.5	0 0	0 0	0 0

Site 646B Core	66xCC	67x-1	67x-2	67x-3	67x-5	67x-6	68x-2	68x-3	68x-4	69x-1	70x 1	70xCC	71x 1	71x-2	71x-4	71x-6	72x-1	72xCC	73x-1	73xCC	74x-4
Interval (cm)	20-24	60-64	50-54	40-44	50-54	50-54	50-54	50-54	36-40	40-44	50-54	70-24	50-54	40-44	40-44	32-36	72-76	6-10	46-50	10-14	30 34
Depth (m subbottom)	625.8	632.4	633.8	635.2	638.3	639.8	643.3	644.8	646 16	651.3	661	661.55	670 7	672.1	675 1	678.02	680.42	682.71	689 75	691 71	703.8
Number picked	368	147	190	189	331	180	119	295	351	347	314	483	543	353	174	244	406	237	413	158	626
No./20CC	2944	2352	6080	756	2648	1440	1904	4720	5616	5552	2512	15456	4344	2824	1392	976	3248	948	6608	5056	5008
% calcareous forms of total fauna	26.9	12.3	1	4.8	1.8	46.6	50 4	0	0	22.8	34 7	2.8	0 4	1 4	43 1	9	23 6	15.6	34 6	89.2	8.7
% benthic forams in total fauna	50	67 4	95.5	96.5	99 1	32.9	16	100	100	90 6	62 1	90 1	99 6	97 7	52 7	81 6	78.5	82.3	64 8	27.5	89
% Fragments of whole planktonics	71 1	64 1	35	88.8	81.3	63	57.8	0	0	95.2	61.8	58.3	0	0	29 7	56 7	78	69.8	86	74.8	74
Lenticulina spp.	0.0	0.0	0 0	0 0	0 0	0 6	0 0	0 0	0 0	0 0	0 0	0 0	0 0	0 0	0 6	0 0	0.0	0.0	0 0	0.0	0 0
Nonion spp.	7.9	0.0	0.5	0.0	0 0	7.2	9.2	0 0	0 0	5 2	3.2	0 0	0 0	0.3	2.3	0 0	1.5	0.4	4 1	12 7	0.6
Nonionella spp.	0.0	0.0	0 0	0.0	0 0	0 0	0 0	0.0	0 0	0 0	0 0	0 0	0 0	0 0	0 0	0.0	0 0	0.0	0 0	0.6	0 0
Astrononion echolsi	0.0	0.0	0.0	0.0	0.0	0.0	0.0	0.0	0.0	0.0	0 0	0 0	0 0	0.0	0 0	0.0	0 0	0.0	0 0	0.0	0.0
Astrononion umbilicatulum	0.0	0.0	0 0	0 0	0.0	0 0	0 0	0 0	0 0	0 0	0 0	0 0	0 0	0 0	0 0	0.0	0 2	0 0	0 0	0.0	0.0
Elphidium? sp.	0.0	0.0	0 0	0 0	0 0	0 0	0 0	0 0	0.0	0 0	0 0	0 0	0 0	0 0	0 0	0 0	0.0	0.0	0 0	0.0	0 0
Pullenia bulloides	0.3	0.7	0.0	0 0	0 0	1 7	1 7	0 0	0.0	0.9	2.5	0 4	0 0	0 0	1 7	0.0	1.2	1.3	2.2	2.5	0.3
P. quinqueloba	1.5	3 4	0 0	0 0	0.3	2.8	3 4	0 0	0 0	0 6	1.9	0 2	0 0	0.3	0 0	0 0	0 0	0 4	1 7	4 4	1.4
Melonis barleeanum/affinis	0.3	0 0	0 0	0 0	0.0	0 0	0.0	0.0	0 0	0 0	1.6	0 0	0 0	0 0	0 0	0.0	0.0	0 0	0 2	1.3	0.0
M. pompilioides	0.5	2.0	0.0	0.5	0.0	0.6	2.5	0 0	0 0	1 4	1.3	0.2	0.2	0.0	2.3	0 0	1.5	1.3	0 0	0.6	0.0
Florilus sp.	0.0	0 0	0.0	0.0	0 0	0 0	0 0	0 0	0 0	0 0	0 0	0 0	0 0	0 0	0 0	0 0	0 0	0 0	0.0	0.0	0 0
Sphaeroidina bulloides	0.8	0 0	0 0	0 0	0 0	0 0	0 0	0.0	0 0	0 6	0 0	0.0	0 0	0 0	1 1	0.0	0 0	0 0	0.0	0 0	0 0
Ordorsalis umbonatus	0.0	0 7	0 0	0.5	0 0	1 7	6.7	0 0	0.0	0.9	2.3	0 0	0 0	0.6	7.5	0 4	0 0	1 7	5 6	6.3	1 4
Planulina rugosa	0.0	0.0	0 0	0 0	0 0	0 0	0 0	0 0	0 0	0 0	0 0	0 0	0 0	0 0	0 0	0 0	0 0	0 0	0 0	0.0	0 0
Planulina wuellerstorfi	0.0	0 0	0.0	0 0	0 6	0 0	0.8	0 0	0 0	0 0	0 0	0 0	0 0	0.0	0.6	0.4	0 0	0 0	0 7	1.9	0 0
Cibicides lobatulus	0 0	0 0	0.0	0 0	0 0	0 0	0 0	0 0	0.0	0 0	0 0	0 0	0 0	0 0	0.0	0 0	0 0	0 0	0.0	0.6	0 0
Cibicidoides bradyi	0.0	0 0	0.0	0.0	0 0	0 0	0.0	0 0	0 0	0 0	0.3	0 0	0 0	0 0	0 6	0 0	0 2	0.4	0.2	0.6	0 0
C. spp.	0.3	0.0	0 0	0.5	0 0	1 1	0 0	0 0	0 0	0 0	0 0	0.0	0 0	0 0	0 6	0 0	0.0	0.8	0.2	0.0	0 0
Rosalina? sp.	0.0	0.0	0 0	0 0	0 0	0 0	0 0	0 0	0 0	0 0	0 0	0 0	0 0	0 0	0.0	0 0	0 0	0 0	0 0	0.0	0 0
Gyroidina soldanii	2.4	0.7	0.0	0 0	0 0	3.3	0.8	0 0	0 0	0 9	1.9	0.2	0 0	0 0	0.0	0 0	1 0	0.0	1.2	3.8	0 0
Gavelinopsis praegeri	0.0	0 0	0.0	0 0	0.0	0 0	0 0	0 0	0.0	0 0	0 0	0.0	0 0	0.0	0 0	0 0	0.0	0.0	0 0	0.0	0 0
Laticarinina pauperata	0.0	0.7	0.0	0.0	0 0	0 0	0 0	0 0	0 0	0.3	0 0	0.0	0 0	0 0	0.6	0 0	0 0	0 0	0 0	0 6	0 0
Valvulineria laevigata	0.0	0.0	0.0	0.0	0 0	0 0	0 0	0 0	0 0	0 0	0 0	0.0	0 0	0 0	0 0	0.0	0 0	0 0	0 0	0 0	0.0
Nuttallides umbonifera	0 0	0.0	0.0	0.0	0.0	0 0	0 0	0.0	0 0	1.2	0.3	0.0	0 0	0.0	0 0	1 0	4 7	1.3	2.4	5 7	2.7
Hoeglundina elegans	0 0	0.0	0.0	0 0	0 0	0 0	0 0	0 0	0 0	0 0	0 0	0.0	0 0	0.0	0 0	0.0	0 0	0 0	0 0	0 0	0 0
Epistominella exigua	0.8	0.7	0.0	0.0	0 6	5 0	1 7	0 0	0 0	0.6	2.9	0.2	0 0	0.0	6.3	1.2	0 0	0 0	0.5	3.8	0 0
Epondes polius	0.0	0 0	0.0	0 0	0 0	0 0	0 0	0 0	0 0	0.3	0.0	0 0	0 0	0.0	0 0	0.0	0 0	0 0	0 0	0 0	0 0
E. tumidulus	0.8	0.7	0.0	0 0	0 0	4 4	0.0	0 0	0 0	0 0	0.0	0 0	0 0	0.0	0 0	0.0	0 2	0 0	0 7	6.3	0 0
Epondes weddellensis	4.5	1 4	0.0	1 1	0 0	6 7	12 6	0 0	0 0	7.8	8.0	0 2	0 0	0.3	1 1	0.8	2.0	3 0	7 7	10.8	0.0
E.? sp. A	0.3	0.0	0.0	0.0	0 0	0 0	2.5	0 0	0 0	0 0	0.0	0 0	0 0	0 0	0 0	0 0	0 0	0 0	0 0	0 0	0 0
Discorbinella bertheloti	0.0	0.0	0.0	0 0	0 0	0 0	0 0	0 0	0 0	0.0	0 ?	0 0	0 0	0.0	0 0	0 0	0 0	0 0	0 0	0.0	0 0
Globocassidulina subglobosa	3.5	0 0	0.0	0.0	0 0	5 6	2.5	0.0	0 0	1 4	4 1	0.2	0.0	0.0	1 7	0 4	3 7	1.3	4.8	14 6	0.3
Cassidulina laevigata	0 0	0.0	0.0	0 0	0 0	0 0	0.0	0 0	0 0	0 0	0.0	0 0	0 0	0.0	0 0	0 0	0 0	0 0	0 0	0 0	0 0
C. reniforme	0.3	0.0	0.0	0 0	0 0	0 0	0.0	0 0	0 0	0.3	0.3	0 0	0.0	0 0	0 0	0 0	0 0	0 0	0 2	0 6	0 0
C. sp.	0 0	0.0	0.0	0 0	0 0	0 0	0.0	0.0	0 0	0 0	0 0	0 0	0.0	0 0	0 0	0 0	0 0	0 0	0 0	0 0	0.0
Cassidulinoides tenuis	0 0	0 0	0.0	0 0	0 0	0.0	0.0	0 0	0 0	0 0	0 0	0 0	0.0	0 0	0 6	0 0	0 0	0 0	0 0	0 0	0.0
Unidentified rotaliids	0 0	0.0	0 0	0 0	0 0	0 6	0.0	0 0	0 0	0 0	2.2	0 8	0 0	0 0	0 0	2.0	0.5	0.8	0.5	1.9	0 0
Uvigerina peregrina	0 0	0 0	0.0	0 0	0 0	0 0	0.0	0.0	0 0	0 0	0.0	0 0	0 0	0 0	0 0	0 0	0.0	0 0	0 0	0.0	0 6
U. proboscidea	0.0	0 0	0.0	0 0	0 0	0 0	0.0	0 0	0 0	0 0	0 0	0 0	0 0	0 0	0 0	0 0	0.0	0.0	0 0	0.0	0 0
U. sp.	0.0	0 0	0.0	0 0	0 0	0 0	0.0	0 0	0 0	0 0	0 3	0 0	0.0	0 0	0 0	0 4	1.0	0.0	0.0	1.3	0.5

Site 646B Core	75x-5	76x-2	77x-5	78xCC	79x-CC	80x-2
Interval (cm)	30-34	50-54	20-24	26-30	40-44	30-34
Depth (m subbottom)	714.9	720.3	734.1	739.75	750.64	758.8
Number picked	1526	1731	165	348	238	332
No./20CC	12208	13843	330	696	476	332
% calcareous forms of total fauna	0	0	6.1	98	73.5	62.9
% benthic forams in total fauna	100	100	100	48.5	11.7	21.7
% Fragments of whole planktonics	0	0	0	45	22.4	24.8
Lenticulina spp.	0.0	0.0	0.0	0.6	0.0	0.0
Nonion spp.	0.0	0.0	0.0	0.3	4.2	1.2
Nonionella spp.	0.0	0.0	0.0	0.0	0.0	0.0
Astrononion echolsi	0.0	0.0	0.0	0.0	0.0	0.6
Astrononion umbilicatulum	0.0	0.0	0.0	0.0	0.0	0.0
Elphidium? sp.	0.0	0.0	0.0	0.0	0.0	0.0
Pullenia bulloides	0.0	0.0	0.0	0.6	0.4	2.4
P. quinqueloba	0.0	0.0	0.0	1.4	0.0	0.9
Melonis barleeanum/affinis	0.0	0.0	0.0	0.3	0.0	0.6
M. pompilioides	0.0	0.0	0.0	0.0	0.0	0.9
Florilus sp.	0.0	0.0	0.0	0.0	0.0	0.0
Sphaeroidina bulloides	0.0	0.0	0.0	0.0	0.0	0.0
Oridorsalis umbonatus	0.0	0.0	0.0	0.0	18.9	3.0
Planulina rugosa	0.0	0.0	0.0	0.3	0.0	0.0
Planulina wuellerstorfi	0.0	0.0	0.0	0.0	1.7	0.0
Cibicides lobatulus	0.0	0.0	0.0	0.0	1.3	6.0
Cibicidoides bradyi	0.0	0.0	0.0	0.0	0.0	0.3
C. spp.	0.0	0.0	0.0	2.9	0.0	0.0
Rosalina ? sp.	0.0	0.0	0.0	0.0	0.0	0.0
Gyroidina soldanii	0.0	0.0	0.0	2.9	1.3	0.9
Gavelinopsis praegeri	0.0	0.0	0.0	0.0	0.0	0.0
Laticarinina pauperata	0.0	0.0	0.0	0.3	0.4	1.2
Valvulineria laevigata	0.0	0.0	0.0	0.0	0.0	0.0
Nuttallides umbonifera	0.0	0.0	0.0	2.3	0.0	0.0
Hoeglundina elegans	0.0	0.0	0.0	0.0	0.0	0.0
Epistominella exigua	0.0	0.0	0.0	23.3	18.9	6.3
Eponides polius	0.0	0.0	0.0	0.3	0.0	0.0
E. tumidulus	0.0	0.0	0.0	0.9	0.0	3.3
Eponides weddellensis	0.0	0.0	0.0	7.2	1.7	1.5
E.? sp. A	0.0	0.0	0.0	0.0	0.0	0.0
Discorbinella bertheloti	0.0	0.0	0.0	0.0	0.0	0.0
Globocassidulina subglobosa	0.0	0.0	0.0	6.6	10.5	2.1
Cassidulina laevigata	0.0	0.0	0.0	0.0	0.0	0.0
C. reniforme	0.0	0.0	0.0	0.0	0.0	0.0
C. sp.	0.0	0.0	0.0	0.3	0.0	0.0
Cassidulinoides tenuis	0.0	0.0	0.0	0.0	0.4	0.0
Unidentified rotaliids	0.0	0.0	0.0	0.9	1.3	0.9
Uvigerina peregrina	0.0	0.0	0.0	0.3	0.4	0.0
U. proboscidea	0.0	0.0	0.0	0.0	0.0	0.0
U. sp.	0.0	0.0	0.0	0.0	0.0	0.0

Site 646B Core	41x-2	41x-6	42x-1	42x-3	42x-5	42x-7	43x-2	43xCC	44xCC	45x-1	45xCC	46x-2	46x-4	46xCC	47x-2	47xCC	48x-1	48xCC	49x-1	49xCC
Interval (cm)	130-134	70-74	100-104	116-120	90-94	20-24	50-54	10-14	30-34	20-24	20-24	80-84	20-24	20-24	70-74	10-14	110-114	15-19	60-64	20-24
Rectuvigerina spp.	0.0	0.7	0.0	0.0	0.0	0.0	0.0	0.0	0.0	0.0	0.0	0.0	0.0	0.0	0.0	0.0	0.0	0.0	0.0	0.0
Trifrina angulosa	0.6	0.0	1.1	0.0	0.0	0.0	0.0	0.0	0.0	0.0	0.0	0.0	0.0	0.0	0.0	0.6	0.4	0.0	0.0	0.0
Ehrenbergina trigona	0.6	0.0	0.0	0.0	0.0	0.0	0.0	0.0	0.0	0.0	0.0	0.0	0.0	0.0	0.0	0.0	0.0	0.0	0.0	0.0
Bulimina alazaensis	0.0	0.0	0.0	0.0	0.7	0.0	0.0	0.0	0.0	0.0	0.0	0.0	0.0	0.0	0.0	0.0	0.0	0.0	0.0	0.0
B. tessellata	0.0	5.8	0.0	0.0	0.0	0.0	0.0	4.0	1.4	0.0	0.0	0.0	0.0	0.0	0.0	0.0	0.0	0.0	0.0	0.0
B. sp.	0.0	0.0	0.0	0.0	0.0	0.0	0.0	0.0	0.0	0.0	0.0	0.0	0.0	0.0	0.3	0.0	0.0	0.0	0.0	0.0
Globobulimina auriculata	0.0	0.0	0.0	0.0	0.0	0.0	0.0	0.0	0.0	0.0	0.0	0.0	0.0	0.0	1.0	0.0	0.0	0.0	0.0	0.4
Robertinoides charlottensis	0.0	0.3	0.0	0.0	0.0	0.0	0.0	0.0	0.0	0.0	0.0	0.0	0.0	0.0	0.0	0.0	0.0	0.0	0.0	0.0
Bolivina pygmaea	0.0	0.0	0.0	0.0	0.0	0.0	0.0	0.0	0.0	0.0	0.0	0.0	0.0	0.0	0.0	0.0	0.4	0.0	0.0	0.0
B. cf. pygmaea	0.0	0.0	0.0	0.0	0.0	0.0	0.0	0.0	0.0	0.0	0.0	0.0	0.0	0.0	0.0	0.0	0.0	0.0	0.0	0.0
Bolivina pseudoplicata	0.0	0.0	0.0	0.0	0.0	0.0	0.0	0.0	0.0	0.0	0.0	0.0	0.0	0.0	0.0	0.0	0.0	0.0	0.0	0.0
B. pseudothalmanni	0.0	0.0	0.0	0.0	0.0	0.0	0.0	0.0	0.0	0.0	0.0	0.0	0.0	0.0	0.0	0.0	0.0	0.0	0.0	0.0
B. simplex	0.0	0.0	0.0	0.0	0.0	0.0	0.0	0.0	0.0	0.0	0.0	0.0	0.0	0.0	0.0	0.0	0.0	0.0	0.0	0.0
B. pseudopunctata	0.0	0.0	0.0	0.0	0.0	0.0	0.0	0.0	0.0	0.0	0.0	0.8	0.4	0.0	0.0	0.0	0.0	0.0	0.0	0.0
B. lowmani	0.0	0.0	0.0	0.0	0.0	0.0	0.0	0.0	0.0	0.0	0.0	0.0	0.0	0.0	0.0	0.0	0.0	0.0	0.0	0.0
B. inflata	0.0	0.0	0.0	0.0	0.0	0.0	0.0	0.0	0.0	0.0	0.0	0.0	0.0	0.0	0.0	0.0	0.0	0.0	0.0	0.0
B. cf alata	0.0	0.0	0.0	0.0	0.0	0.0	0.0	1.1	0.7	0.0	0.0	0.0	0.0	0.3	0.0	0.0	1.1	0.0	0.0	0.0
B. spp.	1.2	0.3	2.3	0.0	0.0	1.5	0.0	0.0	0.7	0.7	0.0	0.0	0.0	0.3	0.0	0.0	1.1	0.0	0.0	0.0
Nodosaria sp.	0.0	0.0	0.0	0.0	0.0	0.0	0.0	0.0	0.0	0.0	0.0	0.0	0.0	0.0	0.0	0.0	0.0	0.0	0.0	0.0
Fursenkoina fusiformis	0.0	0.0	0.0	0.0	0.0	0.0	0.0	0.0	0.0	0.0	0.0	0.0	0.0	0.0	0.5	0.0	0.0	0.0	0.0	0.0
Pleurostomella spp.	0.0	0.3	0.0	0.0	0.4	0.8	0.0	0.6	0.0	0.0	0.0	0.4	0.4	0.3	0.5	0.0	0.4	0.0	0.0	0.0
Stilostomella spp.	0.0	0.0	0.0	0.0	0.0	0.0	0.0	0.0	0.0	0.0	0.0	0.0	0.0	0.0	0.0	0.0	0.4	0.0	0.0	0.0
Dentalina communis	0.0	0.0	0.0	0.0	0.0	0.0	0.0	0.0	0.0	0.0	0.0	0.0	0.0	0.0	0.0	0.0	0.0	0.0	0.0	0.0
Guttulina sp.	0.0	0.0	0.0	0.0	0.0	0.0	0.0	0.0	0.0	0.0	0.0	0.0	0.0	0.0	0.0	0.0	0.4	0.0	0.0	0.4
Oolina spp.	1.8	1.4	0.0	0.0	0.0	0.0	0.0	1.1	0.0	0.0	0.0	0.4	0.4	0.0	1.4	0.0	0.0	0.4	0.3	0.0
Lagena spp.	0.6	0.0	0.0	0.0	0.7	0.0	0.0	0.6	1.4	0.0	0.0	0.4	0.4	0.3	0.5	0.6	1.1	1.2	0.0	0.0
Fissurina spp.	0.0	1.4	0.0	0.0	1.1	1.9	0.0	2.3	1.4	0.3	0.2	0.0	0.4	0.3	1.4	0.0	0.7	0.0	0.0	0.0
Quinqueloculina seminula	0.0	0.0	0.0	0.0	0.0	0.0	0.0	0.0	0.0	0.0	0.0	0.4	0.0	0.0	0.0	0.0	0.0	0.0	0.0	0.0
Q sp.	0.0	0.0	0.0	0.0	0.0	0.0	1.3	1.1	0.0	0.3	0.0	1.1	0.9	1.0	1.0	0.6	0.0	0.8	0.0	0.0
Pyrgo spp.	0.0	1.4	0.0	0.0	0.0	0.0	0.0	0.0	0.0	0.0	0.0	0.0	0.0	0.0	0.0	0.0	0.0	0.4	0.0	0.0
Sigmoilina tenuis	0.0	0.0	0.0	0.0	0.0	0.0	0.0	1.1	0.7	0.0	0.0	0.0	0.0	0.0	0.0	0.0	0.0	0.0	0.0	0.0
Tosaia hanzawai	0.0	1.4	1.1	0.0	0.0	0.8	0.0	1.1	0.7	0.3	0.2	0.4	0.9	0.0	1.0	0.0	1.5	0.0	0.0	0.4
Cornuspirella diffusa	0.0	0.0	0.0	0.0	0.0	0.0	0.0	0.0	0.0	0.0	0.0	0.0	0.0	0.0	0.0	0.0	0.0	0.0	0.0	0.0
Unidentified serial forms	0.0	0.0	0.0	0.0	0.4	0.0	0.0	0.0	0.0	0.7	0.2	0.0	0.4	0.0	0.0	0.6	0.0	0.0	0.0	0.4
Karreriella bradyi	0.0	0.3	0.0	0.0	0.0	0.0	0.0	0.0	0.0	0.7	0.0	0.0	0.4	0.0	0.5	0.0	0.0	0.4	0.3	0.0
Martinottiella communis	0.0	0.7	0.0	0.0	0.0	0.0	0.0	0.0	0.0	0.0	0.0	0.0	0.4	0.0	0.0	0.0	0.0	0.0	0.0	0.0
Siphotextularia sp.	0.0	2.0	0.0	0.0	0.0	0.0	0.5	1.7	4.3	0.0	0.0	0.4	0.0	0.0	0.0	0.0	0.0	0.0	0.3	0.0
Trochammina cf squamata	1.8	3.8	21.6	9.4	33.0	28.6	23.3	1.7	0.0	12.8	72.0	36.4	55.2	47.1	5.8	0.6	0.0	0.0	0.0	0.4
Trochammina sp.W	0.0	0.3	13.6	0.0	0.0	0.8	0.0	5.2	0.0	9.1	1.7	5.3	0.4	8.0	7.7	13.9	5.9	23.3	29.9	29.4
Cyclammina cancellata	0.0	0.0	0.0	0.0	0.0	0.0	0.5	0.0	0.0	0.3	0.2	0.0	0.0	0.3	1.4	0.0	0.4	0.0	0.7	0.4
Ammotium sp. A	0.0	0.0	3.4	0.0	1.5	0.0	0.0	0.0	0.0	0.0	5.4	1.5	2.6	3.2	0.5	0.0	0.0	0.0	0.0	0.0
Recurvoides sp.	0.0	0.0	0.0	0.0	0.0	0.0	0.3	0.0	0.0	0.7	0.0	0.0	0.0	0.0	1.0	0.6	0.0	0.4	0.7	0.4
Haplophragmoides	0.0	0.0	0.0	0.0	0.0	0.0	0.0	0.0	0.0	0.0	0.0	0.0	0.0	0.0	0.0	0.0	0.0	0.0	0.0	0.0
Miliammina fusca	0.0	0.0	0.0	0.0	0.0	0.0	0.0	0.0	0.0	0.0	0.0	0.0	0.0	0.0	0.0	0.0	0.0	0.0	0.0	0.0
Ammobaculites sp.	0.0	0.0	0.0	0.0	0.0	0.0	1.0	0.0	0.0	0.0	0.2	1.5	0.4	0.0	0.5	1.2	0.0	0.8	0.3	0.4
Sigmoilopsis schlumbergeri	0.0	0.0	0.0	0.0	0.0	0.0	0.0	0.0	0.7	0.0	0.0	0.0	0.0	0.0	0.0	0.0	0.0	0.0	0.0	0.0

Site 646B Core	49x-1	50x-2	50x-3	50xCC	51x-1	52xCC	54x-1	54x-1	54x-3	55x-2	55x-3	55xCC	56x-1	56x-2	56xCC	57x-3	57x-4	57xCC	58x-1	58x-2	59xCC
Interval (cm)	62-65	30-34	22-26	30-34	80-84	20-24	60-64	140-144	16-26	80-84	27-31	10-14	110-114	60-64	20-24	40-44	22-26	20-24	50-54	40-44	20-24
Rectuvigerina spp.	0.0	0.0	0.0	2.5	0.0	0.0	0.0	0.0	0.0	0.0	0.0	0.0	0.0	0.0	0.0	0.0	0.0	0.0	0.0	0.0	0.0
Trifrina angulosa	0.0	0.0	0.0	0.0	0.0	0.0	0.0	0.0	0.0	0.0	0.0	0.0	0.0	0.0	0.0	0.0	0.0	0.0	0.0	0.0	0.0
Ehrenbergina trigona	0.0	0.0	0.0	0.0	0.0	0.0	0.0	0.0	0.0	0.0	0.0	0.0	0.0	0.0	0.0	0.0	0.0	0.0	0.0	0.0	0.0
Bulimina alazanensis	0.0	0.0	0.0	0.0	0.0	0.0	0.0	0.0	0.0	0.0	0.0	0.0	0.0	0.0	0.0	0.0	0.0	0.0	0.0	0.0	0.0
B. tessellata	0.0	0.0	0.0	0.0	0.0	0.0	0.0	0.0	0.0	0.0	0.0	0.0	0.0	0.0	0.0	0.0	0.0	0.0	0.0	0.0	0.0
B. sp.	0.3	0.0	0.0	0.0	0.0	0.0	0.0	0.0	0.0	0.0	0.0	0.0	0.0	0.0	0.0	0.0	0.0	0.0	0.0	0.0	0.0
Globobulimina auriculata	0.0	0.9	0.4	5.9	0.0	0.5	0.0	0.0	0.0	0.3	0.0	0.0	0.0	0.0	0.0	0.0	0.0	0.0	0.0	0.0	0.0
Robertinoides charlottensis	0.0	0.0	0.0	0.0	0.0	0.0	0.0	0.0	0.0	0.0	0.0	0.0	0.0	0.0	0.0	0.0	0.0	0.0	0.0	0.0	0.0
Bolivina pygmaea	0.0	0.0	0.0	0.0	0.0	0.0	0.6	0.0	0.0	0.0	0.0	0.0	0.0	0.0	0.0	0.0	0.0	0.0	0.0	0.0	0.0
B. cf. pygmaea	0.0	0.0	0.0	0.0	0.0	0.0	0.0	0.0	0.0	1.1	0.0	0.0	0.0	0.0	0.0	0.0	0.0	0.0	0.0	0.0	0.0
Bolivina pseudoplicata	0.0	0.0	0.4	0.0	0.0	0.0	0.0	0.0	0.0	0.0	0.0	0.0	0.0	0.0	0.0	0.0	0.0	0.0	0.0	0.0	0.0
B. pseudothalmanni	0.0	0.0	0.0	0.0	0.3	0.0	0.0	0.0	0.9	0.0	0.0	0.0	0.0	0.0	0.0	0.0	0.0	0.0	0.0	0.0	0.0
B. simplex	0.0	0.0	0.0	0.0	0.0	0.0	0.0	0.0	0.0	0.0	0.0	0.0	0.0	0.0	0.0	0.0	0.0	0.0	0.0	0.0	0.0
B. pseudopunctata	0.0	0.5	0.0	0.0	0.0	0.0	0.0	0.0	0.3	0.0	0.9	0.0	0.0	0.0	0.4	0.7	0.0	0.0	0.0	0.0	0.4
B. lowmani	0.0	0.0	0.0	0.0	0.0	0.0	0.0	0.0	0.0	0.0	0.0	0.0	0.0	0.0	0.0	0.0	0.0	0.0	0.0	0.0	0.0
B. inflata	0.0	0.0	0.0	0.0	0.0	0.0	0.0	0.0	0.0	0.0	0.0	0.0	0.0	0.0	0.0	0.0	0.0	0.0	0.0	0.0	0.0
B. cf. elata	0.0	0.5	0.4	0.0	0.0	0.0	0.0	0.0	0.0	0.0	0.0	0.0	0.0	0.0	0.0	0.0	0.0	0.0	0.0	0.0	0.0
B. spp.	0.0	0.5	0.4	0.0	0.0	0.0	0.0	0.0	0.3	0.3	0.0	0.0	0.0	0.0	0.0	0.0	0.0	0.0	0.0	0.0	0.0
Nodosaria sp.	0.0	0.0	0.0	0.0	0.0	0.0	0.0	0.0	0.0	0.0	0.0	0.0	0.0	0.0	0.0	0.0	0.0	0.0	0.0	0.0	0.0
Fursenkoina fusiformis	0.0	0.0	0.0	0.0	0.0	0.0	0.0	0.0	0.0	0.0	0.0	0.0	0.0	0.0	0.0	0.0	0.0	0.0	0.0	0.0	0.0
Pleurostomella spp.	0.3	0.5	0.4	0.0	0.0	0.0	0.0	0.0	0.9	0.0	0.0	0.0	0.0	0.0	0.0	0.0	0.0	0.0	0.0	0.0	0.0
Stilostomella spp.	0.0	0.0	0.0	0.0	0.0	0.0	0.0	0.0	0.0	0.0	0.0	0.5	1.2	0.5	0.0	0.0	0.0	0.0	0.0	0.0	0.0
Dentalina communis	0.0	0.0	0.0	0.0	0.0	0.0	0.0	0.0	0.0	0.0	0.0	0.0	0.0	0.0	0.0	0.0	0.0	0.0	0.0	0.0	0.0
Guttulina sp.	0.0	0.0	0.4	0.0	0.0	0.0	0.0	0.0	0.0	0.0	0.0	0.0	0.0	0.0	0.0	0.0	0.0	0.0	0.0	0.0	0.0
Oolina spp.	0.0	0.9	0.4	0.0	0.0	0.0	0.0	0.0	0.0	0.0	0.0	0.0	0.0	0.5	0.0	0.0	0.0	0.0	0.0	0.0	0.0
Lagena spp.	0.0	0.0	0.8	0.0	0.0	0.5	0.0	0.0	0.6	0.0	0.9	0.0	0.4	0.9	0.4	0.0	0.0	0.0	0.0	0.0	0.0
Fissurina spp.	0.6	1.8	0.4	0.0	0.0	0.5	0.3	0.0	0.3	0.3	1.3	0.5	0.0	0.5	0.4	0.0	0.8	0.0	0.0	0.0	0.4
Quinqueloculina seminula	0.0	0.0	0.0	0.0	0.0	0.0	0.0	0.0	0.0	0.0	0.0	0.0	0.0	0.0	0.0	0.0	0.0	0.0	0.0	0.0	0.0
Q. sp.	0.0	1.4	1.2	0.0	0.3	1.0	0.0	0.0	0.0	1.1	1.7	1.0	0.0	0.0	0.8	0.7	0.0	0.4	0.0	0.0	0.4
Pyrgo spp.	0.0	0.0	0.4	0.0	0.6	0.5	0.0	0.0	0.0	0.0	0.0	0.5	0.0	0.0	0.0	0.0	0.0	0.0	0.0	0.0	0.0
Sigmoilina tenuis	0.0	0.0	0.8	0.0	0.0	0.0	0.0	0.0	0.0	0.0	0.0	0.0	0.0	0.0	0.0	0.0	0.0	0.0	0.0	0.0	0.0
Tosaia hanzawai	0.0	2.3	1.2	0.5	0.0	0.5	0.0	0.0	1.2	0.3	0.0	0.0	0.0	0.0	0.8	0.0	0.0	0.0	0.0	0.0	0.0
Cornuspirella diffusa	0.0	0.0	0.4	0.0	0.0	0.0	0.0	0.0	0.0	0.0	0.4	0.0	0.0	0.0	0.0	0.0	0.0	0.0	0.0	0.0	0.0
Unidentified serial forms	0.0	0.0	0.4	1.5	0.0	0.0	0.0	0.0	0.0	1.1	0.9	0.0	0.0	0.5	0.4	0.0	0.0	0.0	0.0	0.0	0.0
Karreriella bradyi	0.0	0.0	0.0	0.0	0.0	0.0	0.0	0.0	0.0	0.0	0.4	0.0	0.0	0.0	0.0	0.0	0.0	0.0	0.0	0.0	0.0
Martinottiella communis	0.0	0.0	0.0	0.0	0.0	0.0	0.0	0.0	0.0	0.0	0.0	0.0	0.0	0.0	0.0	0.0	0.0	0.0	0.0	0.0	0.0
Siphotextularia sp.	0.0	0.0	0.8	0.0	0.9	0.0	0.0	6.2	0.0	0.3	0.0	0.0	0.0	0.0	0.0	0.0	0.0	0.0	0.0	0.0	0.0
Trochammina cf. squamata	18.2	23.9	1.9	21.6	1.6	61.2	90.1	94.4	68.0	55.1	7.9	1.6	21.1	3.2	19.7	51.4	83.6	15.4	53.2	9.7	28.0
Trochammina sp. W	24.2	4.5	9.3	19.1	36.0	0.0	0.6	1.2	0.0	0.3	14.4	21.5	9.3	11.4	9.7	0.0	1.6	18.8	11.6	2.3	3.6
Cyclammina cancellata	0.9	0.0	0.0	0.0	0.0	0.0	0.0	0.0	0.0	0.0	0.0	0.0	0.0	0.0	0.0	0.0	0.0	0.0	0.7	0.7	0.0
Ammotium sp. A	0.9	0.9	0.0	1.0	0.0	2.4	1.9	2.5	2.1	5.3	0.9	0.5	2.0	0.0	1.7	15.0	2.2	1.7	1.5	3.2	2.2
Recurvoides sp.	1.5	0.5	0.0	2.5	0.0	0.0	0.3	0.0	0.0	0.2	0.9	1.0	0.4	0.0	0.0	0.0	0.0	0.4	0.4	2.7	0.4
Haplophragmoides	0.0	0.0	0.0	0.0	0.0	0.0	0.0	0.0	0.0	0.0	0.0	0.0	0.0	0.0	0.0	0.0	0.0	0.0	0.0	0.0	0.0
Miliammina fusca	0.0	0.0	0.0	0.0	0.0	0.0	0.0	0.0	0.0	0.0	0.0	0.0	0.0	0.0	0.0	0.0	0.0	0.0	0.0	0.0	0.0
Ammobaculites sp.	0.3	0.5	0.8	1.0	0.0	0.0	0.0	0.0	0.0	0.6	0.9	3.1	2.0	1.8	2.1	1.4	1.6	2.5	2.8	0.3	2.2
Sigmoilopsis schlumbergeri	0.0	0.0	0.0	0.0	0.0	0.0	0.0	0.0	0.0	0.0	0.0	0.0	0.0	0.0	0.0	0.0	0.0	0.0	0.0	0.0	0.0

Site 646B Core	60x-3	60xCC	61x-1	61x-2	61x-3	61xCC	62x-1	62x-2	62x-3	62x-4	62x-5	63x-1	63x-2	63xCC	64x-1	65x-1	65x-3	65x-5	65x-7	65x-CC	66x-1
Interval (cm)	32-36	30-34	80-84	20-24	30-34	30-34	44-48	50-54	80-84	56-60	26-30	60-64	26-30	10-14	80-84	80-84	60-64	40-44	20-24	20-24	90-94
Rectuvigerina spp.	0.0	0.0	0.0	0.0	0.0	0.0	0.0	0.0	0.0	0.0	0.0	0.0	0.0	0.0	0.0	0.0	0.0	0.0	0.0	0.0	0.0
Trifrina angulosa	0.0	0.0	0.0	0.0	0.0	0.0	0.0	0.0	0.0	0.0	0.0	0.0	0.0	0.0	0.0	0.0	0.0	0.0	0.0	0.0	0.0
Ehrenbergina trigona	0.0	0.0	0	0.0	0.0	0.0	0.0	0.0	0.0	0.0	0.0	0.0	0.0	0.0	0.0	0.0	0.0	0.0	0.0	0.0	0.0
Bulimina alazanensis	0.0	0.0	0.0	0.0	0.0	0.0	0.0	0.0	0.0	0.0	0.0	0.0	0.0	0.0	0.0	0.0	0.0	0.5	0.0	0.0	0.0
B. tessellata	0.0	0.0	0.0	0.0	0.0	0.0	0.0	0.0	0.0	0.0	0.0	0.0	0.0	0.0	0.0	0.0	0.0	0.0	0.0	0.0	0.0
B. sp.	0.0	0.0	0.0	0.0	0.0	0.0	0.0	0.0	0.0	0.0	0.0	0.0	0.0	0.0	0.0	0.0	0.0	0.0	0.0	0.0	0.0
Globobulimina auriculata	0.0	0.0	0.0	0.0	0.0	0.0	0.0	0.0	0.0	0.0	0.0	0.0	0.0	0.0	0.0	0.0	0.0	0.0	0.0	0.0	0.0
Robertinoides charlottensis	0.0	0.0	0.0	0.0	0.0	0.0	0.0	0.0	0.0	0.0	0.0	0.0	0.0	0.0	0.0	0.0	0.0	0.0	0.0	0.0	0.0
Bolivina pygmaea	0.0	0.0	0.0	0.0	0.0	0.0	0.0	0.0	0.0	0.0	0.0	0.0	0.0	0.0	0.0	0.0	0.0	0.0	0.0	0.0	0.0
B. cf. pygmaea	0.0	0.0	0.0	0.0	0.0	0.0	0.0	0.0	0.0	0.0	0.0	0.0	0.0	0.0	0.0	0.0	0.0	0.0	0.0	0.0	0.0
Bolivina pseudoplicata	0.0	0.0	0.0	0.0	0.0	0.0	0.0	0.0	0.0	0.0	0.0	0.0	0.0	0.0	0.0	0.0	0.0	0.0	0.0	0.0	0.7
B. pseudothalmanni	0.0	0.0	0.0	0.0	0.0	0.0	0.0	0.0	0.0	0.0	0.0	0.0	0.0	0.0	0.0	0.0	0.0	0.0	0.0	0.0	0.0
B. simplex	0.0	0.0	0.0	0.0	0.0	0.0	0.0	0.0	0.0	0.0	0.0	0.5	0.0	0.0	0.0	0.0	0.0	0.0	0.0	0.0	0.0
B. pseudopunctata	0.0	0.0	0.0	0.0	0.0	0.0	0.0	0.0	0.0	0.0	0.0	0.0	0.0	0.0	0.0	0.0	0.0	0.0	0.0	0.0	0.0
B. lowmani	0.0	0.0	0.0	0.0	0.0	0.0	0.0	0.0	0.0	0.0	0.0	0.0	0.0	0.0	0.0	0.0	0.0	0.5	0.0	0.0	0.4
B. inflata	0.0	0.0	0.0	0.0	0.0	0.0	0.0	0.0	0.0	0.0	0.0	0.0	0.0	0.0	0.0	0.0	0.0	0.0	0.0	0.0	0.0
B. cf. alata	0.0	0.0	0.0	0.0	0.0	0.0	0.0	0.0	0.0	0.0	0.0	0.0	0.0	0.0	0.0	0.0	0.0	0.0	0.0	0.0	0.0
B. spp.	2.8	0.3	0.0	0.0	0.0	0.0	0.0	0.0	0.0	0.0	0.0	0.0	0.0	0.3	0.0	0.0	0.0	0.0	0.0	0.0	0.0
Nodosaria sp.	0.0	0.0	0.0	0.0	0.0	0.0	0.0	0.0	0.0	0.0	0.0	0.0	0.0	0.0	0.0	0.0	0.0	0.0	0.0	0.0	0.0
Fursenkoina fusiformis	0.0	0.0	0.0	0.0	0.0	0.0	0.0	0.0	0.0	0.0	0.0	0.5	0.0	0.3	0.0	0.0	0.0	1.8	0.0	0.0	0.0
Pleurostomella spp.	0.0	0.0	0.0	0.0	0.0	0.0	0.0	0.0	0.0	0.0	0.0	0.0	0.0	0.0	0.0	0.6	0.0	0.5	0.0	0.0	0.4
Stilostomella spp.	0.0	0.0	0.0	0.0	0.0	0.0	0.0	0.0	0.0	0.0	0.0	0.0	0.0	0.0	0.0	0.0	0.0	1.8	0.3	0.6	0.7
Dentalina communis	0.0	0.0	0.0	0.0	0.0	0.0	0.0	0.0	0.0	0.0	0.0	0.0	0.0	0.0	0.0	0.0	0.0	0.0	0.0	0.0	0.4
Guttulina sp.	0.0	0.0	0.0	0.0	0.0	0.0	0.0	0.0	0.0	0.4	0.6	0.0	0.0	0.0	0.0	0.0	0.0	0.0	0.0	0.0	0.4
Oolina spp.	0.0	0.7	0.0	0.0	0.0	0.0	0.5	0.0	0.0	0.4	0.6	0.0	0.0	0.3	0.0	1.2	0.0	1.8	0.0	0.0	0.0
Lagena spp.	0.0	0.3	0.0	0.0	0.0	0.0	0.5	0.3	1.8	0.0	0.0	0.0	0.3	0.0	0.0	0.0	0.3	0.0	0.0	0.0	0.0
Fissurina spp.	0.0	0.0	0.0	0.0	0.0	0.0	0.5	0.0	0.9	1.7	2.4	0.9	0.0	0.0	0.0	1.2	0.0	0.0	0.0	0.3	0.7
Quinqueloculina seminula	0.0	0.0	0.0	0.0	0.0	0.0	0.0	0.0	0.0	0.0	0.0	0.0	0.0	0.0	0.0	0.0	0.0	0.0	0.0	0.0	0.0
Q. sp.	0.0	0.7	0.0	0.0	0.0	0.0	0.5	0.0	0.9	0.0	1.2	0.0	0.0	0.3	0.0	1.2	0.0	1.4	0.6	0.0	0.4
Pyrgo spp.	0.0	0.0	0.0	0.0	0.0	0.0	0.0	0.0	0.0	0.0	0.0	0.0	0.0	0.0	0.0	0.0	0.0	0.0	0.0	0.3	0.0
Sigmoilina tenuis	0.0	0.0	0.0	0.0	0.0	0.0	0.0	0.0	0.0	0.0	0.0	0.0	0.0	0.0	0.0	0.0	0.0	0.0	0.0	0.0	0.0
Tosaia hanzawai	0.0	0.0	0.0	0.0	0.0	0.0	1.0	0.0	0.4	3.0	5.3	0.5	0.0	0.0	0.0	0.0	0.0	0.5	0.0	0.0	0.0
Cornuspirella diffusa	0.0	0.0	0.0	0.0	0.0	0.0	0.0	0.0	0.0	0.0	0.6	0.5	0.0	1.0	2.2	0.0	0.0	0.5	0.0	0.0	0.7
Unidentified serial forms	0.0	0.0	0.0	0.0	0.0	0.0	1.0	0.0	0.0	0.0	0.6	0.0	0.0	1.3	0.0	0.0	0.0	0.0	0.0	0.0	0.0
Karreriella bradyi	0.7	0.3	0.0	0.0	0.0	0.0	0.0	0.0	0.0	0.0	0.0	0.0	0.0	0.0	0.0	0.0	0.0	0.0	0.3	0.0	1.1
Martinottiella communis	0.0	0.0	0.0	0.0	0.0	0.0	0.0	0.0	0.0	0.0	0.0	0.0	0.0	0.0	1.1	0.0	0.0	0.0	0.0	0.0	0.0
Siphotextularia sp.	0.0	0.3	0.0	0.0	0.0	0.0	0.0	0.0	0.0	0.0	0.0	0.0	0.0	0.0	0.0	0.0	0.0	0.0	0.0	0.0	0.0
Trochammina cf. squamata	10.5	36.5	25.1	0.0	16.5	0.0	0.0	66.8	27.3	0.0	10.1	18.6	50.3	16.5	0.0	54.3	94.0	15.6	73.5	79.7	28.0
Trochammina sp.W	8.4	1.4	22.3	25.8	17.7	43.3	16.4	0.0	0.0	16.6	0.0	0.0	0.0	5.6	24.7	0.6	0.5	0.0	2.1	5.4	6.3
Cyclammina cancellata	0.0	0.0	0.3	0.3	0.8	0.0	0.0	0.0	0.0	0.0	0.0	0.0	0.0	0.0	2.7	0.0	0.0	0.0	0.0	0.0	0.0
Ammotium sp. A	0.0	2.4	3.1	0.0	2.8	0.8	0.5	10.4	0.0	0.0	0.0	0.0	1.4	0.3	0.0	3.0	2.7	2.3	2.4	0.3	0.0
Recurvoides sp.	0.0	0.0	0.3	0.7	0.0	0.0	0.0	0.0	0.0	0.0	0.0	0.0	0.0	0.0	1.1	0.0	0.0	0.0	0.0	0.0	0.4
Haplophragmoides	0.7	0.0	0.0	0.0	0.0	0.0	0.0	0.0	0.0	0.0	0.0	0.0	0.0	0.0	5.5	0.0	0.0	0.0	0.0	0.0	0.0
Miliammina fusca	0.0	0.0	0.0	0.0	0.0	0.0	0.0	0.0	0.0	0.0	0.0	0.0	0.0	0.3	0.0	0.0	0.0	0.0	0.0	0.0	0.0
Ammobaculites sp.	3.5	0.0	5.2	2.8	0.4	1.9	0.0	6.6	1.8	2.1	0.0	2.3	3.5	2.5	1.1	0.0	0.8	0.5	0.6	1.4	1.5
Sigmoilopsis schlumbergeri	0.0	0.0	0.0	0.0	0.0	0.0	0.0	0.0	0.0	0.0	0.0	0.0	0.0	0.0	0.0	0.0	0.0	0.9	0.0	0.0	0.0

Site 646B Core	66xCC	67x-1	67x-2	67x-3	67x-5	67x-6	68x-2	68x-3	68x-4	69x-1	70x-1	70xCC	71x-1	71x-2	71x-4	71x-5	72x-1	72xCC	73x-1	73xCC	74x-4
Interval (cm)	20-24	60-64	50-54	40-44	50-54	50-54	50-54	50-54	36-40	40-44	50-54	20-24	50-54	40-44	40-44	32-36	72-76	6-10	46-50	10-14	30-34
Rectuvigerina spp.	0.0	0.0	0.0	0.0	0.0	0.0	0.0	0.0	0.0	0.0	0.0	0.0	0.0	0.0	0.6	0.0	0.0	0.0	0.0	1.9	0.0
Trifrina angulosa	0.0	0.0	0.0	0.0	0.0	0.0	0.0	0.0	0.0	0.0	0.0	0.0	0.0	0.0	0.0	0.0	0.0	0.0	0.0	0.0	0.0
Ehrenbergina trigona	0.0	0.0	0.0	0.0	0.0	0.0	0.0	0.0	0.0	0.0	0.0	0.0	0.0	0.0	0.0	0.0	0.0	0.0	0.0	0.0	0.0
Bulimina alazaensis	0.0	0.0	0.0	0.0	0.0	0.0	0.0	0.0	0.0	0.0	0.3	0.0	0.0	0.0	0.0	0.0	0.0	0.0	0.0	0.0	0.0
B. tessellata	0.0	0.0	0.0	0.0	0.0	0.0	0.0	0.0	0.0	0.0	0.0	0.0	0.0	0.0	0.0	0.0	0.0	0.0	0.0	0.0	0.0
B. sp.	0.0	0.0	0.0	0.0	0.0	0.0	0.0	0.0	0.0	0.0	0.0	0.0	0.0	0.0	0.0	0.0	0.0	0.0	0.0	0.0	0.0
Globobulimina auriculata	0.0	0.0	0.0	0.0	0.0	0.0	0.0	0.0	0.0	0.0	0.0	0.0	0.0	0.0	0.0	0.0	0.0	0.0	0.0	0.6	0.0
Robertinoides charlottensis	0.0	0.0	0.0	0.0	0.0	0.0	0.0	0.0	0.0	0.0	0.0	0.0	0.0	0.0	0.0	0.0	0.0	0.0	0.0	0.0	0.0
Bolivina pygmaea	0.0	0.0	0.0	0.0	0.0	0.0	0.0	0.0	0.0	0.0	0.0	0.0	0.0	0.0	0.0	0.0	0.0	0.0	0.0	0.6	0.0
B. cf pygmaea	0.0	0.0	0.0	0.0	0.0	0.0	0.0	0.0	0.0	0.0	0.0	0.0	0.0	0.0	0.0	0.0	0.0	0.0	0.0	0.0	0.0
Bolivina pseudoplicata	0.0	0.0	0.0	0.0	0.0	0.0	0.0	0.0	0.0	0.0	0.0	0.0	0.0	0.0	0.0	0.0	0.0	0.0	0.0	0.0	0.0
B. pseudothalmanni	0.0	0.0	0.0	0.0	0.0	0.0	0.0	0.0	0.0	0.0	0.0	0.0	0.0	0.0	0.0	0.0	0.0	0.0	0.0	0.0	0.0
B. simplex	0.0	0.0	0.0	0.0	0.0	0.0	0.0	0.0	0.0	0.0	0.0	0.0	0.0	0.0	0.0	0.0	0.0	0.0	0.0	0.0	0.0
B. pseudopunctata	0.0	0.0	0.0	0.0	0.0	0.0	0.0	0.0	0.0	0.0	0.0	0.0	0.0	0.0	0.0	0.0	0.0	0.0	0.0	0.0	0.0
B. lowmani	0.0	0.0	0.0	0.0	0.0	0.0	0.0	0.0	0.0	0.0	0.0	0.0	0.0	0.0	0.0	0.0	0.0	0.0	0.0	0.0	0.0
B. inflata	0.0	0.0	0.0	0.0	0.0	0.0	0.0	0.0	0.0	0.0	0.0	0.0	0.0	0.0	0.0	0.0	0.0	0.0	0.0	0.0	0.0
B. cf alata	0.0	0.0	0.0	0.0	0.0	0.0	0.0	0.0	0.0	0.0	0.0	0.0	0.0	0.0	0.0	0.0	0.0	0.0	0.0	0.0	0.0
B. spp.	0.8	0.0	0.0	0.0	0.0	0.0	0.8	0.0	0.0	0.3	0.0	0.0	0.0	0.0	0.0	0.0	0.0	0.0	0.0	0.0	0.0
Nodosaria sp.	0.0	0.0	0.0	0.0	0.0	0.0	0.0	0.0	0.0	0.0	0.0	0.0	0.0	0.0	0.0	0.0	0.0	0.4	0.0	0.0	0.0
Fursenkoina fusiformis	0.0	0.0	0.0	0.0	0.0	0.0	0.0	0.0	0.0	0.0	0.0	0.0	0.0	0.0	0.0	0.0	0.0	0.0	0.0	0.0	0.0
Pleurostomella spp.	0.0	0.0	0.0	0.0	0.0	1.1	0.0	0.0	0.0	0.3	0.0	0.0	0.0	0.0	0.0	0.0	0.2	0.0	0.2	0.6	0.2
Stilostomella spp.	0.3	0.0	0.0	0.0	0.0	0.6	0.0	0.0	0.0	0.0	0.0	0.0	0.0	0.0	0.0	0.0	0.0	0.0	0.0	0.0	0.0
Dentalina communis	0.0	0.0	0.0	0.0	0.0	0.0	0.0	0.0	0.0	0.0	0.0	0.0	0.0	0.0	0.0	0.0	0.0	0.0	0.0	0.0	0.0
Guttulina sp	0.0	0.0	0.0	0.0	0.0	0.0	0.0	0.0	0.0	0.0	0.0	0.0	0.0	0.0	0.0	0.0	0.0	0.0	0.0	0.0	0.0
Oolina spp.	0.5	0.0	0.0	0.0	0.0	0.0	0.8	0.0	0.0	0.3	0.0	0.0	0.0	0.0	0.0	0.0	0.2	0.0	0.0	0.0	0.0
Lagena spp.	0.0	0.0	0.0	0.0	0.3	0.0	0.0	0.0	0.0	0.0	0.0	0.0	0.0	0.0	0.6	0.4	0.0	0.4	0.0	0.0	0.2
Fissurina spp.	0.0	0.0	0.0	0.5	0.0	0.0	0.0	0.0	0.0	0.3	0.3	0.0	0.2	0.0	0.6	0.8	0.0	0.4	0.0	0.6	0.5
Quinqueloculina seminula	0.0	0.0	0.0	0.0	0.0	0.0	1.7	0.0	0.0	0.0	0.0	0.0	0.0	0.0	0.0	0.0	0.0	0.0	0.0	0.0	0.0
Q sp.	0.3	0.0	0.0	0.5	0.0	2.2	0.0	0.0	0.0	0.0	0.0	0.2	0.0	0.0	1.1	0.0	0.5	0.4	0.0	0.0	0.3
Pyrgo spp.	0.0	0.0	0.0	0.0	0.0	0.0	0.0	0.0	0.0	0.0	0.0	0.0	0.0	0.0	0.0	0.0	0.0	0.0	0.0	0.0	0.0
Sigmoilina tenuis	0.0	0.0	0.0	0.0	0.0	0.6	0.0	0.0	0.0	0.0	0.0	0.0	0.0	0.0	0.0	0.0	0.0	0.0	0.0	0.0	0.0
Tosaia hanzawai	0.0	0.0	0.0	0.0	0.0	0.6	0.0	0.0	0.0	0.6	0.6	0.2	0.0	0.0	0.6	0.0	0.2	0.0	0.5	0.0	0.0
Corrupsirella diffusa	0.5	0.0	0.5	1.6	0.6	0.6	1.7	0.0	0.0	0.3	1.3	0.0	0.0	0.0	1.1	0.4	1.2	1.3	0.7	3.2	0.0
Unidentified serial forms	0.0	0.0	0.0	0.0	0.0	0.0	0.0	0.0	0.0	0.0	0.0	0.0	0.0	0.0	0.0	0.0	0.0	0.0	0.0	0.6	0.0
Karrerella bradyi	0.0	0.0	0.0	0.5	0.0	0.0	0.0	0.0	0.0	0.0	0.0	0.0	0.0	0.0	0.0	0.0	0.0	0.0	0.2	0.6	0.0
Martinottiella communis	0.0	0.0	0.5	0.0	0.0	0.0	0.0	0.0	0.0	0.0	0.0	0.0	0.0	0.0	0.0	0.0	0.0	0.0	0.0	0.0	0.0
Siphotextularia sp.	0.0	0.0	0.0	0.0	0.0	0.0	0.0	0.0	0.0	0.0	0.0	0.0	0.0	0.0	0.6	0.0	0.0	0.0	0.0	0.0	0.0
Trochammina cf squamata	51.1	50.3	8.9	45.5	80.7	41.7	5.9	3.4	35.6	67.7	61.1	96.7	99.1	97.7	55.7	91.4	75.6	84.4	62.7	10.1	91.2
Trochammina sp.W	3.8	19.0	28.4	24.3	6.9	8.3	3.4	31.5	29.6	0.0	0.0	0.0	0.0	0.0	0.0	0.0	0.0	0.0	0.0	0.0	0.0
Cyclammina cancellata	0.0	0.0	1.1	1.1	0.0	0.6	0.0	0.7	2.0	0.0	0.6	0.0	0.0	0.0	0.0	0.0	0.0	0.0	0.0	0.0	0.0
Ammotium sp. A	0.3	0.0	0.0	0.0	0.0	0.0	0.0	0.0	0.0	0.0	0.0	0.4	0.6	0.8	0.0	1.2	0.7	0.4	0.0	0.0	0.0
Recurvoides sp	0.0	0.0	0.5	0.0	0.0	0.0	0.0	0.3	0.9	1.4	0.0	0.0	0.0	0.0	0.0	0.0	0.0	0.0	0.0	0.0	0.0
Haplophragmoides	0.0	0.0	0.0	0.0	0.0	0.0	0.0	0.0	0.0	0.0	0.0	0.0	0.0	0.0	0.0	0.0	0.0	0.0	0.0	0.0	0.0
Miliammina fusca	0.0	0.0	0.0	0.0	0.0	0.0	0.0	0.0	0.0	0.0	0.0	0.0	0.0	0.0	0.0	0.0	0.0	0.0	0.0	0.0	0.0
Ammobaculites sp.	0.5	1.4	2.6	0.0	0.3	0.0	4.2	0.7	0.0	2.0	0.0	0.0	0.0	0.0	0.0	0.0	0.0	0.0	0.0	0.0	0.0
Sigmoilopsis schlumbergeri	0.0	0.0	1.1	0.0	0.0	0.0	3.4	0.0	0.0	0.0	0.0	0.0	0.0	0.0	0.0	0.0	0.0	0.0	0.0	0.0	0.0

Site 646B Core	75x-5	76x-2	77x-5	78xCC	79x-CC	80x-2
Interval (cm)	30-34	50-54	20-24	26-30	40-44	30-34
Rectuvigerina spp.	0.0	0.0	0 0	0.0	0.0	0 0
Trifrina angulosa	0.0	0.0	0 0	0 0	0.0	0.0
Ehrenbergina trigona	0.0	0.0	0.0	0.0	0 0	0.0
Bulimina alazaensis	0.0	0.0	0.0	0.0	0 0	0.0
B. tessellata	0.0	0.0	0.0	0 0	0.0	0 0
B. sp.	0.0	0.0	0 0	0.0	0 0	0.0
Globobulimina auriculata	0.0	0 0	0.0	0 0	0 0	1.5
Robertinoides charlottensis	0.0	0 0	0.0	0.0	0 0	0.0
Bolivina pygmaea	0.0	0.0	0.0	0.6	0.0	0 0
B. cf pygmaea	0.0	0.0	0.0	0.0	0.0	0.0
Bolivina pseudoplicata	0.0	0.0	0.0	0.0	0.0	0.0
B. pesudothalmanni	0.0	0.0	0 0	0.0	0 0	0.0
B. simplex	0.0	0.0	0.0	0.0	0 0	0.0
B. pseudopunctata	0.0	0.0	0.0	0.0	0.0	0.0
B. lowmani	0.0	0.0	0 0	0.0	0 0	0.3
B. inflata	0.0	0.0	0 0	0.0	0 0	0.3
B. cf alata	0.0	0.0	0.0	0 0	0 0	0.0
B. spp.	0.0	0.0	0.0	0.3	0 0	0.0
Nodosaria sp.	0.0	0.0	0.0	0 0	0 4	0.0
Fursenkoina fusiformis	0.0	0.0	0.0	0.0	0 0	0.9
Pleurostomella spp.	0.0	0.0	0.0	0.0	0 4	0.0
Stilostomella spp.	0.0	0.0	0.0	0.6	0 0	0.0
Dentalina communis	0.0	0.0	0.0	0.0	0 0	0.0
Guttulina sp.	0.0	0.0	0 0	0.0	0 0	0.0
Oolina spp.	0.0	0.0	0.0	0.0	2.5	0.0
Lagena spp.	0.0	0.0	0.0	0.9	0.0	1.5
Fissurina spp.	0.0	0.0	0.0	3.2	1.3	0.9
Quinqueloculina seminula	0.0	0.0	0 0	0 0	0.0	2.1
Q sp.	0.0	0 0	0 0	3.2	2.5	0.0
Pyrgo spp.	0.0	0 0	0.0	0.0	0.0	0 0
Sigmoilina tenuis	0.0	0.0	0 0	0.0	0.0	0.3
Tosaia hanzawai	0.0	0.0	0 0	0.0	0.0	0 0
Comuspirella diffusa	0.1	0 1	6.1	16 4	4.6	19 6
Unidentified serial forms	0.0	0 0	0.0	0.9	0 4	4.8
Karrerella bradyi	0.0	0 0	0 0	2.0	0.0	0.3
Martinottiella communis	0.0	0.0	0.0	0 0	0.0	0 0
Siphotextularia sp.	0.0	0.0	0 0	0.0	0.0	0 0
Trochammina cf squamata	99.9	99.9	89 1	20 4	26.9	34.3
Trochammina sp.W	0.0	0.0	0.0	0.0	0.0	0 0
Cyclammina cancellata	0.0	0.0	0.0	0.0	0.0	0 0
Ammotium sp. A	0.0	0 0	0 0	0 0	0.0	0 0
Recurvoides sp.	0 0	0.0	0 0	0 0	0 0	0 0
Haplophragmoides	0.0	0.0	0.0	0.0	0.0	0 0
Miliammina fusca	0 0	0 0	0 0	0 0	0.0	0 0
Ammobaculites sp.	0 0	0 0	0 0	0 0	0.0	0 0
Sigmoilopsis schlumbergeri	0 0	0 0	0.0	0.0	0.0	0 0

Site 646B Core	41x-2	41x-6	42x-1	42x-3	42x-5	42x-7	43x-2	43xCC	44xCC	45x-1	45xCC	46x-2	46x-4	46xCC	47x-2	47xCC	48x-1	48xCC	49x-1	49xCC
Interval (cm)	130-134	70-74	100-104	116-120	90-94	20-24	50-54	10-14	30-34	20-24	20-24	80-84	20-24	20-24	70-74	10-14	110-114	15-19	60-64	20-24
S. sp.	0.0	0.0	0.0	0.0	0.0	0.4	0.5	0.0	0.0	0.0	0.0	0.0	0.0	.3	0.0	3.6	0.4	0.4	0.7	0.7
Spiroplectammina sp.	0.0	0.0	0.0	0.0	0.0	0.0	0.0	0.0	0.0	0.0	0.0	0.0	0.0	0.0	0.0	0.0	0.0	0.0	0.0	0.0
Lagenammina sp.	0.0	0.7	0.0	0.0	0.0	0.8	5.2	0.6	0.0	2.7	0.7	2.3	2.2	4.5	4.8	4.8	0.4	1.2	0.7	1.5
Psammosphaera spp.	0.0	0.0	0.0	0.0	0.0	1.5	9.0	0.0	0.0	9.4	0.0	5.7	2.6	3.2	2.9	1.2	9.5	0.8	0.7	2.6
Sacammina sp.	0.0	0.0	0.0	0.0	0.0	0.0	4.9	0.0	0.0	1.0	0.2	0.4	0.0	0.3	1.4	1.8	1.1	2.0	1.3	1.5
Rhizammina spp.	0.0	0.0	29.5	0.0	0.0	0.0	33.1	2.9	0.0	16.8	5.7	9.1	4.3	15.1	30.3	39.4	16.1	33.7	49.8	30.9
Dendrophrya sp.	0.0	0.0	1.1	0.0	0.0	0.0	0.0	0.0	0.0	0.0	0.2	0.0	0.0	0.6	1.4	5.5	0.4	1.2	1.0	1.1
Bigenerina? sp.	0.0	0.0	0.0	0.0	0.0	0.0	0.0	0.0	0.0	0.0	0.0	0.0	0.0	0.0	0.0	0.0	0.0	0.0	0.0	0.0
Glomospira sp.	0.0	0.0	0.0	0.0	0.0	0.0	0.0	0.0	0.0	0.0	0.0	0.0	0.0	0.0	0.0	0.0	0.0	0.0	0.0	0.0
Reophax sp.	0.0	0.0	0.0	0.0	0.0	0.0	0.3	0.0	0.0	1.0	0.0	0.0	0.9	0.0	0.0	0.0	0.4	0.0	0.0	0.0
Textularia sp.	0.0	0.0	0.0	0.0	0.0	0.0	0.0	0.0	0.0	0.0	0.0	0.0	0.0	0.0	0.0	0.0	0.0	0.0	0.0	0.0
Ammodiscus sp.	0.0	0.0	0.0	0.0	0.0	0.0	0.0	0.0	0.0	0.0	0.0	0.0	0.0	0.0	0.0	0.0	0.0	0.0	0.0	0.0
Vulvulina spinosa	0.0	0.0	0.0	0.0	0.0	0.0	0.0	0.0	0.0	0.0	0.0	0.0	0.0	0.0	0.0	0.0	0.0	0.0	0.0	0.0
Unidentified agglutinated forms	0.0	0.0	9.1	0.0	0.0	1.5	3.1	3.4	0.0	6.7	1.5	3.4	3.0	8.3	0.0	10.3	7.0	0.0	8.6	13.0

Site 646B Core	50x-1	50x-2	50x-3	50xCC	51x-1	52xCC	54x 1	54x 1	54x 3	55x-2	55x-3	55xCC	56x-1	56x-2	56xCC	57x-3	57x-4	57xCC	58x-1	58x-2	59xCC
Interval (cm)	62-66	30-34	22-26	30-34	80-84	20-24	60-64	140-144	16-20	80-84	27-31	10-14	110-114	60-64	20-24	40-44	22-26	20-24	50-54	40-44	20-24
S. sp.	0.3	0.0	0.0	1.0	0.9	0.0	0.0	0.0	0.0	0.3	0.0	0.0	1.2	0.0	0.4	0.0	0.0	0.0	0.0	0.0	0.0
Spiroplectammina sp.	0.0	0.0	0.0	0.0	0.0	0.0	0.0	0.0	0.0	0.0	0.0	0.0	0.0	0.5	0.0	0.0	0.0	0.0	0.0	0.0	0.0
Lagenammina sp.	2.1	0.9	2.3	2.9	5.3	0.0	0.0	0.0	0.0	1.1	1.7	1.0	3.3	0.9	0.0	0.0	0.0	0.4	1.3	0.7	3.0
Psammosphaera spp.	5.2	0.9	8.9	5.9	7.5	0.0	0.0	0.0	0.0	0.6	11.8	16.2	11.8	4.6	7.1	0.0	0.0	9.6	0.2	0.0	1.5
Sacammina sp.	0.3	0.0	0.4	0.0	0.0	0.0	0.0	0.0	0.0	0.0	0.0	0.0	0.0	0.0	0.0	0.0	0.0	0.0	0.0	0.0	0.0
Rhizammina spp.	30.9	9.0	12.0	3.9	15.8	0.0	0.0	0.0	0.0	3.1	5.7	21.5	8.9	10.0	13.9	4.3	5.5	27.1	15.3	26.2	7.5
Dendrophrya sp.	0.0	0.0	0.0	0.0	0.0	0.0	0.0	0.0	0.0	0.0	0.0	0.0	0.0	0.0	0.0	0.0	1.6	0.0	0.2	0.0	0.4
Bigenerina? sp.	0.0	0.0	0.0	0.0	0.0	0.0	0.0	0.0	0.0	0.0	0.0	0.0	0.0	0.0	0.0	0.0	0.0	0.0	0.0	0.0	0.0
Glomospira sp.	0.0	0.0	0.0	0.0	0.0	0.0	0.0	0.0	0.0	0.0	0.0	0.0	0.0	0.0	0.0	0.0	0.0	0.0	0.0	25.2	0.0
Recphax sp.	0.0	0.0	0.0	0.0	0.0	0.0	0.0	0.0	0.0	0.0	0.9	0.0	0.8	0.5	0.0	0.0	0.0	0.0	0.0	0.0	0.4
Textularia sp.	0.0	0.0	0.0	0.0	0.0	0.0	0.0	0.0	0.0	0.0	0.0	0.0	0.0	0.0	0.0	0.0	0.0	0.0	0.0	0.0	0.0
Ammodiscus sp.	0.0	0.0	0.0	0.0	0.0	0.0	0.0	0.0	0.0	0.0	0.0	0.0	0.0	0.0	0.0	0.0	0.0	0.0	0.0	0.0	0.0
Vulvulina spinosa	0.0	0.0	0.0	0.0	0.0	0.0	0.0	0.0	0.0	0.0	0.0	0.0	0.0	0.0	0.0	0.0	0.0	0.0	0.0	0.0	0.0
Unidentified agglutinated forms	8.5	6.8	6.6	14.2	22.7	0.5	0.3	0.0	0.0	5.6	19.2	16.2	23.2	9.1	13.0	2.9	1.6	10.8	12.5	25.2	22.0

Site 646B Core	60x-3	60xCC	61x-1	61x-2	61x-3	61xCC	62x-1	62x-2	62x-3	62x-4	62x-5	63x-1	63x-2	63xCC	64x-1	65x-1	65x-3	65x-5	65x-7	65x-CC	66x-1
Interval (cm)	32-36	30-34	80-84	20-24	30-34	30-34	44-48	50-54	80-84	56-60	26-30	60-64	26-30	10-14	80-84	80-84	60-64	40-44	20-24	20-24	90-94
S. sp.	0.0	0.0	0.0	0.0	0.0	0.0	2.1	0.0	1.8	0.0	1.8	1.9	4.5	3.0	0.9	0.0	0.0	0.0	0.0	0.0	0.0
Spiroplectammina sp.	0.0	0.0	0.0	0.0	0.0	0.0	0.0	0	0.0	0.0	0.0	0.0	0.0	0.0	0.0	0.0	0.0	0.0	0.0	0.0	0.0
Lagenammina sp.	0.0	0.0	2.8	1.0	0.4	1.9	0.0	0.7	7.0	2.1	1.8	5.1	0.7	3.8	0.0	0.0	0.0	0.0	0.0	0.0	0.0
Psammosphaera spp.	1.4	4.4	1.2	2.1	9.1	6.7	7.2	1.1	4.8	6.4	0.0	9.8	0.0	2.5	0.0	0.0	0.0	0.0	0.0	0.3	0.7
Sacammina sp	0.0	0.0	0.0	0.0	0.0	0.0	0.0	0.0	0.0	0.0	0.0	0.0	0.7	0.0	0.0	0.0	0.0	0.0	0.0	0.0	0.0
Rhizammina spp.	14.0	15.5	16.5	28.2	24.0	15.0	9.2	4.7	12.3	22.6	27.2	7.0	14.9	39.1	5.5	0.0	0.0	0.0	5.7	2.0	4.9
Dendrophrya sp.	0.0	0.0	0.0	0.7	1.2	0.0	0.0	0.0	0.0	0.0	2.4	0.0	0.3	0.8	0.0	0.0	0.0	0.0	0.0	0.0	0.0
Bigenerina? sp.	0.0	0.0	0.0	0.0	0.0	0.0	0.0	0.0	0.0	0.0	0.0	0.0	1.4	4.6	0.0	0.0	0.0	0.0	0.0	0.0	0.0
Glomospira sp.	0.0	0.0	0.0	0.0	0.0	0.0	0.0	0.0	0.0	0.0	0.0	0.0	0.0	0.0	0.0	0.0	0.0	0.0	0.0	0.0	0.0
Reophax sp.	0.7	0.0	0.0	1.0	0.0	0.0	0.0	0.0	0.0	0.0	3.6	4.7	0.3	0.0	0.0	0.0	0.0	0.0	0.0	0.3	0.0
Textularia sp.	0.0	0.0	0.0	0.0	0.0	0.0	0.0	0.0	0.4	0.4	0.6	0.0	0.0	0.0	0.0	1.2	0.0	0.0	0.0	0.0	0.0
Ammodiscus sp.	0.0	0.0	0.0	0.0	0.0	0.0	0.0	0.0	0.0	0.0	0.0	0.0	0.0	0.0	0.0	0.0	0.0	0.0	0.0	0.0	0.0
Vulvulina spinosa	0.0	0.0	0.0	0.0	0.0	0.0	0.0	0.0	0.0	0.0	0.0	0.0	0.0	0.0	0.0	0.0	0.0	0.0	0.0	0.0	0.0
Unidentified agglutinated forms	21.7	19.3	21.4	24.7	25.2	13.9	20.5	0.8	10.1	18.3	17.8	20.9	11.8	10.2	8.2	1.2	0.8	0.5	2.7	2.9	9.3

Site 646B Core	66xCC	67x-1	67x-2	67x-3	67x 5	67x-6	68x-2	68x 3	68x-4	69x-1	70x-1	70xCC	71x-1	71x-2	71x-4	71x-6	72x-1	72xCC	73x-1	73xCC	74x-4
Interval (cm)	20-24	60-64	50-54	40-44	50-54	50-54	50-54	50-54	36-40	40-44	50-54	20 24	50-54	40-44	40-44	32-36	72-76	6-10	46-50	10-14	30-34
S. sp.	0.8	0.7	8.9	0.0	1.8	0.0	1 7	2.4	8.3	0 0	0.0	0 0	0 0	0 0	0 0	0 0	0.0	0 0	0 0	0 0	0 0
Spir.plectammina sp.	0.0	0.0	0.6	0.0	0.0	0.0	0.0	0.0	0 0	0 0	0 0	0 0	0 0	0 0	0 0	0 0	0.0	0 0	0.0	0.0	0 0
Lagenammina sp.	0.0	0.0	1 1	2.1	0.0	0.0	0.8	6 1	2.6	0.0	0 0	0.0	0 0	0.0	0 0	0.0	0.0	0 0	0.0	0.0	0.0
Psammosphaera spp.	0.0	0.7	0.5	3.2	0.0	0.0	1 7	4 1	0 0	0 0	0 0	0.0	0 0	0 0	0 0	0 0	0 0	0 0	0.0	0.0	0 0
Sacammina sp.	0.0	0.0	0.0	0.0	0 0	0 0	0 0	0 0	0 0	0 0	0.0	0 0	0 0	0 0	0 0	0 0	0.0	0 0	0 0	0.0	0.0
Rhizammina spp.	6.5	2.0	28 4	5.3	4.5	2.8	22 7	42 4	10.8	0.9	0.0	0 2	0 0	0 0	0 0	0 0	0.0	0 0	0 0	0.0	0.0
Dendrophrya sp	0.0	0.0	0.0	0.0	0.0	0 0	0 0	0 0	0 0	0.0	0 0	0 0	0 0	0 0	0 0	0 0	0.0	0 0	0 0	0 0	0.0
Bigenerina? sp.	0.0	0.0	0.0	0.0	0 0	0 0	0 0	0 0	0 0	0 0	0 0	0 0	0 0	0 0	0 0	0 0	0.0	0 0	0 0	0 0	0 0
Glomospira sp.	0.0	0.0	0.0	0.0	0.0	0.0	0 0	0 0	0.3	0 0	0.0	0 0	0 0	0 0	0 0	0 0	0 0	0 0	0 0	0 0	0 0
Reophax sp.	0.0	0.0	1 1	0.5	0 0	0 0	0.0	2.4	4.8	2.0	1.6	0 0	0.0	0 0	0 0	0 0	0.0	0 0	0 0	0.0	0.0
Textularia sp.	0.5	0.0	0 0	0 0	0 0	0 0	0 0	0 0	0 0	0 0	0 0	0 0	0 0	0 0	0 0	0 0	0 0	0 0	0 0	0.0	0 0
Ammodiscus sp.	0.0	0.0	0.0	0.0	0 0	0 0	0 8	0 0	0 0	0 0	0 0	0 0	0.0	0 0	0.0	0 0	0.0	0 0	0 0	0.0	0.0
Vulvulina spinosa	0.0	0.0	0.0	0.0	0 0	0 0	0.0	0 0	1 1	0 0	0.0	0.0	0 0	0 0	0.0	0 0	0.0	0 0	0 0	0 0	0.0
Unidentified agglutinated forms	9.8	12.9	5.3	12.2	1.5	1 1	4.2	6 1	0 0	2.9	0.6	0 0	0 0	0 0	0 0	0 0	0.0	0 0	0.0	0 0	0.0

Site 646B Core	75x-5	76x-2	77x-5	78xCC	79x-CC	80x-2
Interval (cm)	30-34	50-54	20-24	26-30	40-44	30-34
S. sp.	0.0	0.0	0 0	0.0	0.0	0.0
Spiroplectammina sp.	0.0	0.0	0.0	0.0	0.0	0.0
Lagenammina sp.	0.0	0.0	0.0	0.0	0 0	0.0
Psammosphaera spp.	0.0	0.0	0.0	0.0	0.0	0.0
Sacammina sp.	0.0	0.0	0.0	0.0	0 0	0.0
Rhizammina spp.	0.0	0.0	0.0	0 0	0 4	0.0
Dendrophrya sp.	0.0	0.0	0 0	0.0	0 0	0 0
Bigenerina? sp.	0.0	0.0	0 0	0.0	0 0	0 0
Glomospira sp.	0.0	0.0	3 0	0.0	0 0	0 0
Reophax sp.	0.0	0.0	0.0	0.0	0 0	0 0
Textularia sp.	0.0	0.0	0 0	0.0	0 0	0 0
Ammodiscus sp.	0.0	0.0	0 0	0.0	0.0	0 0
Vulvulina spinosa	0.0	0.0	0.0	0 0	0 0	0 0
Unidentified agglutinated forms	0.0	0.0	1.8	0.0	0.4	0 0

REFERENCES CITED

Adams, C.G., Rodda, P., and Kiteley, R.J., 1979. The extinction of the foraminiferal genus *Lepidocyclina* and the Miocene/Pliocene boundary problem in Fiji. Marine Micropaleontology, v. 4, p. 319-339.

Adams, C.G., Benson, R.H., Kidd, R.B., Ryan, W.F.B., and Wright, R.C., 1977. The Messinian Salinity Crisis and evidence of late Miocene eustatic changes in the world ocean. Nature, v. 269, p. 383-386.

Aharon, P., Goldstein S.L., 1993, Sea–level events in the South Pacific linked with the Messinian salinity Crisis: Geology, v. 21, p. 771–775.

Aksu, A.E., and Hillaire–Marcel, C., 1989. Upper Miocene to Holocene oxygen and carbon isotopic stratigraphy of Sites 646 and 647, Labrador Sea: In Proceedings of the Ocean Drilling Program, Scientific Reports, Srivastava, S.P., Arthur, M., and Clement, B. et al. (eds.),Washington, D.C., U.S. Government Printing Office, v. 105, p. 689–695.

Aksu, A.E., and Kaminski, M.A., 1989. Neogene and Quaternary planktonic foraminifer biostratigraphy and biochronology in Baffin Bay and the Labrador Sea. In Srivastava, S.P., Arthur, M.A., et al. (eds.), Proceedings of the Ocean Drilling Program, Leg 105, Washington, D.C. (U.S. Government Printing Office), v. 105, p. 287–304.

Argand, E., 1924. La tectonique de l'Asie. Third Congress Géol. Intern., Bruxelles, Comp. Rend., p. 171–372.

Arthur, M.A., Srivastava, S.P., Kaminski, M., Jarrard, R., and Osler, J., 1989. Seismic stratigraphy and history of deep circulation and sediment drift development in Baffin Bay and Labrador Sea. In Srivastava, S.P., Arthur, M.A. et al. (eds.), Proceedings of the Ocean Drilling Program, Leg 105. Washington, D.C. (U.S. Government Printing Office), v. 105, p. 957–988.

Aubry, P.–M., 1993. Neogene allostratigraphy and depositional history of the De Soto Canyon area, northern Gulf of Mexico. Micropaleontology,. v. 39, p. 327-366.

Bailey, J. W., 1851. Microscopical examination of soundings made by the United States Coast Survey of the Atlantic coast of the United States. Smithsonian Contributions of Knowledge, v. 2, p. 1-15.

Baldauf, J.G., Clement, B.G., Aksu, A., de Vernal, A., Firth, J.V., Hall, F., Head, M.J., Jarrard, R.D., Kaminski, M.A., Lazarus, D., Monjanel, A.-L., Berggren, W.A., Gradstein, F.E., Knüttel, S., Mudie, P.J., and Russell, M.D., 1989. Magnetostratigraphic and biostratigraphic synthesis of Ocean Drilling Program Leg 105: Labrador Sea and Baffin Bay. In Srivastava, S.P., Arthur, M.A. et al. (eds.), Proceedings of the Ocean Drilling Program, Leg 105. Washington, D.C. (U.S. Government Printing Office), v. 105, p. 935–956.

Bandy, O. L., 1949. Eocene and Oligocene foraminifera from Little Stave Creek, Clarke County, Alabama, Bulletins of American Paleontology v. 32, p. 5-206.

Bandy, O.L., 1960. General correlation of foraminiferal structure with environment. Report of the International geological Congress, 21st Session, Copenhagen, Part 2, p. 7–19.

Bandy, O.L., 1973. Chronology and paleoenvironmental trends, late Miocene–early Pliocene, Western Mediterranean. In Drooger, C.W. and Broekman, J.A., (eds.), Messinian Events in the Mediterranean, no. 7 of Geodynamic Scientific Report, North– Holland Publ. Co., Amsterdam, p. 21–25.

Bandy, O.L., 1976, General correlation of foraminiferal structure with environment. Report of the International geological Congress, 21st Session, Copenhagen, Part 2, p. 7–19.

Bandy, O.L., and Arnal, R.E., 1960, Concepts of foraminiferal paleoecology. Bulletin of American Association of Petroleum Geologists, v. 44, p. 1921–1932.

Bandy, O.L., Butler, E.A., and Wright, R.C., 1969. Alaskan upper Miocene glacial deposits and the *Turborotalia pachyderma* datum plane. Sicence, v. 166, p. 607-609.

Banner, F. T. and Blow, W. H. 1965. Two new taxa of the Globorotaliinae (Globigerinacea, Foraminifera) assisting determination of the late Miocene/middle Miocene boundary. Nature, v. 207, p. 1351-4.

Barker, R.W., 1966. Taxonomic notes on the species figured by H.B. Brady in his "Report on the foraminifera dredged by H.M.S. *Challenger* during the years 1873-1876." Accompanied by a reproduction of Brady's plates. Society of Economics, Paleontology, and Mineralogy, Special Publication, v. 9, p. 1-238.

Barron, J.A., and Keller, G., 1983. Paleotemperature oscillations in the middle and late Miocene of the Northeastern Pacific. Micropaleontology, v. 29, p. 150–181.

Batsch, A.I.G.C., 1791, Sechs Kupfertafeln mit conchylien des Seesandes, Cezeichnet und Gestochen von A. J. G. K. Batsch, Jena, 6 pls.

Beaufort, L., and Aubry, M.-P., 1990. Fluctuations in the composition of late Miocene calcareous nannofossil assemblages as a response to orbital forcing, Paleoceanography, v. 5, p. 845-866.

Bender, M.L., and Keigwin, L.D., 1979. Speculations about the upper Miocene change in abyssal Pacific dissolved bicarbonate $\delta^{13}C$. Earth and Planetary Scientific Letters, v. 45, p. 383– 393.

Benson, R.H., and Rakic–El Bied, K., 1991a. Biodynamic, saline giant and late Miocene catastrophism: Carbonates and Evaporites, v. 6, p. 127–168.

Benson, R.H., and Rakic–El Bied, K., 1991b. The Messinian parastratotype at Cuevas del Almanzora, Vera Basin, SE Spain: Refutation of the deep basin, shallow–water hypothesis: Micropaleontology, v. 37, p. 289–302.

Benson, R.H., and Rakic–El Bied, K.; In Collaboration with Aubry, M.-P., Berggren, W.A., Bonaduce, G., Hodell, D.A., Flores, J.A., Kent, D., Mazzei, R., Napoleone, G., Zhang, J., and Semenenko, V.N. The Bou Regreg Section,

Morocco: Proposed global boundary stratotype section and point of the Pliocene. Accepted by Royaume du Maroc Ministere de L'Energie et des Mines Direction de La Geologie. Notes et Memoires du Service Geologique, no. 383, in press.

Benson, R.H., Rakic–El Bied, K., and Bonaduce, G., 1991. An important current reversal (influx) in the Rifian Corridor (Morocco) at the Tortonian–Messinian boundary: the end of Tethys ocean. Paleoceanography. v. 6, p. 164–192.

Benson, R.H., Hayek, L.–A., C., Hodell, D.A., and Rakic–El Bied, K., 1995. Extending the climatic precession curve back to the late Miocene by signature template comparison. Paleoceanography, v. 10, p. 5–20.

Berger, W.H., 1970. Planktonic foraminifera in selective solution and the lysocline. Marine Geology, v. 8, p. 111-183.

Berger, W.H., Bé, A.W.H., and Sliter, W.V., 1975. Dissolution of deep sea carbonates: An introduction. In Spec. Publ. No. 13, ed. Sliter, W.V., Bé, A.W.H., and Berger, W.H., Lawrence Kansas, Cushman Foundation for Foraminiferal Research.

Berger, W. H., and Vincent, V., 1986. Deep-sea carbonates: Reading the carbon-isotope signal, Geologische Rundschau, v. 75, p. 249-269.

Berggren, W.A., 1972. Cenozoic biostratigraphy and paleobiogeography of the North Atlantic. In Initial Reports of Deep Sea Drilling Project, Leg 12, Laughton, A.S., Berggren, A.W. et al. (eds.), Washington, D.C., U.S. Government Printing Office, v. 12, p. 965-1001.

Berggren, W.A., 1977. Late Neogene planktonic foraminiferal biostratigraphy of DSDP Site 357 (Rio Grande Rise). In Supko, P.R., Perch-Nielsen, K., et al., Initial Reports of Deep Sea Drilling Project, 29, U.S. Government Printing Office, Washington, D.C., p. 591-614.

Berggren, W.A., 1993. Neogene planktonic foraminiferal biostratigraphy of eastern Jamaica. In Wright, R.M., and Robinson (eds.), Biostratigraphy of Jamaica, Geological Society of America Memoir 182: 179–217.

Berggren, W.A., and Haq, B., 1976. The Andalusian Stage (late Miocene): Biostratigraphy, biochronology and paleoecology. Paleogeography, Paleoclimatology, Paleoecology, v. 20, p. 67-129.

Berggren, W.A., and Hollister, C.D., 1974. Paleogeography, paleobiogeography, and the history of circulation in the oceans. In Hay, W.W. (ed.), Studies in Paleoceanography. Society of Economics, Paleontology and Mineralogy, Special Publications, v. 20, p. 126–186.

Berggren, W.A., Aubry, M.–P., and Hamilton, N., 1983. Neogene magnetobiostratigraphy of DSDP Site 516 (Rio Grande Rise, South Atlantic). In Barker, P., Johnson, D. et al., Initial Reports of Deep Sea Drilling Projct, Leg, 72, U.S. Government Printing Office, Washington, D.C., v. 72, p. 675–706.

Berggren, W.A., Benson, R.H., Haq, B.U., Riedel, W.R, Sanfilippo, A, Schrader, H.J., and Tjalsma, R.C., 1976. The El Cuervo section (Andalusia, Spain):

Micropaleontologic anatomy of an early late Miocene lower bathyal deposit. Marine Micropaleontology, v. 1, p. 195–247.

Berggren, W.A., Kent, D.V., and Van Couvering, J.A., 1985. Neogene geochronology and chronostratigraphy. In: Snelling, N.J., Ed., The Chronology of the Geological Record, Mem., Blackwell Scientific Publications, v. 10, p. 211–260.

Berggren, W.A., Kent, D.V., Swisher, C.C., III, and Aubry, M.–P., 1995. A revised Neogene geochronology and chronostratigraphy. In Time Scales and Global Stratigraphic Correlations, W.A. Berggren, D.V. Kent and J. Hardenbol (eds.), SEPM Special Volume 54, p. 129-212.

Berthelin, J. P. 1880. Mémoire sur les foraminiféres fossiles de létage Albien de Montcley (Doubs). Memoires de Societé Géologique de France, v. 1, p. 1-84.

Bermúdez, P. J., and Bolli, H.M., 1969. Consideraciones sobre los sedimentos del Mioceno medio al Reciente de las costas central y oriental de Venezuela. Boletin de Geologia, Direccion de Geologia, Ministerio de Minas e Hidrocarbures, v. 10, p. 137-223.

Blanc, P.–L., and Duplessy, J.–C., 1982. The deep-water circulation during the Neogene and the impact of the Messinian Salinity Crisis. Deep Sea Research, v. 29A, p. 1391–1414.

Blow, W. H. 1959. Age, correlation, and biostratigraphy of the Upper Tocuyo (San Lorenzo) and Pozon formations, Eastern Falcon, Venezuela. Bull. American Paleontology, v. 39, p. 67-251.

Blow, W.H., 1969. Late Middle Eocene to Recent planktonic foraminiferal biostratigraphy. Proceedings of First International Conference on Planktonic Microfossils, Geneva, 1967, v. 1, p. 199-422.

Blow, W. H. and Banner, F. T. 1966. The morphology, taxonomy and biostratigraphy of *Globorotalia barisanensis* LeRoy, *Globorotalia fohsi* Cushman and Ellisor, and related taxa. Micropaleontology, v. 12, p. 286-303.

Bolli, H. M. 1957. Planktonic foraminifera from the Oligocene - Miocene Cipero and Lengua formations of Trinidad, B. W. I. Bulletin of U.S. National Museum, v. 15, p. 97-123.

Bolli, H. M. 1970. The foraminifera of Sites 23-31, Initial Reports of Deep-Sea Drilling Project, Leg 4, v. 4, p. 577-643.

Bolli, H.M., and Bermúdez, P.J., 1965. Zonation based on planktonic foraminifera of middle Miocene to Pliocene warm–water sediments. Asoc. Venez. Geol. Mineria y Petr., Bol. Informativo, Caracas, Venezuela, v. 8 (5), p. 1-119.

Bolli, H.M., and Premoli Silva, I., 1973. Oligocene to Recent planktonic foraminifera and stratigraphy of the Leg 15 sites in the Caribbean sea. Initial Reports of Deep Sea Drilling Project, v. 15, p. 475-497.

Bolli, H. M., and Saunders, J. B., 1985, Oligocene to Holocene low latitude planktic foraminifera, plankton stratigraphy, Bolli, H. M., Saunders, J. B., and Perch-Nielsen, K. (eds.), p. 155-262.

Boltovskoy, E., 1978. Late Cenozoic benthonic foraminifera of the Ninetyeast Ridge (Indian Ocean). Marine Geology, v. 26, p. 139-175.

Boltovskoy, E., 1988. Size Change in the phylogeny of foraminifera. Lethaia, v. 21, p. 375-382.

Boltovskoy, E., and Giussani de Khan, G., 1990. Benthic unilocular calcareous foraminifers in Late Cenozoic deep sea deposits of the Pacific and Atlantic oceans. Revista Espanola Micropaleontologia, v. 12, no. 3, p. 361-406.

Boltovskoy, E., and Ocampo, J.V., 1993. Benthic foraminifers from DSDP Site 219 (Eocene-Pleistocene), Arabian Sea. Revista Espanola Micropaleontologia, v. 25, p. 127-156.

Borsetti, A.M., Curzi, P.V., Landuzzi, V., Mutti, M., Ricci Lucchi, F., Sartori, R., Tomadin, L., and Zuffa, G.G., 1990. Messinian and pre–Messinian sediments from ODP Leg 107 sites 652 and 654 in the Tyrrhenian Sea: Sedimentologic and petrographic study and possible comparisons with Italian sequences. In Proceedings of the Ocean Drilling Program (Scientific results), Kastens, K.A., Mascle, J., Auroux, C., et al. (eds.), U.S. Government Printing Office (Washington, D.C.), . v. 107, p. 169–186.

Bourcart, J., 1962. La Méditerranée et la révolution du Pliocène. In Livre à la Mémoire du Professeur P. Fallo, 1 of Society Géolo. France, p. 103–116.

Brady, H. B., 1870. In Brady, G. S. and Robertson, D., 1870. The ostracoda and foraminifera of tidal rivers. With analysis and descriptions of foraminifera by H. B. Brady, Part II. Annual Magazine of Natural History, Ser. 4, v. 6, p. 273-309.

Brady, H. B. 1877. Supplementary notes on the foraminifera of the Chalk (?) of the New Britain group. Geological Magazine, new series, decade v. 2, p. 534-536.

Brady, H. B., 1879. Notes on some reticularian Rhizopoda of the Challenger Expedition. Quarterly Journal of Microscopical Society of London, v. 19, p. 20-99.

Brady, H. B., 1881a. Notes on some of the reticularian Rhizopoda of the *Challenger* Expedition: Part 3. Quarterly Journal of Microscopical Science, new ser., v. 2, p. 31-71.

Brady, H. B., 1881b. On some Arctic Foraminifera from soundings obtained on the Austro-Hungarian North Polar Expedition of 1872-76. Annual Magazine of Natural History, Ser. 5, v. 8, p. 393-418.

Brady, H. B., 1884. Report on the Foraminifera dredged by the *H.M.S. Challenger* during the years 1873-1876. Report of the Scientific Results of the Exploration Voyage of H.M.S. Challenger, Zoology, v. 9, p. 1-814, pl. 1-115.

Brady, H. B., Parker, W. K. and Jones, T. R., 1890. On some foraminifera from the Abrohlos bank. Transactions of the Zoological Society of London, v. 12, p. 211-239.

Broecker, W.S., 1987. The biggest chill. Natural History Magazine, v. 97, p. 74-82.

Broecker, W.S., 1990. Salinity history of the northern Atlantic during the last deglaciation. Paleoceanography, v. 5, p. 459–467.

Broecker, W.S., Bond, G., Klas, M., Bonani, G., and Wolfli, W., 1990. A salt oscillator in the glacial Atlantic? 1. The concept. Paleoceanography, v. 5, p. 469–477.

Broecker, W.S., and Denton, G.H., 1990. The role of ocean–atmosphere reorganizations in glacial cycles. Quaternary Science Reviews, v. 9, p. 305-341.

Broecker, W.S., and Denton, G.H., 1990, What drives glacial cycles? Scientific American, January, p. 49–56.

Broecker, W.S., and Peng, T.–H., 1982. Tracers in the sea. Eldigio Press, p. 1–690.

Brotzen, F., 1936, Foraminiferen aus dem schwedischen untersten Senon von Eriksdal in Schonen, Arsbok Sveriges Geologiska Undersökning, v. 30, p. 1-206.

Bukry, D., 1973. Phytoplankton stratigraphy, DSDP Leg 20, Western Pacific Ocean. In Initial Report of DSDP Project, U.S. Government Printing Office, Washington, D.C., v. 20, p. 307–317.

Bukry, D., 1975. Coccolith and silicoflagellate stratigraphy, Northwestern Pacific Ocean, DSDP. Leg 32. In Initial Report of DSDP Project, U.S. Government Printing Office, Washington, D.C., v. 32, p. 677–701.

Burckle, L., 1995. Overview of late Miocene/early Pliocene paleoclimate. Abstract Volume. International Conference on the Biotic and Climatic Effects of the Messinian Event on the Circum-Mediterranean held in Benghazi, Libya in January of 1995, p. 26.

Cande, S.C., and Kent, D.V., 1992. A new geomagnetic polarity time scale for the Late Cretaceous and Cenozoic. Journal of Geophysical Research, v. 97 (B10), p. 13917–13951.

Cande, S.C., and Kent, D.V., 1995. Revised calibration of the geomagnetic polarity time scale for the late Cretaceous and Cenozoic. Journal of Geophysical Research, v. 100, p. 6093-6095.

Carter, A.N., 1978. Phosphatic nodule beds in Victoria and the late Miocene-Pliocene eustatic event. Nature, 276, p. 258-59.

Casey, R., Hueni, C., and Leavenly, A., 1981. *Brizalina lowmani*, meroplankton foraminiferan useful as an indicator of shelfal circulation and eutrophication (with comments on biostratigraphy and evolution). Transactions of Gulf Coast Association of Geological Society, v. 31, p. 249–255.

Catalano, R., and Sprovieri, R., 1969. Stratigrafia e micropaleotologia dell'intervallo tripoplaceo di torrente Rossi (enna). Accademia Gioenia Sci. Nat. Catania, Atti, Catania, Italy, ser. 7, v. 1, pt. 2, p. 513-527.

Channell, J.E.T., Torii, M., and Hawthorne, T., 1990. Magnetostratigraphy of sediments recovered at Sites 650, 651, 652, and 654 (Leg 107), Tyrrhenian Sea. Proceedings of Ocean Drilling Program, Scientific Results, US Government Printing Office, Washington D.C., v. 107, p. 335-346.

Chaproniere, G.C.H., Styzen, M.J., Sager, W.W., Nishi, H., Quinterno, P.J., and Abrahamsen, N., 1994. Late Neogene biostratigraphic and magnetostratigraphic synthesis, Leg 135. In Hawkins, J., Parson, L., Allan, J., et al., 1994. Proceedings of ODP, Scientific Reports, US Government Printing Office, Washington D.C., v. 135, p. 857-878.

Charles, C.D., and Fairbanks, R.G., 1992. Evidence from Southern Ocean sediments for the effect of North Atlantic deep–water flux on climate. Nature, v. 355, p. 416–419.

Ciesielski, P.F., Ledbetter, M.T., and Ellwood, B.B., 1982 The development of Antarctic glaciation and the Neogene paleoenvironment of the Maurice Ewing Bank. Marine Geology, v. 46, p. 1-51.

Cita, M.B., 1973. Pliocene biostratigraphy and chronostratigraphy. In Ryan, W.B., Hsü, K.J., et al., Initial Reports of the Deep Sea Drilling Project, Washington, D.C. (U.S. Government Printing Office), v. 13, p. 1343–1364.

Cita, M.B., 1975. The Miocene/Pliocene boundary, history and definition. In Saito, T., and Burckle, L. (eds.), Late Neogene Epoch Boundaries. Micropaleontology Press, Special Publication, New York, p. 1–30.

Cita, M.B., 1976. Planktonic foraminiferal biostratigraphy of the Mediterranean Neogene. In Takayanagi, Y., and Saito, . (eds.), Progress in Micropaleontology. Micropaleontology Press, Special Publication, New York, p. 47–68.

Cita, M.B., and McKenzie, J. A., 1986. The terminal Miocene events. In Mesozoic and Cenozoic Oceans, Geodynamics Series, edited by K.J., Hsü, AGU, Washington, D.C., v. 15, p. 123–140.

Cita, M.B., and Podenzani, M., 1980. Destructive effects of oxygen starvation and ash falls on benthic life: A pilot study. Quaternary Research, v. 13, p. 230–241.

Cita M.B., and Ryan, W.B.F., 1978. The Bou Regreg section of the Atlantic coast of Morocco. Evidence, timing and significance of a late Miocene regressive phase. Riv. Ital. Paleont., v. 84, p. 1051-1082.

Cita, M.B., and Ryan, W.B.F., 1979. Late Neogene environmental evolution. In Initial Reports of the DSDP, Leg 47, Arthur, M. A., Cepek, P., Cita, M.B. et al., (eds.), Washington, D.C. (U.S. Government Printing Office), v. 47, p. 447–459.

Clark, D.L., Whitman, R.R., Morgan, K.A., and Mackey, S.D., 1980. Stratigraphic and glacial-marine sediments of the Amerasian Basin, central Arctic Ocean. Geological Society of America, Special Papers, v. 181, p. 1-57.

Clement, B.M., Hall, F.J., and Jarrard, R.D., 1989. The magnetostratigraphy of Ocean Drilling Program Leg 105 sediments. In Srivastava, S.P., Arthus, M.A., et al. (eds.), Proceedings of the Ocean Drilling Program, Leg 105, Washington, D.C. (U.S. Government Printing Office), v. 105, p. 583–595.

Clement, B.M., and Robinson, F., 1987. The magnetostratigraphy of Leg 94 sediments. In Ruddiman, W.F., Kidd, R.B., et al. (eds.), Initial Reports of Deep Sea Drilling Project, Leg 94, part 2, Washington, D.C. (U.S. Government Printing Office), v. 94, p. 635–650.

Coates, A., G., Jackson, J.B., Collins, L.S., Cronin, T.M., Dowesett, H.J., Bywell, L.M., Jung, P., Obando, J.A., 1992. Closure of the Isthmus of Panama: The near–shore marine record of Costa Rica and western Panama. Bulletin of Geological Society of America, v. 104, p. 814–828.

Colalongo, M.L., Di Grande, A., D'Onofrio, S., Gianelli, L., Iaccarino, S., Mazzei, R., Romeo, M., and Salvatiorini, G., 1979. Stratigraphy of late Miocene sections straddling the Tortonian/Messinian boundary, Bolletino Societa Paleontologia di Italia, v. 18, p. 258–302.

Cole, J.W., and Lewis, K.B., 1981. Evolution of the Taupo-Hikurangi subduction system. Tectonophysicus, v. 72, p. 1-22.

Collins, E.S., Scott, D.B., and Zhang, J., in press. Neogene benthic foraminifers from Ocean Drilling Project Sites 898 and 900, Leg 149, Iberia Abyssal Plain.

Collins, L.S., 1993. Neogene paleoenvironments of the Bocas Toro Basin, Panama. J. Paleontology, v. 67, p. 699–710.

Cooper, L.H.N., 1955. Deep water movements in the North Atlantic as a link between climatic changes around Iceland and biological productivity of the English Channel and Celtic Sea. J. Mar. Res., v. 4, p. 347–362.

Corliss, B.H., 1982. Linkage of North Atlantic and Southern Ocean deep–water circulation during glacial intervals. Nature, v. 298, p. 458–460.

Corliss, B.H., 1991. Morphology and microhabitat preference of benthic foraminifera from the northwest Atlantic Ocean. Marine Micropaleontology, v. 17, p. 195–236.

Corliss, B.H., and Chen, C., 1988. Morphotype patterns of Norwegian Sea deep–sea benthic foraminifera and ecological implications. Geology, v. 16, p. 716–719.

Cremer, M., 1989. Texture and microstructure of Neogene-Quaternary sediments, ODP Sites 645 and 646, Baffin Bay and Labrador Sea. In Srivastava, S.P., Arthur, M.A. et al. (eds.), Proceedings of the Ocean Drilling Program, Leg 105. Washington, D.C. (U.S. Government Printing Office), v. 105, p. 7-20.

Cushman, J. A., 1911. A monograph of the foraminifera of the North Pacific Ocean. Pt. 2. Textulariidae. Bulletin of the United States National Museum, v. 71, p. 1-108.

Cushman, J.A., 1918–1931. The foraminifera in the Atlantic Ocean. US National Museum Bulletin 104, parts 1–8.

Cushman, J. A. 1919. Fossil foraminifera from the West Indies. Carnegie Institute, Washington Publication, v. 291, p. 21-71.

Cushman, J. A., 1922. The Foraminifera of the Atlantic Ocean, Part 3, Textulariidae. Bulletin United States National Museum, v. 104, p. 1-149.

Cushman, J. A., 1923. The foraminifera of the Atlantic Ocean. Part 4. Lageniidae, Bulletin of United States National Museum, v. 104, p. 1-3.

Cushman, J. A., 1925. Recent foraminifera from British Columbia. Contributions from the Cushman Laboratory for Foraminiferal Research, v. 1, p. 38-34.

Cushman, J. A., 1926. Foraminifera of the typical Monterey of California. Contributions from the Cushman Laboratory for Foraminiferal Research, v. 2, p. 53-69.

Cushman, J. A., 1927a. Some characteristic Mexican fossil Foraminifera. Journal of Paleontology, v. 1, p. 147-172.

Cushman, J. A., 1927b. New and Interesting foraminifera from Mexico and Texas. Contributions from the Cushman Laboratory of Foraminiferal Research, v. 3, p. 111-117.

Cushman, J. A., 1930, The foraminifera of the Choctawhatchee Formation of Florida. Bulletin of Florida State Geological Survey. No. 4. p. 1-71.

Cushman, J. A., 1932. Notes on the genus *Virgulina*. Contributions from Cushman Laboratory for Foraminiferal Research, v. 8, p. 7-23.

Cushman, J. A., 1933. Some new Recent Foraminifera from the tropical Pacific. Contributions from Cushman Laboratory for Foraminiferal Research, v. 9, p. 77-95.

Cushman, J. A., 1937. A monograph of the subfamily Virgulininae of the foraminiferal family Buliminidae. Cushman Laboratory for Foraminiferal Research, special Publication 9, p. 228.

Cushman, J.A., 1943. Contributions from the Cushman Laboratory for Foraminiferal Research, v. 19 (part 4), p. 92.

Cushman, J. A. and Ellisor, A. O. 1939. New species of foraminifera from the Oligocene and Miocene. Contributions from the Cushman Laboratory for Foraminiferal Research, v. 15, p. 1-14.

Cushman, J. A., and P. W. Jarvis, 1929. New foraminifera from Trinidad. Contributions from the Cushman Laboratory for Foraminiferal Research, v. 5, p. 6-17.

Cushman, J. A., and Jarvis, P. W. 1936. Three new Foraminifera from the Miocene Bowden Marl, of Jamaica. Contributions from the Cushman Laboratory for Foraminiferal Research, v. 12, p. 3-5.

Cushman, J. A. and Renz, H.H., 1941. New Oligocene-Miocene foraminifera from Venezuela. Contribution from the Cushman Laboratory for Foraminiferal Research, v. 17, p. 1-27.

Cushman, J.A., Stewart, R.E., and Stewart, K.C., 1930. Tertiary foraminifera from Humboldt County, California. A preliminary survey of the fauna. Transactions of the San Diego Society of Natural History, v. 6, p. 41-94.

Czjzek, J., 1848. Beitrag zur Kenntniss der fossilen Foraminiferen des Wiener Beckens. Naturwissenschaftliche Abhandlungen, Wien, v. 1, p. 137-150.

D'Onofrio, S., Gianelli, L., Iaccarino, S., Morlotti, E., Romeo, M., Salvatorini, G., Sampo, M. and Sprovieri, R., 1975. Planktonic foraminifera of the Miocene from some Italian sections and the problem of the lower boundary of the Messinian. Bolletino Societa Paleontologia di Italie, v. 14, p. 177–196.

DeMenocal, P., 1995. Marine eolian records of subtropical African and Arabian climate variability since the late Miocene. Abstract volume, International Conference on the Biotic and Climatic Effects of the Messinian Event on the Circum–Mediterranean, Jan., 1995, p. 30–31.

Denton, G.H., and Armstrong, R.L., 1969. Miocene-Pliocene glaciations in southern Alaska. Journal of American Scientists, v. 267, p. 1121-1142.

Deshayes, G. P. 1832. Encyclopedie methodique; Histoire naturelle des vers, Mme. v. Agasse, v. 2, p. 1-594; v. 3, p. 595-1152.

Dietz, R.A., and Woodhouse, M., 1981. Mediterranean theory may be all wet: Geotimes, May, p. 4.

Drooger, C.W., 1973. The Messinian events in the Mediterranean: A review. In Drooger, Broekman, J.A., Hageman, J., Hantelmann, J.J., Marks, P., Meulenkamp, J.E., and Schmidt, R.R., (eds.), Messinian Events in the Mediterranean, Geodynamics Scientific Report No, 7 on the colloquium held in Utrecht, March, 1973, Amsterdam London, p. 263–272.

Drooger, C.W., 1975. The late Miocene events in the Mediterranean. In Progress in Geodynamics: Proceedings of the National Symposium on Geodynamics held in Amsterdam, April 3–4, 1975: North–Holland Publ. Co., Amsterdam, p. 119–125.

Dubois, J., Launay, J., and Recy, J., 1975. Some new evidence on lithospheric bulges close to islands arcs. Tectonophysics, v. 26, p. 189-196.

Duque–Caro, H., 1990. Neogene stratigraphy, paleoceanography and paleobiogeography in northwest South America and the evolution of the Panama Seaway. Paleogeography, Paleoclimatology, Paleoecology, v. 77, p. 203–234.

Earland, A., 1936. Foraminifera, Part IV. Additional records from the Weddell Sea sector from material obtained by the S.Y. Scotia. Discovery Reports., v. 13, p. 1-76.

Egger, J. G., 1857. Die Foraminiferen der Miocan - Schichten bei Ortenburg in Nieder - Bayern, Neues Jahrbuch fur Mineralogie, Geognosie, Geologie, und Petrefakten - Kunde, p. 266-311.

Ellis, B.F., and Messina, A.R., 1940, *et seq.* Catalogue of Foraminifera, Special Publication, American Museum of Natural History, New York.

Erickson, A.J., and Von Herzen, R.P., 1978. Down–hole temperature measurements, Deep Sea Drilling Project, Leg 42A. In Hsü, K.J., Montadert, L., Garrison, R.E., et al, (Eds.) Initial Reports of the Deep Sea Drilling Project, Washington, D.C. (U.S. Government Printing Office, v. 42A, p. 857–871.

Fabricius, F.H., Heimann, K.O., and Braune, K., 1978. Comparison of Site 374 with circum– Ionian land sections: Implications for the Messinian "salinity crisis" on the basis of a "Dynamic model": In Hsü, K.J., Montadert, L., Garrison, R.E., et al, Initial Reports of the Deep Sea Drilling Project, Washington, D.C. (U.S. Government Printing Office), v. 42A, p. 927–942.

Fairbanks, R.G., and Matthews, R.K., 1978. The marine oxygen isotopic record in Pleistocene coral, Barbados, west Indies, Quaternary Research, v. 10, p. 181-196.

Farrell, J.W., Clemens, S.C., and Gromet, L.P., 1995. Improved chronostratigraphic reference curve of late Neogene seawater $^{87}Sr/^{86}Sr$ from ODP Site 758. Geology, v. 23, p. 403-406.

Fichtel, L. von, and J. P. C. von Moll, 1798. Testacea microscopica, aliaque minuta ex generibus *Argonauta et Nautilus*, ad natruam picta et descripta (Microscopische und andere klein Schalthiere aus du geschlechtern Argonaute und Schiffer). Vienna: Camesina.

Foldvik, A., and Gammelsrod, T., 1988. Notes on Southern Ocean hydrography, sea–ice and bottom water formation. Palaeogeography, Palaeoclimatology, Palaeoecology, v. 67, p. 3-17.

Fuglister, F.G., 1960. Atlantic ocean Atlas of temperature and salinity profiles and data from the international geophysical year of 1957–1958. Contributions of Woods Hole Oceanography Institution # 1108, v. 1, pp. 209.

Galloway, J. J., and Wissler, S. G. 1927. Pleistocene foraminifera from the Lomita Quarry, Palos Verdes Hills, California. Journal of Paleontology, v. 1, p. 35-87.

Gartner, S., 1992. Miocene nannofossil chronology in the North Atlantic, DSDP Site 608. Marine Micropaleontology, v. 18, p. 307–331.

Gartner, S., Chow, J., and Stanton, R.J.Jr., 1987. Late Neogene paleoceanography of the eastern Caribbean, the Gulf of Mexico, and the eastern Equatorial Pacific. Marine Micropaleontology, v. 12, p. 255–304.

Gautier, F., Clauzon, G., Suc, J.-P., Cravatte, J., and Violanti, D., 1994. Age et durée de la crise de salinity messiniienne. Comptes Rendus Academie Sciences Paris, t. 318, séries II, p. 1103-1109.

Gieskes, J.M., Meincke, J., and Wenck, A., 1970. Hydrographische und chemische Beobachtungen auf einer Ankerstation im östlichen Nordatlantischen Ozean. "Meteor" Forsch–Ergebnisse, Reihe A, no. 8, seite, p. 1–11.

Glacon, G., Grazzini, C.V., Iaccarino, S., Rehault, J.–P., Randrianasolo, A., Sierro, J.F., Weaver, P., Channell, J., Torii, M., and Hawthorne, T., 1990. Planktonic foraminiferal events and stable isotope records in the upper Miocene, Site 654. In Proceedings of the Ocean Drilling Program (Scientific results), Kastens, K.A., Mascle, J., Auroux, C., et al. (eds.), U.S. Government Printing Office (Washington D.C.), v. 107, p. 415–427.

Goës, A., 1896. The Foraminifera XX. Reports on the dredging operations off the West Coast of Central America to the Galapagos, to the West Coast of Mexico, and in the Gulf of California, in charge of Alexander Agassiz, carried on by the U.S. Fish Commission Steamer "Albatross," during 1891, Lieut. Commander Z.L. Tanner, U.S.N., Commanding, Bulletin of the Museum of Comparative Zoology at Harvard College, v. 29, p. 1-103.

Gooday, A.J., 1988. A response by benthic foraminifera to the deposition of phytodetritus in the deep sea, Nature, v. 332, p. 70–73.

Gooday, A.J., 1993. Deep–sea benthic foraminiferal species which exploit phytodetritus: Characteristic features and controls on distribution. Marine Micropaleontology, v. 22, p. 187–205.

Gooday, A.J., and Turley, C.M., 1990. Responses by benthic foraminifera to inputs of organic material to the ocean floor: A review. Philosophical Transactions of Royal Society, London, v. A331, p. 119–138.

Gordon, A.L., 1975. General ocean circulation. In Numerical Models of Ocean Circulation, National Academy of Sciences, Washington, D.C., p. 39–53.

Gordon, A.L., 1986. Interocean exchange of thermocline water. Journal of Geophysical Research, v. 91 (no. C4), p. 5037–5046.

Gorshkov, S.G., 1974. World ocean atlas v. 2: Atlantic and Indian Oceans, edited by S.G. Gorshkov. Pergamon Press, p. 166–167.

Gregor, H.J., 1995. Pre–, intra–, and post–Messinian megafloras – No break in palaeofloristic and palaeoclimatological conditions in the Mediterranean. Abstract volume, International Conference on the Biotic and Climatic Effects of the Messinian Event on the Circum–Mediterranean, Jan., 1995, p. 45–47.

Gvirtzman, G., and Buchbinder, B., 1978. The late Tertiary of the coastal plain and continental shelf of Israel and its bearing on the history of the eastern Mediterranean. In Ross, D.A. et al. (eds.), Initial Reports of DSDP: National Scientific Foundation, Washington, D.C., v. 42A, p. 1195–1222.

Haake, F.–W., 1980. Benthische foraminiferen in Oberflachen–sedimenten und Kerenen des Ostatlantiks vor Sengal/Gambia (Westafrica). "Meteor" Forsch.–Ergebnisse, Reihe C, no. 32, seite 1–29.

Haq, B.U., Worsley, T.R., Burckle, L.H., Douglas, R.G., Keigwin, L.D., Opdyke, N.D., Savin, S.M., Sommer, M.A., Vincent, E., and Woodruff, F., 1980. Late Miocene marine carbon– isotopic shift and synchroneity of some phyloplanktonic biostratigraphic events: Geology, v. 8, p. 427– 431.

Harman, R.A., 1964, Distribution of foraminifera in the Santa Barbara Basin. Micropaleontology, v.10, p. 81–96.

Hayward, B. W., and Buzas, M., A., 1979. Taxonomy and paleoecology of early miocene benthic foraminifera of northern New Zealand and the North Tasman Sea. Smithsonian Contributions to Paleobiology, No. 36, pp. 154.

Hayes, D.E., Frakes, L.A. et al., 1975. Sites 270, 271, 272. In Hayes, D.E., Frakes, L.A. et al., Initial Reports of DSDP Leg 28, U.S. Government Printing Office, Washington, D.C., v. 28, p. 221-234.

Hedberg, H. D., 1937. Foraminifera of the middle Tertiary Carapita formation of northeastern Venezuela. Journal of Paleontology, v. 11, p. 684-685.

Hermelin, J.O.R., 1986. Pliocene benthic foraminifera from the Black Plateau: Faunal assemblages and paleocirculation. Marine Micropaleontology, v. 10., 343–370.

Hermelin, J.O.R., and Scott, D.B., 1985. Recent benthic foraminifera from the central North Atlantic. Micropaleontology, v. 31, p. 199-220.

Heron-Allen, E., and Earland, A., 1913. On some foraminifera from the North Sea, etc., dredged by the Fisheries Cruiser "Goldseeker" (International North Sea Investigations-Scotland). III. On Cornuspira difusa, a new type from the North Sea, Journal of the Royal Miroscopical Society, London, p. 272-276.

Heron-Allen, E. and Earland, A., 1930. The Foraminifera of the Plymouth District, II. Journal of the Royal Microscopical Society of London, Ser. 3, v. 50, p. 161-199.

Hilgen, F.J., 1987. Sedimentary rhythms and high–resolution chronostratigraphic correlations in the Mediterranean Pliocene. Newsletters Stratigraphy, v. 17, p. 109–127.

Hilgen, F.J., 1991a. Extension of the astronomically calibrated (polarity) time scale to the Miocene/Pliocene boundary. Earth and Planetary Scientific Letters, v. 107, p. 349–368.

Hilgen, F.J., 1991b. Astronomical calibration of Gauss to Matuyama sapropels in the Mediterranean and implications for the Geomagnetic Polarity Time Scale. Earth and Planetary Science Letters, v. 104, p. 226–244.

Hilgen, F.J., and Langereis, C.G., 1988. The age of the Miocene–Pliocene boundary at the Capo Rossello area (Sicily). Earth and Planetary Science Letters, v. 91, p. 214–222.

Hilgen F.J., and Langereis, C.G., 1993. A critical re–evaluation of the Miocene/Pliocene boundary as defined in the Mediterranean. Earth and Planetary Science Letters, v. 118, p. 167–179.

Hinz, K., Winterer, E.L., Baumgartner, P.O., Bradshaw, M.J., Channell, J.E.T., Jaffrezo, M., Jansa, L.F., Leckie, R.M., Moore, J.N., Rullkötter, J., Schaftenaar, C., Steiger, T.H., Vuchev, V., and Wiegand, G.E., 1984. Initial Reports of DSDP, Leg 79, US Government Printing Office, Washington, D.C., v. 79, p. 1-934.

Hiscott, R.N., Cremer, M., and Aksu, A.E., 1989. Evidence from sedimentary structures for processes of sediment transport and deposition during post-Miocene time at Sites 645, 646 and 647. In Srivastava, S.P., Arthur, M.A. et al. (eds.), Proceedings of the Ocean Drilling Program, Leg 105. Washington, D.C. (U.S. Government Printing Office), v. 105, p. 53-63.

Hodell, D.A., and Kennett, J.P., 1986. Late Miocene–early Pliocene stratigraphy and paleoceanograhy of the South Atlantic and Southwest Pacific oceans: A synthesis. Paleoceanography, v. 1, p. 285–311.

Hodell, D.A., Elstrom, K.M., and Kennett, J.P., 1986. Latest Miocene benthic O change, global ice volume, sea level, and the "Messinian Salinity Crisis". Nature, v. 320, p. 411–414.

Hodell, D.A., Benson, R.H., Kennett, J.P., and K. Rakic–El Bied, 1989. Stable isotope stratigraphy of late Miocene–early Pliocene sequences in northwest Morocco: The Bou Regreg Section. Paleoceanography, v. 4, p. 467–482.

Hodell, D.A., Williams, D.F., and Kennett, J.P., 1985, Late Pliocene reorganization of deep vertical water–mass structure in the western South Atlantic: Faunal and isotopic evidence. Geological Society of American Bulletin, v. 96, p. 495–503.

Hodell, D. A., Müller, D.W., Ciesielski, P. F., and Mead, G.A., 1994b. Synthesis of oxygen and carbon isotopic results from Site 704: Implication for major climatic-geochemical transitions during the late Neogene. In Ciesielski, P.F., Kristofferson, Y., et al. (eds.), Proceedings of ODP Leg 114, Scientific Results, Washington, D.C. (Government Printing Office), v. 114, p. 475-480.

Hodell, D.A., Benson, R.H., Kent, D.V., Boersma, A., Rakic–El Bied, K., 1994a. Identification of oxygen isotope stages during the late Miocene based on a continuous drill core sequence from northwestern Morocco: A high–resolution chronology for the Messinian Stage. Paleoceanography, v. 9, p. 835–856.

Höglund, H., 1947. Foraminifera in the Gullmar Fjord and the Skagerak. Zool. Bidrag Uppsala, pp. 26.

Hornibrook, N. de B., Brazier, R.C., and Strong, C.P., 1989. Manual of New Zealand Permian to Pleistocene foraminiferal biostratigraphy: New Zealand Geological Survey Paleontological Bulletin, v. 56, p. 1-175.

Hooper, P.W.P., and Weaver, P.P.E., 1987. Paleoceanographic significance of late Miocene to early Pliocene planktonic foraminifers at Deep Sea Drilling Project Site 609: In Ruddiman, W.F., Kidd, R.B., et al., 1987, Initial Reports of the Deep Sea Drilling Project, Washington, D.C. (U.S. Government Printing Office), v. 94, p. 925–934.

Hsü, K.J., 1973. The desiccated deep–basin model for the Messinian events. In Drooger, Broekman, J.A., Hageman, J., Hantelmann, J.J., Marks, P., Meulenkamp, J.E., and Schmidt, R.R., (Eds.), Messinian Events in the Mediterranean, Geodynamics Scientific Report No, 7 on the colloquium held in Utrecht, March, 1973, Amsterdam London, p. 60–67.

Hsü, K.J., 1987. The desiccation of the Mediterranean Sea. Endeavor. New series, v. 11, no. 2, p. 67–72.

Hsü, K.J., 1988. Mediterranean model: Posterity will judge. Geotimes, September, 5.

Hsü, K. J., and Bernoulli, D., 1978. Genesis of the Tethys and the Mediterranean. In Hsü, K.J., and et al. (eds.), Initial Reports of the Deep Sea Drilling Project, Washington, D.C. (U.S. Government Printing Office), v. 42A, p. 943-950.

Hsü, K.J., Cita, M.B., and Ryan, W.B., 1973a. The origin of the Mediterranean evaporites: In Ryan, W.B., Hsü, K.J., et al., Initial Reports of the Deep Sea Drilling Project, Washington, D.C. (U.S. Government Printing Office), v. 13, p. 1203– 1231.

Hsü, K.J.. Ryan, W.B.F., and Cita, M.B., 1973b. Late Miocene desiccation of the Mediterranean. Nature, v. 242, p. 240–244.

Hsü, K.J., Montadert, L., Bernoulli, D., Cita, M. B., Erickson, A., Garrison, R. E., Kidd, R. B., Milleres., F., Müller, C., and Wright, R., 1977. History of the Mediterranean salinity crisis. Nature, v. 267, p. 399-403.

Hsü, K.J., Montadert, L., Garrison, R.E., et al., 1978. Initial Reports of the Deep Sea Drilling Project, Washington, D.C. (U.S. Government Printing Office), v. 42A, p. 1–1249.

Huddlestun, P.F., 1984. Planktonic foraminiferal biostratigraphy, Deep Sea Drilling Project Leg 81. In Roberts, D.G., Schnitker, D. et al., Initial Reports of DSDP Leg 81. US Government Printing Office (Washington, D.C.), v. 81, p. 429-438.

Iaccarino, S., 1985. Mediterranean Miocene and pliocene planktic foraminifera, plankton stratigraphy, Bolli, H. M., Saunders, J. B., and Perch-Nielsen, K. (eds.), p. 283-314.

Ingle, J.C., 1967. Foraminiferal biofacies variation and the Miocene–Pliocene boundary in Southern California. Bull. American Paleontology, v. 52, p. 217–394.

Iwasa, S., 1955. Biostratigraphy of the Iswasagawa Group in Honjo and its environs, Akita Prefecture. Journal of Geological Society, Tokyo, v. 61, p. 1-18.

Jenkins, D. G. 1960. Planktonic foraminifera from the Lakes Entrance Oil shaft, Victoria, Australia. Micropaleontology, v. 6, p. 345-71.

Jenkins, D. G., 1985. Southern mid-latitude Paleocene to Holocene planktic foraminifera. Plankton stratigraphy, Bolli, H. M., Saunders, J. B., and Per-Nielsen, K.(eds.), p. 263-282.

Jones, T. R., and W. K. Parker, 1860. On the Rhizopodal fauna of the Mediterranean, compared with that of the Italian and some other Tertiary deposits, Quarterly Journal of the Geological Society of London, v. 16, p. 292-307.

Kaminski, M.A., Grassle, J.F., and Whitlatch, R.B., 1988b. Life history and recolonization among agglutinated foraminifera in the Panama Basin,

Abhandlungen der Geologischen Bundesanstalt, Wien, Band 41, Rögl, F. and Gradstein, F.M. (eds.), p. 229-243.

Kaminski, M.A., Gradstein, F.M., Scott, D.B., and Mackinnon, K.D., 1989. Neogene benthic foraminifer biostratigraphy and deep water history of sites 645, 646, and 647, Baffin Bay and Labrador Sea. In Srivastava, S.P., Arthus, M.A., et al. (eds.), Proceedings of the Ocean Drilling Program, Leg 105, Washington, D.C. (U.S. Government Printing Office), v. 105, p. 731–756.

Kaminski, M.A., Gradstein, F.M., Berggren, W.A., Geroch, S., and Beckmann, J.P., 1988a. Flysch-type agglutinated foraminiferal assemblages from Trinidad: Taxonomy, stratigraphy and paleobathymetry, Abhandlungen der Geologischen Bundesanstalt, Wien, Band 41, Rögl, F. and Gradstein, F.M. (eds.), p. 155-227.

Kanmacher, F., 1798. Adams Essays on the Microscope: The Second Edition, with Considerable Additions and Improvements: London (Dillon and Keating).

Kastens, K.A., 1992. Did a glacio–eustatic sea level drop trigger the Messinian salinity crisis? New evidence from Ocean Drilling Program site 654 in the Tyrrhenian Sea. Paleoceanography, v. 7, p. 333–356.

Kastens, K., and Mascle, J., 1990a. Did a glacioeustatic sea level drop trigger the Messinian Salinity Crisis in the Mediterranean? In Barker, P.F., Kennett, J.P., et al. (eds.), Proceedings of the Ocean Drilling Program, Scientific Results, Leg 113, Washington, D.C. (U.S. Government Printing Office), v. 113, p. 993.

Kastens, K.A., and Mascle, J, 1990b. The geological evolution of the Tyrrhenian Sea: An introduction to the scientific results of ODP Leg 107. In Proceedings of the Ocean Drilling Program (Scientific results), Kastens, K.A., Mascle, J., Auroux, C., et al. (eds.), U.S. Government Printing Office (Washington, D.C.), v. 107, p. 3–28.

Katz, M.E., and Miller, K.G., 1993. Latest Oligocene to earliest Pliocene benthic foraminiferal biofacies of the northwestern Gulf of Mexico. Micropaleontology, v. 39, p. 367–403.

Keigwin, L.D., 1978. Pliocene closing of the Isthmus of Panama, based on biostratigraphic evidence from nearby Pacific Ocean and Caribbean Sea cores. Geology, v. 6, p. 630–634.

Keigwin, L.D., 1979. Late Cenozoic stable isotope stratigraphy and paleoceanography of DSDP sites of the east equatorial and central North Pacific Ocean. Earth and Planetary Science Letters, v. 45, p. 361–382.

Keigwin, L.D., 1982. Neogene planktonic foraminifers from DSDP Sites 502, 503. In Prell, W.S., Gardner, J.V. et al., Initial Reports of DSDP, Leg 68, Washington, D.C. (U.S. Government Printing Office, v. 68, p. 269–288.

Keigwin, L.D., 1987. Toward a high–resolution chronology for latest Miocene paleoceanographic events: Paleoceanography, v. 2, p. 639–660.

Keigwin, L.D., and Schackleton, N.J., 1980. Uppermost Miocene carbon isotope stratigraphy of a piston core in the equatorial Pacific. Nature, v. 284, p. 613–614.

Keigwin, L.D., Aubry, M.–P., and Kent, D.V., 1987. North Atlantic late Miocene stable isotope stratigraphy. biostratigraphy, and magnetostratigraphy. In Ruddiman, W.F., Kidd, R.B. et al. (edit.), Initial Reports of Deep Sea Drilling Project Leg 94, part 2, Washington, D.C. (U.S. Government Printing Office), v. 94, p. 935–963.

Keller, G., 1978. Late Neogene biostratigraphy and paleoceanography of DSDP Site 310 Central North Pacific and correlation with the southwest Pacific. Marine Micropaleontology, v. 3, p. 97–119.

Keller, G., 1979a. Late Neogene planktonic foraminiferal biostratigraphy and paleoceanography of the northwest Pacific DSDP Site 296. Palaeogeography, Palaeoclimatology, Palaeoecology, v. 27, p. 129–154.

Keller, G., 1979b. Late Neogene paleoceanography of the North Pacific DSDP Sites 173, 310, and 296. Marine Micropaleontology, v. 4, p. 159–172.

Keller, G., 1979c. Early Pliocene to Pleistocene planktonic foraminiferal datum levels in the North Pacific: DSDP Sites 173, 310, 296. Marine Micropaleontology, v. 4, p. 281–294.

Kemp, E.M., Frakes, L.A., and Hayes, D.E., 1975. In Hayes, D.E., Frakes, L.A. et al., 1975. Initial Reports of DSDP Leg 28, U.S. Government Printing Office, Washington, D.C., v. 28, p. 909-917.

Kennett, J.P., 1966. The *Globorotalia crassaformis* bioseries in north Westland and Marlborough, New Zealand: Micropaleontology, v. 12, p. 235-245.

Kennett, J.P., 1967a. New foraminifera from the Ross Sea, Antarctica. Contributions from the Cushman Laboratory for Foraminiferal Research, v. 18, p. 133-135.

Kennett, J.P., 1967b. Recognition and correlation of the Kapitean Stage (upper Miocene, New Zealand). New Zealand Journal of Geology and Geophysics, v. 10, p. 1051–1063.

Kennett, J.P., 1977. Cenozoic evolution of Antarctic glaciation, the circum–Antarctic ocean, and their impact on global paleoceanography. Journal of Geophysical Research, v. 82, p. 3843–3860.

Kennett, J.P., 1983. Marine Geology, Prentice-Hall Inc., Englewood Cliffs, NJ, p. 1-813.

Kennett, J.P., and Srinivasan, M.S., 1983. Neogene planktonic foraminifera: A phylogenetic Atlas. Stroudsburg, P.A. (Hutchinson Ross), p. 1-265.

Kennett, J.P., and Vella, P.P., 1975. Late Cenozoic planktonic foraminifera and paleoceanography at DSDP Site 284 in the cool subtropical South Pacific. In Kennett, J.P., Houtz, R.E., and others (eds.), Initial Reports of DSDP, Washington. D.C., U.S. Government Printing Office, v. 29, p. 769–799.

Knüttel, S., Russell, M.D., and Firth, J.V., 1985. Neogene calcareous nannofossils from ODP Leg 105: Implications for Pleistocene paleoceanographic trends. In Srivastava, S.P., Arthus, M.A., et al. (eds.), Proceedings of the Ocean Drilling

Program, Leg 105, Washington, D.C. (U.S. Government Printing Office), v. 105, p. 245–262.

Krijgsman, W., Hilgen, F.J., Langereis, C.G., and Zachariasse, W.J., 1994. The age of the Tortonian/Messinian boundary. Earth and Planetary Science Letters, v. 121, p. 533–547.

Kuang, L., and Cada, M., Selecting the factors of wavelet function for pattern recognition. Applied Optics (in press).

Kurihara, K., and Kennett, J.P., 1992. Paleoceanographic significance of Neogene benthic foraminiferal changes in a southwest Pacific bathyal depth transact: Marine Micropaleontology, v. 19, p. 181–199.

Langereis, C.G., and Hilgen, F.J., 1991. The Rossello composite: A Mediterranean and global reference section for the early to late early Pliocene. Earth and Planetary Science letters, v. 104, p. 211–225.

Lehman, S.J., and Keigwin, L.D., 1992a. Sudden changes in North Atlantic circulation during the last deglaciation. Nature, v. 356, p. 757–762.

Lehman, S.J., and Keigwin, L.D., 1992b. Deep circulation revisited. Nature, 358, p. 197–198.

Lincoln, J.M., and Schlanger, S.O., 1987. Miocene sea-level falls related to the geologic history of Midway atoll. Geology, v. 15, p. 639-660.

Li né, C., 1758. Systema naturae per regna tria naturae, secundum classes, ordines, genera, species, cum characteribus, differentiis, synonymis, locis (Vol. 1) (10th ed.): Lipsiae (G. Engelmann), p. 1-824.

Loeblich, Jr., A.R., and Tappan, H., 1988. Foraminiferal genera and their classification. Van Nostrand Reinhold Company, New York, p. 1-970.

Lohmann, G.P., 1978. Abyssal benthonic foraminifera as hydrographic indicators in the western South Atlantic Ocean. Journal of Foraminiferal Research, v. 8, p. 6–34.

Loubere, P., 1987. Changes in mid–depth North Atlantic and Mediterranean circulation during the late Pliocene–isotopic and sedimentological evidence. Marine Geology, v. 77, p. 15–38.

Loutit, T.S., 1981. Late Miocene paleoceanography: Subantarctic water Mass, Southwest Pacific. Marine Micropaleontology, v. 6, p. 1-27.

Loutit, T.S., and Keigwin, L.D., 1982. Stable isotopic evidence for latest Miocene sea–level fall in the Mediterranean region. Nature, v. 300, p. 163–166.

Loutit, T.S., and Kennett, J.P, 1979. Application of carbon isotope stratigraphy to late Miocene shallow marine sediments, New Zealand. Science, v. 204, p. 1196–1199.

Lutze, G.F., 1980. Depth distribution of benthic foraminifera on the continental margin off NW Africa. "Meteor" Forsch.–Ergebnisse, Reihe C, v. 32, p. 31–80.

Lutze, G.F., and Coulbourn, W.T., 1984. Recent benthic foraminifera from the continental margin of northwest Africa: Community structure and distribution. Marine Micropaleontology, v. 8, p. 361–401.

Mackensen, A., 1992. Neogene benthic foraminifers from the Southern Ocean (Kerguelen Plateau): Biostratigraphy and paleoecology. In Proceedings of Ocean Drilling Program, Scientific results, Wise, S.W., Schlich, R. et al. (Eds.), v. 120, p. 649–673.

Marshall, L.G., 1988. Land mammals and the Great American Interchange. American Scientist, v. 76, p. 380–388.

Martin, J.H., 1990. Glacial–interglacial CO_2 change: The iron hypothesis. Paleoceanography, v. 5, p. 1–14.

Martini, E., 1971. Standard Tertiary and Quaternary calcareous nannoplankton zonation. In Farinacci, A. (ed.). Proceedings of the First Planktonic Conference. Roma, 1971. Edit. Tecnoscienza, Rome, p. 739–785.

Mayer–Eymar, C. K., 1868. Tableau desterrains tertiaires Supérieurs [IV ed.]: Zürich.

Mazzei, R., Raffi, I., Rio, D., Hamilton, N., and Cita, M.B., 1979. Calibration of Late Neogene calcareous plankton datum planes with the paleomagnetic record of Site 397 and Mediterranean sections. In: Von Rad, U., Ryan, W.B.F., Arthur, M.A. et al., Initial Reports of DSDP, Leg 47, U.S. Government Printing Office (Washington, D.C.), v. 47, p. 375–391.

McCartney, M.S., 1992. Recirculating components to the deep boundary current of the northern North Atlantic. Progress of Oceanography, v. 29, p. 283–383.

McCartney, M.S., and Talley, L.D., 1984. Warm–to–cold conversion in the northern North Atlantic Ocean. Journal of Physical Oceanography, v. 14, p. 922–935.

McCartney, M.S., Bennett, S.L., and Woodgate–Jones, M.E., 1991. Eastward flow through the Mid–Atlantic Ridge at 11°N and its influence on the abyssal Eastern Basin. Journal of Physical Oceanography, v. 21, p. 1089–1121.

McCave, I.N., and Tucholke, B.E., 1986. Deep current–controlled sedimentation in the western North Atlantic. In Vogt, P.R., and Tucholke, B.E. (eds.), The Geology of North America, vol. M, The Western North Atlantic Region. Boulder, Co., (Geological Society of America, p. 451–468.

McCoy, F.W., and Zimmerman, H.B., 1979. A history of sediment lithofacies in the South Atlantic Ocean. In Initial Reports of Deep Sea Drilling Project, Supko, P.R., Perch– Nielsen et al. (eds.), Washington, D.C., U.S. Government Printing Office, v. 39, P. 1047– 1079.

McDougall, I., Watkins, N.D., and Kristjanson, L., Geochronology and paleomanetism of a Miocene-Pliocene lava sequence at Bessastadaa, eastern Iceland. Journal of American Scientists, v. 276, p. 1078-1095, 1976.

McKenzie, J.A., and Oberhänsli, H., 1985. Paleoceanographic expressions of the Messinian salinity crisis. In South Atlantic Paleoceanography, Hsü, K.J., and Weissert, H.J. (Eds.), Cambridge University Press, p. 99–123.

McKenzie, J.D., Jenkyns, H.C., and Bennet, G.G., 1979/1980. Stable isotope study of the cyclic diatomite–claystones from the Tripoli Formation, Sicily: A prelude to the Messinian Salinity Crisis. Paleogeography, Paleoclimatology, Paleoecology, v. 29, p. 125–141.

McKenzie, J.D., Hodell, D.A., Mueller, P.A., and Mueller, D.W., 1988. Application of strontium isotopes to late Miocene–early Pliocene stratigraphy. Geology, v. 16, p. 1022–1025.

McLaughlin, P. P. and Sen Gupta, B. B., 1994. Benthic foraminiferal record in the Miocene-Pliocene sequence of the Azua Basin, Dominican Republic. Journal of Foraminiferal Research, v. 24, p. 75-109.

Mercer, J.H., 1978. West Antarctic ice sheet and CO_2 greenhouse effect: A threat of disaster. Nature, v. 271, p. 321–325.

Mercer, J.H., and Sutter, J.F., 1982. Late Miocene–early Pliocene glaciation in southern Argentina: Implication for global ice–sheet history. Palaeogeography, Palaeoclimatology, Palaeoecology, v. 38, p. 185–206.

Miller, K.G., and Fairbanks, R.G., 1985. Oligocene to Miocene carbon isotope cycles and abyssal circulation changes. In The Carbon Cycle and Atmosphere CO_2: Natural Variations Archean to Present, Geophysical Monograph Series, Sunduist, E., and Broecker, W.S. (eds.), v. 32, p. 469–486.

Miller, K.G., and Katz, M.E., 1987. Oligocene to Miocene benthic foraminiferal and abyssal circulation changes in the North Atlantic. Micropaleontology, v. 33., p. 97–149.

Miller, K.G., and Lohmann, G.P., 1982, Environmental distribution of recent benthic foraminifera on the northeast United States continental slope. Geological Society of America Bulletin, v. 93, p. 200–206.

Miller, K.G., and Tucholke, B.E., 1983. Development of Cenozoic abyssal circulation south of the Greenland–Scotland Ridge. In Bott, M.H.P., Saxov, S., Talwani, M., and Thiede, J. (eds.), Structure and Development of the Greenland–Scotland Ridge, NATO Conference Ser.: New York (Plemun Press), p. 549–589.

Miller, K.G., Fairbanks, R.G., and Mountain, G.S., 1987. Tertiary oxygen isotope synthesis, sea-level history, and continental margin erosion, Paleoceanography, v. 2, p. 1-19.

Miller, K.G., Fairbanks, R.G., and Thomas, E., 1987. Benthic foraminiferal carbon isotopic records and the development of abyssal circulation in the eastern North Atlantic. In Ruddiman, W.F., Kidd, R.B., et al., (eds.). Initial Reports of DSDP Leg 94, v. 94, pt. 2, p. 981–996.

Miller, K.G., Feigenson, M.D., Wright, J.D., and Clement, B.M., 1991. Miocene isotope reference section, Deep Sea Drilling Project Site 608: An evaluation of isotope and biostratigraphic resolution. Paleoceanography, v. 6, p. 33–52.

Montadert, L., Letouzey, J., and Mauffret, A., 1978. Messinian event: Seismic evidence. In Hsü, K.J., and et al. (eds.), Initial R.ports of DSDP, Natl. Sci. Found., Washington, D.C., v. 42a, p. 1037–1050.

Müller, D.W., and Hsü, K.J., 1987. Event stratigraphy and paleoceanography in the Fortun Basin (South-east Spain): A scenario for the Messinian Salinity Crisis. Paleoceanography, v. 2, p. 679-696.

Müller, D.W., and Mueller, P.A., 1991. Origin and age of the Mediterranean Messinian evaporites: Implications from Sr isotopes. Earth and Planetary Science Letters, v. 107, p. 1-12.

Müller, D.W., Hodell, D. A., and Ciesielski, P. F., 1994. Late Miocene to early Pliocene (9.8-4.5 Ma) paleoceanography of the Subantarctic southeast Atlantic: Stable isotopic, sedimentologic, and microfossil evidence. In Ciesielski, P.F., Kristofferson, Y., et al. (eds.), Proceedings of ODP Leg 114, Scientific Results, Washington, D.C. (Government Printing Office), v. 114, p. 459-474.

Murray, J.W., 1973. A method of determining proximity of marginal seas to an ocean. Marine Geology, v. 22, p. 103–119.

Murray, J.W., 1976. Comparative studies of living and dead benthic foraminiferal distributions. Foraminifera, Hedley, R.H. and Adams, C.G. (edit.), v. 2, p. 45–109.

Murray, J.W., 1984. Paleogene and Neogene benthic foraminifera from Rockall Plateau. In: Roberts, D.G., Schnitker, D., et al., Initial Reports of DSDP, Washington, D.C., U.S. Government Printing House, v. 81, p. 503–534.

Murray, J.W., 1987. Benthic foraminifera and Neogene bottom–water masses at Deep Sea Drilling Project Leg 94 North Atlantic sites. In Ruddiman, W.F., Kidd, R.B., Baldauf, J.G. et al., Initial Reports of the Deep Sea Drilling Project Leg 94, Washington. D.C., U.S. Government Printing Office, v. 94, p. 965–979.

Murray, J.W., Weston, J.F., Haddon, C.A., and Powell, A.D.J., 1986. Miocene to Recent bottom water masses of the northeast Atlantic: an analysis of benthic foraminifera. In C.P. Summerhayes and N.J.Shackleton (eds.), North Atlantic Paleoceanography. Geological Society, London Special Publication, v. 21, p.219–230.

Nesteroff, W.D., 1973a. Distribution of the fine–grained sediment component in the Mediterranean. In Ryan, W.A.F., and et al. (eds.), Initial Reports of the Deep Sea Drilling Project, Natl. Sci. Found, Washington, D.C., v. 13, p. 666–670.

Nesteroff, W.D., 1973b. Un modele pour les evaporites Messinienes en Mediterranee: Des Bassins peu profonds avec depot d'evaporites lagunaires. In Drooger, C.W., Broekman, J.A. and et al. (eds.), Messinian Events in the Mediterranean, North–Holland Publ. Co., Amsterdam, p. 68–81.

Nilsen, T.H., and Kerr, D.R., 1978. Paleoclimatic and paleoceanographic implications of a Lower Tertiary Laterite (latosol) on the Iceland–Faeroe Ridge, North Atlantic region. Geological Magazine, v. 115, p. 153–236.

Norvang, A., 1945. The zoology of Iceland: foraminifera. Ejnar Munksgaard, Copenhagen and Reykjavik, v. 2, p. 1-79.

ODP Leg 151 Shipboard Scientific Party, 1994. Exploring Arctic history through scientific drilling. EOS, v. 75, no. 25, p. 281, 285.

Open University Course Team, 1978. Oceanic Circulation (unit 6). In Oceanography: Physical Processes. The Open University Press, . p. 1–34.

Open University Course Team, 1989. Ocean Circulation. Pergamon Press, p. 1–238.

Orbigny, A. D., d', 1826. Tableau méthodique de la classees des céphalopods. Annales des Sciences Naturelles, Paris, Ser. 1, v. 7, p. 245-314.

Orbigny, A. D., d', 1839a. Voyage dans l'Amérique Méridionale-Foraminifères, (Vol. 5, Pt. 8): Paris (Pitois-Levrault et Cie); Strasbourg (V. Levrault), p. 1-86.

Orbigny, A.D, d', 1839b. Foraminiferes. In: Histoire physique, politique et naturelle de lile de Cuba, ed. R. de la Sagra. Bertrand, Paris, pp. 224.

Orbigny, A.D., d', 1846. Foraminiferes fossiles du Bassin Tertiaire de Vienne (Autriche): Classics in Paleonotoogy, no. 2, Paris: Gide et Comp^{e}, p. 1-321, plates 17.

Oslick, J.S., Miller, K.G., Feigenson, M.D., and Wright, J.D., 1994. Oligocene-Miocene strontium isotopes: Stratigraphic revisions and correlation to the inferred glacioeustatic record, Paleoceanography, v. 9, p. 427-444.

Parker, W. K. and Jones, T. R., 1865. On some foraminifera from the North Atlantic and Arctic Oceans, including Davis Strait and Baffin's Bay. Philosophical Transactions of the Royal Society, v. 155, p. 325-441.

Parker, W. K., and T. R. Jones, 1865. On some foraminifera from the North Atlantic and Arctic Oceans, including Davis Straits and Baffin's Bay, Philosophical Transactions of the Royal Society, v. 155, p. 325-411.

Pedley, H.M., and Grasso, M., 1993. Controls on faunal and sediment cyclicity within the Tripoli and Calcare di Base basin (late Miocene) of central Sicily. Paleogeography, Paleoclimatology, Paleoecology, v. 105, p. 337–360.

Perch–Nielsen, K., 1985. Cenozoic calcareous nannofossils. In Plankton Stratigraphy. Bolli, H.M., Saunders, J.B., and Perch–Nielsen (eds.), Cambridge University Press, p. 427–555.

Pflum, C.E., and Frerichs, W.E., 1976. Gulf of Mexico deep–water foraminifers. Cushman Foundation for Foraminiferal Research Special Publication, no. 14, pp. 125.

Phleger, F.B., 1942. Foraminifera of submarine cores from the continental slope, part 2. Geological Society of America Bulletin, v. 53, p. 1073–1098.

Phleger, F.B., 1951, Ecology of foraminifera, northwest Gulf of Mexico. Part 1, Foraminiferal distribution. GSA Memoir 46, p. 1–88.

Phleger, F.B., and Parker, F.L., 1951. Ecology of foraminifera, northwest Gulf of Mexico. Part 2, Foraminiferal species. GSA Memoir 46, p. 1–64.

Phleger, F.B., Parker, F.L., and Peirson, J.F., 1953. North Atlantic foraminifera. Rep. Swed. Deep Sea Expedition, v. 7, p. 1–122.

Pickard, G.L., and Emery, W.J., 1982. Descriptive Physical Oceanography, 4th (SI) Enlarged Edition. Pergamon Press, p. 249.

Pierre, C., and Rouchy, A.M., 1987. Sedimentary and diagenetic evolution of Messinian evaporites in the Tyrrhenian Sea (ODP Leg 107, Sites 652, 653, and 654): Petrographic, mineralogical, and stable isotope records. In Proceedings of the Ocean Drilling Program (Scientific results), Kastens, K.A., Mascle, J., Auroux, C., et al. (eds.), U.S. Government Printing Office (Washington, D.C.), v. 107, p. 187–209.

Pirazzoli, P.A., 1991. World atlas of Holocene sea-level changes. Amsterdam: Elsevier Oceanography Series 58. Elsevier Publishing, pp. 300.

Pomar, L., and Ward, W.C., 1994. Response of a late Miocene Mediterranean reef platform to high–frequency eustasy. Geology, v. 22, p. 131–134.

Poore, R.Z., Tauxe, L., Percival, Jr. S.F., LaBrecque, J.L., Wright, R., Peterson, N.P., Smith, C.C., Tucker, P., and Hsu, K.J., 1983. Late Cretaceous–Cenozoic magnetostratigraphy and biostratigraphy of the South Atlantic Ocean: DSDP Leg 73. Paleogeography, Paleoclimatology, Paleoecology, v. 42, p. 127–149.

Price, J.F., 1992. Overflows. Oceanus, Summer, p. 28–34.

Price, J.F., Baringer, M.O., Lueck, R.G., Johnson, G.C., Ambar, I., Parrilla, G., Cantos, A., Kennelly, M.A., and Sanford, T.B., 1993. Mediterranean Outflow mixing dynamics. Science, v. 259, p. 1277–1282.

Pudsey, C.J., Barker, .F., and Hamilton, N., 1988. Weddell Sea abyssal sediments a record of Antarctic bottom water flow. Marine Geology, v. 81, p. 289–314.

Reid, J.L, 1979. On the contribution of the Mediterranean Sea outflow to the Norwegian-Greenland seas. Deep Sea Research, v. 26, p. 1199-1223.

Renz, H. H., 1948. Stratigraphy and fauna of the Agua Salada Grop, State of Falcon, Venezuela. The Geological Society of America Memoir 32, pp. 219.

Reuss, A. E., 1850. Neues Foraminiferen aus den Schichten des Österreichischen Tertiärbeckens, Denkschriften der Kaiserlichen Akademie der Wissenschaften, Mathematisch-Naturwissenschaftliche Classe, v. 1, p. 365-390.

Reuss, A. E., 1851. Über die fossilen Foraminiferen und Entomostraceen der Septarienthone der Umgegend von Berlin. Zeitschrift der Deutschen Geologischen Gesellschaft, Berlin, v. 3, p. 49-91.

Roberts, A.P., Turner, G.M., and Vella, P.A., 1994. Magnetostratigraphic chronology of late Miocene to early Pliocene biostratigraphic and oceanographic events in New Zealand. Geological Society of America Bulletin, v. 106, p. 665–683.

Roberts, D.G., Bott, M.H.P., and Uruski, C., 1983. Structure and origin of the Wyville–Thomson Ridge. In Bott. M.H.P., et al. (eds.), Structure and Development of the Greenland–Scotland Ridge: New York (Plenum Press), p. 133–158.

Roberts, D.G, Schnitker, D., et al., 1984. Initial Reports of Deep Sea Drilling Project, Leg 81, Washington, D.C., U.S. Government Printing Office, v. 81, p. 1–923.

Robertson, A., Hieke, W., Mascle, G., McCoy, F., McKenzie, J., Rehault, J.–P, and Sartori, R., 1990. Summary and synthesis of late Miocene to Recent sedimentary and paleoceanographic evolution of the Tyrrhenian Sea, Western Mediterranean: Leg 107 of the Ocean Drilling Program. In Proceedings of the Ocean Drilling Program (Scientific results), Kastens, K.A., Mascle, J., Auroux, C., et al. (eds.), U.S. Government Printing Office (Washington, D.C.), v. 107, p. 639–668.

Rouchy, J.–M., 1982a. La Crise évaporitique messinienne de Méditerranée: nouvelles propositions pour une interprétation génétique. Bulletin of National Musesum of Natural History, Sér, 4, v. 4, p. 107–136.

Rouchy, J.–M., 1982b. Commentaires sur une interprétation paléogéographique du domaine Méditerranéen au cours du dépot des évaporites Messiniennes proposée à partir de étude des surfaces érosin périméditerrannéenes: Bulletin, Society Géology France, Sér. 7, v. 24, p. 653–657.

Ruddiman, W, F., and McIntyre, A., 1977. Late Quaternary surface ocean kinematics and climatic change in the high-latitude North Atlantic. Journal of Geophysical Research, v. 82, p. 3877-3887.

Ruddiman, W, F., Kidd, R.B., Baldauf, J.G., Clement, B.M., Dolan, J.F., Eggers, M.R., Hill, P.R., Keigwin, L.D., Mitchell, M., Philipps, I., Robinson, F., Salehipour, S.A., Takayama, T., Thomas, E., Unsold, G., and Weaver, P.P.E., 1987a. Intial Reports of Deep Sea Drilling Project, Leg. 94, v. 94 (parts 1), p. 1-614.

Ruddiman, W, F., Kidd, R.B., Baldauf, J.G., Clement, B.M., Dolan, J.F., Eggers, M.R., Hill, P.R., Keigwin, L.D., Mitchell, M., Philipps, I., Robinson, F., Salehipour, S.A., Takayama, T., Thomas, E., Unsold, G., and Weaver, P.P.E., 1987b. Intial Reports of Deep Sea Drilling Project, Leg. 94, v. 94 (parts 2), p. 615-1261.

Ruggieri, G., and Sprovieri, R., 1976. Messinian Salinity Crisis and its paleoceanographical implications. Palaeogeography Palaeoclimatology Palaeoecology, v. 20., p. 13–22.

Ryan, W.B.F., 1973. Geodynamic implications of the Messinian crisis of salinity. In Messinian Events in the Mediterranean, Drooger, C.W. (ed.), North–Holland Publishing Company, Amsterdam, London, p. 26–38.

Ryan, W.B., Hsü, K.J., Cita, M.B., Dumitrica, P., Lort, J.M., Maync, W., Nesteroff, W.D., Pautot, G., Stradner, H., and Wezel, F.C., 1973. Initial Reports of Deep Sea Drilling Project, Leg 13, Washington, D.C. (U.S. Government Printing Office), v. 13, Parts 1 and 2, p. 1–516.

Rzehak, A., 1886, [Ueber Foraminiferen], Verhandlungen des Naturforschenden Vereins in Brunn, Sitzungberichte, v. 24, p. 8.

Saito, T., and Burckle, L.H., and Hays, J.D., 1975. Late Miocene to Pleistocene biostratigraphy of equatorial Pacific sediments. In Saito, T., and Burckle, L.H. (eds.), Late Neogene Epoch Boundaries, p. 226-244.

Sarnthein, M., and Winn, K., 1990. Reconstruction of low and middle latitude export productivity, 30,000 years to present: Implications for global carbon reservoirs. In: Schlesinger (ed.), Climate–Ocean interaction. Kluwer Academic Publishers, p. 319–342.

Schmitz, W.J. Jr., and McCartney, M.S., 1993. On the North Atlantic circulation. Reviews of Geophysics, v. 31, p. 29–49.

Schnitker, D., 1974. West Atlantic abyssal circulation during the past 120,000 years: Nature, v. 248, p. 385–387.

Schnitker, D., 1979a. Cenozoic deep water foraminifers, Bay of Biscay. In: Montadert, L., Roberts, D.G. et al., Initial Reports of DSDP, Washington, D.C., U.S. Government Printing House, v. 48, p. 377–413.

Schnitker, D., 1979b. The deep waters of the western North Atlantic during the past 24,000 years, and the re–initiation of the Western Boundary Undercurrent. Marine Micropaleontology. v. 4, p. 265–280.

Schnitker, D., 1980. Quaternary deep–sea benthic foraminifers and bottom water masses. Annual Review of Earth and Planetary Science, v. 8, p. 343–370.

Schnitker, D., 1986. North–east Atlantic Neogene benthic foraminiferal faunas: Tracers of deep water paleoceanography. In North Atlantic Paleoceanography, Summerhays, C.P., and Shackleton, N.J. (eds.), p. 191–203.

Schröder, C.J., 1986. Deep-water arenaceous foraminifera in the Northwest Atlantic Ocean, Can. Tech. Rept. Hydrogr. Ocean Sci., v. 71, p. 1-191.

Schwager, C., 1866. Fossile Foraminiferen von Kar-Nicobar, Reise der Österreichischen Fregatte Novara um Erde in den Jahren 1857, 1858, 1859 unter den Befehlen des Commodore B. Von Wullerstofi-Urbair, Geologscher Theil, v. 2, no.1, Geologische Beobachtungen, no. 2, Palaontologische Mittheilungen, p. 187-268.

Sclater, J.G., and Tapscott, C., 1979. The history of the Atlantic. Scientific America, v. 240, p. 156– 174.

Scott, D.B., and Leger, G.T., 1990. Benthic foraminifers and implications for intraplate deformation, ODP Site 717, distal Bengal Fan. In Cochran, J.R., Stow, D.A.V. et al., Proceedings of the Ocean Drilling Program, Scientific Results, v. 116, p. 189-206.

Scott, D.B., and Medioli, F.S., 1978. Vertical zonations of marsh foraminifera as accurate indicators of former sea-level. Nature, v. 272, p. 528-531.

Scott, D.B., and Medioli, F.S., 1980. Quantitative studies of marsh foraminiferal distribution in Nova Scotia. Cushman Foundation for Foraminifera Research, Special Publication, #17, p. 1-58.

Scott, D.B., and Medioli, F.S., 1986. Foraminifera as sea-level indicators. In Van de Plassche, O. (edit.), Sea-level Research: A manual for the collection and evaluation of data. Geological Books, Norwich, p. 435-455.

Scott, D. B., Suter, J. R., and Kosters, E. C., 1991. Marsh foraminifera and arcellaceans of the lower Mississippi Delta:Controls on spatial distributions. Micropaleontology, v. 37, p. 373-392.

Scott, D.B., Mudie, P., de Vernal, A., Hillaire-Marcel, Baki, V., MacKinnon, K.D., Medioli, F.S., and Mayer, L., 1989. Lithostratigraphy, biostratigraphy, and stable isotope stratigraphy of cores from ODP Leg 105 Site surveys, Labrador Sea and Baffin Bay. In Proceedings of the Ocean Drilling Program, Scientific Results, Srivastava, S.P., Arthur, M.A. et al. (eds.), v. 105, p. 561-582.

Scott, G.H., 1982. Review of Kapitean stratotype and boundary with Opoitian Stage (upper Neogene, New Zealand). New Zealand Journal of Geology and Geophysicus, v. 25, p. 475–485.

Seguenza, G., 1862, Dei terreni Terziarii del distretto di Messina; Part II - Descrizione dei foraminiferi monotalamici delle marne Mioceniche del distretto di Messina. Messina: T. Capra.

Seiler, W.C., 1975. Tiefenverteilung benthischer foraminiferen am Portugiesischen Kontinentalhang, "Meteor" Forsch.–Ergebnisse, Reihe C, no. 23, seite 47–94.

Selli, R. 1960. The Mayer–Eymar Messinian 1867: Proposal for a neostratotype: Rpt. 21_{st} Session, International Geological Congress, Geneva Proceedings, v. 28, p. 311–333.

Selli, R., 1973. An outline of the Italian Messinian. In Drooger, Broekman, J.A., Hageman, J., Hantelmann, J.J., Marks, P., Meulenkamp, J.E., and Schmidt, R.R., (eds.)., Messinian Events in the Mediterranean, Geodynamics Scientific Report, No, 7 on the colloquium held in Utrecht, March, 1973, Amsterdam London, p. 150–171.

Sen Gupta, B.K., Lee, R.F., and May, M.S., 1981. Upwelling and unusual assemblages of benthic foraminifera on the northern Florida continental slope. J. of Paleontology, v. 55, p. 853–857.

Shackleton, N.J., and Cita, M.B., 1979. Oxygen and carbon isotope stratigraphy of benthic foraminifers at Site 397: Detailed history of climatic change during the late Neogene. In Arthur, M.A, Cepek, P. et al., Initial Reports of DSDP Leg 47. Washington. D.C., U.S. Government Printing Office, v. 47, p. 433-446.

Shackleton, N.J., and Kennett, J.P. 1975. Late Cenozoic oxygen and carbon isotope changes at DSP 284: Implications for glacial history of the Northern Hemisphere and Antarctica. In Kennett, J.P., Houtz, R.E., and others (eds.), Initial Reports of DSDP, Washington. D.C., U.S. Government Printing Office, v. 29, p. 801–807.

Shackleton, N.J., Hall, M.A., and Pate, D., 1995. Pliocene stable isotope stratigraphy of ODP Site 846. Proc. Ocean Drilling Prog. Leg 138, Sci. Res., v. 138, p. 337-355.

Sierro, F.J., 1985. The replacement of *"Globorotalia menardii"* group by *"Globorotalia miotumida"* group: An aid to recognizing the Tortonian/Messinian boundary in the Mediterranean and adjacent Atlantic. Marine Micropaleontology, v. 9, p. 525–535.

Sierro, F.J., Flores, J.A., Covis, J., González Delgado, J.A., and Francés, G., 1993. Late Miocene globorotaliid event–stratigraphy and biogeography in the NE Atlantic and Mediterranean. Marine Micropaleontology, v. 21, p. 143–168.

Siesser, W.G., 1995. Paleoproductivity of the Indian Ocean during the Tertiary period. Global and Planetary Change, v. 11, p. 71–88.

Silvestri, A., 1898. Foraminiferi Pliocenici della Provincia di Siena. Parte II, Memorie dell'Accademia Pontificia dei Nuovi Lincei, Roma, v. 15, p. 155-381.

Silvestri, A., 1904. Ricerche strutturali su alcune forme dei Trubi di Bonfornello (Palmero). Momorie della Pontificia Accademia Romana dei Nuovi Lincei, v. 22. p. 235-276.

Sonnenfeld, P., 1975. The significance of upper Miocene (Messinian) evaporites in the Mediterranean Sea. Journal of Geology, v. 83, p. 287–311.

Srinivasan, M.S., and Chaturvedi, S.N., 1992. Neogene planktonic foraminiferal biochronology of the DSDP Sites along the Ninetyeast Ridge, northern Indian Ocean. In Ishizaki, K, M., and Saito, T. (eds.), Centenary of Japanese Micropaleontology, Terra Scientific Publishing Company, Tokyo, p. 175–188.

Srivastava, S. P., Arthur, M. A.,Clement, B. Aksu, A., Baldauf, J., Bohrmann, G., Busch, W., Cederberg, T., Cremer, M., Dadey, K., De Vernal, A., Firth, J., Hall, F., Head, M., Hiscott, R., Jarrard, R., Kaminski, M., Lazarus, D., Monjanel, A., L., Nielsen, O., B., Stein, R., Thiebault, F., Zachos, J., and Zimmerman, 1989a. Proceedings of the Ocean Drilling Program, Leg 105. Washington, D.C. (U.S. Government Printing Office), v. 105, part 1, pp. 917.

Srivastava, S. P., Arthur, M. A.,Clement, B. Aksu, A., Baldauf, J., Bohrmann, G., Busch, W., Cederberg, T., Cremer, M., Dadey, K., De Vernal, A., Firth, J., Hall, F., Head, M., Hiscott, R., Jarrard, R., Kaminski, M., Lazarus, D., Monjanel, A., L., Nielsen, O., B., Stein, R., Thiebault, F., Zachos, J., and Zimmerman, 1989b. Proceedings of the Ocean Drilling Program, Leg 105. Washington, D.C. (U.S. Government Printing Office), v. 105, part 1, pp. 1038.

Stanley, D.J, Got, H., Leenhart, O., and Weiler, Y., 1974. Subsidence of the Western Mediterranean Basin in Pliocene–Quaternary time: Further evidence: Geology, v. 2, p. 345– 350.

Stommel, H., 1958a. The circulation of the abyss: Scientific American, July, p. 85–90.

Stommel, H., 1958b. The abyssal circulation. Deep Sea Research, v. 5, p. 80–82.

Stommel, H., 1958c. The Gulf Stream. University of California Press and Cambridge Press, p. 202.

Stow, D.A., and Holbrook, J.A., 1984. Hatton Drift contourites, Northeast Atlantic, Deep Sea Drilling Project Leg 81. In Initial Reports of DSDP, Roberts, D.G, Schnitker, D., et al. (eds.), v. 81, p. 695–699.

Streeter, S.S., 1973. Bottom water and benthic foraminifera in the North Atlantic – glacial–interglacial contrast. Quaternary Research, v. 3., p. 131–141.

Streeter, S.S., 1976. Deep water benthic foraminiferal faunas in the Atlantic during the late Pleistocene – the significance of uvigerinid peaks. EOS, Transitions of American Geographysics. Union, v. 57, p. 258.

Streeter, S.S., and Shackleton, N.J., 1979. Paleocirculation of the deep North Atlantic 150,000 years record of benthic foraminifera and oxygen–18: Science, v. 203, p. 168–171.

Streeter, S.S., Belanger, P.E., Kellogg, T.B., and Duplessy, J.C., 1982, Late Pleistocene paleo– oceanography of the Norwegian–Greenland Sea: Benthic foraminiferal evidence. Quaternary Research, v. 18, p. 72–90.

Suess, E., 1901. "Das Antlith der Erde.", Bd., Wien.

Takayama, T., and Sato, T., 1987. Coccolith biostratigraphy of the North Atlantic Ocean, Deep Sea Drilling Project Leg 94, In Ruddiman, W.F.,, Fidd, R.B., et al. (eds.), Initial Reports of Deep Sea Drilling Project, Leg 94, part 2, Washington, D.C. (U.S. Government Printing Office), v. 94, p. 651–702.

Takayanagi, Y., 1953. New genus and species of Foraminifera found in the Tonohama group, Kochi Prefecture, Shikoku, Japan. Institution of Geology and Paleontology (Sendai), short paper, v. 5, p. 25-36.

Takayanagi, Y., and Saito, T. 1962. Planktonic foraminifera from the Nobori Formation, Shikoku, Japanese Scientific Reports, Tohoku Imp. University, ser. 2(Geology), special volume 5, p. 67-105.

Talwani, M., Udintsev, G. et al., 1976. Initial Reports of Deep Sea Drilling Project Leg 38, Washington, D.C., U.S. Government Printing Office, v. 38, p. 1-1256.

Thiede, J., 1980. Paleoceanography, margin stratigraphy and paleophysiography of the Tertiary North Atlantic and Norwegian–Greenland Seas. Philosophical Transaction of Royal Society, London, v. 345, p. 177–185.

Thomas, E., 1986. Early to middle Miocene benthic foraminiferal faunas from DSDP Sites 608 and 610, North Atlantic. In North Atlantic Paleoceanography, Summerhays, C.P., and Shackleton, N.J. (eds.), p. 205–218.

Thomas, E., 1987a. Early to Middle Miocene benthic foraminiferal faunas from DSDP Sites 608 and 610, North Atlantic. In Summerhayes, C., and Shackleton, N.J.

(Eds.), North Atlantic Paleoceanography. Journal of Geological Society, London Special Papers, p. 205–218.

Thomas, E., 1987b. Late Oligocene to Recent benthic foraminifers from Deep Sea Drilling Project Sites 608 and 610, northeastern North Atlantic. In Ruddiman, W.F., Kidd, R.B., Baldauf, J.G. et al., Initial Reports of the Deep Sea Drilling Project Leg 94, Washington. D.C., U.S. Government Printing Office, v. 94, p. 997–1015.

Thomas, F. C., Medioli, F. S., and Scott, D. B., 1990. Holocene and latest wisconsinan benthic foraminiferal assemblages and paleocirculation history, Lower Scotian Slope and Rise. Micropaleontology, v. 20, p. 212-245.

Thunell, R.C., 1981. Late Miocene–early Pliocene planktonic foraminiferal biostratigraphy and paleoceanography of low–latitude marine sequences. Marine Micropaleontology, v. 6., p. 71–90.

Thunell, R.C., D. F. Williams, and Howell, M., 1987. Atlantic–Mediterranean water exchange during the late Neogene. Paleoceanography, v. 2., p. 661–678.

Todd, R. 1957. Smaller Foraminifera. In: Geology of Saipa Mariana Islands, Part 3: Paleontology. Professional Papers U. S. Geological Survey, 280-H, p. 265-320.

Turnau, R., and Ledbetter, M.T., 1989. Deep circulation change in the south Atlantic Ocean: response to initiation of Northern Hemisphere glaciation. Paleoceanograhy, v. 4, p. 565–583.

Uchio, T., 1951. New species and genus of the foraminifera of the Cenozoic formations in the middle part of the Boso Peninsula, Chiba - Ken, Japan, Transactions and Proceedings of the Palaeontological Society of Japan, n. ser. v. 2, p. 33-42.

Ujiie, H., 1990. Bathyal benthic foraminifera in a piston core from east off Miyako islands, ryukyu island Arc. Bulletia of the college of science, University of the Ryukyus, No. 49, pp. 60, pls.32.

Vail, P.R., Mitchum, R.M., Jr., and Thompson, S. III, 1977. Global cycles of relative changes of sea level. In Seismic Stratigraphy–Application to Hydrocarbon Exploration, Payton, C.E. (ed.) AAPG, Memoir, v. 26, p. 83–97.

Van Couvering, J.A., Berggren, W.A., Drake, R.E., Aguirre, E., and Curtis, G.H., 1976, The terminal Miocene events: Marine Micropaleontology, v. 1, p. 263–286.

Van der Zwaan, G.J., 1980. The impact of climatic changes on the deep sea benthos. Proc. Kon. Nederlandse Akad. Wetenschappen, Ser. B, v. 83, p. 379–397.

Van der Zwaan, G. J., 1981. Paleoecology of late Miocene Mediferranean foraminifera. Utrecht Micropaleontological Bullentins, I. G. C. P. projcet No. 1, pp. 202.

Van Hinte, J., 1979. Subsidence of the Iceland–Faeroe Ridge. Abstract, Geological Society, London, v. 133, p. 159 (Abstract).

Van Morkhoven, F.P.C.M., Berggren, W.A., and Edwards, A.S., 1986. Cenozoic cosmopolitan deep–water benthic foraminifera. Elf Aquitaine Press, p. 1–421.

Veum, T., Jansen, E., Arnold, M., Beyer, I., Duplessy, J.C., 1992. Water mass exchange between the North Atlantic and the Norwegian Sea during the past 28,000 years. Nature, v. 456, p. 783– 785.

Vincent, E., Killingley, J.S., and Berger. W.H., 1980, The magnetic epoch–6 shift: A change in the ocean's 13C/12C ratio 6.2 million years ago. Marine Micropaleontology, v. 5, p. 185–203.

Vogt, P.R., 1972. The Faeroe–Iceland–Greenland seismic ridge and the western boundary undercurrent. Nature, v. 239, p. 79–81.

Walters, R. 1965. The *Globorotalia zealandica* and *G. miozea* lineages. New Zealand Journal of Geology and Geophysics, v. 8, p. 109-27.

Wang, P., Zhang, J., Zhao, Q. et al., 1988. Foraminifera and ostracoda in bottom sediments of the East China Sea. Ocean Press, (in Chinese with English summary), p. 1–438.

Weaver, P.P.E, 1987. Late Miocene to recent planktonic foraminifers from the North Atlantic: Deep Sea Drilling Project 94. In Ruddiman, W.F.,, Fidd, R.B., et al. (eds.), Initial Reports of Deep Sea Drilling Project, Leg 94, part 2, Washington, D.C. (U.S. Government Printing Office), v. 94, p. 703–728.

Weaver, P.P.E, and Clement, B.M., 1987. Magnetostratigraphy of planktonic foraminiferal datums: Deep Sea Drilling Project Leg 94, North Atlantic. In Ruddiman, W.F.,, Fidd, R.B., et al. (eds.), Initial Reports of Deep Sea Drilling Project, Leg 94, part 2, Washington, D.C. (U.S. Government Printing Office), v. 94, p. 815-830.

Weijermars, R., 1988. Neogene tectonics in the Western Mediterranean may have caused the Messinian Salinity Crisis and an associated glacial event. Tectonophysics, v. 148, p. 211-219.

Weston, J.F., and Murray, J.W., 1984. Benthic foraminifera as deep–sea water–mass indicators. In: Oetli, H.J. (ed.), Benthos, 1983. 2nd Int. Symp. Benthic Foraminifera. (Paul, France, 1983) Elf Aquitaine, Esso REP and Total CFP, Pau and Bordeaux, p. 605–610.

White, R., and McKenzie, D., 1989. Magnetism at rift zones: The generation of volcanic continental margins and flood basalts. Journal of Geophysical Research, v. 94, p. 7685– 7730.

Williamson, W. C., 1858. On Recent Foraminifera of Great Britain. Royal Society Publisher, p. 1-107.

Winterer, E.L., and Hinz, K., 1984. The evolution of the Mazagan continental margin: A synthesis of geophysical and geological data with results of drilling during Deep Sea Drilling Project Leg 79. In Hinz, K., Winterer, E.L., et al. (eds.), Initial Reports of Deep Sea Drilling Project, Leg 79, part 2, Washington, D.C. (U.S. Government Printing Office), v. 79, p. 893–922.

Wolf, T.C.W., 1991. Palăo-ozeanographisch-Klimatische entwicklung des Nördlichen Nordatlantiks seit dem späten Neogen (ODP Legs 105 und 104, DSDP Leg 81, Geomar Report 5, p. 1-92.

Wooddruff, F., and Savin, S.M., 1989. Miocene deepwater oceanography. Paleoceanography, v. 4, p. 87–140.

Worthington, L.V., 1970. The Norwegian Sea as a mediterranean basin. Deep Sea Research., v. 17, p. 77–84.

Worthington, L.V., 1976. On the North Atlantic circulation. The John Hopkins Oceanographic Studies No. 6, The John Hopkins University Press, p. 1–110.

Worthington, L.V., and Wright, W.R., 1970. North Atlantic Ocean atlas of potential temperature and salinity in the deep water, including temperature, salinity and oxygen profiles from the Erika Dan cruise of 1962. Woods Hole Oceanographic Institution Atlas Series, v. 2, 58 plates.

Wright, J.D., and Miller, K.G., 1992. Miocene stable isotope stratigraphy, Site 747, Kerguelen Plateau. In Proceedings of Ocean Drilling Program, Scientific results, Wise, S.W., Schlich, R. et al. (Eds.), v. 120, p. 855–866.

Wright, J.D., Miller, K.G., and Fairbanks, R.G., 1991. Evolution of modern deepwater circulation: Evidence from the late Miocene Southern Ocean. Paleoceanography, v. 6, p. 275–290.

Wright, R., Neogene benthic foraminifers from from DSDP Leg 42A, Mediterranean Sea. Initial Reports of the Deep Sea Drilling Project, Washington, D.C. (U.S. Government Printing Office), v. 42A, p. 709-726.

Zahn, R., Sarnthein, M., and Erlenkeuser, H., 1987. Benthic isotope evidence for changes of the Mediterranean outflow during the late Quaternary. Paleoceanography, v. 2, p. 543–559.

Zhang, J. and Scott, D. B., 1995. New planktonic foraminiferal genus and species from the upper Oligocene, DSDP 366A, Leg 41. Micropaleontology (Spring issue), v. 41, p. 77-83.

Zhang, J., Miller, K.G., and Berggren, W.B., 1993. Neogene planktonic foraminiferal biostratigraphy of northeastern Gulf of Mexico. Micropaleontology, v. 39, p. 299–326.